Université Fédérale

Toulouse Midi-Pyrénées

THÈSE

En vue de l'obtention du

DOCTORAT DE L'UNIVERSITÉ DE TOULOUSE

Délivré par :

Institut Supérieur de l'Aéronautique et de l'Espace

Présentée et soutenue par :
Andrea BRUGNOLI

le lundi 9 novembre 2020

Titre :

A port-Hamiltonian formulation of flexible structures. Modelling and structure-preserving finite element discretization

Une formulation port-Hamiltonienne des structures flexibles. Modélisation et discrétisation symplectique par éléments finis

---

École doctorale et discipline ou spécialité :

EDSYS : Automatique

Unité de recherche :

Équipe d'accueil ISAE-ONERA CSDV

Directeur(s) de Thèse :

M. Daniel ALAZARD (directeur de thèse)
Mme Valérie POMMIER-BUDINGER (co-directrice de thèse)

Jury :

M. Thomas HÉLIE Directeur de recherche LSTMS - Président
M. Daniel ALAZARD Professeur ISAE-SUPAERO - Directeur de thèse
M. Yann LE GORREC Professeur ENSMM - Rapporteur
M. Alessandro MACCHELLI Professore Associato Università di Bologna - Rapporteur
M. Denis MATIGNON Professeur ISAE-SUPAERO
Mme Valérie POMMIER-BUDINGER Professeure ISAE-SUPAERO- Co-directrice de thèse

Abstract

This thesis aims at extending the port-Hamiltonian (pH) approach to continuum mechanics in higher geometrical dimensions (particularly in 2D). The pH formalism has a strong multiphysics character and represents a unified framework to model, analyze and control both finite- and infinite-dimensional systems. Despite the large literature on this topic, elasticity problems in higher geometrical dimensions have almost never been considered. This work establishes the connection between port-Hamiltonian distributed systems and elasticity problems. The originality resides in three major contributions. First, the novel pH formulation of plate models and coupled thermoelastic phenomena is presented. The use of tensor calculus is mandatory for continuum mechanical models and the inclusion of tensor variables is necessary to obtain an intrinsic, i.e. coordinate free, and equivalent pH description. Second, a finite element based discretization technique, capable of preserving the structure of the infinite-dimensional problem at a discrete level, is developed and validated. This methodology relies on an abstract integration by parts formula and can be applied to linear and non-linear hyperbolic and parabolic systems. Several finite elements for beams and plates structures are proposed and tested. The discretization of elasticity problems in port-Hamiltonian form requires the use of non-standard finite elements. Nevertheless, the numerical implementation is performed thanks to well-established open-source libraries, providing external users with an easy to use tool for simulating flexible systems in port-Hamiltonian form. Third, flexible multibody systems are recast in pH form by making use of a floating frame description valid under small deformations assumptions. This reformulation include all kinds of linear elastic models and exploits the intrinsic modularity of pH systems.

Résumé

Cette thèse vise à étendre l'approche port-Hamiltonienne (pH) à la mécanique des milieux continus dans des dimensions géométriques plus élevées (en particulier on se focalise sur la dimension 2). Le formalisme pH, avec son fort caractère multi-physique, représente un cadre unifié pour modéliser, analyser et contrôler les systèmes de dimension finie et infinie. Malgré l'abondante littérature sur ce sujet, les problèmes d'élasticité en deux ou trois dimensions géométriques n'ont presque jamais été considérés. Dans ce travail de thèse la connexion entre problèmes d'élasticité et systèmes distribués port-Hamiltoniens est établie. L'originalité apportée réside dans trois contributions majeures. Tout d'abord, une nouvelle formulation pH des modèles de plaques et des phénomènes thermoélastiques couplés est présentée. L'utilisation du calcul tensoriel est obligatoire pour modéliser les milieux continus et l'introduction de variables tensorielles est nécessaire pour obtenir une description pH équivalente qui soit intrinsèque, c'est-à-dire indépendante des coordonnées choisies. Deuxièmement, une technique de discrétisation basée sur les éléments finis et capable de préserver la structure du problème de la dimension infinie au niveau discret est développée et validée. Cette méthodologie repose sur une formule d'intégration par parties abstraite et peut être appliquée aux systèmes hyperboliques et paraboliques linéaires et non linéaires. Plusieurs éléments finis pour les structures minces (poutres et plaques) sont proposés et testés. La discrétisation des problèmes d'élasticité écrits en forme port-Hamiltonienne nécessite l'utilisation d'éléments finis non standards. Néanmoins, l'implémentation numérique est réalisée grâce à des bibliothèques open source bien établies, fournissant aux utilisateurs externes un outil facile à utiliser pour simuler des systèmes flexibles sous forme pH. Troisièmement, une nouvelle formulation pH de la dynamique multicorps flexible est dérivée. Cette reformulation, valable sous de petites hypothèses de déformations, inclut toutes sortes de modèles élastiques linéaires et exploite la modularité intrinsèque des systèmes pH.

Acknowledgments

This incredible experience has finally come to an end. Certainly there is no ending without a beginning. I must therefore thank Daniel, Valérie and Denis for encouraging me to undertake this path and for always supporting and motivating me during these last three years. A sincere acknowledgment goes to Alessandro Macchelli and Yann Le Gorrec, for the time devoted to reviewing this work and for their infectious passion for research and science. Boundless thanks go obviously to my family, which in any circumstance has always been by my side and has been able to direct me when the way forward was not clear.

These 5 years spent in France were absolutely memorable. Heartfelt thanks to Fabizio, who gave me a roof and educated me on the most arcane mysteries of mathematical thought. Thanks to the marvelous Italian-Spanish family (Albert, Andrea Ac., Anthea, Alessio, Antonio, Daniel Francesco M., Lorenzo, Luca M., Matteo, Raul, Sara) for making me feel at home and for spoiling me with their delicacies. Special thanks to Paolo, for his energy and enthusiasm, who made me understand how important it is to live fully, without fear of the unknown. The Italian family then expanded at the beginning of this PhD. The reckless Andrea An., Andrea G., Francesco T., Manfredo, Michele and Nina have been companions of many exciting adventures, as well as of idle days, where time seemed to stand still. Every hour spent with you has always been meaningful to me. In this extended family I met Francesco S. and I understood that affinities transcend any regional border.

Thanks to Adeline, Clément, Sebastien, Virgile I got to know French culture closely. I never felt like a stranger with them. Among the many experiences made in this doctorate, the stay in Brazil was undoubtedly the densest. Thanks to Flavio's generosity and Mauricio's good heart, I was able to live peacefully and discover that even in adversity you can always smile.

At ISAE I found many passionate people, who always had advice and a word to cheer me up. I refer to Michel, Ghislain and Xavier, Caroline, Nicolas, Michelle, Laurent, Guillame and Remy. Thanks to the friends of a lifetime, who have always been present: Andrea G., Bianca, Davide, Eugenio, Jacopo and Marta.

The end of this doctorate coincides with the beginning of a new adventure in the Netherlands. Here I was welcomed by a new family, this time Italian-French: I sincerely thank Federico, Luigi, Quentin, Davide and Sara for their extraordinary welcome.

Special thanks to Ionna, because with you I feel that becoming a better person is achievable.

Remerciements

Cette incroyable expérience a enfin pris fin. Il n'y a certainement pas de fin sans début. Je dois donc remercier Daniel, Valérie et Denis de m'avoir encouragé à entreprendre ce chemin et de m'avoir toujours soutenu et motivé durant ces trois dernières années. Je remercie sincèrement Alessandro Macchelli et Yann Le Gorrec, pour le temps consacré à la revue de ces travaux et pour leur passion contagieuse pour la recherche et la science. Des remerciements infinis vont évidemment à ma famille qui, en toute circonstance, a toujours été à mes côtés et a su me diriger quand la voie à suivre n'était pas claire.

Ces 5 années passées en France ont été absolument mémorables. Un grand merci à Fabizio, qui m'a permis d'avoir un toit sur ma tête et m'a appris les mystères les plus obscurs de la pensée mathématique. Merci à la merveilleuse famille italo-espagnole (Albert, Andrea Ac., Anthea, Alessio, Antonio, Daniel Francesco M., Lorenzo, Luca M., Matteo, Raul, Sara) de m'avoir fait sentir chez moi et de m'avoir gâté avec leur gourmandises. Un merci spécial à Paolo, pour son énergie et son enthousiasme, qui m'a fait comprendre à quel point il est important de vivre pleinement, sans crainte de l'inconnu. La famille italienne s'est ensuite agrandie au début de ce doctorat. Les intrépides Andrea An., Andrea G., Francesco T., Manfredo, Michele et Nina ont été les compagnons de nombreuses aventures passionnantes, ainsi que de jours de paresse, où le temps semblait s'être arrêté. Chaque heure passée avec vous a toujours été significative pour moi. Dans cette famille élargie, j'ai rencontré Francesco S. et j'ai compris que les affinités transcendent toute frontière régionale.

Grâce à Adeline, Clément, Sébastien, Virgile, j'ai connu de près la culture française. Je ne me suis jamais senti étranger avec eux. Parmi les nombreuses expériences faites dans ce doctorat, le séjour au Brésil a sans doute été le plus dense. Grâce à la générosité de Flavio et au bon cœur de Mauricio, j'ai pu vivre sereinement et découvrir que même dans l'adversité, on peut toujours sourire.

À l'ISAE, j'ai trouvé de nombreuses personnes passionnées, qui avaient toujours des conseils et un mot pour me remonter le moral. Je parle de Michel, Ghislain et Xavier, Caroline, Nicolas, Michelle, Laurent, Guillame et Rémy. Merci aux amis de toute une vie, toujours présents: Andrea G., Bianca, Davide, Eugenio, Jacopo et Marta.

La fin de ce doctorat coïncide avec le début d'une nouvelle aventure aux Pays-Bas. Ici, j'ai été accueilli par une nouvelle famille, cette fois italo-française: je remercie sincèrement Federico, Luigi, Quentin, Davide et Sara pour leur accueil extraordinaire.

Un merci spécial à Ionna, car grâce à toi je pense que devenir une meilleure personne est

réalisable.

Ringraziamenti

Questa incredibile esperienza è finalmente giunta al termine. Certo non vi è conclusione senza un inizio. Devo allora ringraziare Daniel, Valérie e Denis per avermi incoraggiato a intraprendere questo percorso e per avermi sempre sostenuto, accompagnato e motivato durante questi ultimi tre anni. Un sincero ringraziamento va a Alessandro Macchelli e Yann Le Gorrec, per il tempo dedicato alla revisione di questo lavoro e per la loro passione contagiosa per la ricerca e la scienza. Un ringraziamento sconfinato va ovviamente alla mia famiglia, che in qualsiasi circonstanza è sempre stata al mio fianco e ha saputo direzionarmi quanda la strada da seguire non era chiara.

Questi 5 anni passati in Francia sono stati assolutamente memorabili. Un sentito grazie a Fabizio, che mi ha dato un tetto e istruito su i più arcani misteri del pensiero matematico. Grazie alla meravigliosa famiglia italo-spagnola (Albert, Andrea Ac., Anthea, Alessio, Antonio, Daniel Francesco M., Lorenzo, Luca M., Matteo, Raul, Sara) per avermi fatto sentire a casa e per avermi viziato con i loro manicaretti. Un ringraziamento speciale a Paolo, alla sua energia e entusiasmo, che mi fatto comprendere quanto sia importante vivere pienamente, senza paura dell'ignoto. La famiglia italiana si è poi estesa all'inizio di questo dottorato. I temerari Andrea An., Andrea G., Francesco T., Manfredo, Michele e Nina sono stati compagni di molte avventure concitate, così come di giornate oziose, dove il tempo sembrava fermarsi. Ogni ora passata con voi è sempre stata significativa. In questa famiglia estesa ho conosciuto Francesco S. e ho capito che le affinità trascendono ogni frontiera regionale.

Grazie a Adeline, Clément, Sebastien, Virgile ho conosciuto la cultura francese da vicino. Con loro non mi sono mai sentito straniero. Tra le tante esperienze fatte in questo dottorato, il soggiorno in Brasile è stata senz'altro la più densa. Grazie alla generosità di Flavio e al buoncuore di Mauricio ho potuto vivere serenamente e scoprire che anche nelle avversità si può sempre sorridere.

All'ISAE ho trovato tante persone appassionate, che avevano sempre un consiglio e una parola per rincuorarmi. Mi riferisco a Michel, Ghislain e Xavier, Caroline, Nicolas, Michelle, Laurent, Guillame e Remy. Un grazie agli amici di una vita, che sono sempre stati presenti: Andrea G., Bianca, Davide, Eugenio, Jacopo e Marta.

La fine di questo dottorato coincide con l'inizio di una nuova avventura in Olanda. Qui sono stato accolto da una nuova famiglia, questa volta italo-francese: ringrazio di cuore Davide, Federico, Luigi, Quentin e Sara per il loro straordinario benvenuto.

Un grazie speciale a Ionna, perché con te sento che diventare una persona migliore è

un'impresa realizzabile.

Alla mia famiglia

Contents

List of Figures

List of Tables

List of Acronyms

AFW	*Arnold-Falk-Winther*
BDM	*Brezzi-Douglas-Marini*
BJT	*Bécache-Joly-Tsogka*
CG	*Continuous Galerkin*
DAE	*Differential-Algebraic Equation*
DG	*Discontinuous Galerkin*
dpHs	*distributed port-Hamiltonian systems*
FEM	*Finite Element Method*
FFR	*Floating Frame of Reference*
FMS	*Flexible Multibody System*
HHJ	*Hellan-Herrmann-Johnson*
PDE	*Partial Differential Equation*
PFEM	*Partitioned Finite Element Method*
pH	*port-Hamiltonian*
pHs	*port-Hamiltonian systems*
pHDAE	*port-Hamiltonian Descriptor System*
RT	*Raviart-Thomas*

Résumé en français

Contents

R.1 Contexte et motivations

Ce travail vise à explorer le formalisme port-Hamiltonien (pH) comme paradigme de modélisation, en particulier pour le cas des structures flexibles. Ce formalisme bénéficie de nombreuses propriétés intéressantes, car il combine intrinsèquement la géométrie avec la théorie des réseaux et du contrôle [vdS06]. Une caractéristique puissante de ce formalisme, en particulier pour la tâche de modélisation, est sa modularité. Les systèmes port-Hamiltonien (pHs) de dimension finie peuvent être facilement interconnectés entre eux [CvdSB07]. L'interconnexion est également possible dans le cas de dimension infinie [KZvdSB10, Aug20]. Finalement, il est également possible de coupler des systèmes pH finis et infinis [Pas06]. Cette fonctionnalité est particulièrement utile pour simplifier la tâche de modélisation dans les analyses préliminaires, ou, au contraire, pour réaliser des modèles haute fidélité de phénomènes multiphysiques complexes.

Le cadre port-Hamiltonien a été largement utilisé pour modéliser et contrôler des systèmes distribués issus de divers modèles physiques: poutres de Timoshenko [MM04] et Euler-Bernoulli [ACRMA17], propagations d'ondes acoustiques [TRLGK18], réacteurs chimiques [RMS13], plasma dans les tomahawks [VNLF16] et interactions fluide-structure [CRMPB17]. La grande majorité de ces exemples se réfèrent à des modèles unidimensionnels. En effet, pour les systèmes pH linéaires unidimensionnels avec un opérateur anti-adjoint généralisé, [LGZM05] donne des conditions sur l'affectation des entrées et sorties aux limites pour

que l'opérateur système génère un semi-groupe de contraction. Ce résultat a été largement utilisé pour construire des contrôleurs de frontière passifs pour les systèmes hyperboliques [VZLGM09, MLGRZ16, MLGR20].

Depuis leur introduction, les systèmes port-Hamiltoniens distribués (dpH) ont été définis sur des domaines spatiaux multidimensionnels en utilisant le langage des formes différentielles [vdSM02]. Dans [Vil07], la modélisation pH et l'approche en semi-groupe de systèmes à dimension infinie sont combinées. Dans cet article, le cas des domaines multidimensionnels n'est que brièvement discuté. De nombreux exemples de pHs sur des domaines multidimensionnels sont détaillés dans [DMSB09, Chapitre 4]. Cependant, les résultats d'existence et d'unicité n'y sont pas présentés. Une première contribution en ce sens peut être trouvée dans [KZ15], où les auteurs démontrent l'existence et l'unicité de l'équation d'onde linéaire dans des dimensions géométriques arbitraires. Le récent article [Skr19] généralise ce résultat pour traiter le cas des pHs linéaires génériques du premier ordre dans des dimensions géométriques arbitraires. Malgré toute cette littérature préexistante, les modèles issus de la mécanique structurale sur des domaines multidimensionnels n'ont quasiment jamais été considérés (à l'exception notable de [MMB05] pour la modélisation de la plaque de Mindlin).

Le potentiel du formalisme pH comme paradigme de modélisation a été récemment exploré par les chercheurs. Par exemple, dans [EK18], les auteurs considèrent un modèle port-Hamiltonien pour la propagation des ondes de pression dans les réseaux des tuyaux. En employant un schéma d'éléments finis mixtes, les auteurs réalisent une discrétisation préservant la structure du modèle d'origine. Un algorithme de réduction de modèle pour ce modèle discrétisé de réseau de pipelines est ensuite discuté dans [EKLS$^+$18]. Ces travaux récents confirment la validité de ce cadre pour aborder des scénarios d'application complexes et soulignent l'importance des algorithmes de discrétisation préservant la structure. Disposer de méthodologies capables de construire des discrétisations fiables est important non seulement pour la simulation, mais aussi à des fins de contrôle. En particulier, dans [TWRLG20], les auteurs développent une méthode de synthèse systématique pour la conception de contrôleurs-observateurs pour le contrôle frontière des pHs sur des domaines spatiaux unidimensionnels. Pour construire l'observateur, une version discrétisée appropriée du système est supposée disponible.

Cette thèse tente d'établir un lien clair entre les modèles de la mécanique structurale linéaire en dimension n-D et les systèmes port-Hamiltoniens, à la fois pour les tâches de modélisation et de discrétisation. Ces deux finalités sont en effet fortement liées dans le contexte des pHs. Pour obtenir une formulation pH pour les modèles d'élasticité, il faut introduire la variable d'effort, associée à l'énergie de déformation, comme inconnue principale supplémentaire. Ajouter la variable de contrainte comme inconnue est le point de départ des éléments finis mixtes [Arn90]. Cela conduit à la décomposition de l'opérateur elliptique initial (c'est-à-dire le Laplacien ou bi-Laplacien), en deux opérateurs formellement adjoints. Par conséquent, la dynamique est régulée par un opérateur adjoint formellement antisymétrique,

conduisant ainsi à un système Hamiltonien. Après avoir effectué une intégration par parties, une discrétisation mixte est immédiatement réalisée [Jol03]. Ce raisonnement très concis élucide de manière informelle le lien étroit entre la modélisation port-Hamiltonienne de la mécanique des milieux continuum et les éléments finis mixtes.

R.2 Plan de la thèse

L'organigramme de la thèse est illustré sur la Fig. 1. La thèse est divisée en quatre parties principales.

Partie I (Chapitres 1, 2) Cette partie donne une introduction générale des travaux sur les systèmes pH. Le chapitre 2 rappelle brièvement ce que sont les systèmes pH de dimension finie ou infinie et comment ces systèmes sont profondément liés à la structure géométrique de Dirac ou de Stokes-Dirac (pour le cas de dimension finie et infinie respectivement).

Partie II (Chapitres 3, 4, 5) Cette partie est consacrée à la formulation de modèles pH appropriés d'élasticité et de thermoélasticité. Cette partie est subdivisée en trois chapitres.

- Le chapitre 3 détaille la formulation pH pour l'élasticité linéaire n-D générale.
- Une formulation pH des modèles des plaques minces (Kirchhoff-Love) et épaisses (Mindlin-Reissner) est donnée dans le chapitre 4.
- Le problème thermoélastique linéaire entièrement couplé est modélisé comme un système pH couplé dans le chapitre 5.

Partie III (Chapitres 6, 7, 8) Cette partie est consacrée à la discussion et à l'implémentation du principal outil de discrétisation: la méthode des éléments finis partitionnés (PFEM). Cette méthode est une extension naturelle des éléments finis mixtes pour la discrétisation des pHs. Cette partie se compose de trois chapitres.

- Une description détaillée du principe de fonctionnement de PFEM est donnée au chapitre 6 dans le corps principal de la thèse. Les bases d'approximation de cette discrétisation ne sont pas explicitement définies dans ce chapitre, car la méthode peut être implémentée en utilisant soit des éléments finis, soit des méthodes spectrales.
- Une étude de convergence de plusieurs éléments finis est illustrée au chapitre 7 pour la flexion de structures minces (poutres et plaques). Il ne s'agit en aucun cas d'une analyse mathématique rigoureuse de la convergence. Cependant, grâce à des résultats préexistants dans la littérature, les estimations d'erreur sont conjecturées et validées par des expériences numériques.

- Le chapitre 8 est dédié aux applications de la méthode PFEM. En particulier, l'accent est mis sur la stabilisation par injection d'amortissement, l'application des conditions aux limites mixtes et la validation du modèle pH thermoélastique pour une solution analytique.

Partie IV (Chapitres 9, 10) Dans cette partie, une formulation pH des systèmes multi-corps flexibles est discutée et validée. Le chapitre 9 détaille la dérivation d'un système pH associé à un corps flottant flexible sous l'hypothèse des petites déformations. Plusieurs applications sont alors considérées dans le chapitre 10.

R.3 Modélisation port-Hamiltonien des structures flexibles

Dans cette section, un résumé concis des résultats concernant la modélisation de l'élasticité et la thermoélasticité linéaire est reporté. Une discussion détaillée peut être retrouvée dans les chapitres 3, 4 et 5.

L'élasticité linéaire comme système port-Hamiltonien

Dans cette section, une formulation port-Hamiltonienne de l'élasticité est déduite du problème classique d'élastodynamique. Il faut souligner que, déjà dans les années soixante-dix, une formulation purement hyperbolique de l'élasticité a été détaillée [HM78]. Le point manquant est le lien clair avec la théorie des EDP Hamiltoniens. Une formulation Hamiltonienne peut être trouvée dans [Gri15, Chapitre 16], mais sans aucun lien avec le concept de structure de Stokes-Dirac induit par la géométrie sous-jacente.

Variables d'énergie et de co-énergie Considérons un ensemble ouvert connecté $\Omega \subset \mathbb{R}^d$, $d \in \{2, 3\}$. Dans le cadre de l'élasticité linéaire, le déplacement $\boldsymbol{u}$ dans un continuum déformable est donné par

$$\rho \frac{\partial^2 \boldsymbol{u}}{\partial t^2} - \operatorname{Div}(\boldsymbol{\mathcal{D}} \operatorname{Grad} \boldsymbol{u}) = 0, \qquad \boldsymbol{x} \in \Omega.$$

où ρ est la densité et $\boldsymbol{\mathcal{D}}$ est le tenseur de rigidité (cf. Eq. 3.5). Les opérateurs différentielles Div, Grad sont définis dans l'appendice A. Pour dériver une formulation pH, l'énergie totale, qui comprend l'énergie cinétique et de déformation, est nécessaire

$$H = \frac{1}{2} \int_\Omega \left\{ \rho \, \|\partial_t \boldsymbol{u}\|^2 + \boldsymbol{\Sigma} : \boldsymbol{\varepsilon} \right\} \, \mathrm{d}\Omega.$$

La notation $\boldsymbol{A} : \boldsymbol{B} = \operatorname{Tr}(\boldsymbol{A}^\top \boldsymbol{B}) = \sum_{i,j} A_{ij} B_{ij}$ désigne la contraction des tenseurs. Souvenez-vous que $\boldsymbol{\varepsilon} = \operatorname{Grad} \boldsymbol{u}$ et $\boldsymbol{\Sigma} = \boldsymbol{\mathcal{D}} \boldsymbol{\varepsilon}$. Les variables d'énergie sont alors l'impulsion linéaire et le

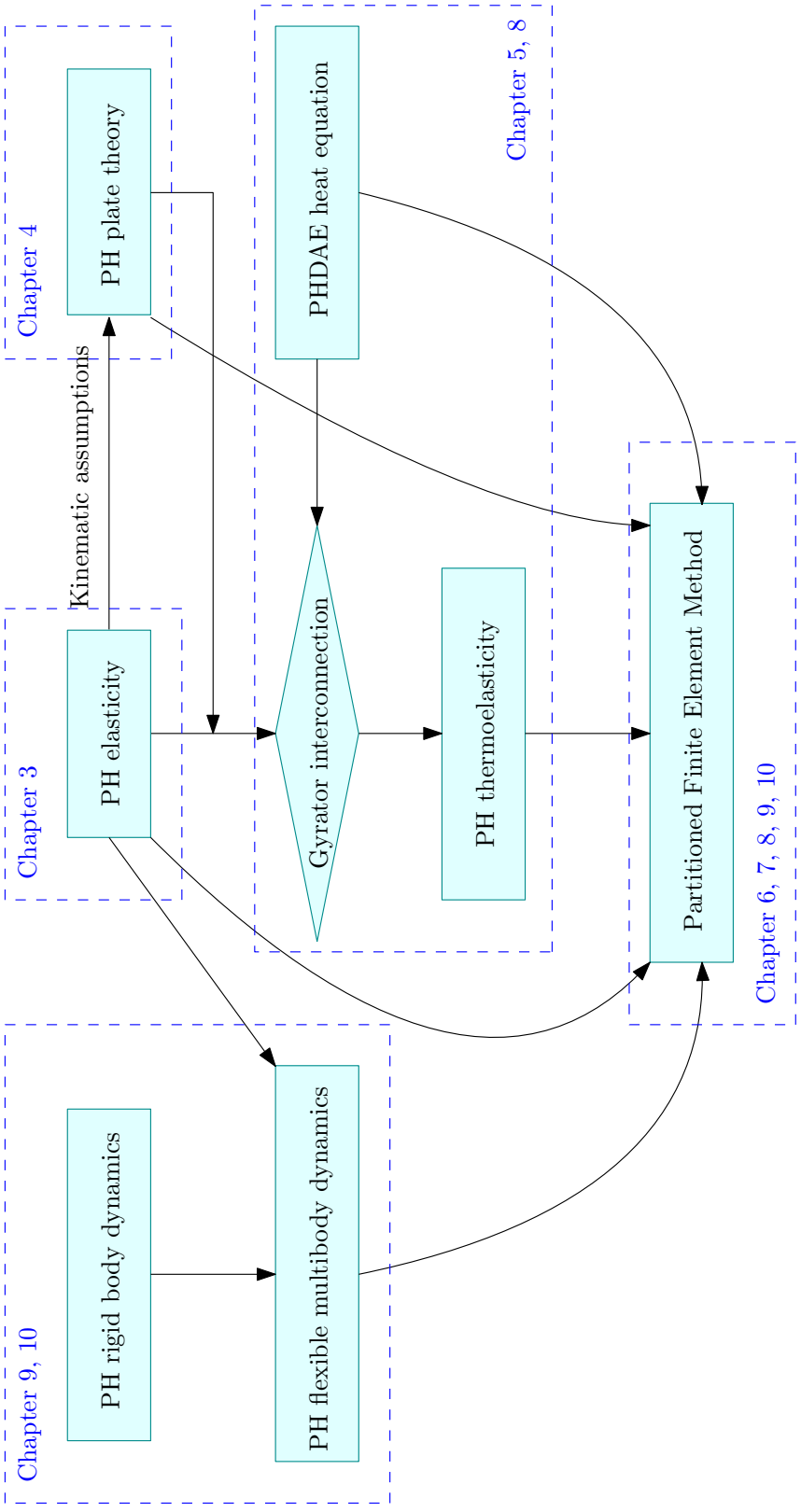

Figure 1: Organigramme de la thèse.

champ de déformation

$$\boldsymbol{\alpha}_v = \rho \boldsymbol{v}, \qquad \boldsymbol{A}_\varepsilon = \boldsymbol{\varepsilon},$$

où $\boldsymbol{v} := \partial_t \boldsymbol{u}$. L'Hamiltonien peut être réécrit comme une fonctionnelle quadratique dans les variables d'énergie

$$H = \frac{1}{2} \int_\Omega \left\{ \frac{1}{\rho} \|\boldsymbol{\alpha}_v\|^2 + (\boldsymbol{\mathcal{D}} \boldsymbol{A}_\varepsilon) : \boldsymbol{A}_\varepsilon \right\} \mathrm{d}\Omega.$$

Les variables de co-énergie sont données par

$$\boldsymbol{e}_v := \frac{\delta H}{\delta \boldsymbol{\alpha}_v} = \boldsymbol{v}, \qquad \boldsymbol{E}_\varepsilon := \frac{\delta H}{\delta \boldsymbol{A}_\varepsilon} = \boldsymbol{\Sigma}.$$

Formulation port-Hamiltonien finale Il est maintenant possible d'expliciter la forme pH du système

$$\frac{\partial}{\partial t} \begin{pmatrix} \boldsymbol{\alpha}_v \\ \boldsymbol{A}_\varepsilon \end{pmatrix} = \begin{bmatrix} \boldsymbol{0} & \mathrm{Div} \\ \mathrm{Grad} & \boldsymbol{0} \end{bmatrix} \begin{pmatrix} \boldsymbol{e}_v \\ \boldsymbol{E}_\varepsilon \end{pmatrix}.$$

La première équation du système est la conservation du moment linéaire. La seconde représente une condition de compatibilité. Le théorème 2 assure que l'opérateur différentiel est formellement anti-adjoint (on peut également trouver ce résultat dans [PZ20, Lemme 3.3], disponible sous la forme de pré-impression arXiv).

Les variables aux bord sont ensuite trouvées en évaluant le bilan de puissance

$$\begin{aligned}
\dot{H} &= \int_\Omega \{ \boldsymbol{e}_v \cdot \partial_t \boldsymbol{\alpha}_v + \boldsymbol{E}_\varepsilon : \partial_t \boldsymbol{A}_\varepsilon \} \ \mathrm{d}\Omega, \\
&= \int_\Omega \{ \boldsymbol{e}_v \cdot \mathrm{Div}\, \boldsymbol{E}_\varepsilon + \boldsymbol{E}_\varepsilon : \mathrm{Grad}\, \boldsymbol{e}_v \} \ \mathrm{d}\Omega, \\
&= \int_\Omega \mathrm{div}(\boldsymbol{E}_\varepsilon\, \boldsymbol{e}_v) \ \mathrm{d}\Omega, \qquad \text{Théorème de Stokes (voir Appendix A Eq. (A.6))}, \\
&= \int_{\partial\Omega} \boldsymbol{e}_v \cdot (\boldsymbol{E}_\varepsilon \boldsymbol{n}) \ \mathrm{d}S = \langle \boldsymbol{e}_v,\, \boldsymbol{E}_\varepsilon\, \boldsymbol{n} \rangle_{L^2(\partial\Omega, \mathbb{R}^d)}.
\end{aligned}$$

L'imposition du champ de vitesse le long de la frontière $\boldsymbol{e}_v = \partial_t \boldsymbol{u}$ correspond à une condition de Dirichlet. Si c'est la traction qui est imposée $\boldsymbol{E}_\varepsilon\, \boldsymbol{n} = \boldsymbol{\Sigma}\, \boldsymbol{n} = \boldsymbol{t}$, on a une condition de Neumann. Considérons une partition de la frontière $\partial\Omega = \overline{\Gamma}_N \cup \overline{\Gamma}_D$ et $\Gamma_N \cap \Gamma_D = \{\emptyset\}$, où une condition de Dirichlet et une condition de Neumann s'appliquent respectivement aux sous-ensemble ouvert Γ_D et Γ_N (voir Fig. 3.2). Ensuite, la formulation pH finale devient

$$\frac{\partial}{\partial t}\begin{pmatrix}\boldsymbol{\alpha}_v\\ \boldsymbol{A}_\varepsilon\end{pmatrix} = \underbrace{\begin{bmatrix}\mathbf{0} & \mathrm{Div}\\ \mathrm{Grad} & \mathbf{0}\end{bmatrix}}_{\mathcal{J}}\begin{pmatrix}\boldsymbol{e}_v\\ \boldsymbol{E}_\varepsilon\end{pmatrix},$$

$$\boldsymbol{u}_\partial = \underbrace{\begin{bmatrix}\boldsymbol{\gamma}_0^{\Gamma_D} & \mathbf{0}\\ \mathbf{0} & \boldsymbol{\gamma}_n^{\Gamma_N}\end{bmatrix}}_{\mathcal{B}_\partial}\begin{pmatrix}\boldsymbol{e}_v\\ \boldsymbol{E}_\varepsilon\end{pmatrix}, \qquad \boldsymbol{y}_\partial = \underbrace{\begin{bmatrix}\mathbf{0} & \boldsymbol{\gamma}_n^{\Gamma_D}\\ \boldsymbol{\gamma}_0^{\Gamma_N} & \mathbf{0}\end{bmatrix}}_{\mathcal{C}_\partial}\begin{pmatrix}\boldsymbol{e}_v\\ \boldsymbol{E}_\varepsilon\end{pmatrix},$$

où $\boldsymbol{\gamma}_0^{\Gamma_*}$, $* = \{D, N\}$ désigne la trace sur l'ensemble Γ_*, soit $\boldsymbol{\gamma}_0^{\Gamma_*}\boldsymbol{e}_v = \boldsymbol{e}_v|_{\Gamma_*}$. De plus, $\boldsymbol{\gamma}_n^{\Gamma_*}$ désigne la trace normale sur l'ensemble Γ_*, à savoir $\boldsymbol{\gamma}_n^{\Gamma_*}\boldsymbol{E}_\varepsilon = \boldsymbol{E}_\varepsilon\boldsymbol{n}|_{\Gamma_*}$. Les opérateurs de frontière $\mathcal{B}_\partial, \mathcal{C}_\partial$ sont non bornés.

Le modèles de plaques en forme port-Hamiltonien

Dans cette section on résume les modèles port-Hamiltonien de plaques minces. On s'intéresse en particulier aux modèles dus à Mindlin [Min51] (plaques épaisses) et Kirchhoff (plaques minces).

Plaque de Mindlin Ce modèle décrit les déformations des plaques modérément épaisses, i.e. le rapport entre l'épaisseur et la longueur est de l'ordre de 10^{-1}. Le système final est donné par 2 EDP couplées ayant comme inconnus le déplacement vertical w et la rotation $\boldsymbol{\theta}$ des segments perpendiculaires à la surface non déformée (pour les détails de calculs voir [Red06, Chapter 10])

$$\rho h\frac{\partial^2 w}{\partial t^2} = \operatorname{div}\boldsymbol{q}, \qquad (x,y)\in\Omega,$$
$$\frac{\rho h^3}{12}\frac{\partial^2\boldsymbol{\theta}}{\partial t^2} = \operatorname{Div}\boldsymbol{M} + \boldsymbol{q},$$

où h est l'épaisseur, $\boldsymbol{M} = \boldsymbol{\mathcal{D}}_b\operatorname{Grad}\boldsymbol{\theta}$ et $\boldsymbol{q} = K_{\mathrm{sh}}Gh\,(\operatorname{grad} w - \boldsymbol{\theta})$. $\Omega\subset\mathbb{R}^2$ est un domaine connecté et borné. Le tenseur de rigidité à flexion $\boldsymbol{\mathcal{D}}_b$ est donné, dans la cas d'un matériel isotrope, par l'Eq. (4.11). K_{sh} est le facteur correctif du au cisaillement et G le module du cisaillement.

Considérons l'Hamiltonien (énergie totale)

$$H = \frac{1}{2}\int_\Omega\left\{\rho h\left(\frac{\partial w}{\partial t}\right)^2 + \frac{\rho h^3}{12}\left\|\frac{\partial\boldsymbol{\theta}}{\partial t}\right\|^2 + \boldsymbol{M}:\boldsymbol{\kappa} + \boldsymbol{q}\cdot\boldsymbol{\gamma}\right\}\mathrm{d}\Omega,$$

où $\boldsymbol{\kappa} = \operatorname{Grad}\boldsymbol{\theta}$, $\boldsymbol{\gamma} = \operatorname{grad} w - \boldsymbol{\theta}$. Le choix des variables d'énergie est le même que dans [MMB05] mais ici des variables scalaires, vectorielles et tensorielles sont regroupées:

$\alpha_w = \rho h\dfrac{\partial w}{\partial t}$,	Moment linéaire,	$\boldsymbol{\alpha}_\theta = \dfrac{\rho h^3}{12}\dfrac{\partial\boldsymbol{\theta}}{\partial t}$,	Moment angulaire,
$\boldsymbol{A}_\kappa = \boldsymbol{\kappa}$,	Tenseur de courbure,	$\boldsymbol{\alpha}_\gamma = \boldsymbol{\gamma}$.	Déformation au cisaillement.

L'Hamiltonien est maintenant une fonctionnelle quadratique dans les variables d'énergies

$$H = \frac{1}{2}\int_\Omega \left\{ \frac{1}{\rho h}\alpha_w^2 + \frac{12}{\rho h^3}\left\|\boldsymbol{\alpha}_\theta\right\|^2 + (\boldsymbol{\mathcal{D}}_b \boldsymbol{A}_\kappa) : \boldsymbol{A}_\kappa + (\boldsymbol{\mathcal{D}}_s \boldsymbol{\alpha}_\gamma)\cdot\boldsymbol{\alpha}_\gamma \right\} \,\mathrm{d}\Omega,$$

Les variables de co-énergie sont trouvées en calculant la dérivée variationnelle de l'Hamiltonien:

$$e_w := \frac{\delta H}{\delta \alpha_w} = \frac{\partial w}{\partial t}, \quad \text{Vitesse linéaire,} \qquad \boldsymbol{e}_\theta := \frac{\delta H}{\delta \boldsymbol{\alpha}_\theta} = \frac{\partial \boldsymbol{\theta}}{\partial t}, \quad \text{Vitesse angulaire,}$$
$$\boldsymbol{E}_\kappa := \frac{\delta H}{\delta \boldsymbol{A}_\kappa} = \boldsymbol{M}, \quad \text{Tenseur de moments,} \qquad \boldsymbol{e}_\gamma := \frac{\delta H}{\delta \boldsymbol{\alpha}_\gamma} = \boldsymbol{q} \quad \text{Effort tranchant.}$$

Une fois les variables concaténées, le système pH est exprimé comme suit

$$\frac{\partial}{\partial t}\begin{pmatrix} \alpha_w \\ \boldsymbol{\alpha}_\theta \\ \boldsymbol{A}_\kappa \\ \boldsymbol{\alpha}_\gamma \end{pmatrix} = \begin{bmatrix} 0 & 0 & 0 & \mathrm{div} \\ \boldsymbol{0} & \boldsymbol{0} & \mathrm{Div} & \boldsymbol{I}_{2\times 2} \\ \boldsymbol{0} & \mathrm{Grad} & \boldsymbol{0} & \boldsymbol{0} \\ \mathrm{grad} & -\boldsymbol{I}_{2\times 2} & \boldsymbol{0} & \boldsymbol{0} \end{bmatrix} \begin{pmatrix} e_w \\ \boldsymbol{e}_\theta \\ \boldsymbol{E}_\kappa \\ \boldsymbol{e}_\gamma \end{pmatrix}.$$

Nous allons maintenant établir le bilan énergétique total en termes de variables au bord car elles feront partie de la structure de Stokes-Dirac sous-jacente de ce modèle. Le bilan de puissance devient

$$\dot{H} = \int_{\partial\Omega} \{ w_t\, q_n + \omega_n\, M_{nn} + \omega_s\, M_{ns} \} \,\mathrm{d}s.$$

Le résultat est obtenu en appliquant le théorème de Stokes. Les variables au bord (illustrées dans la Fig. 4.2) sont définies comme suit:

$$\begin{aligned} \text{Effort de cisaillement} \quad & q_n := \boldsymbol{q}\cdot\boldsymbol{n} = \boldsymbol{e}_\gamma\cdot\boldsymbol{n}, \\ \text{Moment de flexion} \quad & M_{nn} := \boldsymbol{M} : (\boldsymbol{n}\otimes\boldsymbol{n}) = \boldsymbol{E}_\kappa : (\boldsymbol{n}\otimes\boldsymbol{n}), \\ \text{Moment de torsion} \quad & M_{ns} := \boldsymbol{M} : (\boldsymbol{s}\otimes\boldsymbol{n}) = \boldsymbol{E}_\kappa : (\boldsymbol{s}\otimes\boldsymbol{n}), \end{aligned}$$

Étant donné deux vecteurs $\boldsymbol{a}\in\mathbb{R}^n$, $\boldsymbol{b}\in\mathbb{R}^m$, la notation $\boldsymbol{a}\otimes\boldsymbol{b} = \boldsymbol{a}\boldsymbol{b}^\top \in \mathbb{R}^{n\times m}$ désigne le produit extérieur (ou dyadique) de deux vecteurs. Les vecteurs $\boldsymbol{n}$ et $\boldsymbol{s}$ désignent les vecteurs unitaires normaux et tangentiels à la frontière, comme le montre la Fig. 4.3. Les variables conjuguées au sens de la puissance sont

$$\begin{aligned} \text{Vitesse verticale} \quad & w_t := \frac{\partial w}{\partial t} = e_w, \\ \text{Rotation en flexion} \quad & \omega_n := \frac{\partial \boldsymbol{\theta}}{\partial t}\cdot\boldsymbol{n} = \boldsymbol{e}_\theta\cdot\boldsymbol{n}, \\ \text{Rotation en torsion} \quad & \omega_s := \frac{\partial \boldsymbol{\theta}}{\partial t}\cdot\boldsymbol{s} = \boldsymbol{e}_\theta\cdot\boldsymbol{s}. \end{aligned}$$

Considérons une partition de la frontière $\partial\Omega = \overline{\Gamma}_C \cup \overline{\Gamma}_S \cup \overline{\Gamma}_F$, $\Gamma_C \cap \Gamma_S \cap \Gamma_F = \{\emptyset\}$. Les sous-ensembles ouverts Γ_C, Γ_S, Γ_F peuvent être vides. Les conditions aux limites de la plaque Mindlin [DHNLS99] (voir Fig. 4.4) qui sont considérées sont:

- Encastrement (C) sur $\Gamma_C \subseteq \partial\Omega$: $w_t,\ \omega_n,\ \omega_s$ connus;
- Bord simplement appuyé (S) sur $\Gamma_S \subseteq \partial\Omega$: $w_t,\ \omega_s,\ M_{nn}$ connus;
- Bord libre (F) sur $\Gamma_F \subseteq \partial\Omega$: $M_{nn},\ M_{ns},\ q_n$ connus.

Ensuite, la formulation finale pH devient

$$\frac{\partial}{\partial t}\begin{pmatrix}\alpha_w\\ \boldsymbol{\alpha}_\theta\\ \boldsymbol{A}_\kappa\\ \boldsymbol{\alpha}_\gamma\end{pmatrix} = \underbrace{\begin{bmatrix}0 & 0 & 0 & \operatorname{div}\\ \mathbf{0} & \mathbf{0} & \operatorname{Div} & \boldsymbol{I}_{2\times 2}\\ \mathbf{0} & \operatorname{Grad} & \mathbf{0} & \mathbf{0}\\ \operatorname{grad} & -\boldsymbol{I}_{2\times 2} & \mathbf{0} & \mathbf{0}\end{bmatrix}}_{\mathcal{J}}\begin{pmatrix}e_w\\ \boldsymbol{e}_\theta\\ \boldsymbol{E}_\kappa\\ \boldsymbol{e}_\gamma\end{pmatrix},$$

$$\boldsymbol{u}_\partial = \underbrace{\begin{bmatrix}\gamma_0^{\Gamma_C} & 0 & 0 & 0\\ 0 & \gamma_n^{\Gamma_C} & 0 & 0\\ 0 & \gamma_s^{\Gamma_C} & 0 & 0\\ \gamma_0^{\Gamma_S} & 0 & 0 & 0\\ 0 & \gamma_s^{\Gamma_S} & 0 & 0\\ 0 & 0 & \gamma_{nn}^{\Gamma_S} & 0\\ 0 & 0 & \gamma_{nn}^{\Gamma_F} & 0\\ 0 & 0 & \gamma_{ns}^{\Gamma_F} & 0\\ 0 & 0 & 0 & \gamma_n^{\Gamma_F}\end{bmatrix}}_{\mathcal{B}_\partial}\begin{pmatrix}e_w\\ \boldsymbol{e}_\theta\\ \boldsymbol{E}_\kappa\\ \boldsymbol{e}_\gamma\end{pmatrix}, \qquad \boldsymbol{y}_\partial = \underbrace{\begin{bmatrix}0 & 0 & 0 & \gamma_n^{\Gamma_C}\\ 0 & 0 & \gamma_{nn}^{\Gamma_C} & 0\\ 0 & 0 & \gamma_{ns}^{\Gamma_C} & 0\\ 0 & 0 & 0 & \gamma_n^{\Gamma_S}\\ 0 & 0 & \gamma_{ns}^{\Gamma_S} & 0\\ 0 & \gamma_n^{\Gamma_S} & 0 & 0\\ 0 & \gamma_n^{\Gamma_F} & 0 & 0\\ 0 & \gamma_s^{\Gamma_F} & 0 & 0\\ \gamma_0^{\Gamma_F} & 0 & 0 & 0\end{bmatrix}}_{\mathcal{C}_\partial}\begin{pmatrix}e_w\\ \boldsymbol{e}_\theta\\ \boldsymbol{E}_\kappa\\ \boldsymbol{e}_\gamma\end{pmatrix},$$

où $\gamma_0^{\Gamma_*} a = a|_{\Gamma_*}$ désigne la trace sur l'ensemble Γ_*, $* = \{C, S, F\}$. De plus, les notations $\gamma_n^{\Gamma_*}\boldsymbol{a} = \boldsymbol{a}\cdot\boldsymbol{n}|_{\Gamma_*}$, $\gamma_s^{\Gamma_*}\boldsymbol{a} = \boldsymbol{a}\cdot\boldsymbol{s}|_{\Gamma_*}$ indiquent respectivement les traces normales et tangentielles sur l'ensemble Γ_*. Les symboles $\gamma_{nn}^{\Gamma_*}, \gamma_{ns}^{\Gamma_*}$ désignent la trace normale-normale et la trace normale-tangentielle des fonctions tensorielles $\gamma_{nn}^{\Gamma_*}\boldsymbol{A} = \boldsymbol{A} : (\boldsymbol{n}\otimes\boldsymbol{n})|_{\Gamma_*}$, $\gamma_{ns}^{\Gamma_*}\boldsymbol{A} = \boldsymbol{A} : (\boldsymbol{n}\otimes\boldsymbol{s})|_{\Gamma_*}$.

Plaque de Kirchhoff Le modèle de Kirchhoff correspond à une EDP scalaire qui décrit l'évolution du déplacement vertical pour des plaques minces (rapport entre épaisseur et longueur de l'ordre de $10^{-2} - 10^{-3}$). Le modèle peut être dérivé en utilisant le principe de Hamilton et est donné par l'équation suivante (pour les calculs détaillés, le lecteur peut consulter [Red06, Chapter 3])

$$\rho h\frac{\partial^2 w}{\partial t^2} = -\operatorname{div}\operatorname{Div}(\boldsymbol{\mathcal{D}}_b \operatorname{Grad}\operatorname{grad} w), \qquad (x, y) \in \Omega.$$

Encore une fois, le point de départ pour obtenir une formulation port-Hamiltonien est l'Hamiltonien (énergie totale)

$$H = \frac{1}{2}\int_\Omega \left\{\rho h\left(\frac{\partial w}{\partial t}\right)^2 + \boldsymbol{M} : \boldsymbol{\kappa}\right\}\,\mathrm{d}\Omega,$$

où $\boldsymbol{\kappa} = \operatorname{Grad}\operatorname{grad} w$, $\boldsymbol{M} = \boldsymbol{\mathcal{D}}_b \operatorname{Grad}\operatorname{grad} w$. En ce qui concerne le choix des variables

d'énergie, une variable scalaire et une variable tensorielle sont considérées:

$$\alpha_w = \rho h \frac{\partial w}{\partial t}, \quad \text{Moment linéaire,} \qquad \boldsymbol{A}_\kappa = \boldsymbol{\kappa}, \quad \text{Tenseur de corbure.}$$

Les variables de co-énergie sont trouvées en calculant la dérivée variationnelle de l'Hamiltonien:

$$e_w := \frac{\delta H}{\delta \alpha_w} = \frac{\partial w}{\partial t}, \quad \text{Vitesse linéaire,} \qquad \boldsymbol{E}_\kappa := \frac{\delta H}{\delta \boldsymbol{A}_\kappa} = \boldsymbol{M}, \quad \text{Tenseur de moment.}$$

Le système port-Hamiltonien associé s'écrit de la manière suivante

$$\frac{\partial}{\partial t}\begin{pmatrix}\alpha_w \\ \boldsymbol{A}_\kappa\end{pmatrix} = \begin{bmatrix} 0 & -\operatorname{div}\circ\operatorname{Div} \\ \operatorname{Grad}\circ\operatorname{grad} & \boldsymbol{0}\end{bmatrix}\begin{pmatrix} e_w \\ \boldsymbol{E}_\kappa\end{pmatrix}.$$

La première équation représente la dynamique, la seconde le fait que les dérivés d'ordre supérieur commutent. Le théorème 5, détaillé dans le manuscrit, assure que l'opérateur qui régit la dynamique est anti-symétrique. Le bilan de puissance fournit les variables au bord

$$\dot{H} = \int_{\partial\Omega} \{w_t\, \widetilde{q}_n + \partial_{\boldsymbol{n}} w_t\, M_{nn}\}\ \mathrm{d}s.$$

Les variables au bord sont définies

$$\begin{aligned} \text{Effort de cisaillement} \quad & \widetilde{q}_n := -\boldsymbol{n}\cdot\operatorname{Div}(\boldsymbol{E}_\kappa) - \partial_{\boldsymbol{s}} M_{ns}, \\ \text{Moment de flexion} \quad & M_{nn} := \boldsymbol{M} : (\boldsymbol{n}\otimes\boldsymbol{n}) = \boldsymbol{E}_\kappa : (\boldsymbol{n}\otimes\boldsymbol{n}). \end{aligned}$$

Les variables conjuguées au sens de la puissance sont données par

$$\begin{aligned} \text{Vitesse verticale} \quad & w_t := \frac{\partial w}{\partial t} = e_w, \\ \text{Rotation en flexion} \quad & \partial_{\boldsymbol{n}} w_t := \nabla e_w \cdot \boldsymbol{n}. \end{aligned}$$

Considérons une partition de la frontière $\partial\Omega = \overline{\Gamma}_C \cup \overline{\Gamma}_S \cup \overline{\Gamma}_F,\ \Gamma_C \cap \Gamma_S \cap \Gamma_F = \{\emptyset\}$, où $\Gamma_C, \Gamma_S, \Gamma_F$ sont des sous-ensembles ouverts de $\partial\Omega$. Les conditions aux limites pour la plaque de Kirchhoff [GSV18] sont les suivantes (voir Fig. 4.5):

- Encastrée (C) sur $\Gamma_C \subseteq \partial\Omega$: $w_t,\ \partial_{\boldsymbol{n}} w_t$ connu;
- Appui simple (S) sur $\Gamma_S \subseteq \partial\Omega$: $w_t,\ M_{nn}$ connu;
- Libre (F) sur $\Gamma_F \subseteq \partial\Omega$: $\widetilde{q}_n,\ M_{nn}$ connu.

Ensuite, la formulation finale du pH devient

$$\frac{\partial}{\partial t}\begin{pmatrix}\alpha_w\\ \boldsymbol{A}_\kappa\end{pmatrix} = \underbrace{\begin{bmatrix}0 & -\operatorname{div}\circ\operatorname{Div}\\ \operatorname{Grad}\circ\operatorname{grad} & \boldsymbol{0}\end{bmatrix}}_{\mathcal{J}}\begin{pmatrix}e_w\\ \boldsymbol{E}_\kappa\end{pmatrix},$$

$$\boldsymbol{u}_\partial = \underbrace{\begin{bmatrix}\gamma_0^{\Gamma_C} & 0\\ \gamma_1^{\Gamma_C} & 0\\ \gamma_0^{\Gamma_S} & 0\\ 0 & \gamma_{nn}^{\Gamma_S}\\ 0 & \gamma_{nn,1}^{\Gamma_F}\\ 0 & \gamma_{nn}^{\Gamma_F}\end{bmatrix}}_{\mathcal{B}_\partial}\begin{pmatrix}e_w\\ \boldsymbol{E}_\kappa\end{pmatrix}, \qquad \boldsymbol{y}_\partial = \underbrace{\begin{bmatrix}0 & \gamma_{nn,1}^{\Gamma_C}\\ 0 & \gamma_{nn}^{\Gamma_C}\\ 0 & \gamma_{nn,1}^{\Gamma_S}\\ \gamma_1^{\Gamma_S} & 0\\ \gamma_0^{\Gamma_F} & 0\\ \gamma_1^{\Gamma_F} & 0\end{bmatrix}}_{\mathcal{C}_\partial}\begin{pmatrix}e_w\\ \boldsymbol{E}_\kappa\end{pmatrix},$$

où $\gamma_0^{\Gamma_*}a = a|_{\Gamma_*}$ et $\gamma_1^{\Gamma_*}a = \partial_{\boldsymbol{n}}a|_{\Gamma_*}$ désignent respectivement la trace et la trace dérivée normale sur l'ensemble Γ_*. Le symbole $\gamma_{nn,1}^{\Gamma_*}$ désigne la trace $\gamma_{nn,1}^{\Gamma_*}\boldsymbol{A} = -\boldsymbol{n}\cdot\operatorname{Div}\boldsymbol{A} - \partial_{\boldsymbol{s}}(\boldsymbol{A}:(\boldsymbol{n}\otimes\boldsymbol{s}))|_{\Gamma_*}$, tandis que $\gamma_{nn}^{\Gamma_*}\boldsymbol{A} = \boldsymbol{A}:(\boldsymbol{n}\otimes\boldsymbol{n})|_{\Gamma_*}$ indique la trace normale-normale d'une fonction tensorielle.

Le problème thermoélastique linéaire couplé

Pour les problèmes thermoélastiques linéaires, on s'aperçoit que les modèles classique peuvent être réécrits comme deux systèmes port-Hamiltonien couplés. Considérons à nouveau l'équation d'élasticité sur $\Omega \subset \mathbb{R}^d$, $d \in \{1,2,3\}$, avec une entrée distribuée $\boldsymbol{u}_E$ qui joue le rôle d'une force externe

$$\frac{\partial}{\partial t}\begin{pmatrix}\boldsymbol{\alpha}_v\\ \boldsymbol{A}_\varepsilon\end{pmatrix} = \begin{bmatrix}\boldsymbol{0} & \operatorname{Div}\\ \operatorname{Grad} & \boldsymbol{0}\end{bmatrix}\begin{pmatrix}\boldsymbol{e}_v\\ \boldsymbol{E}_\varepsilon\end{pmatrix} + \begin{bmatrix}\boldsymbol{I}_{d\times d}\\ \boldsymbol{0}\end{bmatrix}\boldsymbol{u}_E,$$

$$\boldsymbol{y}_E = \begin{bmatrix}\boldsymbol{I}_{d\times d} & \boldsymbol{0}\end{bmatrix}\begin{pmatrix}\boldsymbol{e}_v\\ \boldsymbol{E}_\varepsilon\end{pmatrix},$$

avec l'Hamiltonien

$$H_E = \frac{1}{2}\int_\Omega \{\boldsymbol{\alpha}_v\cdot\boldsymbol{e}_v + \boldsymbol{A}_\varepsilon : \boldsymbol{E}_\varepsilon\}\ \mathrm{d}\Omega.$$

L'équation de la chaleur admet la représentation différentielle-algébrique (pHDAE) suivante

$$\begin{bmatrix}1 & 0\\ \boldsymbol{0} & \boldsymbol{0}\end{bmatrix}\frac{\partial}{\partial t}\begin{pmatrix}\alpha_T\\ \boldsymbol{j}_Q\end{pmatrix} = \begin{bmatrix}0 & -\operatorname{div}\\ -\operatorname{grad} & -(T_0k)^{-1}\end{bmatrix}\begin{pmatrix}e_T\\ \boldsymbol{j}_Q\end{pmatrix} + \begin{bmatrix}1\\ \boldsymbol{0}\end{bmatrix}u_T,$$

$$y_T = \begin{bmatrix}1 & \boldsymbol{0}\end{bmatrix}\begin{pmatrix}e_T\\ \boldsymbol{j}_Q\end{pmatrix},$$

où les variables sont définies comme suit

$$\alpha_T := \rho c_\epsilon(T - T_0), \qquad e_T := \frac{T - T_0}{T_0} =: \theta, \qquad \boldsymbol{j}_Q := -k\operatorname{grad}T.$$

Les paramètres c_ϵ, k, T_0 sont la capacité thermique à déformation constante, le coefficient de diffusivité et une température de référence. L'entrée u_T joue le rôle d'une source de chaleur distribuée. L'Hamiltonien corresponds à une fonctionnelle quadratique (c'est n'est pas l'énergie interne)

$$H_T = \frac{1}{2}\int_\Omega e_T \alpha_T \, \mathrm{d}\Omega.$$

Considérez l'interconnexion suivante

$$\boldsymbol{u}_E = -\operatorname{Div}(\boldsymbol{\mathcal{C}}_\beta \, y_T), \qquad u_T = -\boldsymbol{\mathcal{C}}_\beta : \operatorname{Grad}(\boldsymbol{y}_E).$$

où on a introduit l'opérateur de couplage

$$\boldsymbol{\mathcal{C}}_\beta := T_0 \beta (2\mu + 3\lambda) \boldsymbol{I}_{d\times d},$$

avec β le coefficient de dilatation thermique et λ, μ les coefficients de Lamé. L'interconnexion préserve l'énergie car elle peut être écrite de manière compacte comme

$$\boldsymbol{u}_E = \mathcal{A}_\beta(y_T), \qquad u_T = -\mathcal{A}_\beta^*(\boldsymbol{y}_E), \qquad \text{where} \qquad \mathcal{A}_\beta(\cdot) = -\operatorname{Div}(\boldsymbol{\mathcal{C}}_\beta \cdot),$$

où $\mathcal{A}_\beta^*$ indique l'adjoint formel. Le problème thermoélastique couplé peut maintenant être écrit comme

$$\begin{bmatrix} \mathbf{1} & \mathbf{0} & \mathbf{0} & \mathbf{0} \\ \mathbf{0} & \mathbf{1} & \mathbf{0} & \mathbf{0} \\ 0 & 0 & 1 & 0 \\ \mathbf{0} & \mathbf{0} & \mathbf{0} & \mathbf{0} \end{bmatrix} \frac{\partial}{\partial t} \begin{pmatrix} \boldsymbol{\alpha}_v \\ \boldsymbol{A}_\varepsilon \\ \alpha_T \\ \boldsymbol{j}_Q \end{pmatrix} = \begin{bmatrix} \mathbf{0} & \operatorname{Div} & \mathcal{A}_\beta & \mathbf{0} \\ \operatorname{Grad} & \mathbf{0} & \mathbf{0} & \mathbf{0} \\ -\mathcal{A}_\beta^* & 0 & 0 & -\operatorname{div} \\ \mathbf{0} & \mathbf{0} & -\operatorname{grad} & -(T_0 k)^{-1} \end{bmatrix} \begin{pmatrix} \boldsymbol{e}_v \\ \boldsymbol{E}_\varepsilon \\ e_T \\ \boldsymbol{j}_Q \end{pmatrix}.$$

Le bilan de puissance global est facilement calculé comme

$$\dot{H} = \dot{H}_E + \dot{H}_T \leq \int_{\partial\Omega} \{[\boldsymbol{E}_\varepsilon - e_T \boldsymbol{\mathcal{C}}_\beta] \cdot \boldsymbol{n}\} \cdot \boldsymbol{e}_v \, \mathrm{d}S - \int_{\partial\Omega} e_T \, \boldsymbol{j}_Q \cdot \boldsymbol{n} \, \mathrm{d}S.$$

Le système final et le bilan de puissance associé sont identiques aux résultats reportés dans [Car73, page 326, 332]. Soit une partition de la frontière $\partial\Omega = \Gamma_D^E \cup \Gamma_N^E = \Gamma_D^T \cup \Gamma_N^T$ pour le domaine élastique et thermique. Les conditions aux limites générales sont données par (voir Fig. 5.1)

$$\begin{aligned} \boldsymbol{e}_v \text{ connu sur } \Gamma_D^E \times (0,+\infty), \qquad & e_T \text{ connu sur } \Gamma_D^T \times (0,+\infty), \\ (\boldsymbol{E}_\varepsilon - \boldsymbol{\mathcal{C}}_\beta e_T) \cdot \boldsymbol{n} \text{ connu sur } \Gamma_N^E \times (0,+\infty), \qquad & \boldsymbol{j}_Q \cdot \boldsymbol{n} \text{ connu sur } \Gamma_N^T \times (0,+\infty). \end{aligned}$$

À partir du bilan de puissance, les conditions aux limites classiques sont extraites. Cela permet de définir des opérateurs de frontière appropriés pour le problème thermoélastique

$$\boldsymbol{u}_\partial = \underbrace{\begin{bmatrix} \gamma_0^{\Gamma_D^E} & \mathbf{0} & \mathbf{0} & \mathbf{0} \\ \mathbf{0} & \gamma_n^{\Gamma_N^E} & -\gamma_n^{\Gamma_N^E}(\boldsymbol{\mathcal{C}}_\beta \cdot) & \mathbf{0} \\ 0 & 0 & \gamma_0^{\Gamma_D^T} & 0 \\ \mathbf{0} & \mathbf{0} & \mathbf{0} & \gamma_n^{\Gamma_N^T} \end{bmatrix}}_{\mathcal{B}_\partial} \begin{pmatrix} \boldsymbol{e}_v \\ \boldsymbol{E}_\varepsilon \\ e_T \\ \boldsymbol{j}_Q \end{pmatrix}, \quad \boldsymbol{y}_\partial = \underbrace{\begin{bmatrix} \mathbf{0} & \gamma_n^{\Gamma_D^E} & -\gamma_n^{\Gamma_D^E}(\boldsymbol{\mathcal{C}}_\beta \cdot) & \mathbf{0} \\ \gamma_0^{\Gamma_N^E} & \mathbf{0} & \mathbf{0} & \mathbf{0} \\ \mathbf{0} & \mathbf{0} & \mathbf{0} & \gamma_n^{\Gamma_D^T} \\ 0 & 0 & \gamma_0^{\Gamma_N^T} & 0 \end{bmatrix}}_{\mathcal{C}_\partial} \begin{pmatrix} \boldsymbol{e}_v \\ \boldsymbol{E}_\varepsilon \\ e_T \\ \boldsymbol{j}_Q \end{pmatrix}.$$

R.4 Développement de la méthode PFEM

Dans cette section on résume les résultats concernant la développement d'une méthode de discrétisation reposant sur les éléments finis. Cette partie est traitée en détail dans les chapitres 6, 7, 8.

Une discrétisation préservant la structure est capable de construire un système pH équivalent qui possède les propriétés structurelles du modèle d'origine:

Système pH de dimension infinie

EDP avec entrées distribuées:

$$\partial_t \boldsymbol{\alpha}(\boldsymbol{x},t) = \mathcal{J}\delta_{\boldsymbol{\alpha}} H + \mathcal{B}\boldsymbol{u}_\Omega(\boldsymbol{x},t),$$
$$\boldsymbol{y}_\Omega(\boldsymbol{x},t) = \mathcal{B}^*\delta_{\boldsymbol{\alpha}} H.$$

Conditions aux limites:

$$\boldsymbol{u}_\partial = \mathcal{B}_\partial \delta_{\boldsymbol{\alpha}} H, \quad \boldsymbol{y}_\partial = \mathcal{C}_\partial \delta_{\boldsymbol{\alpha}} H.$$

Bilan de puissance (Théorème de Stokes):

$$\dot{H} = \int_{\partial\Omega} \boldsymbol{u}_\partial \cdot \boldsymbol{y}_\partial \, \mathrm{d}S + \int_\Omega \boldsymbol{u}_\Omega \cdot \boldsymbol{y}_\Omega \, \mathrm{d}\Omega.$$

Discretisation préservant la structure

EDO résultante:

$$\dot{\boldsymbol{\alpha}}_d = \mathbf{J}\nabla H_d + \mathbf{B}_\Omega \mathbf{u}_\Omega + \mathbf{B}_\partial \mathbf{u}_\partial,$$
$$\mathbf{y}_\Omega = \mathbf{B}_\Omega^\top \nabla H_d,$$
$$\mathbf{y}_\partial = \mathbf{B}_\partial^\top \nabla H_d.$$

Hamiltonien discrétisé:

$$H_d := H(\boldsymbol{\alpha} \equiv \boldsymbol{\alpha}_d).$$

Bilan de puissance discret:

$$\dot{H} = \mathbf{u}_\partial^\top \mathbf{y}_\partial + \mathbf{u}_\Omega^\top \mathbf{y}_\Omega.$$

Dans cette thèse, la méthode des éléments finis partitionnés (PFEM), présentée à l'origine dans [CRML18, CRML19], est choisie pour obtenir des modèles discrétisés des dpHs. Les éléments finis variationnels ont été largement utilisés pour discrétiser des systèmes hyperboliques linéaires fermés [Jol03]. On montrera que PFEM étend le cadre détaillé dans [Jol03] aux systèmes Hamiltoniens ouverts (c'est-à-dire contrôlés par les limites). De plus, il est également applicable aux systèmes non linéaires §6.1.2 et aux systèmes paraboliques §8.3 (voir aussi [SHM19a, SHM19b]). Cette procédure de discrétisation se résume à trois étapes simples

1. Le système est écrit sous une forme faible;

2. Une intégration par parties est appliquée pour mettre en évidence le contrôle frontière approprié;

3. Une méthode de Galerkin est utilisée pour obtenir un système de dimension finie. Pour les bases d'approximation, la méthode des éléments finis est utilisée ici, mais des méthodes spectrales peuvent également être utilisées.

Une fois le système mis en forme faible, un sous-ensemble d'équations est intégré par parties, de sorte que les variables limites sont naturellement incluses dans la formulation et apparaissent comme des entrées de contrôle, les sorties colocalisées étant définies en conséquence. La discrétisation des variables d'énergie et de co-énergie (et les fonctions de test associées) conduit directement à une représentation de rang complet pour le système pH de dimension finie. Cette approche rend possible l'utilisation de logiciels FEM, comme FEniCS [LMW+12], ou Firedrake [RHM+17]. La procédure est universelle, car elle repose sur une formule générale d'intégration par parties qui caractérise les pHs multidimensionnels.

Pour pouvoir appliquer cette méthodologie, deux hypothèses doivent être vérifiées.

Hypothèse R.1 (Structure partitionnée du système)
Le système doit posséder une structure partitionnée (cf. hypothèse 2)

$$\mathcal{J} = \begin{bmatrix} 0 & -\mathcal{L}^* \\ \mathcal{L} & 0 \end{bmatrix}, \qquad \begin{aligned} \mathcal{L}^* &: L^2(\Omega, \mathbb{B}) \to L^2(\Omega, \mathbb{A}), \\ \mathcal{L} &: L^2(\Omega, \mathbb{A}) \to L^2(\Omega, \mathbb{B}), \end{aligned}$$

où $\mathbb{A}$, $\mathbb{B}$ *sont des espace des scalaires, vecteurs, tenseurs ou un produit cartésien d'eux.*

Hypothèse R.2 (Formule d'intégration par partie abstraite)
Une formule d'intégration par partie abstraite, qui permet d'identifier des opérateurs au bord, est vérifiée (cf. hypothèse 3)

$$\langle \boldsymbol{u}_2,\, \mathcal{L}\, \boldsymbol{u}_1 \rangle_{L^2(\Omega,\mathbb{B})} - \langle \mathcal{L}^*\, \boldsymbol{u}_2,\, \boldsymbol{u}_1 \rangle_{L^2(\Omega,\mathbb{A})} = \langle \mathcal{N}_{\partial,1} \boldsymbol{u}_1,\, \mathcal{N}_{\partial,2} \boldsymbol{u}_2 \rangle_{L^2(\partial\Omega,\mathbb{R}^m)}\,.$$

Les opérateurs de frontière $\mathcal{B}_\partial$, $\mathcal{C}_\partial$ *sont alors supposés vérifier, de manière exclusive, soit*

$$\mathcal{B}_\partial = \begin{bmatrix} 0 & \mathcal{N}_{\partial,2} \end{bmatrix}, \qquad \mathcal{C}_\partial = \begin{bmatrix} \mathcal{N}_{\partial,1} & 0 \end{bmatrix},$$

ou bien

$$\mathcal{B}_\partial = \begin{bmatrix} \mathcal{N}_{\partial,1} & 0 \end{bmatrix}, \qquad \mathcal{C}_\partial = \begin{bmatrix} 0 & \mathcal{N}_{\partial,2} \end{bmatrix}.$$

Un système qui vérifie ces deux hypothèses, s'écrit alors sous la forme

$$\partial_t \begin{pmatrix} \boldsymbol{\alpha}_1 \\ \boldsymbol{\alpha}_2 \end{pmatrix} = \begin{bmatrix} 0 & -\mathcal{L}^* \\ \mathcal{L} & 0 \end{bmatrix} \begin{pmatrix} \delta_{\boldsymbol{\alpha}_1} H \\ \delta_{\boldsymbol{\alpha}_2} H \end{pmatrix}.$$

Les variables au bord sont alors données par

$$\boldsymbol{u}_\partial = \mathcal{N}_{\partial,2}\delta_{\boldsymbol{\alpha}_2} H, \qquad \boldsymbol{y}_\partial = \mathcal{N}_{\partial,1}\delta_{\boldsymbol{\alpha}_1} H,$$

ou bien

$$\boldsymbol{u}_\partial = \mathcal{N}_{\partial,1}\delta_{\boldsymbol{\alpha}_1} H, \qquad \boldsymbol{y}_\partial = \mathcal{N}_{\partial,2}\delta_{\boldsymbol{\alpha}_2} H.$$

L'application de la méthode donne lieu à deux formulations avec causalité opposée. En particulier, si on applique PFEM en intégrant par partie l'opérateur $-\mathcal{L}^*$, on obtient

$$\begin{aligned}
\begin{pmatrix} \dot{\boldsymbol{\alpha}}_{d,1} \\ \dot{\boldsymbol{\alpha}}_{d,2} \end{pmatrix} &= \begin{bmatrix} \mathbf{0} & -\mathbf{M}_1^{-1}\mathbf{D}_{\mathcal{L}}^\top \mathbf{M}_2^{-1} \\ \mathbf{M}_2^{-1}\mathbf{D}_{\mathcal{L}}\mathbf{M}_1^{-1} & \mathbf{0} \end{bmatrix} \begin{pmatrix} \partial_{\boldsymbol{\alpha}_{d,1}} H_d(\boldsymbol{\alpha}_d) \\ \partial_{\boldsymbol{\alpha}_{d,2}} H_d(\boldsymbol{\alpha}_d) \end{pmatrix} + \begin{bmatrix} \mathbf{B}_1 \\ \mathbf{0} \end{bmatrix} \mathbf{u}_\partial, \\
\mathbf{M}_\partial \mathbf{y}_\partial &= \begin{bmatrix} \mathbf{B}_1^\top & \mathbf{0} \end{bmatrix} \begin{pmatrix} \partial_{\boldsymbol{\alpha}_{d,1}} H_d(\boldsymbol{\alpha}_d) \\ \partial_{\boldsymbol{\alpha}_{d,2}} H_d(\boldsymbol{\alpha}_d) \end{pmatrix}.
\end{aligned}$$

Si par contre c'est l'opérateur $\mathcal{L}$ qui est intégré par partie, on trouve

$$\begin{aligned}
\begin{pmatrix} \dot{\boldsymbol{\alpha}}_{d,1} \\ \dot{\boldsymbol{\alpha}}_{d,2} \end{pmatrix} &= \begin{bmatrix} \mathbf{0} & \mathbf{M}_1^{-1}\mathbf{D}_{-\mathcal{L}^*}\mathbf{M}_2^{-1} \\ -\mathbf{M}_2^{-1}\mathbf{D}_{-\mathcal{L}^*}^\top \mathbf{M}_1^{-1} & \mathbf{0} \end{bmatrix} \begin{pmatrix} \partial_{\boldsymbol{\alpha}_{d,1}} H_d(\boldsymbol{\alpha}_d) \\ \partial_{\boldsymbol{\alpha}_{d,2}} H_d(\boldsymbol{\alpha}_d) \end{pmatrix} + \begin{bmatrix} \mathbf{0} \\ \mathbf{B}_2 \end{bmatrix} \mathbf{u}_\partial, \\
\mathbf{M}_\partial \mathbf{y}_\partial &= \begin{bmatrix} \mathbf{0} & \mathbf{B}_2^\top \end{bmatrix} \begin{pmatrix} \partial_{\boldsymbol{\alpha}_{d,1}} H_d(\boldsymbol{\alpha}_d) \\ \partial_{\boldsymbol{\alpha}_{d,2}} H_d(\boldsymbol{\alpha}_d) \end{pmatrix}.
\end{aligned}$$

Dans le Chapitre 6 la construction des matrices est expliquée de manière détaillée.

Exemple: les équations de Saint-Venant irrotationnelle (cf. §8.1.2) Un exemple concret d'application est représenté par les équations de Saint-Venant irrotationnelles

$$\begin{aligned}
\frac{\partial}{\partial t}\begin{pmatrix} \alpha_h \\ \boldsymbol{\alpha}_v \end{pmatrix} &= -\begin{bmatrix} 0 & \operatorname{div} \\ \operatorname{grad} & \mathbf{0} \end{bmatrix} \begin{pmatrix} \delta_{\alpha_h} H \\ \delta_{\boldsymbol{\alpha}_v} H \end{pmatrix}, \\
u_\partial &= -\delta_{\boldsymbol{\alpha}_v} H \cdot \boldsymbol{n}, \\
y_\partial &= \delta_{\alpha_h} H,
\end{aligned}$$

où l'Hamiltonien prendre la forme

$$H(\alpha_h, \boldsymbol{\alpha}_v) = \frac{1}{2}\int_\Omega \left\{ \frac{1}{\rho}\alpha_h \left\|\boldsymbol{\alpha}_v\right\|^2 + \rho g \alpha_h^2 \right\} \mathrm{d}\Omega,$$

avec g l'accélération de gravité. On peut donc utiliser la méthode PFEM pour simuler le système. Un cas d'application consiste à stabiliser ce modèle autour d'une certaine hauteur à travers la loi de commande suivante

$$u_\partial = -k(y_\partial - y_\partial^{\mathrm{des}}), \qquad y_\partial^{\mathrm{des}} = \rho g h^{\mathrm{des}}, \quad k > 0.$$

où h^{des} est l'hauteur du fluide désirée. Ce contrôle assure que la fonction de Lyapunov

$$V = \frac{1}{2}\int_{\Omega}\left\{\frac{1}{2}\rho g(\alpha_h - \alpha_h^{\text{des}})^2 + \frac{1}{2\rho}\alpha_h \left\|\boldsymbol{\alpha}_v\right\|^2\right\} d\Omega \geq 0,$$

où $\alpha_h^{\text{des}} = h^{\text{des}}$, a une dérivée en temps semi-défini négative. Selon le principe de LaSalle pour un système de dimension infini [Hen06], le point

$$\alpha_h = h^{\text{des}}, \qquad \boldsymbol{\alpha}_v = \mathbf{0},$$

est asymptotiquement stable.

Les instantanés de la simulation sont rassemblés dans la Fig. 3. L'évolution de l'Hamiltonien et de la fonction de Lyapunov (Fig. 2) montrent clairement que, alors que la fonction de Lyapunov diminue de manière monotone, l'Hamiltonien oscille autour de l'équilibre souhaité.

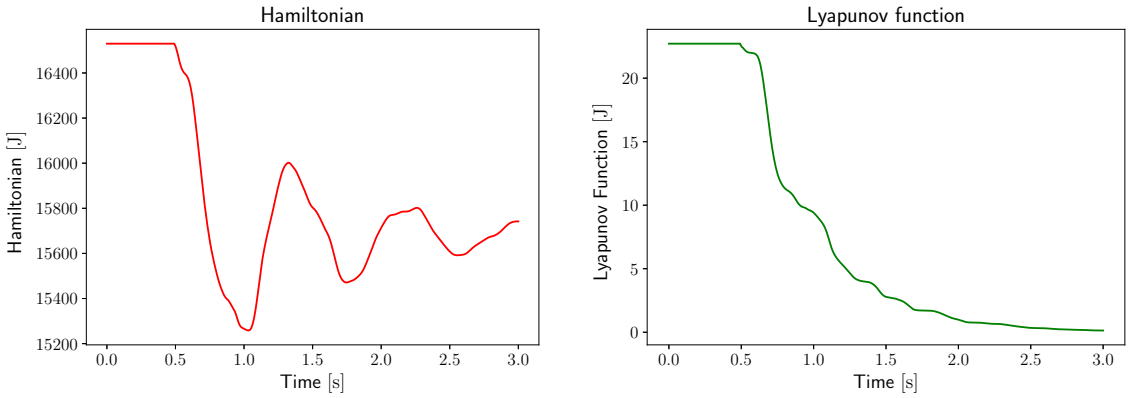

(a) Énergie totale (Hamiltonien) (b) Fonctionnelle de Lyapunov

Figure 2: Énergie totale et fonction de Lyapunov pour les équations des Saint Venant.

Le cas linéaire

Dans le cas linéaire, une simplification majeure se produit puisque la loi de comportement reliant les variables d'énergie et de co-énergie est facilement inversible. Cela permet une description basée uniquement sur des variables de co-énergie.

Pour rendre le système linéaire, une hypothèse supplémentaire est introduite.

Hypothèse R.3 (Hamiltonien quadratique séparable)
On suppose que l'Hamiltonien est une fonctionnelle quadratique positive par rapport aux variables d'énergie $\boldsymbol{\alpha}_1$, $\boldsymbol{\alpha}_2$. *De plus, l'Hamiltonien est considéré comme séparable par rapport à* $\boldsymbol{\alpha}_1$, $\boldsymbol{\alpha}_2$ *(cette hypothèse est toujours satisfaite pour les systèmes considérés). Par conséquent,*

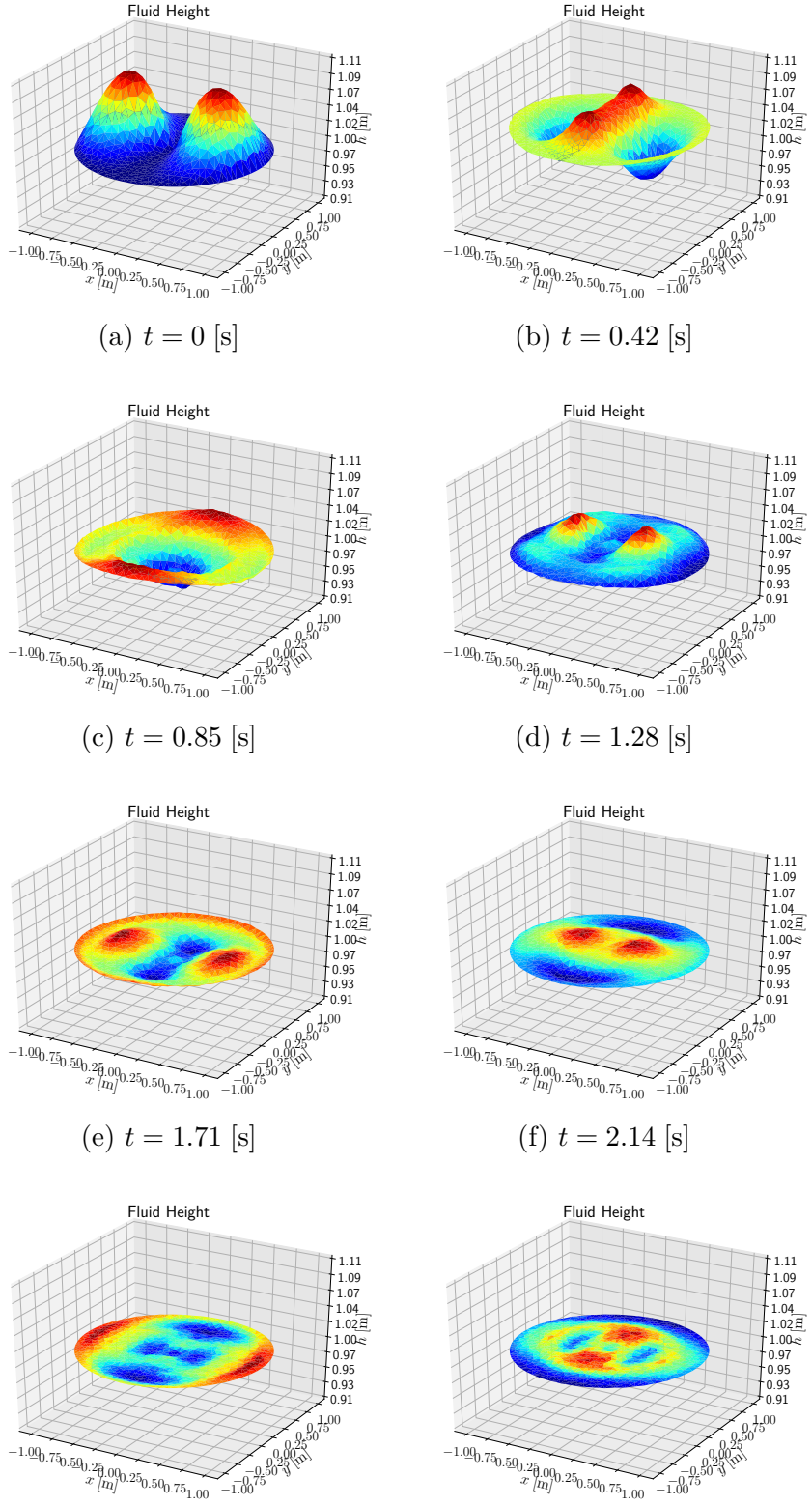

(a) $t = 0$ [s] (b) $t = 0.42$ [s]

(c) $t = 0.85$ [s] (d) $t = 1.28$ [s]

(e) $t = 1.71$ [s] (f) $t = 2.14$ [s]

(g) $t = 2.57$ [s] (h) $t = 3$ [s]

Figure 3: Instantanés à différents moments de la simulation pour les équations irrotationnelles de Saint Venant contrôlées à la frontière.

il peut être exprimé comme

$$H = \frac{1}{2}\left\langle \boldsymbol{\alpha}_1,\, \mathcal{Q}_1\boldsymbol{\alpha}_1\right\rangle_{L^2(\Omega,\mathbb{A})} + \frac{1}{2}\left\langle \boldsymbol{\alpha}_2,\, \mathcal{Q}_2\boldsymbol{\alpha}_2\right\rangle_{L^2(\Omega,\mathbb{B})},$$

où $\mathcal{Q}_1$, $\mathcal{Q}_2$ *sont des opérateurs symétriques positifs, bornés inférieurement et supérieurement*

$$m_1\boldsymbol{I}_{\mathbb{A}} \leq \mathcal{Q}_1 \leq M_1\boldsymbol{I}_{\mathbb{A}}, \qquad m_2\boldsymbol{I}_{\mathbb{B}} \leq \mathcal{Q}_2 \leq M_2\boldsymbol{I}_{\mathbb{B}}, \qquad m_1 > 0,\ m_2 > 0,\ M_1 > 0,\ M_2 > 0,$$

où $\boldsymbol{I}_{\mathbb{A}}$, $\boldsymbol{I}_{\mathbb{B}}$ sont les opérateurs d'identité dans $\mathbb{A}$, $\mathbb{B}$ respectivement. En raison de cette hypothèse, les variables de co-énergie sont données par

$$\boldsymbol{e}_1 := \delta_{\alpha_1} H = \mathcal{Q}_1\boldsymbol{\alpha}_1, \qquad \boldsymbol{e}_2 := \delta_{\alpha_2} H = \mathcal{Q}_2\boldsymbol{\alpha}_2$$

Puisque $\mathcal{Q}_1$, $\mathcal{Q}_2$ sont positifs bornés inférieurement et supérieurement, il est possible de les inverser pour obtenir

$$\boldsymbol{\alpha}_1 = \mathcal{Q}_1^{-1}\boldsymbol{e}_1 = \mathcal{M}_1\boldsymbol{e}_1, \qquad \boldsymbol{\alpha}_2 = \mathcal{Q}_2^{-1}\boldsymbol{e}_2 = \mathcal{M}_2\boldsymbol{e}_2, \qquad \mathcal{M}_1 := \mathcal{Q}_1^{-1},\ \mathcal{M}_2 := \mathcal{Q}_2^{-1}.$$

L'Hamiltonien s'écrit alors en termes de variables de co-énergie comme

$$H = \frac{1}{2}\left\langle \boldsymbol{e}_1,\, \mathcal{M}_1\boldsymbol{e}_1\right\rangle_{L^2(\Omega,\mathbb{A})} + \frac{1}{2}\left\langle \boldsymbol{e}_2,\, \mathcal{M}_2\boldsymbol{e}_2\right\rangle_{L^2(\Omega,\mathbb{B})}.$$

Sous les hypothèses R.1, R.2, R.3, un système de pH linéaire est exprimé comme

$$\begin{bmatrix} \mathcal{M}_1 & 0 \\ 0 & \mathcal{M}_2 \end{bmatrix} \partial_t \begin{pmatrix} \boldsymbol{e}_1 \\ \boldsymbol{e}_2 \end{pmatrix} = \begin{bmatrix} 0 & -\mathcal{L}^* \\ \mathcal{L} & 0 \end{bmatrix} \begin{pmatrix} \boldsymbol{e}_1 \\ \boldsymbol{e}_2 \end{pmatrix}, \qquad \begin{matrix} \boldsymbol{e}_1 \in H^{\mathcal{L}}, \\ \boldsymbol{e}_2 \in H^{-\mathcal{L}^*}. \end{matrix}$$

Les variables au bord deviennent

$$\boldsymbol{u}_\partial = \mathcal{N}_{\partial,2}\boldsymbol{e}_2, \qquad \boldsymbol{y}_\partial = \mathcal{N}_{\partial,1}\boldsymbol{e}_1,$$

ou alors

$$\boldsymbol{u}_\partial = \mathcal{N}_{\partial,1}\boldsymbol{e}_1, \qquad \boldsymbol{y}_\partial = \mathcal{N}_{\partial,2}\boldsymbol{e}_2.$$

L'application de la méthode PFEM amène à la discrétisation suivante une fois que l'opérateur $-\mathcal{L}^*$ est intégré par partie

$$\begin{bmatrix} \mathbf{M}_{\mathcal{M}_1} & \mathbf{0} \\ \mathbf{0} & \mathbf{M}_{\mathcal{M}_2} \end{bmatrix} \begin{pmatrix} \dot{\mathbf{e}}_1 \\ \dot{\mathbf{e}}_2 \end{pmatrix} = \begin{bmatrix} \mathbf{0} & -\mathbf{D}_{\mathcal{L}}^\top \\ \mathbf{D}_{\mathcal{L}} & \mathbf{0} \end{bmatrix} \begin{pmatrix} \mathbf{e}_1 \\ \mathbf{e}_2 \end{pmatrix} + \begin{bmatrix} \mathbf{B}_1 \\ \mathbf{0} \end{bmatrix} \mathbf{u}_\partial,$$

$$\mathbf{M}_\partial \mathbf{y}_\partial = \begin{bmatrix} \mathbf{B}_1^\top & \mathbf{0} \end{bmatrix} \begin{pmatrix} \mathbf{e}_1 \\ \mathbf{e}_2 \end{pmatrix}.$$

Si par contre c'est l'opérateur $\mathcal{L}$ qui est intégré par partie, on obtient le système suivant

$$\begin{bmatrix} \mathbf{M}_{\mathcal{M}_1} & \mathbf{0} \\ \mathbf{0} & \mathbf{M}_{\mathcal{M}_2} \end{bmatrix} \begin{pmatrix} \dot{\mathbf{e}}_1 \\ \dot{\mathbf{e}}_2 \end{pmatrix} = \begin{bmatrix} \mathbf{0} & \mathbf{D}_{-\mathcal{L}^*} \\ -\mathbf{D}_{-\mathcal{L}^*}^\top & \mathbf{0} \end{bmatrix} \begin{pmatrix} \mathbf{e}_1 \\ \mathbf{e}_2 \end{pmatrix} + \begin{bmatrix} \mathbf{0} \\ \mathbf{B}_2 \end{bmatrix} \mathbf{u}_\partial,$$
$$\mathbf{M}_\partial \mathbf{y}_\partial = \begin{bmatrix} \mathbf{0} & \mathbf{B}_2^\top \end{bmatrix} \begin{pmatrix} \mathbf{e}_1 \\ \mathbf{e}_2 \end{pmatrix}.$$

L'hypothèse R.2 garantit une condition de causalité uniforme, c'est à dire avec une condition aux limites homogène (i.e. seulement Neumann ou seulement Dirichlet). Néanmoins cette méthode permet de prendre un compte des conditions aux limites mixtes, soit à travers l'introduction des multiplicateurs de Lagrange (cf. §6.2.1), soit en utilisant une méthode de décomposition de domaine virtuelle (cf. 6.2.2). En particulier l'exemple suivant utilise des multiplicateurs de Lagrange pour imposer des conditions aux limites mixtes.

Exemple: la plaque de Kirchhoff avec contrôle sur le bord libre (cf. §8.1.1) On considère comme exemple la stabilisation frontière d'une plaque de Kirchhoff encastrée sur un bord et contrôlée sur la partie restante de la frontière. Considérez le problème

$$\begin{bmatrix} \rho h & 0 \\ \mathbf{0} & \boldsymbol{\mathcal{D}}_{\boldsymbol{b}}^{-1} \end{bmatrix} \frac{\partial}{\partial t} \begin{pmatrix} e_w \\ \boldsymbol{E}_\kappa \end{pmatrix} = \begin{bmatrix} 0 & -\operatorname{div}\operatorname{Div} \\ \operatorname{Hess} & \mathbf{0} \end{bmatrix} \begin{pmatrix} e_w \\ \boldsymbol{E}_\kappa \end{pmatrix} \qquad (x, y) \in \Omega = [0,1] \times [0,1]$$

soumis aux conditions homogènes de Dirichlet suivantes

$$\begin{aligned} \partial_t e_w|_{\Gamma_D} &= 0, \\ \partial_x e_w|_{\Gamma_D} &= 0, \end{aligned} \qquad \Gamma_D = \{x = 0\},$$

et avec contrôle frontière donné par

$$\begin{aligned} u_{\partial,q} &= \widetilde{q}_n|_{\Gamma_N} = -\boldsymbol{n} \cdot \operatorname{Div} \boldsymbol{E}_\kappa - \partial_{\boldsymbol{s}}(\boldsymbol{E}_\kappa : (\boldsymbol{n} \otimes \boldsymbol{s}))|_{\Gamma_N}, \\ u_{\partial,m} &= m_{nn}|_{\Gamma_N} = \boldsymbol{E}_\kappa : (\boldsymbol{n} \otimes \boldsymbol{n})|_{\Gamma_N}, \end{aligned} \qquad \Gamma_N = \{y = 0 \cup x = 1 \cup y = 1\}.$$

Les sorties conjuguées sont données par

$$\begin{aligned} y_{\partial,q} &= e_w|_{\Gamma_N}, \\ y_{\partial,m} &= \partial_{\boldsymbol{n}} e_w|_{\Gamma_N}. \end{aligned}$$

La loi de commande suivante stabilise asymptotiquement le système (cf. [Lag89])

$$\begin{aligned} u_{\partial,q} &= -k_q e_w|_{\Gamma_N} = -k_q y_{\partial,q}, & k_q > 0, \\ u_{\partial,m} &= -k_m \partial_{\boldsymbol{n}} e_w|_{\Gamma_N} = -k_m y_{\partial,m}, & k_m > 0. \end{aligned}$$

Le Hamiltonien discret décroit à zéro en 4 secondes (Fig. 4). Des instantanés de la vitesse verticale sont rapportés dans la Fig. 5.

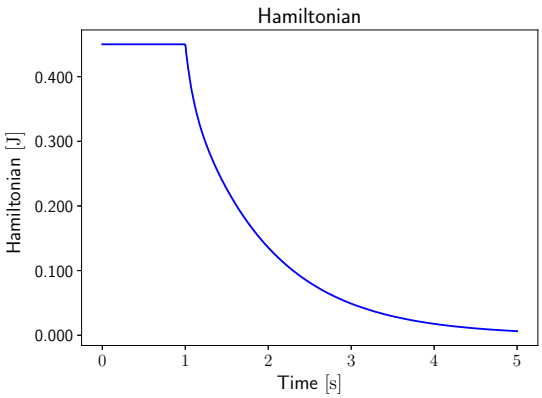

Figure 4: Évolution de l'Hamiltonien pour la plaque de Kirchhoff encastrée.

Choix des éléments finis et ordre des convergence

Même si une étude de convergence mathématiquement rigoureuse ne fait pas l'objet de ce manuscrit, dans le chapitre 7 plusieurs éléments finis sont validés et testés pour le modèles de poutres et de plaques.

La discrétisation de la poutre d'Euler-Bernoulli peut être obtenue de trois manières différentes:

1. Soit en utilisant des éléments d'Hermite pour la vitesse et des éléments de type Galerkin Discontinus pour l'effort (cf. Eq. (7.2)).
2. Soit, d'une manière symétrique, en utilisant des éléments Galerkin Discontinus pour la vitesse et des éléments d'Hermite pour l'effort (cf. Eq. (7.5)).
3. On peut aussi réduire la régularité demandée aux éléments en utilisant des éléments de Lagrange pour toutes les variables (cf. Eq. (7.8)).

Pour la plaque à Mindlin plusieurs stratégies sont possibles pour la discrétisation

1. Si une discrétisation purement mixte est considérée on peut:
   - soit utiliser les éléments *Bécache-Tsogka-Joly* BTJ (cf. Eq. (7.11)) si on souhaite imposer la symétrie du tenseur des efforts d'une manière forte.
   - soit utiliser les éléments *Arnold-Falk-Winther* AFW (cf. Eq. (7.14)) si la symétrie du tenseur des efforts est imposée d'une manière faible.

   La différence structurelle entre les deux réside dans le fait que le première utilise des éléments carrés, tandis que le deuxième est basée sur des éléments triangulaires.

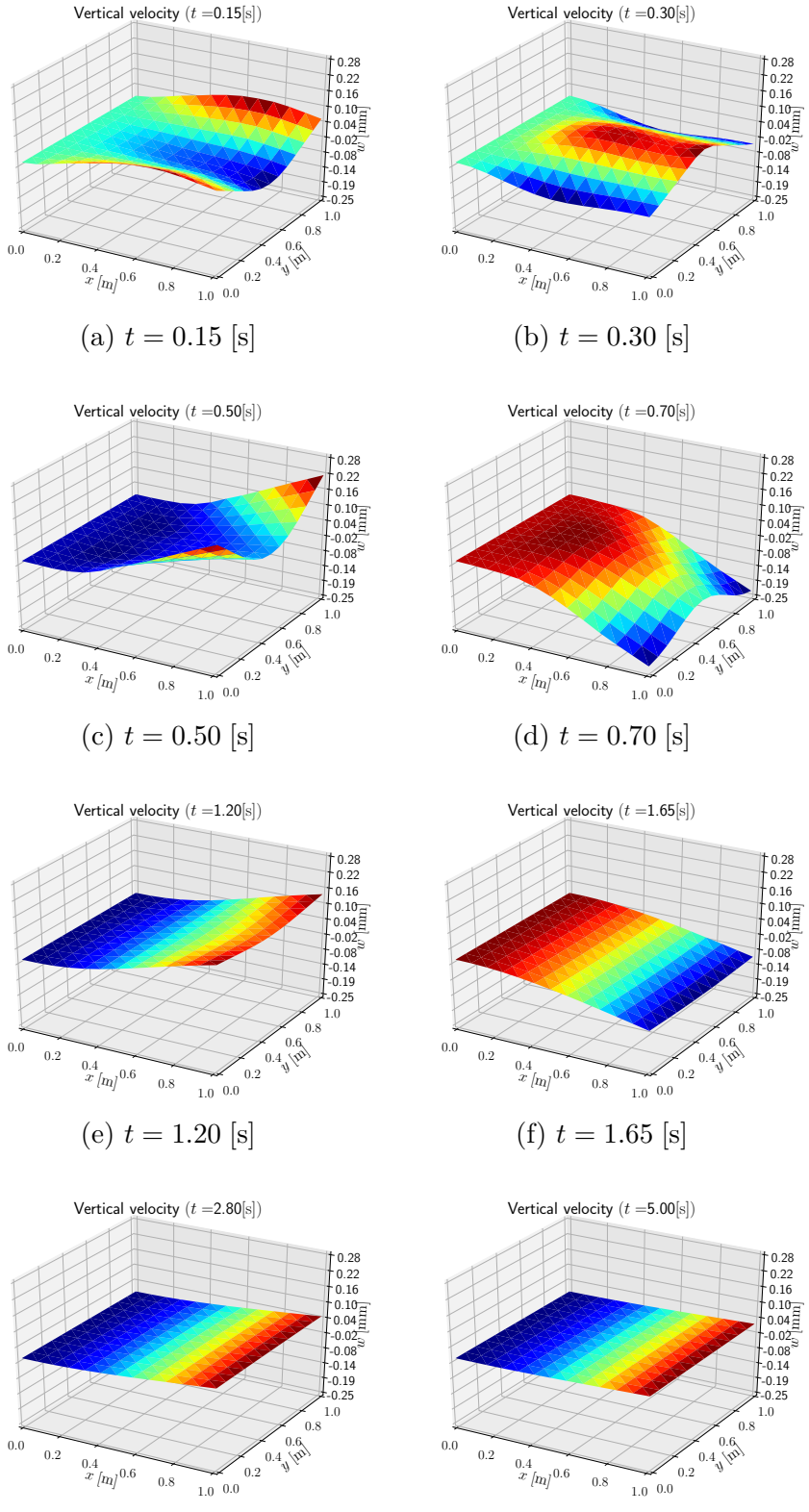

(a) $t = 0.15$ [s] (b) $t = 0.30$ [s]

(c) $t = 0.50$ [s] (d) $t = 0.70$ [s]

(e) $t = 1.20$ [s] (f) $t = 1.65$ [s]

(g) $t = 2.80$ [s] (h) $t = 5$ [s]

Figure 5: Instantanés à différents moments de la simulation de la plaque de Kirchhoff contrôlée au bord.

2. Si on utilise une méthode de type mixte-dual (aussi nommée primal-dual dans [Jol03]) les éléments *Continuous Galerkin, Discontinuous Galerkin* CGDG (cf. Eq. (7.21)) peuvent être utilisé. Ces éléments sont plus lourds au niveau computationnelle mais la symétrie du tenseur des efforts ne pose pas des problèmes.

Pour la plaque à Kirchhoff deux éléments sont proposés

1. Les éléments dus à Hellan-Herrmann-Johnson (7.16) [Hel67, Her67, Joh73] peuvent être utilisés pour obtenir une discrétisation non conforme du problème.
2. Une discrétisation de type dual mixte peut également être utilisée (voir Eq. (7.24)). Les éléments sous-jacents sont très lourds car ils possèdent beaucoup des degrés de liberté.

Une autre possibilité consisterait à utiliser des éléments div-Div conformes. Des éléments finis conformes pour l'espace $H^{\mathrm{div}\,\mathrm{Div}}$ ont été récemment proposés [CH20]. Une implémentation efficace de ces éléments n'est pas encore disponible et pour cela cette discrétisation n'est pas considérée.

Pour tout ce qui concerne l'ordre de convergence pour les éléments finis utilisés on renvoie le lecteur au chapitre 7, où plusieurs conjectures sont proposées pour les estimations d'erreurs.

R.5 Modélisation port-Hamiltonien des systèmes multi-corps flexibles

Dans le chapitre 9, une description pH de la dynamique flexible sous de grands déplacements de corps rigides et petites déformations est détaillée. En partant de l'équation générale de la dynamique rigide-flexible d'un corps flottant, un système port-Hamiltonien équivalent est trouvé par une sélection appropriée des moments canoniques. Le comportement flexible est basé sur l'hypothèse d'élasticité linéaire permettant d'inclure toutes sortes de modèles linéaires. Le problème est alors écrit comme un système couplé d'équations différentielles ordinaires et à dérivées partielles (ODE et EDP), étendant la définition générale des systèmes descripteurs port-Hamiltoniens de dimension finie fournie dans [MM19]. La modularité des systèmes pH rend l'approche proposée analogue à une technique de sous-structuration: chaque composant individuel peut être interconnecté aux autres corps en utilisant l'interconnexion standard des systèmes pH, comme cela est fait dans [MMS07]. Cette fonctionnalité permet l'utilisation de plates-formes de modélisation comme Simulink® ou Modelica®. Les contraintes sont imposées sur les vitesses, conduisant à un système port-Hamiltonien algébrique différentiel d'indice 2 quasi-linéaire (pHDAE) [Ste06, BMXZ18]. Dans le cas linéaire, les contraintes algébriques peuvent être éliminées, en préservant la structure globale pH, en utilisant des méthodes de réduction [LBS08]. Lorsqu'une formulation de cadre flottant est utilisée, des techniques de réduction de modèle peuvent être utilisées pour réduire la complexité de calcul du modèle [CBG16, EKLS+18].

Formulation port-Hamiltonien continue et discrète pour la dynamique d'un corps flottant flexible

Grâce à la proposition 10, presentée dans le corps centrale de la thèse, on s'aperçoit que les équations de la dynamique flexible d'un corps flottant [Sim13, Chapitre 4] peuvent être récrites d'une manière équivalente comme

- Bilan du moment linéaire:

$$m\dot{\boldsymbol{v}}_P + [\boldsymbol{s}_u]_\times^\top \dot{\boldsymbol{\omega}}_P + \int_\Omega \rho \dot{\boldsymbol{v}}_f \, \mathrm{d}\Omega = \left[m\boldsymbol{v}_P + [\boldsymbol{s}_u]_\times^\top \boldsymbol{\omega}_P + 2\int_\Omega \rho \boldsymbol{v}_f \, \mathrm{d}\Omega \right]_\times \boldsymbol{\omega}_P + \int_{\partial\Omega} \boldsymbol{\tau} \, \mathrm{d}\Gamma.$$

- Bilan du moment angulaire:

$$\begin{aligned} [\boldsymbol{s}_u]_\times \dot{\boldsymbol{v}}_P + \boldsymbol{J}_u \dot{\boldsymbol{\omega}}_P + \int_\Omega \rho [\boldsymbol{x}_f]_\times \dot{\boldsymbol{v}}_f \, \mathrm{d}\Omega = \\ \left[[\boldsymbol{s}_u]_\times^\top \boldsymbol{\omega}_P + 2\int_\Omega \rho \boldsymbol{v}_f \, \mathrm{d}\Omega \right]_\times \boldsymbol{v}_P + \left[[\boldsymbol{s}_u]_\times \boldsymbol{v}_P + \boldsymbol{J}_u \boldsymbol{\omega}_P + 2\int_\Omega \rho [\boldsymbol{x}_f]_\times \boldsymbol{v}_f \, \mathrm{d}\Omega \right]_\times \boldsymbol{\omega}_P + \\ 2\int_\Omega \left[\rho \boldsymbol{v}_P + \rho [\boldsymbol{x}_f]_\times^\top \boldsymbol{\omega}_P \right]_\times \boldsymbol{v}_f \, \mathrm{d}\Omega + \int_{\partial\Omega} [\boldsymbol{x}_f]_\times \boldsymbol{\tau} \, \mathrm{d}\Gamma. \end{aligned}$$

- EDP pour la déformation:

$$\rho\dot{\boldsymbol{v}}_P + \rho [\boldsymbol{x}_f]_\times^\top \dot{\boldsymbol{\omega}}_P + \rho\dot{\boldsymbol{v}}_f = \left[\rho\boldsymbol{v}_P + \rho [\boldsymbol{x}_f]_\times^\top \boldsymbol{\omega}_P + 2\rho\boldsymbol{v}_f \right]_\times \boldsymbol{\omega}_P + \mathrm{Div}\, \boldsymbol{\Sigma}.$$

On renvoie au chapitre 9 pour la signification des variables et des paramètres. La notation $[\boldsymbol{a}]_\times$ désigne la matrice asymétrique associée au vecteur $\boldsymbol{a}$ (voir Sec. A.4). Considérons l'énergie totale (Hamiltonienne), donnée par la somme de l'énergie cinétique et de déformation:

$$H = H_{\mathrm{kin}} + H_{\mathrm{def}} = \frac{1}{2}\int_\Omega \left\{ \rho ||\boldsymbol{v}_P + [\boldsymbol{\omega}_P]_\times \boldsymbol{x}_f + \boldsymbol{v}_f||^2 + \boldsymbol{\Sigma} : \boldsymbol{\varepsilon} \right\} \, \mathrm{d}\Omega.$$

Les moments (généralement appelées variables d'énergie dans le cadre pH) sont ensuite calculés par dérivation de l'Hamiltonien. Comme les variables appartiennent à des espaces de dimension finie et infinie, la dérivée est soit un gradient classique, soit une dérivée variationnelle:

$$\begin{aligned} \boldsymbol{p}_t &:= \frac{\partial H}{\partial \boldsymbol{v}_P} = m\boldsymbol{v}_P + [\boldsymbol{s}_u]_\times^\top \boldsymbol{\omega}_P + \int_\Omega \rho \boldsymbol{v}_f \, \mathrm{d}\Omega, \\ \boldsymbol{p}_r &:= \frac{\partial H}{\partial \boldsymbol{\omega}_P} = [\boldsymbol{s}_u]_\times \boldsymbol{v}_P + \boldsymbol{J}_u \boldsymbol{\omega}_P + \int_\Omega \rho [\boldsymbol{x}_f]_\times \boldsymbol{v}_f \, \mathrm{d}\Omega, \\ \boldsymbol{p}_f &:= \frac{\delta H}{\delta \boldsymbol{v}_f} = \rho\boldsymbol{v}_P + \rho [\boldsymbol{x}_f]_\times^\top \boldsymbol{\omega}_P + \rho\boldsymbol{v}_f, \\ \boldsymbol{\varepsilon} &:= \frac{\delta H}{\delta \boldsymbol{\Sigma}} = \boldsymbol{\mathcal{D}}^{-1}\boldsymbol{\Sigma} = \boldsymbol{\mathcal{C}}\boldsymbol{\Sigma}, \end{aligned}$$

où la dernière dérivée est calculée par rapport à un tenseur et $\boldsymbol{\mathcal{C}}$ est l'inverse du tenseur de rigidité (3.6). Afin d'obtenir une formulation complète, des coordonnées généralisées sont nécessaires. Il est naturel de sélectionner les variables suivantes:

- ${}^i\boldsymbol{r}_P$ la position du point P dans le référentiel inertiel;

- $\boldsymbol{R}$ la matrice du cosinus directeur qui transforme les vecteurs du repère corps au repère inertiel (d'autres paramétrisations d'attitude sont possibles, ici la matrice du cosinus directeur est considérée pour faciliter la présentation);

- $\boldsymbol{u}_f$ le déplacement flexible;

La formulation port-Hamiltonienne globale est alors

$$\underbrace{\left[\begin{array}{c|c} \boldsymbol{I} & \boldsymbol{0} \\ \hline \boldsymbol{0} & \mathcal{M} \end{array}\right]}_{\mathcal{E}} \frac{\partial}{\partial t} \underbrace{\begin{pmatrix} {}^i\boldsymbol{r}_P \\ \boldsymbol{R}_{\mathrm{v}} \\ \boldsymbol{u}_f \\ \hline \boldsymbol{v}_P \\ \boldsymbol{\omega}_P \\ \boldsymbol{v}_f \\ \boldsymbol{\Sigma} \end{pmatrix}}_{e} = \underbrace{\left[\begin{array}{ccc|ccc|c} \boldsymbol{0} & \boldsymbol{0} & \boldsymbol{0} & \boldsymbol{R} & \boldsymbol{0} & \boldsymbol{0} & \boldsymbol{0} \\ \boldsymbol{0} & \boldsymbol{0} & \boldsymbol{0} & \boldsymbol{0} & [\boldsymbol{R}_{\mathrm{v}}]_\times & \boldsymbol{0} & \boldsymbol{0} \\ \boldsymbol{0} & \boldsymbol{0} & \boldsymbol{0} & \boldsymbol{0} & \boldsymbol{0} & \boldsymbol{I}_{3\times 3} & \boldsymbol{0} \\ \hline -\boldsymbol{R}^\top & \boldsymbol{0} & \boldsymbol{0} & \boldsymbol{0} & [\widehat{\boldsymbol{p}}_t]_\times & \boldsymbol{0} & \boldsymbol{0} \\ \boldsymbol{0} & -[\boldsymbol{R}_{\mathrm{v}}]_\times^\top & \boldsymbol{0} & [\widehat{\boldsymbol{p}}_t]_\times & [\widehat{\boldsymbol{p}}_r]_\times & \mathcal{I}^\Omega_{p_f} & \boldsymbol{0} \\ \boldsymbol{0} & \boldsymbol{0} & -\boldsymbol{I}_{3\times 3} & \boldsymbol{0} & -(\mathcal{I}^\Omega_{p_f})^* & \boldsymbol{0} & \mathrm{Div} \\ \boldsymbol{0} & \boldsymbol{0} & \boldsymbol{0} & \boldsymbol{0} & \boldsymbol{0} & \mathrm{Grad} & \boldsymbol{0} \end{array}\right]}_{\mathcal{J}} \underbrace{\begin{pmatrix} \partial_{\boldsymbol{r}_P} H \\ \partial_{\boldsymbol{R}_{\mathrm{v}}} H \\ \delta_{\boldsymbol{u}_f} H \\ \hline \boldsymbol{v}_P \\ \boldsymbol{\omega}_P \\ \boldsymbol{v}_f \\ \boldsymbol{\Sigma} \end{pmatrix}}_{z}.$$

On renvoie à nouveau au chapitre 9 pour la signification des variables. Ce système dynamique s'inscrit dans le cadre détaillé dans [MM19] et l'étend, puisqu'un système couplé des EDO et des EDP est considéré. La dynamique peut être réécrite de manière compacte comme

$$\begin{aligned} \mathcal{E}(\boldsymbol{e})\frac{\partial \boldsymbol{e}}{\partial t} &= \mathcal{J}(\boldsymbol{e})\boldsymbol{z}(\boldsymbol{e}) + \mathcal{B}_r(\boldsymbol{e})\boldsymbol{u}_\partial, \\ \boldsymbol{y}_r &= \mathcal{B}_r^*(\boldsymbol{e})\boldsymbol{z}(\boldsymbol{e}), \\ \boldsymbol{u}_\partial &= \mathcal{B}_\partial \boldsymbol{z}(\boldsymbol{e}) = \boldsymbol{\Sigma}\cdot\boldsymbol{n}|_{\partial\Omega} = \boldsymbol{\tau}|_{\partial\Omega}, \\ \boldsymbol{y}_\partial &= \mathcal{C}_\partial \boldsymbol{z}(\boldsymbol{e}) = \boldsymbol{v}_f|_{\partial\Omega}, \end{aligned}$$

où l'Hamiltonien vérifie

$$\partial_{\boldsymbol{e}} H = \boldsymbol{\mathcal{E}}^* \boldsymbol{z}.$$

L'application de la méthode PFEM (en utilisant une intégration par partie sur l'opérateur Div) fournit le système discrétisé suivant

$$\begin{aligned} \mathbf{E}(\mathbf{e})\dot{\mathbf{e}} &= \mathbf{J}(\mathbf{e})\mathbf{z}(\mathbf{e}) + \mathbf{B}_\partial(\mathbf{e})\mathbf{u}_\partial, \\ \mathbf{y}_\partial &:= \mathbf{M}_\partial \widetilde{\mathbf{y}}_\partial = \mathbf{B}_\partial^\top \mathbf{z}(\mathbf{e}). \end{aligned}$$

Le calcul du vecteur $\mathbf{z}$ est basé sur le gradient de l'Hamiltonien discret

$$\frac{\partial H_d}{\partial \mathbf{e}} = \mathbf{E}^\top \mathbf{z}.$$

Construction modulaire des systèmes multicorps

Cette méthode peut être utilisée pour modéliser d'une manière modulaire les systèmes multi-corps et les interconnecter entre eux. Par exemple la modélisation de poutres dans un repère flottant à travers ce formalisme donne lieu aux systèmes suivants :

$$\begin{cases} \mathbf{E}_i \dot{\mathbf{e}}_i = \mathbf{J}_i \mathbf{z}_i(\mathbf{e}_i) + \mathbf{B}_i^{\text{int}} \mathbf{u}_i^{\text{int}} + \mathbf{B}_i^{\text{ext}} \mathbf{u}_i^{\text{ext}} \\ \mathbf{y}_i^{\text{int}} = \mathbf{B}_i^{\text{int}\top} \mathbf{z}_i \\ \mathbf{y}_i^{\text{ext}} = \mathbf{B}_i^{\text{ext}\top} \mathbf{z}_i \end{cases} \qquad \forall i = 1, 2.$$

Si on veut interconnecter deux systèmes à travers un pivot (cf. Fig. 6), les variables d'interconnexion deviennent les forces et les vitesses linéaires aux extrémités.

$$\begin{aligned} \mathbf{u}_1^{\text{int}} &= [F_{C_1}^x,\, F_{C_1}^y]^\top := \mathbf{F}_{C_1}, \qquad & \mathbf{y}_1^{\text{int}} &= [v_{C_1}^x,\, v_{C_1}^y]^\top := \mathbf{v}_{C_1}, \\ \mathbf{u}_2^{\text{int}} &= [F_{P_2}^x,\, F_{P_2}^y]^\top := \mathbf{F}_{P_2}, \qquad & \mathbf{y}_2^{\text{int}} &= [v_{P_2}^x,\, v_{P_2}^y]^\top := \mathbf{v}_{P_2}. \end{aligned}$$

La matrice d'interconnexion est la matrice de rotation relative entre les deux repères locaux

$$\mathbf{R}(\theta) = \begin{bmatrix} \cos(\theta) & -\sin(\theta) \\ \sin(\theta) & \cos(\theta) \end{bmatrix}, \qquad \theta(t) = \theta(0) + \int_0^t (\omega_{P_2}^z - \omega_{P_1}^z)\, \mathrm{d}\tau.$$

L'interconnexion de type *transformer*

$$\mathbf{u}_1^{\text{int}} = -\mathbf{R}(\theta)\mathbf{u}_2^{\text{int}}, \qquad \mathbf{y}_2^{\text{int}} = \mathbf{R}(\theta)^\top \mathbf{y}_1^{\text{int}},$$

impose les contraintes au niveau des vitesses et donne lieu à un système différentielle-algébrique d'ordre deux.

$$\begin{bmatrix} \mathbf{E}_1 & \mathbf{0} & \mathbf{0} \\ \mathbf{0} & \mathbf{E}_2 & \mathbf{0} \\ \mathbf{0} & \mathbf{0} & \mathbf{0} \end{bmatrix} \begin{pmatrix} \dot{\mathbf{e}}_1 \\ \dot{\mathbf{e}}_2 \\ \dot{\boldsymbol{\lambda}} \end{pmatrix} = \begin{bmatrix} \mathbf{J}_1(\mathbf{e}_1) & \mathbf{0} & -\mathbf{B}_1^{\text{int}}\mathbf{R} \\ \mathbf{0} & \mathbf{J}_2(\mathbf{e}_2) & \mathbf{B}_2^{\text{int}} \\ \mathbf{R}^\top \mathbf{B}_1^{\text{int}\top} & -\mathbf{B}_2^{\text{int}\top} & \mathbf{0} \end{bmatrix} \begin{pmatrix} \mathbf{z}_1 \\ \mathbf{z}_2 \\ \boldsymbol{\lambda} \end{pmatrix} + \begin{bmatrix} \mathbf{B}_{\partial 1}^{\text{ext}} & \mathbf{0} \\ \mathbf{0} & \mathbf{B}_{\partial 2}^{\text{ext}} \\ \mathbf{0} & \mathbf{0} \end{bmatrix} \begin{pmatrix} \mathbf{u}_1^{\text{ext}} \\ \mathbf{u}_2^{\text{ext}} \end{pmatrix},$$

$$\begin{pmatrix} \mathbf{y}_1^{\text{ext}} \\ \mathbf{y}_2^{\text{ext}} \end{pmatrix} = \begin{bmatrix} \mathbf{B}_{\partial 1}^{\text{ext}\top} & \mathbf{0} & \mathbf{0} \\ \mathbf{0} & \mathbf{B}_{\partial 2}^{\text{ext}\top} & \mathbf{0} \end{bmatrix} \begin{pmatrix} \mathbf{z}_1 \\ \mathbf{z}_2 \\ \boldsymbol{\lambda} \end{pmatrix}.$$

Exemple: analyse modale d'un mécanisme à quatre barres (cf. §10.1.1) Le mécanisme à quatre barres a un degré de liberté et représente une chaîne fermée de corps. Les données, extraites de [KL90, CDPGA17], sont rappelées dans le Tableau 1. En Fig. 7 le mécanisme et le schéma fonctionnel correspondant utilisé pour construire le système pH final (avec des interconnexions de type *transformer* entre les sous-systèmes) sont présentés. Les masses localisées sont directement incluses dans les modèles du coupleur et du suiveur en

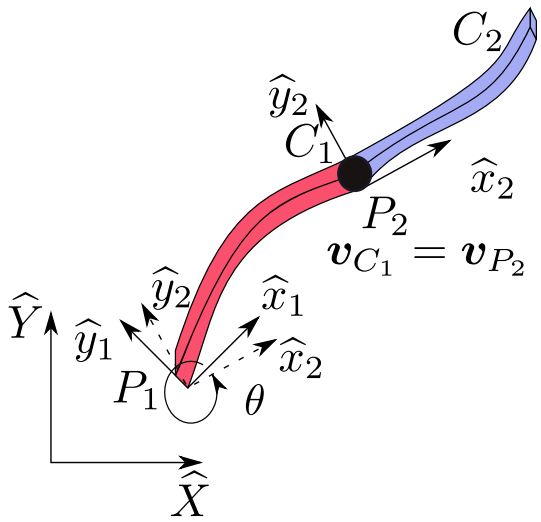

Figure 6: Deux poutres interconnectées par un pivot

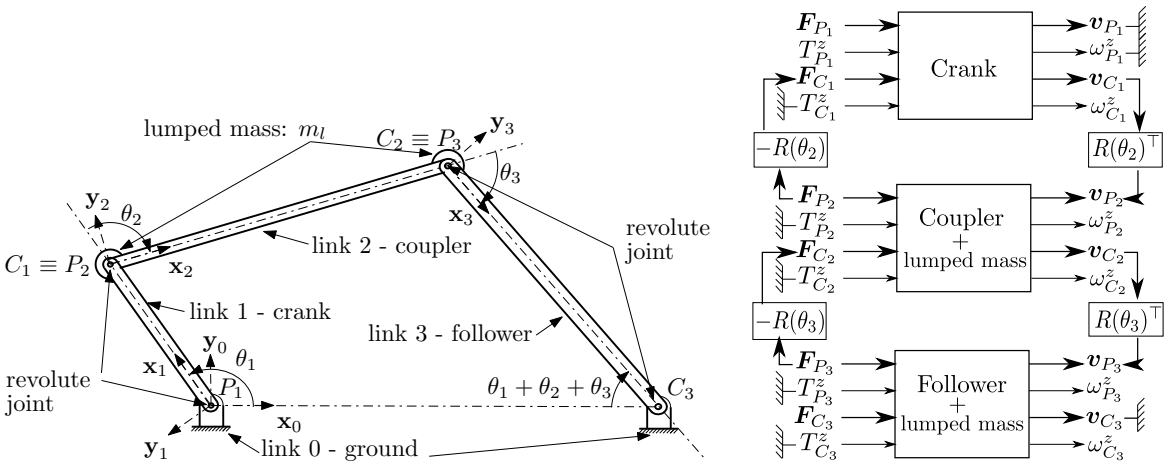

Figure 7: Illustration du mécanisme à quatre barres (à gauche) et schéma fonctionnel utilisé pour l'analyse des valeurs propres (à droite)

considérant une simple modification de la matrice de masse rigide

$$\mathbf{M}^{i+m_l}_{rr}[1:2,1:2] = \mathbf{M}^{i}_{rr}[1:2,1:2] + \mathbf{I}_{2\times 2} m_l,$$

où $i = 2, 3$ désigne le modèle coupleur ou suiveur. Étant donné un certain angle de manivelle θ_1, les angles relatifs entre les différents liens sont trouvés en résolvant les deux contraintes cinématiques

$$\begin{aligned} L_1\cos(\theta_1) + L_2\cos(\theta_1+\theta_2) + L_3\cos(\theta_1+\theta_2+\theta_3) &= L_0, \\ L_1\sin(\theta_1) + L_2\sin(\theta_1+\theta_2) + L_3\sin(\theta_1+\theta_2+\theta_3) &= 0. \end{aligned}$$

Une fois que les angles décrivant la configuration géométrique sont connus, une interconnexion de type *transformer* est appliquée pour insérer un pivot entre des liaisons adjacentes. Pour

Table 1: Propriétés des liens du mécanisme à quatre barres: chaque lien est une poutre uniforme avec densité de masse $\rho = 2714\,[\mathrm{kg/m^3}]$ et module de Young $E = 7.1\,10^{10}\,[\mathrm{N/m^2}]$.

i	0	1	2	3
Nom	terre	manivelle	coupleur	suiveur
Longueur L_i [m]	0.254	0.108	0.2794	0.2705
Section transverse A_i [$\mathrm{m^2}$]	–	$1.0774\,10^{-4}$	$4.0645\,10^{-5}$	$4.0645\,10^{-5}$
Rigidité à flexion $(EI)_i$ [$\mathrm{Nm^2}$]	–	11.472	0.616	0.616

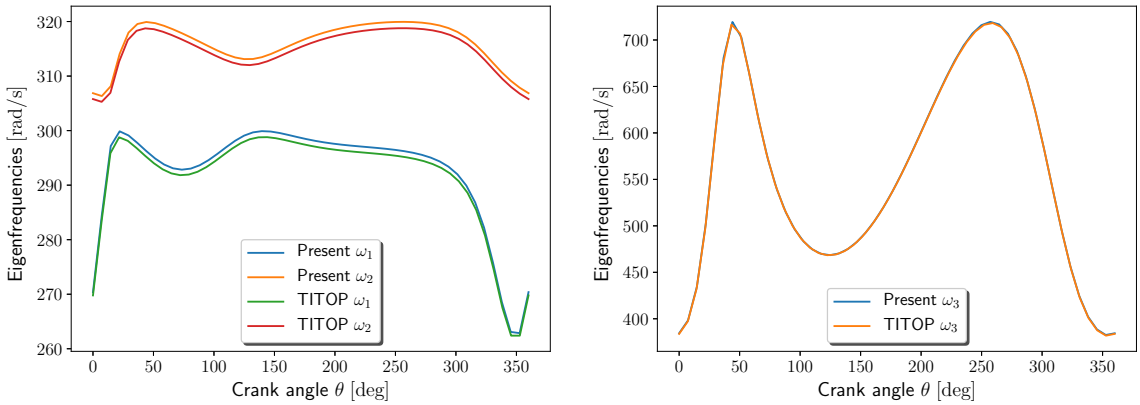

Figure 8: Valeurs propres $\omega_i,\ i = 1, 2, 3$ pour le mécanisme à quatre barres en fonction de l'angle de la manivelle.

le champ de déformation, une condition d'encastrement est imposée pour chaque poutre. Le système résultant est alors contraint à la masse en imposant les égalités suivantes

$$\mathbf{v}_{P_1} = \mathbf{0}, \quad \omega^z_{P_1} = 0, \quad \mathbf{v}_{C_3} = \mathbf{0}.$$

Le système résultant est exprimé sous forme pH comme $\mathbf{E}\dot{\mathbf{e}} = \mathbf{J}\mathbf{e}$. Les fréquences propres sont ensuite trouvées en résolvant le problème généralisé des valeurs propres $\mathbf{E}\boldsymbol{\Phi}\boldsymbol{\Lambda} = \mathbf{J}\boldsymbol{\Phi}$. Puisque $\mathbf{J}$ est asymétrique, les valeurs propres seront imaginaires $\boldsymbol{\Lambda} = j\boldsymbol{\Omega}$. Les trois premières pulsations sont rapportées sur la Fig. 8 pour différentes valeurs de l'angle de manivelle θ_1. Les résultats correspondent à ceux de [CDPGA17] (notés TITOP sur la figure).

R.6 Conclusions et perspectives

Ce travail a étudié les avantages du formalisme pH en tant que paradigme de modélisation. Une attention particulière a été portée aux modèles issus de la mécanique des solides. Ces modèles sont de nature hyperbolique et présentent une structure partitionnée lorsqu'ils sont reformulés sous forme pH. Cette structure partitionnée est intimement liée à une formule abstraite d'intégration par parties. Ces deux concepts sont cruciaux pour démontrer l'existence et l'unicité des pH linéaires sur des domaines multidimensionnels [Skr19]. De plus, ils sont au

cœur de la stratégie de discrétisation proposée par éléments finis. Parce qu'elle est basée sur la structure partitionnée du problème, cette méthodologie porte le nom de méthode des éléments finis partitionnés (PFEM). Dans la mesure où le système considéré possède cette structure, la méthode est applicable. Par conséquent, elle n'est pas limitée aux systèmes hyperboliques, mais peut être étendue aux systèmes paraboliques [SHM19b]. Les non-linéarités associées à l'Hamiltonien sont également faciles à gérer, puisque la loi de comportement est discrétisée séparément de la dynamique. La discrétisation proposée a été mise en œuvre à l'aide d'éléments finis. Il existe un lien clair entre la méthode des éléments finis partitionnés, les éléments finis mixtes et la discrétisation par éléments finis standard. Pour cette raison, un certain nombre d'éléments finis connus peuvent être utilisés pour réaliser une discrétisation préservant la structure. De nombreuses conjectures pour les ordres de convergence sont proposées et validées par des expériences numériques, évaluant la performance des schémas numériques. Les algorithmes développés peuvent être utilisés pour développer des stratégies de contrôle basées sur des modèles. Ceci est illustré par la méthode d'injection d'amortissement simple. Un domaine d'application qui bénéficie fortement de la modularité des pH est la dynamique des systèmes multicorps. Il a été montré que le modèle Lagrangien classique basé sur la *floating frame of reference formulation* peut être reformulé comme un système couplé d'ODE et de PDE sous forme pH. Cette formulation est utilisé car elle permet d'incorporer tous les modèles mécaniques linéaires discutés dans cette thèse. La discrétisation utilisée s'apparente alors à une discrétisation standard avec une intégration réduite des contraintes. Il est alors possible de relier entre eux des sous-composants pour modéliser des mécanismes de manière modulaire.
Des nombreux points nécessitent des investigations complémentaires. Les orientations futures concernent les sujets suivants.

Modélisation Seuls les modèles de plaques linéaires ont été formulés comme systèmes pH. Il est intéressant de voir comment des structures linéaires minces sur des variétés, c'est-à-dire des coques, peuvent être formulées en termes de systèmes Hamiltoniens. Des EDP bien posés ont été formulés pour le problème de membrane et les coques de Koiter [Cia00]. Il devrait être possible de formuler ces problèmes sous forme de systèmes Hamiltoniens en utilisant des outils de géométrie différentielle. Pour éviter l'utilisation de la géométrie différentielle, le calcul différentiel tangentiel [DZ11] peut également être utilisé. Le calcul différentiel tangentiel a été adopté avec succès pour fournir une formulation intrinsèque des problèmes des coques de type Kirchhoff [SF19a] et Mindlin [SF19b].
En ce qui concerne les modèles non linéaires, il serait très intéressant de voir si les équations Föppl – von Kármán décrivant les grandes déformations de plaques minces [BTTD15] admettent une reformulation pH.

Discrétisation Certaines questions méritent une analyse plus approfondie concernant la discrétisation des modèles de plaques. La discrétisation de la plaque de Kirchhoff est réalisée à l'aide d'une discrétisation duale-mixte et de la méthode HHJ non conforme. La première méthode est coûteuse d'un point de vue temps de calcul et pour cette raison n'a pas été

analysée dans la littérature. Pour la seconde stratégie, les conditions aux limites non homogènes en présence de conditions aux limites libres ne sont pas faciles à gérer. Pour faire face aux limites de ces deux méthodologies, la discrétisation proposée dans [RZ18] peut être utilisée. Cette formulation permet d'utiliser les fonctions C^0 pour approcher ce problème avec des conditions aux limites génériques non homogènes. Il serait très intéressant d'étendre cette méthode au cas dynamique.
Pour la plaque Mindlin, un point clé à aborder est le phénomène de verrouillage numérique. Les éléments finis mixtes permettent de construire des approximations du problème statique qui ne sont pas affectées par ce phénomène [BadVMR13]. Pour le cas dynamique, les choses se compliquent car l'épaisseur joue également un rôle dans les termes inertiels.
Une étude de convergence complète pour l'équation d'onde contrôlée aux limites est réalisée dans [HMS20]. Des études de convergence rigoureuses pour les modèles proposés dans ce travail devraient également être réalisées.
Pour l'implémentation numérique, l'approximation par éléments finis a été utilisée. Cependant, des méthodes spectrales pourraient également être utilisées. Cela fournirait des systèmes discrétisés de petite dimension avec des matrices denses, réduisant drastiquement les charges de calcul. En particulier, des techniques d'analyse modale peuvent être utilisées pour construire une approximation pour une bande de fréquence donnée.

Réduction de modèles Les stratégies de réduction de modèles n'ont pas été abordées dans ce manuscrit. Compte tenu de la taille des matrices issues de la discrétisation, cela reste un enjeu fondamental. Des méthodologies prometteuses, reposant sur une décomposition orthogonale appropriée et des sous-espaces H_2-optimaux pour pHODE non linéaire [CBG16] et sur les méthodes de Krylov pour pHDAE linéaire [EKLS+18], sont déjà disponibles. En pratique, il est intéressant de réduire le système avec précision dans une bande de fréquence limitée, représentative de la dynamique du système et de l'instrumentation [Vui14]. Les techniques de réduction de modèles à fréquence limitée et préservant la structure ont été récemment étendues aux systèmes de pH [XJ20]. Il serait d'un grand intérêt d'appliquer ces techniques aux modèles proposés dans ce travail.

Dynamique multicorps flexible La formulation proposée donne lieu à un système différentiel-algébrique d'index deux. La résolution de ce genre de problèmes est notoirement difficile [BCP95]. Il existe un besoin d'outils de calcul fiables et efficaces pour l'intégration temporelle. Des méthodes préservant le caractère passif du système sont bien entendu préférables.
Un autre sujet intéressant serait l'inclusion de grandes déformations. En principe, cela devrait être possible en utilisant une formulation co-rotationnelle ou des techniques de sous-structuration [WH88].

Contrôle Le formalisme pH s'est avéré plutôt efficace pour la conception de lois de contrôle pour les systèmes non linéaires [OGC04] et le contrôle frontière des EDP sur des domaines unidimensionnels [MLGR20]. Un sujet encore ouvert est l'introduction de spécifications de performance dans ce formalisme. Ces spécifications sont généralement exprimées dans le

domaine fréquentiel. Pour les systèmes à dimension infinie, des travaux récents portent sur l'implémentation de contrôleurs basés sur les techniques H^∞ [AN18, AN20]. Ces stratégies sont applicables aux EDP paraboliques et hyperboliques. Pour les pHs, il serait intéressant de voir si les contrôles robustes et passifs peuvent être combinés. De plus, il serait important de considérer le cas de contrôles et d'observations non colocalisés [CR16]. En introduisant des estimateurs d'état appropriés [YY19], il devrait être possible de reconstruire l'entrée conjuguée pour garantir un retour de sortie passif.

Part I

Introduction and state of the art

Chapter 1

Introduction

I was born not knowing and have had only a little time to change that here and there.

Richard Feynman
Letter to Armando Garcia J.

Contents

1.1 Motivation and context

This work aims at exploring the port-Hamiltonian (pH) framework as a modelling paradigm, with particular emphasis for the case of flexible structures. This framework enjoys many interesting properties, since it intrinsically merges geometry with network and control theory [vdS06]. A powerful feature of this formalism, especially for the modelling task, is its modularity. Finite-dimensional port-Hamiltonian systems (pHs) can be easily interconnected together [CvdSB07]. The interconnection is also possible in the infinite-dimensional case [KZvdSB10, Aug20]. Eventually, it is also possible to merge finite and infinite pH systems [Pas06]. This features is especially useful to simplify the modelling task in preliminary analyses, or, conversely, to achieve high-fidelity models of complex multiphysics phenomena. Examples of multiphysics problems are brain edema simulations [JCLT20] (cf. Fig. 1.1) or plasma physics [Nät19] (cf. Fig. 1.2).

The port-Hamiltonian framework has been extensively used to model and control distributed systems arising from a variety of physical models: Timoshenko [MM04] and Euler-

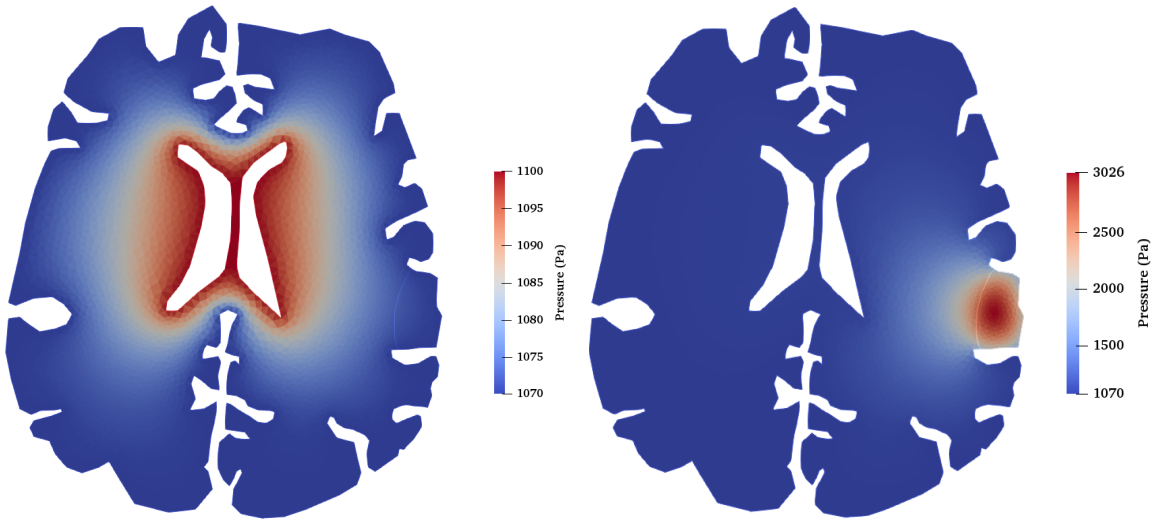

(a) Normal brain (b) Injured brain

Figure 1.1: Simulated pressure within the brain for a physiological (left) and injured (right) condition. The authors propose a coupled multiphysics framework to solve the underlying Biot system. The numerical model is obtained using a combination of classical and mixed finite elements (courtesy of Mingchao Cai [JCLT20]).

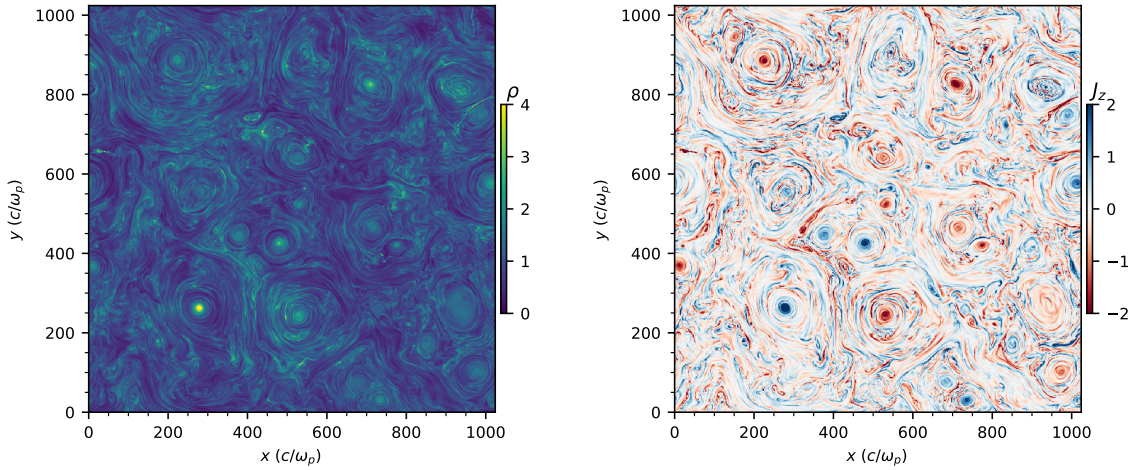

(a) Plasma density (b) Out-of-plane plasma current density

Figure 1.2: Simulated snapshot of the density field (left) and current density (right) for plasma kinetic turbulence. The underlying code employs the Yee finite difference scheme [Yee66] to approximate the Vlasov-Maxwell equations and a full relativistic Boris scheme [Bor70] to update the particles velocity and position (courtesy of Joonas Nättilä [Nät19]).

Bernoulli [ACRMA17] beam models, acoustic wave propagations [TRLGK18], stirred tank reactors [RMS13], plasma in tomahawks [VNLF16] and fluid-structure interactions [CRMPB17]. The large majority of these examples refer to 1-dimensional models. Indeed, for 1-dimensional linear pH systems with a generalized skew-adjoint system operator, [LGZM05] gives conditions on the assignment of boundary inputs and outputs for the system operator to generate a contraction semigroup. This result has been largely used to construct passive boundary controllers for hyperbolic systems [VZLGM09, MLGRZ16, MLGR20].

Since their introduction, distributed port-Hamiltonian systems (dpHs) have been defined on multidimensional spatial domains using the language of differential forms [vdSM02]. In [Vil07] pH modelling and semigroup approach of infinite-dimensional systems are merged together. Therein, the case of multidimensional domains is only briefly discussed. Many other examples of pHs on multidimensional domains are detailed in [DMSB09, Chapter 4]. However, well-posedness results are not presented there. A first contribution in this sense can be found in [KZ15], where the authors demonstrate the well-posedness of the linear wave equation in arbitrary geometric dimensions. The recent paper [Skr19] generalizes this result to treat the case of generic first order linear pHs in arbitrary geometric dimensions. Despite all this preexisting literature, models arising from structural mechanics on multidimensional domains have almost never been considered (apart from the notable exception of [MMB05] for the modelling of the Mindlin plate).

The potential of the pH framework as modelling paradigm has been recently explored by researchers. For instance, in [EK18] the authors consider a port-Hamiltonian model for pressure waves propagation in networks of pipes. By employing a mixed finite element scheme, the authors achieve a structure-preserving discretization of the original model. A model reduction algorithm for this discretized model of pipeline network is then discussed in [EKLS+18]. These recent works substantiate the validity of this framework to tackle complex application scenarios and highlight the importance of structure-preserving discretization algorithms. Disposing of methodologies capable of constructing reliable discretizations is important not only for simulation, but also for control purposes. In particular, in [TWRLG20] the authors develop a systematic synthesis method for observer-based boundary controller design for pHs on one dimensional spatial domains. To construct the observer, a suitable discretized version of the system is assumed to be available.

This thesis tries to establish a clear connection between linear structural mechanics models and port-Hamiltonian systems, both for the modelling and discretization tasks. These two purposes are indeed strongly related in the context of pHs. To get a pH formulation for elasticity models, one has to introduce the stress variable, associated to the deformation energy, as an additional principal unknown. Adding the stress variable as an unknown is the starting point of mixed finite elements [Arn90]. This leads to the decomposition of the initial elliptic operator (i.e. the Laplacian or bi-Laplacian), into two formal adjoint operators. By consequence, the dynamics is regulated by a formally skew adjoint operator, hence leading

to a Hamiltonian system. After performing an integration by parts, a mixed discretization is immediately achieved [Jol03]. This very concise reasoning informally elucidates the strong connection between port-Hamiltonian modelling of continuum mechanics and mixed finite elements.

1.2 Literature review

A brief literature review of the topics considered in the thesis is made here. Throughout the chapters of the thesis, the literature is also referenced.

1.2.1 Structure-preserving discretization

The research community is focusing on structure-preserving discretization techniques since several years. The first study dates back to [GTVDSM04], where the authors made use of a mixed finite element spatial discretization for 1D and 2D hyperbolic system of conservation laws. A pseudo-spectral method relying on higher-order global polynomial approximations was studied in [MLM12]. This method was used and extended to take into account unbounded control operators in [CRMPB17]. A simplicial discretization based on discrete exterior calculus was proposed in [SvdSS12]. This approach comes with additional complexities, since a primal and a dual meshes have to be defined but the discretization is structure-preserving, regardless of the spatial dimension of the problem. Weak formulations which lead to Galerkin numerical approximations began to be explored in the last years. In [KML18] the prototypical example of hyperbolic systems of two conservation laws was discretized by a weak formulation. In this approach the boundary is split according to the causality of boundary ports, so that mixed boundary conditions are easily handled. The construction of the necessary power-preserving mappings is, however, not straightforward on arbitrary meshes. A 2D finite difference method with staggered grids was used in [TRLGK18].

1.2.2 Mixed finite elements for elasticity

Thanks to [CRML18], it has become evident that there is a strict link between discretization of port-Hamiltonian (pH) systems and mixed finite elements. Velocity-stress formulation for the wave dynamics and elastodynamics problems are indeed Hamiltonian and their mixed discretization preserves such a structure. For instance in [KK15] the authors employed mixed finite elements to obtain a symplectic semi-discretization for the wave equation. This allows using known finite element scheme to preserve the pH structure at the discrete level.

This discretization technique is a mature research topic, that is rather advantageous over classical finite elements, for a variety of reasons [Wri09]:

- locking-free behavior for incompressible material,
- no locking in thin elements,
- no sensitivity against mesh distortions,
- good coarse mesh accuracy,
- simple implementation of non-linear constitutive equations and
- efficiency (e.g. few necessary integration points).

Mixed finite elements for the wave equation have been studied in [Gev88, BJT00]. For elastodynamics the construction of stable elements gets more complicated because of the presence of the symmetric stress tensor. Existing elements enforce symmetry either strongly [BJT01, AW02] or weakly [AFW07, AL14]. A complete comparative study on this topic can be found in [Lee12].

For what concerns the mixed discretization of Kirchhoff like plates, non-conforming elements are the most common solution to lower the regularity requirement for this problem [Arn90]. In particular the Hellan-Herrmann-Johnson method [Hel67, Her67, Joh73] is the most successful one. Generic boundary conditions are not easy to handle. Nevertheless, the method is convergent for all usual boundary conditions [BR90]. Recently a mixed discretization requiring C^0 elements and valid for all kind of boundary condition has been proposed in [RZ18] for static bending problems. However, this method requires the resolution of three systems, hence the extension to the dynamical case is not straightforward.

There are many more important papers on this topic. Those cited here are significant since many proposed discretizations in this thesis are based on them.

1.2.3 Modular multibody dynamics modelling

In structural control co-design of flexible multibody systems, it is especially useful to dispose of a modular description, to simplify analysis. In this spirit, the transfer matrix method [RRWY10] and the component mode synthesis [Hur65] are two well known substructuring techniques that allow the construction of complex multibody systems by interconnecting subcomponents together. A reformulation of the Finite Element-Transfer Matrix (FE-TM) method [TYBK90] allows an easy construction of reduced models that are suited for decentralized control design. For the component mode synthesis, the controlled component synthesis (CCS), a framework for the design of decentralized controller of flexible structures, has been proposed in [You90]. Another modeling paradigm based on the component mode synthesis is the two-input two-output port (TITOP) approach [APCL15]. It conceives the dynamical model of each substructure as a transfer between the accelerations and the external forces at the connection points. This feature allows considering different boundary conditions

by inverting specific channels in the transfer matrix. A rigorous validation was provided in [PAL+16, SAPB+18], where the robustness of the methodology in handling various boundary conditions was assessed.

The Lagrangian formulation is the most commonly used methodology to retrieve the equations of motion of flexible multibody systems. The strong form Lagrangian formulation of flexible dynamics using a floating frame approach is detailed in [Sim13, Eq. 4.10] using the least action principle, but without highlighting the Hamiltonian structure of the problem. Using the variational principles of geometric mechanics, the equations of motion in Hamiltonian form can be derived either for rigid body dynamics [Hol08, Proposition 7.1.1] and general non linear elasticity [Mar81, Chapter 3]. The port-Hamiltonian (pH) framework [DMSB09] has been recently employed to describe the dynamics of rigid and flexible links [MMS07, MMS09]. Being intrinsically modular, the pH approach naturally allows constructing complex system by interconnecting together atomic elements. The formulation therein accounts for the nonlinearities due to large deformations. However, this methodology relies on Lie algebra and differential geometry concepts and requires non standard discretization techniques. Thus, the overall implementation is not straightforward.

Together with the approach used to derive the equations of motion, the incorporation of the elastic motion represents another important point when dealing with flexible multibody systems. Three descriptions are commonly used: the floating frame formulation, the corotational frame formulation and the inertial frame formulation [ES18]. The choice greatly depends on the foreseen application. The corotational and inertial frame formulations take into account large deformations of the elastic body, hence are well-suited for accurate simulations. For these formulations many model reduction strategies have been developed in the last two decades [RRTW19]. The inclusion of active control strategies is often unfeasible due to the computational burden [WN03]. The floating frame formulation is less accurate but easily integrates many model reduction techniques [NFFE12], making it possible to obtain a low-dimensional problem for control design.

1.3 Outline

The flowchart of this thesis is illustrated in Fig. 1.3. The thesis in divided into four main parts.

Part I (Chapters 1, 2) This part gives a general introduction of the following work. Chapter 2 briefly remind what finite- or infinite- dimensional pH systems are and how these systems are deeply related to the geometric Dirac or Stokes-Dirac structure (for the finite- and infinite- dimensional case respectively).

Part II (Chapters 3, 4, 5) This part is devoted to the formulation of suitable models for elasticity and thermoelasticity. This part is subdivided into three chapters.

- Chapter 3 details the pH formulation for general n-D linear elasticity.
- A pH formulation of thin (Kirchhoff-Love) and thick (Mindlin-Reissner) plate models is given in Chapter 4.
- The linear fully coupled thermoelastic problem is modelled as a coupled pH system in Chapter 5.

Part III (Chapters 6, 7, 8) This part is dedicated to the discussion and implementation of the main discretization tool: the Partitioned Finite Element method (PFEM). This method is a natural extension of mixed finite elements for the discretization of pHs. This part consists of three chapters.

- A detailed description of the operating principle of PFEM is given in Chapter 6. The approximation bases for this discretization are not explicitly defined in this chapter, since the method can be implemented through finite elements and spectral methods.
- A convergence study of several finite elements is illustrated in Chapter 7 for the bending of thin structures (beams and plates). This is by no means a rigorous mathematical convergence analysis. However, thanks to preexisting results in the literature, error estimates are conjectured and validated through numerical experiments.
- Chapter 8 is dedicated to the applications of the PFEM. In particular, the focus is on stabilization by damping injection, enforcement of mixed boundary conditions and validation of the thermoelastic pH model for an analytical solution.

Part IV (Chapters 9, 10) In this part a pH formulation of flexible multibody systems is discussed an validated. Chapter 9 details the derivation of a pH system associated to a flexible floating body under small deformation assumption. Several applications are then considered in Chapter 10.

1.4 Contributions

As an outcome of this pHD work several contributions have appeared or have been submitted in international reviews and conferences.

Accepted journal papers [BAPBM19c, BAPBM19d, BAPBM20]:

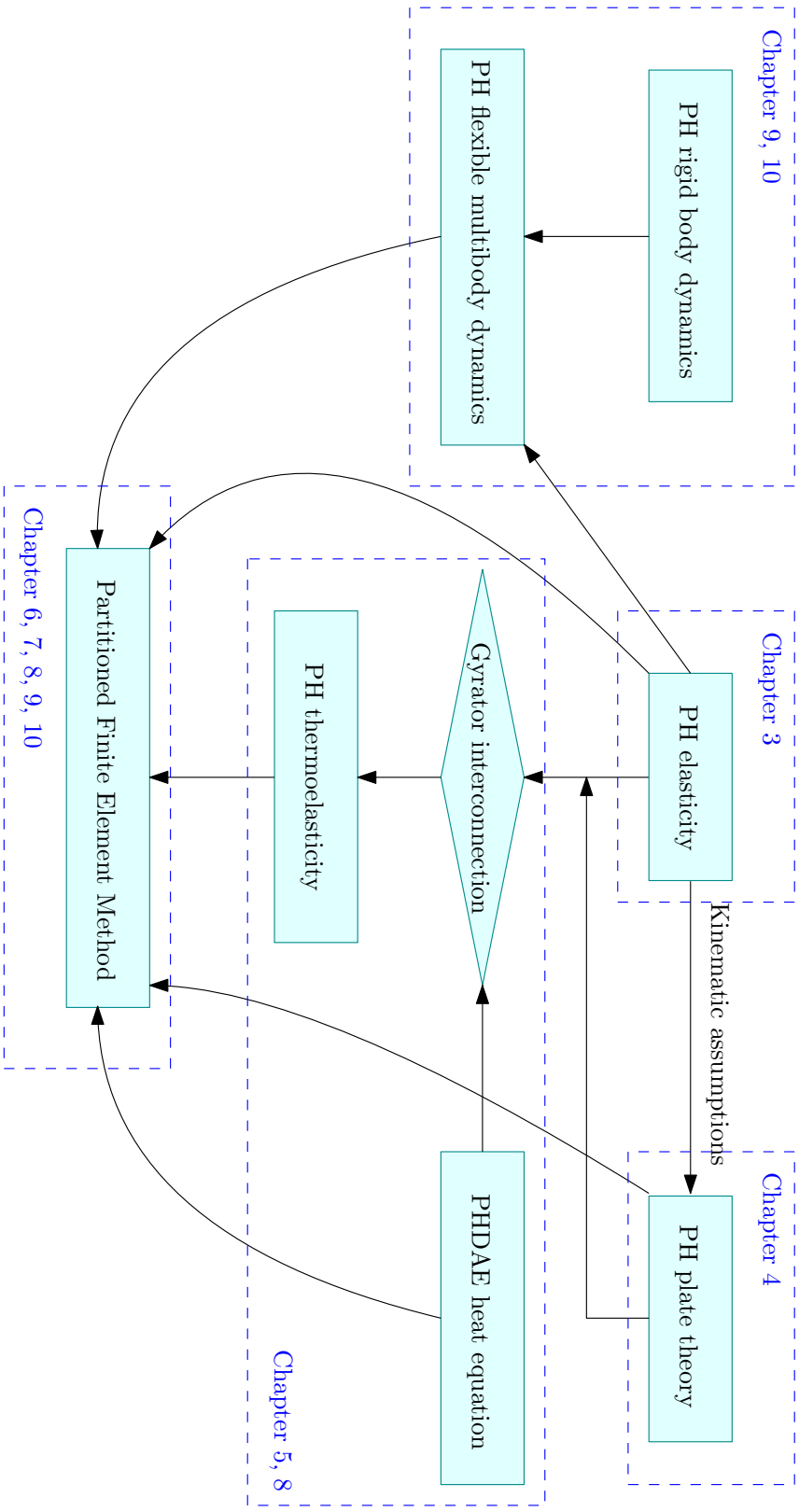

Figure 1.3: Thesis Flowchart.

1. A. Brugnoli, D. Alazard, V. Pommier-Budinger, and D. Matignon. *Port-Hamiltonian formulation and symplectic discretization of plate models. Part I: Mindlin model for thick plates.* Applied Mathematical Modelling, 75:940 – 960, Nov 2019.

2. A. Brugnoli, D. Alazard, V. Pommier-Budinger, and D. Matignon. *Port-Hamiltonian formulation and symplectic discretization of plate models. Part II: Kirchhoff model for thin plates.* Applied Mathematical Modelling, 75:961 – 981, Nov 2019.

3. A. Brugnoli, D. Alazard, V. Pommier-Budinger, and D. Matignon. *Port-Hamiltonian flexible multibody dynamics.* Multibody System Dynamics, Oct. 2020.

The content of the first two articles is mainly found in Chapters 4, 6. Chapters 9, 10 follow the third publication.

Submitted journal papers [BHSV20]:

1. A. Brugnoli, G. Haine, A. Serhani, and X. Vasseur. *Numerical approximation of port-Hamiltonian systems for hyperbolic or parabolic PDEs with boundary control.* arXiv preprint arXiv:2007.08326, 2020. Under Review.

Chapters 9, 10 follow closely this publication.

Publications in conference with full paper in proceedings [BAPBM19b, BAPBM19a, CRBML19, BCRHK20, BAPBM21]:

1. A. Brugnoli, D. Alazard, V. Pommier-Budinger, and D. Matignon. *Partitioned finite element method for the Mindlin plate as a port-Hamiltonian system.* In 3rd IFAC Workshop on Control of Systems Governed by Partial Differential Equations CPDE 2019, pages 88 – 95, Oaxaca, MX, 2019.

2. A. Brugnoli, D. Alazard, V. Pommier-Budinger, and D. Matignon. *Interconnection of the Kirchhoff plate within the port-Hamiltonian framework.* In Proceedings of the 59th IEEE Conference on Decision and Control, Dec 2019.
   The results of this conference paper are reported in Chapters 8, 10.

3. F.L. Cardoso-Ribeiro, A. Brugnoli, D. Matignon, and L. Lefèvre. *Port-Hamiltonian modeling, discretization and feedback control of a circular water tank.* In Proceedings of the 59th IEEE Conference on Decision and Control, Dec 2019.
   The content of this paper can be found in Chapter 8.

4. A. Brugnoli, F. L. Cardoso-Ribeiro, G. Haine, and P. Kotyzca. *Partitioned finite element method for power-preserving structured discretization with mixed boundary conditions.* Accepted for the 21st IFAC World congress, Jul 2020.
   The idea behind this work is illustrated in Chapter 6. The practical application is illustrated in Chapter 8

5. A. Brugnoli, D. Alazard, V. Pommier-Budinger, and D. Matignon. *Structure-preserving discretization of port-Hamiltonian plate models.* Accepted for the 24st International Symposium on Mathematical Theory of Networks and Systems, Aug 2021.
   A part of Chapter 7 reports the results of this paper.

Chapter 2

Reminder on port-Hamiltonian systems

Books serve to show a man that those original thoughts of his aren't very new after all.

Abraham Lincoln

Contents

The main mathematical aspects behind the pH formalism are recalled in this chapter. First, the finite dimensional case is considered. The geometric concept of Dirac structure [Cou90] is first presented. Finite dimensional port-Hamiltonian system are then introduced by making clear their intimate connection with the concept of Dirac structure. Second, the infinite dimensional case is recalled. The equivalent of Dirac structures for the infinite-dimensional case is the concept of Stokes-Dirac structure. Analogously to what happens in the finite-dimensional case, infinite-dimensional (or distributed) port-Hamiltonian systems are intimately related to the concept of Stokes-Dirac structure.

This notion of Stokes-Dirac structure was first introduced in the literature by making use of a differential geometry approach [vdSM02]. This approach can be extended to encompass the case of higher-order differential operators [NY04]. However, in this work the language of PDE will be privileged over the one of differential forms.

In the last section some examples are presented to demonstrate the general character of the port-Hamiltonian formalism.

2.1 Finite dimensional setting

Finite dimensional port-Hamiltonian are characterized by geometrical structures called Dirac structures. It is important to define this geometric concept and see how pHs relate to it.

2.1.1 Dirac structure

Consider a finite dimensional space F over the field $\mathbb{R}$ and $E \equiv F'$ its dual, i.e. the space of linear operator $\mathbf{e} : F \to \mathbb{R}$. The elements of F are called flows, while the elements of E are called efforts. Those are port variables and their combination gives the power flowing inside the system. The space $B := F \times E$ is called the bond space of power variables. Therefore the power is defined as $\langle \mathbf{e}, \mathbf{f} \rangle = \boldsymbol{e}(\mathbf{f})$, where $\langle \mathbf{e}, \mathbf{f} \rangle$ is the dual product between $\mathbf{f}$ and $\mathbf{e}$.

Definition 1 (Dirac Structure [Cou90], Def. 1.1.1)
Given the finite-dimensional space F and its dual E with respect to the inner product $\langle \cdot, \cdot \rangle_{E \times F} : F \times E \to \mathbb{R}$, consider the symmetric bilinear form:

$$\langle\langle\, (\mathbf{f}_1, \mathbf{e}_1), (\mathbf{f}_2, \mathbf{e}_2)\, \rangle\rangle := \langle \mathbf{e}_1,\, \mathbf{f}_2 \rangle_{E \times F} + \langle \mathbf{e}_2,\, \mathbf{f}_1 \rangle_{E \times F}\,, \qquad \textit{where} \qquad \mathbf{f}_i, \mathbf{e}_i \in B,\ i = 1, 2 \tag{2.1}$$

A Dirac structure on $B := F \times E$ is a subspace $D \subset B$, which is maximally isotropic under $\langle\langle \cdot, \cdot \rangle\rangle$. Equivalently, a Dirac structure on $B := F \times E$ is a subspace $D \subset B$ which equals its orthogonal complement with respect to $\langle\langle \cdot, \cdot \rangle\rangle : D = D^{\perp}$.

This definition can be extended to consider distributed forces and dissipation [Vil07].

Proposition 1 (Characterization of Dirac structures)
Consider the space of power variables $F \times E$ and let X denote an n-dimensional space, the space of energy variables. Suppose that $F := F_s \times F_e$ and that $E := E_s \times E_e$, with $\dim F_s = \dim E_s = n$ and $\dim F_e = \dim E_e = m$. Moreover, let $\mathbf{J}(\mathbf{x})$ denote a skew-symmetric matrix of dimension n and $\mathbf{B}(\mathbf{x})$ a matrix of dimension $n \times m$. Then, the set

$$D := \left\{ (\mathbf{f}_s, \mathbf{f}_e, \mathbf{e}_s, \mathbf{e}_e) \in F \times E \middle| \quad \mathbf{f}_s = \mathbf{J}(\mathbf{x})\mathbf{e}_s + \mathbf{B}(\mathbf{x})\mathbf{f}_e,\ \mathbf{e}_e = -\mathbf{B}(\mathbf{x})^{\top}\mathbf{e}_s \right\} \tag{2.2}$$

is a Dirac structure.

It is now possible to make the connection between Dirac structures and pH system explicit.

2.1.2 Finite-dimensional port-Hamiltonian systems

Consider the time-invariant dynamical system:

$$\begin{cases} \dot{\mathbf{x}} &= \mathbf{J}(\mathbf{x})\nabla H(\mathbf{x}) + \mathbf{B}(\mathbf{x})\mathbf{u}, \\ \mathbf{y} &= \mathbf{B}(\mathbf{x})^\top \nabla H(\mathbf{x}), \end{cases} \tag{2.3}$$

where $H(\mathbf{x}) : X \subset \mathbb{R}^n \to \mathbb{R}$, the Hamiltonian, is a real-valued function bounded from below. Such a system is called port-Hamiltonian, as it arises from the Hamiltonian modelling of a physical system and it interacts with the environment through the input $\mathbf{u}$ and the output $\mathbf{y}$, included in the formulation. The connection with the concept of Dirac structure is achieved by considering the following port behavior:

$$\begin{aligned} \mathbf{f}_s &= \dot{\mathbf{x}}, & \mathbf{e}_s &= \nabla H(\mathbf{x}), \\ \mathbf{f}_e &= \mathbf{u}, & \mathbf{e}_e &= -\mathbf{y}. \end{aligned} \tag{2.4}$$

With this choice of the port variables, system (2.3) defines, by Proposition 1, a Dirac structure. Dissipation and distributed forces can be included and the corresponding system defines an extended Dirac structure, once the proper port variables have been introduced.

System 2.3 is a pH system in canonical form. Recently, finite-dimensional differential algebraic port-Hamiltonian systems (pHDAE) have been introduced both for linear [BMXZ18] and non-linear systems [MM19]. This enriched description share all the crucial features of ordinary pHs, but easily account for algebraic constraints, time-dependent transformations and explicit dependence on time in the Hamiltonian.

2.2 Infinite-dimensional setting

Infinite-dimensional spaces appear whenever differential operators have to be considered. In this section we first explain what defines a differential operator. Then Stokes-Dirac structures, characterized by a skew-symmetric differential operator, are introduced. Finally distributed port-Hamiltonian systems and their connection to the concept of Stokes-Dirac structure are illustrated.

Before starting we recall how inner products of square-integrable function are computed. Let Ω denote a compact subset of $\mathbb{R}^d$ and let $L^2(\Omega, \mathbb{A})$ be the space of square-integrable

functions over the set $\mathbb{A}$ in Ω, with inner product denoted by $\langle \cdot, \cdot \rangle_{L^2(\Omega,\mathbb{A})}$. The set $\mathbb{A}$ can either denote scalars $\mathbb{R}$, vectors $\mathbb{R}^d$, tensors $\mathbb{R}^{d\times d}$ or a Cartesian product of those. For scalars $(a, b) \in L^2(\Omega)$, vectors $(\boldsymbol{a}, \boldsymbol{b}) \in L^2(\Omega, \mathbb{R}^d)$ and tensors $(\boldsymbol{A}, \boldsymbol{B}) \in L^2(\Omega, \mathbb{R}^{d\times d})$ the L^2 inner product is given by

$$\langle a,\, b\rangle_{L^2(\Omega)} = \int_\Omega ab \,\mathrm{d}\Omega, \qquad \langle \boldsymbol{a},\, \boldsymbol{b}\rangle_{L^2(\Omega,\mathbb{R}^d)} = \int_\Omega \boldsymbol{a}\cdot\boldsymbol{b} \,\mathrm{d}\Omega, \qquad \langle \boldsymbol{A},\, \boldsymbol{B}\rangle_{L^2(\Omega,\mathbb{R}^{d\times d})} = \int_\Omega \boldsymbol{A}\!:\!\boldsymbol{B} \,\mathrm{d}\Omega. \tag{2.5}$$

The notation $\boldsymbol{A}:\boldsymbol{B} = \sum_{i,j} A_{ij}B_{ij}$ denotes the tensor contraction. Furthermore, the space of square-integrable vector-valued functions over the boundary of Ω is denoted by $L^2(\partial\Omega, \mathbb{R}^m)$. This space is endowed with the inner product

$$\langle \boldsymbol{a}_\partial,\, \boldsymbol{b}_\partial\rangle_{L^2(\partial\Omega,\mathbb{R}^m)} = \int_{\partial\Omega} \boldsymbol{a}_\partial \cdot \boldsymbol{b}_\partial \,\mathrm{d}S, \qquad \boldsymbol{a}_\partial, \boldsymbol{b}_\partial \in \mathbb{R}^m. \tag{2.6}$$

2.2.1 Constant linear differential operators

Let Ω denote a compact subset of $\mathbb{R}^d$ representing the spatial domain of the distributed parameter system. Consider two functional spaces F_1, F_2 over the sets $\mathbb{A}$, $\mathbb{B}$ defined on $\Omega \subset \mathbb{R}^d$ and a map $\mathcal{L}$ relating the two

$$\begin{aligned} \mathcal{L} : F_1(\Omega, \mathbb{A}) &\longrightarrow F_2(\Omega, \mathbb{B}), \\ \boldsymbol{u} &\longrightarrow \boldsymbol{v}. \end{aligned} \tag{2.7}$$

Sets $\mathbb{A}, \mathbb{B}$ can either denote scalars $\mathbb{R}$, vectors $\mathbb{R}^d$, tensors $\mathbb{R}^{d\times d}$ or a Cartesian product of those. Given $\boldsymbol{u} \in F_1$, $\boldsymbol{v} \in F_2$, the map $\mathcal{L}$ is a constant linear differential operator if it can be represented by a linear combination of derivatives of $\boldsymbol{u}$

$$\boldsymbol{v} = \mathcal{L}\boldsymbol{u} \iff \boldsymbol{v} := \sum_{|\alpha|=0}^{n} \mathcal{P}_\alpha \partial^\alpha \boldsymbol{u}, \tag{2.8}$$

where $\alpha := (\alpha_1, \ldots, \alpha_d)$ is a multi-index of order $|\alpha| := \sum_{i=1}^d \alpha_i$ and $\partial^\alpha := \partial_{x_1}^{\alpha_1} \ldots \partial_{x_d}^{\alpha_d}$ is a differential operator of order $|\alpha|$ resulting from a combination of spatial derivatives. $\mathcal{P}_\alpha : \mathbb{A} \to \mathbb{B}$ is a constant algebraic operator from set $\mathbb{A}$ to $\mathbb{B}$.

Example 1 (Divergence operator in $\mathbb{R}^d$)
Given $\boldsymbol{u} \in C^\infty(\Omega, \mathbb{R}^d)$, $v \in C^\infty(\Omega)$, where $C^\infty(\Omega, \mathbb{R}^d)$, $C^\infty(\Omega)$ denotes the set of indefinitely smooth vector- and scalar-valued function defined on Ω, the divergence operator in Cartesian coordinate is expressed as

$$v = \operatorname{div} \boldsymbol{u} = \sum_{i=1}^{d} \boldsymbol{e}_i \cdot \partial_{x_i} \boldsymbol{u}, \tag{2.9}$$

where $\boldsymbol{e}_i$ is the $i-th$ element of the canonical basis in $\mathbb{R}^d$.

The differential operators employed in this thesis are reported in Appendix A.
A very important notion related to a differential operator is the concept of formal adjoint.

Definition 2 (Formal Adjoint)
Let $\mathcal{L} = L^2(\Omega, \mathbb{A}) \to L^2(\Omega, \mathbb{B})$ be a differential operator and $\boldsymbol{u} \in C_0^\infty(\Omega, \mathbb{A})$, $\boldsymbol{v} \in C_0^\infty(\Omega, \mathbb{B})$ be smooth variables with compact support on Ω. The formal adjoint of the differential operator $\mathcal{L}$, denoted by $\mathcal{L}^* = L^2(\Omega, \mathbb{B}) \to L^2(\Omega, \mathbb{A})$, is defined by the relation

$$\langle \mathcal{L}\boldsymbol{u},\, \boldsymbol{v} \rangle_{L^2(\Omega,\mathbb{B})} = \langle \boldsymbol{u},\, \mathcal{L}^*\boldsymbol{v} \rangle_{L^2(\Omega,\mathbb{A})}\,. \tag{2.10}$$

This definition represent an extension to generic sets $\mathbb{A}$, $\mathbb{B}$ of Def. 5.80 in [RR04] (reported in Appendix A).

Remark 1 (Differences between adjoint and formal adjoint)
The definition of formal adjoint is such that the integration by parts formula is respected. Contrarily to the adjoint of an operator, the formal adjoint definition does not require the actual domain of the operator nor the boundary conditions. The formal adjoint respects the integration by parts formula and is defined only for sufficiently smooth functions with compact support. In this sense the formal adjoint of div *is* $-\operatorname{grad}$*, since for smooth functions with compact support, it holds*

$$\langle \operatorname{div} \boldsymbol{y},\, x \rangle_{L^2(\Omega,\mathbb{R})} \underbrace{=}_{I.B.P.} - \langle \boldsymbol{y},\, \operatorname{grad} x \rangle_{L^2(\Omega,\mathbb{R}^d)}\,,$$

for $\boldsymbol{y} \in C_0^\infty(\Omega, \mathbb{R}^d)$, $x \in C_0^\infty(\Omega)$ (I.B.P. stands for integration by parts). The definition of the domain of the operators, that requires the knowledge of the boundary conditions, has not been specified.

For pHs formally skew-adjoint (or simply skew-symmetric) operators play a fundamental role.

Definition 3 (Formally skew-adjoint operator)
Let $\mathcal{J} : L^2(\Omega, \mathbb{F}) \to L^2(\Omega, \mathbb{F})$ be a linear differential operator. Notice that the set $\mathbb{F}$ in the domain and co-domain is the same. Then, $\mathcal{J}$ is formally skew-adjoint (or skew-symmetric) if and only if $\mathcal{J} = -\mathcal{J}^*$.

If functions with compact support are considered, i.e. $\boldsymbol{u}_1, \boldsymbol{u}_2 \in C_0^\infty(\Omega, \mathbb{F})$ a formally skew-adjoint operator is characterized by the relation

$$\langle \mathcal{J}\boldsymbol{u}_1,\, \boldsymbol{u}_2 \rangle_{L^2(\Omega,\mathbb{F})} + \langle \boldsymbol{u}_1,\, \mathcal{J}\boldsymbol{u}_2 \rangle_{L^2(\Omega,\mathbb{F})} = 0. \tag{2.11}$$

2.2.2 Constant Stokes-Dirac structures

Constant Stokes-Dirac structures are the infinite-dimensional generalization of constant Dirac structures (i.e. Dirac structures for which the matrices $\mathbf{J}$, $\mathbf{B}$ in (2.3) are constant). Stokes-Dirac structure are characterized by the fact that they equal their orthogonal complement with respect to a given bilinear product. So we recall the definition of orthogonal companion for the case of smooth functions.

Definition 4 (Orthogonal complement)
Let $\Omega \subset \mathbb{R}^d$, $d \in \{1, 2, 3\}$ be an open connected set and $C^\infty(\partial\Omega, \mathbb{R}^m)$ the space of infinitely smooth functions over its boundary. Consider the space

$$B = C^\infty(\Omega, \mathbb{F}) \times C^\infty(\partial\Omega, \mathbb{R}^m) \times C^\infty(\Omega, \mathbb{F}) \times C^\infty(\partial\Omega, \mathbb{R}^m), \tag{2.12}$$

and the bilinear pairing defined by

$$\begin{aligned} \langle\langle \cdot, \cdot \rangle\rangle : B \times B &\longrightarrow \mathbb{R}, \\ (\boldsymbol{a},\ \boldsymbol{a}_\partial,\ \boldsymbol{b},\ \boldsymbol{b}_\partial) \times (\boldsymbol{c},\ \boldsymbol{c}_\partial,\ \boldsymbol{d},\ \boldsymbol{d}_\partial) &\longrightarrow \begin{array}{l} \langle \boldsymbol{a},\ \boldsymbol{d} \rangle_{L^2(\Omega,\mathbb{F})} + \langle \boldsymbol{b},\ \boldsymbol{c} \rangle_{L^2(\Omega,\mathbb{F})} + \\ \langle \boldsymbol{a}_\partial,\ \boldsymbol{d}_\partial \rangle_{L^2(\partial\Omega,\mathbb{R}^m)} + \langle \boldsymbol{b}_\partial,\ \boldsymbol{c}_\partial \rangle_{L^2(\partial\Omega,\mathbb{R}^m)}\,. \end{array} \end{aligned} \tag{2.13}$$

Given a linear subspace $W \subset B$, its orthogonal complement is the set

$$W^\perp = \{\boldsymbol{v} = (\boldsymbol{v}_1,\ \boldsymbol{v}_{1\partial},\ \boldsymbol{v}_2,\ \boldsymbol{v}_{2\partial}) \in B |\, \langle\langle\, \boldsymbol{v}, \boldsymbol{w}\, \rangle\rangle = 0,\ \forall \boldsymbol{w} = (\boldsymbol{w}_1,\ \boldsymbol{w}_{1\partial},\ \boldsymbol{w}_2,\ \boldsymbol{w}_{2\partial}) \in W\}. \tag{2.14}$$

We can now define what a Stokes-Dirac structure is.

Definition 5 (Stokes-Dirac structure)
A subset $D \subset B$, with B defined in (2.12), is a Stokes-Dirac structure iff

$$D = D^\perp, \tag{2.15}$$

where the orthogonal complement is defined by Eq. (2.14)

For a subset to be a Stokes-Dirac structures a link between flow and effort variables must hold. Consider $\boldsymbol{f} \in C^\infty(\Omega, \mathbb{F})$ and $\boldsymbol{e} \in C^\infty(\Omega, \mathbb{F})$ and te following relation between the two

$$\boldsymbol{f} = \mathcal{J}\boldsymbol{e}, \qquad \mathcal{J} = -\mathcal{J}^*, \tag{2.16}$$

where $\mathcal{J}$ is a formally skew-adjoint operator. Moreover, a Stokes-Dirac structure requires the specification of boundary variables in order to express a general power conservation property for *open* physical systems. We make therefore the following assumption, over the existence of appropriate boundary operators.

Assumption 1 (Existence of boundary operators)

Assume that exist two linear boundary operators $\mathcal{B}_\partial$, $\mathcal{C}_\partial$ such that for $\boldsymbol{u}_1,\ \boldsymbol{u}_2 \in C^\infty(\overline{\Omega}, \mathbb{F})$ the following integration by parts formula holds

$$\langle \mathcal{J}\boldsymbol{u}_1,\ \boldsymbol{u}_2\rangle_{L^2(\Omega,\mathbb{B})} + \langle \boldsymbol{u}_1,\ \mathcal{J}\boldsymbol{u}_2\rangle_{L^2(\Omega,\mathbb{A})} = \langle \mathcal{B}_\partial \boldsymbol{u}_1,\ \mathcal{C}_\partial \boldsymbol{u}_2\rangle_{L^2(\partial\Omega,\mathbb{R}^m)} + \langle \mathcal{C}_\partial \boldsymbol{u}_1,\ \mathcal{B}_\partial \boldsymbol{u}_2\rangle_{L^2(\partial\Omega,\mathbb{R}^m)}\,. \tag{2.17}$$

This assumption proves necessary to appropriately define a Stokes-Dirac structure. Only few particular cases, like the transport equation, do not verify it. We can now characterize Stokes-Dirac structure for smooth functions spaces.

Remark 2
The assumption involves smooth functions only. Care must be taken with less regular functions, especially for what concerns the boundary operators. When working with less regular spaces (i.e. Sobolev spaces), the boundary operator are unbounded and the integration by parts results in a duality bracket instead of an L^2 inner product [TW09, Chapter 4].

Proposition 2 (Characterization of Stokes-Dirac structures [LGZM05])
Let B be defined as in Eq. (2.12) and $\mathcal{J}$ be a formally skew adjoint operator verifying Assumption 1. The set

$$D_\mathcal{J} = \{(\boldsymbol{f},\ \boldsymbol{f}_\partial,\ \boldsymbol{e},\ \boldsymbol{e}_\partial) \in B |\ \boldsymbol{f} = \mathcal{J}\boldsymbol{e},\ \boldsymbol{f}_\partial = \mathcal{B}_\partial \boldsymbol{e},\ \boldsymbol{e}_\partial = -\mathcal{C}_\partial \boldsymbol{e}\} \tag{2.18}$$

is a Stokes-Dirac structure with respect to the bilinear pairing (2.13).

Proof. A Stokes-Dirac is characterized by the fact that $D_\mathcal{J} = D_\mathcal{J}^\perp$. Then one has to show that $D_\mathcal{J} \subset D_\mathcal{J}^\perp$ and $D_\mathcal{J}^\perp \subset D_\mathcal{J}$. Following [LGZM05], the proof is obtained following three steps.

Step 1. To show that $D_\mathcal{J} \subset D_\mathcal{J}^\perp$, take $(\boldsymbol{f},\ \boldsymbol{f}_\partial,\ \boldsymbol{e},\ \boldsymbol{e}_\partial) \in D_\mathcal{J}$. Then

$$\begin{aligned}
\langle\langle\, (\boldsymbol{f},\boldsymbol{f}_\partial,\boldsymbol{e},\boldsymbol{e}_\partial), (\boldsymbol{f},\boldsymbol{f}_\partial,\boldsymbol{e},\boldsymbol{e}_\partial)\,\rangle\rangle =& 2\,\langle \boldsymbol{e},\ \boldsymbol{f}\rangle_{L^2(\Omega,\mathbb{F})} + 2\,\langle \boldsymbol{e}_\partial,\ \boldsymbol{f}_\partial\rangle_{L^2(\partial\Omega,\mathbb{R}^m)}\,,\\
=& 2\,\langle \boldsymbol{e},\ \mathcal{J}\boldsymbol{e}\rangle_{L^2(\Omega,\mathbb{F})} + 2\,\langle \boldsymbol{e}_\partial,\ \boldsymbol{f}_\partial\rangle_{L^2(\partial\Omega,\mathbb{R}^m)}\,,\\
\overset{\text{Eq. (2.17)}}{=}& 2\,\langle \mathcal{B}_\partial\boldsymbol{e},\ \mathcal{C}_\partial\boldsymbol{e}\rangle_{L^2(\partial\Omega,\mathbb{R}^m)} + 2\,\langle \boldsymbol{e}_\partial,\ \boldsymbol{f}_\partial\rangle_{L^2(\partial\Omega,\mathbb{R}^m)}\,,\\
\overset{\text{Eq. (2.18)}}{=}& 2\,\langle \mathcal{B}_\partial\boldsymbol{e},\ \mathcal{C}_\partial\boldsymbol{e}\rangle_{L^2(\partial\Omega,\mathbb{R}^m)} - 2\,\langle \mathcal{B}_\partial\boldsymbol{e},\ \mathcal{C}_\partial\boldsymbol{e}\rangle_{L^2(\partial\Omega,\mathbb{R}^m)}\,,\\
=& 0.
\end{aligned}$$

This implies $D_\mathcal{J} \subset D_\mathcal{J}^\perp$.

Step 2. Take $(\boldsymbol{\phi},\ \boldsymbol{\phi}_\partial,\ \boldsymbol{\epsilon},\ \boldsymbol{\epsilon}_\partial) \in D_\mathcal{J}^\perp$ and $\boldsymbol{e}_0 \in C_0^\infty(\Omega, \mathbb{F})$. This implies $\mathcal{B}_\partial \boldsymbol{e}_0 = (\mathbf{0},\ \mathbf{0})$ and $\mathcal{C}_\partial \boldsymbol{e}_0 = (\mathbf{0},\ \mathbf{0})$. Taking $(\mathcal{J}\boldsymbol{e}_0, \mathbf{0}, \boldsymbol{e}_0, \mathbf{0}) \in D_\mathcal{J}$ then

$$\langle\langle\, (\boldsymbol{\phi},\boldsymbol{\phi}_\partial,\boldsymbol{\epsilon},\boldsymbol{\epsilon}_\partial), (\mathcal{J}\boldsymbol{e}_0,\mathbf{0},\boldsymbol{e}_0,\mathbf{0})\,\rangle\rangle = \langle \boldsymbol{\epsilon},\ \mathcal{J}\boldsymbol{e}_0\rangle_{L^2(\Omega,\mathbb{F})} + \langle \boldsymbol{e}_0,\ \boldsymbol{\phi}\rangle_{L^2(\Omega,\mathbb{F})} = 0, \quad \forall \boldsymbol{e}_0 \in C_0^\infty(\Omega,\mathbb{F}).$$

It follows that $\boldsymbol{\epsilon} \in C_0^\infty(\Omega, \mathbb{F})$ and $\boldsymbol{\phi} = \mathcal{J}\boldsymbol{\epsilon}$.

Step 3. Take $(\boldsymbol{\phi}, \boldsymbol{\phi}_\partial, \boldsymbol{\epsilon}, \boldsymbol{\epsilon}_\partial) \in D_\mathcal{J}^\perp$ and $(\boldsymbol{f}, \boldsymbol{f}_\partial, \boldsymbol{e}, \boldsymbol{e}_\partial) \in D_\mathcal{J}$. From step 2 and (2.17)

$$
\begin{aligned}
0 &= \langle \mathcal{J}\boldsymbol{e}, \boldsymbol{\epsilon}\rangle_{L^2(\Omega,\mathbb{F})} + \langle \boldsymbol{e}, \mathcal{J}\boldsymbol{\epsilon}\rangle_{L^2(\Omega,\mathbb{F})} + \langle \boldsymbol{e}_\partial, \boldsymbol{\phi}_\partial\rangle_{L^2(\partial\Omega,\mathbb{R}^m)} + \langle \boldsymbol{\epsilon}_\partial, \boldsymbol{f}_\partial\rangle_{L^2(\partial\Omega,\mathbb{R}^m)}\,, \\
&\overset{\text{Eq. (2.17)}}{=} \langle \mathcal{B}_\partial\boldsymbol{e}, \mathcal{C}_\partial\boldsymbol{\epsilon}\rangle_{L^2(\partial\Omega,\mathbb{R}^m)} + \langle \mathcal{B}_\partial\boldsymbol{\epsilon}, \mathcal{C}_\partial\boldsymbol{e}\rangle_{L^2(\partial\Omega,\mathbb{R}^m)} + \langle \boldsymbol{e}_\partial, \boldsymbol{\phi}_\partial\rangle_{L^2(\partial\Omega,\mathbb{R}^m)} + \langle \boldsymbol{\epsilon}_\partial, \boldsymbol{f}_\partial\rangle_{L^2(\partial\Omega,\mathbb{R}^m)}\,, \\
&= \langle \mathcal{B}_\partial\boldsymbol{e}, \mathcal{C}_\partial\boldsymbol{\epsilon}\rangle_{L^2(\partial\Omega,\mathbb{R}^m)} + \langle \mathcal{B}_\partial\boldsymbol{\epsilon}, \mathcal{C}_\partial\boldsymbol{e}\rangle_{L^2(\partial\Omega,\mathbb{R}^m)} + \langle -\mathcal{C}_\partial\boldsymbol{e}, \boldsymbol{\phi}_\partial\rangle_{L^2(\partial\Omega,\mathbb{R}^m)} + \langle \boldsymbol{\epsilon}_\partial, \mathcal{B}_\partial\boldsymbol{e}\rangle_{L^2(\partial\Omega,\mathbb{R}^m)}\,, \\
&= \langle \mathcal{B}_\partial\boldsymbol{e}, \mathcal{C}_\partial\boldsymbol{\epsilon} + \boldsymbol{\epsilon}_\partial\rangle_{L^2(\partial\Omega,\mathbb{R}^m)} + \langle \mathcal{B}_\partial\boldsymbol{\epsilon} - \boldsymbol{\phi}_\partial, \mathcal{C}_\partial\boldsymbol{e}\rangle_{L^2(\partial\Omega,\mathbb{R}^m)}\,, \qquad \text{By linearity,} \\
&= \langle \boldsymbol{e}_\partial, \mathcal{C}_\partial\boldsymbol{\epsilon} + \boldsymbol{\epsilon}_\partial\rangle_{L^2(\partial\Omega,\mathbb{R}^m)} - \langle \mathcal{B}_\partial\boldsymbol{\epsilon} - \boldsymbol{\phi}_\partial, \boldsymbol{f}_\partial\rangle_{L^2(\partial\Omega,\mathbb{R}^m)}\,.
\end{aligned}
$$

Given the fact that $\boldsymbol{e}_\partial$, $\boldsymbol{f}_\partial$ are arbitrary then

$$\boldsymbol{\phi}_\partial = \mathcal{B}_\partial\boldsymbol{\epsilon}, \qquad \boldsymbol{\epsilon}_\partial = -\mathcal{C}_\partial\boldsymbol{\epsilon},$$

meaning that $D_\mathcal{J}^\perp \subset D_\mathcal{J}$. This concludes the proof. □

2.2.3 Distributed port-Hamiltonian systems

A distributed lossless port-Hamiltonian system is defined by a set of variables that describes the unknowns, by a formally skew-adjoint differential operator, an energy functional and a set of boundary inputs and corresponding conjugated outputs. Such a system is described by the following set of equations, defined on an open connected set $\Omega \subset \mathbb{R}^d$

$$
\begin{aligned}
\partial_t\boldsymbol{\alpha} &= \mathcal{J}\,\delta_{\boldsymbol{\alpha}}H, & \boldsymbol{\alpha} &\in C^\infty(\Omega, \mathbb{F}), \\
\boldsymbol{u}_\partial &= \mathcal{B}_\partial\,\delta_{\boldsymbol{\alpha}}H, & \boldsymbol{u}_\partial &\in C^\infty(\partial\Omega, \mathbb{R}^m), \\
\boldsymbol{y}_\partial &= \mathcal{C}_\partial\,\delta_{\boldsymbol{\alpha}}H, & \boldsymbol{y}_\partial &\in C^\infty(\partial\Omega, \mathbb{R}^m).
\end{aligned}
\tag{2.19}
$$

The unknowns $\boldsymbol{\alpha}$ are called energy variables in the port-Hamiltonian framework, the formally skew-adjoint operator $\mathcal{J}$ is named interconnection operator (see Def. 3 for a precise definition of formal skew adjointness). $\mathcal{B}_\partial, \mathcal{C}_\partial$ are boundary operators, that provide the boundary input $\boldsymbol{u}_\partial$ and output $\boldsymbol{y}_\partial$ [TW09, Chapter 4]. The functional $H(\boldsymbol{\alpha}) : C^\infty(\Omega, \mathbb{F}) \to \mathbb{R}$ corresponds to the Hamiltonian functional and in all the examples considered in this thesis coincide with the total energy of the system. Notation $\delta_{\boldsymbol{\alpha}}H$ indicates the variational derivative of H.

Definition 6 (Variational derivative, Def. 4.1 in [Olv93])
Consider a functional $H(\boldsymbol{\alpha}) : C^\infty(\Omega, \mathbb{F}) \to \mathbb{R}$

$$H(\boldsymbol{\alpha}) = \int_\Omega \mathcal{H}(\boldsymbol{\alpha})\,\mathrm{d}\Omega.$$

Given a variation $\boldsymbol{\alpha} = \bar{\boldsymbol{\alpha}} + \eta\boldsymbol{\delta\alpha}$ *the variational derivative* $\frac{\delta H}{\delta \boldsymbol{\alpha}}$ *is defined as*

$$H(\bar{\boldsymbol{\alpha}} + \eta\boldsymbol{\delta\alpha}) = H(\bar{\boldsymbol{\alpha}}) + \eta \left\langle \delta_{\boldsymbol{\alpha}} H,\, \boldsymbol{\delta\alpha} \right\rangle_{L^2(\Omega,\mathbb{F})} + O(\eta^2).$$

Remark 3
If the integrand does not contain derivatives of the argument $\boldsymbol{\alpha}$ *then the variational derivative is equal to the partial derivative of the Hamiltonian density* $\mathcal{H}$

$$\frac{\delta H}{\delta \boldsymbol{\alpha}} = \frac{\partial \mathcal{H}}{\partial \boldsymbol{\alpha}}.$$

Remark 4 (Co-energy variables)
The variational derivative of the Hamiltonian defines the co-energy variables $\boldsymbol{e} := \delta_{\boldsymbol{\alpha}} H$*. These are equivalent to the effort variables of the Stokes-Dirac structure as we will immediately show.*

Suppose that operators $\mathcal{J}$, $\mathcal{B}_\partial$, $\mathcal{C}_\partial$ in Eq. 2.19 verify Assumption 1. Then, System (2.19) is lossless since the energy rate is given by

$$\begin{aligned} \dot{H} &= \left\langle \delta_{\boldsymbol{\alpha}} H,\, \partial_t \boldsymbol{\alpha} \right\rangle_{L^2(\Omega,\mathbb{F})}, \\ &\overset{\text{Eq. (2.17)}}{=} \left\langle \mathcal{B}_\partial \delta_{\boldsymbol{\alpha}} H,\, \mathcal{C}_\partial \delta_{\boldsymbol{\alpha}} H \right\rangle_{L^2(\partial\Omega,\mathbb{R}^m)}, \\ &= \left\langle \boldsymbol{u}_\partial,\, \boldsymbol{y}_\partial \right\rangle_{L^2(\partial\Omega,\mathbb{R}^m)}. \end{aligned} \tag{2.20}$$

The connection between the concept of Stokes-Dirac structure and dpHs becomes clear if the following port behavior is considered

$$\begin{aligned} \boldsymbol{f} &= \partial_t \boldsymbol{\alpha}, \qquad & \boldsymbol{e} &= \delta_{\boldsymbol{\alpha}} H, \\ \boldsymbol{f}_\partial &= \boldsymbol{u}_\partial, \qquad & \boldsymbol{e}_\partial &= -\boldsymbol{y}_\partial. \end{aligned} \tag{2.21}$$

By Proposition (2) System (2.19) under the port behavior (2.21) defines a Stokes-Dirac structure. No rigorous characterization has been given so far for operators $\mathcal{J}$, $\mathcal{B}_\partial$, $\mathcal{C}_\partial$ in system (2.19). A formal characterization of these operators has been given in [LGZM05] for pH of generic order only in one geometrical dimensional. In Chapter 6 the operator $\mathcal{J}$ will be better characterized using an appropriate partition. By applying a general integration by parts formula, the operators $\mathcal{B}_\partial$, $\mathcal{C}_\partial$ associated to $\mathcal{J}$ can be defined as well. The following examples clarifies this assertion for some known pHs.

2.3 Some examples of known distributed port-Hamiltonian systems

In this section the generality of the pH framework is illustrated through three different examples: the wave equation in a 2D geometry, the Euler-Bernoulli beam and the non-linear Saint-Venant equations.

2.3.1 Wave equation

Given an open bounded connected set $\Omega \subset \mathbb{R}^d,\ d = \{2, 3\}$ with Lipschitz continuous boundary $\partial\Omega$, the propagation of sound in air can be described by the following model [TRLGK18]

$$\begin{aligned} \chi_s \partial_t p(\boldsymbol{x}, t) &= -\operatorname{div} \boldsymbol{v}, \\ \mu_0 \partial_t \boldsymbol{v}(\boldsymbol{x}, t) &= -\operatorname{grad} p, \end{aligned} \tag{2.22}$$

where the scalars χ_s, μ_0 are the constant adiabatic compressibility factor and the steady state mass density respectively. The scalar field $p \in \mathbb{R}$ and vector field $\boldsymbol{v} \in \mathbb{R}^d$ represents the variation of pressure and velocity from the steady state. The Hamiltonian (total energy) reads

$$H = \frac{1}{2} \int_\Omega \left\{ \chi_s p^2 + \mu_0 \left\| \boldsymbol{v} \right\|^2 \right\} \, \mathrm{d}\Omega.$$

To recast (2.22) in pH form the energy variables has to be introduced $\boldsymbol{\alpha} = [\alpha_p, \boldsymbol{\alpha}_v]^\top$

$$\alpha_p := \chi_s p, \qquad \boldsymbol{\alpha}_v := \mu_0 \boldsymbol{v}.$$

The Hamiltonian is rewritten as

$$H = \frac{1}{2} \int_\Omega \left\{ \frac{1}{\chi_s} \alpha_p^2 + \frac{1}{\mu_0} \left\| \boldsymbol{\alpha}_v \right\|^2 \right\} \, \mathrm{d}\Omega.$$

By definition, the co-energy are

$$e_p = \frac{\delta H}{\delta \alpha_p} = \frac{1}{\chi_s} \alpha_p = p, \qquad \boldsymbol{e}_v = \frac{\delta H}{\delta \boldsymbol{\alpha}_v} = \frac{1}{\mu_0} \boldsymbol{\alpha}_v = \boldsymbol{v}.$$

Equation (2.22) can be recast in port-Hamiltonian form

$$\frac{\partial}{\partial t} \begin{pmatrix} \alpha_p \\ \boldsymbol{\alpha}_v \end{pmatrix} = - \begin{bmatrix} 0 & \operatorname{div} \\ \operatorname{grad} & \mathbf{0} \end{bmatrix} \begin{pmatrix} e_p \\ \boldsymbol{e}_v \end{pmatrix}. \tag{2.23}$$

From the energy rate it is possible to identify the boundary variables.

$$\begin{aligned} \dot{H} &= + \int_\Omega \left\{ e_p \, \partial_t \alpha_p + \boldsymbol{e}_v \cdot \partial_t \boldsymbol{\alpha}_v \right\} \, \mathrm{d}\Omega, \\ &= - \int_\Omega \left\{ e_p \, \operatorname{div} \boldsymbol{e}_v + \boldsymbol{e}_v \cdot \operatorname{grad} e_p \right\} \, \mathrm{d}\Omega, && \text{Chain rule,} \\ &= - \int_\Omega \operatorname{div}(e_p \, \boldsymbol{e}_v) \, \mathrm{d}\Omega, && \text{Stokes theorem,} \\ &= - \int_{\partial\Omega} e_p \, \boldsymbol{e}_v \cdot \boldsymbol{n} \, \mathrm{d}S = - \left\langle e_p, \, \boldsymbol{e}_v \cdot \boldsymbol{n} \right\rangle_{L^2(\partial\Omega, \mathbb{R}^2)}. \end{aligned}$$

The boundary term $\langle e_p, \, \boldsymbol{e}_v \cdot \boldsymbol{n} \rangle_{L^2(\partial\Omega, \mathbb{R}^2)}$ pairs two power variables. One is taken as control input, the other plays the role of power-conjugated output. The assignment of these roles to the boundary power variables is referred to as causality of the boundary port [KML18],[Kot19, Chapter 2]. Under uniform causality assumption, either e_p or $\boldsymbol{e}_v$ can assume the role of

(distributed) boundary input, but not both. This leads to two possible selections:

- First case $u_\partial = e_p, \quad y_\partial = \boldsymbol{e}_v \cdot \boldsymbol{n}$.
  This imposes the variable $e_p := p$ as boundary input and corresponds to a classical Dirichlet condition. The boundary operator for this case are given by

$$\mathcal{B}_\partial \begin{pmatrix} e_p \\ \boldsymbol{e}_v \end{pmatrix} = e_p|_{\partial\Omega}, \qquad \mathcal{C}_\partial \begin{pmatrix} e_p \\ \boldsymbol{e}_v \end{pmatrix} = \boldsymbol{e}_v \cdot \boldsymbol{n}|_{\partial\Omega},$$

  corresponding to the standard trace and normal trace operators.

- Second case $u_\partial = \boldsymbol{e}_v \cdot \boldsymbol{n}, \quad y_\partial = e_p$.
  This imposes the variable $\boldsymbol{e}_v \cdot \boldsymbol{n} := \boldsymbol{v} \cdot \boldsymbol{n}$ as boundary input and corresponds to a Neumann condition. The boundary operators are therefore switched with respect to the previous case

$$\mathcal{B}_\partial \begin{pmatrix} e_p \\ \boldsymbol{e}_v \end{pmatrix} = \boldsymbol{e}_v \cdot \boldsymbol{n}|_{\partial\Omega}, \qquad \mathcal{C}_\partial \begin{pmatrix} e_p \\ \boldsymbol{e}_v \end{pmatrix} = e_p|_{\partial\Omega}.$$

2.3.2 Euler-Bernoulli beam

The Euler-Bernoulli beam model consists of one PDE, describing the vertical displacement along the beam length:

$$\rho A(x) \frac{\partial^2 w}{\partial t^2}(x,t) + \frac{\partial^2}{\partial x^2}\left(EI(x) \frac{\partial^2 w}{\partial x^2} \right) = 0, \quad x \in \Omega = \{0, L\}, \tag{2.24}$$

where $w(x,t)$ is the transverse displacement of the beam. The coefficients $\rho(x), A(x)E(x)$ and $I(x)$ are the mass density, cross section, Young's modulus of elasticity and the moment of inertia of a cross section. The energy variables are then chosen as follows:

$$\alpha_w = \rho A(x) \frac{\partial w}{\partial t}(x,t), \quad \text{Linear Momentum}, \quad \alpha_\kappa = \frac{\partial^2 w}{\partial x^2}(x,t), \quad \text{Curvature}. \tag{2.25}$$

Those variables are collected in the vector $\boldsymbol{\alpha} = (\alpha_w, \alpha_\kappa)^T$, so that the Hamiltonian can be written as a quadratic functional in the energy variables:

$$H = \frac{1}{2} \int_\Omega \left\{ \frac{1}{\rho A} \alpha_w^2 + EI \alpha_\kappa^2 \right\} \, \mathrm{d}\Omega \tag{2.26}$$

The co-energy variables are found by computing the variational derivative of the Hamiltonian:

$$\begin{aligned} e_w &:= \frac{\delta H}{\delta \alpha_w} = \frac{\partial w}{\partial t}(x,t), && \text{Vertical velocity}, \\ e_\kappa &:= \frac{\delta H}{\delta \alpha_\kappa} = EI(x) \frac{\partial^2 w}{\partial x^2}(x,t), && \text{Flexural momentum}. \end{aligned} \tag{2.27}$$

The underlying interconnection structure is then found to be:

$$\frac{\partial}{\partial t}\begin{pmatrix}\alpha_w\\ \alpha_\kappa\end{pmatrix} = \begin{bmatrix}0 & -\partial_{xx}\\ \partial_{xx} & 0\end{bmatrix}\begin{pmatrix}e_w\\ e_\kappa\end{pmatrix}. \tag{2.28}$$

The power flow gives access to the boundary variables:

$$\begin{aligned}\dot{H} &= \int_\Omega \{e_w\partial_t\alpha_w + e_\kappa\partial_t\alpha_\kappa\}\ \mathrm{d}\Omega,\\ &= \int_\Omega \{-e_w\partial_{xx}e_\kappa + e_\kappa\partial_{xx}e_w\}\ \mathrm{d}\Omega, \qquad \text{Integration by parts,}\\ &= \int_{\partial\Omega}\{-e_w\partial_x e_\kappa + e_\kappa\partial_x e_w\}\,\mathrm{d}s = \langle -e_w|_{\partial\Omega},\, \partial_x e_\kappa|_{\partial\Omega}\rangle_{\mathbb{R}^2} + \langle e_\kappa|_{\partial\Omega},\, \partial_x e_w|_{\partial\Omega}\rangle_{\mathbb{R}^2}\end{aligned} \tag{2.29}$$

Since the system is of differential order two, two pairing appears, giving rise to four combination of uniform boundary causality

- First case $u_{\partial,1} = e_w, \quad u_{\partial,2} = \partial_x e_w, \quad y_{\partial,1} = -\partial_x e_\kappa, \quad y_{\partial,2} = e_\kappa$.
  This imposes the vertical $e_w := \partial_t w$ and angular velocity $\partial_x e_w := \partial_{xt} w$ as boundary inputs

$$\mathcal{B}_\partial\begin{pmatrix}e_w\\ e_\kappa\end{pmatrix} = \begin{pmatrix}e_w(L)\\ -e_w(0)\\ \partial_x e_w(L)\\ -\partial_x e_w(0)\end{pmatrix} \in \mathbb{R}^4 \qquad \mathcal{C}_\partial\begin{pmatrix}e_w\\ e_\kappa\end{pmatrix} = \begin{pmatrix}-\partial_x e_\kappa(L)\\ \partial_x e_\kappa(0)\\ e_\kappa(L)\\ -e_\kappa(0)\end{pmatrix} \in \mathbb{R}^4 \tag{2.30}$$

  If the inputs are null a clamped boundary condition is obtained.

- Second case $u_{\partial,1} = e_w, \quad u_{\partial,2} = e_\kappa, \quad y_{\partial,1} = -\partial_x e_\kappa, \quad y_{\partial,2} = \partial_x e_w$.
  This imposes the vertical velocity and flexural momentum $e_\kappa := EI\partial_{xx} w$ as boundary inputs

$$\mathcal{B}_\partial\begin{pmatrix}e_w\\ e_\kappa\end{pmatrix} = \begin{pmatrix}e_w(L)\\ -e_w(0)\\ e_\kappa(L)\\ -e_\kappa(0)\end{pmatrix} \in \mathbb{R}^4 \qquad \mathcal{C}_\partial\begin{pmatrix}e_w\\ e_\kappa\end{pmatrix} = \begin{pmatrix}-\partial_x e_\kappa(L)\\ \partial_x e_\kappa(0)\\ \partial_x e_w(L)\\ -\partial_x e_w(0)\end{pmatrix} \in \mathbb{R}^4 \tag{2.31}$$

  Zero inputs lead to a simply supported condition.

- Third case $u_{\partial,1} = -\partial_x e_\kappa, \quad u_{\partial,2} = e_\kappa, \quad y_{\partial,1} = e_w, \quad y_{\partial,2} = \partial_x e_w$.
  This imposes the shear force $\partial_x e_\kappa := \partial_x(EI\partial_{xx} w)$ and flexural momentum as boundary inputs

$$\mathcal{B}_\partial\begin{pmatrix}e_w\\ e_\kappa\end{pmatrix} = \begin{pmatrix}-\partial_x e_\kappa(L)\\ \partial_x e_\kappa(0)\\ e_\kappa(L)\\ -e_\kappa(0)\end{pmatrix} \in \mathbb{R}^4 \qquad \mathcal{C}_\partial\begin{pmatrix}e_w\\ e_\kappa\end{pmatrix} = \begin{pmatrix}e_w(L)\\ -e_w(0)\\ \partial_x e_w(L)\\ -\partial_x e_w(0)\end{pmatrix} \in \mathbb{R}^4 \tag{2.32}$$

  Null inputs correspond to a free condition.

- Fourth case $u_{\partial,1} = -\partial_x e_\kappa, \quad u_{\partial,2} = \partial_x e_w, \quad y_{\partial,1} = e_w, \quad y_{\partial,2} = e_\kappa.$
  This imposes the shear force and angular velocity as boundary inputs

$$\mathcal{B}_\partial \begin{pmatrix} e_w \\ e_\kappa \end{pmatrix} = \begin{pmatrix} -\partial_x e_\kappa(L) \\ \partial_x e_\kappa(0) \\ \partial_x e_w(L) \\ -\partial_x e_w(0) \end{pmatrix} \in \mathbb{R}^4 \qquad \mathcal{C}_\partial \begin{pmatrix} e_w \\ e_\kappa \end{pmatrix} = \begin{pmatrix} e_w(L) \\ -e_w(0) \\ e_\kappa(L) \\ -e_\kappa(0) \end{pmatrix} \in \mathbb{R}^4 \tag{2.33}$$

2.3.3 2D shallow water equations

This formulation may be found in [CR16, Section 6.2]. This model describes a thin fluid layer of constant density in hydrostatic balance, like the propagation of a tsunami wave far from shore. Consider an open bounded connected set $\Omega \subset \mathbb{R}^2$ and a constant bed profile. The mass conservation implies

$$\frac{\partial h}{\partial t} + \operatorname{div}(h\boldsymbol{v}) = 0,$$

where $h(x, y, t) \in \mathbb{R}$ is a scalar field representing the fluid height, $\boldsymbol{v}(x, y, t) \in \mathbb{R}^2$ is the fluid velocity field. The conservation of linear momentum reads

$$\frac{\partial \rho \boldsymbol{v}}{\partial t} + \rho(\boldsymbol{v} \cdot \nabla)\boldsymbol{v} + \nabla(\rho g h) = 0,$$

where ρ is the mass density and g the gravitational acceleration constant. Using the identity

$$(\boldsymbol{v} \cdot \nabla)\boldsymbol{v} = \frac{1}{2}\nabla(\|\boldsymbol{v}\|^2) + (\nabla \times \boldsymbol{v}) \times \boldsymbol{v},$$

where $\nabla\times$ is the rotational of $\boldsymbol{v}$ (also denoted $\operatorname{curl} \boldsymbol{v}$), the momentum is rearranged as follows

$$\frac{\partial \rho \boldsymbol{v}}{\partial t} = -\nabla\left(\frac{1}{2}\rho \|\boldsymbol{v}\|^2 + \rho g h\right) - \rho(\nabla \times \boldsymbol{v}) \times \boldsymbol{v}.$$

The last term on the right-hand side can be rewritten

$$\rho(\nabla \times \boldsymbol{v}) \times \boldsymbol{v} = \begin{bmatrix} 0 & -\rho\omega \\ \rho\omega & 0 \end{bmatrix} \boldsymbol{v},$$

with $\omega = \partial_x v_y - \partial_y v_x$ the local vorticity term. To derive a suitable pH formulation, the total energy, made up of kinetic and potential contribution, has to be invoked

$$H = \frac{1}{2}\int_\Omega \left\{\rho h \|\boldsymbol{v}\|^2 + \rho g h^2\right\} \, \mathrm{d}\Omega.$$

As energy variable the fluid height and the linear momentum are chosen

$$\alpha_h = h, \qquad \boldsymbol{\alpha}_v = \rho \boldsymbol{v}. \tag{2.34}$$

The Hamiltonian is a non separable functional of the energy variables

$$H(\alpha_h, \boldsymbol{\alpha}_v) = \frac{1}{2}\int_\Omega \left\{ \frac{1}{\rho}\alpha_h \left\|\boldsymbol{\alpha}_v\right\|^2 + \rho g \alpha_h^2 \right\} \mathrm{d}\Omega. \tag{2.35}$$

The co-energy variables are given by

$$e_h := \frac{\delta H}{\delta \alpha_h} = \frac{1}{2\rho}\left\|\boldsymbol{\alpha}_v\right\|^2 + \rho g \alpha_h, \qquad \boldsymbol{e}_v := \frac{\delta H}{\delta \boldsymbol{\alpha}_v} = \frac{1}{\rho}\alpha_h \boldsymbol{\alpha}_v. \tag{2.36}$$

The mass and momentum conservation are then rewritten as follows

$$\frac{\partial}{\partial t}\begin{pmatrix}\alpha_h \\ \boldsymbol{\alpha}_v\end{pmatrix} = \begin{bmatrix} 0 & -\operatorname{div} \\ -\operatorname{grad} & \boldsymbol{\mathcal{G}} \end{bmatrix}\begin{pmatrix} e_h \\ \boldsymbol{e}_v \end{pmatrix}, \tag{2.37}$$

The gyroscopic skew-symmetric term $\boldsymbol{\mathcal{G}}$ introduces a non-linearity as it depends on the energy variables

$$\boldsymbol{\mathcal{G}}(\alpha_h, \boldsymbol{\alpha}_v) = \frac{\omega}{\alpha_h}\begin{bmatrix} 0 & -1 \\ 1 & 0 \end{bmatrix}, \qquad \omega = \partial_x \alpha_{v,y} - \partial_y \alpha_{v,x}.$$

Despite the non-standard formulation, the energy rate provides anyway the boundary variables

$$\begin{aligned}
\dot{H} &= +\int_\Omega \left\{ e_h\, \partial_t \alpha_h + \boldsymbol{e}_v \cdot \partial_t \boldsymbol{\alpha}_v \right\} \mathrm{d}\Omega, \\
&= -\int_\Omega \left\{ e_h\, \operatorname{div} \boldsymbol{e}_v + \boldsymbol{e}_v \cdot (\operatorname{grad} e_h - \boldsymbol{\mathcal{G}} \boldsymbol{e}_v) \right\} \mathrm{d}\Omega, && \text{skew-symmetry of } \boldsymbol{\mathcal{G}}, \\
&= -\int_\Omega \left\{ e_h\, \operatorname{div} \boldsymbol{e}_v + \boldsymbol{e}_v \cdot \operatorname{grad} e_h \right\} \mathrm{d}\Omega, && \text{Chain rule}, \\
&= -\int_\Omega \operatorname{div}(e_h\, \boldsymbol{e}_v)\, \mathrm{d}\Omega, && \text{Stokes theorem}, \\
&= -\int_{\partial\Omega} e_h\, \boldsymbol{e}_v \cdot \boldsymbol{n}\, \mathrm{d}S = -\left\langle e_h,\, \boldsymbol{e}_v \cdot \boldsymbol{n} \right\rangle_{\partial\Omega}.
\end{aligned} \tag{2.38}$$

Again two possible cases of uniform boundary causality arise:

- First case $u_\partial = e_h, \quad y_\partial = \boldsymbol{e}_v \cdot \boldsymbol{n}$.
  This imposes the variable $e_h := h$ as boundary input and corresponds to a given water level for a fluid boundary.

- Second case $u_\partial = \boldsymbol{e}_v \cdot \boldsymbol{n}, \quad y_\partial = e_p$.
  This imposes the variable $\boldsymbol{e}_v \cdot \boldsymbol{n} := h\boldsymbol{v} \cdot \boldsymbol{n}$ as boundary input and corresponds to a given volumetric flow rate.

2.4 Conclusion

In this chapter, the main mathematical tools needed to understand infinite-dimensional pHs were recalled. A general characterization of the underlying operators behind a boundary control pH system is still an open topic. In Chapter 6, these operators are characterized, in connection to the discretization method developed.

Part II

Port-Hamiltonian elasticity and thermoelasticity

Chapter 3

Elasticity in port-Hamiltonian form

I try not to break the rules but merely to test their elasticity.

Bill Veeck

Contents

Continuum mechanics is the mathematical description of how materials behave kinematically under external excitations. In this framework, the microscopic structure of a material body is neglected and a macroscopic viewpoint, that describes the body as a continuum, is adopted. This leads to a PDE based model. In this chapter, the general linear elastodynamics problem is recalled. A suitable port-Hamiltonian formulation is then derived.

3.1 Continuum mechanics

In this section, the main concepts behind a deformable continuum are briefly recalled following [Lee12]. For a detailed discussion on this topic, the reader may consult [Abe12, LPKL12].

3.1.1 Non-linear formulation of elasticity

The bounded region of $\mathbb{R}^d$, $d \in \{2, 3\}$ occupied by a solid is called configuration. The reference configuration Ω is the domain that a body occupies at the initial state. To describe how the body deforms in time the deformation map $\mathbf{\Phi} : \Omega \times [0, T_f] \to \Omega' \subset \mathbb{R}^d$ is introduced. This map

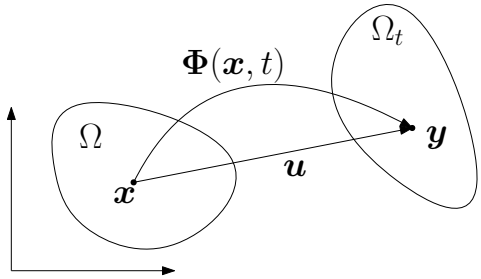

Figure 3.1: A 2D continuum in his reference configuration Ω and in the current configuration Ω_t. Given a generic point $\boldsymbol{x}$ in the reference configuration, the map $\boldsymbol{\Phi}(\boldsymbol{x},t)$ provides its current position $\boldsymbol{y}$ at a given time instant t.

is differentiable and orientation preserving, and the image of Ω under $\boldsymbol{\Phi}(\cdot,t)$ $\forall t \in [0,T_f]$ is called the deformed configuration Ω_t. Given a specific point in the reference frame its image is denoted by $\boldsymbol{y} = \boldsymbol{\Phi}(\boldsymbol{x},t)$. The gradient of the deformation map is called the deformation gradient $\boldsymbol{F} := \nabla_x \boldsymbol{\Phi} = \frac{\partial \boldsymbol{y}}{\partial \boldsymbol{x}}$. A rigid deformation maps a point $\boldsymbol{x} \in \Omega \to \boldsymbol{A}(t)\boldsymbol{x} + \boldsymbol{b}(t)$, where $\boldsymbol{A}(t)$ is an orthogonal matrix and $\boldsymbol{b}(t) \in \mathbb{R}^d$ a vector. A differentiable deformation map $\boldsymbol{\Phi}$ is a rigid deformation iff $\boldsymbol{F}^\top \boldsymbol{F} - \boldsymbol{I} = 0$, where $\boldsymbol{I}$ is the identity in $\mathbb{R}^{d\times d}$ (for the proof see [Cia88], page 44). For this reason, a suitable measure of the deformation is the Green-St.Venant strain tensor $\frac{1}{2}(\boldsymbol{F}^\top \boldsymbol{F} - \boldsymbol{I})$.
A quantity of interest is the displacement $\boldsymbol{u} : \Omega \times [0,T_f] \to \mathbb{R}^d$ with respect to the reference configuration. It is defined as $\boldsymbol{u}(\boldsymbol{x},t) = \boldsymbol{\Phi}(\boldsymbol{x},t) - \boldsymbol{x}$ (cf. Fig. 3.1). The gradient of the displacement verifies $\nabla_x \boldsymbol{u} = \boldsymbol{F} - \boldsymbol{I}$. The strain tensor can now be written in terms of the displacement

$$\begin{aligned}\frac{1}{2}(\boldsymbol{F}^\top \boldsymbol{F} - \boldsymbol{I}) &= \frac{1}{2}\left[(\nabla_x \boldsymbol{u} + \boldsymbol{I})^\top (\nabla_x \boldsymbol{u} + \boldsymbol{I}) - \boldsymbol{I}\right] \\ &= \frac{1}{2}\left[\nabla_x \boldsymbol{u} + (\nabla_x \boldsymbol{u})^\top + (\nabla_x \boldsymbol{u})^\top (\nabla_x \boldsymbol{u})\right],\end{aligned}$$

or in components

$$\frac{1}{2}(F_{ik}^\top F_{kj} - I_{ij}) = \frac{1}{2}\left(\frac{\partial u_i}{\partial x_j} + \frac{\partial u_j}{\partial x_i} + \frac{\partial u_i}{\partial x_j}\frac{\partial u_j}{\partial x_i}\right).$$

To state the balance laws the actual deformed configuration is considered. The linear and angular momenta in a subdomain $\omega_t \subset \Omega_t$ are computed as

$$\int_{\omega_t} \rho\, \boldsymbol{v}\, \mathrm{d}\omega_t, \quad \text{and} \quad \int_{\omega_t} \rho\, \boldsymbol{y} \times \boldsymbol{v}\, \mathrm{d}\omega_t,$$

where ρ is the mass density and the velocity $\boldsymbol{v} = \frac{D\boldsymbol{u}}{Dt}(\boldsymbol{y},t) = \frac{\partial \boldsymbol{u}}{\partial t}(\boldsymbol{x},t)$ is the material time derivative of the displacement (see [Abe12, Chapter 1]). Let $\omega_{t,1}$, $\omega_{t,2}$ be two subregions in a deformed continuum Ω_t with contacting surface S_{12}. There is a force acting on this surface for a continuum that is called stress vector. If $\boldsymbol{n}$ is the outward normal at $\boldsymbol{y}$ on S_{12} with respect to $\omega_{t,1}$, then the surface force that $\omega_{t,1}$ exerts on $\omega_{t,2}$ is denoted by $\boldsymbol{t}(\boldsymbol{y},\boldsymbol{n}) \in \mathbb{R}^d$. By the Newton third law, the surface force that $\omega_{t,2}$ applies on $\omega_{t,1}$ is given by $\boldsymbol{t}(\boldsymbol{y},-\boldsymbol{n}) = -\boldsymbol{t}(\boldsymbol{y},\boldsymbol{n})$.

It is assumed that the linear and angular momentum balances hold for any subregion $\omega_t \in \Omega_t$

$$\frac{d}{dt}\int_{\omega_t} \rho \boldsymbol{v}\, \mathrm{d}\omega_t = \int_{\partial\omega_t} \boldsymbol{t}(\boldsymbol{y},\boldsymbol{n})\, \mathrm{d}S + \int_{\omega_t} \boldsymbol{f}\, \mathrm{d}\omega_t,$$
$$\frac{d}{dt}\int_{\omega_t} \rho \boldsymbol{y}\times\boldsymbol{v}\, \mathrm{d}\omega_t = \int_{\partial\omega_t} \boldsymbol{y}\times\boldsymbol{t}(\boldsymbol{y},\boldsymbol{n})\, \mathrm{d}S + \int_{\omega_t} \boldsymbol{y}\times\boldsymbol{f}\, \mathrm{d}\omega_t,$$

where $\partial\omega_t$ stands for the boundary surface of the subdomain ω_t, $\boldsymbol{n}$ is the outward normal to the surface $\partial\omega_t$ and $\boldsymbol{f}$ represents an exterior body force. The following theorem characterizes the stress vector (see [Cia88, Chapter 2]):

Theorem 1 (Cauchy's theorem)
If the linear and angular momenta balances hold, then there exists a matrix-valued function $\boldsymbol{\Sigma}$ *from* Ω_t *to* $\mathbb{S}$ *such that* $\boldsymbol{t}(\boldsymbol{y},\boldsymbol{n}) = \boldsymbol{\Sigma}(\boldsymbol{y})\boldsymbol{n}$, $\forall \boldsymbol{y} \in \Omega_t$ *where the right-hand side is the matrix-vector multiplication.*

The set $\mathbb{S} = \mathbb{R}^{d\times d}_{\mathrm{sym}}$ denotes the field of symmetric matrices in $\mathbb{R}^{d\times d}$. The symmetry of the stress tensor $\boldsymbol{\Sigma}$ is due to the balance of angular momentum. The divergence theorem can then be applied

$$\int_{\partial\omega_t} \boldsymbol{\Sigma}\,\boldsymbol{n}\, \mathrm{d}S = \int_{\omega_t} \nabla_y \cdot \boldsymbol{\Sigma}\, \mathrm{d}\omega_t,$$

where $\nabla_y\cdot$ is the tensor divergence with respect to the deformed configuration, $\nabla_y \cdot \boldsymbol{\Sigma} = \sum_{i=1}^{d} \frac{\partial \Sigma_{ij}}{\partial y_i}$. Because the considered subregion ω_t is arbitrary, using the linear balance momentum and the conservation of mass, the following PDE is found

$$\rho\frac{D\boldsymbol{v}}{Dt} - \nabla_y \cdot \boldsymbol{\Sigma} = \boldsymbol{f}, \qquad \boldsymbol{y} \in \Omega_t.$$

This equation is written with respect to the deformed configuration Ω_t. For a detailed derivation of this equation the reader may consult [Abe12, Chapter 4]. To obtain a closed formulation, the constitutive law, namely the link between the stress tensor $\boldsymbol{\Sigma}$ and the strain tensor $\frac{1}{2}(\boldsymbol{F}^\top\boldsymbol{F} - \boldsymbol{I})$, has to be introduced. In the next section such relation will be discussed for the case of linear elasticity. It is important to remark that an Hamiltonian formulation of non-linear elasticity has been proposed in [Mar81, Chapter 3].

3.1.2 The linear elastodynamics problem

Whenever deformations are small, $\|\nabla_x \boldsymbol{u}\| \ll 1$, then the reference and deformed configurations are almost indistinguishable $\boldsymbol{y} = \boldsymbol{x} + \boldsymbol{u} = \boldsymbol{x} + O(\nabla_x \boldsymbol{u}) \approx \boldsymbol{x}$. This allows writing the linear momentum balance in the reference configuration

$$\rho\frac{\partial \boldsymbol{v}}{\partial t}(\boldsymbol{x},\boldsymbol{t}) - \mathrm{Div}\, \boldsymbol{\Sigma}(\boldsymbol{x},t) = \boldsymbol{f}, \qquad \boldsymbol{x} \in \Omega.$$

The material derivative simplifies to a partial one. The operator Div is the divergence of a tensor field with respect to the reference configuration (see Appendix A for a description of the differential operators)

$$\operatorname{Div} \boldsymbol{\Sigma}(\boldsymbol{x}, t) = \nabla_x \cdot \boldsymbol{\Sigma}(\boldsymbol{x}, t) = \left(\sum_{i=1}^{d} \frac{\partial \Sigma_{ij}}{\partial x_i} \right)_{1 \leq j \leq d}.$$

Furthermore, the non-linear terms in the Green-St. Venant strain tensor can be dropped

$$\frac{1}{2}(\boldsymbol{F}^\top \boldsymbol{F} - \boldsymbol{I}) = \frac{1}{2}\left[\nabla_x \boldsymbol{u} + (\nabla_x \boldsymbol{u})^\top + (\nabla_x \boldsymbol{u})^\top (\nabla_x \boldsymbol{u})\right] \approx \frac{1}{2}\left[\nabla_x \boldsymbol{u} + (\nabla_x \boldsymbol{u})^\top\right].$$

The linearized strain tensor (also called infinitesimal strain tensor) is the symmetric gradient of the displacement

$$\boldsymbol{\varepsilon} := \operatorname{Grad} \boldsymbol{u}, \qquad \text{where} \qquad \operatorname{Grad} \boldsymbol{u} = \frac{1}{2}\left[\nabla_x \boldsymbol{u} + (\nabla_x \boldsymbol{u})^\top\right]. \tag{3.1}$$

To obtain a closed system of equations, it is now necessary to characterize the relation between stress and strain. This relation is normally called *constitutive law*. In the following, the particular case of elastic materials is considered. These materials are able to return back to their original size and shapes after forces are removed. For this class of materials, the stress tensor is solely determined from the deformed configuration at a given time (Hooke's law)

$$\boldsymbol{\Sigma}(\boldsymbol{x}) = \boldsymbol{\mathcal{D}}(\boldsymbol{x})\, \boldsymbol{\varepsilon}(\boldsymbol{u}(\boldsymbol{x})).$$

The *stiffness tensor* or *elasticity tensor* $\boldsymbol{\mathcal{D}} : \mathbb{S} \to \mathbb{S}$ is a rank 4 tensor that is symmetric positive definite and uniformly bounded above and below. Because of symmetry, its components satisfy

$$\mathcal{D}_{ijkl} = \mathcal{D}_{jikl} = \mathcal{D}_{klij}.$$

From the uniform boundedness of $\boldsymbol{\mathcal{D}}$, the map $\boldsymbol{\mathcal{D}} : L^2(\Omega, \mathbb{S}) \to L^2(\Omega, \mathbb{S})$ is a symmetric positive definite bounded linear operator ($L^2(\Omega, \mathbb{S})$ is the space of square-integrable symmetric tensor-valued functions). The compliance tensor $\boldsymbol{\mathcal{C}}$ is defined by $\boldsymbol{\mathcal{C}} = \boldsymbol{\mathcal{D}}^{-1}$. Thus $\boldsymbol{\mathcal{C}} : \mathbb{S} \to \mathbb{S}$ is as well symmetric positive definite and uniformly bounded above and below. An isotropic elastic medium has the same kinematic properties in any direction and at each point. If an elastic medium is isotropic, then the stiffness and compliance tensors assume the form

$$\boldsymbol{\mathcal{D}}(\cdot) = 2\mu(\cdot) + \lambda \operatorname{Tr}(\cdot)\boldsymbol{I}, \qquad \boldsymbol{\mathcal{C}}(\cdot) = \frac{1}{2\mu}\left[(\cdot) - \frac{\lambda}{2\mu + d\lambda} \operatorname{Tr}(\cdot)\boldsymbol{I}\right], \qquad d = \{2, 3\}, \tag{3.2}$$

where Tr is the trace operator and the positive scalar functions μ, λ, defined on Ω, are called the Lamé coefficients. In engineering applications it is easier to compute experimentally two other parameters: the Young modulus E and Poisson's ratio ν. Those are expressed in terms of the Lamé coefficients as

$$\nu = \frac{\lambda}{2(\lambda + \mu)}, \qquad E = \frac{\mu(3\lambda + 2\mu)}{\lambda + \mu}, \tag{3.3}$$

and conversely

$$\lambda = \frac{E\nu}{(1+\nu)(1-2\nu)}, \qquad \mu = \frac{E}{2(1+\nu)}. \tag{3.4}$$

The stiffness and compliant tensor are expressed as

$$\boldsymbol{\mathcal{D}}(\cdot) = \frac{E}{1+\nu}\left[(\cdot) + \frac{\nu}{1-2\nu}\operatorname{Tr}(\cdot)\boldsymbol{I}\right], \tag{3.5}$$

$$\boldsymbol{\mathcal{C}}(\cdot) = \frac{1+\nu}{E}\left[(\cdot) - \frac{\nu}{1+\nu(d-2)}\operatorname{Tr}(\cdot)\boldsymbol{I}\right]. \tag{3.6}$$

The linear elastodynamics problem is formulated through a vector-valued PDE

$$\rho\frac{\partial^2 \boldsymbol{u}}{\partial t^2} - \operatorname{Div}(\boldsymbol{\mathcal{D}}\operatorname{Grad}\boldsymbol{u}) = \boldsymbol{f}. \tag{3.7}$$

The classical elastodynamics problem is expressed considering the displacement $\boldsymbol{u}$ as the unknown. This PDE goes together with appropriate boundary conditions that will be specified in 3.2.

3.2 Port-Hamiltonian formulation of linear elasticity

In this section a port-Hamiltonian formulation for elasticity is deduced from the classical elastodynamics problem. It must be highlighted that already in the seventies a purely hyperbolic formulation for elasticity was detailed [HM78]. The missing point is the clear connection with the theory of Hamiltonian PDEs. An Hamiltonian formulation can be found in [Gri15, Chapter 16], but without any connection to the concept of Stokes-Dirac structure induced by the underlying geometry.

3.2.1 Energy and co-energy variables

Consider an open connected set $\Omega \subset \mathbb{R}^d$, $d \in \{2, 3\}$. The displacement within a deformable continuum is given by Eq. (3.7).

$$\rho\frac{\partial^2 \boldsymbol{u}}{\partial t^2} - \operatorname{Div}(\boldsymbol{\mathcal{D}}\operatorname{Grad}\boldsymbol{u}) = 0, \qquad \boldsymbol{x} \in \Omega. \tag{3.8}$$

The contribution of the body force $\boldsymbol{f}$ has been removed for ease of presentation. To derive a pH formulation, the total energy, that includes the kinetic and deformation energy, is needed

$$H = \frac{1}{2}\int_\Omega \left\{\rho\,\|\partial_t \boldsymbol{u}\|^2 + \boldsymbol{\Sigma} : \boldsymbol{\varepsilon}\right\}\,\mathrm{d}\Omega. \tag{3.9}$$

The notation $\boldsymbol{A} : \boldsymbol{B} = \operatorname{Tr}(\boldsymbol{A}^\top \boldsymbol{B}) = \sum_{i,j} A_{ij}B_{ij}$ denotes the tensor contraction. Recall that $\boldsymbol{\varepsilon} = \operatorname{Grad}\boldsymbol{u}$ and $\boldsymbol{\Sigma} = \boldsymbol{\mathcal{D}}\boldsymbol{\varepsilon}$. The energy variables are then the linear momentum and the

deformation field

$$\boldsymbol{\alpha}_v = \rho \boldsymbol{v}, \qquad \boldsymbol{A}_\varepsilon = \boldsymbol{\varepsilon},$$

where $\boldsymbol{v} := \partial_t \boldsymbol{u}$. The Hamiltonian can be rewritten as a quadratic functional in the energy variables

$$H = \frac{1}{2} \int_\Omega \left\{ \frac{1}{\rho} \|\boldsymbol{\alpha}_v\|^2 + (\boldsymbol{\mathcal{D}} \boldsymbol{A}_\varepsilon) : \boldsymbol{A}_\varepsilon \right\} \, \mathrm{d}\Omega. \tag{3.10}$$

The co-energy variables are given by

$$\boldsymbol{e}_v := \frac{\delta H}{\delta \boldsymbol{\alpha}_v} = \boldsymbol{v}, \qquad \boldsymbol{E}_\varepsilon := \frac{\delta H}{\delta \boldsymbol{A}_\varepsilon} = \boldsymbol{\Sigma}. \tag{3.11}$$

The tensor-valued co-energy $\boldsymbol{E}_\varepsilon$ is obtained by taking the variational derivative with respect to a tensor.

Proposition 3
The variational derivative of the Hamiltonian with respect to the strain tensor is the stress tensor $\delta_{\boldsymbol{A}_\varepsilon} H = \boldsymbol{\Sigma}$.

Proof. Let $\mathbb{S} : \mathbb{R}^{d \times d}_{\mathrm{sym}}$ be the space of symmetric tensor and $L^2(\Omega, \mathbb{S})$ the space of the square-integrable symmetric tensors endowed with the tensor contraction as inner product

$$\langle \boldsymbol{A}, \boldsymbol{B} \rangle_{L^2(\Omega,\mathbb{S})} = \int_\Omega \boldsymbol{A} : \boldsymbol{B} \, \mathrm{d}\Omega. \tag{3.12}$$

The contribution due to the deformation part in Hamiltonian is given by:

$$H_{\mathrm{def}}(\boldsymbol{A}_\varepsilon) = \frac{1}{2} \int_\Omega (\boldsymbol{\mathcal{D}} \boldsymbol{A}_\varepsilon) : \boldsymbol{A}_\varepsilon \ \mathrm{d}\Omega.$$

A variation $\boldsymbol{\Delta A}_\varepsilon$ of the strain tensor with respect to a given value $\bar{\boldsymbol{A}}_\varepsilon$ leads to:

$$\begin{aligned} H_{\mathrm{def}}(\bar{\boldsymbol{A}}_\varepsilon + \eta \boldsymbol{\Delta A}_\varepsilon) = &+ \frac{1}{2} \int_\Omega (\boldsymbol{\mathcal{D}} \bar{\boldsymbol{A}}_\varepsilon) : \bar{\boldsymbol{A}}_\varepsilon \ \mathrm{d}\Omega \\ &+ \eta \frac{1}{2} \int_\Omega \left\{ (\boldsymbol{\mathcal{D}} \bar{\boldsymbol{A}}_\varepsilon) : \boldsymbol{\Delta A}_\varepsilon + (\boldsymbol{\mathcal{D}} \boldsymbol{\Delta A}_\varepsilon) : \bar{\boldsymbol{A}}_\varepsilon \right\} \ \mathrm{d}\Omega + O(\eta^2). \end{aligned}$$

The term $(\boldsymbol{\mathcal{D}} \boldsymbol{\Delta A}_\varepsilon) : \bar{\boldsymbol{A}}_\varepsilon$ can be further rearranged using the symmetry of $\boldsymbol{\mathcal{D}}$ and the commutativity of the tensor contraction

$$(\boldsymbol{\mathcal{D}} \boldsymbol{\Delta A}_\varepsilon) : \bar{\boldsymbol{A}}_\varepsilon = (\boldsymbol{\mathcal{D}} \bar{\boldsymbol{A}}_\varepsilon) : \boldsymbol{\Delta A}_\varepsilon,$$

so that

$$H_{\mathrm{def}}(\bar{\boldsymbol{A}}_\varepsilon + \eta \boldsymbol{\Delta A}_\varepsilon) = \frac{1}{2} \int_\Omega (\boldsymbol{\mathcal{D}} \bar{\boldsymbol{A}}_\varepsilon) : \bar{\boldsymbol{A}}_\varepsilon \ \mathrm{d}\Omega + \eta \int_\Omega (\boldsymbol{\mathcal{D}} \bar{\boldsymbol{A}}_\varepsilon) : \boldsymbol{\Delta A}_\varepsilon \ \mathrm{d}\Omega + O(\eta^2).$$

By definition of variational derivative it can be written:

$$H_{\text{def}}(\bar{\boldsymbol{A}}_\varepsilon + \eta \boldsymbol{\Delta A}_\varepsilon) = H_{\text{def}}(\bar{\boldsymbol{A}}_\varepsilon) + \eta \left\langle \frac{\delta H_{\text{def}}}{\delta \boldsymbol{A}_\varepsilon}, \boldsymbol{\Delta A}_\varepsilon \right\rangle_{L^2(\Omega,\mathbb{S})} + O(\eta^2),$$

Then, by identification

$$\frac{\delta H_{\text{def}}}{\delta \boldsymbol{A}_\varepsilon} = \boldsymbol{\mathcal{D}} \bar{\boldsymbol{A}}_\varepsilon = \boldsymbol{\Sigma}.$$

Since the Hamiltonian is separable $\delta_{\boldsymbol{A}_\varepsilon} H_{\text{def}} = \delta_{\boldsymbol{A}_\varepsilon} H$, leading to the final result. □

3.2.2 Final system and associated Stokes-Dirac structure

It is now possible to state the final pH form

$$\frac{\partial}{\partial t} \begin{pmatrix} \boldsymbol{\alpha}_v \\ \boldsymbol{A}_\varepsilon \end{pmatrix} = \begin{bmatrix} \mathbf{0} & \text{Div} \\ \text{Grad} & \mathbf{0} \end{bmatrix} \begin{pmatrix} \boldsymbol{e}_v \\ \boldsymbol{E}_\varepsilon \end{pmatrix}. \tag{3.13}$$

The first equation of the system is the conservation of linear momentum. The second represents a compatibility condition

$$\begin{aligned} \partial_t \boldsymbol{A}_\varepsilon &= \text{Grad}(\boldsymbol{e}_v), \\ \partial_t \boldsymbol{\varepsilon} &= \text{Grad}(\boldsymbol{v}), \\ \partial_t \,\text{Grad}\, \boldsymbol{u} &= \text{Grad}(\partial_t \boldsymbol{u}). \end{aligned} \tag{3.14}$$

Assuming that $\boldsymbol{u} \in C^2$, higher order derivatives commute (Clairaut's theorem). Hence, the equation is verified. The following theorem ensures the differential operator is formally skew-adjoint (one can also find this result in the recent article [PZ20, Lemma 3.3], available as arXiv preprint).

Theorem 2
The formal adjoint of the tensor divergence Div *is* −Grad*, the opposite of the symmetric gradient.*

Proof. We denote by $\mathbb{V} = \mathbb{R}^d$ the space of vector field in $\mathbb{R}^d$ and by $\mathbb{S} = \mathbb{R}^{d\times d}$ the space of symmetric tensor field in $\mathbb{R}^{d\times d}$. Let us consider the Hilbert space of the square-integrable symmetric tensors $L^2(\Omega, \mathbb{S})$ with scalar product defined in (3.12). Moreover consider the Hilbert space of the square-integrable vector function $L^2(\Omega, \mathbb{V})$, endowed with the usual scalar product

$$\langle \boldsymbol{a}, \boldsymbol{b} \rangle_{L^2(\Omega,\mathbb{V})} = \int_\Omega \boldsymbol{a} \cdot \boldsymbol{b} \ \mathrm{d}\Omega.$$

Let us consider the tensor divergence operator defined as:

$$\begin{aligned} \mathrm{Div}:\ L^2(\Omega,\mathbb{S}) &\to L^2(\Omega,\mathbb{V}),\\ \boldsymbol{\Psi} &\to \mathrm{Div}\,\boldsymbol{\Psi}=\boldsymbol{\psi}, \end{aligned} \qquad \text{with } \psi_j=\mathrm{div}(\Psi_{ij})=\sum_{i=1}^{d}\frac{\partial\Psi_{ij}}{\partial x_i}.$$

We try to identify Div^*

$$\begin{aligned} \mathrm{Div}^*:\ L^2(\Omega,\mathbb{V}) &\to L^2(\Omega,\mathbb{S}),\\ \boldsymbol{\phi} &\to \mathrm{Div}^*\boldsymbol{\phi}=\boldsymbol{\Phi}, \end{aligned}$$

such that

$$\langle \mathrm{Div}\,\boldsymbol{\Psi},\,\boldsymbol{\phi}\rangle_{L^2(\Omega,\mathbb{V})}=\langle \boldsymbol{\Psi},\,\mathrm{Div}^*\boldsymbol{\phi}\rangle_{L^2(\Omega,\mathbb{S})}, \qquad \begin{aligned}&\forall\boldsymbol{\Psi}\in\mathrm{Dom}(\mathrm{Div})\subset L^2(\Omega,\mathbb{S}),\\ &\forall\boldsymbol{\phi}\in\mathrm{Dom}(\mathrm{Div}^*)\subset L^2(\Omega,\mathbb{V}).\end{aligned}$$

Now let us take $\boldsymbol{\Psi}\in C_0^1(\Omega,\mathbb{S})\subset\mathrm{Domain}(\mathrm{Div})$ the space of differentiable symmetric tensors with compact support in Ω. Additionally $\boldsymbol{\phi}$ will belong to $C_0^1(\Omega,\mathbb{V})\subset\mathrm{Dom}(\mathrm{Div}^*)$, the space of differentiable vector functions with compact support in Ω. Then

$$\begin{aligned} \langle \mathrm{Div}\,\boldsymbol{\Psi},\boldsymbol{\phi}\rangle_{L^2(\Omega,\mathbb{V})} &= \int_\Omega \boldsymbol{\psi}\cdot\boldsymbol{\phi}\ \mathrm{d}\Omega,\\ &= \int_\Omega \sum_{i=1}^{d}\sum_{j=1}^{d}\frac{\partial\Psi_{ij}}{\partial x_i}\phi_j\ \mathrm{d}\Omega,\\ &= -\int_\Omega \sum_{i=1}^{d}\sum_{j=1}^{d}\Psi_{ij}\frac{\partial\phi_j}{\partial x_i}\ \mathrm{d}\Omega, && \text{since the functions vanish at the boundary,}\\ &= -\int_\Omega \sum_{i=1}^{d}\sum_{j=1}^{d}\Psi_{ij}F_{ij}\ \mathrm{d}\Omega, && \text{where}\quad F_{ij}=\frac{\partial\phi_j}{\partial x_i},\\ &= -\langle\boldsymbol{\Psi},\boldsymbol{F}\rangle_{L^2(\Omega,\mathbb{S})}, && \boldsymbol{F}=\mathrm{grad}\,\boldsymbol{\phi}. \end{aligned}$$

But in this latter case, it could not be stated that $\boldsymbol{F}\in L^2(\Omega,\mathbb{S})$. Now, since $\boldsymbol{\Psi}\in L^2(\Omega,\mathbb{S})$, $\Psi_{ji}=\Psi_{ij}$, thus the last equality can be further decomposed as

$$\sum_{i,j}\Psi_{ij}\frac{\partial\phi_j}{\partial x_i}=\sum_{i,j}\Psi_{ij}\frac{1}{2}\left(\frac{\partial\phi_i}{\partial x_j}+\frac{\partial\phi_j}{\partial x_i}\right)=\sum_{i,j}\Psi_{ij}\Phi_{ij}, \qquad \text{with } \Phi_{ij}:=\frac{1}{2}\left(\frac{\partial\phi_i}{\partial x_j}+\frac{\partial\phi_j}{\partial x_i}\right).$$

Thus $\boldsymbol{\Phi}=\mathrm{Grad}\,\boldsymbol{\phi}\in L^2(\Omega,\mathbb{S})$ and it can be stated that:

$$\begin{aligned} \langle \mathrm{Div}\,\boldsymbol{\Psi},\,\boldsymbol{\phi}\rangle_{L^2(\Omega,\mathbb{V})} &= -\int_\Omega \sum_{i,j}\Psi_{ij}\frac{1}{2}\left(\frac{\partial\phi_i}{\partial x_j}+\frac{\partial\phi_j}{\partial x_i}\right)\ \mathrm{d}\Omega\\ &= -\int_\Omega \sum_{i,j}\Psi_{ij}\Phi_{ij}\ \mathrm{d}\Omega=\langle\boldsymbol{\Psi},\,-\mathrm{Grad}\,\boldsymbol{\phi}\rangle_{L^2(\Omega,\mathbb{S})}. \end{aligned}$$

It can be concluded that the formal adjoint of Div is $\mathrm{Div}^*=-\mathrm{Grad}$. □

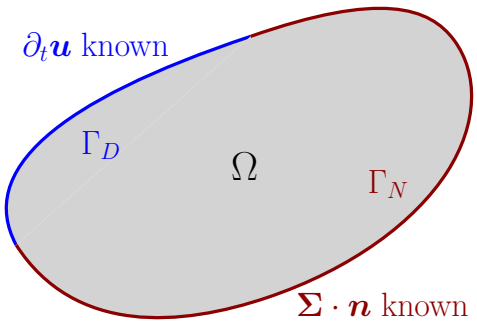

Figure 3.2: A 2D continuum with Neumann and Dirichlet boundary conditions

The boundary values are then found by evaluating the energy rate

$$\begin{aligned}
\dot{H} &= \int_\Omega \{\boldsymbol{e}_v \cdot \partial_t \boldsymbol{\alpha}_v + \boldsymbol{E}_\varepsilon : \partial_t \boldsymbol{A}_\varepsilon\} \, \mathrm{d}\Omega, \\
&= \int_\Omega \{\boldsymbol{e}_v \cdot \operatorname{Div} \boldsymbol{E}_\varepsilon + \boldsymbol{E}_\varepsilon : \operatorname{Grad} \boldsymbol{e}_v\} \, \mathrm{d}\Omega, \\
&= \int_\Omega \operatorname{div}(\boldsymbol{E}_\varepsilon \, \boldsymbol{e}_v) \, \mathrm{d}\Omega, && \text{Stokes theorem (see Appendix A Eq. (A.6))}, \\
&= \int_{\partial\Omega} \boldsymbol{e}_v \cdot (\boldsymbol{E}_\varepsilon \boldsymbol{n}) \, \mathrm{d}S.
\end{aligned} \tag{3.15}$$

The imposition of the velocity field along the boundary $\boldsymbol{e}_v = \partial_t \boldsymbol{u}$ corresponds to a Dirichlet condition. Setting $\boldsymbol{E}_\varepsilon \boldsymbol{n} = \boldsymbol{\Sigma} \boldsymbol{n} = \boldsymbol{t}$ (the traction) corresponds to a Neumann condition. Consider a partition of the boundary $\partial\Omega = \overline{\Gamma}_N \cup \overline{\Gamma}_D$ and $\Gamma_N \cap \Gamma_D = \{\emptyset\}$, where a Dirichlet and a Neumann condition applies on the open subset Γ_D and Γ_N respectively (see Fig. 3.2). Then the final pH formulation reads

$$\begin{aligned}
\frac{\partial}{\partial t} \begin{pmatrix} \boldsymbol{\alpha}_v \\ \boldsymbol{A}_\varepsilon \end{pmatrix} &= \underbrace{\begin{bmatrix} \mathbf{0} & \operatorname{Div} \\ \operatorname{Grad} & \mathbf{0} \end{bmatrix}}_{\mathcal{J}} \begin{pmatrix} \boldsymbol{e}_v \\ \boldsymbol{E}_\varepsilon \end{pmatrix}, \\
\boldsymbol{u}_\partial &= \underbrace{\begin{bmatrix} \boldsymbol{\gamma}_0^{\Gamma_D} & \mathbf{0} \\ \mathbf{0} & \boldsymbol{\gamma}_n^{\Gamma_N} \end{bmatrix}}_{\mathcal{B}_\partial} \begin{pmatrix} \boldsymbol{e}_v \\ \boldsymbol{E}_\varepsilon \end{pmatrix}, \\
\boldsymbol{y}_\partial &= \underbrace{\begin{bmatrix} \mathbf{0} & \boldsymbol{\gamma}_n^{\Gamma_D} \\ \boldsymbol{\gamma}_0^{\Gamma_N} & \mathbf{0} \end{bmatrix}}_{\mathcal{C}_\partial} \begin{pmatrix} \boldsymbol{e}_v \\ \boldsymbol{E}_\varepsilon \end{pmatrix},
\end{aligned} \tag{3.16}$$

where $\boldsymbol{\gamma}_0^{\Gamma_*}$ denotes the trace over the set Γ_*, namely $\boldsymbol{\gamma}_0^{\Gamma_*} \boldsymbol{e}_v = \boldsymbol{e}_v|_{\Gamma_*}$. Furthermore, $\boldsymbol{\gamma}_n^{\Gamma_*}$ denotes the normal trace over the set Γ_*, namely $\boldsymbol{\gamma}_n^{\Gamma_*} \boldsymbol{E}_\varepsilon = \boldsymbol{E}_\varepsilon \boldsymbol{n}|_{\Gamma_*}$.

Remark 5
The boundary operators $\mathcal{B}_\partial, \mathcal{C}_\partial$ in Eq.(3.16) are unbounded if the co-energy belong to H^{Grad}, H^{Div}.

Remark 6 (Trace operators and duality pairing for the elastodynamics problem)
For linear elastodynamics the integrations by parts formula leads to the following duality pairings [BBF+13, Chapter 1]

$$\langle \operatorname{Grad} \boldsymbol{e}_v,\, \boldsymbol{E}_\varepsilon \rangle_{L^2(\Omega,\mathbb{S})} + \langle \boldsymbol{e}_v,\, \operatorname{Div} \boldsymbol{E}_\varepsilon \rangle_{L^2(\Omega,\mathbb{V})} = \langle \boldsymbol{\gamma}_0 \boldsymbol{e}_v,\, \boldsymbol{\gamma}_n \boldsymbol{E}_\varepsilon \rangle_{H^{\frac{1}{2}} \times H^{-\frac{1}{2}}(\partial\Omega,\mathbb{V})}\,, \tag{3.17}$$

where $H^{\frac{1}{2}}(\partial\Omega,\mathbb{V})$ is the space of traces of functions belonging to $H^{\mathrm{Grad}}(\Omega,\mathbb{V})$ and $H^{-\frac{1}{2}}(\partial\Omega,\mathbb{V})$ is its topological dual.

Theorem 3 (Stokes-Dirac structure for elastodynamics)
Let $H^{\mathrm{Grad}}(\Omega,\mathbb{V})$ denote the space of vectors with symmetric gradient in $L^2(\Omega,\mathbb{S})$ and $H^{\mathrm{Div}}(\Omega,\mathbb{S})$ be the space of symmetric tensors with divergence in $L^2(\Omega,\mathbb{V})$. Consider the following definitions

$$\begin{aligned} H &:= H^{\mathrm{Grad}}(\Omega,\mathbb{V}) \times H^{\mathrm{Div}}(\Omega,\mathbb{S}),\\ F &:= L^2(\Omega,\mathbb{V}) \times L^2(\Omega,\mathbb{S}),\\ V_\partial &:= H^{\frac{1}{2}}(\partial\Omega,\mathbb{V}),\\ V_\partial' &:= H^{-\frac{1}{2}}(\partial\Omega,\mathbb{V}), \end{aligned}$$

The set

$$D_{\mathcal{J}} = \left\{ \begin{pmatrix} \boldsymbol{f} \\ \boldsymbol{f}_\partial \\ \boldsymbol{e} \\ \boldsymbol{e}_\partial \end{pmatrix} \mid \boldsymbol{e} \in H, \quad \boldsymbol{f} = \mathcal{J}\boldsymbol{e} \in F, \quad \boldsymbol{f}_\partial = \boldsymbol{\gamma}_0 \boldsymbol{e}_v \in V_\partial, \quad \boldsymbol{e}_\partial = -\boldsymbol{\gamma}_n \boldsymbol{E}_\varepsilon \in V_\partial' \right\}, \tag{3.18}$$

where $\boldsymbol{e} = (\boldsymbol{e}_v,\, \boldsymbol{E}_\varepsilon)$ and $\mathcal{J}$ are defined in (3.16), is a Stokes–Dirac structure with respect to the pairing

$$\begin{aligned} \left\langle\!\left\langle (\boldsymbol{f}^1, \boldsymbol{f}^1_\partial, \boldsymbol{e}^1, \boldsymbol{e}^1_\partial), (\boldsymbol{f}^2, \boldsymbol{f}^2_\partial, \boldsymbol{e}^2, \boldsymbol{e}^2_\partial) \right\rangle\!\right\rangle := &\left\langle \boldsymbol{f}^1,\, \boldsymbol{e}^2 \right\rangle_F + \left\langle \boldsymbol{f}^2,\, \boldsymbol{e}^1 \right\rangle_F \\ &+ \left\langle \boldsymbol{f}^1_\partial,\, \boldsymbol{e}^2_\partial \right\rangle_{V_\partial \times V_\partial'} + \left\langle \boldsymbol{f}^2_\partial,\, \boldsymbol{e}^1_\partial \right\rangle_{V_\partial \times V_\partial'}, \end{aligned} \tag{3.19}$$

where

$$\langle \boldsymbol{f}_\partial,\, \boldsymbol{e}_\partial \rangle_{V_\partial \times V_\partial'} = -\left\langle \boldsymbol{\gamma}_0 \boldsymbol{e}_v,\, \boldsymbol{\gamma}_n \boldsymbol{E}_\varepsilon \right\rangle_{H^{\frac{1}{2}} \times H^{-\frac{1}{2}}(\partial\Omega,\mathbb{V})}. \tag{3.20}$$

Proof. A Stokes-Dirac is characterized by the fact that $D_{\mathcal{J}} = D_{\mathcal{J}}^{\perp}$. Then one has to show that $D_{\mathcal{J}} \subset D_{\mathcal{J}}^{\perp}$ and $D_{\mathcal{J}}^{\perp} \subset D_{\mathcal{J}}$. The main steps of Theorem 3.6 in [LGZM05] (and Proposition 2) are followed here to support the substantiation of the conjecture. The integration by parts formula is applied as in (3.15).

Step 1. To show that $D_{\mathcal{J}} \subset D_{\mathcal{J}}^{\perp}$, take $(\boldsymbol{f},\, \boldsymbol{f}_\partial,\, \boldsymbol{e},\, \boldsymbol{e}_\partial) \in D_{\mathcal{J}}$. Then

$$\begin{aligned}\langle\langle\, (\boldsymbol{f}, \boldsymbol{f}_\partial, \boldsymbol{e}, \boldsymbol{e}_\partial), (\boldsymbol{f}, \boldsymbol{f}_\partial, \boldsymbol{e}, \boldsymbol{e}_\partial)\,\rangle\rangle =& 2\,\langle \boldsymbol{f},\, \boldsymbol{e}\rangle_F + 2\,\langle \boldsymbol{f}_\partial,\, \boldsymbol{e}_\partial\rangle_{V_\partial \times V_\partial'}\,,\\ =& 2\,\langle \mathcal{J}\boldsymbol{e},\, \boldsymbol{e}\rangle_F + 2\,\langle \boldsymbol{f}_\partial,\, \boldsymbol{e}_\partial\rangle_{V_\partial \times V_\partial'}\,,\\ =& +2\int_\Omega \{\boldsymbol{e}_v \cdot \operatorname{Div} \boldsymbol{E}_\varepsilon + \boldsymbol{E}_\varepsilon : \operatorname{Grad} \boldsymbol{e}_v\}\ \mathrm{d}\Omega\\ & -2\int_{\partial\Omega} \boldsymbol{e}_v \cdot (\boldsymbol{E}_\varepsilon\, \boldsymbol{n})\ \mathrm{d}S, = 0, \quad \text{from (3.17)}.\end{aligned}$$

This implies $D_{\mathcal{J}} \subset D_{\mathcal{J}}^{\perp}$.

Step 2. Take $(\boldsymbol{\phi},\, \boldsymbol{\phi}_\partial,\, \boldsymbol{\epsilon},\, \boldsymbol{\epsilon}_\partial) \in D_{\mathcal{J}}^{\perp}$ and $\boldsymbol{e}_0 = (\boldsymbol{e}_{v,0},\ \boldsymbol{E}_{\varepsilon,0}) \in H$ with compact support on Ω. This implies $\boldsymbol{\gamma_0} \boldsymbol{e}_{v,0} = \boldsymbol{0}$ and $\boldsymbol{\gamma}_n \boldsymbol{E}_{\varepsilon,0} = \boldsymbol{0}$. Taking $(\mathcal{J}\boldsymbol{e}_0, \boldsymbol{0}, \boldsymbol{e}_0, \boldsymbol{0}) \in D_{\mathcal{J}}$ then

$$\langle\langle\, (\boldsymbol{\phi}, \boldsymbol{\phi}_\partial, \boldsymbol{\epsilon}, \boldsymbol{\epsilon}_\partial), (\mathcal{J}\boldsymbol{e}_0, \boldsymbol{0}, \boldsymbol{e}_0, \boldsymbol{0})\,\rangle\rangle = \langle \mathcal{J}\boldsymbol{e}_0,\, \boldsymbol{\epsilon}\rangle_F + \langle \boldsymbol{\phi},\, \boldsymbol{e}_0\rangle_F = 0, \quad \forall \boldsymbol{e}_0 \in H.$$

It follows that $\boldsymbol{\epsilon} \in H$ and $\boldsymbol{\phi} = \mathcal{J}\boldsymbol{\epsilon}$.

Step 3. Take $(\boldsymbol{\phi},\, \boldsymbol{\phi}_\partial,\, \boldsymbol{\epsilon},\, \boldsymbol{\epsilon}_\partial) \in D_{\mathcal{J}}^{\perp}$ and $(\boldsymbol{f},\, \boldsymbol{f}_\partial,\, \boldsymbol{e},\, \boldsymbol{e}_\partial) \in D_{\mathcal{J}}$. Variables $\boldsymbol{e}, \boldsymbol{\epsilon}$ are indeed tuples containing a vector and a tensor, namely $\boldsymbol{e} = (\boldsymbol{e}_v,\, \boldsymbol{E}_\varepsilon)$, $\boldsymbol{\epsilon} = (\boldsymbol{\epsilon}_v,\, \boldsymbol{\mathcal{E}}_\varepsilon)$. From step 2 and (3.19)

$$\begin{aligned}0 &= \langle \mathcal{J}\boldsymbol{\epsilon},\, \boldsymbol{e}\rangle_F + \langle \mathcal{J}\boldsymbol{e},\, \boldsymbol{\epsilon}\rangle_F + \langle \boldsymbol{\phi}_\partial,\, \boldsymbol{e}_\partial\rangle_{V_\partial \times V_\partial'} + \langle \boldsymbol{f}_\partial,\, \boldsymbol{\epsilon}_\partial\rangle_{V_\partial \times V_\partial'}\,,\\ &= \int_{\partial\Omega} \{\boldsymbol{e}_v \cdot (\boldsymbol{\mathcal{E}}_\varepsilon\, \boldsymbol{n}) + \boldsymbol{\epsilon}_v \cdot (\boldsymbol{E}_\varepsilon\, \boldsymbol{n})\}\ \mathrm{d}S + \langle \boldsymbol{\phi}_\partial,\, -\boldsymbol{\gamma}_n \boldsymbol{E}_\varepsilon\rangle_{V_\partial \times V_\partial'} + \langle \boldsymbol{\gamma}_0 \boldsymbol{e}_v,\, \boldsymbol{\epsilon}_\partial\rangle_{V_\partial \times V_\partial'}\,.\end{aligned}$$

Given the fact that $\boldsymbol{e} = (\boldsymbol{e}_v,\ \boldsymbol{E}_\varepsilon)$ is arbitrary then

$$\boldsymbol{\phi}_\partial = \boldsymbol{\gamma}_0 \boldsymbol{\epsilon}_v, \qquad \boldsymbol{\epsilon}_\partial = -\boldsymbol{\gamma}_n \boldsymbol{\mathcal{E}}_\varepsilon,$$

meaning that $D_{\mathcal{J}}^{\perp} \subset D_{\mathcal{J}}$. □

Remark 7 (General mixed causality and existence and uniqueness of solutions)
The proof consider uniform boundary condition based on the integration by parts formula given in Remark 6. This is sufficient for characterizing the Stokes-Dirac structure. Indeed, for the existence and uniqueness of solution of system (3.16), the control inputs and outputs have to satisfy additional compatibility conditions [Gri11]. In particular, when both Neumann and Dirichlet conditions are imposed and their boundary partitions touch (just like in Fig. 3.2), then the appropriate space for the Dirichlet control is $H_{00}^{1/2}$ (see e.g. [RRR19]). The conjugated output will then belong to the topological dual of this space, that does not possess a characterization. These issues are out of the scope of this work.

Linear elasticity falls within the assumptions of the theoretical work of [Skr19]. Therefore,

it is a well posed boundary control pH system. A question that naturally arises is how to reformulate this system using the language of differential geometry. This is possible through the usage of vector-valued differential forms. The interested reader may consult [Bre08].

3.3 Conclusion

In this chapter, the pH formulation of elasticity has been obtained. This model represents a generalization of the wave equation to higher dimensional variables. This leads to the introduction of symmetric tensorial quantities describing the state of stress and deformation within the body.
For a plane continuum with moderate thickness, it is possible to reduce the general three-dimensional mode to two uncoupled systems: one representing the in-plane behavior ruled by 2D elasticity and one representing the out-of-plane deflection. This will be the object of the next chapter dedicated to the study of a pH formulation of plate bending. It is important to remember that plate models are just particular cases of three-dimensional elasticity.

Chapter 4

Port-Hamiltonian plate theory

You get tragedy where the tree, instead of bending, breaks.

Culture and Value
Ludwig Wittgenstein

Contents

Plates are plane structural elements with a small thickness compared to the planar dimensions. Thanks to this feature, it is not necessary to model plate structures using three-dimensional elasticity. Dimensional reduction strategies are employed to describe plate structures as two-dimensional problems. These strategies rely on an educated guess of the displacement field. For beams and plates this field is expressed in terms of unknown functions $\phi_i^j(x, y, t)$ that solely depends on the midplane coordinates (x, y)

$$u_i(x, y, z, t) = \sum_{j=0}^{m} (z)^j \phi_i^j(x, y, t).$$

where u_i, $i = \{x, y, z\}$ are the components of the displacement field. A first-order approximation is commonly used, meaning that a linear dependence on z is considered. Two main models arise from such a framework:

- the Mindlin-Reissner model for thick plates;

- the Kirchhoff-Love model for thin plates.

In this chapter it is shown how to formulate first-order plate models as pHs.

4.1 First order plate theory

As previously stated, first order theories assume a linear dependence on the vertical coordinate (cf. [Red06])

$$u_i(x,y,z,t) = \phi_i^0(x,y,t) + z\phi_i^1(x,y,t).$$

This hypothesis implies that the fibers, i.e. segments perpendicular to the mid-plane before deformation, remain straight after deformation. Additionally, for plate with moderate thickness the fibers are considered inextensible, meaning that $\phi_z^1 = 0$. These assumptions lead to the following displacement field

$$\begin{aligned} u_x(x,y,z,t) &= u_x^0(x,y,t) - z\theta_x(x,y,t), \\ u_y(x,y,z,t) &= u_y^0(x,y,t) - z\theta_y(x,y,t), \\ u_z(x,y,z,t) &= u_z^0(x,y,t), \end{aligned} \tag{4.1}$$

where $u_i^0(x,y,t) = \phi_i^0(x,y,t)$, $\theta_i(x,y,t) = -\phi_i^1(x,y,t)$. Assuming a linear elastic behavior, the 3D strain tensors for such a displacement field takes the form

$$\varepsilon_{\alpha\beta} = \frac{1}{2}\left(\partial_\beta u_\alpha + \partial_\alpha u_\beta\right) - z\frac{1}{2}\left(\partial_\beta\theta_\alpha + \partial_\alpha\theta_\beta\right) = \varepsilon^0_{\alpha\beta} - z\kappa_{\alpha\beta}, \tag{4.2}$$

$$\varepsilon_{\alpha z} = \frac{1}{2}\left(\partial_a u_z - \theta_\alpha\right) = \frac{1}{2}\gamma_\alpha, \tag{4.3}$$

where $\alpha = \{x,y\}$, $\beta = \{x,y\}$. The tensors $\boldsymbol{\varepsilon}^0$, $\boldsymbol{\kappa}$, $\boldsymbol{\gamma}$ are called membrane, bending (or curvature) and shear strain tensor

$$\boldsymbol{\varepsilon}^0 = \operatorname{Grad}\boldsymbol{u}^0, \tag{4.4}$$

$$\boldsymbol{\kappa} = \operatorname{Grad}\boldsymbol{\theta}, \tag{4.5}$$

$$\boldsymbol{\gamma} = \operatorname{grad} u_z - \boldsymbol{\theta}. \tag{4.6}$$

where $\boldsymbol{u}^0 = (u_x, u_y)^\top$, $\boldsymbol{\theta} = (\theta_x, \theta_y)^\top$. For now, it is assumed that the material is isotropic, linear elastic (in §4.3 this hypothesis is removed). Recall the Hooke's law for 3D continua (see Eq. (3.5))

$$\boldsymbol{\Sigma} = \frac{E}{1+\nu}\left[\boldsymbol{\varepsilon} + \frac{\nu}{1-2\nu}\operatorname{Tr}(\boldsymbol{\varepsilon})\boldsymbol{I}_{3\times 3}\right].$$

where E, ν are the Young modulus and Poisson ratio. The hypothesis of inextensible fibers implies $\varepsilon_{zz} = 0$. However, imposing a plane strain condition provides a model that is too stiff. Rather than a plain strain assumption, a plain stress hypothesis is used to derive the constitutive law for plates. The displacement field (4.1) is left unchanged, but, instead of ε_{zz},

Σ_{zz} is set to zero. If $\Sigma_{zz} = 0$, one gets

$$\varepsilon_{zz} = -\frac{\nu}{1-\nu}(\varepsilon_{xx} + \varepsilon_{yy}).$$

Consequently, it is computed

$$\mathrm{Tr}(\boldsymbol{\varepsilon}) = \frac{1-2\nu}{1-\nu}(\varepsilon_{xx} + \varepsilon_{yy}).$$

The constitutive law for the in-plane stress takes the form

$$\boldsymbol{\Sigma}_{2D} = \boldsymbol{\mathcal{D}}_{2D}\, \boldsymbol{\varepsilon}_{2D},$$

where $\boldsymbol{\Sigma}_{2D} = \Sigma_{\alpha\beta}$, $\boldsymbol{\varepsilon}_{2D} = \varepsilon_{\alpha\beta}$ and

$$\boldsymbol{\mathcal{D}}_{2D} = \frac{E}{1-\nu^2}\left[(1-\nu)(\cdot) + \nu\,\mathrm{Tr}(\cdot)\boldsymbol{I}_{2\times 2}\right]. \tag{4.7}$$

Concerning the shear deformation, the constitutive law reduces to

$$\boldsymbol{\sigma}_s = G\boldsymbol{\gamma}, \tag{4.8}$$

where $\boldsymbol{\sigma}_s := \boldsymbol{\Sigma}_{\alpha,3}$ and $G = \frac{E}{2(1+\nu)}$ is the shear modulus. In the following sections, the most common plate models will be presented.

4.1.1 Mindlin-Reissner model

The Mindlin-Reissner model [Rei47, Min51] represents a first-order shear deformation theory for describing the bending of plate. The in-plane midplane displacement are zero $\boldsymbol{u}^0(x,y) = \boldsymbol{0}$ for an isotropic plate that experiences only bending. Hence, the displacement field reduces to

$$\begin{aligned} u_x(x,y,z) &= -z\partial_x\theta_x, \\ u_y(x,y,z) &= -z\partial_y\theta_y, \\ u_z(x,y,z) &= u_z^0(x,y). \end{aligned} \tag{4.9}$$

In pure bending, the strain tensor is given by

$$\boldsymbol{\varepsilon}_b := \boldsymbol{\varepsilon}_{2D}(\boldsymbol{u}^0 = \boldsymbol{0}) = -z\boldsymbol{\kappa},$$

with $\boldsymbol{\kappa}$ given by (4.5). Consequently, the stress tensor reads

$$\boldsymbol{\Sigma}_b := \boldsymbol{\Sigma}_{2D}(\boldsymbol{u}^0 = \boldsymbol{0}) = -z\boldsymbol{\mathcal{D}}_{2D}\boldsymbol{\kappa},$$

where $\boldsymbol{\mathcal{D}}_{2D}$ is defined in Eq. (4.7).

The undeformed middle plane of the plate is denoted by Ω. The total domain of the

plate is the product $\Omega \times (-h/2, h/2)$, where h is the constant thickness. To effectively reduce the problem from three- to two-dimensional, the stresses have to be integrated along the fibers. Since the stress varies linearly across the thickness, the stress has to be multiplied by z before the integration to get a non null contribution. The resulting quantity is called bending momenta tensor and is given by

$$\boldsymbol{M} := -\int_{-h/2}^{h/2} z\boldsymbol{\Sigma}_b \, \mathrm{d}z = \boldsymbol{\mathcal{D}}_b \, \boldsymbol{\kappa}, \tag{4.10}$$

where

$$\boldsymbol{\mathcal{D}}_b = D_b \left[(1-\nu)(\cdot) + \nu \operatorname{Tr}(\cdot)\boldsymbol{I}_{2\times 2}\right], \qquad \text{where} \qquad D_b = \frac{Eh^3}{12(1-\nu^2)}. \tag{4.11}$$

The shear stress has to be integrated along the fibers as well. Given the excessive rigidity of the shear contribution, a correction factor $K_{\mathrm{sh}} = 5/6$ [Red06, Chapter 10] is introduced

$$\boldsymbol{q} = \int_{-h/2}^{h/2} K_{\mathrm{sh}} \boldsymbol{\sigma_s} = K_{\mathrm{sh}} G h \boldsymbol{\gamma}, \tag{4.12}$$

where $\boldsymbol{\gamma}$ is defined in Eq. (4.6). The equations of motion can be obtained using Hamilton's principle. It consists in minimizing the total Lagrangian, given by $L = E_{\mathrm{def}} - E_{\mathrm{kin}}$, where E_{def} and E_{kin} are the deformation and kinetic energies

$$E_{\mathrm{def}} = \frac{1}{2}\int_\Omega \int_{-h/2}^{h/2} \boldsymbol{\Sigma} : \boldsymbol{\varepsilon} \, \mathrm{d}\Omega \, \mathrm{d}z = \frac{1}{2}\int_\Omega \{\boldsymbol{M} : \boldsymbol{\kappa} + \boldsymbol{q}\cdot\boldsymbol{\gamma}\} \, \mathrm{d}\Omega, \tag{4.13}$$

$$E_{\mathrm{kin}} = \frac{1}{2}\int_\Omega \int_{-h/2}^{h/2} \rho \, \|\partial_t \boldsymbol{u}\|^2 \, \mathrm{d}\Omega \, \mathrm{d}z = \frac{1}{2}\int_\Omega \left\{ \frac{\rho h^3}{12} \|\partial_t \boldsymbol{\theta}\|^2 + \rho h (\partial_t u_z)^2 \right\} \mathrm{d}\Omega, \tag{4.14}$$

where ρ is the mass density. The Hamilton principle states that

$$\int_0^T \delta L \, \mathrm{d}t = \int_0^T \{\delta E_{\mathrm{def}} - \delta E_{\mathrm{kin}}\} \, \mathrm{d}t = 0.$$

The final result is the following system of PDEs (for the detailed computations see [Red06, Chapter 10])

$$\begin{aligned} \rho h \frac{\partial^2 u_z}{\partial t^2} &= \operatorname{div} \boldsymbol{q}, \qquad (x,y) \in \Omega, \\ \frac{\rho h^3}{12}\frac{\partial^2 \boldsymbol{\theta}}{\partial t^2} &= \operatorname{Div} \boldsymbol{M} + \boldsymbol{q}, \end{aligned} \tag{4.15}$$

with $\boldsymbol{M} = \boldsymbol{\mathcal{D}}_b \operatorname{Grad} \boldsymbol{\theta}$ and $\boldsymbol{q} = K_{\mathrm{sh}} G h \, (\operatorname{grad} u_z - \boldsymbol{\theta})$. This PDE goes together with specified boundary conditions. Those will be detailed in 4.2.1.

4.1.2 Kirchhoff-Love model

The Kirchhoff model was formulated around 1850 and it is referred to as classical plate theory. The hypotheses on the displacement field consist of the following three points (see Fig. 4.1):

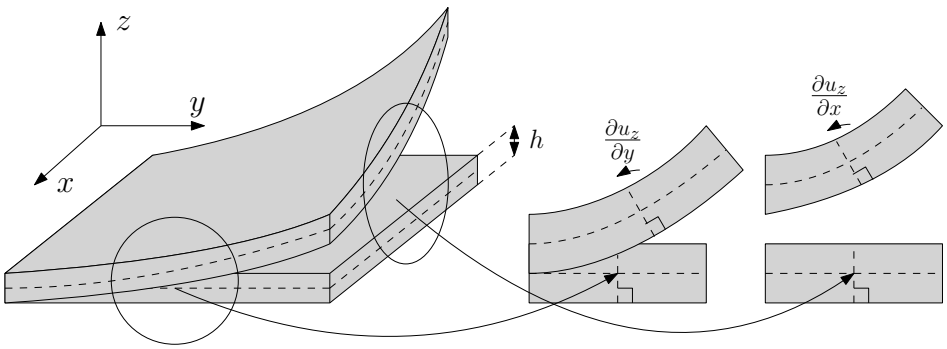

Figure 4.1: Kinematic assumption for the Kirchhoff plate

1. The fibers, segments perpendicular to the mid-plane before deformation, remain straight after deformation.

2. The fibers are inextensible.

3. While rotating, fibers remain perpendicular to the middle surface after deformation.

While the first two points are valid also for the Mindlin plate, the third assumption is specific to the Kirchhoff-Love model. Such an approximation is valid for plates having span-to-thickness ratio of the order of $L/h \approx 100-1000$ and implies zero transverse shear deformation

$$\boldsymbol{\gamma} = 0 \implies \varepsilon_{xz} = -\theta_x + \frac{\partial u_z}{\partial x} = 0, \qquad \varepsilon_{yz} = -\theta_y + \frac{\partial u_z}{\partial y} = 0.$$

The rotation vector is then related to the vertical displacement $\boldsymbol{\theta} = \operatorname{grad} u_z$. Plugging this into (4.5), it is found

$$\boldsymbol{\kappa} = \operatorname{Grad} \operatorname{grad} u_z = \operatorname{Hess} u_z. \tag{4.16}$$

Since the focus is on bending behavior, the in-plane displacement of the mid-plane are assumed to be zero $\boldsymbol{u}^0(x, y) = \boldsymbol{0}$. Hence, the displacement field assumes the form

$$\begin{aligned} u_x(x, y, z) &= -z\partial_x u_z, \\ u_y(x, y, z) &= -z\partial_y u_z, \\ u_z(x, y, z) &= u_z^0(x, y). \end{aligned} \tag{4.17}$$

For the Kirchhoff plate, the same link between the momenta and bending tensor holds

$$\boldsymbol{M} = \boldsymbol{\mathcal{D}}_b \boldsymbol{\kappa},$$

where $\boldsymbol{\mathcal{D}}_b$ and $\boldsymbol{\kappa}$ are given in (4.11), (4.16) respectively. The equations of motion can be obtained using Hamilton's principle [Red06, Chapter 2]. The deformation energy, kinetic

energy and external work read

$$E_{\text{def}} = \frac{1}{2}\int_\Omega \int_{-h/2}^{h/2} \boldsymbol{\Sigma} : \boldsymbol{\varepsilon}\, \mathrm{d}\Omega\, \mathrm{d}z = \frac{1}{2}\int_\Omega \{\boldsymbol{M} : \boldsymbol{\kappa}\}\, \mathrm{d}\Omega, \tag{4.18}$$

$$E_{\text{kin}} = \frac{1}{2}\int_\Omega \int_{-h/2}^{h/2} \rho\, \|\partial_t \boldsymbol{u}\|^2\, \mathrm{d}\Omega\, \mathrm{d}z \approx \frac{1}{2}\int_\Omega \rho h (\partial_t u_z)^2\, \mathrm{d}\Omega. \tag{4.19}$$

Remark 8 (Rotational energy)
For the kinetic energy the rotational contribution

$$E_{rot} = \frac{1}{2}\int_\Omega \int_{-h/2}^{h/2} \left\{\rho\,(\partial_t u_x)^2 + (\partial_t u_y)^2\right\}\, \mathrm{d}\Omega\, \mathrm{d}z = \frac{h^3}{24}\int_\Omega \rho \left\{\,(\partial_{tx} u_z)^2 + (\partial_{ty} u_z)^2\right\}\, \mathrm{d}\Omega = O(h^3),$$

is neglected given the small thickness assumption.

The final result from the Hamilton's principle is the following PDE (for the detailed computations the reader may consult [Red06, Chapter 3])

$$\rho h \frac{\partial^2 u_z}{\partial t^2} = -\operatorname{div}\operatorname{Div}(\boldsymbol{\mathcal{D}}_b\, \operatorname{Grad}\operatorname{grad} u_z), \qquad (x, y) \in \Omega. \tag{4.20}$$

Developing the calculations, one obtains

$$\rho h \frac{\partial^2 u_z}{\partial t^2} = -D_b \Delta^2 u_z, \qquad (x, y) \in \Omega,$$

where $\Delta^2 = \frac{\partial^4}{\partial x^4} + 2\frac{\partial^2}{\partial x^2}\frac{\partial^2}{\partial y^2} + \frac{\partial^4}{\partial y^4}$ is the bi-Laplacian. Appropriate boundary conditions for this problem will be detailed in 4.2.2.

4.2 Port-Hamiltonian formulation of isotropic plates

In this section the pH formulation of the isotropic Mindlin and Kirchhoff plate models is detailed. In [MMB05], the Mindlin plate model was put in pH form by appropriate selection of the energy variables. However, the final system does not consider the nature of the different variables that come into play, leading to a non intrinsic final formulation. Additionally, this model was presented using the jet bundle formalism in [SS17]. The Kirchhoff model was never explored in the pH framework and represents an original contribution of this thesis. The interested reader can find in [RZ18] a rigorous mathematical treatment of the biharmonic problem and its decomposition in 2D geometries, but only for the static case (the 3D case, that does not relate to plate bending, is treated in [PZ18]).

4.2.1 Port-Hamiltonian Mindlin plate

Let $w := u_z$ denote the vertical displacement of the plate. Consider a bounded, connected domain $\Omega \subset \mathbb{R}^2$ and the Hamiltonian (total energy)

$$H = \frac{1}{2}\int_\Omega \left\{ \rho h \left(\frac{\partial w}{\partial t}\right)^2 + \frac{\rho h^3}{12}\left\|\frac{\partial \boldsymbol{\theta}}{\partial t}\right\|^2 + \boldsymbol{M} : \boldsymbol{\kappa} + \boldsymbol{q}\cdot\boldsymbol{\gamma} \right\} \mathrm{d}\Omega, \tag{4.21}$$

where $\boldsymbol{M}$, $\boldsymbol{\kappa}$, $\boldsymbol{q}$, $\boldsymbol{\gamma}$ are defined in Eqs. (4.10), (4.5), (4.12), (4.6) respectively. The choice of the energy variables is the same as in [MMB05] but here scalar-, vector- and tensor-valued variables are gathered together:

$$\begin{aligned} &\alpha_w = \rho h \frac{\partial w}{\partial t}, && \text{Linear momentum,} && \boldsymbol{\alpha}_\theta = \frac{\rho h^3}{12}\frac{\partial \boldsymbol{\theta}}{\partial t}, && \text{Angular momentum,} \\ &\boldsymbol{A}_\kappa = \boldsymbol{\kappa}, && \text{Curvature tensor,} && \boldsymbol{\alpha}_\gamma = \boldsymbol{\gamma}. && \text{Shear deformation.} \end{aligned} \tag{4.22}$$

The energy is now a quadratic function of the energy variables

$$H = \frac{1}{2}\int_\Omega \left\{ \frac{1}{\rho h}\alpha_w^2 + \frac{12}{\rho h^3}\left\|\boldsymbol{\alpha}_\theta\right\|^2 + (\boldsymbol{\mathcal{D}}_b \boldsymbol{A}_\kappa) : \boldsymbol{A}_\kappa + (\boldsymbol{\mathcal{D}}_s \boldsymbol{\alpha}_\gamma)\cdot\boldsymbol{\alpha}_\gamma \right\} \mathrm{d}\Omega, \tag{4.23}$$

where $\boldsymbol{\mathcal{D}}_s := GhK_{\mathrm{sh}}\boldsymbol{I}_{2\times 2}$, G is the shear modulus and K_{sh} the correction factor. The co-energy variables are found by computing the variational derivative of the Hamiltonian:

$$\begin{aligned} &e_w := \frac{\delta H}{\delta \alpha_w} = \frac{\partial w}{\partial t}, && \text{Linear velocity,} && \boldsymbol{e}_\theta := \frac{\delta H}{\delta \boldsymbol{\alpha}_\theta} = \frac{\partial \boldsymbol{\theta}}{\partial t}, && \text{Angular velocity,} \\ &\boldsymbol{E}_\kappa := \frac{\delta H}{\delta \boldsymbol{A}_\kappa} = \boldsymbol{M}, && \text{Momenta tensor,} && \boldsymbol{e}_\gamma := \frac{\delta H}{\delta \boldsymbol{\alpha}_\gamma} = \boldsymbol{q} && \text{Shear stress.} \end{aligned} \tag{4.24}$$

Proposition 4
The variational derivative of the Hamiltonian with respect to the curvature tensor is the momenta tensor $\frac{\delta H}{\delta \boldsymbol{A}_\kappa} = \boldsymbol{M}$.

Proof. The proof is analogous to the one already detailed in Prop. 3 □

Once the variables are concatenated together, the pH system is expressed as follows

$$\frac{\partial}{\partial t}\begin{pmatrix} \alpha_w \\ \boldsymbol{\alpha}_\theta \\ \boldsymbol{A}_\kappa \\ \boldsymbol{\alpha}_\gamma \end{pmatrix} = \begin{bmatrix} 0 & 0 & 0 & \mathrm{div} \\ \boldsymbol{0} & \boldsymbol{0} & \mathrm{Div} & \boldsymbol{I}_{2\times 2} \\ \boldsymbol{0} & \mathrm{Grad} & \boldsymbol{0} & \boldsymbol{0} \\ \mathrm{grad} & -\boldsymbol{I}_{2\times 2} & \boldsymbol{0} & \boldsymbol{0} \end{bmatrix} \begin{pmatrix} e_w \\ \boldsymbol{e}_\theta \\ \boldsymbol{E}_\kappa \\ \boldsymbol{e}_\gamma \end{pmatrix}. \tag{4.25}$$

The first two equations are equivalent to (4.15). The last two equations, like (3.14) for 3D elasticity, represent the fact that the higher order derivatives commute. We shall now establish the total energy balance in terms of boundary variables as they will be part of the

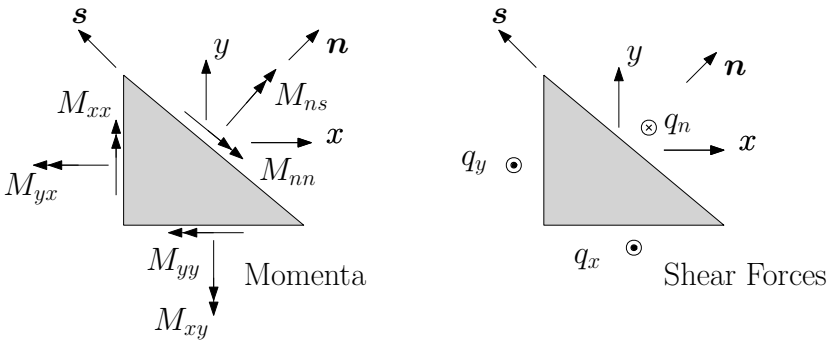

Figure 4.2: Cauchy law for momenta and forces at the boundary.

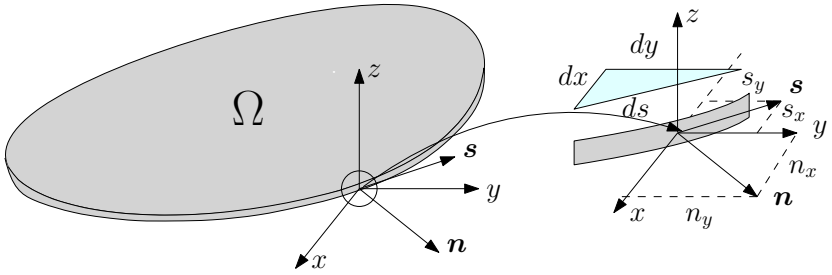

Figure 4.3: Reference frames and notations.

underlying Stokes-Dirac structure of this model. The energy rate reads

$$\begin{aligned}\dot{H} &= \int_\Omega \left\{ \frac{\partial \alpha_w}{\partial t} e_w + \frac{\partial \boldsymbol{\alpha}_\theta}{\partial t} \cdot \boldsymbol{e}_\theta + \frac{\partial \boldsymbol{A}_\kappa}{\partial t} : \boldsymbol{E}_\kappa + \frac{\partial \boldsymbol{\alpha}_\gamma}{\partial t} \cdot \boldsymbol{e}_\gamma \right\} \mathrm{d}\Omega \\ &= \int_\Omega \{ \mathrm{div}(\boldsymbol{e}_\gamma) e_w + \mathrm{Div}(\boldsymbol{E}_\kappa) \cdot \boldsymbol{e}_\theta + \ \mathrm{Grad}(\boldsymbol{e}_\theta) : \boldsymbol{E}_\kappa + \mathrm{grad}(e_w) \cdot \boldsymbol{e}_\gamma \} \ \mathrm{d}\Omega \qquad \text{Stokes theorem,} \\ &= \int_{\partial\Omega} \{ w_t \, q_n + \omega_n \, M_{nn} + \omega_s \, M_{ns} \} \ \mathrm{d}s,\end{aligned} \tag{4.26}$$

where s is the curvilinear abscissa. The last integral is obtained by applying the Stokes theorem. The boundary variables appearing in the last line of (4.26) and illustrated in Fig. 4.2 are defined as follows:

$$\begin{aligned} \text{Shear force} \quad & q_n := \boldsymbol{q} \cdot \boldsymbol{n} = \boldsymbol{e}_\gamma \cdot \boldsymbol{n}, \\ \text{Flexural momentum} \quad & M_{nn} := \boldsymbol{M} : (\boldsymbol{n} \otimes \boldsymbol{n}) = \boldsymbol{E}_\kappa : (\boldsymbol{n} \otimes \boldsymbol{n}), \\ \text{Torsional momentum} \quad & M_{ns} := \boldsymbol{M} : (\boldsymbol{s} \otimes \boldsymbol{n}) = \boldsymbol{E}_\kappa : (\boldsymbol{s} \otimes \boldsymbol{n}), \end{aligned} \tag{4.27}$$

Given two vectors $\boldsymbol{a} \in \mathbb{R}^n$, $\boldsymbol{b} \in \mathbb{R}^m$, the notation $\boldsymbol{a} \otimes \boldsymbol{b} = \boldsymbol{a}\boldsymbol{b}^\top \in \mathbb{R}^{n \times m}$ denotes the outer (or dyadic) product of two vectors. Vectors $\boldsymbol{n}$ and $\boldsymbol{s}$ designate the normal and tangential unit vectors to the boundary, as shown in Fig. 4.3. The corresponding power conjugated

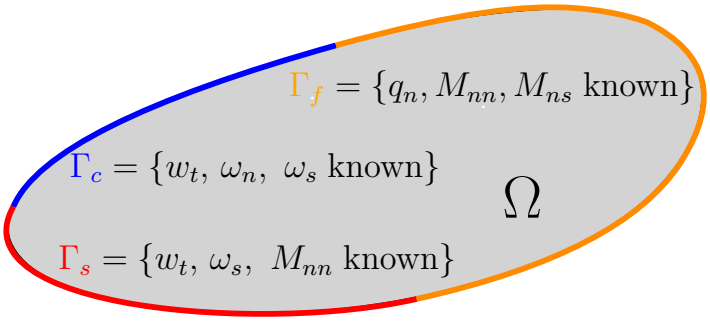

Figure 4.4: Boundary conditions for the Mindlin plate.

variables are

$$\begin{aligned} \text{Vertical velocity} \quad & w_t := \frac{\partial w}{\partial t} = e_w, \\ \text{Flexural rotation} \quad & \omega_n := \frac{\partial \boldsymbol{\theta}}{\partial t} \cdot \boldsymbol{n} = \boldsymbol{e}_\theta \cdot \boldsymbol{n}, \\ \text{Torsional rotation} \quad & \omega_s := \frac{\partial \boldsymbol{\theta}}{\partial t} \cdot \boldsymbol{s} = \boldsymbol{e}_\theta \cdot \boldsymbol{s}. \end{aligned} \tag{4.28}$$

Consider a partition of the boundary $\partial\Omega = \overline{\Gamma}_C \cup \overline{\Gamma}_S \cup \overline{\Gamma}_F$, $\Gamma_C \cap \Gamma_S \cap \Gamma_F = \{\emptyset\}$. The open subset Γ_C, Γ_S, Γ_F could be empty. Given definitions (4.27), (4.28), the boundary conditions for the Mindlin plate [DHNLS99] (see Fig. 4.4) that are considered are:

- Clamped (C) on $\Gamma_C \subseteq \partial\Omega$: $w_t,\ \omega_n,\ \omega_s$ known;
- Simply supported hard (S) on $\Gamma_S \subseteq \partial\Omega$: $w_t,\ \omega_s,\ M_{nn}$ known;
- Free (F) on $\Gamma_F \subseteq \partial\Omega$: $M_{nn},\ M_{ns},\ q_n$ known.

Then the final pH formulation reads

$$
\begin{aligned}
\frac{\partial}{\partial t}\begin{pmatrix}\alpha_w\\ \boldsymbol{\alpha}_\theta\\ \boldsymbol{A}_\kappa\\ \boldsymbol{\alpha}_\gamma\end{pmatrix} &= \underbrace{\begin{bmatrix}0 & 0 & 0 & \operatorname{div}\\ \mathbf{0} & \mathbf{0} & \operatorname{Div} & \boldsymbol{I}_{2\times 2}\\ \mathbf{0} & \operatorname{Grad} & \mathbf{0} & \mathbf{0}\\ \operatorname{grad} & -\boldsymbol{I}_{2\times 2} & \mathbf{0} & \mathbf{0}\end{bmatrix}}_{\mathcal{J}}\begin{pmatrix}e_w\\ \boldsymbol{e}_\theta\\ \boldsymbol{E}_\kappa\\ \boldsymbol{e}_\gamma\end{pmatrix},\\
\boldsymbol{u}_\partial &= \underbrace{\begin{bmatrix}\gamma_0^{\Gamma_C} & 0 & 0 & 0\\ 0 & \gamma_n^{\Gamma_C} & 0 & 0\\ 0 & \gamma_s^{\Gamma_C} & 0 & 0\\ \gamma_0^{\Gamma_S} & 0 & 0 & 0\\ 0 & \gamma_s^{\Gamma_S} & 0 & 0\\ 0 & 0 & \gamma_{nn}^{\Gamma_S} & 0\\ 0 & 0 & \gamma_{nn}^{\Gamma_F} & 0\\ 0 & 0 & \gamma_{ns}^{\Gamma_F} & 0\\ 0 & 0 & 0 & \gamma_n^{\Gamma_F}\end{bmatrix}}_{\mathcal{B}_\partial}\begin{pmatrix}e_w\\ \boldsymbol{e}_\theta\\ \boldsymbol{E}_\kappa\\ \boldsymbol{e}_\gamma\end{pmatrix},\\
\boldsymbol{y}_\partial &= \underbrace{\begin{bmatrix}0 & 0 & 0 & \gamma_n^{\Gamma_C}\\ 0 & 0 & \gamma_{nn}^{\Gamma_C} & 0\\ 0 & 0 & \gamma_{ns}^{\Gamma_C} & 0\\ 0 & 0 & 0 & \gamma_n^{\Gamma_S}\\ 0 & 0 & \gamma_{ns}^{\Gamma_S} & 0\\ 0 & \gamma_n^{\Gamma_S} & 0 & 0\\ 0 & \gamma_n^{\Gamma_F} & 0 & 0\\ 0 & \gamma_s^{\Gamma_F} & 0 & 0\\ \gamma_0^{\Gamma_F} & 0 & 0 & 0\end{bmatrix}}_{\mathcal{C}_\partial}\begin{pmatrix}e_w\\ \boldsymbol{e}_\theta\\ \boldsymbol{E}_\kappa\\ \boldsymbol{e}_\gamma\end{pmatrix},
\end{aligned}
\tag{4.29}
$$

where $\gamma_0^{\Gamma_*} a = a|_{\Gamma_*}$ denotes the trace over the set Γ_*. Furthermore, notations $\gamma_n^{\Gamma_*}\boldsymbol{a} = \boldsymbol{a}\cdot\boldsymbol{n}|_{\Gamma_*}$, $\gamma_s^{\Gamma_*}\boldsymbol{a} = \boldsymbol{a}\cdot\boldsymbol{s}|_{\Gamma_*}$ indicate respectively the normal and tangential traces over the set Γ_*. Symbols $\gamma_{nn}^{\Gamma_*}, \gamma_{ns}^{\Gamma_*}$ denote the normal-normal trace and the normal-tangential trace of tensor-valued functions and $\gamma_{nn}^{\Gamma_*}\boldsymbol{A} = \boldsymbol{A}:(\boldsymbol{n}\otimes\boldsymbol{n})|_{\Gamma_*}$, $\gamma_{ns}^{\Gamma_*}\boldsymbol{A} = \boldsymbol{A}:(\boldsymbol{n}\otimes\boldsymbol{s})|_{\Gamma_*}$. The boundary operators $\mathcal{B}_\partial, \mathcal{C}_\partial$ are unbounded.

Remark 9
It can be observed that the interconnection structure given by $\mathcal{J}$ in (4.29) mimics that of the Timoshenko beam [JZ12, Chapter 7].

Remark 10 (Trace operators and duality pairings for the Mindlin plate)
For the Mindlin plate the integrations by parts formula leads to the following duality pairings

$$
\begin{aligned}
\langle \operatorname{grad} e_w,\, \boldsymbol{e}_\gamma\rangle + \langle e_w,\, \operatorname{div}\boldsymbol{e}_\gamma\rangle + \langle \operatorname{Grad}\boldsymbol{e}_\theta,\, \boldsymbol{E}_\kappa\rangle + \langle \boldsymbol{e}_\theta,\, \operatorname{Div}\boldsymbol{E}_\kappa\rangle &= + \langle \gamma_0 e_w,\, \gamma_n\boldsymbol{e}_\gamma\rangle_{H^{\frac12}\times H^{-\frac12}(\partial\Omega)}\\
&\quad + \langle \boldsymbol{\gamma}_0\boldsymbol{e}_\theta,\, \boldsymbol{\gamma}_n\boldsymbol{E}_\kappa\rangle_{H^{\frac12}\times H^{-\frac12}(\partial\Omega,\mathbb{V})},
\end{aligned}
\tag{4.30}
$$

where $H^{\frac12}(\partial\Omega)$, $H^{\frac12}(\partial\Omega,\mathbb{V})$ is the space of traces of functions belonging to $H^1(\Omega)$, $H^{\operatorname{Grad}}(\Omega,\mathbb{V})$

respectively and $H^{-\frac{1}{2}}(\partial\Omega)$, $H^{-\frac{1}{2}}(\partial\Omega, \mathbb{V})$ *are their topological dual.*

Theorem 4 (Stokes-Dirac structure for the Mindlin plate)
Consider $\mathbb{V} = \mathbb{R}^2$, $\mathbb{S} = \mathbb{R}^{2\times 2}_{sym}$ *and let* $H^1(\Omega)$ *be the space of functions with gradient in* $L^2(\Omega, \mathbb{V})$ *and* $H^{\mathrm{div}}(\Omega, \mathbb{V})$ *the space of vector-valued functions with divergence in* $L^2(\Omega)$. *Furthermore,* $H^1(\Omega, \mathbb{V})$ *is the space of vectors with symmetric gradient in* $L^2(\Omega, \mathbb{S})$ *and* $H^{\mathrm{Div}}(\Omega, \mathbb{S})$ *denotes the space of symmetric tensors with divergence in* $L^2(\Omega, \mathbb{V})$. *Consider the definitions*

$$\begin{aligned} H &:= H^1(\Omega) \times H^{\mathrm{Grad}}(\Omega, \mathbb{V}) \times H^{\mathrm{Div}}(\Omega, \mathbb{S}) \times H^{\mathrm{div}}(\Omega, \mathbb{V}), \\ F &:= L^2(\Omega) \times L^2(\Omega, \mathbb{V}) \times L^2(\Omega, \mathbb{S}) \times L^2(\Omega, \mathbb{V}), \\ V_\partial &:= H^{\frac{1}{2}}(\partial\Omega) \times H^{\frac{1}{2}}(\partial\Omega, \mathbb{V}), \\ V'_\partial &:= H^{-\frac{1}{2}}(\partial\Omega) \times H^{-\frac{1}{2}}(\partial\Omega, \mathbb{V}). \end{aligned}$$

The set

$$\begin{aligned} D_{\mathcal{J}} = \Bigg\{ \begin{pmatrix} \boldsymbol{f} \\ \boldsymbol{f}_\partial \\ \boldsymbol{e} \\ \boldsymbol{e}_\partial \end{pmatrix} \mid \boldsymbol{e} \in H, \quad \boldsymbol{f} = \mathcal{J}\boldsymbol{e} \in F, \quad \boldsymbol{f}_\partial = \begin{bmatrix} \gamma_0 & 0 \\ \boldsymbol{0} & \boldsymbol{\gamma}_0 \end{bmatrix} \begin{pmatrix} e_w \\ \boldsymbol{e}_\theta \end{pmatrix} \in V_\partial, \\ \boldsymbol{e}_\partial = - \begin{bmatrix} \boldsymbol{\gamma}_n & 0 \\ \boldsymbol{0} & \gamma_n \end{bmatrix} \begin{pmatrix} \boldsymbol{E}_\kappa \\ \boldsymbol{e}_\gamma \end{pmatrix} \in V'_\partial \Bigg\}, \end{aligned} \tag{4.31}$$

where $\boldsymbol{e} = (e_w, \boldsymbol{e}_\theta, \boldsymbol{E}_\kappa, \boldsymbol{e}_\gamma)$ *and* $\mathcal{J}$ *is defined in* (4.29), *is a Stokes–Dirac structure with respect to the pairing*

$$\begin{aligned} \left\langle\!\left\langle (\boldsymbol{f}^1, \boldsymbol{f}^1_\partial, \boldsymbol{e}^1, \boldsymbol{e}^1_\partial), (\boldsymbol{f}^2, \boldsymbol{f}^2_\partial, \boldsymbol{e}^2, \boldsymbol{e}^2_\partial) \right\rangle\!\right\rangle := &\left\langle \boldsymbol{f}^1, \boldsymbol{e}^2 \right\rangle_F + \left\langle \boldsymbol{f}^2, \boldsymbol{e}^1 \right\rangle_F \\ &+ \left\langle \boldsymbol{f}^1_\partial, \boldsymbol{e}^2_\partial \right\rangle_{V_\partial \times V'_\partial} + \left\langle \boldsymbol{f}^2_\partial, \boldsymbol{e}^1_\partial \right\rangle_{V_\partial \times V'_\partial}. \end{aligned} \tag{4.32}$$

where

$$\langle \boldsymbol{f}_\partial, \boldsymbol{e}_\partial \rangle_{V_\partial \times V'_\partial} = - \langle \gamma_0 e_w, \gamma_n \boldsymbol{e}_\gamma \rangle_{H^{\frac{1}{2}} \times H^{-\frac{1}{2}}(\partial\Omega)} - \langle \boldsymbol{\gamma}_0 \boldsymbol{e}_\theta, \boldsymbol{\gamma}_n \boldsymbol{E}_\kappa \rangle_{H^{\frac{1}{2}} \times H^{-\frac{1}{2}}(\partial\Omega, \mathbb{V})}.$$

Proof. The proof is analogous to the proof of to Theorem 3. Here, the integration by parts formula (4.30) is used. □

The Mindlin plate falls within the assumption of [Skr19], hence it is a well-posed boundary control pH systems.

4.2.2 Port-Hamiltonian Kirchhoff plate

Again the starting point is the Hamiltonian (total energy)

$$H = \frac{1}{2}\int_\Omega \left\{ \rho h \left(\frac{\partial w}{\partial t}\right)^2 + \boldsymbol{M} : \boldsymbol{\kappa} \right\} \mathrm{d}\Omega, \tag{4.33}$$

where $\boldsymbol{M}$, $\boldsymbol{\kappa}$ are defined in Eqs. (4.10), (4.16). For what concerns the choice of the energy variables, a scalar and a tensor variable are considered:

$$\alpha_w = \rho h \frac{\partial w}{\partial t}, \quad \text{Linear momentum,} \qquad \boldsymbol{A}_\kappa = \boldsymbol{\kappa}, \quad \text{Curvature tensor.} \tag{4.34}$$

The co-energy variables are found by computing the variational derivative of the Hamiltonian:

$$e_w := \frac{\delta H}{\delta \alpha_w} = \frac{\partial w}{\partial t}, \quad \text{Linear velocity,} \qquad \boldsymbol{E}_\kappa := \frac{\delta H}{\delta \boldsymbol{A}_\kappa} = \boldsymbol{M}, \quad \text{Momenta tensor.} \tag{4.35}$$

The port-Hamiltonian system is then written as

$$\frac{\partial}{\partial t}\begin{pmatrix} \alpha_w \\ \boldsymbol{A}_\kappa \end{pmatrix} = \begin{bmatrix} 0 & -\operatorname{div}\circ\operatorname{Div} \\ \operatorname{Grad}\circ\operatorname{grad} & \boldsymbol{0} \end{bmatrix} \begin{pmatrix} e_w \\ \boldsymbol{E}_\kappa \end{pmatrix}. \tag{4.36}$$

The first equation is equivalent to (4.20). The last equation represents the fact that higher order derivatives commute

$$\begin{aligned} \partial_t \boldsymbol{A}_\kappa &= \operatorname{Grad}\operatorname{grad} e_w, \\ \partial_t \boldsymbol{\kappa} &= \operatorname{Grad}\operatorname{grad} \partial_t w, \\ \partial_t \operatorname{Grad}\operatorname{grad} w &= \operatorname{Grad}\operatorname{grad} \partial_t w. \end{aligned}$$

The last equation holds for $w \in C^3(\Omega)$.

Theorem 5
The operator $\operatorname{Grad}\circ\operatorname{grad}$*, corresponding to the Hessian operator, is the adjoint of the double divergence* $\operatorname{div}\circ\operatorname{Div}$.

Proof. Let $\mathbb{S} = \mathbb{R}^{d\times d}_{\mathrm{sym}}$ and consider the Hilbert space of the square-integrable symmetric square tensors $L^2(\Omega, \mathbb{S})$ over an open connected set Ω. Consider the Hilbert space $L^2(\Omega)$ of scalar square-integrable functions, endowed with the standard inner product. Consider the double divergence operator defined as:

$$\begin{aligned} \operatorname{div}\operatorname{Div}:\ & L^2(\Omega,\mathbb{S}) \to L^2(\Omega), \\ & \boldsymbol{\Psi} \to \operatorname{div}\operatorname{Div}\boldsymbol{\Psi} = \psi, \end{aligned} \qquad \text{with } \psi = \operatorname{div}\operatorname{Div}\boldsymbol{\Psi} = \sum_{i=1}^{d}\sum_{j=1}^{d} \frac{\partial^2 \boldsymbol{\Psi}_{ij}}{\partial x_i \partial x_j}.$$

We shall identify $\operatorname{div}\operatorname{Div}^*$

$$\begin{aligned}\operatorname{div}\operatorname{Div}^* :\ L^2(\Omega) &\to L^2(\Omega,\mathbb{S}),\\ f &\to \operatorname{div}\operatorname{Div}^* f = \boldsymbol{F},\end{aligned}$$

such that

$$\langle \operatorname{div}\operatorname{Div}\boldsymbol{\Psi}, f\rangle_{L^2(\Omega)} = \langle \boldsymbol{\Psi}, \operatorname{div}\operatorname{Div}^* f\rangle_{L^2(\Omega,\mathbb{S})}\,, \qquad \begin{aligned}&\forall\,\boldsymbol{\Psi}\in \operatorname{Dom}(\operatorname{div}\operatorname{Div})\subset L^2(\Omega,\mathbb{S})\\ &\forall\, f\in \operatorname{Dom}(\operatorname{div}\operatorname{Div}^*)\subset L^2(\Omega)\end{aligned}$$

The function has to belong to the operator domain, so for instance $f\in C_0^2(\Omega)\in\operatorname{Dom}(\operatorname{div}\operatorname{Div}^*)$ the space of twice differentiable scalar functions with compact support and $\boldsymbol{\Psi}$ can be chosen in the set $C_0^2(\Omega,\mathbb{S})\in\operatorname{Dom}(\operatorname{div}\operatorname{Div})$, the space of twice differentiable symmetric tensors with compact support on Ω. A classical result is the fact that the adjoint of the vector divergence is $\operatorname{div}^* = -\operatorname{grad}$ as stated in [KZ15]. By theorem 2, it holds $\operatorname{Div}^* = -\operatorname{Grad}$. Considering that $\operatorname{div}\operatorname{Div} = \operatorname{div}\circ\operatorname{Div}$ is the composition of two different operators and that the adjoint of a composed operator is the adjoint of each operator in reverse order, i.e. $(B\circ C)^* = C^*\circ B^*$, then it can be stated

$$(\operatorname{div}\circ\operatorname{Div})^* = \operatorname{Div}^*\circ\operatorname{div}^* = \operatorname{Grad}\circ\operatorname{grad}\,.$$

Since only formal adjoints are being looked for, this concludes the proof. □

The energy rate provides the boundary port variables

$$\begin{aligned}\dot H &= \int_\Omega \{\partial_t\alpha_w\, e_w + \partial_t \boldsymbol{A}_\kappa : \boldsymbol{E}_\kappa\}\ \mathrm{d}\Omega\\ &= \int_\Omega \{-\operatorname{div}\operatorname{Div}\boldsymbol{E}_\kappa\, e_w + \operatorname{Grad}\operatorname{grad} e_w : \boldsymbol{E}_\kappa\}\ \mathrm{d}\Omega, && \text{Stokes theorem}\\ &= \int_{\partial\Omega} \{-\boldsymbol{n}\cdot\operatorname{Div}\boldsymbol{E}_\kappa\, e_w + (\boldsymbol{n}\otimes\operatorname{grad} e_w) : \boldsymbol{E}_\kappa\}\ \mathrm{d}s,\\ &= \int_{\partial\Omega} \{-\boldsymbol{n}\cdot\operatorname{Div}\boldsymbol{E}_\kappa\, e_w + \partial_{\boldsymbol{n}} e_w\,(\boldsymbol{n}\otimes\boldsymbol{n}) : \boldsymbol{E}_\kappa + \partial_{\boldsymbol{s}} e_w\,(\boldsymbol{n}\otimes\boldsymbol{s}) : \boldsymbol{E}_\kappa\}\ \mathrm{d}s, && \text{Dyadic properties}\\ &= \int_{\partial\Omega} \{\widehat{q}_n\, w_t + \partial_{\boldsymbol{n}} w_t\, M_{nn} + \partial_{\boldsymbol{s}} w_t\, M_{ns}\}\ \mathrm{d}s.\end{aligned} \tag{4.37}$$

where s is the curvilinear abscissa, $w_t := \partial_t w$ and $\partial_{\boldsymbol{s}} w_t$ denotes the directional derivative along the tangential versor at the boundary. Additionally, the following definitions have been introduced

$$\widehat{q}_n := -\boldsymbol{n}\cdot\operatorname{Div}(\boldsymbol{E}_\kappa),\quad M_{nn} := (\boldsymbol{n}\otimes\boldsymbol{n}) : \boldsymbol{E}_\kappa,\quad M_{ns} := (\boldsymbol{n}\otimes\boldsymbol{s}) : \boldsymbol{E}_\kappa. \tag{4.38}$$

Variables w_t and $\partial_{\boldsymbol{s}} w_t$ are not independent as they are differentially related with respect to derivation along $\boldsymbol{s}$ (see for instance [TWK59, Chapter 4]). The tangential derivative has to be moved on the torsional momentum M_{ns}. For sake of simplicity, $\partial\Omega$ is supposed to be regular.

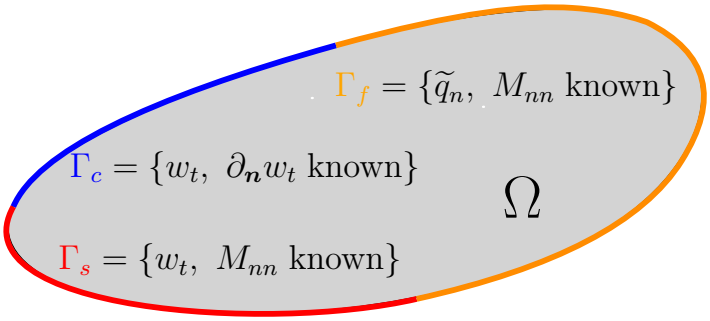

Figure 4.5: Boundary conditions for the Kirchhoff plate.

Then the integration by parts provides

$$\int_{\partial\Omega} \partial_{\boldsymbol{s}} w_t \, M_{ns} \ \mathrm{d}s = -\int_{\partial\Omega} \partial_{\boldsymbol{s}} M_{ns} \, w_t \ \mathrm{d}s. \tag{4.39}$$

The final energy balance reads

$$\dot{H} = \int_{\partial\Omega} \{w_t \, \widetilde{q}_n + \partial_{\boldsymbol{n}} w_t \, M_{nn}\} \ \mathrm{d}s, \tag{4.40}$$

where the boundary variables are

$$\text{Effective shear force} \quad \widetilde{q}_n := \widehat{q}_n - \partial_{\boldsymbol{s}} M_{ns}, \tag{4.41a}$$
$$\text{Flexural momentum} \quad M_{nn} := \boldsymbol{M} : (\boldsymbol{n} \otimes \boldsymbol{n}) = \boldsymbol{E}_\kappa : (\boldsymbol{n} \otimes \boldsymbol{n}), \tag{4.41b}$$

and $\widehat{q}_n$ is defined in (4.38). The corresponding power conjugated variables are:

$$\text{Vertical velocity} \quad w_t := \frac{\partial w}{\partial t} = e_w, \tag{4.42a}$$
$$\text{Flexural rotation} \quad \partial_{\boldsymbol{n}} w_t := \nabla e_w \cdot \boldsymbol{n}. \tag{4.42b}$$

,

Consider a partition of the boundary $\partial\Omega = \overline{\Gamma}_C \cup \overline{\Gamma}_S \cup \overline{\Gamma}_F$, $\Gamma_C \cap \Gamma_S \cap \Gamma_F = \{\emptyset\}$, where $\Gamma_C, \Gamma_S, \Gamma_F$ are open subset of $\partial\Omega$. Given definitions (4.41), (4.42), the boundary conditions for the Kirchhoff plate [GSV18] are the following (see Fig. 4.5):

- Clamped (C) on $\Gamma_C \subseteq \partial\Omega$: $w_t,\ \partial_{\boldsymbol{n}} w_t$ known;
- Simply supported (S) on $\Gamma_S \subseteq \partial\Omega$: $w_t,\ M_{nn}$ known;
- Free (F) on $\Gamma_F \subseteq \partial\Omega$: $\widetilde{q}_n,\ M_{nn}$ known.

Then the final pH formulation reads

$$\begin{aligned}
\frac{\partial}{\partial t}\begin{pmatrix}\alpha_w\\ \boldsymbol{A}_\kappa\end{pmatrix} &= \underbrace{\begin{bmatrix}0 & -\operatorname{div}\circ\operatorname{Div}\\ \operatorname{Grad}\circ\operatorname{grad} & \mathbf{0}\end{bmatrix}}_{\mathcal{J}}\begin{pmatrix}e_w\\ \boldsymbol{E}_\kappa\end{pmatrix},\\
\boldsymbol{u}_\partial &= \underbrace{\begin{bmatrix}\gamma_0^{\Gamma_C} & 0\\ \gamma_1^{\Gamma_C} & 0\\ \gamma_0^{\Gamma_S} & 0\\ 0 & \gamma_{nn}^{\Gamma_S}\\ 0 & \gamma_{nn,1}^{\Gamma_F}\\ 0 & \gamma_{nn}^{\Gamma_F}\end{bmatrix}}_{\mathcal{B}_\partial}\begin{pmatrix}e_w\\ \boldsymbol{E}_\kappa\end{pmatrix},\\
\boldsymbol{y}_\partial &= \underbrace{\begin{bmatrix}0 & \gamma_{nn,1}^{\Gamma_C}\\ 0 & \gamma_{nn}^{\Gamma_C}\\ 0 & \gamma_{nn,1}^{\Gamma_S}\\ \gamma_1^{\Gamma_S} & 0\\ \gamma_0^{\Gamma_F} & 0\\ \gamma_1^{\Gamma_F} & 0\end{bmatrix}}_{\mathcal{C}_\partial}\begin{pmatrix}e_w\\ \boldsymbol{E}_\kappa\end{pmatrix},
\end{aligned} \tag{4.43}$$

where $\gamma_0^{\Gamma_*}a = a|_{\Gamma_*}$ and $\gamma_1^{\Gamma_*}a = \partial_{\boldsymbol{n}}a|_{\Gamma_*}$ denote the trace and the normal derivative trace over the set Γ_* respectively. The symbol $\gamma_{nn,1}^{\Gamma_*}$ denotes the map $\gamma_{nn,1}^{\Gamma_*}\boldsymbol{A} = -\boldsymbol{n}\cdot\operatorname{Div}\boldsymbol{A} - \partial_{\boldsymbol{s}}(\boldsymbol{A}:(\boldsymbol{n}\otimes\boldsymbol{s}))|_{\Gamma_*},$, while $\gamma_{nn}^{\Gamma_*}\boldsymbol{A} = \boldsymbol{A}:(\boldsymbol{n}\otimes\boldsymbol{n})|_{\Gamma_*}$ indicates the normal-normal trace of a tensor-valued function. As the elasticity system (3.16) and the Mindlin plate (4.29) the boundary operators $\mathcal{B}_\partial, \mathcal{C}_\partial$ are unbounded.

Remark 11
The interconnection structure $\mathcal{J}$ in (4.43) mimics that of the Bernoulli beam [CRMPB17]. The double divergence and the Hessian coincide, in dimension one, with the second derivative.

Remark 12 (Trace operators and duality pairings for the Kirchhoff plate)
For the Kirchoff plate the integrations by parts formula leads to the following duality pairings [ACPC02, Theorem 2.2]

$$\langle\operatorname{Hess} e_w,\, \boldsymbol{E}_\kappa\rangle - \langle e_w,\, \operatorname{div}\operatorname{Div}\boldsymbol{E}_\kappa\rangle = \langle\gamma_1 e_w,\, \gamma_{nn}\boldsymbol{E}_\kappa\rangle_{H^{\frac{1}{2}}\times H^{-\frac{1}{2}}(\partial\Omega)} + \langle\gamma_0 e_w,\, \gamma_{nn,1}\boldsymbol{E}_\kappa\rangle_{H^{\frac{3}{2}}\times H^{-\frac{3}{2}}(\partial\Omega)}, \tag{4.44}$$

where $H^{\frac{1}{2}}(\partial\Omega)$, $H^{\frac{3}{2}}(\partial\Omega)$ are the spaces of traces of functions belonging to $H^1(\Omega)$ and $H^2(\Omega)$ respectively and $H^{-\frac{1}{2}}(\partial\Omega)$, $H^{-\frac{3}{2}}(\partial\Omega)$ are their topological duals.

Theorem 6 (Stokes-Dirac structure for the Kirchhoff plate)
Consider $\mathbb{S} = \mathbb{R}^{2\times 2}_{sym}$ and let $H^2(\Omega)$ be the space of functions with Hessian in $L^2(\Omega,\mathbb{S})$ and $H^{\operatorname{div}\operatorname{Div}}(\Omega,\mathbb{S})$ the space of vector-valued functions with double divergence in $L^2(\Omega)$. Consider

the definitions

$$\begin{aligned} H &:= H^2(\Omega) \times H^{\operatorname{div}\operatorname{Div}}(\Omega, \mathbb{S}), \\ F &:= L^2(\Omega) \times L^2(\Omega, \mathbb{S}), \\ V_\partial &:= H^{\frac{1}{2}}(\partial\Omega) \times H^{\frac{3}{2}}(\partial\Omega), \\ V_\partial' &:= H^{-\frac{1}{2}}(\partial\Omega) \times H^{-\frac{3}{2}}(\partial\Omega). \end{aligned}$$

The set

$$D_{\mathcal{J}} = \left\{ \begin{pmatrix} \boldsymbol{f} \\ \boldsymbol{f}_\partial \\ \boldsymbol{e} \\ \boldsymbol{e}_\partial \end{pmatrix} \mid \boldsymbol{e} \in H, \quad \boldsymbol{f} = \mathcal{J}\boldsymbol{e} \in F, \quad \boldsymbol{f}_\partial = \begin{bmatrix} \gamma_1 \\ \gamma_0 \end{bmatrix} e_w \in V_\partial, \quad \boldsymbol{e}_\partial = -\begin{bmatrix} \gamma_{nn} \\ \gamma_{nn,1} \end{bmatrix} \boldsymbol{E}_\kappa \in V_\partial' \right\}, \tag{4.45}$$

where $\boldsymbol{e} = (e_w, \boldsymbol{E}_\kappa)$ *and* $\mathcal{J}$ *is defined in* (4.43)*, is a Stokes–Dirac structure with respect to the pairing*

$$\begin{aligned} \left\langle\!\left\langle (\boldsymbol{f}^1, \boldsymbol{f}_\partial^1, \boldsymbol{e}^1, \boldsymbol{e}_\partial^1), (\boldsymbol{f}^2, \boldsymbol{f}_\partial^2, \boldsymbol{e}^2, \boldsymbol{e}_\partial^2) \right\rangle\!\right\rangle := &\left\langle \boldsymbol{f}^1, \boldsymbol{e}^2 \right\rangle_F + \left\langle \boldsymbol{f}^2, \boldsymbol{e}^1 \right\rangle_F \\ &+ \left\langle \boldsymbol{f}_\partial^1, \boldsymbol{e}_\partial^2 \right\rangle_{V_\partial \times V_\partial'} + \left\langle \boldsymbol{f}_\partial^2, \boldsymbol{e}_\partial^1 \right\rangle_{V_\partial \times V_\partial'}, \end{aligned} \tag{4.46}$$

where

$$\langle \boldsymbol{f}_\partial, \boldsymbol{e}_\partial \rangle_{V_\partial \times V_\partial'} = -\langle \gamma_1 e_w, \gamma_{nn} \boldsymbol{E}_\kappa \rangle_{H^{\frac{1}{2}} \times H^{-\frac{1}{2}}(\partial\Omega)} - \langle \gamma_0 e_w, \gamma_{nn,1} \boldsymbol{E}_\kappa \rangle_{H^{\frac{3}{2}} \times H^{-\frac{3}{2}}(\partial\Omega)}.$$

Proof. The proof is analogous to Theorem 3. The integration by parts formula (4.44) is here used. □

4.3 Laminated anisotropic plates

Until now homogeneous isotropic materials have been considered. For this class of materials, the membrane and bending problems are decoupled. In aeronautical applications, structure are made up of laminae of different materials to enhance the mechanical properties of the resulting structure. In some cases, a certain coupling is desired, to increase the aerodynamical performance of the wing as it deforms.

Consider again the deformation field given by (4.1)

$$\begin{aligned} \boldsymbol{u}(x, y, z, t) &= \boldsymbol{u}^0(x, y, t) - z\boldsymbol{\theta}(x, y, t), \\ u_z(x, y, z, t) &= u_z^0(x, y, t), \end{aligned}$$

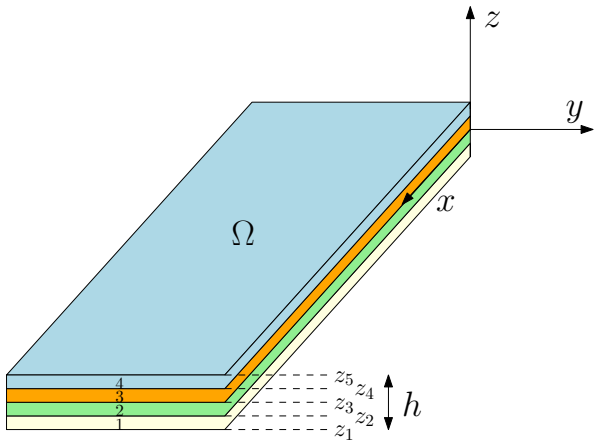

Figure 4.6: Laminated plate with 4 layers.

where $\boldsymbol{u} = (u_x, u_y)$. The link between in-plane deformation (4.2) and the membrane and bending contribution (4.4), (4.5).

$$\boldsymbol{\varepsilon}_{2D} = \boldsymbol{\varepsilon}^0 - z\boldsymbol{\kappa} \qquad \text{where} \qquad \boldsymbol{\varepsilon}^0 = \operatorname{Grad} \boldsymbol{u}^0, \quad \boldsymbol{\kappa} = \operatorname{Grad} \boldsymbol{\theta}. \tag{4.47}$$

Assume that each layer is an anisotropic material under plane stress condition. Then, it holds (see [Red03, Chapter 1] for details)

$$\boldsymbol{\Sigma}^i_{2D} = \boldsymbol{\mathcal{D}}^i_{2D} \boldsymbol{\varepsilon}^i_{2D},$$

where i indicates the layer under consideration. The matrix $\boldsymbol{\mathcal{D}}^i_{2D}$ depends on the properties of each material. To reduce the problem to bi-dimensional, the stresses have to be integrated along the thickness. Consider the membrane and bending resultant of the stress

$$\boldsymbol{N} := \sum_{i=1}^{n_{\text{layer}}} \int_{z_i}^{z_{i+1}} \boldsymbol{\Sigma}^i_{2D} \, \mathrm{d}z, \qquad \boldsymbol{M} := \sum_{i=1}^{n_{\text{layer}}} \int_{z_i}^{z_{i+1}} -z\boldsymbol{\Sigma}^i_{2D} \, \mathrm{d}z. \tag{4.48}$$

where n_{layer} is the number of layers and z_i represents the height of the i^{th} layer (see Fig. 4.6) Since the stress are discontinuous due to the change of constitutive law along the thickness, the integration has to be performed lamina-wise. Once the computations are carried out, it is found

$$\begin{pmatrix} \boldsymbol{N} \\ \boldsymbol{M} \end{pmatrix} = \begin{bmatrix} \boldsymbol{\mathcal{D}}_m & \boldsymbol{\mathcal{D}}_c \\ \boldsymbol{\mathcal{D}}_c & \boldsymbol{\mathcal{D}}_b \end{bmatrix} \begin{pmatrix} \boldsymbol{\varepsilon}^0 \\ \boldsymbol{\kappa} \end{pmatrix}, \tag{4.49}$$

where

$$\boldsymbol{\mathcal{D}}_m = \sum_{i=1}^{n_{\text{layer}}} \boldsymbol{\mathcal{D}}^i_{2D}(z_{i+1} - z_i), \quad \boldsymbol{\mathcal{D}}_c = -\frac{1}{2} \sum_{i=1}^{n_{\text{layer}}} \boldsymbol{\mathcal{D}}^i_{2D}(z^2_{i+1} - z^2_i), \quad \boldsymbol{\mathcal{D}}_b = \frac{1}{3} \sum_{i=1}^{n_{\text{layer}}} \boldsymbol{\mathcal{D}}^i_{2D}(z^3_{i+1} - z^3_i), \tag{4.50}$$

Differently from isotropic plate, for laminated anisotropic plates the membrane and bending

behavior are coupled. The coupling term $\boldsymbol{\mathcal{D}}_c$ disappears if a symmetric configuration is considered. For the shear contribution it is obtained

$$\boldsymbol{q} := \int_{-h/2}^{h/2} \boldsymbol{\sigma}_s \, \mathrm{d}z = \boldsymbol{\mathcal{D}}_s \boldsymbol{\gamma}, \qquad \text{where} \qquad \boldsymbol{\gamma} = \operatorname{grad} u_z - \boldsymbol{\theta}. \tag{4.51}$$

The tensor $\boldsymbol{\mathcal{D}}_s$ is not diagonal as in the isotropic case, cf. §4.2.1.

In the following section it is shown how anisotropic laminated plates can be formulated as pHs.

4.3.1 Port-Hamiltonian laminated Mindlin plate

For a shear deformable laminated plate the kinetic and deformation energy read

$$\begin{aligned} E_{\text{kin}} &= \frac{1}{2} \int_\Omega \left\{ \rho h \left\| \frac{\partial \boldsymbol{u}^0}{\partial t} \right\|^2 + \rho h \left(\frac{\partial u_z}{\partial t} \right)^2 + \frac{\rho h^3}{12} \left\| \frac{\partial \boldsymbol{\theta}}{\partial t} \right\|^2 \right\} \mathrm{d}\Omega, \\ E_{\text{def}} &= \frac{1}{2} \int_\Omega \left\{ \boldsymbol{N} : \boldsymbol{\varepsilon}^0 + \boldsymbol{M} : \boldsymbol{\kappa} + \boldsymbol{q} \cdot \boldsymbol{\gamma} \right\} \mathrm{d}\Omega. \end{aligned}$$

By using Hamilton's principle the equations of motion are retrieved (see [Red03, Chapter 3] for an exhaustive explanation)

$$\begin{aligned} \rho h \frac{\partial^2 \boldsymbol{u}^0}{\partial t^2} &= \operatorname{Div} \boldsymbol{N}, \\ \rho h \frac{\partial^2 u_z}{\partial t^2} &= \operatorname{div} \boldsymbol{q}, \\ \frac{\rho h^3}{12} \frac{\partial^2 \boldsymbol{\theta}}{\partial t^2} &= \operatorname{Div} \boldsymbol{M} + \boldsymbol{q}, \end{aligned} \tag{4.52}$$

where $\boldsymbol{N}$, $\boldsymbol{M}$, $\boldsymbol{q}$ are defined in Eqs. (4.49), (4.51). To get a port-Hamiltonian formulation, the following energy variables are chosen

$$\begin{aligned} \boldsymbol{\alpha}_u &= \rho h \frac{\partial \boldsymbol{u}^0}{\partial t}, & \alpha_w &= \rho h \frac{\partial u_z}{\partial t}, & \boldsymbol{\alpha}_\theta &= \frac{\rho h^3}{12} \frac{\partial \boldsymbol{\theta}}{\partial t}, \\ \boldsymbol{A}_{\varepsilon^0} &= \boldsymbol{\varepsilon}^0, & \boldsymbol{A}_\kappa &= \boldsymbol{\kappa}, & \boldsymbol{\alpha}_\gamma &= \boldsymbol{\gamma}. \end{aligned} \tag{4.53}$$

This choice highlights the nature of the problem in which the membrane part (equivalent to a 2D elasticity problem) and the bending part interact. The total energy $H = E_{\text{kin}} + E_{\text{def}}$ is now a quadratic function of the energy variables

$$\begin{aligned} E_{\text{kin}} &= \frac{1}{2} \int_\Omega \left\{ \frac{1}{\rho h} \left\| \frac{\partial \boldsymbol{\alpha}_u}{\partial t} \right\|^2 + \frac{1}{\rho h} \left(\frac{\partial \alpha_w}{\partial t} \right)^2 + \frac{12}{\rho h^3} \left\| \frac{\partial \boldsymbol{\alpha}_\theta}{\partial t} \right\|^2 \right\} \mathrm{d}\Omega, \\ E_{\text{def}} &= \frac{1}{2} \int_\Omega \left\{ (\boldsymbol{\mathcal{D}}_m \boldsymbol{A}_{\varepsilon^0} + \boldsymbol{\mathcal{D}}_c \boldsymbol{A}_\kappa) : \boldsymbol{A}_{\varepsilon^0} + (\boldsymbol{\mathcal{D}}_c \boldsymbol{A}_{\varepsilon^0} + \boldsymbol{\mathcal{D}}_b \boldsymbol{A}_\kappa) : \boldsymbol{A}_\kappa + (\boldsymbol{\mathcal{D}}_s \boldsymbol{\alpha}_\gamma) \cdot \boldsymbol{\alpha}_\gamma \right\} \mathrm{d}\Omega, \end{aligned}$$

The co-energies are equal to

$$\begin{aligned} e_w &:= \frac{\delta H}{\delta \boldsymbol{\alpha}_u} = \frac{\partial \boldsymbol{u}^0}{\partial t}, & e_w &:= \frac{\delta H}{\delta \alpha_w} = \frac{\partial u_z}{\partial t}, & \boldsymbol{e}_\theta &:= \frac{\delta H}{\delta \boldsymbol{\alpha}_\theta} = \frac{\partial \boldsymbol{\theta}}{\partial t}, \\ \boldsymbol{E}_\kappa &:= \frac{\delta H}{\delta \boldsymbol{A}_{\varepsilon^0}} = \boldsymbol{N}, & \boldsymbol{E}_\kappa &:= \frac{\delta H}{\delta \boldsymbol{A}_\kappa} = \boldsymbol{M}, & \boldsymbol{e}_\gamma &:= \frac{\delta H}{\delta \boldsymbol{\alpha}_\gamma} = \boldsymbol{q} \end{aligned} \tag{4.54}$$

The final pH formulation is found as usual considering the dynamics (4.52) and Clairaut's theorem

$$\frac{\partial}{\partial t}\begin{pmatrix} \boldsymbol{\alpha}_u \\ \alpha_w \\ \boldsymbol{\alpha}_\theta \\ \boldsymbol{A}_{\varepsilon^0} \\ \boldsymbol{A}_\kappa \\ \boldsymbol{\alpha}_\gamma \end{pmatrix} = \begin{bmatrix} \boldsymbol{0} & \boldsymbol{0} & \boldsymbol{0} & \mathrm{Div} & \boldsymbol{0} & \boldsymbol{0} \\ 0 & 0 & 0 & 0 & 0 & \mathrm{div} \\ \boldsymbol{0} & \boldsymbol{0} & \boldsymbol{0} & \boldsymbol{0} & \mathrm{Div} & \boldsymbol{I}_{2\times 2} \\ \mathrm{Grad} & \boldsymbol{0} & \boldsymbol{0} & \boldsymbol{0} & \boldsymbol{0} & \boldsymbol{0} \\ \boldsymbol{0} & \boldsymbol{0} & \mathrm{Grad} & \boldsymbol{0} & \boldsymbol{0} & \boldsymbol{0} \\ \boldsymbol{0} & \mathrm{grad} & -\boldsymbol{I}_{2\times 2} & \boldsymbol{0} & \boldsymbol{0} & \boldsymbol{0} \end{bmatrix} \begin{pmatrix} \boldsymbol{e}_u \\ e_w \\ \boldsymbol{e}_\theta \\ \boldsymbol{E}_{\varepsilon^0} \\ \boldsymbol{E}_\kappa \\ \boldsymbol{e}_\gamma \end{pmatrix}. \tag{4.55}$$

The coupling between the membrane and bending part is clear when considering the link between energy and co-energy variables

$$\begin{pmatrix} \boldsymbol{e}_u \\ e_w \\ \boldsymbol{e}_\theta \\ \boldsymbol{E}_{\varepsilon^0} \\ \boldsymbol{E}_\kappa \\ \boldsymbol{e}_\gamma \end{pmatrix} = \begin{bmatrix} \frac{1}{\rho h}\boldsymbol{I}_{2\times 2} & \boldsymbol{0} & \boldsymbol{0} & \boldsymbol{0} & \boldsymbol{0} & \boldsymbol{0} \\ 0 & \frac{1}{\rho h} & 0 & 0 & 0 & 0 \\ \boldsymbol{0} & \boldsymbol{0} & \frac{12}{\rho h^3}\boldsymbol{I}_{2\times 2} & \boldsymbol{0} & \boldsymbol{0} & \boldsymbol{0} \\ \boldsymbol{0} & \boldsymbol{0} & \boldsymbol{0} & \boldsymbol{\mathcal{D}}_m & \boldsymbol{\mathcal{D}}_c & \boldsymbol{0} \\ \boldsymbol{0} & \boldsymbol{0} & \boldsymbol{0} & \boldsymbol{\mathcal{D}}_c & \boldsymbol{\mathcal{D}}_b & \boldsymbol{0} \\ \boldsymbol{0} & \boldsymbol{0} & \boldsymbol{0} & \boldsymbol{0} & \boldsymbol{0} & \boldsymbol{\mathcal{D}}_s \end{bmatrix} \begin{pmatrix} \boldsymbol{\alpha}_u \\ \alpha_w \\ \boldsymbol{\alpha}_\theta \\ \boldsymbol{A}_{\varepsilon^0} \\ \boldsymbol{A}_\kappa \\ \boldsymbol{\alpha}_\gamma \end{pmatrix}. \tag{4.56}$$

Again appropriate boundary variables and a suitable Stokes-Dirac structure can be found for this model. The final formulation is just a superposition of systems (3.16) and (4.29).

4.3.2 Port-Hamiltonian laminated Kirchhoff plate

According to the Kirchhoff hypotheses the kinetic and deformation energies reduce to

$$\begin{aligned} E_{\mathrm{kin}} &= \frac{1}{2}\int_\Omega \left\{ \rho h \left\| \frac{\partial \boldsymbol{u}^0}{\partial t} \right\|^2 + \rho h \left(\frac{\partial u_z}{\partial t} \right)^2 \right\} \mathrm{d}\Omega, \\ E_{\mathrm{def}} &= \frac{1}{2}\int_\Omega \left\{ \boldsymbol{N} : \boldsymbol{\varepsilon}^0 + \boldsymbol{M} : \boldsymbol{\kappa} \right\} \mathrm{d}\Omega, \end{aligned}$$

where $\boldsymbol{\kappa}$ is defined in Eq. (4.5). Furthermore, as stated in Remark 8, the rotational contribution in the kinetic energy has been neglected. The equations of motion are (see [Red03, Chapter 3] for an exhaustive explanation)

$$\begin{aligned} \rho h \frac{\partial^2 \boldsymbol{u}^0}{\partial t^2} &= \mathrm{Div}\, \boldsymbol{N}, \\ \rho h \frac{\partial^2 u_z}{\partial t^2} &= -\,\mathrm{div}\,\mathrm{Div}\, \boldsymbol{M}, \end{aligned} \tag{4.57}$$

where $\boldsymbol{N}$, $\boldsymbol{M}$ are defined in Eqs. (4.49). To get a port-Hamiltonian formulation, the following energy variables are chosen

$$\begin{aligned} \boldsymbol{\alpha}_u &= \rho h \frac{\partial \boldsymbol{u}^0}{\partial t}, & \alpha_w &= \rho h \frac{\partial u_z}{\partial t}, \\ \boldsymbol{A}_{\varepsilon^0} &= \boldsymbol{\varepsilon}^0, & \boldsymbol{A}_\kappa &= \boldsymbol{\kappa}. \end{aligned} \tag{4.58}$$

The total energy $H = E_{\text{kin}} + E_{\text{def}}$ is now a quadratic function of the energy variables

$$\begin{aligned} E_{\text{kin}} &= \frac{1}{2}\int_\Omega \left\{ \frac{1}{\rho h} \left\| \frac{\partial \boldsymbol{\alpha}_u}{\partial t} \right\|^2 + \frac{1}{\rho h}\left(\frac{\partial \alpha_w}{\partial t}\right)^2 \right\} \mathrm{d}\Omega, \\ E_{\text{def}} &= \frac{1}{2}\int_\Omega \left\{ (\boldsymbol{\mathcal{D}}_m \boldsymbol{A}_{\varepsilon^0} + \boldsymbol{\mathcal{D}}_c \boldsymbol{A}_\kappa) : \boldsymbol{A}_{\varepsilon^0} + (\boldsymbol{\mathcal{D}}_c \boldsymbol{A}_{\varepsilon^0} + \boldsymbol{\mathcal{D}}_b \boldsymbol{A}_\kappa) : \boldsymbol{A}_\kappa \right\} \mathrm{d}\Omega, \end{aligned}$$

The co-energies are equal to

$$\begin{aligned} e_w &:= \frac{\delta H}{\delta \boldsymbol{\alpha}_u} = \frac{\partial \boldsymbol{u}^0}{\partial t}, & e_w &:= \frac{\delta H}{\delta \alpha_w} = \frac{\partial u_z}{\partial t}, \\ \boldsymbol{E}_\kappa &:= \frac{\delta H}{\delta \boldsymbol{A}_{\varepsilon^0}} = \boldsymbol{N}, & \boldsymbol{E}_\kappa &:= \frac{\delta H}{\delta \boldsymbol{A}_\kappa} = \boldsymbol{M}, \end{aligned} \tag{4.59}$$

The final pH formulation is found to be

$$\frac{\partial}{\partial t}\begin{pmatrix} \boldsymbol{\alpha}_u \\ \alpha_w \\ \boldsymbol{A}_{\varepsilon^0} \\ \boldsymbol{A}_\kappa \end{pmatrix} = \begin{bmatrix} \boldsymbol{0} & \boldsymbol{0} & \mathrm{Div} & \boldsymbol{0} \\ 0 & 0 & 0 & -\operatorname{div}\circ\mathrm{Div} \\ \mathrm{Grad} & \boldsymbol{0} & \boldsymbol{0} & \boldsymbol{0} \\ \boldsymbol{0} & \mathrm{Grad}\circ\operatorname{grad} & \boldsymbol{0} & \boldsymbol{0} \end{bmatrix} \begin{pmatrix} \boldsymbol{e}_u \\ e_w \\ \boldsymbol{E}_{\varepsilon^0} \\ \boldsymbol{E}_\kappa \end{pmatrix}. \tag{4.60}$$

Again, the coupling appears when considering the link between energy and co-energy variables

$$\begin{pmatrix} \boldsymbol{e}_u \\ e_w \\ \boldsymbol{E}_{\varepsilon^0} \\ \boldsymbol{E}_\kappa \end{pmatrix} = \begin{bmatrix} \frac{1}{\rho h}\boldsymbol{I}_{2\times 2} & \boldsymbol{0} & \boldsymbol{0} & \boldsymbol{0} \\ 0 & \frac{1}{\rho h} & 0 & 0 \\ \boldsymbol{0} & \boldsymbol{0} & \boldsymbol{\mathcal{D}}_m & \boldsymbol{\mathcal{D}}_c \\ \boldsymbol{0} & \boldsymbol{0} & \boldsymbol{\mathcal{D}}_c & \boldsymbol{\mathcal{D}}_b \end{bmatrix} \begin{pmatrix} \boldsymbol{\alpha}_u \\ \alpha_w \\ \boldsymbol{A}_{\varepsilon^0} \\ \boldsymbol{A}_\kappa \end{pmatrix}. \tag{4.61}$$

The energy rate provides the appropriate boundary conditions from which one can construct the Stokes-Dirac structure. The necessary computations are not performed here as the final result is just a juxtaposition of systems (3.16), (4.43).

4.4 Conclusion

In this chapter, a pH formulation for the most commonly used plate models has been detailed. Many open questions remain. In particular, how to generalize the results to shell problems, for which the domain is a surface embedded in the three dimensional space (a manifold). Computations get more involved in this case since the usage of differential geometry concepts is unavoidable. These models are important since they are widely used in the aerospace in-

dustry and ubiquitous in nature.

The reformulation of plate models using the language of differential geometry is another open research topic. Indeed, while for the Mindlin plate it should be possible to use vector-valued forms to obtain an equivalent system [Fal08], for the Kirchhoff plate higher order Stokes-Dirac structure are needed [NY04].

Chapter 5

Thermoelasticity in port-Hamiltonian form

Eh bien, mon ami, la terre sera un jour ce cadavre refroidi. Elle deviendra inhabitable et sera inhabitée comme la lune, qui depuis longtemps a perdu sa chaleur vitale.

Vingt mille lieues sous les mers
Jules Verne

Contents

Thermoelasticity is the study of deformable bodies undergoing thermal excitations. It is a clear example of a multiphysics phenomenon since the heat transfer and elastic vibrations within the body mutually interact. In this chapter, a linear model of thermoelasticity is obtained under the pH formalism. Each physics is described separately and the final system is obtained considering a power-preserving interconnection of two pHs.

5.1 Port-Hamiltonian linear coupled thermoelasticity

In this section, a pH formulation of heat transfer is first introduced. The classical model of thermoelasticity is then recalled. The same model is found by interconnecting the heat equation and the linear elastodynamics problem seen as pHs. It is shown that the interconnection

preserves a quadratic functional that plays the role of a fictitious energy. The resulting system is dissipative with respect to this functional. The construction makes use of the intrinsic modularity of pHs [KZvdSB10].

5.1.1 The heat equation as a port-Hamiltonian descriptor system

Consider the heat equation in a bounded connected set $\Omega \subset \mathbb{R}^d$, $d \in \{1, 2, 3\}$, describing the evolution of the temperature field $T(\boldsymbol{x}, t)$

$$\rho c_\epsilon \frac{\partial T}{\partial t} = k\Delta T + r_Q, \qquad \boldsymbol{x} \in \Omega, \tag{5.1}$$

where ρ, c_ϵ, k, r_Q are the mass density, the specific heat density at constant strain, the thermal diffusivity and an heat source. Symbol Δ denotes the Laplacian in $\mathbb{R}^d$. The Dirichlet and Neumann condition of this problem are

$$\begin{aligned} T \text{ known on } \Gamma_D^T, &\qquad \text{Dirichlet condition,} \\ -k \operatorname{grad} T \cdot \boldsymbol{n} \text{ known on } \Gamma_N^T, &\qquad \text{Neumann condition,} \end{aligned}$$

where a partition of the boundary $\partial\Omega = \Gamma_D^T \cup \Gamma_N^T$ has been considered. This model can be put in pH form by means of a canonical interconnection structure. An algebraic relationship that describes the Fourier law has to be incorporated in the model (cf. [Kot19, Chapter 2]). Here, a differential-algebraic formulation is exploited to obtain the same system.

Let T_0 be a constant reference temperature (the introduction of this variables is instrumental for coupled thermoelasticity). The functional

$$H_T = \frac{1}{2} \int_\Omega \rho c_\epsilon T_0 \left(\frac{T - T_0}{T_0} \right)^2 \mathrm{d}\Omega$$

has the physical dimension of an energy and represents a Lyapunov functional of this system. Even though it does not represent the internal energy, it has some important properties. Select as energy variable

$$\alpha_T := \rho c_\epsilon (T - T_0),$$

whose corresponding co-energy is

$$e_T := \frac{\delta H_T}{\delta \alpha_T} = \frac{\alpha_T}{\rho c_\epsilon T_0} = \frac{T - T_0}{T_0} =: \theta.$$

Introducing the heat flux $\boldsymbol{j}_Q := -k \operatorname{grad} T$ as additional variable, the heat equation (5.1) is

equivalently reformulated as

$$\begin{aligned} \begin{bmatrix} 1 & 0 \\ \mathbf{0} & \mathbf{0} \end{bmatrix} \frac{\partial}{\partial t} \begin{pmatrix} \alpha_T \\ \boldsymbol{j}_Q \end{pmatrix} &= \begin{bmatrix} 0 & -\operatorname{div} \\ -\operatorname{grad} & -(T_0 k)^{-1} \end{bmatrix} \begin{pmatrix} e_T \\ \boldsymbol{j}_Q \end{pmatrix} + \begin{bmatrix} 1 \\ \mathbf{0} \end{bmatrix} u_T, \\ y_T &= \begin{bmatrix} 1 & \mathbf{0} \end{bmatrix} \begin{pmatrix} e_T \\ \boldsymbol{j}_Q \end{pmatrix}. \end{aligned} \tag{5.2}$$

with $u_T := r_Q$ and y_T represents the corresponding power-conjugate variable. In matrix notation, it is obtained

$$\begin{aligned} \mathcal{E}_T \partial_t \boldsymbol{\alpha}_T &= (\mathcal{J}_T - \mathcal{R}_T)\, \boldsymbol{e}_T + \mathcal{B}_T\, u_T, \\ y_d &= \mathcal{B}_T^*\, \boldsymbol{e}_T \end{aligned} \tag{5.3}$$

where $\boldsymbol{\alpha}_T = (\alpha_T,\ \boldsymbol{j}_Q)$, $\boldsymbol{e}_T = (e_T,\ \boldsymbol{j}_Q)$ and

$$\mathcal{E}_T = \begin{bmatrix} 1 & 0 \\ \mathbf{0} & \mathbf{0} \end{bmatrix}, \quad \mathcal{J}_T = \begin{bmatrix} 0 & -\operatorname{div} \\ -\operatorname{grad} & \mathbf{0} \end{bmatrix}, \quad \mathcal{R}_T = \begin{bmatrix} 0 & 0 \\ \mathbf{0} & (T_0 k)^{-1} \end{bmatrix}, \quad \mathcal{B}_T = \begin{bmatrix} 1 \\ \mathbf{0} \end{bmatrix}.$$

The system is an example of pH descriptor system (cf. [BMXZ18] for the finite-dimensional case). The Hamiltonian reads

$$H_T = \frac{1}{2} \int_\Omega \boldsymbol{e}_T \cdot \mathcal{E}_T \boldsymbol{\alpha}_T \, \mathrm{d}\Omega. \tag{5.4}$$

The power rate is then deduced

$$\begin{aligned} \dot{H}_T &= \int_\Omega \boldsymbol{e}_T \cdot \mathcal{E}_T\, \partial_t \boldsymbol{\alpha}_T \, \mathrm{d}\Omega, \\ &= \int_\Omega \boldsymbol{e}_T \cdot \{(\mathcal{J}_T - \mathcal{R}_T)\boldsymbol{e} + \mathcal{B}_T u_T\} \, \mathrm{d}\Omega, \\ &= \int_\Omega u_T\, y_T \, \mathrm{d}\Omega - \int_\Omega \left(e_T \operatorname{div} \boldsymbol{j}_Q + \boldsymbol{j}_Q \operatorname{grad} e_T + \frac{\|\boldsymbol{j}_Q\|^2}{k T_0} \right) \mathrm{d}\Omega, \\ &\leq \int_\Omega u_T\, y_T \, \mathrm{d}\Omega - \int_{\partial\Omega} e_T\ \boldsymbol{j}_Q \cdot \boldsymbol{n} \, \mathrm{d}S. \end{aligned} \tag{5.5}$$

This choice of Hamiltonian allows retrieving the classical boundary conditions and leads to a dissipative system. Other formulations, based on an entropy or internal energy functionals, are possible for the heat equation [DMSB09, SHM19a]. These provide an accrescent or a lossless system. Unfortunately these formulations are non linear and their discretization is a difficult task [SHM19b].

5.1.2 Classical thermoelasticity

The derivation of the classical theory of thermoelasticity is not carried out here. The reader may consult in [HE09, Chapter 1] or [Abe12, Chapter 8] for a detailed discussion on this topic.

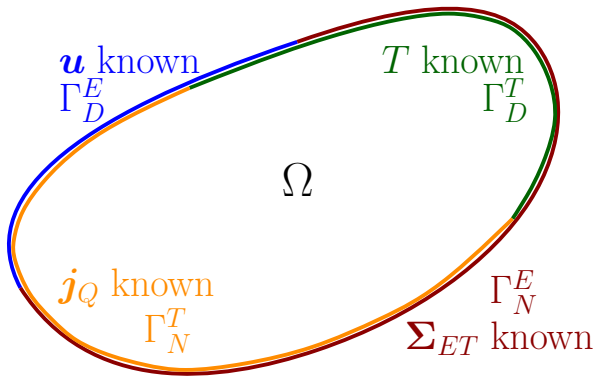

Figure 5.1: Boundary conditions for the thermoelastic problem.

Consider a bounded connected set $\Omega \subset \mathbb{R}^d$, $d \in \{1, 2, 3\}$. The classical equations for linear fully-coupled thermoelasticity for an isotropic thermoelastic material are [Bio56, Car73]

$$\begin{aligned} \rho \frac{\partial^2 \boldsymbol{u}}{\partial t^2} &= \operatorname{Div}(\boldsymbol{\Sigma}_{ET}), \\ \rho c_\epsilon \frac{\partial T}{\partial t} &= -\operatorname{div}(\boldsymbol{j}_Q) - \boldsymbol{\mathcal{C}}_\beta : \frac{\partial \boldsymbol{\varepsilon}}{\partial t}, \\ \boldsymbol{\Sigma}_{ET} &= \boldsymbol{\Sigma}_E + \boldsymbol{\Sigma}_T, \\ \boldsymbol{\Sigma}_E &= 2\mu\boldsymbol{\varepsilon} + \lambda \operatorname{Tr}(\boldsymbol{\varepsilon}) \boldsymbol{I}_{d\times d}, \\ \boldsymbol{\Sigma}_T &= -\boldsymbol{\mathcal{C}}_\beta \theta, \qquad \theta := (T - T_0)/T_0 \\ \boldsymbol{\varepsilon} &= \operatorname{Grad}(\boldsymbol{u}), \\ \boldsymbol{j}_Q &= -k \operatorname{grad} T. \end{aligned} \tag{5.6}$$

For simplicity the coupling term

$$\boldsymbol{\mathcal{C}}_\beta := T_0 \beta (2\mu + 3\lambda) \boldsymbol{I}_{d\times d}$$

has been introduced. Field $\boldsymbol{u}$ is the displacement, $\boldsymbol{\varepsilon}$ is the infinitesimal strain tensor, $\boldsymbol{\Sigma}_E, \boldsymbol{\Sigma}_T$ are the stress tensor contribution due to mechanical deformation and a thermal field. Coefficients λ, μ are the Lamé parameters, and β the thermal expansion coefficient. Given a partition of the boundary $\partial\Omega = \Gamma_D^E \cup \Gamma_N^E = \Gamma_D^T \cup \Gamma_N^T$ for the elastic and thermal domain. The general boundary conditions read (see Fig. 5.1)

$$\begin{aligned} \boldsymbol{u} \text{ known on } \Gamma_D^E \times (0, +\infty), \qquad & T \text{ known on } \Gamma_D^T \times (0, +\infty), \\ \boldsymbol{\Sigma}_{ET} \cdot \boldsymbol{n} \text{ known on } \Gamma_N^E \times (0, +\infty), \qquad & \boldsymbol{j}_Q \cdot \boldsymbol{n} \text{ known on } \Gamma_N^T \times (0, +\infty). \end{aligned} \tag{5.7}$$

In the following section an equivalent system is constructed by interconnecting the heat equation and the elastodynamics system in a structured manner.

5.1.3 Thermoelasticity as two coupled port-Hamiltonian systems

Consider again the equation of elasticity on $\Omega \subset \mathbb{R}^d$, $d \in \{1,2,3\}$ (cf. Eq. (3.16)), together with a distributed input $\boldsymbol{u}_E$ that plays the role of a distributed force

$$\begin{aligned} \frac{\partial}{\partial t}\begin{pmatrix}\boldsymbol{\alpha}_v \\ \boldsymbol{A}_\varepsilon\end{pmatrix} &= \begin{bmatrix}\mathbf{0} & \operatorname{Div} \\ \operatorname{Grad} & \mathbf{0}\end{bmatrix}\begin{pmatrix}\boldsymbol{e}_v \\ \boldsymbol{E}_\varepsilon\end{pmatrix} + \begin{bmatrix}\boldsymbol{I}_{d\times d} \\ \mathbf{0}\end{bmatrix}\boldsymbol{u}_E, \\ \boldsymbol{y}_E &= \begin{bmatrix}\boldsymbol{I}_{d\times d} & \mathbf{0}\end{bmatrix}\begin{pmatrix}\boldsymbol{e}_v \\ \boldsymbol{E}_\varepsilon\end{pmatrix}, \end{aligned} \tag{5.8}$$

with Hamiltonian

$$H_E = \frac{1}{2}\int_\Omega \{\boldsymbol{\alpha}_v \cdot \boldsymbol{e}_v + \boldsymbol{A}_\varepsilon : \boldsymbol{E}_\varepsilon\}\ \mathrm{d}\Omega.$$

Recall the pHDAE formulation of the heat equation (5.2)

$$\begin{aligned} \begin{bmatrix}1 & 0 \\ \mathbf{0} & \mathbf{0}\end{bmatrix}\frac{\partial}{\partial t}\begin{pmatrix}\alpha_T \\ \boldsymbol{j}_Q\end{pmatrix} &= \begin{bmatrix}0 & -\operatorname{div} \\ -\operatorname{grad} & -(T_0 k)^{-1}\end{bmatrix}\begin{pmatrix}e_T \\ \boldsymbol{j}_Q\end{pmatrix} + \begin{bmatrix}1 \\ \mathbf{0}\end{bmatrix}u_T, \\ y_T &= \begin{bmatrix}1 & \mathbf{0}\end{bmatrix}\begin{pmatrix}e_T \\ \boldsymbol{j}_Q\end{pmatrix}, \end{aligned} \tag{5.9}$$

with Hamiltonian H_T defined in (5.4). The linear thermoelastic problem can be expressed as a coupled port-Hamiltonian system. Consider the following interconnection

$$\boldsymbol{u}_E = -\operatorname{Div}(\boldsymbol{\mathcal{C}}_\beta\, y_T), \qquad u_T = -\boldsymbol{\mathcal{C}}_\beta : \operatorname{Grad}(\boldsymbol{y}_E). \tag{5.10}$$

The interconnection is power preserving as it can be compactly written as

$$\boldsymbol{u}_E = \mathcal{A}_\beta(y_T), \qquad u_T = -\mathcal{A}_\beta^*(\boldsymbol{y}_E), \qquad \text{where} \qquad \mathcal{A}_\beta(\cdot) = -\operatorname{Div}(\boldsymbol{\mathcal{C}}_\beta\,\cdot), \tag{5.11}$$

where $\mathcal{A}_\beta^*$ denotes the formal adjoint. The assertion is justified by the following proposition.

Proposition 5
Let $C_0^\infty(\Omega)$, $C_0^\infty(\Omega,\mathbb{R}^d)$ be the space of smooth functions and vector-valued functions respectively. Given $y_T \in C_0^\infty(\Omega)$, $\boldsymbol{y}_E \in C_0^\infty(\Omega,\mathbb{R}^d)$, the coupling operator

$$\begin{aligned} \mathcal{A}_\beta : C_0^\infty(\Omega) &\to C_0^\infty(\Omega,\mathbb{R}^d), \\ y_T &\to -\operatorname{Div}(\boldsymbol{\mathcal{C}}_\beta y_T) \end{aligned} \tag{5.12}$$

has formal adjoint

$$\begin{aligned} \mathcal{A}_\beta^* : C_0^\infty(\Omega,\mathbb{R}^d) &\to C_0^\infty(\Omega) \\ \boldsymbol{y}_E &\to +\boldsymbol{\mathcal{C}}_\beta : \operatorname{Grad}(\boldsymbol{y}_E) \end{aligned} \tag{5.13}$$

Proof. It is necessary to show

$$\langle \boldsymbol{y}_E,\, \mathcal{A}_\beta y_T\rangle_{L^2(\Omega,\mathbb{R}^d)} = \left\langle \mathcal{A}_\beta^* \boldsymbol{y}_E,\, y_T \right\rangle_{L^2(\Omega)}, \tag{5.14}$$

where for $\boldsymbol{u}_E, \boldsymbol{y}_E \in C_0^\infty(\Omega),\ u_T, y_T \in C_0^\infty(\Omega)$

$$\langle \boldsymbol{u}_E,\, \boldsymbol{y}_E \rangle_{L^2(\Omega,\mathbb{R}^d)} = \int_{\Omega_E} \boldsymbol{u}_E \cdot \boldsymbol{y}_E \,\mathrm{d}\Omega, \qquad \langle u_T,\, y_T \rangle_{L^2(\Omega)} = \int_{\Omega_T} u_T y_T \,\mathrm{d}\Omega. \tag{5.15}$$

The proof is a simple application of Theorem 8

$$\begin{aligned} \langle \boldsymbol{y}_E,\, \mathcal{A}_\beta y_T \rangle_{L^2(\Omega,\mathbb{R}^d)} &= -\int_\Omega \boldsymbol{y}_E \cdot \mathrm{Div}(\boldsymbol{\mathcal{C}}_\beta y_T) \,\mathrm{d}\Omega, \\ &= \int_\Omega \mathrm{Grad}(\boldsymbol{y}_E) : \boldsymbol{\mathcal{C}}_\beta y_T \,\mathrm{d}\Omega, \\ &= \int_\Omega \mathcal{A}_\beta^*(\boldsymbol{y}_E) y_T \,\mathrm{d}\Omega, \\ &= \left\langle \mathcal{A}_\beta^* \boldsymbol{y}_E,\, y_T \right\rangle_{L^2(\Omega)}. \end{aligned} \tag{5.16}$$

This concludes the proof. □

If the compact support assumption is removed, it is obtained

$$\begin{aligned} \langle u_T, y_T \rangle_{L^2(\Omega)} + \langle \boldsymbol{u}_E, \boldsymbol{y}_E \rangle_{L^2(\Omega,\mathbb{R}^3)} &= -\int_\Omega \{(\boldsymbol{\mathcal{C}}_\beta : \mathrm{Grad}\, \boldsymbol{e}_v) e_T + \mathrm{Div}(\boldsymbol{\mathcal{C}}_\beta e_T) \cdot \boldsymbol{e}_v\} \,\mathrm{d}\Omega, \\ &= -\int_\Omega \mathrm{div}(e_T \boldsymbol{\mathcal{C}}_\beta \cdot \boldsymbol{e}_v) \,\mathrm{d}\Omega, \\ &= -\int_{\partial\Omega} (e_T \boldsymbol{\mathcal{C}}_\beta \cdot \boldsymbol{n}) \cdot \boldsymbol{e}_v \,\mathrm{d}S. \end{aligned} \tag{5.17}$$

Using the expression of $y_T, \boldsymbol{y}_E$, considering that T_0 is constant and applying Schwarz theorem for smooth function, the inputs are equal to

$$\boldsymbol{u}_E = \mathrm{Div}(\boldsymbol{\Sigma}_T), \qquad u_T = -\boldsymbol{\mathcal{C}}_\beta : \mathrm{Grad}(\boldsymbol{v}) = -\boldsymbol{\mathcal{C}}_\beta : \frac{\partial \boldsymbol{\varepsilon}}{\partial t}.$$

The coupled thermoelastic problem can now be written as

$$\begin{bmatrix} \mathbf{1} & \mathbf{0} & \mathbf{0} & \mathbf{0} \\ \mathbf{0} & \mathbf{1} & \mathbf{0} & \mathbf{0} \\ 0 & 0 & 1 & 0 \\ \mathbf{0} & \mathbf{0} & \mathbf{0} & \mathbf{0} \end{bmatrix} \frac{\partial}{\partial t} \begin{pmatrix} \boldsymbol{\alpha}_v \\ \boldsymbol{A}_\varepsilon \\ \alpha_T \\ \boldsymbol{j}_Q \end{pmatrix} = \begin{bmatrix} \mathbf{0} & \mathrm{Div} & \mathcal{A}_\beta & \mathbf{0} \\ \mathrm{Grad} & \mathbf{0} & \mathbf{0} & \mathbf{0} \\ -\mathcal{A}_\beta^* & 0 & 0 & -\mathrm{div} \\ \mathbf{0} & \mathbf{0} & -\mathrm{grad} & -(T_0 k)^{-1} \end{bmatrix} \begin{pmatrix} \boldsymbol{e}_v \\ \boldsymbol{E}_\varepsilon \\ e_T \\ \boldsymbol{j}_Q \end{pmatrix}, \tag{5.18}$$

with total energy given by $H = H_E + H_T$. The power balance for each subsystem is given by

$$\dot{H}_E = \int_\Omega \boldsymbol{u}_E \cdot \boldsymbol{y}_E \,\mathrm{d}\Omega + \int_{\partial\Omega} \boldsymbol{e}_v \cdot (\boldsymbol{E}_\varepsilon \cdot \boldsymbol{n}) \,\mathrm{d}S, \tag{5.19}$$

$$\dot{H}_T \leq \int_\Omega u_T\ y_T \,\mathrm{d}\Omega - \int_{\partial\Omega} \theta\ \boldsymbol{j}_Q \cdot \boldsymbol{n} \,\mathrm{d}S, \tag{5.20}$$

The overall power balance is easily computed considering Eqs. (5.19) (5.20) and (5.17)

$$\dot{H} = \dot{H}_E + \dot{H}_T \leq \int_{\partial\Omega} \{[\boldsymbol{E}_\varepsilon - e_T \boldsymbol{\mathcal{C}}_\beta] \cdot \boldsymbol{n}\} \cdot \boldsymbol{e}_v \, \mathrm{d}S - \int_{\partial\Omega} e_T \, \boldsymbol{j}_Q \cdot \boldsymbol{n} \, \mathrm{d}S. \tag{5.21}$$

This result is the same stated in [Car73, page 332]. From the power balance the classical boundary conditions are retrieved. This allows defining appropriate boundary operators for the thermoelastic problem

$$\boldsymbol{u}_\partial = \underbrace{\begin{bmatrix} \boldsymbol{\gamma}_0^{\Gamma_D^E} & \mathbf{0} & \mathbf{0} & \mathbf{0} \\ \mathbf{0} & \boldsymbol{\gamma}_n^{\Gamma_N^E} & -\boldsymbol{\gamma}_n^{\Gamma_N^E}(\boldsymbol{\mathcal{C}}_\beta \cdot) & \mathbf{0} \\ 0 & 0 & \gamma_0^{\Gamma_D^T} & 0 \\ \mathbf{0} & \mathbf{0} & \mathbf{0} & \boldsymbol{\gamma}_n^{\Gamma_N^T} \end{bmatrix}}_{\mathcal{B}_\partial} \begin{pmatrix} \boldsymbol{e}_v \\ \boldsymbol{E}_\varepsilon \\ e_T \\ \boldsymbol{j}_Q \end{pmatrix}, \quad \boldsymbol{y}_\partial = \underbrace{\begin{bmatrix} \mathbf{0} & \boldsymbol{\gamma}_n^{\Gamma_D^E} & -\boldsymbol{\gamma}_n^{\Gamma_D^E}(\boldsymbol{\mathcal{C}}_\beta \cdot) & \mathbf{0} \\ \boldsymbol{\gamma}_0^{\Gamma_N^E} & \mathbf{0} & \mathbf{0} & \mathbf{0} \\ \mathbf{0} & \mathbf{0} & \mathbf{0} & \boldsymbol{\gamma}_n^{\Gamma_D^T} \\ 0 & 0 & \gamma_0^{\Gamma_N^T} & 0 \end{bmatrix}}_{\mathcal{C}_\partial} \begin{pmatrix} \boldsymbol{e}_v \\ \boldsymbol{E}_\varepsilon \\ e_T \\ \boldsymbol{j}_Q \end{pmatrix}. \tag{5.22}$$

System (5.18) together with (5.22) is a pH system with boundary control and observation. Indeed, the classical thermoelastic problem can be modeled as two coupled systems, demonstrating the modularity of the pH paradigm.

Remark 13
Notice that the boundary operators in Eq. (5.22) contains a coupling between the thermal and mechanical variables. This is due to the fact that the coupling operator $\mathcal{A}_\beta$ is of differential kind.

5.2 Thermoelastic port-Hamiltonian bending

In this section, the thermoelastic bending of thin beam and plate structures is described as coupled interconnection of pHs. Starting from classical thermoelastic models a suitable pH formulation can be obtained. This couples a mechanical system defined on a reduced domain (uni-dimensional for beams, bi-dimensional for plates), to a thermal domain defined in the three-dimensional space.

5.2.1 Thermoelastic Euler-Bernoulli beam

The model for the linear thermoelastic vibrations of an isotropic thin rod is detailed in [Cha62, LR00]. The domain of the beam is uni-dimensional $\Omega_E = \{0, L\}$, while the thermal domain is three-dimensional $\Omega_T = \{0, L\} \times S$, where S is the set representing the beam cross section. The set S is assumed to constant along the axis for simplicity. The ruling equations

are

$$\begin{aligned} \rho A \frac{\partial^2 w}{\partial t^2} &= -EI \frac{\partial^4 w}{\partial x^4} - \beta E T_0 \frac{\partial^2}{\partial x^2} \int_S z\theta \, \mathrm{d}x \, \mathrm{d}y, \qquad x \in \{0, L\} = \Omega_E, \\ \rho c_{\epsilon,B} T_0 \frac{\partial \theta}{\partial t} &= k T_0 \Delta \theta + \beta T_0 E z \frac{\partial^3 w}{\partial x^2 \partial t}, \qquad (x, y, z) \in \Omega_E \times S = \Omega_T, \end{aligned} \tag{5.23}$$

where $w(x,t)$ is the vertical displacement of the beam $I = \int_S z^2 \, \mathrm{d}x \, \mathrm{d}y$ the second moment of area, E the Young modulus and A the cross section. The constant $c_{\epsilon,B}$ is due to the thermoelastic coupling (cf. [Cha62, LR00] for a detailed explanation). The other terms have meaning than in §5.1. Since the normalized temperature $\theta(x,y,z,t)$ depends on all spatial coordinates, the symbol $\Delta = \partial_{xx} + \partial_{yy} + \partial_{zz}$ is the Laplacian in three dimensions. The physical parameters are assumed to be constant for simplicity.

The coupling operator is defined as

$$\mathcal{A}_{\beta,B}(y_T) := -\beta E T_0 \partial_{xx} \left(\int_S z y_T \, \mathrm{d}x \, \mathrm{d}y \right). \tag{5.24}$$

To unveil an interconnection that is power-preserving with respect to a certain function, the formal adjoint of the coupling operator is needed.

Proposition 6
Let $C_0^\infty(\Omega_T)$, $C_0^\infty(\Omega_E)$ be the space of smooth functions with compact support defined on Ω_T and Ω_E respectively. Given $y_T \in C_0^\infty(\Omega_T)$, $y_E \in C_0^\infty(\Omega_E)$ the formal adjoint of the coupling operator is

$$\mathcal{A}^*_{\beta,B}(y_E) = -\beta E T_0 z \, \partial_{xx} y_E. \tag{5.25}$$

Proof. The formal adjoint is defined by the relation

$$\langle y_E, \mathcal{A}_{\beta,B} y_T \rangle_{L^2(\Omega_E)} = \left\langle \mathcal{A}^*_{\beta,B} y_E, y_T \right\rangle_{L^2(\Omega_T)}, \tag{5.26}$$

where for $u_E, y_E \in C_0^\infty(\Omega_E)$, $u_T, y_T \in C_0^\infty(\Omega_T)$

$$\langle u_E, y_E \rangle_{L^2(\Omega_E)} = \int_{\Omega_E} u_E y_E \, \mathrm{d}x, \qquad \langle u_T, y_T \rangle_{L^2(\Omega_T)} = \int_{\Omega_T} y_T y_T \, \mathrm{d}x \, \mathrm{d}y \, \mathrm{d}z. \tag{5.27}$$

Using Def. (5.24) and the integration by parts, one finds

$$\begin{aligned} \langle y_E, \mathcal{A}_{\beta,B} y_T \rangle_{L^2(\Omega_E)} &= \int_{\Omega_E} y_E \mathcal{A}_{\beta,B} y_T \, \mathrm{d}x, \\ &= -\int_{\Omega_E} y_E \beta E T_0 \partial_{xx} \left(\int_S z y_T \, \mathrm{d}y \, \mathrm{d}z \right) \mathrm{d}x, \\ &= -\int_{\Omega_E} (\partial_{xx} y_E) \beta E T_0 \left(\int_S z y_T \, \mathrm{d}y \, \mathrm{d}z \right) \mathrm{d}x, \end{aligned} \tag{5.28}$$

Since $\Omega_T = \Omega_E \times S$ and from the properties of multiple integrals, it is found

$$\begin{aligned} -\int_{\Omega_E} \partial_{xx}(y_E)\beta E T_0 \left(\int_S z\, y_T \,\mathrm{d}y\,\mathrm{d}z\right) \mathrm{d}x &= -\int_{\Omega_E}\int_S (\partial_{xx} y_E)\beta E T_0 z\, y_T \,\mathrm{d}x\,\mathrm{d}y\,\mathrm{d}z, \\ &= -\int_{\Omega_T} (\partial_{xx} y_E)\beta E T_0 z\, y_T \,\mathrm{d}x\,\mathrm{d}y\,\mathrm{d}z, \\ &= \left\langle \mathcal{A}^*_{\beta,B} y_E,\, y_T \right\rangle_{L^2(\Omega_T)}. \end{aligned} \tag{5.29}$$

This concludes the proof. □

Using Eqs. (5.24) and (5.25), System (5.23), is rewritten as

$$\begin{aligned} \rho A \frac{\partial^2 w}{\partial t^2} &= -EI\frac{\partial^4 w}{\partial x^4} + \mathcal{A}_{\beta,B}\theta, \\ \rho c_{\epsilon,B} T_0 \frac{\partial \theta}{\partial t} &= kT_0 \Delta\theta - \mathcal{A}^*_{\beta,B}\frac{\partial w}{\partial t}. \end{aligned} \tag{5.30}$$

Consider the Hamiltonian functional

$$H = H_E + H_T = \frac{1}{2}\int_{\Omega_E} \left\{ \rho A \left(\frac{\partial w}{\partial t}\right)^2 + EI\left(\frac{\partial^2 w}{\partial x^2}\right)^2 \right\} \mathrm{d}x + \frac{1}{2}\int_{\Omega_T} \rho c_{\epsilon,B} T_0 \theta^2 \,\mathrm{d}x\,\mathrm{d}y\,\mathrm{d}z. \tag{5.31}$$

The energy variables are chosen to make the Hamiltonian functional quadratic

$$\alpha_w = \rho A \partial_t w, \qquad \alpha_\kappa = \partial_{xx} w, \qquad \alpha_T = \rho c_{\epsilon,B} T_0 \theta. \tag{5.32}$$

The corresponding co-energy variables evaluate to

$$e_w := \frac{\delta H}{\delta \alpha_w} = \partial_t w, \qquad e_\kappa := \frac{\delta H}{\delta \alpha_\kappa} = EI\partial_{xx} w, \qquad e_T := \frac{\delta H}{\delta \alpha_T} = \theta. \tag{5.33}$$

System (5.30) can now be rewritten as

$$\begin{bmatrix} 1 & 0 & 0 & 0 \\ 0 & 1 & 0 & 0 \\ 0 & 0 & 1 & 0 \\ \mathbf{0} & \mathbf{0} & \mathbf{0} & \mathbf{0} \end{bmatrix} \frac{\partial}{\partial t} \begin{pmatrix} \alpha_w \\ \alpha_\kappa \\ \alpha_T \\ \boldsymbol{j}_Q \end{pmatrix} = \begin{bmatrix} 0 & -\partial_{xx} & \mathcal{A}_{\beta,B} & 0 \\ \partial_{xx} & 0 & 0 & 0 \\ -\mathcal{A}^*_{\beta,B} & 0 & 0 & -\operatorname{div} \\ \mathbf{0} & \mathbf{0} & -\operatorname{grad} & -(kT_0)^{-1} \end{bmatrix} \begin{pmatrix} e_w \\ e_\kappa \\ e_T \\ \boldsymbol{j}_Q \end{pmatrix}, \tag{5.34}$$

This system is the equivalent of (5.18) for bending of beams. Hence, following the same reasoning, it can be obtained starting from each subsystem in pH form by means of an appropriate interconnection.

5.2.2 Thermoelastic Kirchhoff plate

For the bending of thin plate, several different models have been proposed [Cha62, Lag89, Sim99, Nor06]. Here, the Chadwick model [Cha62] is considered. The thin plate occupies the

open connected set $\Omega_E \times \left\{-\frac{h}{2}, \frac{h}{2}\right\}$, where h is the plate thickness. The system of equations describe the midplane vertical displacement and the evolution of the temperature in the 3D domain

$$\begin{aligned} \rho h \frac{\partial^2 w}{\partial t^2} &= -D_b \Delta_{2D}^2 w - \frac{\beta T_0 E}{1-\nu} \Delta_{2D} \left(\int_{-h/2}^{h/2} z\theta \, \mathrm{d}z \right), && (x,y) \in \Omega_E, \\ \rho c_{\epsilon,P} T_0 \frac{\partial \theta}{\partial t} &= -k T_0 \Delta_{3D} + \frac{\beta T_0 E z}{1-\nu} \Delta_{2D} \left(\frac{\partial w}{\partial t} \right), && (x,y,z) \in \Omega_E \times \left\{-\frac{h}{2}, \frac{h}{2}\right\} = \Omega_T, \end{aligned} \tag{5.35}$$

where $w(x,y,t)$ is the vertical deflection, $D_b = \frac{Eh^3}{12(1-\nu^2)}$ the bending rigidity (cf. Eq. (4.11)), ν the Poisson modulus and $c_{\epsilon,P}$ a constant (depending on the heat capacity at constant strain and other coupling parameters, cf. [Cha62]). Symbols $\Delta_{2D} = \partial_{xx} + \partial_{yy}$, $\Delta_{3D} = \partial_{xx} + \partial_{yy} + \partial_{zz}$ are the two- and three-dimensional Laplacian.

The coupling operator is here defined as

$$\mathcal{A}_{\beta,P}(y_T) := -\frac{\beta T_0 E}{1-\nu} \Delta_{2D} \left(\int_{-h/2}^{h/2} z y_T \, \mathrm{d}z \right). \tag{5.36}$$

Analouglsy with respect to the Euler-Bernoulli beam its formal adjoint is sought for.

Proposition 7
Let $C_0^\infty(\Omega_T)$, $C_0^\infty(\Omega_E)$ be the space of smooth functions with compact support defined on Ω_T and Ω_E respectively. Given $y_T \in C_0^\infty(\Omega_T)$, $y_E \in C_0^\infty(\Omega_E)$ the formal adjoint of the coupling operator is

$$\mathcal{A}_{\beta,B}^*(y_E) = -\frac{\beta T_0 E z}{1-\nu} \Delta_{2D} y_E. \tag{5.37}$$

Proof. The proof is completely identical to Prop. 6. □

System 5.35 is rewritten as

$$\begin{aligned} \rho h \frac{\partial^2 w}{\partial t^2} &= -D_b \Delta_{2D}^2 w + \mathcal{A}_{\beta,P} \theta, \\ \rho c_{\epsilon,P} T_0 \frac{\partial \theta}{\partial t} &= -k T_0 \Delta_{3D} \theta - \mathcal{A}_{\beta,P}^* \left(\frac{\partial w}{\partial t} \right), \end{aligned} \tag{5.38}$$

The Hamiltonian functional equals

$$\begin{aligned} H = H_E + H_T =& \frac{1}{2} \int_{\Omega_E} \left\{ \rho h \left(\frac{\partial w}{\partial t} \right)^2 + (\boldsymbol{\mathcal{D}}_b \mathrm{Hess}_{2D} w) : \mathrm{Hess}_{2D} w \right\} \mathrm{d}x \, \mathrm{d}y \\ &+ \frac{1}{2} \int_{\Omega_T} \rho c_{\epsilon,P} T_0 \theta^2 \, \mathrm{d}x \, \mathrm{d}y \, \mathrm{d}z, \end{aligned} \tag{5.39}$$

where Hess_{2D} is the Hessian in two dimensions and $\boldsymbol{\mathcal{D}}_b$ was defined in (4.11) (cf. §4.1.1). The

energy and co-energy variables are

$$\begin{aligned} \alpha_w &= \rho h \partial_t w, & \boldsymbol{A}_\kappa &= \mathrm{Hess}_{2D} w, & \alpha_T &= \rho c_{\epsilon,P} T_0 \theta, \\ e_w &= \partial_t w, & \boldsymbol{E}_\kappa &= \boldsymbol{\mathcal{D}}_b \mathrm{Hess}_{2D} w, & e_T &= \theta. \end{aligned} \tag{5.40}$$

System (5.38) is rewritten as

$$\begin{bmatrix} 1 & 0 & 0 & 0 \\ \mathbf{0} & \mathbf{1} & \mathbf{0} & \mathbf{0} \\ 0 & 0 & 1 & 0 \\ \mathbf{0} & \mathbf{0} & \mathbf{0} & \mathbf{0} \end{bmatrix} \frac{\partial}{\partial t} \begin{pmatrix} \alpha_w \\ \boldsymbol{A}_\kappa \\ \alpha_T \\ \boldsymbol{j}_Q \end{pmatrix} = \begin{bmatrix} 0 & -\operatorname{div} \mathrm{Div}_{2D} & \mathcal{A}_{\beta,P} & 0 \\ \mathrm{Hess}_{2D} & \mathbf{0} & \mathbf{0} & 0 \\ -\mathcal{A}^*_{\beta,P} & 0 & 0 & -\operatorname{div}_{3D} \\ \mathbf{0} & \mathbf{0} & -\operatorname{grad}_{3D} & -(kT_0)^{-1} \end{bmatrix} \begin{pmatrix} e_w \\ \boldsymbol{E}_\kappa \\ e_T \\ \boldsymbol{j}_Q \end{pmatrix}, \tag{5.41}$$

The subscript $2D$, $3D$ refers to two- and three-dimensional operators respectively. The final system reproduces the same structured coupling already observed for (5.18), (5.34).

Remark 14
The thermoelastic bending can be reduced to two problems defined on the same domain (cf. [HZ97] for beams and [AL00] for plates) by introducing the following approximation of the temperature field

$$\theta(x, y, z) = \theta_0 + z\theta_1, \tag{5.42}$$

where $\theta_0 = \theta_0(x)$, $\theta_1 = \theta_1(x)$ for beams and $\theta_0 = \theta_0(x, y)$, $\theta_1 = \theta_1(x, y)$ for plates. However, this introduces a strong simplification as the thermal phenomena typically occur in the whole three-dimensional space.

5.3 Conclusion

In this chapter, it was shown classical linear thermoelastic problem are equivalent to two coupled port-Hamiltonian systems. This is especially interesting for the simulation of thermoelastic phenomena: each subsystem can be discretized separately and then coupled to the other using the discretized coupling operator. This allows to track easily how the energy flows within the two physics. To assess the validity of the models proposed in this chapter, in Chapter 8 the numerical discretization of the Danilovskaya problem [Dan50] written in pH form is performed.

Part III

Finite element structure preserving discretization

Chapter 6

Partitioned finite element method

Every truth is simple... is that not doubly a lie?

Twilight of the Idols
Friedrich Nietzsche

Contents

Discretization is the process of transferring continuous models into discrete counterparts. The discrete model should be faithful to the continuous one. To this aim, it is usually essential that the main properties of the continuous system be preserved at the discrete level. An algorithm that is capable of conserving properties in terms of structure only is called structure-preserving [CMKO11]. In this chapter, a method to spatially discretize infinite-dimensional pHs into finite-dimensional ones in a structure-preserving manner is illustrated.

6.1 Discretization under uniform boundary condition

A discrete version of a infinite-dimensional pH system is meant to preserve the underlying properties related to power continuity. To achieve this purpose, the discretization procedure consists of two steps [KML18]:

- Finite-dimensional approximation of the Stokes-Dirac structure, i.e. the formally skew symmetric differential operator that defines the structure. The duality of the power variables has to be mapped onto the finite approximation. The subspace of the discrete variables will be represented by a Dirac structure.
- The Hamiltonian requires as well a suitable discretization, which gives rise to a discrete Hamiltonian.

A structure-preserving discretization is able to construct an equivalent pH system that possesses the structural properties of the original model:

Infinite-dimensional pH system

PDE with distributed inputs:

$$\frac{\partial \boldsymbol{\alpha}}{\partial t}(\boldsymbol{x},t) = \mathcal{J}\frac{\delta H}{\delta \boldsymbol{\alpha}} + \mathcal{B}\boldsymbol{u}_\Omega(\boldsymbol{x},t),$$
$$\boldsymbol{y}_\Omega(\boldsymbol{x},t) = \mathcal{B}^*\frac{\delta H}{\delta \boldsymbol{\alpha}}.$$

Boundary conditions:

$$\boldsymbol{u}_\partial = \mathcal{B}_\partial\frac{\delta H}{\delta \boldsymbol{\alpha}}, \quad \boldsymbol{y}_\partial = \mathcal{C}_\partial\frac{\delta H}{\delta \boldsymbol{\alpha}}.$$

Power balance (Stokes Theorem):

$$\dot{H} = \int_{\partial\Omega} \boldsymbol{u}_\partial \cdot \boldsymbol{y}_\partial \,\mathrm{d}S + \int_\Omega \boldsymbol{u}_\Omega \cdot \boldsymbol{y}_\Omega \,\mathrm{d}\Omega.$$

Structure-preserving discretization

Resulting ODE:

$$\dot{\boldsymbol{\alpha}}_d = \mathbf{J}\nabla H_d + \mathbf{B}_\Omega \mathbf{u}_\Omega + \mathbf{B}_\partial \mathbf{u}_\partial,$$
$$\mathbf{y}_\Omega = \mathbf{B}_\Omega^\top \nabla H_d,$$
$$\mathbf{y}_\partial = \mathbf{B}_\partial^\top \nabla H_d.$$

Discretized Hamiltonian:

$$H_d := H(\boldsymbol{\alpha} \equiv \boldsymbol{\alpha}_d).$$

Power balance:

$$\dot{H} = \mathbf{u}_\partial^\top \mathbf{y}_\partial + \mathbf{u}_\Omega^\top \mathbf{y}_\Omega.$$

In this thesis the Partitioned Finite Element Method (PFEM), originally presented in [CRML18, CRML19], is chosen to obtain discretized models of dpHs. Variational finite element method has been extensively used for discretizing closed linear hyperbolic systems [Jol03]. It will be shown that PFEM extends the framework detailed in [Jol03] to open (i.e. boundary controlled) Hamiltonian systems. Furthermore, it is also applicable to non-linear systems §6.1.2 and parabolic systems §8.3 (see also [SHM19a, SHM19b]). This discretization procedure boils down to three simple steps

1. The system is written in weak form;
2. An integration by parts is applied to highlight the appropriate boundary control;
3. A Galerkin method is employed to obtain a finite-dimensional system. For the approximation basis the finite element method is here employed but spectral methods can be used as well.

Once the system has been put into weak form, a subset of the equations is integrated by parts, so that boundary variables are naturally included into the formulation and appear

as control inputs, the collocated outputs being defined accordingly. The discretization of energy and co-energy variables (and the associated test functions) leads directly to a full rank representation for the finite-dimensional pH system. This approach makes possible the usage of FEM softwares, like FEniCS [LMW+12], or Firedrake [RHM+17]. The procedure is universal, as it relies on a general integration by parts formula that characterizes multi-dimensional pHs. This is why the methodology is illustrated in all its generality and then detailed for some particular examples of interest:

1. in §6.1.1 the 2D non-linear irrotational shallow water equations;
2. the Euler-Bernoulli beam in §6.1.4.1;
3. the Kirchhoff plate in §6.1.4.2;
4. in §6.1.4.3 the Mindlin plate.

This methodology is easily applicable under a uniform causality assumption. The case of mixed boundary conditions requires additional care and will be treated in the subsequent §6.2.

6.1.1 General procedure

Given an open connected set $\Omega \in \mathbb{R}^d$, $d \in \{1, 2, 3\}$, consider a generic pH system defined on Ω

$$\partial_t \boldsymbol{\alpha} = \mathcal{J}\boldsymbol{e}, \qquad \boldsymbol{\alpha} \in L^2(\Omega, \mathbb{F}), \quad \mathcal{J} : L^2(\Omega, \mathbb{F}) \to L^2(\Omega, \mathbb{F}) |\ \mathcal{J} = -\mathcal{J}^*, \tag{6.1a}$$

$$\boldsymbol{e} := \delta_{\boldsymbol{\alpha}} H, \qquad \boldsymbol{e} \in H^{\mathcal{J}} := \left\{ \boldsymbol{e} \in L^2(\Omega, \mathbb{F}) |\ \mathcal{J}\boldsymbol{e} \in L^2(\Omega, \mathbb{F}) \right\}, \tag{6.1b}$$

$$\boldsymbol{u}_\partial = \mathcal{B}_\partial \boldsymbol{e}, \qquad \boldsymbol{u}_\partial \in L^2(\partial\Omega, \mathbb{R}^m), \tag{6.1c}$$

$$\boldsymbol{y}_\partial = \mathcal{C}_\partial \boldsymbol{e}, \qquad \boldsymbol{y}_\partial \in L^2(\partial\Omega, \mathbb{R}^m). \tag{6.1d}$$

The operator $\mathcal{J} : L^2(\Omega, \mathbb{F}) \to L^2(\Omega, \mathbb{F})$ is a differential, formally skew adjoint operator $\mathcal{J} = -\mathcal{J}^*$ over the space $L^2(\Omega, \mathbb{F})$. The set $\mathbb{F}$ is an appropriate Cartesian product of either scalar, vectorial or tensorial quantities. Its precise definition depends on the example upon consideration. It is assumed that the boundary variables belong to an L^2 space over the boundary. This simplification comes in handy when finite element approximations are sought for. Indeed the boundary variables belongs to more complicated spaces (cf. Remarks 6, 10, 12).

For scalars $(a, b) \in L^2(\Omega)$, vectors $(\boldsymbol{a}, \boldsymbol{b}) \in L^2(\Omega, \mathbb{R}^d)$ and tensors $(\boldsymbol{A}, \boldsymbol{B}) \in L^2(\Omega, \mathbb{R}^{d\times d})$ the L^2 inner product is given by

$$\langle a,\, b\rangle_{L^2(\Omega)} = \int_\Omega ab \,\mathrm{d}\Omega, \qquad \langle \boldsymbol{a},\, \boldsymbol{b}\rangle_{L^2(\Omega,\mathbb{R}^d)} = \int_\Omega \boldsymbol{a}\cdot\boldsymbol{b} \,\mathrm{d}\Omega, \qquad \langle \boldsymbol{A},\, \boldsymbol{B}\rangle_{L^2(\Omega,\mathbb{R}^{d\times d})} = \int_\Omega \boldsymbol{A} : \boldsymbol{B} \,\mathrm{d}\Omega. \tag{6.2}$$

For scalars $a_\partial, b_\partial \in L^2(\partial\Omega)$ and vectors $\boldsymbol{a}_\partial, \boldsymbol{b}_\partial \in L^2(\partial\Omega, \mathbb{R}^m)$ defined on the boundary the inner product is defined as

$$\langle a_\partial,\, b_\partial \rangle_{L^2(\partial\Omega)} = \int_{\partial\Omega} a_\partial b_\partial \,\mathrm{d}S, \qquad \langle \boldsymbol{a}_\partial,\, \boldsymbol{b}_\partial \rangle_{L^2(\partial\Omega,\mathbb{R}^m)} = \int_{\partial\Omega} \boldsymbol{a}_\partial \cdot \boldsymbol{b}_\partial \,\mathrm{d}S. \tag{6.3}$$

The Hamiltonian functional of Eq. (6.1b) is allowed to be non-linear in the energy variables

$$H = \int_\Omega \mathcal{H}(\boldsymbol{\alpha}) \,\mathrm{d}\Omega,$$

where $\mathcal{H}(\boldsymbol{\alpha}) : L^2(\Omega, \mathbb{F}) \to \mathbb{R}$ is a non-linear function.

To apply this methodology the non-linearities are restricted to the Hamiltonian and a uniform causality condition is supposed to characterize the system. By uniform causality condition we mean the imposition of a single type of boundary condition [Kot19] (as opposed to the mixed boundary conditions case). It is required as well that the system admits a partition of the variables. This requirement is always encountered in the following examples. These hypotheses are summarized in the following assumptions.

Assumption 2 (Partitioning of the system)
Consider system (6.1a). It is assumed that the Hilbert space $L^2(\Omega, \mathbb{F}) := L^2(\Omega, \mathbb{F})$ admits the splitting $L^2(\Omega, \mathbb{F}) = L^2(\Omega, \mathbb{A}) \times L^2(\Omega, \mathbb{B})$ This means that $\mathbb{F} = \mathbb{A} \times \mathbb{B}$.

The operator $\mathcal{J}$ is assumed to be skew-symmetric (or formally skew-adjoint) on $L^2(\Omega, \mathbb{F})$ and linear:

$$\mathcal{J} = \mathcal{J}_a + \mathcal{J}_d, \tag{6.4}$$

where $\mathcal{J}_a$ is the algebraic contribution (a skew-symmetric matrix) and $\mathcal{J}_d$ the differential contribution. The algebraic part is assumed to take the form

$$\mathcal{J}_a = \begin{bmatrix} 0 & -\boldsymbol{L}^\top \\ \boldsymbol{L} & 0 \end{bmatrix}, \qquad \begin{aligned} \boldsymbol{L}^\top &: L^2(\Omega, \mathbb{B}) \to L^2(\Omega, \mathbb{A}), \\ \boldsymbol{L} &: L^2(\Omega, \mathbb{A}) \to L^2(\Omega, \mathbb{B}), \end{aligned} \tag{6.5}$$

where $\boldsymbol{L}$ is a bounded operator. Analogously, the linear differential operator $\mathcal{J}_d$ is assumed to be of the form

$$\mathcal{J}_d = \begin{bmatrix} 0 & -\mathcal{L}^* \\ \mathcal{L} & 0 \end{bmatrix}, \qquad \begin{aligned} \mathcal{L}^* &: L^2(\Omega, \mathbb{B}) \to L^2(\Omega, \mathbb{A}), \\ \mathcal{L} &: L^2(\Omega, \mathbb{A}) \to L^2(\Omega, \mathbb{B}), \end{aligned} \tag{6.6}$$

where $\mathcal{L}^*$ denotes the formal adjoint of the linear differential operator $\mathcal{L}$. The operator $\mathcal{L}$ is unbounded and can be either a first or a second order differential operator (in the latter case it can be expressed as $\mathcal{L} = \mathcal{L}_1 \circ \mathcal{L}_2$). Given the splitting $L^2(\Omega, \mathbb{A}) \times L^2(\Omega, \mathbb{B}) = L^2(\Omega, \mathbb{F})$ the Hilbert space $H^{\mathcal{J}}$ can be split as well as

$$H^{\mathcal{J}} = H^{\mathcal{L}} \times H^{-\mathcal{L}^*}, \qquad \begin{aligned} H^{\mathcal{L}} &:= \left\{ \boldsymbol{u}_1 \in L^2(\Omega, \mathbb{A}) |\ \mathcal{L}\boldsymbol{u}_1 \in L^2(\Omega, \mathbb{B}) \right\}, \\ H^{-\mathcal{L}^*} &:= \left\{ \boldsymbol{u}_2 \in L^2(\Omega, \mathbb{B}) |\ -\mathcal{L}^*\boldsymbol{u}_2 \in L^2(\Omega, \mathbb{A}) \right\} \end{aligned} \tag{6.7}$$

Remark 15
Notice that this assumption is also made in [Skr19] (using a vectorial notation for tensors) to demonstrate the well-posedness of linear pHs in arbitrary geometrical domains.

The boundary operators are then supposed to fulfill the following assumption, that guarantees a uniform causality condition.

Assumption 3 (Abstract integration by parts formula)
Assume that there exists two boundary operators $\mathcal{N}_{\partial,1}$, $\mathcal{N}_{\partial,2}$ such that for $(\boldsymbol{u}_1, \boldsymbol{u}_2) \in H^{\mathcal{L}} \times H^{-\mathcal{L}^*}$ a general integration by parts formula holds

$$\langle \boldsymbol{u}_2,\, \mathcal{L}\,\boldsymbol{u}_1\rangle_{L^2(\Omega,\mathbb{B})} - \langle \mathcal{L}^*\,\boldsymbol{u}_2,\, \boldsymbol{u}_1\rangle_{L^2(\Omega,\mathbb{A})} = \langle \mathcal{N}_{\partial,1}\boldsymbol{u}_1,\, \mathcal{N}_{\partial,2}\boldsymbol{u}_2\rangle_{L^2(\partial\Omega,\mathbb{R}^m)}\,. \tag{6.8}$$

The boundary operators $\mathcal{B}_\partial, \mathcal{C}_\partial$ of Eqs. (6.1c), (6.1d), are then assumed to verify, in an exclusive manner, either

$$\mathcal{B}_\partial = \begin{bmatrix} 0 & \mathcal{N}_{\partial,2}\end{bmatrix}, \qquad \mathcal{C}_\partial = \begin{bmatrix}\mathcal{N}_{\partial,1} & 0\end{bmatrix}, \tag{6.9}$$

or

$$\mathcal{B}_\partial = \begin{bmatrix}\mathcal{N}_{\partial,1} & 0\end{bmatrix}, \qquad \mathcal{C}_\partial = \begin{bmatrix} 0 & \mathcal{N}_{\partial,2}\end{bmatrix}. \tag{6.10}$$

Thanks to the partitioned structure of the system, this assumption enables to identify the boundary operators more precisely than Assumption 1.

Remark 16 (Duality pairing for rigged Hilbert spaces)
The integration by part formula establishes a duality pairing between Sobolev spaces (cf. Remarks 6, 10, 12). This duality pairing is then compatible with an L^2 inner-product in presence of a rigged Hilbert space (or Gelfand triple [GV64]). For sake of simplicity (and without being mathematically rigorous), the boundary integrals are expressed as L^2 inner product over the boundary.

Thanks to Assumption 2, System (6.1) is rewritten as

$$\partial_t \begin{pmatrix}\boldsymbol{\alpha}_1\\ \boldsymbol{\alpha}_2\end{pmatrix} = \begin{bmatrix} 0 & -\boldsymbol{L}^\top - \mathcal{L}^* \\ \boldsymbol{L} + \mathcal{L} & 0\end{bmatrix}\begin{pmatrix}\boldsymbol{e}_1\\ \boldsymbol{e}_2\end{pmatrix}, \qquad \begin{matrix}\boldsymbol{\alpha}_1 \in L^2(\Omega,\mathbb{A}),\\ \boldsymbol{\alpha}_2 \in L^2(\Omega,\mathbb{B}),\end{matrix} \tag{6.11a}$$

$$\begin{pmatrix}\boldsymbol{e}_1\\ \boldsymbol{e}_2\end{pmatrix} := \begin{pmatrix}\delta_{\boldsymbol{\alpha}_1} H\\ \delta_{\boldsymbol{\alpha}_2} H\end{pmatrix}, \qquad \begin{matrix}\boldsymbol{e}_1 \in H^{\mathcal{L}},\\ \boldsymbol{e}_2 \in H^{-\mathcal{L}^*}.\end{matrix} \tag{6.11b}$$

In light of Assumption 3, if Eq. (6.9) holds the boundary variables are given by

$$\boldsymbol{u}_\partial = \mathcal{N}_{\partial,2}\boldsymbol{e}_2, \qquad \boldsymbol{y}_\partial = \mathcal{N}_{\partial,1}\boldsymbol{e}_1, \qquad \boldsymbol{u}_\partial,\, \boldsymbol{y}_\partial \in L^2(\partial\Omega,\mathbb{R}^m). \tag{6.12}$$

Otherwise, if Eq. (6.10) applies, then

$$\boldsymbol{u}_\partial = \mathcal{N}_{\partial,1}\boldsymbol{e}_1, \qquad \boldsymbol{y}_\partial = \mathcal{N}_{\partial,2}\boldsymbol{e}_2, \qquad \boldsymbol{u}_\partial,\, \boldsymbol{y}_\partial \in L^2(\partial\Omega,\mathbb{R}^m). \tag{6.13}$$

In both cases, the power balance reads

$$\begin{aligned}\dot{H} &= \langle \boldsymbol{e}_1,\, \partial_t \boldsymbol{\alpha}_1 \rangle_{L^2(\Omega,\mathbb{A})} + \langle \boldsymbol{e}_2,\, \partial_t \boldsymbol{\alpha}_2 \rangle_{L^2(\Omega,\mathbb{B})}\,, \\ &= \langle \boldsymbol{e}_1,\, -\mathcal{L}^* \boldsymbol{e}_2 \rangle_{L^2(\Omega,\mathbb{A})} + \langle \boldsymbol{e}_2,\, \mathcal{L} \boldsymbol{e}_1 \rangle_{L^2(\Omega,\mathbb{B})}\,, \\ &= \langle \mathcal{N}_{\partial,1} \boldsymbol{e}_1,\, \mathcal{N}_{\partial,2} \boldsymbol{e}_2 \rangle_{L^2(\partial\Omega,\mathbb{R}^m)}\,, \\ &= \langle \boldsymbol{y}_\partial,\, \boldsymbol{u}_\partial \rangle_{L^2(\partial\Omega,\mathbb{R}^m)}\,.\end{aligned} \tag{6.14}$$

We are now in a position to illustrate the PFEM.

Step 1: Weak Form

First consider the weak form of system (6.11a), obtained by taking the L^2 inner product introducing an appropriate test function $\boldsymbol{v} = (\boldsymbol{v}_1, \boldsymbol{v}_2) \in \mathbb{A} \times \mathbb{B} = \mathbb{F}$ and integrating over the domain Ω

$$\begin{aligned}\langle \boldsymbol{v}_1,\, \partial_t \boldsymbol{\alpha}_1 \rangle_{L^2(\Omega,\mathbb{A})} &= -\langle \boldsymbol{v}_1,\, \boldsymbol{L}^\top \boldsymbol{e}_2 \rangle_{L^2(\Omega,\mathbb{A})} - \langle \boldsymbol{v}_1,\, \mathcal{L}^* \boldsymbol{e}_2 \rangle_{L^2(\Omega,\mathbb{A})}\,, \\ \langle \boldsymbol{v}_2,\, \partial_t \boldsymbol{\alpha}_2 \rangle_{L^2(\Omega,\mathbb{B})} &= \langle \boldsymbol{v}_2,\, \boldsymbol{L} \boldsymbol{e}_1 \rangle_{L^2(\Omega,\mathbb{B})} + \langle \boldsymbol{v}_2,\, \mathcal{L} \boldsymbol{e}_1 \rangle_{L^2(\Omega,\mathbb{B})}\,.\end{aligned} \tag{6.15}$$

To close the system, the constitutive law (6.11b) and the output variables (6.1d) are put in weak form

$$\begin{aligned}\langle \boldsymbol{v}_1,\, \boldsymbol{e}_1 \rangle_{L^2(\Omega,\mathbb{A})} &= \langle \boldsymbol{v}_1,\, \delta_{\boldsymbol{\alpha}_1} H \rangle_{L^2(\Omega,\mathbb{A})}\,, \\ \langle \boldsymbol{v}_2,\, \boldsymbol{e}_2 \rangle_{L^2(\Omega,\mathbb{B})} &= \langle \boldsymbol{v}_2,\, \delta_{\boldsymbol{\alpha}_2} H \rangle_{L^2(\Omega,\mathbb{B})}\,, \\ \langle \boldsymbol{v}_\partial,\, \boldsymbol{y}_\partial \rangle_{L^2(\partial\Omega,\mathbb{R}^m)} &= \langle \boldsymbol{v}_\partial,\, \mathcal{C}_\partial \boldsymbol{e} \rangle_{L^2(\partial\Omega,\mathbb{R}^m)}\,,\end{aligned} \tag{6.16}$$

where the test function $\boldsymbol{v}_\partial \in L^2(\partial\Omega, \mathbb{R}^m)$ is defined on the boundary $\partial\Omega$ and $\mathcal{C}_\partial$ is defined either by Eq. (6.9) or (6.10).

Step 2: Integration by parts

Next the integration by part has to be carried out. The choice is dictated by the boundary control to be imposed on the system. Consider again Eq. (6.15). The integration by parts can be carried out either on term $-\langle \boldsymbol{v}_1,\, \mathcal{L}^* \boldsymbol{e}_2 \rangle_{L^2(\Omega,\mathbb{A})}$, or on term $\langle \boldsymbol{v}_2,\, \mathcal{L} \boldsymbol{e}_1 \rangle_{L^2(\Omega,\mathbb{B})}$. Depending on which line undergoes the integration by parts (this is why the name Partitioned Finite Element method), two structure-preserving weak forms can be obtained. These differ by the boundary causality imposed to the system.

A) Integration by parts of the term $-\langle \boldsymbol{v}_1,\, \mathcal{L}^* \boldsymbol{e}_2 \rangle_{L^2(\Omega,\mathbb{A})}$ In this case case, using Eq. (6.8), it is obtained

$$-\langle \boldsymbol{v}_1,\, \mathcal{L}^* \boldsymbol{e}_2 \rangle_{L^2(\Omega,\mathbb{A})} = -\langle \mathcal{L} \boldsymbol{v}_1,\, \boldsymbol{e}_2 \rangle_{L^2(\Omega,\mathbb{B})} + \langle \mathcal{N}_{\partial,1} \boldsymbol{v}_1,\, \mathcal{N}_{\partial,2} \boldsymbol{e}_2 \rangle_{L^2(\partial\Omega,\mathbb{R}^m)}\,. \tag{6.17}$$

Then the weak form of the system dynamics reads

$$\begin{aligned}\langle \boldsymbol{v}_1,\, \partial_t \boldsymbol{\alpha}_1\rangle_{L^2(\Omega,\mathbb{A})} &= -\langle \boldsymbol{v}_1,\, \boldsymbol{L}^\top \boldsymbol{e}_2\rangle_{L^2(\Omega,\mathbb{A})} - \langle \mathcal{L}\boldsymbol{v}_1,\, \boldsymbol{e}_2\rangle_{L^2(\Omega,\mathbb{B})} + \langle \mathcal{N}_{\partial,1}\boldsymbol{v}_1,\, \boldsymbol{u}_\partial\rangle_{L^2(\partial\Omega,\mathbb{R}^m)}\,,\\ \langle \boldsymbol{v}_2,\, \partial_t \boldsymbol{\alpha}_2\rangle_{L^2(\Omega,\mathbb{B})} &= \langle \boldsymbol{v}_2,\, \boldsymbol{L}\boldsymbol{e}_1\rangle_{L^2(\Omega,\mathbb{B})} + \langle \boldsymbol{v}_2,\, \mathcal{L}\boldsymbol{e}_1\rangle_{L^2(\Omega,\mathbb{B})}\,,\end{aligned} \tag{6.18}$$

The following proposition is crucial as the lossless character of the infinite-dimensional system (due to the formally skew-adjoint operator) translates into an equivalent property for the corresponding bilinear form in the weak form.

Proposition 8
Given the Hilbert space $H_2^{\mathcal{L}} := H^{\mathcal{L}} \times L^2(\Omega,\mathbb{B})$ and variables $\boldsymbol{v} = (\boldsymbol{v}_1, \boldsymbol{v}_2) \in H_2^{\mathcal{L}}$, $\boldsymbol{e} = (\boldsymbol{e}_1, \boldsymbol{e}_2) \in H_2^{\mathcal{L}}$, the bilinear form

$$\begin{aligned} j_{\mathcal{L}} : H_2^{\mathcal{L}} \times H_2^{\mathcal{L}} &\longrightarrow \mathbb{R},\\ (\boldsymbol{v}, \boldsymbol{e}) &\longrightarrow -\langle \mathcal{L}\boldsymbol{v}_1,\, \boldsymbol{e}_2\rangle_{L^2(\Omega,\mathbb{B})} + \langle \boldsymbol{v}_2,\, \mathcal{L}\boldsymbol{e}_1\rangle_{L^2(\Omega,\mathbb{B})}\end{aligned}$$

is skew-symmetric.

Proof. The proof is obtained by the following computation

$$\begin{aligned} j_{\mathcal{L}}(\boldsymbol{v}, \boldsymbol{e}) &= -\langle \mathcal{L}\boldsymbol{v}_1,\, \boldsymbol{e}_2\rangle_{L^2(\Omega,\mathbb{B})} + \langle \boldsymbol{v}_2,\, \mathcal{L}\boldsymbol{e}_1\rangle_{L^2(\Omega,\mathbb{B})}\,,\\ &= -\Big(-\langle \boldsymbol{v}_2,\, \mathcal{L}\boldsymbol{e}_1\rangle_{L^2(\Omega,\mathbb{B})} + \langle \mathcal{L}\boldsymbol{v}_1,\, \boldsymbol{e}_2\rangle_{L^2(\Omega,\mathbb{B})}\Big)\,,\\ &= -\Big(-\langle \mathcal{L}\boldsymbol{e}_1,\, \boldsymbol{v}_2\rangle_{L^2(\Omega,\mathbb{B})} + \langle \boldsymbol{e}_2,\, \mathcal{L}\boldsymbol{v}_1\rangle_{L^2(\Omega,\mathbb{B})}\Big) = -j_{\mathcal{L}}(\boldsymbol{e}, \boldsymbol{v}).\end{aligned}$$

□

Now assume that the system satisfies the boundary causality condition 6.12. Then, this choice of the integration by parts leads to the following weak formulation

$$\begin{aligned}\langle \boldsymbol{v}_1,\, \partial_t \boldsymbol{\alpha}_1\rangle_{L^2(\Omega,\mathbb{A})} &= -\langle \boldsymbol{v}_1,\, \boldsymbol{L}^\top \boldsymbol{e}_2\rangle_{L^2(\Omega,\mathbb{A})} - \langle \mathcal{L}\boldsymbol{v}_1,\, \boldsymbol{e}_2\rangle_{L^2(\Omega,\mathbb{B})} + \langle \mathcal{N}_{\partial,1}\boldsymbol{v}_1,\, \boldsymbol{u}_\partial\rangle_{L^2(\partial\Omega,\mathbb{R}^m)}\,,\\ \langle \boldsymbol{v}_2,\, \partial_t \boldsymbol{\alpha}_2\rangle_{L^2(\Omega,\mathbb{B})} &= \langle \boldsymbol{v}_2,\, \boldsymbol{L}\boldsymbol{e}_1\rangle_{L^2(\Omega,\mathbb{B})} + \langle \boldsymbol{v}_2,\, \mathcal{L}\boldsymbol{e}_1\rangle_{L^2(\Omega,\mathbb{B})}\,,\\ \langle \boldsymbol{v}_1,\, \boldsymbol{e}_1\rangle_{L^2(\Omega,\mathbb{A})} &= \langle \boldsymbol{v}_1,\, \delta_{\boldsymbol{\alpha}_1} H\rangle_{L^2(\Omega,\mathbb{A})}\,,\\ \langle \boldsymbol{v}_2,\, \boldsymbol{e}_2\rangle_{L^2(\Omega,\mathbb{B})} &= \langle \boldsymbol{v}_2,\, \delta_{\boldsymbol{\alpha}_2} H\rangle_{L^2(\Omega,\mathbb{B})}\,,\\ \langle \boldsymbol{v}_\partial,\, \boldsymbol{y}_\partial\rangle_{L^2(\partial\Omega,\mathbb{R}^m)} &= \langle \boldsymbol{v}_\partial,\, \mathcal{N}_{\partial,1}\boldsymbol{e}_1\rangle_{L^2(\partial\Omega,\mathbb{R}^m)}\,.\end{aligned} \tag{6.19}$$

B) Integration by parts of the term $\langle \boldsymbol{v}_2,\, \mathcal{L}\boldsymbol{e}_1\rangle_{L^2(\Omega,\mathbb{B})}$ Using Eq. (6.8), it is obtained

$$\langle \boldsymbol{v}_2,\, \mathcal{L}\boldsymbol{e}_1\rangle_{L^2(\Omega,\mathbb{B})} = \langle \mathcal{L}^*\boldsymbol{v}_2,\, \boldsymbol{e}_1\rangle_{L^2(\Omega,\mathbb{A})} + \langle \mathcal{N}_{\partial,2}\boldsymbol{v}_2,\, \mathcal{N}_{\partial,1}\boldsymbol{e}_1\rangle_{L^2(\partial\Omega,\mathbb{R}^m)}\,. \tag{6.20}$$

Then the weak form of the system dynamics reads

$$\begin{aligned}\langle \boldsymbol{v}_1,\, \partial_t \boldsymbol{\alpha}_1 \rangle_{L^2(\Omega,\mathbb{A})} &= -\langle \boldsymbol{v}_1,\, \boldsymbol{L}^\top \boldsymbol{e}_2 \rangle_{L^2(\Omega,\mathbb{A})} - \langle \boldsymbol{v}_1,\, \mathcal{L}^* \boldsymbol{e}_2 \rangle_{L^2(\Omega,\mathbb{A})}\,, \\ \langle \boldsymbol{v}_2,\, \partial_t \boldsymbol{\alpha}_2 \rangle_{L^2(\Omega,\mathbb{B})} &= \langle \boldsymbol{v}_2,\, \boldsymbol{L} \boldsymbol{e}_1 \rangle_{L^2(\Omega,\mathbb{B})} + \langle \mathcal{L}^* \boldsymbol{v}_2,\, \boldsymbol{e}_1 \rangle_{L^2(\Omega,\mathbb{A})} + \langle \mathcal{N}_{\partial,2} \boldsymbol{v}_2,\, \boldsymbol{u}_\partial \rangle_{L^2(\partial\Omega,\mathbb{R}^m)}\,,\end{aligned} \tag{6.21}$$

Again the bilinear form arising from the formally skew-adjoint operator is skew-symmetric.

Proposition 9
Given the Hilbert space $H_1^{-\mathcal{L}^*} = L^2(\Omega,\mathbb{A}) \times H^{-\mathcal{L}^*}$ *and variables* $\boldsymbol{v} = (\boldsymbol{v}_1, \boldsymbol{v}_2) \in H_1^{-\mathcal{L}^*}$, $\boldsymbol{e} = (\boldsymbol{e}_1, \boldsymbol{e}_2) \in H_1^{-\mathcal{L}^*}$, *the bilinear form*

$$\begin{aligned} j_{-\mathcal{L}^*} : H_1^{-\mathcal{L}^*} \times H_1^{-\mathcal{L}^*} &\longrightarrow \mathbb{R}, \\ (\boldsymbol{v}, \boldsymbol{e}) &\longrightarrow -\langle \boldsymbol{v}_1,\, \mathcal{L}^* \boldsymbol{e}_2 \rangle_{L^2(\Omega,\mathbb{A})} + \langle \mathcal{L}^* \boldsymbol{v}_2,\, \boldsymbol{e}_1 \rangle_{L^2(\Omega,\mathbb{A})} \end{aligned}$$

is skew-symmetric.

Proof. The proof follows from the computation

$$\begin{aligned} j_{-\mathcal{L}^*}(\boldsymbol{v}, \boldsymbol{e}) &= -\langle \boldsymbol{v}_1,\, \mathcal{L}^* \boldsymbol{e}_2 \rangle_{L^2(\Omega,\mathbb{A})} + \langle \mathcal{L}^* \boldsymbol{v}_2,\, \boldsymbol{e}_1 \rangle_{L^2(\Omega,\mathbb{A})}\,, \\ &= -\Big(-\langle \mathcal{L}^* \boldsymbol{v}_2,\, \boldsymbol{e}_1 \rangle_{L^2(\Omega,\mathbb{A})} + \langle \boldsymbol{v}_1,\, \mathcal{L}^* \boldsymbol{e}_2 \rangle_{L^2(\Omega,\mathbb{A})} \Big)\,, \\ &= -\Big(-\langle \boldsymbol{e}_1,\, \mathcal{L}^* \boldsymbol{v}_2 \rangle_{L^2(\Omega,\mathbb{A})} + \langle \mathcal{L}^* \boldsymbol{e}_2,\, \boldsymbol{v}_1 \rangle_{L^2(\Omega,\mathbb{A})} \Big) = -j_{-\mathcal{L}^*}(\boldsymbol{e}, \boldsymbol{v}). \end{aligned}$$

□

Now assume that the system satisfies the boundary causality condition (6.13). Then, the final weak formulation reads

$$\begin{aligned} \langle \boldsymbol{v}_1,\, \partial_t \boldsymbol{\alpha}_1 \rangle_{L^2(\Omega,\mathbb{A})} &= -\langle \boldsymbol{v}_1,\, \boldsymbol{L}^\top \boldsymbol{e}_2 \rangle_{L^2(\Omega,\mathbb{A})} - \langle \boldsymbol{v}_1,\, \mathcal{L}^* \boldsymbol{e}_2 \rangle_{L^2(\Omega,\mathbb{A})}\,, \\ \langle \boldsymbol{v}_2,\, \partial_t \boldsymbol{\alpha}_2 \rangle_{L^2(\Omega,\mathbb{B})} &= \langle \boldsymbol{v}_2,\, \boldsymbol{L} \boldsymbol{e}_1 \rangle_{L^2(\Omega,\mathbb{B})} + \langle \mathcal{L}^* \boldsymbol{v}_2,\, \boldsymbol{e}_1 \rangle_{L^2(\Omega,\mathbb{A})} + \langle \mathcal{N}_{\partial,2} \boldsymbol{v}_2,\, \boldsymbol{u}_\partial \rangle_{L^2(\partial\Omega,\mathbb{R}^m)}\,, \\ \langle \boldsymbol{v}_1,\, \boldsymbol{e}_1 \rangle_{L^2(\Omega,\mathbb{A})} &= \langle \boldsymbol{v}_1,\, \delta_{\boldsymbol{\alpha}_1} H \rangle_{L^2(\Omega,\mathbb{A})}\,, \\ \langle \boldsymbol{v}_2,\, \boldsymbol{e}_2 \rangle_{L^2(\Omega,\mathbb{B})} &= \langle \boldsymbol{v}_2,\, \delta_{\boldsymbol{\alpha}_2} H \rangle_{L^2(\Omega,\mathbb{B})}\,, \\ \langle \boldsymbol{v}_\partial,\, \boldsymbol{y}_\partial \rangle_{L^2(\partial\Omega,\mathbb{R}^m)} &= \langle \boldsymbol{v}_\partial,\, \mathcal{N}_{\partial,2} \boldsymbol{e}_2 \rangle_{L^2(\partial\Omega,\mathbb{R}^m)}\,. \end{aligned} \tag{6.22}$$

Step 3: Galerkin discretization

To conclude the illustration of this methodology, a Galerkin discretization is introduced. This means that corresponding (i.e. with the same index) test, energy and co-energy functions are discretized using the same basis. Furthermore the boundary variables are discretized as well

using bases defined over the boundary

$$\begin{aligned}
\boldsymbol{v}_1 &\approx \sum_{i=1}^{n_1} \boldsymbol{\phi}_1^i(\boldsymbol{x}) v_1^i, & \boldsymbol{\alpha}_1 &\approx \sum_{i=1}^{n_1} \boldsymbol{\phi}_1^i(\boldsymbol{x}) \alpha_1^i(t), & \boldsymbol{e}_1 &\approx \sum_{i=1}^{n_1} \boldsymbol{\phi}_1^i(\boldsymbol{x}) e_1^i(t), \quad \boldsymbol{x} \in \Omega, \\
\boldsymbol{v}_2 &\approx \sum_{i=1}^{n_2} \boldsymbol{\phi}_2^i(\boldsymbol{x}) v_2^i, & \boldsymbol{\alpha}_2 &\approx \sum_{i=1}^{n_2} \boldsymbol{\phi}_2^i(\boldsymbol{x}) \alpha_2^i(t), & \boldsymbol{e}_2 &\approx \sum_{i=1}^{n_2} \boldsymbol{\phi}_2^i(\boldsymbol{x}) e_2^i(t), \quad \boldsymbol{x} \in \Omega, \\
\boldsymbol{v}_\partial &\approx \sum_{i=1}^{n_\partial} \boldsymbol{\phi}_\partial^i(\boldsymbol{s}) v_\partial^i, & \boldsymbol{u}_\partial &\approx \sum_{i=1}^{n_\partial} \boldsymbol{\phi}_\partial^i(\boldsymbol{s}) u_\partial^i(t), & \boldsymbol{y}_\partial &\approx \sum_{i=1}^{n_\partial} \boldsymbol{\phi}_\partial^i(\boldsymbol{s}) y_\partial^i(t), \quad \boldsymbol{s} \in \partial\Omega,
\end{aligned} \tag{6.23}$$

where $\boldsymbol{\phi}_1^i \in \mathbb{A},\ \boldsymbol{\phi}_2^i \in \mathbb{B},\ \boldsymbol{\phi}_\partial^i \in \mathbb{R}^m$.

A) Discretization of the weak form (6.19) Plugging the approximation into the weak form (6.19) and considering that the resulting equation holds $\forall\, v_1^i,\ v_2^j,\ v_\partial^k$ ($i \in \{1, n_1\},\ j \in \{1, n_2\},\ k \in \{1, n_\partial\}$), the finite-dimensional system is obtained

$$\begin{aligned}
\begin{bmatrix} \mathbf{M}_1 & \mathbf{0} \\ \mathbf{0} & \mathbf{M}_2 \end{bmatrix} \begin{pmatrix} \dot{\boldsymbol{\alpha}}_{d,1} \\ \dot{\boldsymbol{\alpha}}_{d,2} \end{pmatrix} &= \begin{bmatrix} \mathbf{0} & -\mathbf{D}_0^\top - \mathbf{D}_\mathcal{L}^\top \\ \mathbf{D}_0 + \mathbf{D}_\mathcal{L} & \mathbf{0} \end{bmatrix} \begin{pmatrix} \mathbf{e}_1 \\ \mathbf{e}_2 \end{pmatrix} + \begin{bmatrix} \mathbf{B}_1 \\ \mathbf{0} \end{bmatrix} \mathbf{u}_\partial, \\
\begin{bmatrix} \mathbf{M}_1 & \mathbf{0} \\ \mathbf{0} & \mathbf{M}_2 \end{bmatrix} \begin{pmatrix} \mathbf{e}_1 \\ \mathbf{e}_2 \end{pmatrix} &= \begin{bmatrix} \partial_{\boldsymbol{\alpha}_{d,1}} H_d(\boldsymbol{\alpha}_d) \\ \partial_{\boldsymbol{\alpha}_{d,2}} H_d(\boldsymbol{\alpha}_d) \end{bmatrix}, \\
\mathbf{M}_\partial \mathbf{y}_\partial &= \begin{bmatrix} \mathbf{B}_1^\top & \mathbf{0} \end{bmatrix} \begin{pmatrix} \mathbf{e}_1 \\ \mathbf{e}_2 \end{pmatrix}.
\end{aligned} \tag{6.24}$$

Vectors $\boldsymbol{\alpha}_{d,1}$, $\boldsymbol{\alpha}_{d,2}$, $\mathbf{e}_1$, $\mathbf{e}_2$, $\mathbf{u}_\partial$, $\mathbf{y}_\partial$ are given by the column-wise concatenation of their respective degrees of freedom. The matrices are defined as follows

$$\begin{aligned}
M_1^{ij} &= \left\langle \boldsymbol{\phi}_1^i,\, \boldsymbol{\phi}_1^j \right\rangle_{L^2(\Omega,\mathbb{A})}, & D_0^{mi} &= \left\langle \boldsymbol{\phi}_2^m,\, \boldsymbol{L}\boldsymbol{\phi}_1^i \right\rangle_{L^2(\Omega,\mathbb{B})}, & B_1^{ik} &= \left\langle \mathcal{N}_{\partial,1}\boldsymbol{\phi}_1^i,\, \boldsymbol{\phi}_\partial^k \right\rangle_{L^2(\partial\Omega,\mathbb{R}^m)}, \\
M_2^{mn} &= \langle \boldsymbol{\phi}_2^m,\, \boldsymbol{\phi}_2^n \rangle_{L^2(\Omega,\mathbb{B})}, & D_\mathcal{L}^{mi} &= \left\langle \boldsymbol{\phi}_2^m,\, \mathcal{L}\boldsymbol{\phi}_1^i \right\rangle_{L^2(\Omega,\mathbb{B})}, & M_\partial^{lk} &= \left\langle \boldsymbol{\phi}_\partial^l,\, \boldsymbol{\phi}_\delta^k \right\rangle_{L^2(\partial\Omega,\mathbb{R}^m)},
\end{aligned} \tag{6.25}$$

where $i, j \in \{1, n_1\},\ m, n \in \{1, n_2\},\ l, k \in \{1, n_\partial\}$. Introducing the definitions

$$\begin{aligned}
\delta_{\boldsymbol{\alpha}_{d,1}} H_d &:= \delta_{\boldsymbol{\alpha}_1} H \left(\boldsymbol{\alpha}_1 = \sum_{i=1}^{n_1} \boldsymbol{\phi}_1^i \alpha_1^i,\ \boldsymbol{\alpha}_2 = \sum_{j=1}^{n_2} \boldsymbol{\phi}_2^j \alpha_2^j \right), \\
\delta_{\boldsymbol{\alpha}_{d,2}} H_d &:= \delta_{\boldsymbol{\alpha}_2} H \left(\boldsymbol{\alpha}_1 = \sum_{i=1}^{n_1} \boldsymbol{\phi}_1^i \alpha_1^i,\ \boldsymbol{\alpha}_2 = \sum_{j=1}^{n_2} \boldsymbol{\phi}_2^j \alpha_2^j \right),
\end{aligned}$$

the discretized gradient of the Hamiltonian reads

$$\begin{aligned}
\partial_{\alpha_{d,1}^i} H_d(\boldsymbol{\alpha}_d) &= \left\langle \boldsymbol{\phi}_1^i,\, \delta_{\boldsymbol{\alpha}_{d,1}} H_d \right\rangle_{L^2(\Omega,\mathbb{A})}, & i &\in \{1, n_1\}, \\
\partial_{\alpha_{d,2}^j} H_d(\boldsymbol{\alpha}_d) &= \left\langle \boldsymbol{\phi}_2^j,\, \delta_{\boldsymbol{\alpha}_{d,2}} H_d \right\rangle_{L^2(\Omega,\mathbb{B})}, & j &\in \{1, n_2\}.
\end{aligned} \tag{6.26}$$

A pH system in canonical form is found observing that Sys. (6.24) is compactly rewritten as

$$\mathbf{M}\dot{\boldsymbol{\alpha}}_d = \mathbf{J}_{\mathcal{L}}\mathbf{e} + \mathbf{B}\mathbf{u}_\partial, \tag{6.27}$$
$$\mathbf{M}\mathbf{e} = \nabla H_d(\boldsymbol{\alpha}_d), \tag{6.28}$$
$$\mathbf{M}_\partial \mathbf{y}_\partial = \mathbf{B}^\top \mathbf{e}, \tag{6.29}$$

where $\boldsymbol{\alpha}_d = (\boldsymbol{\alpha}_{d,1}^\top \;\; \boldsymbol{\alpha}_{d,2}^\top)^\top$, $\mathbf{e} = (\mathbf{e}_1^\top \;\; \mathbf{e}_2^\top)^\top$, $\nabla H_d(\boldsymbol{\alpha}_d) = (\partial_{\boldsymbol{\alpha}_{d,1}}^\top H_d(\boldsymbol{\alpha}_d) \;\; \partial_{\boldsymbol{\alpha}_{d,2}}^\top H_d(\boldsymbol{\alpha}_d))^\top$ and

$$\mathbf{M} = \begin{bmatrix} \mathbf{M}_1 & \mathbf{0} \\ \mathbf{0} & \mathbf{M}_2 \end{bmatrix}, \qquad \mathbf{J}_{\mathcal{L}} = \begin{bmatrix} \mathbf{0} & -\mathbf{D}_0^\top - \mathbf{D}_{\mathcal{L}}^\top \\ \mathbf{D}_0 + \mathbf{D}_{\mathcal{L}} & \mathbf{0} \end{bmatrix}, \qquad \mathbf{B} = \begin{bmatrix} \mathbf{B}_1 \\ \mathbf{0} \end{bmatrix}. \tag{6.30}$$

Plugging (6.28) into (6.27), a pH system in canonical form is obtained

$$\begin{aligned} \dot{\boldsymbol{\alpha}}_d &= \mathbf{J}\,\nabla H_d(\boldsymbol{\alpha}_d) + \mathbf{B}\,\mathbf{u}_\partial, \qquad \text{where} \qquad \mathbf{J} = \mathbf{M}^{-1}\mathbf{J}_{\mathcal{L}}\mathbf{M}^{-1}, \\ \widehat{\mathbf{y}}_\partial &= \mathbf{B}^\top \nabla H_d(\boldsymbol{\alpha}_d), \qquad \text{where} \qquad \widehat{\mathbf{y}}_\partial = \mathbf{M}_\partial \mathbf{y}_\partial. \end{aligned} \tag{6.31}$$

The structure-preserving character of the method is evident from the preservation of the power balance at the discrete level. The finite-dimensional counterpart of the energy rate is given by

$$\begin{aligned} \dot{H}_d &= \nabla^\top H_d(\boldsymbol{\alpha}_d)\dot{\boldsymbol{\alpha}}_d, \\ &= \nabla^\top H_d(\boldsymbol{\alpha}_d)\mathbf{J}\,\nabla H_d(\boldsymbol{\alpha}_d) + \nabla^\top H_d(\boldsymbol{\alpha}_d)\mathbf{B}\,\mathbf{u}_\partial, \qquad \text{Skew-symmetry of } \mathbf{J} \\ &= \mathbf{y}_\partial^\top \mathbf{M}_\partial \mathbf{u}_\partial = \widehat{\mathbf{y}}_\partial^\top \mathbf{u}_\partial. \end{aligned} \tag{6.32}$$

This result mimics its infinite-dimensional equivalent (6.14).

B) Discretization of the weak form (6.22) Plugging the approximation into the weak form (6.22) a finite-dimensional system with a different causality is obtained

$$\begin{aligned} \begin{bmatrix} \mathbf{M}_1 & \mathbf{0} \\ \mathbf{0} & \mathbf{M}_2 \end{bmatrix} \begin{pmatrix} \dot{\boldsymbol{\alpha}}_{d,1} \\ \dot{\boldsymbol{\alpha}}_{d,2} \end{pmatrix} &= \begin{bmatrix} \mathbf{0} & -\mathbf{D}_0^\top + \mathbf{D}_{-\mathcal{L}^*} \\ \mathbf{D}_0 - \mathbf{D}_{-\mathcal{L}^*}^\top & \mathbf{0} \end{bmatrix} \begin{pmatrix} \mathbf{e}_1 \\ \mathbf{e}_2 \end{pmatrix} + \begin{bmatrix} \mathbf{0} \\ \mathbf{B}_2 \end{bmatrix} \mathbf{u}_\partial, \\ \begin{bmatrix} \mathbf{M}_1 & \mathbf{0} \\ \mathbf{0} & \mathbf{M}_2 \end{bmatrix} \begin{pmatrix} \mathbf{e}_1 \\ \mathbf{e}_2 \end{pmatrix} &= \begin{pmatrix} \partial_{\boldsymbol{\alpha}_{d,1}} H_d(\boldsymbol{\alpha}_d) \\ \partial_{\boldsymbol{\alpha}_{d,2}} H_d(\boldsymbol{\alpha}_d) \end{pmatrix}, \\ \mathbf{M}_\partial \mathbf{y}_\partial &= \begin{bmatrix} \mathbf{0} & \mathbf{B}_2^\top \end{bmatrix} \begin{pmatrix} \mathbf{e}_1 \\ \mathbf{e}_2 \end{pmatrix}. \end{aligned} \tag{6.33}$$

The differences with respect to formulation (6.24) reside in matrices $\mathbf{D}_{-\mathcal{L}^*}$, $\mathbf{B}_2$, whose definitions are

$$D_{-\mathcal{L}^*}^{im} = \left\langle \boldsymbol{\phi}_1^i, -\mathcal{L}^* \boldsymbol{\phi}_2^m \right\rangle_{L^2(\Omega,\mathbb{A})}, \qquad B_2^{mk} = \left\langle \mathcal{N}_{\partial,2} \boldsymbol{\phi}_2^m, \boldsymbol{\phi}_\partial^k \right\rangle_{L^2(\partial\Omega,\mathbb{R}^m)}, \tag{6.34}$$

where $i \in \{1, n_1\}$, $m \in \{1, n_2\}$, $k \in \{1, n_\partial\}$. System (6.33) can be put in canonical form by replacing the co-energy variables by the discretized gradient.

6.1.2 Example: the irrotational shallow water equations

Consider as an example the shallow water equations detailed in §2.3.3. The flow is assumed to be irrotational ($\nabla \times \boldsymbol{v} = 0$). As a consequence the term $\boldsymbol{\mathcal{G}}$ in Eq. (2.37) vanishes. To fulfill Assumption 3, the incoming volumetric flow is known at the boundary, so that a uniform Neumann condition is imposed. This leads to the following boundary control system, defined on an open connected set $\Omega \subset \mathbb{R}^2$

$$\begin{aligned}
\frac{\partial}{\partial t}\begin{pmatrix}\alpha_h \\ \boldsymbol{\alpha}_v\end{pmatrix} &= -\begin{bmatrix}0 & \operatorname{div} \\ \operatorname{grad} & \mathbf{0}\end{bmatrix}\begin{pmatrix}e_h \\ \boldsymbol{e}_v\end{pmatrix}, & \alpha_h &\in L^2(\Omega), \\
& & \boldsymbol{\alpha}_v &\in L^2(\Omega, \mathbb{R}^2), \\
\begin{pmatrix}e_h \\ \boldsymbol{e}_v\end{pmatrix} := \begin{pmatrix}\delta_{\alpha_h} H \\ \delta_{\boldsymbol{\alpha}_v} H\end{pmatrix} &= \begin{pmatrix}\frac{1}{2\rho}\left\|\boldsymbol{\alpha}_v\right\|^2 + \rho g \alpha_h \\ \frac{1}{\rho}\alpha_h \boldsymbol{\alpha}_v\end{pmatrix}, & e_h &\in H^1(\Omega), \\
& & \boldsymbol{e}_v &\in H^{\operatorname{div}}(\Omega, \mathbb{R}^2), \\
u_\partial &= -\boldsymbol{e}_v \cdot \boldsymbol{n}, & u_\partial &\in L^2(\partial\Omega), \\
y_\partial &= e_h, & y_\partial &\in L^2(\partial\Omega),
\end{aligned} \tag{6.35}$$

where the Hamiltonian is a non-linear functional in the energy variables

$$H(\alpha_h, \boldsymbol{\alpha}_v) = \frac{1}{2}\int_\Omega \left\{\frac{1}{\rho}\alpha_h \left\|\boldsymbol{\alpha}_v\right\|^2 + \rho g \alpha_h^2\right\} \mathrm{d}\Omega.$$

The energy and co-energy variables are related to the physical variables (fluid height and velocity) through Eqs. (2.34), (2.36). In this case $\mathbb{A} = \mathbb{R}$, $\mathbb{B} = \mathbb{R}^2$ and $\mathcal{L} = \operatorname{grad}$, $-\mathcal{L}^* = \operatorname{div}$. This implies $H^{\mathcal{L}} = H^1(\Omega)$, $H^{-\mathcal{L}^*} = H^{\operatorname{div}}(\Omega, \mathbb{R}^2)$. As shown in (2.38), the energy rate equals

$$\dot{H} = -\left\langle \boldsymbol{e}_v, \operatorname{grad} e_h\right\rangle_{L^2(\Omega,\mathbb{R}^2)} - \left\langle \operatorname{div} \boldsymbol{e}_v, e_h\right\rangle_{L^2(\Omega)} = \left\langle -\boldsymbol{e}_v \cdot \boldsymbol{n}, e_h\right\rangle_{L^2(\partial\Omega)}. \tag{6.36}$$

The boundary operators are therefore given by

$$\begin{aligned}
u_\partial &= \mathcal{N}_{\partial,2}\boldsymbol{e}_v = -\gamma_n \boldsymbol{e}_v = -\boldsymbol{e}_v \cdot \boldsymbol{n}|_{\partial\Omega}, \\
y_\partial &= \mathcal{N}_{\partial,1} e_h = \gamma_0 e_h = e_h|_{\partial\Omega}.
\end{aligned} \tag{6.37}$$

This system represents a particular example of the general formulation of the general framework (6.11), together with boundary conditions (6.12). To obtain a finite-dimensional system, the test variables v_h, $\boldsymbol{v}_v$ are introduced and the integration by parts is performed on the div operator, leading to the weak form

$$\begin{aligned}
\left\langle v_h, \partial_t \alpha_h\right\rangle_{L^2(\Omega)} &= \left\langle \operatorname{grad} v_h, \boldsymbol{e}_v\right\rangle_{L^2(\Omega,\mathbb{R}^2)} + \left\langle \gamma_0 v_h, \boldsymbol{u}_\partial\right\rangle_{L^2(\partial\Omega)}, \\
\left\langle \boldsymbol{v}_v, \partial_t \boldsymbol{\alpha}_v\right\rangle_{L^2(\Omega,\mathbb{R}^2)} &= -\left\langle \boldsymbol{v}_v, \operatorname{grad} e_h\right\rangle_{L^2(\Omega,\mathbb{R}^2)}, \\
\left\langle v_h, e_h\right\rangle_{L^2(\Omega)} &= \left\langle v_h, \frac{1}{2\rho}\left\|\boldsymbol{\alpha}_v\right\|^2 + \rho g \alpha_h\right\rangle_{L^2(\Omega)}, \\
\left\langle \boldsymbol{v}_v, \boldsymbol{e}_v\right\rangle_{L^2(\Omega,\mathbb{R}^2)} &= \left\langle \boldsymbol{v}_v, \frac{1}{\rho}\alpha_h \boldsymbol{\alpha}_v\right\rangle_{L^2(\Omega,\mathbb{R}^2)}, \\
\left\langle v_\partial, y_\partial\right\rangle_{L^2(\partial\Omega)} &= \left\langle v_\partial, \gamma_0 e_h\right\rangle_{L^2(\partial\Omega)}.
\end{aligned} \tag{6.38}$$

Introducing a Galerkin approximation as in (6.23)

$$\begin{aligned}
v_h &\approx \sum_{i=1}^{n_h} \phi_h^i(\boldsymbol{x}) v_h^i, \qquad \alpha_h \approx \sum_{i=1}^{n_h} \phi_h^i(\boldsymbol{x}) \alpha_h^i(t), \qquad e_h \approx \sum_{i=1}^{n_h} \phi_h^i(\boldsymbol{x}) e_h^i(t), \quad \boldsymbol{x} \in \Omega, \\
\boldsymbol{v}_v &\approx \sum_{i=1}^{n_v} \boldsymbol{\phi}_v^i(\boldsymbol{x}) v_v^i, \qquad \boldsymbol{\alpha}_v \approx \sum_{i=1}^{n_v} \boldsymbol{\phi}_v^i(\boldsymbol{x}) \alpha_v^i(t), \qquad \boldsymbol{e}_v \approx \sum_{i=1}^{n_v} \boldsymbol{\phi}_v^i(\boldsymbol{x}) e_v^i(t), \quad \boldsymbol{x} \in \Omega, \\
v_\partial &\approx \sum_{i=1}^{n_\partial} \phi_\partial^i(\boldsymbol{s}) v_\partial^i, \qquad u_\partial \approx \sum_{i=1}^{n_\partial} \phi_\partial^i(\boldsymbol{s}) u_\partial^i(t), \qquad y_\partial \approx \sum_{i=1}^{n_\partial} \phi_\partial^i(\boldsymbol{s}) y_\partial^i(t), \quad \boldsymbol{s} \in \partial\Omega,
\end{aligned} \tag{6.39}$$

the finite-dimensional system is obtained

$$\begin{aligned}
\begin{bmatrix} \mathbf{M}_h & \mathbf{0} \\ \mathbf{0} & \mathbf{M}_v \end{bmatrix} \begin{pmatrix} \dot{\boldsymbol{\alpha}}_{d,h} \\ \dot{\boldsymbol{\alpha}}_{d,v} \end{pmatrix} &= - \begin{bmatrix} \mathbf{0} & -\mathbf{D}_{\text{grad}}^\top \\ \mathbf{D}_{\text{grad}} & \mathbf{0} \end{bmatrix} \begin{pmatrix} \mathbf{e}_h \\ \mathbf{e}_v \end{pmatrix} + \begin{bmatrix} \mathbf{B}_h \\ \mathbf{0} \end{bmatrix} \mathbf{u}_\partial, \\
\begin{bmatrix} \mathbf{M}_h & \mathbf{0} \\ \mathbf{0} & \mathbf{M}_v \end{bmatrix} \begin{pmatrix} \mathbf{e}_h \\ \mathbf{e}_v \end{pmatrix} &= \begin{bmatrix} \partial_{\boldsymbol{\alpha}_{d,h}} H_d(\boldsymbol{\alpha}_{d,h},\ \boldsymbol{\alpha}_{d,v}) \\ \partial_{\boldsymbol{\alpha}_{d,v}} H_d(\boldsymbol{\alpha}_{d,h},\ \boldsymbol{\alpha}_{d,v}) \end{bmatrix}, \\
\mathbf{M}_\partial \mathbf{y}_\partial &= \begin{bmatrix} \mathbf{B}_h^\top & \mathbf{0} \end{bmatrix} \begin{pmatrix} \mathbf{e}_h \\ \mathbf{e}_v \end{pmatrix}.
\end{aligned} \tag{6.40}$$

The matrices are defined as follows

$$\begin{aligned}
M_h^{ij} &= \left\langle \phi_h^i,\ \phi_h^j \right\rangle_{L^2(\Omega)}, & D_{\text{grad}}^{mi} &= \left\langle \boldsymbol{\phi}_v^m,\ \text{grad}\, \phi_h^i \right\rangle_{L^2(\Omega,\mathbb{R}^2)}, \\
M_v^{mn} &= \langle \boldsymbol{\phi}_v^m,\ \boldsymbol{\phi}_v^n \rangle_{L^2(\Omega,\mathbb{R}^2)}, & B_h^{ik} &= \left\langle \gamma_0 \phi_h^i,\ \phi_\partial^k \right\rangle_{L^2(\partial\Omega)}, \\
M_\partial^{lk} &= \left\langle \phi_\partial^l,\ \phi_\partial^k \right\rangle_{L^2(\partial\Omega)},
\end{aligned} \tag{6.41}$$

where $i, j \in \{1, n_h\}$, $m, n \in \{1, n_v\}$, $l, k \in \{1, n_\partial\}$. The discretized gradient of the Hamiltonian reads

$$\begin{aligned}
\partial_{\alpha_{d,h}^i} H_d(\boldsymbol{\alpha}_{d,h},\ \boldsymbol{\alpha}_{d,v}) &= \left\langle \boldsymbol{\phi}_h^i,\ \frac{1}{2\rho} \left\| \sum_{r=1}^{n_v} \boldsymbol{\phi}_v^r \alpha_v^r \right\|^2 + \rho g \sum_{r=1}^{n_h} \phi_h^r \alpha_h^r \right\rangle_{L^2(\Omega)}, \qquad i \in \{1, n_h\}, \\
\partial_{\alpha_{d,v}^m} H_d(\boldsymbol{\alpha}_{d,h},\ \boldsymbol{\alpha}_{d,v}) &= \left\langle \boldsymbol{\phi}_v^m,\ \frac{1}{\rho} \left(\sum_{r=1}^{n_h} \phi_h^r \alpha_h^r \right) \left(\sum_{r=1}^{n_v} \boldsymbol{\phi}_v^r \alpha_v^r \right) \right\rangle_{L^2(\Omega,\mathbb{R}^2)}, \qquad m \in \{1, n_v\}.
\end{aligned} \tag{6.42}$$

One possible finite element discretization for this problem can be found in [Pir89]. The non-linear nature of the problem strongly complicates the analysis. The presence of shocks has to be accounted for in the numerical discretization. The proposed methodology has to cope with finite time shocks to become a valid alternative to already well established strategies.

6.1.3 Linear case

The general framework detailed in Sec. 6.1.1 is valid for both linear and non-linear systems. However, in the linear case a major simplification occurs since the constitutive law connect-

ing energy and co-energy variables is easily invertible. This allows a description based on co-energy variables only.

To make the system linear, an additional assumption is introduced.

Assumption 4 (Quadratic separable Hamiltonian)
The Hamiltonian is assumed to be a positive quadratic functional in the energy variables $\boldsymbol{\alpha}_1$, $\boldsymbol{\alpha}_2$. *Furthermore, the Hamiltonian is considered to be separable with respect to* $\boldsymbol{\alpha}_1$, $\boldsymbol{\alpha}_2$ *(this hypothesis is always met for the systems under consideration). Therefore, it can be expressed as*

$$H = \frac{1}{2}\left\langle \boldsymbol{\alpha}_1,\, \mathcal{Q}_1\boldsymbol{\alpha}_1\right\rangle_{L^2(\Omega,\mathbb{A})} + \frac{1}{2}\left\langle \boldsymbol{\alpha}_2,\, \mathcal{Q}_2\boldsymbol{\alpha}_2\right\rangle_{L^2(\Omega,\mathbb{B})}, \tag{6.43}$$

where $\mathcal{Q}_1$, $\mathcal{Q}_2$ *are positive symmetric operators, bounded from below and above*

$$m_1\boldsymbol{I}_{\mathbb{A}} \leq \mathcal{Q}_1 \leq M_1\boldsymbol{I}_{\mathbb{A}}, \qquad m_2\boldsymbol{I}_{\mathbb{B}} \leq \mathcal{Q}_2 \leq M_2\boldsymbol{I}_{\mathbb{B}}, \qquad m_1 > 0,\ m_2 > 0,\ M_1 > 0,\ M_2 > 0,$$

where $\boldsymbol{I}_{\mathbb{A}}$, $\boldsymbol{I}_{\mathbb{B}}$ *are the identity operators in* $\mathbb{A}$, $\mathbb{B}$ *respectively.*

Because of Assumption 4, the co-energy variables are given by

$$\boldsymbol{e}_1 := \delta_{\alpha_1}H = \mathcal{Q}_1\boldsymbol{\alpha}_1, \qquad \boldsymbol{e}_2 := \delta_{\alpha_2}H = \mathcal{Q}_2\boldsymbol{\alpha}_2 \tag{6.44}$$

Since $\mathcal{Q}_1$, $\mathcal{Q}_2$ are positive bounded from below and above, it is possible to invert them to obtain

$$\boldsymbol{\alpha}_1 = \mathcal{Q}_1^{-1}\boldsymbol{e}_1 = \mathcal{M}_1\boldsymbol{e}_1, \qquad \boldsymbol{\alpha}_2 = \mathcal{Q}_2^{-1}\boldsymbol{e}_2 = \mathcal{M}_2\boldsymbol{e}_2, \qquad \mathcal{M}_1 := \mathcal{Q}_1^{-1},\ \mathcal{M}_2 := \mathcal{Q}_2^{-1}. \tag{6.45}$$

The Hamiltonian is then written in terms of co-energy variables as

$$H = \frac{1}{2}\left\langle \boldsymbol{e}_1,\, \mathcal{M}_1\boldsymbol{e}_1\right\rangle_{L^2(\Omega,\mathbb{A})} + \frac{1}{2}\left\langle \boldsymbol{e}_2,\, \mathcal{M}_2\boldsymbol{e}_2\right\rangle_{L^2(\Omega,\mathbb{B})}. \tag{6.46}$$

Under assumptions 2, 3, 4, a pH linear system is expressed as

$$\begin{bmatrix} \mathcal{M}_1 & 0 \\ 0 & \mathcal{M}_2 \end{bmatrix} \partial_t \begin{pmatrix} \boldsymbol{e}_1 \\ \boldsymbol{e}_2 \end{pmatrix} = \begin{bmatrix} 0 & -\boldsymbol{L}^\top - \mathcal{L}^* \\ \boldsymbol{L} + \mathcal{L} & 0 \end{bmatrix} \begin{pmatrix} \boldsymbol{e}_1 \\ \boldsymbol{e}_2 \end{pmatrix}, \qquad \begin{matrix} \boldsymbol{e}_1 \in H^{\mathcal{L}}, \\ \boldsymbol{e}_2 \in H^{-\mathcal{L}^*}. \end{matrix} \tag{6.47}$$

If Eq. (6.9) holds the boundary variables equal

$$\boldsymbol{u}_\partial = \mathcal{N}_{\partial,2}\boldsymbol{e}_2, \qquad \boldsymbol{y}_\partial = \mathcal{N}_{\partial,1}\boldsymbol{e}_1, \qquad \boldsymbol{u}_\partial,\, \boldsymbol{y}_\partial \in L^2(\partial\Omega, \mathbb{R}^m). \tag{6.48}$$

Whereas if Eq. (6.10) holds, then

$$\boldsymbol{u}_\partial = \mathcal{N}_{\partial,1}\boldsymbol{e}_1, \qquad \boldsymbol{y}_\partial = \mathcal{N}_{\partial,2}\boldsymbol{e}_2, \qquad \boldsymbol{u}_\partial,\, \boldsymbol{y}_\partial \in L^2(\partial\Omega, \mathbb{R}^m). \tag{6.49}$$

From equation (6.46), the power balance reads

$$\begin{aligned}\dot{H} &= \langle \boldsymbol{e}_1,\, \mathcal{M}_1 \partial_t \boldsymbol{e}_1 \rangle_{L^2(\Omega,\mathbb{A})} + \langle \boldsymbol{e}_2,\, \mathcal{M}_2 \partial_t \boldsymbol{e}_2 \rangle_{L^2(\Omega,\mathbb{B})}\,, \\ &= \langle \boldsymbol{e}_1,\, -\mathcal{L}^* \boldsymbol{e}_2 \rangle_{L^2(\Omega,\mathbb{A})} + \langle \boldsymbol{e}_2,\, \mathcal{L} \boldsymbol{e}_1 \rangle_{L^2(\Omega,\mathbb{B})}\,, \\ &= \langle \mathcal{N}_{\partial,1} \boldsymbol{e}_1,\, \mathcal{N}_{\partial,2} \boldsymbol{e}_2 \rangle_{L^2(\partial\Omega,\mathbb{R}^m)}\,, \\ &= \langle \boldsymbol{y}_\partial,\, \boldsymbol{u}_\partial \rangle_{L^2(\partial\Omega,\mathbb{R}^m)}\,.\end{aligned} \tag{6.50}$$

To get a finite-dimensional approximation the same procedure detailed in §6.1.1 is followed. The only difference is that there is no need to discretize the constitutive relations since those are already incorporated in the dynamics.

Once the system is put into weak form, if the operator $-\mathcal{L}^*$ is integrated by parts, one obtains the weak form

$$\begin{aligned}\langle \boldsymbol{v}_1,\, \mathcal{M}_1 \partial_t \boldsymbol{e}_1 \rangle_{L^2(\Omega,\mathbb{A})} &= -\langle \boldsymbol{v}_1,\, \boldsymbol{L}^\top \boldsymbol{e}_2 \rangle_{L^2(\Omega,\mathbb{A})} - \langle \mathcal{L} \boldsymbol{v}_1,\, \boldsymbol{e}_2 \rangle_{L^2(\Omega,\mathbb{B})} + \langle \mathcal{N}_{\partial,1} \boldsymbol{v}_1,\, \boldsymbol{u}_\partial \rangle_{L^2(\partial\Omega,\mathbb{R}^m)}\,, \\ \langle \boldsymbol{v}_2,\, \mathcal{M}_2 \partial_t \boldsymbol{e}_2 \rangle_{L^2(\Omega,\mathbb{B})} &= \langle \boldsymbol{v}_2,\, \boldsymbol{L} \boldsymbol{e}_1 \rangle_{L^2(\Omega,\mathbb{B})} + \langle \boldsymbol{v}_2,\, \mathcal{L} \boldsymbol{e}_1 \rangle_{L^2(\Omega,\mathbb{B})}\,, \\ \langle \boldsymbol{v}_\partial,\, \boldsymbol{y}_\partial \rangle_{L^2(\partial\Omega,\mathbb{R}^m)} &= \langle \boldsymbol{v}_\partial,\, \mathcal{N}_{\partial,1} \boldsymbol{e}_2 \rangle_{L^2(\partial\Omega,\mathbb{R}^m)}\,.\end{aligned} \tag{6.51}$$

Otherwise, if operator $\mathcal{L}$ is integrated by parts, it is computed

$$\begin{aligned}\langle \boldsymbol{v}_1,\, \mathcal{M}_1 \partial_t \boldsymbol{e}_1 \rangle_{L^2(\Omega,\mathbb{A})} &= -\langle \boldsymbol{v}_1,\, \boldsymbol{L}^\top \boldsymbol{e}_2 \rangle_{L^2(\Omega,\mathbb{A})} - \langle \boldsymbol{v}_1,\, \mathcal{L}^* \boldsymbol{e}_2 \rangle_{L^2(\Omega,\mathbb{A})}\,, \\ \langle \boldsymbol{v}_2,\, \mathcal{M}_2 \partial_t \boldsymbol{e}_2 \rangle_{L^2(\Omega,\mathbb{B})} &= \langle \boldsymbol{v}_2,\, \boldsymbol{L} \boldsymbol{e}_1 \rangle_{L^2(\Omega,\mathbb{B})} + \langle \mathcal{L}^* \boldsymbol{v}_2,\, \boldsymbol{e}_1 \rangle_{L^2(\Omega,\mathbb{A})} + \langle \mathcal{N}_{\partial,2} \boldsymbol{v}_2,\, \boldsymbol{u}_\partial \rangle_{L^2(\partial\Omega,\mathbb{R}^m)}\,, \\ \langle \boldsymbol{v}_\partial,\, \boldsymbol{y}_\partial \rangle_{L^2(\partial\Omega,\mathbb{R}^m)} &= \langle \boldsymbol{v}_\partial,\, \mathcal{N}_{\partial,2} \boldsymbol{e}_2 \rangle_{L^2(\partial\Omega,\mathbb{R}^m)}\,.\end{aligned} \tag{6.52}$$

After introducing a Galerkin approximation as in (6.23), the discretized version of the weak form (6.51) reads

$$\begin{aligned}\begin{bmatrix} \mathbf{M}_{\mathcal{M}_1} & \mathbf{0} \\ \mathbf{0} & \mathbf{M}_{\mathcal{M}_2} \end{bmatrix} \begin{pmatrix} \dot{\mathbf{e}}_1 \\ \dot{\mathbf{e}}_2 \end{pmatrix} &= \begin{bmatrix} \mathbf{0} & -\mathbf{D}_0^\top - \mathbf{D}_{\mathcal{L}}^\top \\ \mathbf{D}_0 + \mathbf{D}_{\mathcal{L}} & \mathbf{0} \end{bmatrix} \begin{pmatrix} \mathbf{e}_1 \\ \mathbf{e}_2 \end{pmatrix} + \begin{bmatrix} \mathbf{B}_1 \\ \mathbf{0} \end{bmatrix} \mathbf{u}_\partial, \\ \mathbf{M}_\partial \mathbf{y}_\partial &= \begin{bmatrix} \mathbf{B}_1^\top & \mathbf{0} \end{bmatrix} \begin{pmatrix} \mathbf{e}_1 \\ \mathbf{e}_2 \end{pmatrix}.\end{aligned} \tag{6.53}$$

The only difference with respect to Eq. (6.24) concerns the mass matrices

$$M^{ij}_{\mathcal{M}_1} = \left\langle \boldsymbol{\phi}_1^i,\, \mathcal{M}_1 \boldsymbol{\phi}_1^j \right\rangle_{L^2(\Omega,\mathbb{A})}, \quad M^{mn}_{\mathcal{M}_2} = \langle \boldsymbol{\phi}_2^m,\, \mathcal{M}_2 \boldsymbol{\phi}_2^n \rangle_{L^2(\Omega,\mathbb{B})} \quad i,j \in \{1, n_1\},\ m,n \in \{1, n_2\}. \tag{6.54}$$

If the Galerkin approximation is applied to the weak form (6.52), it is obtained

$$\begin{aligned}\begin{bmatrix} \mathbf{M}_{\mathcal{M}_1} & \mathbf{0} \\ \mathbf{0} & \mathbf{M}_{\mathcal{M}_2} \end{bmatrix} \begin{pmatrix} \dot{\mathbf{e}}_1 \\ \dot{\mathbf{e}}_2 \end{pmatrix} &= \begin{bmatrix} \mathbf{0} & -\mathbf{D}_0^\top + \mathbf{D}_{-\mathcal{L}^*} \\ \mathbf{D}_0 - \mathbf{D}_{-\mathcal{L}^*}^\top & \mathbf{0} \end{bmatrix} \begin{pmatrix} \mathbf{e}_1 \\ \mathbf{e}_2 \end{pmatrix} + \begin{bmatrix} \mathbf{0} \\ \mathbf{B}_2 \end{bmatrix} \mathbf{u}_\partial, \\ \mathbf{M}_\partial \mathbf{y}_\partial &= \begin{bmatrix} \mathbf{0} & \mathbf{B}_2^\top \end{bmatrix} \begin{pmatrix} \mathbf{e}_1 \\ \mathbf{e}_2 \end{pmatrix}.\end{aligned} \tag{6.55}$$

In both cases, it is easy to verify that the Hamiltonian

$$H_d = \frac{1}{2}\mathbf{e}_1^\top \mathbf{M}_{\mathcal{M}_1}\mathbf{e}_1 + \frac{1}{2}\mathbf{e}_2^\top \mathbf{M}_{\mathcal{M}_2}\mathbf{e}_2, \tag{6.56}$$

once differentiated in time, provides the energy rate

$$\dot{H}_d = \mathbf{y}_\partial^\top \mathbf{M}_\partial \mathbf{u}_\partial = \widehat{\mathbf{y}}_\partial^\top \mathbf{u}_\partial, \qquad \text{where} \qquad \widehat{\mathbf{y}}_\partial := \mathbf{M}_\partial \mathbf{y}_\partial. \tag{6.57}$$

This result mimics its finite-dimensional counterpart (6.50).

6.1.4 Linear flexible structures

In this section, some linear examples from the elasticity realm are considered. We restrict the discussion to linear problems. This case is anyway significant, as these examples are frequently encountered in engineering applications.

6.1.4.1 Euler-Bernoulli beam

We reconsider the example discussed in §2.3.2. The relation between energy and co-energy variables is given by Eqs. (2.25), (2.27)

$$\alpha_w = \rho A\, e_w, \qquad \alpha_\kappa = \frac{1}{EI}\, e_\kappa \tag{6.58}$$

The coefficients ρ, A, E and I are the mass density, the cross section area, Young's modulus of elasticity and the moment of inertia of the cross section.

Control through forces and torques Given an interval $\Omega = (0,\, L)$, a thin beam under free boundary condition (forces and torques imposed at the boundary) can be modeled in terms of co-energy variables by the following system

$$\begin{bmatrix} \rho A & 0 \\ 0 & (EI)^{-1} \end{bmatrix} \frac{\partial}{\partial t} \begin{pmatrix} e_w \\ e_\kappa \end{pmatrix} = \begin{bmatrix} 0 & -\partial_{xx} \\ \partial_{xx} & 0 \end{bmatrix} \begin{pmatrix} e_w \\ e_\kappa \end{pmatrix}, \qquad \begin{matrix} e_w \in H^2(\Omega), \\ e_\kappa \in H^2(\Omega), \end{matrix} \tag{6.59a}$$

$$\boldsymbol{u}_\partial = \begin{bmatrix} 0 & \gamma_0 \\ 0 & -\gamma_1 \end{bmatrix} \begin{pmatrix} e_w \\ e_\kappa \end{pmatrix}, \qquad \boldsymbol{u}_\partial \in \mathbb{R}^4, \tag{6.59b}$$

$$\boldsymbol{y}_\partial = \begin{bmatrix} \gamma_1 & 0 \\ \gamma_0 & 0 \end{bmatrix} \begin{pmatrix} e_w \\ e_\kappa \end{pmatrix}, \qquad \boldsymbol{y}_\partial \in \mathbb{R}^4. \tag{6.59c}$$

The boundary operators $\boldsymbol{\gamma}_0$, $\boldsymbol{\gamma}_1$ denote the trace and the first derivative trace along the boundary. In a one-dimensional domain the boundary degenerates to two single points

$$\boldsymbol{\gamma}_0 a = a|_{\partial\Omega} = \begin{pmatrix} -a(0) \\ +a(L) \end{pmatrix}, \qquad \boldsymbol{\gamma}_1 a = \partial_{\boldsymbol{n}} a|_{\partial\Omega} = \begin{pmatrix} -\partial_x a(0) \\ +\partial_x a(L) \end{pmatrix}. \tag{6.60}$$

In this case $\mathbb{A} = \mathbb{B} = \mathbb{R}$. The operators $\mathcal{M}_1$, $\mathcal{M}_2$, $\mathcal{L}$, $N_{\partial,1}$, $N_{\partial,2}$ read

$$\mathcal{M}_1 = \rho A, \qquad \mathcal{M}_2 = (EI)^{-1}, \qquad \mathcal{L} = \partial_{xx}, \qquad N_{\partial,1} = \begin{bmatrix} \boldsymbol{\gamma}_1 \\ \boldsymbol{\gamma}_0 \end{bmatrix}, \qquad N_{\partial,2} = \begin{bmatrix} \boldsymbol{\gamma}_0 \\ -\boldsymbol{\gamma}_1 \end{bmatrix}. \tag{6.61}$$

The Hamiltonian is given by

$$H = \frac{1}{2} \int_\Omega \left\{ \rho A \; e_w^2 + (EI)^{-1} \; e_\kappa^2 \right\} \, \mathrm{d}\Omega. \tag{6.62}$$

Applying the integration by parts formula twice, one obtains the power balance

$$\begin{aligned} \dot{H} &= \langle e_w, \, \rho A \; \partial_t e_w \rangle_{L^2(\Omega)} + \left\langle e_\kappa, \, (EI)^{-1} \; \partial_t e_\kappa \right\rangle_{L^2(\Omega)}, \\ &= \langle e_w, \, -\partial_{xx} e_\kappa \rangle_{L^2(\Omega)} + \langle e_\kappa, \, \partial_{xx} e_w \rangle_{L^2(\Omega)}, \\ &= \langle \boldsymbol{\gamma}_1 e_w, \, \boldsymbol{\gamma}_0 e_\kappa \rangle_{\mathbb{R}^2} + \langle \boldsymbol{\gamma}_0 e_w, \, -\boldsymbol{\gamma}_1 e_\kappa \rangle_{\mathbb{R}^2}, \\ &= \langle \boldsymbol{y}_\partial, \, \boldsymbol{u}_\partial \rangle_{\mathbb{R}^4}. \end{aligned} \tag{6.63}$$

Given the test functions v_w, v_κ, the weak form is readily obtained as

$$\begin{aligned} \langle v_w, \, \rho A \partial_t e_w \rangle_{L^2(\Omega)} &= \langle v_w, \, -\partial_{xx} e_\kappa \rangle_{L^2(\Omega)}, \\ \left\langle v_\kappa, \, (EI)^{-1} \partial_t e_\kappa \right\rangle_{L^2(\Omega)} &= \langle v_\kappa, \, \partial_{xx} e_w \rangle_{L^2(\Omega)}. \end{aligned} \tag{6.64}$$

If the integration by parts is applied twice to the first line of Eq. (6.59a), it is obtained

$$\begin{aligned} \langle v_w, \, \rho A \partial_t e_w \rangle_{L^2(\Omega)} &= -\langle \partial_{xx} v_w, \, e_\kappa \rangle_{L^2(\Omega)} + \langle \boldsymbol{\gamma}_1 v_w, \, (u_{\partial,1}, u_{\partial,2}) \rangle_{\mathbb{R}^2} + \langle \boldsymbol{\gamma}_0 v_w, \, (u_{\partial,3}, u_{\partial,4}) \rangle_{\mathbb{R}^2}, \\ \left\langle v_\kappa, \, (EI)^{-1} \partial_t e_\kappa \right\rangle_{L^2(\Omega)} &= \langle v_\kappa, \, \partial_{xx} e_w \rangle_{L^2(\Omega)}. \end{aligned} \tag{6.65}$$

Introducing a Galerkin discretization for test and efforts functions

$$v_w = \sum_{i=1}^{n_w} \phi_w^i v_w^i, \qquad e_w = \sum_{i=1}^{n_w} \phi_w^i e_w^i(t), \qquad v_\kappa = \sum_{i=1}^{n_\kappa} \phi_\kappa^i v_\kappa^i, \qquad e_\kappa = \sum_{i=1}^{n_\kappa} \phi_\kappa^i e_\kappa^i(t), \tag{6.66}$$

and considering that $\boldsymbol{u}_\partial \in \mathbb{R}^4, \boldsymbol{y}_\partial \in \mathbb{R}^4$, the following is obtained

$$\begin{aligned} \begin{bmatrix} \mathbf{M}_{\rho A} & \mathbf{0} \\ \mathbf{0} & \mathbf{M}_{EI^{-1}} \end{bmatrix} \begin{pmatrix} \dot{\mathbf{e}}_w \\ \dot{\mathbf{e}}_\kappa \end{pmatrix} &= \begin{bmatrix} \mathbf{0} & -\mathbf{D}_{\partial_{xx}}^\top \\ \mathbf{D}_{\partial_{xx}} & \mathbf{0} \end{bmatrix} \begin{pmatrix} \mathbf{e}_w \\ \mathbf{e}_\kappa \end{pmatrix} + \begin{bmatrix} \mathbf{B}_w \\ \mathbf{0} \end{bmatrix} \mathbf{u}_\partial, \\ \mathbf{y}_\partial &= \begin{bmatrix} \mathbf{B}_w^\top & \mathbf{0} \end{bmatrix} \begin{pmatrix} \mathbf{e}_w \\ \mathbf{e}_\kappa \end{pmatrix}. \end{aligned} \tag{6.67}$$

The matrices $\mathbf{M}_{\rho A}$, $\mathbf{M}_{EI^{-1}}$, $\mathbf{D}_{\partial_{xx}}$ are defined as ($i, j \in \{1, n_w\}$, $m, n \in \{1, n_\kappa\}$)

$$M^{ij}_{\rho A} = \left\langle \phi^i_w,\, \rho A \phi^j_w \right\rangle_{L^2(\Omega)}, \quad M^{mn}_{EI^{-1}} = \left\langle \phi^m_\kappa,\, (EI)^{-1} \phi^n_\kappa \right\rangle_{L^2(\Omega)}, \quad D^{mi}_{\partial_{xx}} = \left\langle \phi^m_\kappa,\, \partial_{xx} \phi^i_w \right\rangle_{L^2(\Omega)}. \tag{6.68}$$

The $\mathbf{B}_w$ is composed of four column vectors $\mathbf{B}_w = [\mathbf{b}^1_w\ \mathbf{b}^2_w\ \mathbf{b}^3_w\ \mathbf{b}^4_w]$

$$b^{1,i}_w = -\partial_x \phi^i_w(0), \qquad b^{2,i}_w = \partial_x \phi^i_w(L), \qquad b^{3,i}_w = -\phi^i_w(0), \qquad b^{4,i}_w = \phi^i_w(L), \qquad i \in \{1, n_w\}. \tag{6.69}$$

Control through linear and angular velocities Equivalently, the second line of Eq. (6.59a) could have been integrated by parts to control using the linear and angular velocities at the extremities. Consider the system with known forces and torques at the extremities

$$\begin{bmatrix} \rho A & 0 \\ 0 & (EI)^{-1} \end{bmatrix} \frac{\partial}{\partial t} \begin{pmatrix} e_w \\ e_\kappa \end{pmatrix} = \begin{bmatrix} 0 & -\partial_{xx} \\ \partial_{xx} & 0 \end{bmatrix} \begin{pmatrix} e_w \\ e_\kappa \end{pmatrix}, \qquad \begin{matrix} e_w \in H^2(\Omega), \\ e_\kappa \in H^2(\Omega), \end{matrix} \tag{6.70a}$$

$$\boldsymbol{u}_\partial = \begin{bmatrix} \boldsymbol{\gamma}_1 & 0 \\ \boldsymbol{\gamma}_0 & 0 \end{bmatrix} \begin{pmatrix} e_w \\ e_\kappa \end{pmatrix}, \qquad \boldsymbol{u}_\partial \in \mathbb{R}^4, \tag{6.70b}$$

$$\boldsymbol{y}_\partial = \begin{bmatrix} 0 & \boldsymbol{\gamma}_0 \\ 0 & -\boldsymbol{\gamma}_1 \end{bmatrix} \begin{pmatrix} e_w \\ e_\kappa \end{pmatrix}, \qquad \boldsymbol{y}_\partial \in \mathbb{R}^4. \tag{6.70c}$$

Once the system is put into weak form and the second line of Eq. (6.70a) is integrated twice, it is computed

$$\begin{aligned} \langle v_w,\, \rho A \partial_t e_w \rangle_{L^2(\Omega)} &= \langle v_w,\, -\partial_{xx} e_\kappa \rangle_{L^2(\Omega)}, \\ \left\langle v_\kappa,\, (EI)^{-1} \partial_t e_\kappa \right\rangle_{L^2(\Omega)} &= \langle \partial_{xx} v_\kappa,\, e_w \rangle_{L^2(\Omega)} + \langle \boldsymbol{\gamma}_0 v_\kappa,\, (u_{\partial,1}, u_{\partial,2}) \rangle_{\mathbb{R}^2} + \langle -\boldsymbol{\gamma}_1 v_\kappa,\, (u_{\partial,3}, u_{\partial,4}) \rangle_{\mathbb{R}^2}. \end{aligned} \tag{6.71}$$

Replacing a Galerkin approximation, it is obtained

$$\begin{aligned} \begin{bmatrix} \mathbf{M}_{\rho A} & \mathbf{0} \\ \mathbf{0} & \mathbf{M}_{EI^{-1}} \end{bmatrix} \begin{pmatrix} \dot{\mathbf{e}}_w \\ \dot{\mathbf{e}}_\kappa \end{pmatrix} &= \begin{bmatrix} \mathbf{0} & \mathbf{D}_{-\partial_{xx}} \\ -\mathbf{D}^\top_{-\partial_{xx}} & \mathbf{0} \end{bmatrix} \begin{pmatrix} \mathbf{e}_w \\ \mathbf{e}_\kappa \end{pmatrix} + \begin{bmatrix} \mathbf{0} \\ \mathbf{B}_\kappa \end{bmatrix} \mathbf{u}_\partial, \\ \mathbf{y}_\partial &= \begin{bmatrix} \mathbf{0} & \mathbf{B}^\top_\kappa \end{bmatrix} \begin{pmatrix} \mathbf{e}_w \\ \mathbf{e}_\kappa \end{pmatrix}. \end{aligned} \tag{6.72}$$

The rectangular matrix $\mathbf{D}_{-\partial_{xx}}$ is defined as

$$D^{im}_{-\partial_{xx}} = \left\langle \phi^i_w,\, -\partial_{xx} \phi^m_\kappa \right\rangle_{L^2(\Omega)}, \qquad i, \in \{1, n_w\},\ m \in \{1, n_\kappa\}. \tag{6.73}$$

The $\mathbf{B}_\kappa$ is composed of four column vectors $\mathbf{B}_\kappa = [\mathbf{b}^1_\kappa\ \mathbf{b}^2_\kappa\ \mathbf{b}^3_\kappa\ \mathbf{b}^4_\kappa]$

$$b^{1,m}_\kappa = -\phi^m_\kappa(0), \quad b^{2,m}_\kappa = \phi^m_\kappa(L), \quad b^{3,m}_\kappa = \partial_x \phi^m_\kappa(0), \quad b^{4,m}_\kappa = -\partial_x \phi^m_\kappa(L), \quad m \in \{1, n_\kappa\}. \tag{6.74}$$

Both discretizations require the use of Hermite polynomials to meet the regularity re-

quirement. Indeed, to lower the regularity requirement for the finite elements employed in the discretization, both lines can be integrated by parts. This will be discussed in Chap. 7.

6.1.4.2 Kirchhoff plate

The link beetween the energy and co-energy variables for the isotropic Kirchhoff model is the following (4.34)

$$\alpha_w = \rho h e_w, \qquad \boldsymbol{A}_\kappa = \boldsymbol{\mathcal{C}}_b \boldsymbol{E}_\kappa, \qquad \text{where} \qquad \boldsymbol{\mathcal{C}}_b := \boldsymbol{\mathcal{D}}_b^{-1} \tag{6.75}$$

where ρ is the mass density, h the plate thickness and $\boldsymbol{\mathcal{D}}_b$, the bending rigidity tensor, cf. Eq. (4.11). The bending compliance is given by

$$\boldsymbol{\mathcal{C}}_b = \frac{12}{Eh^3}[(1+\nu)(\cdot) - \nu \operatorname{Tr}(\cdot)\boldsymbol{I}_{2\times 2}]. \tag{6.76}$$

Given an open connected set $\Omega \subset \mathbb{R}^2$, the Kirchhoff plate model (4.43) in co-energy form controlled by forces and momenta is then expressed as

$$\begin{bmatrix} \rho h & 0 \\ 0 & \boldsymbol{\mathcal{C}}_b \end{bmatrix} \frac{\partial}{\partial t} \begin{pmatrix} e_w \\ \boldsymbol{E}_\kappa \end{pmatrix} = \begin{bmatrix} 0 & -\operatorname{div}\operatorname{Div} \\ \operatorname{Hess} & \boldsymbol{0} \end{bmatrix} \begin{pmatrix} e_w \\ \boldsymbol{E}_\kappa \end{pmatrix}, \qquad \begin{matrix} e_w \in H^2(\Omega), \\ \boldsymbol{E}_\kappa \in H^{\operatorname{div}\operatorname{Div}}(\Omega, \mathbb{R}^{2\times 2}_{\mathrm{sym}}), \end{matrix} \tag{6.77a}$$

$$\boldsymbol{u}_\partial = \begin{bmatrix} 0 & \gamma_{nn,1} \\ 0 & \gamma_{nn} \end{bmatrix} \begin{pmatrix} e_w \\ \boldsymbol{E}_\kappa \end{pmatrix}, \qquad \boldsymbol{u}_\partial \in L^2(\partial\Omega, \mathbb{R}^2), \tag{6.77b}$$

$$\boldsymbol{y}_\partial = \begin{bmatrix} \gamma_0 & 0 \\ \gamma_1 & 0 \end{bmatrix} \begin{pmatrix} e_w \\ \boldsymbol{E}_\kappa \end{pmatrix}, \qquad \boldsymbol{y}_\partial \in L^2(\partial\Omega, \mathbb{R}^2), \tag{6.77c}$$

We recall the expressions of the trace maps

$$\begin{aligned} &\gamma_0 a = a|_{\partial\Omega}, \qquad && \gamma_{nn,1}\boldsymbol{A} = -\boldsymbol{n}\cdot\operatorname{Div}\boldsymbol{A} - \partial_{\boldsymbol{s}}(\boldsymbol{A} : (\boldsymbol{n}\otimes\boldsymbol{s}))|_{\partial\Omega}, \\ &\gamma_1 a = \partial_{\boldsymbol{n}} a|_{\partial\Omega}, \qquad && \gamma_{nn}\boldsymbol{A} = \boldsymbol{A} : (\boldsymbol{n}\otimes\boldsymbol{n})|_{\partial\Omega}. \end{aligned} \tag{6.78}$$

In this case, the sets are $\mathbb{A} = \mathbb{R}$, $\mathbb{B} = \mathbb{R}^{2\times 2}_{\mathrm{sym}}$. The operators $\mathcal{M}_1$, $\mathcal{M}_2$, $\mathcal{L}$, $N_{\partial,1}$, $N_{\partial,2}$ are

$$\mathcal{M}_1 = \rho h, \qquad \mathcal{M}_2 = \boldsymbol{\mathcal{C}}_b, \qquad \mathcal{L} = \operatorname{Hess}, \qquad N_{\partial,1} = \begin{bmatrix} \gamma_0 \\ \gamma_1 \end{bmatrix}, \qquad N_{\partial,2} = \begin{bmatrix} \gamma_{nn,1} \\ \gamma_{nn} \end{bmatrix}. \tag{6.79}$$

The energy rate from Eq. (4.40) equals $\dot{H} = \langle \boldsymbol{y}_\partial, \boldsymbol{u}_\partial \rangle_{L^2(\partial\Omega,\mathbb{R}^2)}$. Introducing the test functions $(v_w, \boldsymbol{V}_\kappa)$ and integrating by parts the first line of (6.77a) twice, one gets

$$\begin{aligned} &\langle v_w, \rho h \partial_t e_w \rangle_{L^2(\Omega)} = -\langle \operatorname{Hess} v_w, \boldsymbol{E}_\kappa \rangle_{L^2(\Omega,\mathbb{R}^{2\times 2}_{\mathrm{sym}})} + \langle \gamma_0 v_w, u_{\partial,1} \rangle_{L^2(\partial\Omega)} + \langle \gamma_1 v_w, u_{\partial,2} \rangle_{L^2(\partial\Omega)}, \\ &\langle \boldsymbol{V}_\kappa, \boldsymbol{\mathcal{C}_b} \partial_t \boldsymbol{V}_\kappa \rangle_{L^2(\Omega,\mathbb{R}^{2\times 2}_{\mathrm{sym}})} = \langle \boldsymbol{V}_\kappa, \operatorname{Hess} e_w \rangle_{L^2(\Omega,\mathbb{R}^{2\times 2}_{\mathrm{sym}})}. \end{aligned} \tag{6.80}$$

Introducing a Galerkin discretization for test and co-energy functions

$$\begin{aligned} v_w &= \sum_{i=1}^{n_w} \phi_w^i v_w^i, & \boldsymbol{V}_\kappa &= \sum_{i=1}^{n_\kappa} \boldsymbol{\Phi}_\kappa^i v_\kappa^i, & \boldsymbol{v}_\partial &= \sum_{i=1}^{n_\partial} \boldsymbol{\phi}_\partial^i v_\partial^i, \\ e_w &= \sum_{i=1}^{n_w} \phi_w^i e_w^i, & \boldsymbol{E}_\kappa &= \sum_{i=1}^{n_\kappa} \boldsymbol{\Phi}_\kappa^i e_\kappa^i & \boldsymbol{u}_\partial &= \sum_{i=1}^{n_\partial} \boldsymbol{\phi}_\partial^i u_\partial^i, \end{aligned} \qquad \boldsymbol{y}_\partial = \sum_{i=1}^{n_\partial} \boldsymbol{\phi}_\partial^i y_\partial^i. \tag{6.81}$$

the following finite-dimensional system is obtained

$$\begin{aligned} \begin{bmatrix} \mathbf{M}_{\rho h} & \mathbf{0} \\ \mathbf{0} & \mathbf{M}_{\boldsymbol{\mathcal{C}}_b} \end{bmatrix} \begin{pmatrix} \dot{\mathbf{e}}_w \\ \dot{\mathbf{e}}_\kappa \end{pmatrix} &= \begin{bmatrix} \mathbf{0} & -\mathbf{D}_{\text{Hess}}^\top \\ \mathbf{D}_{\text{Hess}} & \mathbf{0} \end{bmatrix} \begin{pmatrix} \mathbf{e}_w \\ \mathbf{e}_\kappa \end{pmatrix} + \begin{bmatrix} \mathbf{B}_w & \mathbf{B}_{\partial_{\boldsymbol{n}} w} \\ \mathbf{0} & \mathbf{0} \end{bmatrix} \mathbf{u}_\partial, \\ \mathbf{M}_\partial \mathbf{y}_\partial &= \begin{bmatrix} \mathbf{B}_w^\top & \mathbf{0} \\ \mathbf{B}_{\partial_{\boldsymbol{n}} w}^\top & \mathbf{0} \end{bmatrix} \begin{pmatrix} \mathbf{e}_w \\ \mathbf{e}_\kappa \end{pmatrix}. \end{aligned} \tag{6.82}$$

The matrices $\mathbf{M}_{\rho h}$, $\mathbf{M}_{\boldsymbol{\mathcal{C}}_b}$, $\mathbf{D}_{\text{Hess}}$ are defined as $(i, j \in \{1, n_w\},\ m, n \in \{1, n_\kappa\})$

$$M_{\rho h}^{ij} = \left\langle \phi_w^i,\, \rho h \phi_w^j \right\rangle_{L^2(\Omega)}, \quad M_{\boldsymbol{\mathcal{C}}_b}^{mn} = \langle \boldsymbol{\Phi}_\kappa^m,\, \boldsymbol{\mathcal{C}}_b \boldsymbol{\Phi}_\kappa^n \rangle_{L^2(\Omega, \mathbb{R}^{2\times 2}_{\text{sym}})}, \quad D_{\text{Hess}}^{mi} = \left\langle \boldsymbol{\Phi}_\kappa^m,\, \text{Hess}\, \phi_w^i \right\rangle_{L^2(\Omega)}. \tag{6.83}$$

Matrices $\mathbf{B}_w$, $\mathbf{B}_{\partial_{\boldsymbol{n}} w}$ are given by

$$B_w^{il} = \left\langle \gamma_0 \phi_w^i,\, \phi_{\partial,1}^l \right\rangle_{L^2(\partial\Omega)}, \qquad B_{\partial_{\boldsymbol{n}} w}^{il} = \left\langle \gamma_1 \phi_w^i,\, \phi_{\partial,2}^l \right\rangle_{L^2(\partial\Omega)}, \qquad l \in \{1, n_\partial\}. \tag{6.84}$$

This kind of discretization requires H^2-conforming elements. The construction of those is rather involved and they are computationally expensive [AFS68, Bel69]. Nevertheless, this kind of discretization is able to handle generic boundary conditions [GSV18]. For this reason, it is the most adapted for the pH framework.

To lower the regularity requirement for the finite elements, many non conforming elements have been proposed. The most employed is the Hellan-Herrmann-Johnson element [AB85, BR90]. For what concerns conforming mixed discretization of the Kirchhoff plate, an interesting analysis can be found in [BDJ05]. Their method consists in integrating by parts both lines of 6.77a. Lagrange polynomials of order 2 (and bubble functions for mass lumping) are then employed for the velocity and bending momenta. However, these two methods do not handle generic non-homogeneous boundary conditions in a straightforward way.

Remark 17 (On the $H^{\text{div}\,\text{Div}}$ space)
Equivalently, the second line of Eq. (6.77a) can be integrated by parts twice to obtain a discretized system whose inputs are the linear velocity and the angular velocity at the boundary. Conforming finite elements for the $H^{\text{div}\,\text{Div}}$ space have been recently proposed [CH20]. An efficient implementation of these elements is not available yet.

6.1.4.3 Mindlin plate

Using Eqs. (4.22) and (4.24), the relation between co-energy and energy variables for the isotropic Mindlin plate is found to be

$$\begin{aligned} &\alpha_w = \rho h e_w, \qquad &&\boldsymbol{\alpha}_\theta = I_\theta \boldsymbol{e}_\theta, \qquad &&I_\theta := \rho h^3/12, \\ &\boldsymbol{A}_\kappa = \boldsymbol{\mathcal{C}}_b \boldsymbol{E}_\kappa, \qquad &&\boldsymbol{\alpha}_\gamma = C_s \boldsymbol{e}_\gamma, \qquad &&C_s := 1/(K_{\text{sh}} G h), \end{aligned} \tag{6.85}$$

where K_{sh} is the shear correction factor, G the shear modulus. The other variables have the same meaning as in §6.1.4.2.

Control through forces and torques A pH representation in co-energy variables with known forces and momenta at the boundary is given by the system

$$\begin{bmatrix} \rho h & 0 & 0 & 0 \\ \mathbf{0} & I_\theta & \mathbf{0} & \mathbf{0} \\ \mathbf{0} & \mathbf{0} & \boldsymbol{\mathcal{C}}_b & \mathbf{0} \\ \mathbf{0} & \mathbf{0} & \mathbf{0} & C_s \end{bmatrix} \frac{\partial}{\partial t} \begin{pmatrix} e_w \\ \boldsymbol{e}_\theta \\ \boldsymbol{E}_\kappa \\ \boldsymbol{e}_\gamma \end{pmatrix} = \begin{bmatrix} 0 & 0 & 0 & \text{div} \\ \mathbf{0} & \mathbf{0} & \text{Div} & \boldsymbol{I}_{2\times 2} \\ \mathbf{0} & \text{Grad} & \mathbf{0} & \mathbf{0} \\ \text{grad} & -\boldsymbol{I}_{2\times 2} & \mathbf{0} & \mathbf{0} \end{bmatrix} \begin{pmatrix} e_w \\ \boldsymbol{e}_\theta \\ \boldsymbol{E}_\kappa \\ \boldsymbol{e}_\gamma \end{pmatrix}, \quad \begin{aligned} &e_w \in H^1(\Omega), \\ &\boldsymbol{e}_\theta \in H^{\text{Grad}}(\Omega, \mathbb{R}^2), \\ &\boldsymbol{E}_\kappa \in H^{\text{Div}}(\Omega, \mathbb{R}^{2\times 2}_{\text{sym}}), \\ &\boldsymbol{e}_\gamma \in H^{\text{div}}(\Omega, \mathbb{R}^2), \end{aligned} \tag{6.86a}$$

$$\boldsymbol{u}_\partial = \begin{bmatrix} 0 & 0 & 0 & \gamma_n \\ 0 & 0 & \gamma_{nn} & 0 \\ 0 & 0 & \gamma_{ns} & 0 \end{bmatrix} \begin{pmatrix} e_w \\ \boldsymbol{e}_\theta \\ \boldsymbol{E}_\kappa \\ \boldsymbol{e}_\gamma \end{pmatrix}, \qquad \boldsymbol{u}_\partial \in L^2(\partial\Omega, \mathbb{R}^3), \tag{6.86b}$$

$$\boldsymbol{y}_\partial = \begin{bmatrix} \gamma_0 & 0 & 0 & 0 \\ 0 & \gamma_n & 0 & 0 \\ 0 & \gamma_s & 0 & 0 \end{bmatrix} \begin{pmatrix} e_w \\ \boldsymbol{e}_\theta \\ \boldsymbol{E}_\kappa \\ \boldsymbol{e}_\gamma \end{pmatrix}, \qquad \boldsymbol{y}_\partial \in L^2(\partial\Omega, \mathbb{R}^3). \tag{6.86c}$$

The trace operators are defined as

$$\begin{aligned} &\gamma_0 a = a|_{\partial\Omega}, \qquad &&\gamma_n \boldsymbol{a} = \boldsymbol{a} \cdot \boldsymbol{n}|_{\partial\Omega}, \qquad &&\gamma_{nn} \boldsymbol{A} = \boldsymbol{A} : (\boldsymbol{n} \otimes \boldsymbol{n})|_{\partial\Omega}, \\ &&&\gamma_s \boldsymbol{a} = \boldsymbol{a} \cdot \boldsymbol{s}|_{\partial\Omega}, &&\gamma_{ns} \boldsymbol{A} = \boldsymbol{A} : (\boldsymbol{n} \otimes \boldsymbol{s})|_{\partial\Omega}. \end{aligned} \tag{6.87}$$

The variables assume values in the sets $\mathbb{A} = \mathbb{R} \times \mathbb{R}^2$, $\mathbb{B} = \mathbb{R}^{2\times 2}_{\text{sym}} \times \mathbb{R}^2$. The mass operators are given by

$$\mathcal{M}_1 = \begin{bmatrix} \rho h & 0 \\ \mathbf{0} & I_\theta \end{bmatrix}, \qquad \mathcal{M}_2 = \begin{bmatrix} \boldsymbol{\mathcal{C}}_b & \mathbf{0} \\ \mathbf{0} & C_s \end{bmatrix}. \tag{6.88}$$

The $\boldsymbol{L}$, $\mathcal{L}$, $\mathcal{N}_{\partial,1}$, $\mathcal{N}_{\partial,2}$ operators are

$$\boldsymbol{L} = \begin{bmatrix} \mathbf{0} & \mathbf{0} \\ \mathbf{0} & -\boldsymbol{I}_{2\times 2} \end{bmatrix}, \qquad \mathcal{L} = \begin{bmatrix} \mathbf{0} & \mathrm{Grad} \\ \mathrm{grad} & \mathbf{0} \end{bmatrix}, \qquad \mathcal{N}_{\partial,1} = \begin{bmatrix} \gamma_0 & 0 \\ 0 & \gamma_n \\ 0 & \gamma_s \end{bmatrix}, \qquad \mathcal{N}_{\partial,2} = \begin{bmatrix} 0 & \gamma_n \\ \gamma_{nn} & 0 \\ \gamma_{ns} & 0 \end{bmatrix}. \tag{6.89}$$

The energy rate is retrieved from Eq. (4.26) $\dot{H} = \langle \boldsymbol{y}_\partial,\, \boldsymbol{u}_\partial \rangle_{L^2(\partial\Omega,\mathbb{R}^2)}$.
Introducing the test functions $(v_w,\, \boldsymbol{v}_\theta,\, \boldsymbol{V}_\kappa,\, \boldsymbol{v}_\gamma)$ and integrating by parts the first two lines of (6.86a) one gets

$$\begin{aligned}
\langle v_w,\, \rho h \partial_t e_w \rangle_{L^2(\Omega)} &= -\langle \mathrm{grad}\, v_w,\, \boldsymbol{e}_\gamma \rangle_{L^2(\Omega,\mathbb{R}^2)} + \langle \gamma_0 v_w,\, u_{\partial,1} \rangle_{L^2(\partial\Omega)}\,, \\
\langle \boldsymbol{v}_\theta,\, I_\theta \partial_t \boldsymbol{e}_\theta \rangle_{L^2(\Omega,\mathbb{R}^2)} &= -\langle \mathrm{Grad}\, \boldsymbol{v}_\theta,\, \boldsymbol{E}_\kappa \rangle_{L^2(\Omega,\mathbb{R}^{2\times 2}_{\mathrm{sym}})} + \langle \boldsymbol{v}_\theta,\, \boldsymbol{e}_\gamma \rangle_{L^2(\Omega)} + \langle \boldsymbol{\gamma}_0 \boldsymbol{v}_\theta,\, \boldsymbol{\gamma}_n \boldsymbol{E}_\kappa \rangle_{L^2(\partial\Omega,\mathbb{R}^2)}\,, \\
\langle \boldsymbol{V}_\kappa,\, \boldsymbol{\mathcal{C}_b} \partial_t \boldsymbol{E}_\kappa \rangle_{L^2(\Omega,\mathbb{R}^{2\times 2}_{\mathrm{sym}})} &= \langle \boldsymbol{V}_\kappa,\, \mathrm{Grad}\, \boldsymbol{e}_\theta \rangle_{L^2(\Omega,\mathbb{R}^{2\times 2}_{\mathrm{sym}})}\,, \\
\langle \boldsymbol{v}_\gamma,\, C_s \partial_t \boldsymbol{e}_\gamma \rangle_{L^2(\Omega,\mathbb{R}^2)} &= \langle \boldsymbol{v}_\gamma,\, \mathrm{grad}\, e_w \rangle_{L^2(\Omega,\mathbb{R}^2)} - \langle \boldsymbol{v}_\gamma,\, \boldsymbol{e}_\theta \rangle_{L^2(\Omega,\mathbb{R}^2)}\,.
\end{aligned} \tag{6.90}$$

The term $\langle \boldsymbol{\gamma}_0 \boldsymbol{v}_\theta,\, \boldsymbol{\gamma}_n \boldsymbol{E}_\kappa \rangle_{L^2(\partial\Omega,\mathbb{R}^2)}$ can be decomposed in its tangential and normal components

$$\langle \boldsymbol{\gamma}_0 \boldsymbol{v}_\theta,\, \boldsymbol{\gamma}_n \boldsymbol{E}_\kappa \rangle_{L^2(\partial\Omega,\mathbb{R}^2)} = \langle \gamma_n \boldsymbol{v}_\theta,\, u_{\partial,2} \rangle_{L^2(\partial\Omega)} + \langle \gamma_s \boldsymbol{v}_\theta,\, u_{\partial,3} \rangle_{L^2(\partial\Omega)} \tag{6.91}$$

Introducing a Galerkin discretization for test and co-energy functions

$$\begin{aligned}
v_w &= \sum_{i=1}^{n_w} \phi_w^i v_w^i, & \boldsymbol{v}_\theta &= \sum_{i=1}^{n_\theta} \boldsymbol{\phi}_\theta^i v_\theta^i, & \boldsymbol{V}_\kappa &= \sum_{i=1}^{n_\kappa} \boldsymbol{\Phi}_\kappa^i v_\kappa^i, & \boldsymbol{v}_\gamma &= \sum_{i=1}^{n_\gamma} \boldsymbol{\phi}_\gamma^i v_\gamma^i, & \boldsymbol{v}_\partial &= \sum_{i=1}^{n_\partial} \boldsymbol{\phi}_\partial^i v_\partial^i, \\
e_w &= \sum_{i=1}^{n_w} \phi_w^i e_w^i, & \boldsymbol{e}_\theta &= \sum_{i=1}^{n_\theta} \boldsymbol{\phi}_\theta^i e_\theta^i, & \boldsymbol{E}_\kappa &= \sum_{i=1}^{n_\kappa} \boldsymbol{\Phi}_\kappa^i e_\kappa^i, & \boldsymbol{e}_\gamma &= \sum_{i=1}^{n_\gamma} \boldsymbol{\phi}_\gamma^i e_\gamma^i, & \boldsymbol{u}_\partial &= \sum_{i=1}^{n_\partial} \boldsymbol{\phi}_\partial^i u_\partial^i, \\
& & & & & & & & \boldsymbol{y}_\partial &= \sum_{i=1}^{n_\partial} \boldsymbol{\phi}_\partial^i y_\partial^i.
\end{aligned} \tag{6.92}$$

the following finite-dimensional system is obtained

$$\begin{aligned}
\mathrm{Diag} \begin{bmatrix} \mathbf{M}_{\rho h} \\ \mathbf{M}_{I_\theta} \\ \mathbf{M}_{\boldsymbol{\mathcal{C}}_b} \\ \mathbf{M}_{C_s} \end{bmatrix} \begin{pmatrix} \dot{\mathbf{e}}_w \\ \dot{\mathbf{e}}_\theta \\ \dot{\mathbf{e}}_\kappa \\ \dot{\mathbf{e}}_\gamma \end{pmatrix} &= \begin{bmatrix} \mathbf{0} & \mathbf{0} & \mathbf{0} & -\mathbf{D}_{\mathrm{grad}}^\top \\ \mathbf{0} & \mathbf{0} & -\mathbf{D}_{\mathrm{Grad}}^\top & -\mathbf{D}_0^\top \\ \mathbf{0} & \mathbf{D}_{\mathrm{Grad}} & \mathbf{0} & \mathbf{0} \\ \mathbf{D}_{\mathrm{grad}} & \mathbf{D}_0 & \mathbf{0} & \mathbf{0} \end{bmatrix} \begin{pmatrix} \mathbf{e}_w \\ \mathbf{e}_\theta \\ \mathbf{e}_\kappa \\ \mathbf{e}_\gamma \end{pmatrix} + \begin{bmatrix} \mathbf{B}_w & \mathbf{0} & \mathbf{0} \\ \mathbf{0} & \mathbf{B}_{\theta_n} & \mathbf{B}_{\theta_s} \\ \mathbf{0} & \mathbf{0} & \mathbf{0} \\ \mathbf{0} & \mathbf{0} & \mathbf{0} \end{bmatrix} \mathbf{u}_\partial, \\
\mathbf{M}_\partial \mathbf{y}_\partial &= \begin{bmatrix} \mathbf{B}_w^\top & \mathbf{0} & \mathbf{0} & \mathbf{0} \\ \mathbf{0} & \mathbf{B}_{\theta_n}^\top & \mathbf{0} & \mathbf{0} \\ \mathbf{0} & \mathbf{B}_{\theta_s}^\top & \mathbf{0} & \mathbf{0} \end{bmatrix} \begin{pmatrix} \mathbf{e}_w \\ \mathbf{e}_\theta \\ \mathbf{e}_\kappa \\ \mathbf{e}_\gamma \end{pmatrix}.
\end{aligned} \tag{6.93}$$

The notation Diag denotes a block-diagonal matrix. The mass matrices $\mathbf{M}_{\rho h},\ \mathbf{M}_{I_\theta},\ \mathbf{M}_{\boldsymbol{\mathcal{C}}_b},\ \mathbf{M}_{C_s}$

are computed as

$$\begin{aligned} M^{ij}_{\rho h} &= \left\langle \phi^i_w,\, \rho h \phi^j_w \right\rangle_{L^2(\Omega)}, & M^{pq}_{\boldsymbol{\mathcal{C}}_b} &= \langle \boldsymbol{\Phi}^p_\kappa,\, \boldsymbol{\mathcal{C}}_b \boldsymbol{\Phi}^q_\kappa \rangle_{L^2(\Omega,\mathbb{R}^{2\times 2}_{\mathrm{sym}})}, \\ M^{mn}_{I_\theta} &= \langle \phi^m_\kappa,\, I_\theta \phi^n_\kappa \rangle_{L^2(\Omega,\mathbb{R}^2)}, & M^{rs}_{C_s} &= \left\langle \boldsymbol{\phi}^r_\gamma,\, C_s \boldsymbol{\phi}^s_\gamma \right\rangle_{L^2(\Omega,\mathbb{R}^2)}, \end{aligned} \tag{6.94}$$

where $i,j \in \{1,n_w\},\ m,n \in \{1,n_\theta\},\ p,q \in \{1,n_\kappa\},\ r,s \in \{1,n_\gamma\}$. Matrices $\mathbf{D}_{\mathrm{grad}},\ \mathbf{D}_{\mathrm{Grad}},\ \mathbf{D}_0$ assume the form

$$\begin{aligned} D^{rj}_{\mathrm{grad}} &= \left\langle \boldsymbol{\phi}^r_\gamma,\, \operatorname{grad} \phi^j_w \right\rangle_{L^2(\Omega,\mathbb{R}^2)}, \\ D^{pn}_{\mathrm{Grad}} &= \langle \boldsymbol{\Phi}^p_\kappa,\, \operatorname{Grad} \boldsymbol{\phi}^n_\theta \rangle_{L^2(\Omega,\mathbb{R}^{2\times 2}_{\mathrm{sym}})}, \end{aligned} \qquad D^{rn}_0 = -\left\langle \boldsymbol{\phi}^r_\gamma,\, \boldsymbol{\phi}^n_\theta \right\rangle_{L^2(\Omega,\mathbb{R}^2)}. \tag{6.95}$$

Matrices $\mathbf{B}_w$, $\mathbf{B}_{\theta_n}$, $\mathbf{B}_{\theta_s}$ are computed as ($l \in \{1,n_\partial\}$)

$$B^{il}_w = \left\langle \gamma_0 \phi^i_w,\, \phi^l_{\partial,1} \right\rangle_{L^2(\partial\Omega)}, \qquad B^{ml}_{\theta_n} = \left\langle \gamma_n \boldsymbol{\phi}^m_\theta,\, \phi^l_{\partial,2} \right\rangle_{L^2(\partial\Omega)}, \qquad B^{ml}_{\theta_s} = \left\langle \gamma_s \boldsymbol{\phi}^m_\theta,\, \phi^l_{\partial,3} \right\rangle_{L^2(\partial\Omega)}. \tag{6.96}$$

Control through linear and angular velocities If instead the opposite causality is considered, the continuous system reads

$$\begin{bmatrix} \rho h & 0 & 0 & 0 \\ \mathbf{0} & I_\theta & \mathbf{0} & \mathbf{0} \\ \mathbf{0} & \mathbf{0} & \boldsymbol{\mathcal{C}}_b & \mathbf{0} \\ \mathbf{0} & \mathbf{0} & \mathbf{0} & C_s \end{bmatrix} \frac{\partial}{\partial t} \begin{pmatrix} e \\ \boldsymbol{e}_\theta \\ \boldsymbol{E}_\kappa \\ \boldsymbol{e}_\gamma \end{pmatrix} = \begin{bmatrix} 0 & 0 & 0 & \operatorname{div} \\ \mathbf{0} & \mathbf{0} & \operatorname{Div} & \boldsymbol{I}_{2\times 2} \\ \mathbf{0} & \operatorname{Grad} & \mathbf{0} & \mathbf{0} \\ \operatorname{grad} & -\boldsymbol{I}_{2\times 2} & \mathbf{0} & \mathbf{0} \end{bmatrix} \begin{pmatrix} e_w \\ \boldsymbol{e}_\theta \\ \boldsymbol{E}_\kappa \\ \boldsymbol{e}_\gamma \end{pmatrix}, \tag{6.97a}$$

$$\boldsymbol{u}_\partial = \begin{bmatrix} \gamma_0 & 0 & 0 & 0 \\ 0 & \gamma_n & 0 & 0 \\ 0 & \gamma_s & 0 & 0 \end{bmatrix} \begin{pmatrix} e_w \\ \boldsymbol{e}_\theta \\ \boldsymbol{E}_\kappa \\ \boldsymbol{e}_\gamma \end{pmatrix}, \qquad \boldsymbol{u}_\partial \in \mathbb{R}^3, \tag{6.97b}$$

$$\boldsymbol{y}_\partial = \begin{bmatrix} 0 & 0 & 0 & \gamma_n \\ 0 & 0 & \gamma_{nn} & 0 \\ 0 & 0 & \gamma_{ns} & 0 \end{bmatrix} \begin{pmatrix} e_w \\ \boldsymbol{e}_\theta \\ \boldsymbol{E}_\kappa \\ \boldsymbol{e}_\gamma \end{pmatrix}, \qquad \boldsymbol{y}_\partial \in \mathbb{R}^3. \tag{6.97c}$$

Integrating by parts the last two lines of (6.97a) one gets

$$\begin{aligned} \langle v_w,\, \rho h \partial_t e_w \rangle_{L^2(\Omega)} &= \langle v_w,\, \operatorname{div} \boldsymbol{e}_\gamma \rangle_{L^2(\Omega,\mathbb{R}^2)}, \\ \langle \boldsymbol{v}_\theta,\, I_\theta \partial_t \boldsymbol{e}_\theta \rangle_{L^2(\Omega,\mathbb{R}^2)} &= \langle \boldsymbol{v}_\theta,\, \operatorname{Div} \boldsymbol{E}_\kappa \rangle_{L^2(\Omega,\mathbb{R}^2)} + \langle \boldsymbol{v}_\theta,\, \boldsymbol{e}_\gamma \rangle_{L^2(\Omega)}, \\ \langle \boldsymbol{V}_\kappa,\, \boldsymbol{\mathcal{C}_b} \partial_t \boldsymbol{E}_\kappa \rangle_{L^2(\Omega,\mathbb{R}^{2\times 2}_{\mathrm{sym}})} &= -\langle \operatorname{Div} \boldsymbol{V}_\kappa,\, \boldsymbol{e}_\theta \rangle_{L^2(\Omega,\mathbb{R}^2)} + \langle \boldsymbol{\gamma}_n \boldsymbol{V}_\kappa,\, \boldsymbol{\gamma}_0 \boldsymbol{e}_\theta \rangle_{L^2(\partial\Omega,\mathbb{R}^2)}, \\ \langle \boldsymbol{v}_\gamma,\, C_s \partial_t \boldsymbol{e}_\gamma \rangle_{L^2(\Omega,\mathbb{R}^2)} &= -\langle \operatorname{div} \boldsymbol{v}_\gamma,\, e_w \rangle_{L^2(\Omega)} - \langle \boldsymbol{v}_\gamma,\, \boldsymbol{e}_\theta \rangle_{L^2(\Omega,\mathbb{R}^2)} + \langle \gamma_0 v_w,\, u_{\partial,1} \rangle_{L^2(\partial\Omega)}. \end{aligned} \tag{6.98}$$

The term $\langle \boldsymbol{\gamma}_n \boldsymbol{V}_\kappa,\, \boldsymbol{\gamma}_0 \boldsymbol{e}_\theta \rangle_{L^2(\partial\Omega,\mathbb{R}^2)}$ can be decomposed in its tangential and normal components

$$\langle \boldsymbol{\gamma}_n \boldsymbol{V}_\kappa,\, \boldsymbol{\gamma}_0 \boldsymbol{e}_\theta \rangle_{L^2(\partial\Omega,\mathbb{R}^2)} = \langle \gamma_{nn} \boldsymbol{V}_\kappa,\, u_{\partial,2} \rangle_{L^2(\partial\Omega)} + \langle \gamma_{ns} \boldsymbol{V}_\kappa,\, u_{\partial,3} \rangle_{L^2(\partial\Omega)}. \tag{6.99}$$

Plugging approximation (6.92) into this system, one computes

$$\operatorname{Diag}\begin{bmatrix}\mathbf{M}_{\rho h}\\ \mathbf{M}_{I_\theta}\\ \mathbf{M}_{\mathcal{C}_b}\\ \mathbf{M}_{C_s}\end{bmatrix}\begin{pmatrix}\dot{\mathbf{e}}_w\\ \dot{\mathbf{e}}_\theta\\ \dot{\mathbf{e}}_\kappa\\ \dot{\mathbf{e}}_\gamma\end{pmatrix}=\begin{bmatrix}\mathbf{0} & \mathbf{0} & \mathbf{0} & \mathbf{D}_{\mathrm{div}}\\ \mathbf{0} & \mathbf{0} & \mathbf{D}_{\mathrm{Div}} & -\mathbf{D}_0^\top\\ \mathbf{0} & -\mathbf{D}_{\mathrm{Div}}^\top & \mathbf{0} & \mathbf{0}\\ -\mathbf{D}_{\mathrm{div}}^\top & \mathbf{D}_0 & \mathbf{0} & \mathbf{0}\end{bmatrix}\begin{pmatrix}\mathbf{e}_w\\ \mathbf{e}_\theta\\ \mathbf{e}_\kappa\\ \mathbf{e}_\gamma\end{pmatrix}+\begin{bmatrix}\mathbf{0} & \mathbf{0} & \mathbf{0}\\ \mathbf{0} & \mathbf{0} & \mathbf{0}\\ \mathbf{0} & \mathbf{B}_{M_{nn}} & \mathbf{B}_{M_{ns}}\\ \mathbf{B}_{q_n} & \mathbf{0} & \mathbf{0}\end{bmatrix}\mathbf{u}_\partial,$$
$$\mathbf{M}_\partial\mathbf{y}_\partial=\begin{bmatrix}\mathbf{0} & \mathbf{0} & \mathbf{0} & \mathbf{B}_{q_n}^\top\\ \mathbf{0} & \mathbf{0} & \mathbf{B}_{M_{nn}}^\top & \mathbf{0}\\ \mathbf{0} & \mathbf{0} & \mathbf{B}_{M_{ns}}^\top & \mathbf{0}\end{bmatrix}\begin{pmatrix}\mathbf{e}_w\\ \mathbf{e}_\theta\\ \mathbf{e}_\kappa\\ \mathbf{e}_\gamma\end{pmatrix}. \tag{6.100}$$

Matrices $\mathbf{D}_{\mathrm{div}}$, $\mathbf{D}_{\mathrm{Div}}$ assume the form ($i,j\in\{1,n_w\}$, $m,n\in\{1,n_\theta\}$, $p,q\in\{1,n_\kappa\}$, $r,s\in\{1,n_\gamma\}$)

$$D_{\mathrm{div}}^{is}=\left\langle\phi_w^i,\,\mathrm{div}\,\boldsymbol{\phi}_\gamma^s\right\rangle_{L^2(\Omega)},\qquad D_{\mathrm{Div}}^{mq}=\langle\boldsymbol{\phi}_\theta^m,\,\mathrm{Div}\,\boldsymbol{\Phi}_\kappa^q\rangle_{L^2(\Omega,\mathbb{R}^2)}. \tag{6.101}$$

Matrix $\mathbf{B}_{q_n}$, $\mathbf{B}_{M_{nn}}$, $\mathbf{B}_{M_{ns}}$ are computed as ($l\in\{1,n_\partial\}$)

$$B_{q_n}^{rl}=\left\langle\gamma_n\boldsymbol{\phi}_\gamma^r,\,\phi_{\partial,1}^l\right\rangle_{L^2(\partial\Omega)},\quad B_{M_{nn}}^{pl}=\left\langle\gamma_{nn}\boldsymbol{\Phi}_\kappa^p,\,\phi_{\partial,2}^l\right\rangle_{L^2(\partial\Omega)},\quad B_{M_{ns}}^{pl}=\left\langle\gamma_{ns}\boldsymbol{\Phi}_\kappa^p,\,\phi_{\partial,3}^l\right\rangle_{L^2(\partial\Omega)}. \tag{6.102}$$

This finite-dimensional system represents a purely mixed discretization of the problem and is really close to the plane elasticity system. Conforming finite elements for the plane elasticity system on simplicial meshes have been constructed in [AW02]. The resulting element is rather cumbersome and computationally expensive as the stress tensor has at least 24 degrees of freedom on a triangle. For this reason, many finite element discretizations impose the symmetry of the stress tensor in a weak manner [AFW07]. To actually implement the discretization, in Chap. 7 the Mindlin plate problem is going to be reformulated so that the momenta tensor is only weakly symmetric.

6.2 Mixed boundary conditions

In this section Assumption 3 on uniform boundary condition is modified to account for general non-homogeneous boundary conditions. The discretization of Stokes-Dirac structure under mixed causality has been already treated in [KML18]. However, to satisfy the power balance at a discrete level, some additional parameters are introduced. This makes the employment of the methodology proposed therein not simple and dependent on the considered application. Furthermore, elasticity models do not fall within the required assumptions, because of the presence of tensorial variables and higher order differential operators.

We propose here two methodologies to tackle mixed boundary conditions within the Partitioned Finite Element Method. The first introduces Lagrange multipliers, and therefore algebraic constraints, to enforce the mixed causality. Finite-dimensional differential algebraic

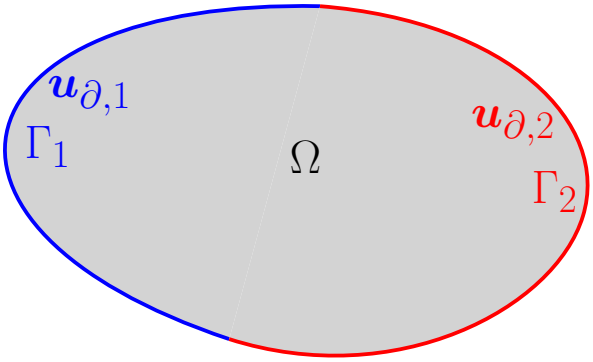

Figure 6.1: Partition of boundary into two connected sets.

port-Hamiltonian systems (pHDAE) have been introduced in [BMXZ18] for linear systems and in [MM19] for non-linear systems. This enriched description shares all the crucial features of ordinary pHs, but can easily take into account algebraic constraints, time-dependent transformations and explicit dependence on time in the Hamiltonian. The second method employs a domain decomposition technique to interconnect systems with different causalities. These two methodologies have been presented in [Jol03] to tackle complex geometries or geometrical details in diffraction problems. Therein, the numerical analysis relies heavily on the discrete energy conservation. In this section the connection between these two methods and the structure-preserving discretization of pHs under mixed boundary conditions becomes clear. For sake of simplicity, the illustration is restricted to the linear case.

The open connected set $\Omega \subset \mathbb{R}^d,\ d = \{1, 2, 3\}$, with Lipschitz boundary $\partial\Omega$ represents the spatial domain. The boundary is partitioned into two sets $\partial\Omega = \overline{\Gamma}_1 \cup \overline{\Gamma}_2,\ \Gamma_1 \cap \Gamma_2 = \{\emptyset\}$. The sets $\Gamma_1,\ \Gamma_2$ are considered to be connected, cf. Fig. 6.1.

Remark 18 (Connectedness of Γ_1, Γ_2)
Disconnected sets can be handled as well. This requires the introduction of a heavy notation and complicates the illustration. For sake of simplicity, the connectedness hypothesis is made.

For scalars $a_{\partial,*}, b_{\partial,*} \in L^2(\Gamma_*)$ and vectors $\boldsymbol{a}_{\partial,*}, \boldsymbol{b}_{\partial,*} \in L^2(\Gamma_*, \mathbb{R}^m)$ defined on the sub-boundary Γ_* the inner product is defined as

$$\langle a_{\partial,*},\, b_{\partial,*} \rangle_{L^2(\Gamma_*)} = \int_{\Gamma_*} a_{\partial,*} b_{\partial,*} \,\mathrm{d}\Gamma_*, \qquad \langle \boldsymbol{a}_{\partial,*},\, \boldsymbol{b}_{\partial,*} \rangle_{L^2(\Gamma_*, \mathbb{R}^m)} = \int_{\Gamma_*} \boldsymbol{a}_{\partial,*} \cdot \boldsymbol{b}_{\partial,*} \,\mathrm{d}\Gamma_*. \quad (6.103)$$

Consider now the following boundary-control linear pH system in co-energy form

$$\begin{bmatrix} \mathcal{M}_1 & 0 \\ 0 & \mathcal{M}_2 \end{bmatrix} \partial_t \begin{pmatrix} \boldsymbol{e}_1 \\ \boldsymbol{e}_2 \end{pmatrix} = \begin{bmatrix} 0 & -\boldsymbol{L}^\top - \mathcal{L}^* \\ \boldsymbol{L} + \mathcal{L} & 0 \end{bmatrix} \begin{pmatrix} \boldsymbol{e}_1 \\ \boldsymbol{e}_2 \end{pmatrix}, \qquad \begin{matrix} \boldsymbol{e}_1 \in H^{\mathcal{L}}, \\ \boldsymbol{e}_2 \in H^{-\mathcal{L}^*}, \end{matrix} \tag{6.104a}$$

$$\begin{pmatrix} \boldsymbol{u}_{\partial,1} \\ \boldsymbol{u}_{\partial,2} \end{pmatrix} = \begin{bmatrix} \mathcal{N}_{\partial,1}^{\Gamma_1} & 0 \\ 0 & \mathcal{N}_{\partial,2}^{\Gamma_2} \end{bmatrix} \begin{pmatrix} \boldsymbol{e}_1 \\ \boldsymbol{e}_2 \end{pmatrix}, \qquad \begin{matrix} \boldsymbol{u}_{\partial,1} \in L^2(\Gamma_1, \mathbb{R}^m), \\ \boldsymbol{u}_{\partial,2} \in L^2(\Gamma_2, \mathbb{R}^m), \end{matrix} \tag{6.104b}$$

$$\begin{pmatrix} \boldsymbol{y}_{\partial,1} \\ \boldsymbol{y}_{\partial,2} \end{pmatrix} = \begin{bmatrix} 0 & \mathcal{N}_{\partial,2}^{\Gamma_1} \\ \mathcal{N}_{\partial,1}^{\Gamma_2} & 0 \end{bmatrix} \begin{pmatrix} \boldsymbol{e}_1 \\ \boldsymbol{e}_2 \end{pmatrix}, \qquad \begin{matrix} \boldsymbol{y}_{\partial,1} \in L^2(\Gamma_1, \mathbb{R}^m), \\ \boldsymbol{y}_{\partial,2} \in L^2(\Gamma_2, \mathbb{R}^m). \end{matrix} \tag{6.104c}$$

The operator $\mathcal{N}_{\partial,*}^{\Gamma_\circ}$ with $*, \circ \in \{1, 2\}$ represents now the restriction of operator $\mathcal{N}_{\partial,*}$, defined in Eq. (6.8) (Assumption 1), over the subset $\Gamma_\circ$. The boundary inputs and outputs are now couples of vectors $\in \mathbb{R}^2$. This does not mean that the boundary conditions have been doubled, but only that the components of $\boldsymbol{u}_\partial, \boldsymbol{y}_\partial$ are only defined on the subsets Γ_1, Γ_2 of the overall boundary. This corresponds to a slight modification of Assumption 3.

Given the additive property of the integral, it is possible to write

$$\begin{aligned} \langle \mathcal{N}_{\partial,1} \boldsymbol{e}_1, \mathcal{N}_{\partial,2} \boldsymbol{e}_2 \rangle_{L^2(\partial\Omega, \mathbb{R}^m)} &= \left\langle \mathcal{N}_{\partial,1}^{\Gamma_1} \boldsymbol{e}_1, \mathcal{N}_{\partial,2}^{\Gamma_1} \boldsymbol{e}_2 \right\rangle_{L^2(\Gamma_1, \mathbb{R}^m)} + \left\langle \mathcal{N}_{\partial,1}^{\Gamma_2} \boldsymbol{e}_1, \mathcal{N}_{\partial,2}^{\Gamma_2} \boldsymbol{e}_2 \right\rangle_{L^2(\Gamma_2, \mathbb{R}^m)}, \\ &= \langle \boldsymbol{u}_{\partial,1}, \boldsymbol{y}_{\partial,1} \rangle_{L^2(\Gamma_1, \mathbb{R}^m)} + \langle \boldsymbol{y}_{\partial,2}, \boldsymbol{u}_{\partial,2} \rangle_{L^2(\Gamma_2, \mathbb{R}^m)}. \end{aligned} \tag{6.105}$$

The continuous power balance is obtained using Eqs. (6.50) and (6.105)

$$\dot{H} = \langle \boldsymbol{u}_{\partial,1}, \boldsymbol{y}_{\partial,1} \rangle_{L^2(\Gamma_1, \mathbb{R}^m)} + \langle \boldsymbol{y}_{\partial,2}, \boldsymbol{u}_{\partial,2} \rangle_{L^2(\Gamma_2, \mathbb{R}^m)}. \tag{6.106}$$

6.2.1 Lagrange multipliers method

This method introduces a Lagrange multiplier for the boundary control that does not arise explicitly in the weak form. To illustrate the idea, consider again the weak form 6.51 (obtained by integration by parts of the $-\mathcal{L}^*$ operator) of Sys. 6.104

$$\begin{aligned} \langle \boldsymbol{v}_1, \mathcal{M}_1 \partial_t \boldsymbol{e}_1 \rangle_{L^2(\Omega, \mathbb{A})} &= -\langle \boldsymbol{v}_1, \boldsymbol{L}^\top \boldsymbol{e}_2 \rangle_{L^2(\Omega, \mathbb{A})} - \langle \mathcal{L} \boldsymbol{v}_1, \boldsymbol{e}_2 \rangle_{L^2(\Omega, \mathbb{B})} + \langle \mathcal{N}_{\partial,1} \boldsymbol{v}_1, \mathcal{N}_{\partial,2} \boldsymbol{e}_2 \rangle_{L^2(\partial\Omega, \mathbb{R}^m)}, \\ \langle \boldsymbol{v}_2, \mathcal{M}_2 \partial_t \boldsymbol{e}_2 \rangle_{L^2(\Omega, \mathbb{B})} &= \langle \boldsymbol{v}_2, \boldsymbol{L} \boldsymbol{e}_1 \rangle_{L^2(\Omega, \mathbb{B})} + \langle \boldsymbol{v}_2, \mathcal{L} \boldsymbol{e}_1 \rangle_{L^2(\Omega, \mathbb{B})}. \end{aligned} \tag{6.107}$$

The term $\langle \mathcal{N}_{\partial,1}\boldsymbol{v}_1, \mathcal{N}_{\partial,2}\boldsymbol{e}_2\rangle_{L^2(\partial\Omega,\mathbb{R}^m)}$ can be split into the two boundary contributions, as in Eq. (6.105). The variable $\boldsymbol{y}_{\partial,1}$ plays here the role of a Lagrange multiplier $\boldsymbol{y}_{\partial,1} = \boldsymbol{\lambda}_{\partial,1}$

$$\begin{aligned}\langle \mathcal{N}_{\partial,1}\boldsymbol{v}_1, \mathcal{N}_{\partial,2}\boldsymbol{e}_2\rangle_{L^2(\partial\Omega,\mathbb{R}^m)} &= \left\langle \mathcal{N}^{\Gamma_1}_{\partial,1}\boldsymbol{v}_1, \mathcal{N}^{\Gamma_1}_{\partial,2}\boldsymbol{e}_2\right\rangle_{L^2(\Gamma_1,\mathbb{R}^m)} + \left\langle \mathcal{N}^{\Gamma_2}_{\partial,1}\boldsymbol{v}_1, \mathcal{N}^{\Gamma_2}_{\partial,2}\boldsymbol{e}_2\right\rangle_{L^2(\Gamma_2,\mathbb{R}^m)},\\ &= \left\langle \mathcal{N}^{\Gamma_1}_{\partial,1}\boldsymbol{v}_1, \boldsymbol{y}_{\partial,1}\right\rangle_{L^2(\Gamma_1,\mathbb{R}^m)} + \left\langle \mathcal{N}^{\Gamma_2}_{\partial,1}\boldsymbol{v}_1, \boldsymbol{u}_{\partial,2}\right\rangle_{L^2(\Gamma_2,\mathbb{R}^m)},\\ &= \left\langle \mathcal{N}^{\Gamma_1}_{\partial,1}\boldsymbol{v}_1, \boldsymbol{\lambda}_{\partial,1}\right\rangle_{L^2(\Gamma_1,\mathbb{R}^m)} + \left\langle \mathcal{N}^{\Gamma_2}_{\partial,1}\boldsymbol{v}_1, \boldsymbol{u}_{\partial,2}\right\rangle_{L^2(\Gamma_2,\mathbb{R}^m)},\end{aligned} \tag{6.108}$$

If the test functions $\boldsymbol{v}_{\partial,1},\ \boldsymbol{v}_{\partial,2} \in \mathbb{R}^m$ are introduced, the input and outputs definitions

$$\boldsymbol{u}_{\partial,1} = \mathcal{N}^{\Gamma_1}_{\partial,1}\boldsymbol{e}_1, \qquad \boldsymbol{y}_{\partial,1} = \boldsymbol{\lambda}_{\partial,1}, \qquad \boldsymbol{y}_{\partial,2} = \mathcal{N}^{\Gamma_2}_{\partial,1}\boldsymbol{e}_1, \tag{6.109}$$

can be put into weak form to obtain

$$\begin{aligned}\langle \boldsymbol{v}_{\partial,1}, \boldsymbol{u}_{\partial,1}\rangle_{L^2(\Gamma_1,\mathbb{R}^m)} &= \left\langle \boldsymbol{v}_{\partial,1}, \mathcal{N}^{\Gamma_1}_{\partial,1}\boldsymbol{e}_1\right\rangle_{L^2(\Gamma_1,\mathbb{R}^m)},\\ \langle \boldsymbol{v}_{\partial,1}, \boldsymbol{y}_{\partial,1}\rangle_{L^2(\Gamma_1,\mathbb{R}^m)} &= \langle \boldsymbol{v}_{\partial,1}, \boldsymbol{\lambda}_{\partial,1}\rangle_{L^2(\Gamma_1,\mathbb{R}^m)},\\ \langle \boldsymbol{v}_{\partial,2}, \boldsymbol{y}_{\partial,2}\rangle_{L^2(\Gamma_1,\mathbb{R}^m)} &= \left\langle \boldsymbol{v}_{\partial,2}, \mathcal{N}^{\Gamma_2}_{\partial,1}\boldsymbol{e}_1\right\rangle_{L^2(\Gamma_1,\mathbb{R}^m)}.\end{aligned} \tag{6.110}$$

As usual, a Galerkin approximation is introduced

$$\begin{aligned}&\boldsymbol{v}_1 \approx \sum_{i=1}^{n_1} \boldsymbol{\phi}^i_1(\boldsymbol{x})v^i_1, \qquad \boldsymbol{e}_1 \approx \sum_{i=1}^{n_1} \boldsymbol{\phi}^i_1(\boldsymbol{x})e^i_1(t), \qquad \triangle_{\partial,1} \approx \sum_{i=1}^{n_{\partial,1}} \boldsymbol{\phi}^i_{\partial,1}(\boldsymbol{s}_1)\triangle^i_{\partial,1}, \quad \boldsymbol{s}_1 \in \Gamma_1,\\ &\boldsymbol{v}_2 \approx \sum_{i=1}^{n_2} \boldsymbol{\phi}^i_2(\boldsymbol{x})v^i_2, \qquad \boldsymbol{e}_2 \approx \sum_{i=1}^{n_2} \boldsymbol{\phi}^i_2(\boldsymbol{x})e^i_2(t), \qquad \square_{\partial,2} \approx \sum_{i=1}^{n_{\partial,2}} \boldsymbol{\phi}^i_{\partial,2}(\boldsymbol{s}_2)\square^i_{\partial,2}(t), \quad \boldsymbol{s}_2 \in \Gamma_2.\end{aligned} \tag{6.111}$$

where $\triangle$ stands for v, u, y, λ and $\square$ for v, u, y. Replacing the approximation 6.111 into Eqs. 6.107, 6.108, 6.110, the following differential-algebraic system is constructed

$$\begin{aligned}&\mathrm{Diag}\begin{bmatrix}\mathbf{M}_{\mathcal{M}_1}\\ \mathbf{M}_{\mathcal{M}_2}\\ \mathbf{0}\end{bmatrix}\begin{pmatrix}\dot{\mathbf{e}}_1\\ \dot{\mathbf{e}}_2\\ \dot{\boldsymbol{\lambda}}_{\partial,1}\end{pmatrix} = \begin{bmatrix}\mathbf{0} & -\mathbf{D}_0^\top - \mathbf{D}_{\mathcal{L}}^\top & \mathbf{B}_{1,\Gamma_1}\\ \mathbf{D}_0 + \mathbf{D}_{\mathcal{L}} & \mathbf{0} & \mathbf{0}\\ -\mathbf{B}^\top_{1,\Gamma_1} & \mathbf{0} & \mathbf{0}\end{bmatrix}\begin{pmatrix}\mathbf{e}_1\\ \mathbf{e}_2\\ \boldsymbol{\lambda}_{\partial,1}\end{pmatrix} + \begin{bmatrix}\mathbf{0} & \mathbf{B}_{1,\Gamma_2}\\ \mathbf{0} & \mathbf{0}\\ \mathbf{M}_{\partial,1} & \mathbf{0}\end{bmatrix}\begin{bmatrix}\mathbf{u}_{\partial,1}\\ \mathbf{u}_{\partial,2}\end{bmatrix},\\ &\begin{bmatrix}\mathbf{M}_{\partial,1} & \mathbf{0}\\ \mathbf{0} & \mathbf{M}_{\partial,2}\end{bmatrix}\begin{pmatrix}\mathbf{y}_{\partial,1}\\ \mathbf{y}_{\partial,2}\end{pmatrix} = \begin{bmatrix}\mathbf{0} & \mathbf{0} & \mathbf{M}_{\partial,1}\\ \mathbf{B}^\top_{1,\Gamma_2} & \mathbf{0} & \mathbf{0}\end{bmatrix}\begin{pmatrix}\mathbf{e}_1\\ \mathbf{e}_2\\ \boldsymbol{\lambda}_{\partial,1}\end{pmatrix}.\end{aligned} \tag{6.112}$$

Apart from matrices $\mathbf{M}_{\partial,1}, \mathbf{M}_{\partial,2}, \mathbf{B}_{1,\Gamma_1}, \mathbf{B}_{1,\Gamma_2}$,

$$\begin{aligned}&M^{lk}_{\partial,1} = \left\langle \boldsymbol{\phi}^l_{\partial,1}, \boldsymbol{\phi}^k_{\partial,1}\right\rangle_{L^2(\Gamma_1,\mathbb{R}^m)},\ (l,k) \in \{1, n_{\partial,1}\}, \quad B^{ik}_{1,\Gamma_1} = \left\langle \mathcal{N}^{\Gamma_1}_{\partial,1}\boldsymbol{\phi}^i_1, \boldsymbol{\phi}^k_{\partial,1}\right\rangle_{L^2(\Gamma_1,\mathbb{R}^m)},\\ &M^{fg}_{\partial,2} = \left\langle \boldsymbol{\phi}^f_{\partial,2}, \boldsymbol{\phi}^g_{\partial,2}\right\rangle_{L^2(\Gamma_2,\mathbb{R}^m)},\ (f,g) \in \{1, n_{\partial,2}\}, \quad B^{ig}_{1,\Gamma_2} = \left\langle \mathcal{N}^{\Gamma_2}_{\partial,1}\boldsymbol{\phi}^i_1, \boldsymbol{\phi}^g_{\partial,2}\right\rangle_{L^2(\Gamma_2,\mathbb{R}^m)},\end{aligned} \quad i \in \{1, n_1\}, \tag{6.113}$$

the other matrices keep the same definition as in (6.53). The discrete Hamiltonian, whose expression is [BMXZ18]

$$H_d = \frac{1}{2}\mathbf{e}_1^\top \mathbf{M}_{\mathcal{M}_1}\mathbf{e}_1 + \frac{1}{2}\mathbf{e}_2^\top \mathbf{M}_{\mathcal{M}_2}\mathbf{e}_2. \tag{6.114}$$

gives rise to the discrete power balance

$$\begin{aligned}
\dot{H}_d &= \mathbf{e}_1^\top \mathbf{M}_{\mathcal{M}_1}\dot{\mathbf{e}}_1 + \mathbf{e}_2^\top \mathbf{M}_{\mathcal{M}_2}\dot{\mathbf{e}}_2, \\
&= -\mathbf{e}_1^\top (\mathbf{D}_0 + \mathbf{D}_{\mathcal{L}})^\top \mathbf{e}_2 + \mathbf{e}_2^\top (\mathbf{D}_0 + \mathbf{D}_{\mathcal{L}})\mathbf{e}_1 + \mathbf{e}_1^\top (\mathbf{B}_{1,\Gamma_1}\boldsymbol{\lambda}_{\partial,1} + \mathbf{B}_{1,\Gamma_2}\mathbf{u}_{\partial,2}), \\
&= \mathbf{y}_{\partial,1}^\top \mathbf{M}_{\partial,1}\mathbf{u}_{\partial,1} + \mathbf{y}_{\partial,2}^\top \mathbf{M}_{\partial,2}\mathbf{u}_{\partial,2}, \\
&= \widehat{\mathbf{y}}_{\partial,1}^\top \mathbf{u}_{\partial,1} + \widehat{\mathbf{y}}_{\partial,2}^\top \mathbf{u}_{\partial,2}, \qquad \text{where} \qquad \widehat{\mathbf{y}}_{\partial,1} := \mathbf{M}_{\partial,1}\mathbf{y}_{\partial,1}, \quad \widehat{\mathbf{y}}_{\partial,2} := \mathbf{M}_{\partial,2}\mathbf{y}_{\partial,2}.
\end{aligned} \tag{6.115}$$

This result is the finite-dimensional equivalent of (6.106).

Equivalently, the weak form Eq.6.52 may be used as a starting point. The computation follows in a completely analogous manner. The only difference is that $\boldsymbol{y}_{\partial,2} = \boldsymbol{\lambda}_{\partial,2}$ plays the role of the Lagrange multiplier. The final finite-dimensional system is then given by

$$\begin{aligned}
&\mathrm{Diag}\begin{bmatrix}\mathbf{M}_{\mathcal{M}_1}\\ \mathbf{M}_{\mathcal{M}_2}\\ \mathbf{0}\end{bmatrix}\begin{pmatrix}\dot{\mathbf{e}}_1\\ \dot{\mathbf{e}}_2\\ \dot{\boldsymbol{\lambda}}_{\partial,2}\end{pmatrix} = \begin{bmatrix}\mathbf{0} & -\mathbf{D}_0^\top + \mathbf{D}_{-\mathcal{L}^*} & \mathbf{0}\\ \mathbf{D}_0 - \mathbf{D}_{-\mathcal{L}^*}^\top & \mathbf{0} & \mathbf{B}_{2,\Gamma_2}\\ \mathbf{0} & -\mathbf{B}_{2,\Gamma_2}^\top & \mathbf{0}\end{bmatrix}\begin{pmatrix}\mathbf{e}_1\\ \mathbf{e}_2\\ \boldsymbol{\lambda}_{\partial,2}\end{pmatrix} + \begin{bmatrix}\mathbf{0} & \mathbf{0}\\ \mathbf{B}_{2,\Gamma_1} & \mathbf{0}\\ \mathbf{0} & \mathbf{M}_{\partial,2}\end{bmatrix}\begin{bmatrix}\mathbf{u}_{\partial,1}\\ \mathbf{u}_{\partial,2}\end{bmatrix}, \\
&\begin{bmatrix}\mathbf{M}_{\partial,1} & \mathbf{0}\\ \mathbf{0} & \mathbf{M}_{\partial,2}\end{bmatrix}\begin{pmatrix}\mathbf{y}_{\partial,1}\\ \mathbf{y}_{\partial,2}\end{pmatrix} = \begin{bmatrix}\mathbf{0} & \mathbf{B}_{2,\Gamma_1}^\top & \mathbf{0}\\ \mathbf{0} & \mathbf{0} & \mathbf{M}_{\partial,2}\end{bmatrix}\begin{pmatrix}\mathbf{e}_1\\ \mathbf{e}_2\\ \boldsymbol{\lambda}_{\partial,2}\end{pmatrix}.
\end{aligned} \tag{6.116}$$

where $\mathbf{B}_{2,\Gamma_1}$, $\mathbf{B}_{2,\Gamma_2}$ are given by

$$B_{2,\Gamma_1}^{mk} = \left\langle \mathcal{N}_{\partial,2}^{\Gamma_1}\boldsymbol{\phi}_2^m,\, \boldsymbol{\phi}_{\partial,1}^k \right\rangle_{L^2(\Gamma_1,\mathbb{R}^m)}, \quad B_{2,\Gamma_2}^{mg} = \left\langle \mathcal{N}_{\partial,2}^{\Gamma_2}\boldsymbol{\phi}_2^m,\, \boldsymbol{\phi}_{\partial,2}^g \right\rangle_{L^2(\Gamma_2,\mathbb{R}^m)}, \tag{6.117}$$

where $m \in \{1, n_2\}$, $k \in \{1, n_{\partial,1}\}$, $g \in \{1, n_{\partial,2}\}$. This first method can be applied to incorporate all possible mixed boundary conditions in a systematic manner. However the finite element discretization is required to satisfy the inf-sup condition [Ste95]. Simulating the resulting system is harder, since the algebraic constrains pose additional difficulties for the time integration.

6.2.2 Virtual domain decomposition

Since the boundary subsets Γ_1, Γ_2 are supposed to be connected sets, a single interface is sufficient to decompose the system appropriately. In Fig. 6.2 the splitting of the domain is accomplished by introducing the interface Γ_{12}. This separation line that separates the domain is an additional degree of freedom, as it can be freely drawn. If the finite element method is used for the basis functions, the interface should be drawn so that the meshing of the subdomains does not generate excessively skewed triangles.

The idea is based on the fact that System 6.104 can be split into two systems with uniform

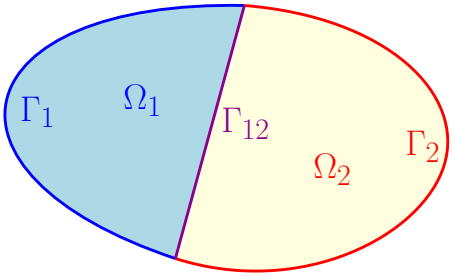

Figure 6.2: Splitting of the domain.

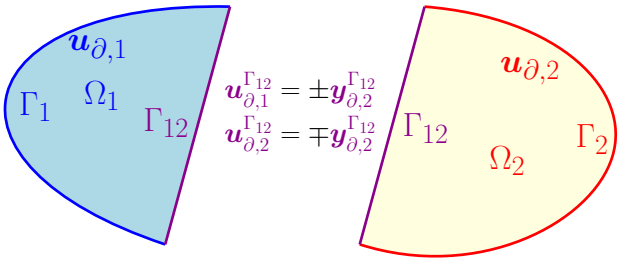

Figure 6.3: Interconnection at the interface Γ_{12}.

causality. The following set of boundary variables is used for Ω_1 subdomain

$$\begin{pmatrix} \boldsymbol{u}_{\partial,1} \\ \boldsymbol{u}_{\partial,1}^{\Gamma_{12}} \end{pmatrix} = \begin{bmatrix} \mathcal{N}_{\partial,1}^{\Gamma_1} & 0 \\ \mathcal{N}_{\partial,1}^{\Gamma_{12}} & 0 \end{bmatrix} \begin{pmatrix} \boldsymbol{e}_1 \\ \boldsymbol{e}_2 \end{pmatrix}, \qquad \begin{pmatrix} \boldsymbol{y}_{\partial,1} \\ \boldsymbol{y}_{\partial,1}^{\Gamma_{12}} \end{pmatrix} = \begin{bmatrix} 0 & \mathcal{N}_{\partial,2}^{\Gamma_1} \\ 0 & \mathcal{N}_{\partial,2}^{\Gamma_{12}} \end{bmatrix} \begin{pmatrix} \boldsymbol{e}_1 \\ \boldsymbol{e}_2 \end{pmatrix}. \tag{6.118}$$

Whereas for the Ω_2 subdomain, the boundary variables are

$$\begin{pmatrix} \boldsymbol{u}_{\partial,2} \\ \boldsymbol{u}_{\partial,2}^{\Gamma_{12}} \end{pmatrix} = \begin{bmatrix} 0 & \mathcal{N}_{\partial,2}^{\Gamma_2} \\ 0 & \mathcal{N}_{\partial,2}^{\Gamma_{12}} \end{bmatrix} \begin{pmatrix} \boldsymbol{e}_1 \\ \boldsymbol{e}_2 \end{pmatrix}, \qquad \begin{pmatrix} \boldsymbol{y}_{\partial,2} \\ \boldsymbol{y}_{\partial,2}^{\Gamma_{12}} \end{pmatrix} = \begin{bmatrix} \mathcal{N}_{\partial,1}^{\Gamma_1} & 0 \\ \mathcal{N}_{\partial,1}^{\Gamma_{12}} & 0 \end{bmatrix} \begin{pmatrix} \boldsymbol{e}_1 \\ \boldsymbol{e}_2 \end{pmatrix}. \tag{6.119}$$

The following relations then hold (cf. Fig. 6.3)

$$\boldsymbol{u}_{\partial,1}^{\Gamma_{12}} = \pm \boldsymbol{y}_{\partial,2}^{\Gamma_{12}}, \qquad \boldsymbol{u}_{\partial,2}^{\Gamma_{12}} = \mp \boldsymbol{y}_{\partial,1}^{\Gamma_{12}}. \tag{6.120}$$

The plus or minus sign is due to the fact that either $\mathcal{N}_{\partial,1}^{\Gamma_{12}}$ or $\mathcal{N}_{\partial,2}^{\Gamma_{12}}$ contains a scalar product with the outgoing normal (or the tangent unit vector) at Γ_{12} (that has opposite direction depending on which subdomain is considered). *These relations are at the core of the methodology, since they state the equivalence between a problem with mixed causalities and the interconnection of two problems with uniform causality.*

To obtain a final system with the desired causality, the weak form has to be carried out separately on each subdomain. In particular, on subdomain Ω_1 the $\mathcal{L}$ operator is integrated by parts, whereas on subdomain Ω_2 the $-\mathcal{L}^*$ operator undergoes the integration by parts. Consequently, on subdomains Ω_1 (Ω_2) the boundary input $\boldsymbol{u}_{\partial,1}$ ($\boldsymbol{u}_{\partial,2}$) explicitly appears. Let $L^2(\Omega_*, \mathbb{A})$ be the L^2 space restricted to the subdomain Ω_*, and let $L^2(\Omega_*, \mathbb{B})$ be the restriction of the L^2 space to Ω_* for $* \in \{1, 2\}$. The weak form of the dynamics (6.104a) for the Ω_1 contribution reads

$$\begin{aligned} \langle \boldsymbol{v}_1, \mathcal{M}_1 \partial_t \boldsymbol{e}_1 \rangle_{L^2(\Omega_1,\mathbb{A})} &= -\langle \boldsymbol{v}_1, \boldsymbol{L}^\top \boldsymbol{e}_2 \rangle_{L^2(\Omega_1,\mathbb{A})} - \langle \boldsymbol{v}_1, \mathcal{L}^* \boldsymbol{e}_2 \rangle_{L^2(\Omega_1,\mathbb{A})} \\ \langle \boldsymbol{v}_2, \mathcal{M}_2 \partial_t \boldsymbol{e}_2 \rangle_{L^2(\Omega_1,\mathbb{B})} &= \langle \boldsymbol{v}_2, \boldsymbol{L} \boldsymbol{e}_1 \rangle_{L^2(\Omega_1,\mathbb{B})} + \langle \mathcal{L}^* \boldsymbol{v}_2, \boldsymbol{e}_1 \rangle_{L^2(\Omega_1,\mathbb{A})} + \langle \mathcal{N}_{\partial,2} \boldsymbol{v}_2, \mathcal{N}_{\partial,1} \boldsymbol{e}_1 \rangle_{L^2(\partial\Omega_1,\mathbb{R}^m)}. \end{aligned} \tag{6.121}$$

For Ω_2, we get

$$\begin{aligned}\langle \boldsymbol{v}_1,\, \mathcal{M}_1\partial_t \boldsymbol{e}_1\rangle_{L^2(\Omega_2,\mathbb{A})} &= -\langle \boldsymbol{v}_1,\, \boldsymbol{L}^\top \boldsymbol{e}_2\rangle_{L^2(\Omega_2,\mathbb{A})} - \langle \mathcal{L}\boldsymbol{v}_1,\, \boldsymbol{e}_2\rangle_{L^2(\Omega_2,\mathbb{B})} + \langle \mathcal{N}_{\partial,1}\boldsymbol{v}_1,\, \mathcal{N}_{\partial,2}\boldsymbol{e}_2\rangle_{L^2(\partial\Omega_2,\mathbb{R}^m)}\,,\\ \langle \boldsymbol{v}_2,\, \mathcal{M}_2\partial_t \boldsymbol{e}_2\rangle_{L^2(\Omega_2,\mathbb{B})} &= \langle \boldsymbol{v}_2,\, \boldsymbol{L}\boldsymbol{e}_1\rangle_{L^2(\Omega_2,\mathbb{B})} + \langle \boldsymbol{v}_2,\, \mathcal{L}\boldsymbol{e}_1\rangle_{L^2(\Omega_2,\mathbb{B})}\,.\end{aligned} \tag{6.122}$$

Since $\partial\Omega_1 = \overline{\Gamma}_1 \cup \overline{\Gamma}_{12}$ and $\partial\Omega_2 = \overline{\Gamma}_2 \cup \overline{\Gamma}_{12}$, the boundary terms can be decomposed

$$\begin{aligned}\langle \mathcal{N}_{\partial,2}\boldsymbol{v}_2,\, \mathcal{N}_{\partial,1}\boldsymbol{e}_1\rangle_{L^2(\partial\Omega_1,\mathbb{R}^m)} &= \langle \mathcal{N}_{\partial,2}\boldsymbol{v}_2,\, \mathcal{N}_{\partial,1}\boldsymbol{e}_1\rangle_{L^2(\Gamma_1,\mathbb{R}^m)} + \langle \mathcal{N}_{\partial,2}\boldsymbol{v}_2,\, \mathcal{N}_{\partial,1}\boldsymbol{e}_1\rangle_{L^2(\Gamma_{12},\mathbb{R}^m)}\,,\\ &= \left\langle \mathcal{N}^{\Gamma_1}_{\partial,2}\boldsymbol{v}_2,\, \mathcal{N}^{\Gamma_1}_{\partial,1}\boldsymbol{e}_1\right\rangle_{L^2(\Gamma_1,\mathbb{R}^m)} + \left\langle \mathcal{N}^{\Gamma_{12}}_{\partial,2}\boldsymbol{v}_2,\, \mathcal{N}^{\Gamma_{12}}_{\partial,1}\boldsymbol{e}_1\right\rangle_{L^2(\Gamma_{12},\mathbb{R}^m)}\,,\\ &= \left\langle \mathcal{N}^{\Gamma_1}_{\partial,2}\boldsymbol{v}_2,\, \boldsymbol{u}_{\partial,1}\right\rangle_{L^2(\Gamma_1,\mathbb{R}^m)} + \left\langle \mathcal{N}^{\Gamma_{12}}_{\partial,2}\boldsymbol{v}_2,\, \boldsymbol{u}^{\Gamma_{12}}_{\partial,1}\right\rangle_{L^2(\Gamma_{12},\mathbb{R}^m)}\,.\end{aligned} \tag{6.123}$$

Analogously, for the remaining boundary term we find

$$\langle \mathcal{N}_{\partial,1}\boldsymbol{v}_1,\, \mathcal{N}_{\partial,2}\boldsymbol{e}_2\rangle_{L^2(\partial\Omega_2,\mathbb{R}^m)} = \left\langle \mathcal{N}^{\Gamma_2}_{\partial,1}\boldsymbol{v}_1,\, \boldsymbol{u}_{\partial,2}\right\rangle_{L^2(\Gamma_2,\mathbb{R}^m)} + \left\langle \mathcal{N}^{\Gamma_{12}}_{\partial,1}\boldsymbol{v}_1,\, \boldsymbol{u}^{\Gamma_{12}}_{\partial,2}\right\rangle_{L^2(\Gamma_{12},\mathbb{R}^m)}\,. \tag{6.124}$$

A Galerkin approximation, analogous to (6.111), is used for each subdomain

$$\begin{aligned}
\boldsymbol{v}_{1,1} &\approx \sum_{i=1}^{n_{1,1}} \boldsymbol{\phi}^i_{1,1}(\boldsymbol{x}_1) v^i_{1,1}, \quad \boldsymbol{x}_1 \in \Omega_1, & \boldsymbol{v}_{1,2} &\approx \sum_{i=1}^{n_{1,2}} \boldsymbol{\phi}^i_{1,2}(\boldsymbol{x}_2) v^i_{1,2}, \quad \boldsymbol{x}_2 \in \Omega_2,\\
\boldsymbol{v}_{2,1} &\approx \sum_{i=1}^{n_{2,1}} \boldsymbol{\phi}^i_{2,1}(\boldsymbol{x}_1) v^i_{2,1}, & \boldsymbol{v}_{2,2} &\approx \sum_{i=1}^{n_{2,2}} \boldsymbol{\phi}^i_{2,2}(\boldsymbol{x}_2) v^i_{2,2},\\
\boldsymbol{e}_{1,1} &\approx \sum_{i=1}^{n_{1,1}} \boldsymbol{\phi}^i_{1,1}(\boldsymbol{x}_1) e^i_{1,1}(t), & \boldsymbol{e}_{1,2} &\approx \sum_{i=1}^{n_{1,2}} \boldsymbol{\phi}^i_{1,2}(\boldsymbol{x}_2) e^i_{1,2}(t),\\
\boldsymbol{e}_{2,1} &\approx \sum_{i=1}^{n_{2,1}} \boldsymbol{\phi}^i_{2,1}(\boldsymbol{x}_1) e^i_{2,1}(t), & \boldsymbol{e}_{2,2} &\approx \sum_{i=1}^{n_{2,2}} \boldsymbol{\phi}^i_{2,2}(\boldsymbol{x}_2) e^i_{2,2}(t).
\end{aligned} \tag{6.125}$$

For the boundary variables, another basis for the common interface is needed

$$\begin{aligned}
\square_{\partial,1} &\approx \sum_{i=1}^{n_{\partial,1}} \boldsymbol{\phi}^i_{\partial,1}(\boldsymbol{s}_1)\square^i_{\partial,1}(t), \quad \boldsymbol{s}_1 \in \Gamma_1, & \square^{\Gamma_{12}}_{\partial,1} &\approx \sum_{i=1}^{n_{\partial,12}} \boldsymbol{\phi}^i_{\partial,12}(\boldsymbol{s}_{12})\square^{i,\Gamma_{12}}_{\partial,1}(t),\\
\square_{\partial,2} &\approx \sum_{i=1}^{n_{\partial,2}} \boldsymbol{\phi}^i_{\partial,2}(\boldsymbol{s}_2)\square^i_{\partial,2}(t), \quad \boldsymbol{s}_2 \in \Gamma_2. & \square^{\Gamma_{12}}_{\partial,2} &\approx \sum_{i=1}^{n_{\partial,12}} \boldsymbol{\phi}^i_{\partial,12}(\boldsymbol{s}_{12})\square^{i,\Gamma_{12}}_{\partial,2}(t),
\end{aligned} \qquad \boldsymbol{s}_{12} \in \Gamma_{12}. \tag{6.126}$$

where $\square$ stands for v, u, y.

Remark 19 (Choice of the interface basis functions)
Notice that the same basis functions $\boldsymbol{\phi}_{\partial,12}$ are used for both interface variables. This is necessary in order to dispose of the same degrees of freedom for the interconnection.

Replacing approximations 6.111, 6.126 into Eqs. 6.121, 6.123, 6.118, a finite-dimensional system for the Ω_1 subdomain is obtained

$$\begin{bmatrix} \mathbf{M}_{\mathcal{M}_1}^{\Omega_1} & \mathbf{0} \\ \mathbf{0} & \mathbf{M}_{\mathcal{M}_2}^{\Omega_1} \end{bmatrix} \begin{pmatrix} \dot{\mathbf{e}}_{1,1} \\ \dot{\mathbf{e}}_{2,1} \end{pmatrix} = \begin{bmatrix} \mathbf{0} & -\mathbf{D}_0^{\Omega_1\top} + \mathbf{D}_{-\mathcal{L}^*}^{\Omega_1} \\ \mathbf{D}_0^{\Omega_1} - \mathbf{D}_{-\mathcal{L}^*}^{\Omega_1\top} & \mathbf{0} \end{bmatrix} \begin{pmatrix} \mathbf{e}_{1,1} \\ \mathbf{e}_{2,1} \end{pmatrix} + \begin{bmatrix} \mathbf{0} & \mathbf{0} \\ \mathbf{B}_{2,\Gamma_1}^{\Omega_1} & \mathbf{B}_{2,\Gamma_{12}}^{\Omega_1} \end{bmatrix} \begin{pmatrix} \mathbf{u}_{\partial,1} \\ \mathbf{u}_{\partial,1}^{\Gamma_{12}} \end{pmatrix},$$
$$\begin{bmatrix} \mathbf{M}_{\partial,1} & \mathbf{0} \\ \mathbf{0} & \mathbf{M}_{\partial,12} \end{bmatrix} \begin{pmatrix} \mathbf{y}_{\partial,1} \\ \mathbf{y}_{\partial,1}^{\Gamma_{12}} \end{pmatrix} = \begin{bmatrix} \mathbf{0} & \mathbf{B}_{2,\Gamma_1}^{\Omega_1\top} \\ \mathbf{0} & \mathbf{B}_{2,\Gamma_{12}}^{\Omega_1\top} \end{bmatrix} \begin{pmatrix} \mathbf{e}_{1,1} \\ \mathbf{e}_{2,1} \end{pmatrix}. \tag{6.127}$$

The mass and interconnection operator matrices are the restrictions to the subdomain of the matrices given in (6.116)

$$\begin{aligned} M_{\mathcal{M}_1}^{\Omega_1,ij} &= \left\langle \boldsymbol{\phi}_{1,1}^i,\, \mathcal{M}_1 \boldsymbol{\phi}_{1,1}^j \right\rangle_{L^2(\Omega_1,\mathbb{A})}, \quad D_0^{\Omega_1,mj} = \left\langle \boldsymbol{\phi}_{2,1}^i,\, \boldsymbol{L}\boldsymbol{\phi}_{1,1}^j \right\rangle_{L^2(\Omega_1,\mathbb{B})}, \qquad i,j \in \{1, n_{1,1}\}, \\ M_{\mathcal{M}_2}^{\Omega_1,mn} &= \left\langle \boldsymbol{\phi}_{2,1}^m,\, \mathcal{M}_2 \boldsymbol{\phi}_{2,1}^n \right\rangle_{L^2(\Omega_1,\mathbb{B})}, \quad D_{-\mathcal{L}^*}^{\Omega_1,in} = \left\langle \boldsymbol{\phi}_{1,1}^m,\, -\mathcal{L}^* \boldsymbol{\phi}_{2,1}^n \right\rangle_{L^2(\Omega_1,\mathbb{A})}, \quad m,n \in \{1, n_{2,1}\}. \end{aligned} \tag{6.128}$$

Matrix $\mathbf{M}_{\partial,1}$ is constructed as in Eq. (6.116). Matrix $\mathbf{M}_{\partial,12}$ is similarly built

$$M_{\partial,12}^{lk} = \left\langle \boldsymbol{\phi}_{\partial,12}^l,\, \boldsymbol{\phi}_{\partial,12}^k \right\rangle_{L^2(\Gamma_{12},\mathbb{R}^m)}, \qquad l,k \in \{1, n_{\partial,12}\}. \tag{6.129}$$

The novel matrices $\mathbf{B}_{2,\Gamma_1}^{\Omega_1}$, $\mathbf{B}_{1,\Gamma_{12}}^{\Omega_1}$ have elements

$$\begin{aligned} B_{2,\Gamma_1}^{\Omega_1,mh} &= \left\langle \mathcal{N}_{\partial,2}^{\Gamma_1} \boldsymbol{\phi}_{2,1}^m,\, \boldsymbol{\phi}_{\partial,1}^h \right\rangle_{L^2(\Gamma_1,\mathbb{R}^m)}, \qquad m \in \{1, n_{2,1}\}, \quad h \in \{1, n_{\partial,1}\}, \\ B_{2,\Gamma_{12}}^{\Omega_1,mk} &= \left\langle \mathcal{N}_{\partial,2}^{\Gamma_{12}} \boldsymbol{\phi}_{2,1}^m,\, \boldsymbol{\phi}_{\partial,12}^k \right\rangle_{L^2(\Gamma_{12},\mathbb{R}^m)}, \qquad\qquad\quad k \in \{1, n_{\partial,12}\}. \end{aligned} \tag{6.130}$$

If instead the approximations are plugged into Eqs. 6.122, 6.124, 6.119, a finite-dimensional system for the Ω_2 subdomain is computed

$$\begin{bmatrix} \mathbf{M}_{\mathcal{M}_1}^{\Omega_2} & \mathbf{0} \\ \mathbf{0} & \mathbf{M}_{\mathcal{M}_2}^{\Omega_2} \end{bmatrix} \begin{pmatrix} \dot{\mathbf{e}}_{1,2} \\ \dot{\mathbf{e}}_{2,2} \end{pmatrix} = \begin{bmatrix} \mathbf{0} & -\mathbf{D}_0^{\Omega_2\top} - \mathbf{D}_{\mathcal{L}}^{\Omega_2\top} \\ \mathbf{D}_0^{\Omega_2} + \mathbf{D}_{\mathcal{L}}^{\Omega_2} & \mathbf{0} \end{bmatrix} \begin{pmatrix} \mathbf{e}_{1,2} \\ \mathbf{e}_{2,2} \end{pmatrix} + \begin{bmatrix} \mathbf{B}_{1,\Gamma_2}^{\Omega_2} & \mathbf{B}_{1,\Gamma_{12}}^{\Omega_2} \\ \mathbf{0} & \mathbf{0} \end{bmatrix} \begin{pmatrix} \mathbf{u}_{\partial,2} \\ \mathbf{u}_{\partial,2}^{\Gamma_{12}} \end{pmatrix},$$
$$\begin{bmatrix} \mathbf{M}_{\partial,2} & \mathbf{0} \\ \mathbf{0} & \mathbf{M}_{\partial,12} \end{bmatrix} \begin{pmatrix} \mathbf{y}_{\partial,2} \\ \mathbf{y}_{\partial,2}^{\Gamma_{12}} \end{pmatrix} = \begin{bmatrix} \mathbf{B}_{1,\Gamma_2}^{\Omega_2\top} & \mathbf{0} \\ \mathbf{B}_{1,\Gamma_{12}}^{\Omega_2\top} & \mathbf{0} \end{bmatrix} \begin{pmatrix} \mathbf{e}_{1,2} \\ \mathbf{e}_{2,2} \end{pmatrix}. \tag{6.131}$$

The mass and interconnection operator matrices are the restrictions to the subdomain of the matrices given in (6.112)

$$\begin{aligned} M_{\mathcal{M}_1}^{\Omega_2,ij} &= \left\langle \boldsymbol{\phi}_{1,2}^i,\, \mathcal{M}_1 \boldsymbol{\phi}_{1,2}^j \right\rangle_{L^2(\Omega_2,\mathbb{A})}, \quad D_0^{\Omega_2,mj} = \left\langle \boldsymbol{\phi}_{2,2}^i,\, \boldsymbol{L}\boldsymbol{\phi}_{1,2}^j \right\rangle_{L^2(\Omega_2,\mathbb{B})}, \qquad i,j \in \{1, n_{1,2}\}, \\ M_{\mathcal{M}_2}^{\Omega_2,mn} &= \left\langle \boldsymbol{\phi}_{2,2}^m,\, \mathcal{M}_2 \boldsymbol{\phi}_{2,2}^n \right\rangle_{L^2(\Omega_2,\mathbb{B})}, \quad D_{\mathcal{L}}^{\Omega_2,mj} = \left\langle \boldsymbol{\phi}_{2,2}^m,\, \mathcal{L}\boldsymbol{\phi}_{1,2}^n \right\rangle_{L^2(\Omega_2,\mathbb{B})}, \quad m,n \in \{1, n_{2,2}\}. \end{aligned} \tag{6.132}$$

Matrix $\mathbf{M}_{\partial,2}$ is constructed as in (6.112). The elements of matrices $\mathbf{B}_{1,\Gamma_2}$, $\mathbf{B}_{1,\Gamma_{12}}$ are computed

as

$$\begin{aligned} B^{ig}_{1,\Gamma_2} &= \left\langle \mathcal{N}^{\Gamma_2}_{\partial,1}\boldsymbol{\phi}^i_{1,2},\, \boldsymbol{\phi}^g_{\partial,2}\right\rangle_{L^2(\Gamma_2)}, \qquad i\in\{1,n_{1,2}\}, \quad g\in\{1,n_{\partial,2}\},\\ B^{ik}_{1,\Gamma_{12}} &= \left\langle \mathcal{N}^{\Gamma_{12}}_{\partial,1}\boldsymbol{\phi}^i_{1,2},\, \boldsymbol{\phi}^k_{\partial,12}\right\rangle_{L^2(\Gamma_{12})}, \qquad\qquad\quad k\in\{1,n_{\partial,12}\}. \end{aligned} \tag{6.133}$$

Systems (6.127), (6.131) are compactly rewritten as

System (6.127)

$$\begin{aligned} \mathbf{M}_{\Omega_1}\dot{\mathbf{e}}_{\Omega_1} &= \mathbf{J}_{\Omega_1}\mathbf{e}_{\Omega_1} + \mathbf{B}^{\Omega_1}_{\Gamma_1}\mathbf{u}_{\partial,1} + \mathbf{B}^{\Omega_1}_{\Gamma_{12}}\mathbf{u}^{\Gamma_{12}}_{\partial,1},\\ \mathbf{M}_{\partial,1}\mathbf{y}_{\partial,1} &= \mathbf{B}^{\Omega_1\top}_{\Gamma_1}\mathbf{e}_{\Omega_1},\\ \mathbf{M}_{\partial,12}\mathbf{y}^{\Gamma_{12}}_{\partial,1} &= \mathbf{B}^{\Omega_1\top}_{\Gamma_{12}}\mathbf{e}_{\Omega_1}, \end{aligned} \tag{6.134}$$

with Hamiltonian $H_{d,1} = \frac{1}{2}\mathbf{e}^\top_{\Omega_1}\mathbf{M}_{\Omega_1}\mathbf{e}_{\Omega_1}$

System (6.131)

$$\begin{aligned} \mathbf{M}_{\Omega_2}\dot{\mathbf{e}}_{\Omega_2} &= \mathbf{J}_{\Omega_2}\mathbf{e}_{\Omega_2} + \mathbf{B}^{\Omega_2}_{\Gamma_2}\mathbf{u}_{\partial,2} + \mathbf{B}^{\Omega_2}_{\Gamma_{12}}\mathbf{u}^{\Gamma_{12}}_{\partial,2},\\ \mathbf{M}_{\partial,2}\mathbf{y}_{\partial,2} &= \mathbf{B}^{\Omega_2\top}_{\Gamma_2}\mathbf{e}_{\Omega_2},\\ \mathbf{M}_{\partial,12}\mathbf{y}^{\Gamma_{12}}_{\partial,2} &= \mathbf{B}^{\Omega_2\top}_{\Gamma_{12}}\mathbf{e}_{\Omega_2}, \end{aligned} \tag{6.135}$$

with Hamiltonian $H_{d,2} = \frac{1}{2}\mathbf{e}^\top_{\Omega_2}\mathbf{M}_{\Omega_2}\mathbf{e}_{\Omega_2}$

To obtain a system with the desired causality, an interconnection is employed to connect the two Systems (6.134), (6.135) along the shared boundary Γ_{12}. Given (6.120), the gyrator interconnection [DMSB09] is computed as

$$\begin{aligned} \mathbf{u}^{\Gamma_{12}}_{\partial,1} &= \pm\mathbf{y}^{\Gamma_{12}}_{\partial,2} = \pm\mathbf{M}^{-1}_{\partial,12}\mathbf{B}^{\Omega_2\top}_{\Gamma_{12}}\mathbf{e}_{\Omega_2},\\ \mathbf{u}^{\Gamma_{12}}_{\partial,2} &= \mp\mathbf{y}^{\Gamma_{12}}_{\partial,1} = \mp\mathbf{M}^{-1}_{\partial,12}\mathbf{B}^{\Omega_1\top}_{\Gamma_{12}}\mathbf{e}_{\Omega_1}, \end{aligned} \tag{6.136}$$

The coupling matrix is then defined by

$$\mathbf{C} := \mathbf{B}^{\Omega_1}_{\Gamma_{12}}\mathbf{M}^{-1}_{\partial,12}\mathbf{B}^{\Omega_2\top}_{\Gamma_{12}}. \tag{6.137}$$

Plugging Eq. (6.136) into 6.134, 6.135, the final system with mixed causality is obtained

$$\begin{aligned} \begin{bmatrix}\mathbf{M}_{\Omega_1} & \mathbf{0}\\ \mathbf{0} & \mathbf{M}_{\Omega_2}\end{bmatrix}\begin{pmatrix}\dot{\mathbf{e}}_{\Omega_1}\\ \dot{\mathbf{e}}_{\Omega_2}\end{pmatrix} &= \begin{bmatrix}\mathbf{J}_{\Omega_1} & \pm\mathbf{C}\\ \mp\mathbf{C}^\top & \mathbf{J}_{\Omega_2}\end{bmatrix}\begin{pmatrix}\mathbf{e}_{\Omega_1}\\ \mathbf{e}_{\Omega_2}\end{pmatrix} + \begin{bmatrix}\mathbf{B}^{\Omega_1}_{\Gamma_1} & \mathbf{0}\\ \mathbf{0} & \mathbf{B}^{\Omega_2}_{\Gamma_2}\end{bmatrix}\begin{pmatrix}\mathbf{u}_{\partial,1}\\ \mathbf{u}_{\partial,2}\end{pmatrix},\\ \begin{bmatrix}\mathbf{M}_{\partial,1} & \mathbf{0}\\ \mathbf{0} & \mathbf{M}_{\partial,2}\end{bmatrix}\begin{pmatrix}\mathbf{y}_{\partial,1}\\ \mathbf{y}_{\partial,2}\end{pmatrix} &= \begin{bmatrix}\mathbf{B}^{\Omega_1\top}_{\Gamma_1} & \mathbf{0}\\ \mathbf{0} & \mathbf{B}^{\Omega_2\top}_{\Gamma_2}\end{bmatrix}\begin{pmatrix}\mathbf{e}_{\Omega_1}\\ \mathbf{e}_{\Omega_2}\end{pmatrix}. \end{aligned} \tag{6.138}$$

The total Hamiltonian is the sum

$$H_d = H_{d,1} + H_{d,2} = \frac{1}{2}\mathbf{e}^\top_{\Omega_1}\mathbf{M}_{\Omega_1}\mathbf{e}_{\Omega_1} + \frac{1}{2}\mathbf{e}^\top_{\Omega_2}\mathbf{M}_{\Omega_2}\mathbf{e}_{\Omega_2}. \tag{6.139}$$

So, the power rate is

$$\begin{aligned}\dot{H}_d &= \mathbf{e}_{\Omega_1}^\top \mathbf{M}_{\Omega_1}\dot{\mathbf{e}}_{\Omega_1} + \mathbf{e}_{\Omega_2}^\top \mathbf{M}_{\Omega_2}\dot{\mathbf{e}}_{\Omega_2},\\ &= \mathbf{e}_{\Omega_1}^\top \mathbf{J}_{\Omega_1}\mathbf{e}_{\Omega_1} + \mathbf{e}_{\Omega_2}^\top \mathbf{J}_{\Omega_2}\mathbf{e}_{\Omega_2} \pm \mathbf{e}_{\Omega_1}^\top \mathbf{C}\,\mathbf{e}_{\Omega_2} \mp \mathbf{e}_{\Omega_2}^\top \mathbf{C}^\top \mathbf{e}_{\Omega_1} + \mathbf{e}_{\Omega_1}^\top \mathbf{B}_{\Gamma_1}^{\Omega_1}\mathbf{u}_{\partial,1} + \mathbf{e}_{\Omega_2}^\top \mathbf{B}_{\Gamma_2}^{\Omega_2}\mathbf{u}_{\partial,2},\\ &= \mathbf{y}_{\partial,1}^\top \mathbf{M}_{\partial,1}\mathbf{u}_{\partial,1} + \mathbf{y}_{\partial,2}^\top \mathbf{M}_{\partial,2}\mathbf{u}_{\partial,2},\\ &= \widehat{\mathbf{y}}_{\partial,1}^\top \mathbf{u}_{\partial,1} + \widehat{\mathbf{y}}_{\partial,2}^\top \mathbf{u}_{\partial,2}, \qquad \text{where} \qquad \widehat{\mathbf{y}}_{\partial,1} := \mathbf{M}_{\partial,1}\mathbf{y}_{\partial,1}, \quad \widehat{\mathbf{y}}_{\partial,2} := \mathbf{M}_{\partial,2}\mathbf{y}_{\partial,2}.\end{aligned} \tag{6.140}$$

Again this results mimics its corresponding infinite-dimensional (6.106).

This technique allows obtaining a system with the correct causality, but has some drawbacks. Suitable finite elements are required for both kinds of discretization detailed in §6.1.1, but the two are not always available (see Remark 17). A rigorous numerical convergence analysis of this technique appears rather involved. Some cases of mixed conditions, in particular conditions on single components of vectors, cannot be handled by this technique. For example, the simply supported condition in beams and plates imposes zero normal component of the traction at the boundary. Furthermore two different meshes are required and to perform the interconnection the degrees of freedom have to be manipulated carefully. This makes the implementation heavier than the Lagrange multiplier method §6.2.1.

6.3 Conclusion

In this chapter a universal discretization method for multi-dimensional pHs has been detailed. The underlying Assumptions 2, 3 are indeed those that characterize the well-posedness of multi-dimensional pHs [Skr19]. For the time being, it has been shown that this technique is capable of constructing a finite-dimensional pHs from an infinite-dimensional one. For this reason, it is a structure-preserving method. The questions of numerical convergence and choice of approximation bases (in this thesis the focus is on the finite element method but spectral methods can be employed as well) are addressed in the next chapter, for the linear case only.

Chapter 7

Numerical convergence study

Aristotle maintained that women have fewer teeth than men; although he was twice married, it never occurred to him to verify this statement by examining his wives' mouths.

The Impact of Science on Society
Bertrand Russell

Contents

The application of the Partitioned Finite Element method leads to finite-dimensional pH systems, that can be discretized using finite elements method. To quantify how well the numerical solution approximates the true one, it is important to estimate the rate of convergence of the finite elements. In this chapter convergence estimates are conjectured for beams and plates systems and numerical experiments are constructed to support the proposed conjectures.

The first section is devoted to the pH Euler-Bernoulli beam. For the discretization of this problem three strategies are proposed. In the second section of this chapter, pH plate problems are discretized using mixed finite elements. This means that the divergence operator explicitly appears in the weak formulation. In the third part the discretization of plate problem is of dual-mixed type [Arn90], meaning that the gradient operator comes out in the weak formulation. The last section gathers all the numerical results.

Remark 20
Homogeneous boundary conditions will always be considered in this chapter. These are enforced weakly (i.e. natural boundary conditions $\boldsymbol{u}_\partial \equiv \mathbf{0}$) or strongly (i.e. essential boundary conditions) depending on the specific formulation under analysis.

Notations The space of all, symmetric and skew-symmetric 2×2 matrices are denoted by $\mathbb{M}, \mathbb{S}, \mathbb{K}$ respectively. The space of $\mathbb{R}^2$ vectors is denoted by $\mathbb{V}$. The symbol $\Omega \subset \mathbb{R}^2$ denotes an open connected set. The standard notation $H^m(\Omega)$ denotes the Sobolev space of square-integrable functions with m^{th} derivative in L^2 and norm

$$||u||_m^2 = \sum_{|\alpha| \leq m} \|\partial^\alpha u\|_{L^2(\Omega)}^2.$$

The space $H^{\text{Grad}}(\Omega, \mathbb{V})$ is the space of vectors with symmetric gradient in L^2

$$H^{\text{Grad}}(\Omega, \mathbb{V}) = \{\boldsymbol{u} \in L^2(\Omega, \mathbb{V}) |\ \text{Grad}(\boldsymbol{u}) \in L^2(\Omega, \mathbb{S})\},$$

and norm

$$||\boldsymbol{u}||_{\text{Grad}}^2 = ||\boldsymbol{u}||^2 + ||\,\text{Grad}(\boldsymbol{u})||^2.$$

For $\mathbb{X} \subseteq \mathbb{M}$, let

$$H^{\text{div}}(\Omega, \mathbb{V}) = \{\boldsymbol{u} \in L^2(\Omega, \mathbb{V}) |\ \text{div}(\boldsymbol{u}) \in L^2(\Omega)\},$$
$$H^{\text{Div}}(\Omega, \mathbb{X}) = \{\boldsymbol{U} \in L^2(\Omega, \mathbb{X}) |\ \text{Div}(\boldsymbol{U}) \in L^2(\Omega; \mathbb{V})\},$$

which are Hilbert spaces with the norms

$$\|\boldsymbol{u}\|_{\text{div}}^2 = \|\boldsymbol{u}\|_{L^2(\Omega,\mathbb{V})}^2 + \|\text{div}(\boldsymbol{u})\|_{L^2(\Omega)}^2,$$
$$\|\boldsymbol{U}\|_{\text{Div}}^2 = \|\boldsymbol{U}\|_{L^2(\Omega,\mathbb{M})}^2 + \|\text{Div}(\boldsymbol{U})\|_{L^2(\Omega,\mathbb{V})}^2.$$

Let X be a Hilbert space, and t_f a positive real number. We denote by $L^\infty([0, t_f]; X)$ or $L^\infty(X)$ the space of functions $f : [0, t_f] \to X$ for which the time-space norm $||\cdot||_{L^\infty([0,t_f];X)}$ satisfies

$$||f||_{L^\infty([0,t_f];X)} = \operatorname*{ess\,sup}_{t \in [0,t_f]} ||f||_X < \infty.$$

The notation

$$||u - u_h|| \lesssim h^k$$

means $||u - u_h|| \leq C(u, t_f)h^k$. The constant $C(u, t_f)$ depends only on the exact solution u and on the final time t_f.

7.1 Discretization of the Euler-Bernoulli beam

In this section the Euler-Bernoulli beam is discretized using conforming finite elements for three different formulations:

- the weak formulation (6.65) corresponding (in absence of inputs) to a free-free beam;
- the weak formulation (6.71) corresponding (for zero inputs) to a clamped-clamped beam;
- a novel weak formulation allowing to use H^1 conforming finite elements (both lines of system (6.64) are integrated by parts once). This formulation corresponds to zero shear forces and zero rotations at the extremities. This kind of boundary conditions appears in the Cahn-Hilliard equation [CH58], but makes little sense in continuum mechanics.

7.1.1 Mixed discretization for the free-free beam

The weak formulation (6.65) seeks

$$\{e_w, e_\kappa\} \in H^2(\Omega) \times L^2(\Omega)$$

so that

$$\begin{aligned} \langle v_w,\, \rho A \partial_t e_w \rangle_{L^2(\Omega)} &= -\langle \partial_{xx} v_w,\, e_\kappa \rangle_{L^2(\Omega)}\,, && \forall\, v_w \in H^2(\Omega), \\ \left\langle v_\kappa,\, (EI)^{-1} \partial_t e_\kappa \right\rangle_{L^2(\Omega)} &= \langle v_\kappa,\, \partial_{xx} e_w \rangle_{L^2(\Omega)}\,, && \forall\, v_\kappa \in L^2(\Omega). \end{aligned} \tag{7.1}$$

Given an interval mesh $\mathcal{I}_h$ with elements E, the following conforming family of finite elements is selected for this problem

$$\begin{aligned} H^2_{h,\mathrm{HerDG1}}(\Omega) &= \{w_h \in H^2(\Omega) |\ \forall E \in \mathcal{I}_h,\ w_h|_Q \in \mathrm{Her}\}, \\ L^2_{h,\mathrm{HerDG1}}(\Omega) &= \{M_h \in L^2(\Omega) |\ \forall E \in \mathcal{I}_h,\ M_h|_E \in \mathrm{DG}_1\}, \end{aligned} \tag{7.2}$$

where Her denotes the cubic Hermite polynomials and DG is the discontinuous Galerkin finite element [LMW+12, Chapter 3]. Since for the discretization of the static problem the use of Hermite polynomial provides optimal convergence of order 2 [Hug12], it seems logical to conjecture the following error estimates:

Conjecture 1 (Convergence of the HerDG1 elements)
Assuming a smooth solution for problem (7.1), the following error estimates hold

$$||e_w - e_w^h||_{L^\infty(H^2(\Omega))} \lesssim h^2, \qquad ||e_\kappa - e_\kappa^h||_{L^\infty(L^2(\Omega))} \lesssim h^2. \tag{7.3}$$

7.1.2 Mixed discretization for the clamped-clamped beam

The weak formulation (6.71) seeks

$$\{e_w, e_\kappa\} \in L^2(\Omega) \times H^2(\Omega)$$

so that

$$\begin{aligned} \langle v_w,\, \rho A \partial_t e_w \rangle_{L^2(\Omega)} &= \langle v_w,\, -\partial_{xx} e_\kappa \rangle_{L^2(\Omega)}\,, && \forall\, v_w \in L^2(\Omega), \\ \left\langle v_\kappa,\, (EI)^{-1} \partial_t e_\kappa \right\rangle_{L^2(\Omega)} &= \langle \partial_{xx} v_\kappa,\, e_w \rangle_{L^2(\Omega)}\,, && \forall\, v_\kappa \in H^2(\Omega). \end{aligned} \tag{7.4}$$

The following family of finite elements, defined on an interval mesh $\mathcal{I}_h$ with elements E, is chosen for this problem

$$\begin{aligned} H^2_{h,\mathrm{DG1Her}}(\Omega) &= \{w_h \in L^2(\Omega) |\ \forall E \in \mathcal{I}_h,\ w_h|_Q \in \mathrm{DG}_1\}, \\ L^2_{h,\mathrm{DG1Her}}(\Omega) &= \{M_h \in H^2(\Omega) |\ \forall E \in \mathcal{I}_h,\ M_h|_E \in \mathrm{Her}\}, \end{aligned} \tag{7.5}$$

Since the formulation is symmetrical to (7.1), the following error estimates can be conjectured:

Conjecture 2 (Convergence of the DG1Her elements)
Assuming a smooth solution for problem (7.4), the following error estimates hold

$$||e_w - e_w^h||_{L^\infty(L^2(\Omega))} \lesssim h^2, \qquad ||e_\kappa - e_\kappa^h||_{L^\infty(H^2(\Omega))} \lesssim h^2. \tag{7.6}$$

7.1.3 Mixed discretization with lower regularity requirement

Consider the weak formulation (6.64). If both lines are integrated by parts once, the resulting weak form seeks

$$\{e_w, e_\kappa\} \in H^1(\Omega) \times H^1(\Omega)$$

so that

$$\begin{aligned} \langle v_w,\, \rho A \partial_t e_w \rangle_{L^2(\Omega)} &= \langle \partial_x v_w,\, \partial_x e_\kappa \rangle_{L^2(\Omega)}\,, && \forall\, v_w \in H^1(\Omega), \\ \left\langle v_\kappa,\, (EI)^{-1} \partial_t e_\kappa \right\rangle_{L^2(\Omega)} &= -\langle \partial_x v_w,\, \partial_x e_\kappa \rangle_{L^2(\Omega)}\,, && \forall\, v_\kappa \in H^1(\Omega). \end{aligned} \tag{7.7}$$

The following family of finite elements is employed for this problem

$$\begin{aligned} H^2_{h,\mathrm{CGCG}}(\Omega) &= \{w_h \in H^1(\Omega) |\ \forall E \in \mathcal{I}_h,\ w_h|_Q \in \mathrm{CG}_k\}, \\ L^2_{h,\mathrm{CGCG}}(\Omega) &= \{M_h \in H^1(\Omega) |\ \forall E \in \mathcal{I}_h,\ M_h|_E \in \mathrm{CG}_k\}, \end{aligned} \tag{7.8}$$

where CG is the Continuous Galerkin finite element [LMW+12, Chapter 3]. The following error estimates are conjectured:

Conjecture 3 (Convergence of the CGCG elements)
Assuming a smooth solution for problem (7.4), the following error estimates hold

$$||e_w - e_w^h||_{L^\infty(H^1(\Omega))} \lesssim h^k, \qquad ||e_\kappa - e_\kappa^h||_{L^\infty(H^1(\Omega))} \lesssim h^k. \tag{7.9}$$

7.2 Plate problems using known mixed finite elements

First we focus on the Mindlin plate. This problem is a combination of plane wave dynamics and plane elastodynamics. A classical mixed formulation requires H^{div} conforming elements both for the wave dynamics [BJT00] and elastodynamics [BJT01, AL14]. To obtain a suitable discretization of the Mindlin problem one has to combine the two. Additional difficulties arise from the symmetry of the stress tensor that can be imposed strongly [BJT01] or weakly [AL14].

Then we discuss the mixed discretization of the Kirchhoff plate problem. For this problem the non-conforming Hellan-Herrmann-Johnson scheme [Hel67, Her67, Joh73] (HHJ) is the most successful. However, it has been analyzed under generic boundary conditions in the static case only [BR90].

7.2.1 Mindlin plate mixed discretization

We consider the weak formulation (6.98), reported in §6.1.3. We present first a scheme that enforces the symmetry of the momenta tensor strongly and then a scheme in which the symmetry of the momenta tensor is imposed weakly.

7.2.1.1 Mindlin plate with strongly imposed symmetry

The weak formulation with strongly imposed symmetry seeks

$$\{e_w, \boldsymbol{e_\theta}, \boldsymbol{E}_\kappa, \boldsymbol{e}_\gamma\} \in L^2(\Omega) \times L^2(\Omega, \mathbb{V}) \times H^{\text{Div}}(\Omega, \mathbb{S}) \times H^{\text{div}}(\Omega, \mathbb{V})$$

so that

$$\begin{aligned}
\langle v_w,\, \rho b \partial_t e_w \rangle_{L^2(\Omega)} &= \langle v_w,\, \text{div}\, \boldsymbol{e}_\gamma \rangle_{L^2(\Omega)} + (v_w, f), && \forall\, v_w \in L^2(\Omega),\\
\langle \boldsymbol{v}_\theta,\, I_\theta \partial_t \boldsymbol{e}_\theta \rangle_{L^2(\Omega,\mathbb{V})} &= \langle \boldsymbol{v}_\theta,\, \text{Div}\, \boldsymbol{E}_\kappa + \boldsymbol{e}_\gamma \rangle_{L^2(\Omega,\mathbb{V})} + \langle \boldsymbol{v}_\theta,\, \boldsymbol{\tau} \rangle_{L^2(\Omega,\mathbb{V})}\,, && \forall\, \boldsymbol{v}_\theta \in L^2(\Omega, \mathbb{V}),\\
\langle \boldsymbol{V}_\kappa,\, \boldsymbol{\mathcal{C}}_b \partial_t \boldsymbol{E}_\kappa \rangle_{L^2(\Omega,\mathbb{S})} &= -\langle \text{Div}\, \boldsymbol{V}_\kappa,\, \boldsymbol{e}_\theta \rangle_{L^2(\Omega,\mathbb{S})}\,, && \forall\, \boldsymbol{V}_\kappa \in H^{\text{Div}}(\Omega, \mathbb{S}),\\
\langle \boldsymbol{v}_\gamma,\, C_s \partial_t \boldsymbol{e}_\gamma \rangle_{L^2(\Omega,\mathbb{V})} &= -\langle \text{div} \boldsymbol{v}_\gamma,\, e_w \rangle_{L^2(\Omega)} + \langle \boldsymbol{v}_\gamma,\, \boldsymbol{e}_\theta \rangle_{L^2(\Omega,\mathbb{V})}\,, && \forall\, \boldsymbol{v}_\gamma \in H^{\text{div}}(\Omega, \mathbb{V}).
\end{aligned} \tag{7.10}$$

The plate thickness is indicated by the symbol b, to avoid confusion with the average

mesh size indicated by h. A distributed force f and torque $\boldsymbol{\tau}$ are considered in order to find a manufactured solution for this problem.

Obtaining stable finite elements that embed the symmetry of the stress tensor for the elastodynamics problem has proven to be a difficult task [AW02]. The easiest construction is the one presented in [BJT01]. This finite element solution can be implemented in Firedrake [RHM+17] thanks to the extruded mesh functionality [MBM+16]. The main disadvantage is that this scheme requires the domain to be given by a union of rectangles, as the mesh elements have to be square. However, this allows constructing a simple element for the momenta tensor. Let $\mathcal{R}_h$ be a regular mesh with square elements Q. The following spaces are introduced as discretization spaces

$$\begin{aligned} L^2_{h,\mathrm{BJT}}(\Omega) &= \{w_h \in L^2(\Omega) |\ \forall Q \in \mathcal{R}_h,\ w_h|_Q \in \mathrm{DG}_{k-1}\}, \\ L^2_{h,\mathrm{BJT}}(\Omega, \mathbb{V}) &= \{\boldsymbol{\theta}_h \in L^2(\Omega, \mathbb{V}) |\ \forall Q \in \mathcal{R}_h,\ \boldsymbol{\theta}_h|_Q \in (\mathrm{DG}_{k-1})^2\}, \\ H^{\mathrm{Div}}_{h,\mathrm{BJT}}(\Omega, \mathbb{S}) &= \{m_{12} \in H^1(\Omega) |\ \forall Q \in \mathcal{R}_h,\ m_{12}|_Q \in \mathrm{CG}_k\} \\ &\quad \cup \{(m_{11}, m_{22}) \in H^{\mathrm{div}}(\Omega, \mathbb{V}) |\ \forall Q \in \mathcal{R}_h,\ (m_{11}, m_{22})|_Q \in \mathrm{BDM}_k\}, \\ H^{\mathrm{div}}_{h,\mathrm{BJT}}(\Omega, \mathbb{V}) &= \{\boldsymbol{q}_h \in H^{\mathrm{div}}(\Omega, \mathbb{V}) |\ \forall Q \in \mathcal{R}_h,\ \boldsymbol{q}_h|_Q \in \mathrm{BDM}_k\}, \end{aligned} \tag{7.11}$$

where BDM are the Brezzi-Douglas-Marini elements [BDM85]. BJT stands for the initials of the authors in [BJT00, BJT01]. Combining the results of both papers, the following error estimates can be conjectured.

Conjecture 4 (Convergence rate for the BJT elements)
Assuming a smooth solution to problem (7.10), the following error estimates hold

$$\begin{aligned} ||e_w - e_w^h||_{L^\infty(L^2(\Omega))} &\lesssim h^k, \qquad ||\boldsymbol{E}_\kappa - \boldsymbol{E}_\kappa^h||_{L^\infty(L^2(\Omega,\mathbb{S}))} \lesssim h^k, \\ ||\boldsymbol{e}_\theta - \boldsymbol{e}_\theta^h||_{L^\infty(L^2(\Omega,\mathbb{V}))} &\lesssim h^k, \qquad ||\boldsymbol{e}_\gamma - \boldsymbol{e}_\gamma^h||_{L^\infty(L^2(\Omega,\mathbb{V}))} \lesssim h^k. \end{aligned} \tag{7.12}$$

7.2.1.2 Mindlin plate with weakly imposed symmetry

To impose the symmetry of the momenta tensor weakly, we modify the third equation in (7.10). The symmetric gradient can be rewritten as

$$\mathrm{Grad}\ \boldsymbol{\theta} = \mathrm{grad}\,\boldsymbol{\theta} - \mathrm{skw}(\mathrm{grad}\,\boldsymbol{\theta}),$$

where $\mathrm{skw}(\boldsymbol{A}) := (\boldsymbol{A} - \boldsymbol{A}^\top)/2$ is the skew-symmetric part of matrix $\boldsymbol{A}$. Consider the weak form of the third equation in (7.10) before applying the integration by parts

$$\langle \boldsymbol{V}_\kappa, \boldsymbol{\mathcal{C}}_b \partial_t \boldsymbol{E}_\kappa \rangle_{L^2(\Omega,\mathbb{M})} = \langle \boldsymbol{V}_\kappa, \mathrm{Grad}\,\boldsymbol{e}_\theta \rangle_{L^2(\Omega,\mathbb{M})}\,.$$

Introducing the new variable $\boldsymbol{E}_r = \text{skw}(\text{grad}\,\boldsymbol{\theta})$, then $\{\boldsymbol{e}_\theta, \boldsymbol{E}_\kappa, \boldsymbol{E}_r\} \in L^2(\Omega,\mathbb{V}) \times H^{\text{Div}}(\Omega,\mathbb{M}) \times L^2(\Omega,\mathbb{K})$ satisfy (remind that $\boldsymbol{e}_\theta = \partial_t\boldsymbol{\theta}$)

$$\begin{aligned}\langle \boldsymbol{V}_\kappa,\, \boldsymbol{\mathcal{C}}_b\partial_t\boldsymbol{E}_\kappa\rangle_{L^2(\Omega,\mathbb{M})} &= \langle \boldsymbol{V}_\kappa,\, \text{grad}\,\boldsymbol{e}_\theta\rangle_{L^2(\Omega,\mathbb{M})} - \langle \boldsymbol{V}_\kappa,\, \partial_t\boldsymbol{E}_r\rangle_{L^2(\Omega,\mathbb{M})}\,,\\ &= -\langle \text{Div}\,\boldsymbol{V}_\kappa,\, \boldsymbol{e}_\theta\rangle_{L^2(\Omega,\mathbb{V})} - \langle \boldsymbol{V}_\kappa,\, \partial_t\boldsymbol{E}_r\rangle_{L^2(\Omega,\mathbb{M})}\,.\end{aligned}$$

The momenta tensor is weakly symmetric if

$$\langle \boldsymbol{V}_r,\, \boldsymbol{E}_\kappa\rangle_{L^2(\Omega,\mathbb{M})} = 0,$$

or equivalently

$$\langle \boldsymbol{V}_r,\, \partial_t\boldsymbol{E}_\kappa\rangle_{L^2(\Omega,\mathbb{M})} = 0.$$

The weak formulation then consists in finding

$$\{e_w, \boldsymbol{e}_{\boldsymbol{\theta}}, \boldsymbol{E}_\kappa, \boldsymbol{e}_\gamma, \boldsymbol{E}_r\} \in L^2(\Omega) \times L^2(\Omega,\mathbb{V}) \times H^{\text{Div}}(\Omega,\mathbb{M}) \times H^{\text{div}}(\Omega,\mathbb{V}) \times L^2(\Omega,\mathbb{K}).$$

so that

$$\begin{aligned}
\langle v_w,\, \rho b\partial_t e_w\rangle_{L^2(\Omega)} &= \langle v_w,\, \text{div}\,\boldsymbol{e}_\gamma\rangle_{L^2(\Omega)} + (v_w, f), && \forall\, v_w \in L^2(\Omega),\\
\langle \boldsymbol{v}_\theta,\, I_\theta\partial_t\boldsymbol{e}_\theta\rangle_{L^2(\Omega,\mathbb{V})} &= \langle \boldsymbol{v}_\theta,\, \text{Div}\,\boldsymbol{E}_\kappa + \boldsymbol{e}_\gamma\rangle_{L^2(\Omega,\mathbb{V})} + \langle \boldsymbol{v}_\theta,\, \boldsymbol{\tau}\rangle_{L^2(\Omega,\mathbb{V})}\,, && \forall\, \boldsymbol{v}_\theta \in L^2(\Omega,\mathbb{V}),\\
\langle \boldsymbol{V}_\kappa,\, \boldsymbol{\mathcal{C}}_b\partial_t\boldsymbol{E}_\kappa\rangle_{L^2(\Omega,\mathbb{M})} &= -\langle \text{Div}\,\boldsymbol{V}_\kappa,\, \boldsymbol{e}_\theta\rangle_{L^2(\Omega,\mathbb{V})} - \langle \boldsymbol{V}_\kappa,\, \partial_t\boldsymbol{E}_r\rangle_{L^2(\Omega,\mathbb{M})}\,, && \forall\, \boldsymbol{V}_\kappa \in H^{\text{Div}}(\Omega,\mathbb{M}),\\
\langle \boldsymbol{v}_\gamma,\, C_s\partial_t\boldsymbol{e}_\gamma\rangle_{L^2(\Omega,\mathbb{V})} &= -\langle \text{div}\boldsymbol{v}_\gamma,\, e_w\rangle_{L^2(\Omega)} + \langle \boldsymbol{v}_\gamma,\, \boldsymbol{e}_\theta\rangle_{L^2(\Omega,\mathbb{V})}\,, && \forall\, \boldsymbol{v}_\gamma \in H^{\text{div}}(\Omega,\mathbb{V}),\\
\langle \boldsymbol{V}_r,\, \partial_t\boldsymbol{E}_\kappa\rangle_{L^2(\Omega,\mathbb{M})} &= 0 && \forall\, \boldsymbol{V}_r \in L^2(\Omega,\mathbb{K}).
\end{aligned} \tag{7.13}$$

Consider a regular triangulation $\mathcal{T}_h$ with elements T. The following spaces are used as discretization spaces

$$\begin{aligned}
L^2_{h,\text{AFW}}(\Omega) &= \{w_h \in L^2(\Omega)|\ \forall T \in \mathcal{T}_h,\ w_h|_T \in \text{DG}_{k-1}\},\\
L^2_{h,\text{AFW}}(\Omega,\mathbb{V}) &= \{\boldsymbol{\theta}_h \in L^2(\Omega,\mathbb{V})|\ \forall T \in \mathcal{T}_h,\ \boldsymbol{\theta}_h|_T \in (\text{DG}_{k-1})^2\},\\
H^{\text{Div}}_{h,\text{AFW}}(\Omega,\mathbb{M}) &= \{(m_{11}, m_{12}) \in H^{\text{div}}(\Omega,\mathbb{V})|\ \forall T \in \mathcal{T}_h,\ (m_{11}, m_{12})|_T \in \text{BDM}_k\}\\
&\quad \cup \{(m_{21}, m_{22}) \in H^{\text{div}}(\Omega,\mathbb{V})|\ \forall T \in \mathcal{T}_h,\ (m_{21}, m_{22})|_T \in \text{BDM}_k\},\\
H^{\text{div}}_{h,\text{AFW}}(\Omega,\mathbb{V}) &= \{\boldsymbol{q}_h \in H^{\text{div}}(\Omega,\mathbb{V})|\ \forall T \in \mathcal{T}_h,\ \boldsymbol{q}_h|_T \in \text{RT}_{k-1}\},\\
L^2_{h,\text{AFW}}(\Omega,\mathbb{K}) &= \{\boldsymbol{R}_h \in L^2(\Omega,\mathbb{K})|\ \forall T \in \mathcal{T}_h,\ w_h|_T \in \text{DG}_{k-1}\},
\end{aligned} \tag{7.14}$$

where RT stands for the Raviart-Thomas elements [RT77]. The acronym AFW stands for Arnold-Falk-Winther, that proposed this kind of discretization for static elasticity [AFW07]. A convergence analysis for the general elastodynamics problem with weak symmetry in the $L^\infty(L^2)$ norm is fully detailed in [AL14]. A convergence study for the wave equation with mixed finite elements in the $L^\infty(L^2)$ is presented in [Gev88]. Combining the results of the

two, the following error estimates can be conjectured:

Conjecture 5 (Rate of convergence for the AFW elements)
Assuming a smooth solution to problem (7.13), the following error estimates hold

$$\begin{aligned} &||e_w - e_w^h||_{L^\infty(L^2(\Omega))} \lesssim h^k, \qquad ||\boldsymbol{E}_\kappa - \boldsymbol{E}_\kappa^h||_{L^\infty(L^2(\Omega,\mathbb{M}))} \lesssim h^k, \qquad ||\boldsymbol{E}_r - \boldsymbol{E}_r^h||_{L^\infty(L^2(\Omega,\mathbb{K}))} \lesssim h^k. \\ &||\boldsymbol{e}_\theta - \boldsymbol{e}_\theta^h||_{L^\infty(L^2(\Omega,\mathbb{V}))} \lesssim h^k, \qquad ||\boldsymbol{e}_\gamma - \boldsymbol{e}_\gamma^h||_{L^\infty(L^2(\Omega,\mathbb{V}))} \lesssim h^k, \end{aligned} \tag{7.15}$$

7.2.2 The Hellan-Herrmann-Johnson scheme for the Kirchhoff plate

For the Kirchhoff plate, the Hellan-Herrmann-Johnson scheme [Hel67, Her67, Joh73] (HHJ) can be used to obtain a structure-preserving discretization. Given the non-conforming nature of this scheme, it is necessary to first introduce the discrete functional spaces and state the problem directly in discrete form. The illustration of the method follows closely [AW19]. The vertical displacement is approximated using continuous Lagrange polynomials, while the momenta tensor is discretized using the HHJ element

$$\begin{aligned} W_h =& \{w_h \in H_0^1(\Omega) |\ \forall T \in \mathcal{T}_h,\ w_h|_T \in P_k\}, \\ S_h =& \{\boldsymbol{M}_h \in L^2(\Omega, \mathbb{S}) |\ \forall T \in \mathcal{T}_h,\ \boldsymbol{M}_h|_T \in (P_{k-1})^{2\times 2}_{\text{sym}}, \\ & \boldsymbol{M}_h \text{ is normal-normal continous across elements}\}. \end{aligned} \tag{7.16}$$

The normal to normal continuity means that if two triangles T_1, T_2 share a common edge E then $\boldsymbol{n}^\top(\boldsymbol{M}_h|_{T_1})\boldsymbol{n} = \boldsymbol{n}^\top(\boldsymbol{M}_h|_{T_2})\boldsymbol{n}$ on E. Taking system (4.36) and multiplying the first equation by $v_w \in W_h$ and integrating over a triangle

$$\begin{aligned} -\langle v_w, \operatorname{div}\operatorname{Div}\boldsymbol{E}_\kappa\rangle_{L^2(T)} &= \langle \nabla v_w, \operatorname{Div}\boldsymbol{E}_\kappa\rangle_{L^2(T,\mathbb{V})} - \langle v_w, \operatorname{Div}\boldsymbol{E}_\kappa \cdot \boldsymbol{n}\rangle_{L^2(\partial T)}, \\ &= -\langle \operatorname{Hess} v_w, \boldsymbol{E}_\kappa\rangle_{L^2(T,\mathbb{S})} - \langle v_w, \operatorname{Div}\boldsymbol{E}_\kappa \cdot \boldsymbol{n}\rangle_{L^2(\partial T)}, \\ &+ \left\langle \partial_{\boldsymbol{s}} v_w, \boldsymbol{s}^\top \boldsymbol{E}_\kappa \boldsymbol{n}\right\rangle_{L^2(\partial T)} + \left\langle \partial_{\boldsymbol{n}} v_w, \boldsymbol{n}^\top \boldsymbol{E}_\kappa \boldsymbol{n}\right\rangle_{L^2(\partial T)}. \end{aligned}$$

A double integration by parts is applied to get the final equation. For the last term a summation over all triangles provides

$$\sum_{T\in\mathcal{T}_h} \left\langle \partial_{\boldsymbol{n}} v_w, \boldsymbol{n}^\top \boldsymbol{E}_\kappa \boldsymbol{n}\right\rangle_{L^2(\partial T)} = \sum_{E\in\mathcal{E}_h} \left\langle [\![\partial_{\boldsymbol{n}} v_w]\!], \boldsymbol{n}^\top \boldsymbol{E}_\kappa \boldsymbol{n}\right\rangle_{L^2(E)},$$

where $\mathcal{E}_h$ is the set of all edges belonging to the mesh and $[\![a]\!] = a|_{T_1} + a|_{T_2}$ denotes the jump of a function across shared edges. For a boundary edge it is simply the value of the function. For the other terms, it holds

$$\langle v_w, \operatorname{Div}\boldsymbol{E}_\kappa \cdot \boldsymbol{n}\rangle_{L^2(\partial T)} = 0, \qquad \left\langle \partial_{\boldsymbol{s}} v_w, \boldsymbol{s}^\top \boldsymbol{E}_\kappa \boldsymbol{n}\right\rangle_{L^2(\partial T)} = 0,$$

since v_w is continuous across the edge boundaries, and the normal switches sign. We are now in a position to state the final weak form. Given the bilinear form

$$d_h(v_w,\ \boldsymbol{E}_\kappa) := -\sum_{T\in\mathcal{T}_h} \langle \operatorname{Hess} v_w,\ \boldsymbol{E}_\kappa\rangle_{L^2(T,\mathbb{S})} + \sum_{E\in\mathcal{E}_h} \left\langle [\![\partial_n v_w]\!],\ \boldsymbol{n}^\top \boldsymbol{E}_\kappa \boldsymbol{n}\right\rangle_{L^2(E)}, \tag{7.17}$$

find $(e_w, \boldsymbol{E}_\kappa) \in W_h \times S_h$ such that

$$\begin{aligned} \langle v_w,\ \rho b \partial_t e_w\rangle_{L^2(\Omega)} &= +d_h(v_w,\ \boldsymbol{E}_\kappa) + \langle v_w,\ f\rangle_{L^2(\Omega)}, && \forall\ v_w \in W_h, \\ \langle \boldsymbol{V}_\kappa,\ \boldsymbol{\mathcal{C}}_b \partial_t \boldsymbol{E}_\kappa\rangle_{L^2(\Omega,\mathbb{S})} &= -d_h(e_w,\ \boldsymbol{V}_\kappa), && \forall\ \boldsymbol{V}_\kappa \in S_h. \end{aligned} \tag{7.18}$$

For the associated static problem, under the hypothesis of smooth solutions, optimal convergence of order $O(k)$ for $w \in H^1$ and $\boldsymbol{M} \in L^2$ has been established. So, it is natural to conjecture the following result for the dynamic problem:

Conjecture 6 (Convergence of the HHJ elements)
Assuming a smooth solution for problem (7.18), the following error estimates hold

$$||e_w - e_w^h||_{L^\infty(H^1(\Omega))} \lesssim h^k, \qquad ||\boldsymbol{E}_\kappa - \boldsymbol{E}_\kappa^h||_{L^\infty(L^2(\Omega,\mathbb{S}))} \lesssim h^k. \tag{7.19}$$

7.3 Dual mixed discretization of plate problems

In this section the discretization of the Kirchhoff and Mindlin plates is no more a classical mixed discretization. The application of PFEM to the other partition of the system provides a discretization in which the grad and Grad operators appear. In [Jol03], the author refers to this kind of discretization as primal-dual.

7.3.1 Dual mixed discretization of the Mindlin plate

First of all we construct a family of finite elements capable of discretizing problem (6.90), that seeks

$$\{e_w, \boldsymbol{e_\theta}, \boldsymbol{E}_\kappa, \boldsymbol{e}_\gamma\} \in H^1(\Omega) \times H^{\mathrm{Grad}}(\Omega,\mathbb{V}) \times L^2(\Omega,\mathbb{S}) \times L^2(\Omega,\mathbb{V}),$$

so that

$$\begin{aligned} \langle v_w,\ \rho h \partial_t e_w\rangle_{L^2(\Omega)} &= -\langle \operatorname{grad} v_w,\ \boldsymbol{e}_\gamma\rangle_{L^2(\Omega,\mathbb{V})}, && \forall\ v_w \in H^1(\Omega), \\ \langle \boldsymbol{v}_\theta,\ I_\theta \partial_t \boldsymbol{e}_\theta\rangle_{L^2(\Omega,\mathbb{V})} &= -\langle \operatorname{Grad} \boldsymbol{v}_\theta,\ \boldsymbol{E}_\kappa\rangle_{L^2(\Omega,\mathbb{S})} + \langle \boldsymbol{v}_\theta,\ \boldsymbol{e}_\gamma\rangle_{L^2(\Omega)}, && \forall\ \boldsymbol{v}_\theta \in H^{\mathrm{Grad}}(\Omega,\mathbb{V}), \\ \langle \boldsymbol{V}_\kappa,\ \boldsymbol{\mathcal{C}_b} \partial_t \boldsymbol{E}_\kappa\rangle_{L^2(\Omega,\mathbb{S})} &= \langle \boldsymbol{V}_\kappa,\ \operatorname{Grad} \boldsymbol{e}_\theta\rangle_{L^2(\Omega,\mathbb{S})}, && \forall\ \boldsymbol{V}_\kappa \in L^2(\Omega,\mathbb{S}), \\ \langle \boldsymbol{v}_\gamma,\ C_s \partial_t \boldsymbol{e}_\gamma\rangle_{L^2(\Omega,\mathbb{V})} &= \langle \boldsymbol{v}_\gamma,\ \operatorname{grad} e_w\rangle_{L^2(\Omega,\mathbb{V})} - \langle \boldsymbol{v}_\gamma,\ \boldsymbol{e}_\theta\rangle_{L^2(\Omega,\mathbb{V})}, && \forall\ \boldsymbol{v}_\gamma \in L^2(\Omega,\mathbb{V}). \end{aligned} \tag{7.20}$$

Consider a regular triangulation $\mathcal{T}_h$ with elements T. The following conforming family of

finite elements is used to the weak formulation (7.20) (see also [CF05] for a similar construction for the elastodynamics problem)

$$\begin{aligned} H^1_{h,\mathrm{CGDG}}(\Omega) &= \{w_h \in H^1(\Omega)|\ \forall T \in \mathcal{T}_h,\ w_h|_T \in \mathrm{CG}_k\},\\ H^{\mathrm{Grad}}_{h,\mathrm{CGDG}}(\Omega,\mathbb{V}) &= \{\boldsymbol{\theta}_h \in H^{\mathrm{Grad}}(\Omega,\mathbb{V})|\ \forall T \in \mathcal{T}_h,\ \boldsymbol{\theta}_h|_T \in (\mathrm{CG}_k)^2\},\\ L^2_{h,\mathrm{CGDG}}(\Omega,\mathbb{S}) &= \{\boldsymbol{M}_h \in L^2(\Omega,\mathbb{S})|\ \forall T \in \mathcal{T}_h, \boldsymbol{M}_h|_T \in (\mathrm{DG}_{k-1})^{2\times 2}_{\mathrm{sym}}\},\\ L^2_{h,\mathrm{CGDG}}(\Omega,\mathbb{V}) &= \{\boldsymbol{q}_h \in L^2(\Omega,\mathbb{V})|\ \forall T \in \mathcal{T}_h,\ \boldsymbol{q}_h|_T \in (\mathrm{DG}_{k-1})^2\}. \end{aligned} \tag{7.21}$$

To approximate spaces $H^1_h(\Omega)$, $H^{\mathrm{Grad}}_h(\Omega,\mathbb{R}^2)$ Lagrange polynomials of order k are selected. For spaces $L^2_h(\Omega,\mathbb{S})$, $L^2_h(\Omega,\mathbb{R}^2)$ Discontinous Galerkin polynomials of order $k-1$ are employed. This selection of finite elements can be seen as a standard discretization of the problem combined with a reduced integration of the stress tensor and shear vector. For this reason, the following conjecture on the error estimates can be proposed.

Conjecture 7 (Convergence of the CGDG elements)
Assuming a smooth solution to problem (7.20), the following error estimates hold

$$\begin{aligned} ||e_w - e^h_w||_{L^\infty(H^1(\Omega))} &\lesssim h^k, \qquad ||\boldsymbol{E}_\kappa - \boldsymbol{E}^h_\kappa||_{L^\infty(L^2(\Omega,\mathbb{S}))} \lesssim h^k,\\ ||\boldsymbol{e}_\theta - \boldsymbol{e}^h_\theta||_{L^\infty(H^{\mathrm{Grad}}(\Omega,\mathbb{V}))} &\lesssim h^k, \qquad ||\boldsymbol{e}_\gamma - \boldsymbol{e}^h_\gamma||_{L^\infty(L^2(\Omega,\mathbb{V}))} \lesssim h^k. \end{aligned} \tag{7.22}$$

7.3.2 Dual mixed discretization of the Kirchhoff plate

The Kirchhoff plate weak formulation (6.80) seeks

$$\{e_w, \boldsymbol{E}_\kappa\} \in H^2(\Omega) \times L^2(\Omega,\mathbb{S})$$

so that

$$\begin{aligned} \langle v_w,\, \rho h \partial_t e_w\rangle_{L^2(\Omega)} &= -\langle \mathrm{Hess}\, v_w,\, \boldsymbol{E}_\kappa\rangle_{L^2(\Omega,\mathbb{S})}\,, \qquad &\forall\ v_w \in H^2(\Omega),\\ \langle \boldsymbol{V}_\kappa,\, \boldsymbol{\mathcal{C}_b}\partial_t \boldsymbol{V}_\kappa\rangle_{L^2(\Omega,\mathbb{R}^S)} &= \langle \boldsymbol{V}_\kappa,\, \mathrm{Hess}\, e_w\rangle_{L^2(\Omega,\mathbb{S})}\,. &\forall\ \boldsymbol{V}_\kappa \in L^2(\Omega,\mathbb{S}). \end{aligned} \tag{7.23}$$

Given a regular triangulation $\mathcal{T}_h$ with elements T, the following family of finite elements is conforming to the weak formulation (7.23)

$$\begin{aligned} H^2_{h,\mathrm{BellDG3}}(\Omega) &= \{w_h \in H^2(\Omega)|\ \forall T \in \mathcal{T}_h,\ w_h|_T \in \mathrm{Bell}\},\\ L^2_{h,\mathrm{BellDG3}}(\Omega,\mathbb{S}) &= \{\boldsymbol{M}_h \in L^2(\Omega,\mathbb{S})|\ \forall T \in \mathcal{T}_h, \boldsymbol{M}_h|_T \in (\mathrm{DG}_3)^{2\times 2}_{\mathrm{sym}}\}, \end{aligned} \tag{7.24}$$

where Bell stands for the Bell element [Bel69]. No conjectured error estimates are proposed to this problem. As it will be shown in §7.4.3, the results obtained with this elements are of difficult interpretation.

Remark 21
Thanks to a general approach for transforming finite elements [Kir18], H^2-conforming elements have been implemented in the Firedrake *library. Therefore, for the discretization of*

the H^2-space, the Argyris element [AFS68] is another valuable possibility. Unfortunately, the strong imposition of boundary conditions for H^2 conforming elements is not possible in FIREDRAKE *at the present time [KM19, Sec. 3.2]. Because of the simpler structure and ordering of its degrees of freedom, the Bell element has been privileged over the Argyris one for the convergence study. In Chapter 8 the Argyris element will be employed imposing the boundary conditions weakly.*

7.4 Numerical experiments

In this section numerical test cases are used to verify the conjectured orders of convergence for the two problems. Upon discretization, cf. §6.1.3, the weak formulations (7.1), (7.4), (7.7) (Euler Bernoulli beam), (7.10), (7.20) (Mindlin plate), and (7.18) (7.23) (Kirchhoff plate) assume the form

$$\underbrace{\begin{bmatrix} \mathbf{M}_1 & \mathbf{0} \\ \mathbf{0} & \mathbf{M}_2 \end{bmatrix}}_{\mathbf{M}} \begin{pmatrix} \dot{\mathbf{e}}_1 \\ \dot{\mathbf{e}}_2 \end{pmatrix} = \underbrace{\begin{bmatrix} \mathbf{0} & \mathbf{D} \\ -\mathbf{D}^\top & \mathbf{0} \end{bmatrix}}_{\mathbf{J}} \begin{pmatrix} \mathbf{e}_1 \\ \mathbf{e}_2 \end{pmatrix} + \begin{pmatrix} \mathbf{f} \\ \mathbf{0} \end{pmatrix}.$$

The mass matrix $\mathbf{M}$ is symmetric and positive definite. In case of weak enforcement of the symmetry (7.13), the final system reads

$$\underbrace{\begin{bmatrix} \mathbf{M}_1 & \mathbf{0} & \mathbf{0} \\ \mathbf{0} & \mathbf{M}_2 & \mathbf{A}_\lambda^\top \\ \mathbf{0} & \mathbf{A}_\lambda & \mathbf{0} \end{bmatrix}}_{\mathbf{M}} \begin{pmatrix} \dot{\mathbf{e}}_1 \\ \dot{\mathbf{e}}_2 \\ \dot{\mathbf{e}}_\lambda \end{pmatrix} = \underbrace{\begin{bmatrix} \mathbf{0} & \mathbf{D} & \mathbf{0} \\ -\mathbf{D}^\top & \mathbf{0} & \mathbf{0} \\ \mathbf{0} & \mathbf{0} & \mathbf{0} \end{bmatrix}}_{\mathbf{J}} \begin{pmatrix} \mathbf{e}_1 \\ \mathbf{e}_2 \\ \mathbf{e}_\lambda \end{pmatrix} + \begin{pmatrix} \mathbf{f} \\ \mathbf{0} \\ \mathbf{0} \end{pmatrix}.$$

where $\mathbf{A}_\lambda$ is the matrix obtained by discretization of $\left\langle \boldsymbol{V}_r, \dot{\boldsymbol{E}}_\kappa \right\rangle_{L^2(\Omega,\mathbb{M})}$.
Because of the presence of the Lagrange multiplier, the mass matrix $\mathbf{M}$ is symmetric but indefinite, giving rise to a saddle point problem. The numerical solution of this kind of problems is notoriously much harder than that of positive definite ones [BGL05]. The FIREDRAKE library [RHM+17] is used to generate the matrices. To integrate the equations in time a Crank-Nicholson scheme has been used, for all simulations. The time step is set to $\Delta t = h/10$ to have a lower impact of the time discretization error with respect to the spatial error. The final time is set to one $t_f = 1$ [s] for all simulations. To compute the $L^\infty(X)$ space-time dependent norm the discrete norm $L^\infty_{\Delta t}(X)$ is used

$$||\cdot||_{L^\infty(X)} \approx ||\cdot||_{L^\infty_{\Delta t}(X)} = \max_{t \in t_i} ||\cdot||_X,$$

where t_i are the discrete simulation instants.

7.4.1 Numerical test for the Euler-Bernoulli beam

We consider the following exact solution for the Euler-Bernoulli beam under simply supported boundary conditions

$$w^{\text{ex}} = \sin(\pi x/L)\sin(t), \qquad \Omega = \{0, L\}. \tag{7.25}$$

The corresponding pH exact solutions are then

$$\begin{aligned} e_w^{\text{ex}} &= \sin(\pi x/L)\cos(t), & e_w^{\text{ex}}|_{\partial\Omega} &= 0, \\ e_\kappa^{\text{ex}} &= -EI\,(\pi/L)^2 \sin(\pi x/L)\sin(t), & e_\kappa^{\text{ex}}|_{\partial\Omega} &= 0. \end{aligned} \tag{7.26}$$

The numerical values used for the simulations are reported in Tab. 7.1.

Beam parameters				
ρ	A	E	I	L
5600 [kg/m^3]	50 [mm^2]	[136 GPa]	4.16 [mm^4]	1 m

Table 7.1: Physical parameters for the Euler Bernoulli beam.

Results for the HerDG1 elements 7.2 The results are reported in Fig. 7.1 and Table B.1. The conjectured error estimates (7.3) are respected.

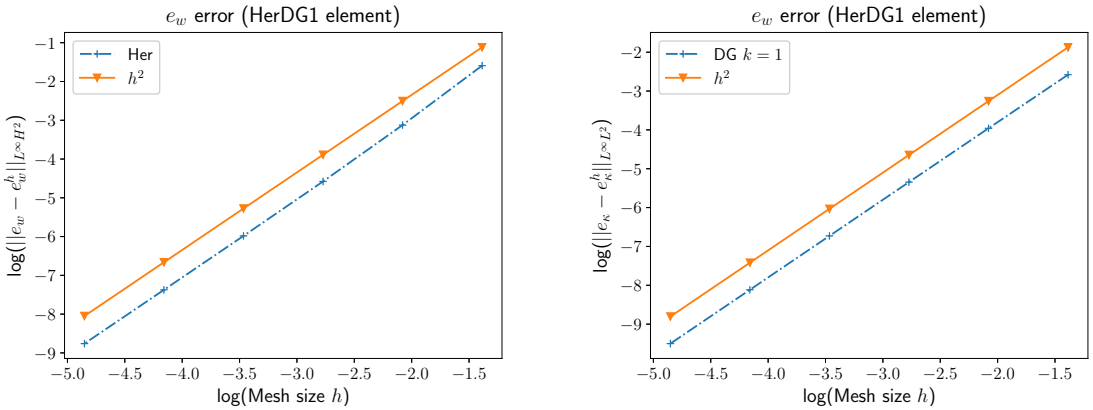

(a) $L^\infty_{\Delta t}(H^2(\Omega))$ error for e_w (b) $L^\infty_{\Delta t}(L^2(\Omega))$ error for e_κ

Figure 7.1: Error for the Euler Bernoulli beam (HerDG1 elements).

Results for the DG1Her elements 7.5 The results, reported in Fig. 7.2 and Table B.2, satisfy the predicted error (7.6).

Results for the CGCG elements 7.8 The results, reported in Fig. 7.3 and Tables B.3, B.4, B.5, verify the conjectured error (7.9).

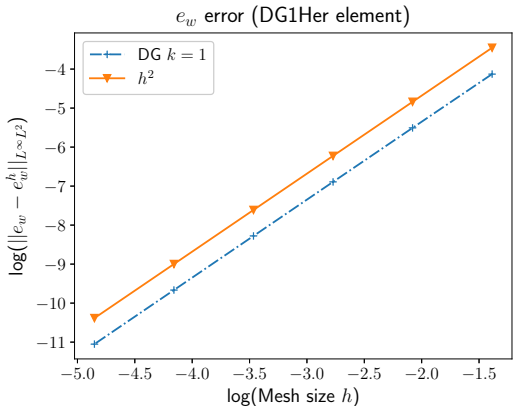

(a) $L^\infty_{\Delta t}(L^2(\Omega))$ error for e_w

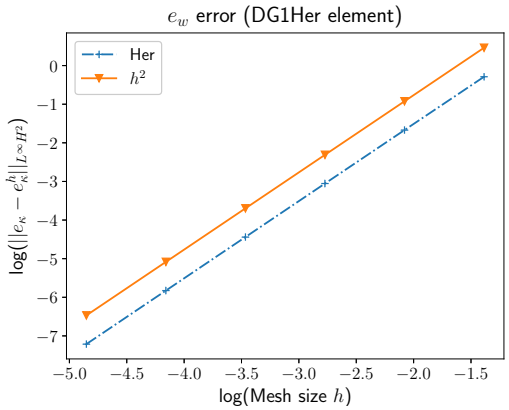

(b) $L^\infty_{\Delta t}(H^2(\Omega))$ error for e_κ

Figure 7.2: Error for the Euler Bernoulli beam (DG1Her elements).

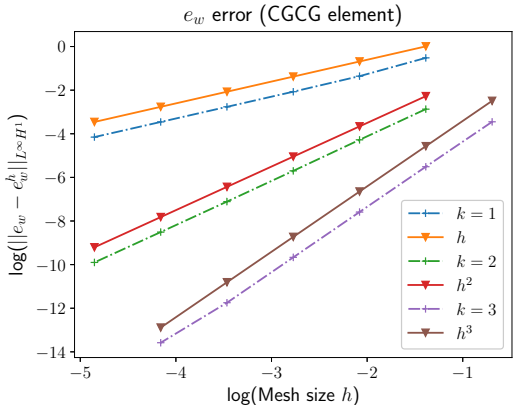

(a) $L^\infty_{\Delta t}(H^1(\Omega))$ error for e_w

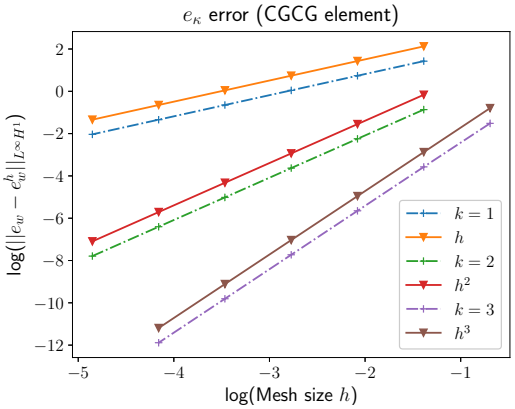

(b) $L^\infty_{\Delta t}(H^1(\Omega))$ error for e_κ

Figure 7.3: Error for the Euler Bernoulli beam (CGCG elements).

7.4.2 Numerical test for the Mindlin plate

To validate the method, we first test a finite element combinations on an analytic solution. Constructing an analytical solution for a vibrating Mindlin plate is far from trivial. Therefore, the solution for the static case [BadVMR13] is exploited.

Consider a distributed static force given by

$$\begin{aligned} f_s(x,y) = \frac{E_Y}{12(1-\nu^2)}\{&12y(y-1)(5x^2-5x+1)\\ \times&[2y^2(y-1)2 + x(x-1)(5y^2-5y+1)] + 12x(x-1)\\ \times&(5y^2-5y+1)[2x^2(x-1)2 + y(y-1)(5x^2-5x+1)]\}. \end{aligned}$$

The static displacement and rotation are given by

$$\begin{aligned} w_s(x,y) &= \frac{1}{3}x^3(x-1)^3y^3(y-1)^3 - \frac{2b^2}{5(1-\nu)}[y^3(y-1)^3x(x-1)(5x^2-5x+1).\\ \boldsymbol{\theta}_s(x,y) &= \begin{pmatrix} y^3(y-1)^3 & x^2(x-1)^2(2x-1)\\ x^3(x-1)^3 & y^2(y-1)^2(2y-1)\end{pmatrix} \end{aligned}$$

The static solution solves the following problem defined on the square domain $\Omega = (0,1)\times(0,1)$ under clamped boundary conditions:

$$\begin{aligned} 0 &= \text{div } \boldsymbol{q}_s + f_s, \qquad & \boldsymbol{\mathcal{C}}_b\boldsymbol{M}_s &= \text{Grad } \boldsymbol{\theta}_s, \qquad & w_s|_{\partial\Omega} &= 0,\\ 0 &= \text{Div}\boldsymbol{M}_s + \boldsymbol{q}_s, \qquad & C_s\boldsymbol{q}_s &= \text{grad } w_s - \boldsymbol{\theta}_s, \qquad & \boldsymbol{\theta}_s|_{\partial\Omega} &= 0. \end{aligned} \tag{7.27}$$

Given the linear nature of the system a solution for the dynamic problem is found by multiplying the static solution by a time dependent term. For simplicity a sinus function is chosen

$$w_d(x,y,t) = w_s(x,y)\sin(t), \quad \boldsymbol{\theta}_d(x,y,t) = \boldsymbol{\theta}_s(x,y)\sin(t).$$

Appropriate forcing terms have to be introduced to compensate the inertial accelerations. The force and torque in the dynamical case become

$$f_d = f_s\sin(t) + \rho b\partial_{tt}w_d, \qquad \boldsymbol{\tau}_d = \frac{\rho b^3}{12}\partial_{tt}\boldsymbol{\theta}_d.$$

For the port-Hamiltonian system the unknowns are the linear and angular velocities, the momenta tensor and the shear force. The exact solution and boundary conditions are thus given by

$$\begin{aligned} e_w^{\text{ex}} &= w_s(x,y)\cos(t), \qquad & \boldsymbol{E}_\kappa^{\text{ex}} &= \boldsymbol{\mathcal{D}}_b \text{ Grad } \boldsymbol{\theta}_d, \qquad & e_w^{\text{ex}}|_{\partial\Omega} &= 0,\\ \boldsymbol{e}_\theta^{\text{ex}} &= \boldsymbol{\theta}_s(x,y)\cos(t), \qquad & \boldsymbol{e}_\gamma^{\text{ex}} &= D_s(\text{grad } w_d - \boldsymbol{\theta}_d), \qquad & \boldsymbol{e}_\theta^{\text{ex}}|_{\partial\Omega} &= 0. \end{aligned} \tag{7.28}$$

Variables $(e_w^{\text{ex}}, \boldsymbol{e}_\theta^{\text{ex}}, \boldsymbol{E}_\kappa^{\text{ex}}, \boldsymbol{e}_\gamma^{\text{ex}})$ under excitations $(f_d, \boldsymbol{\tau}_d)$ solve problem (6.86a). The solution being smooth, conjectures 4 and 5 should hold. The numerical values of the physical parameters are reported in Table 7.2.

Remark 22
The numerical values for the parameters in Tab. 7.2 do not represent any physical material. If more realistic values are used, the solver fails when the AFW elements (7.14) for polynomial degree $k = 3$ is employed. This is due to the extremely high condition number of the indefinite mass matrix. For all the other cases the employed solvers converge to the solution.

Plate parameters				
E	ρ	ν	K_{sh}	b
1 [Pa]	1 [kg/m^3]	0.3	5/6	0.1 [m]

Table 7.2: Physical parameters for the Mindlin plate.

Results for the mixed strong symmetry formulation (BTJ elements (7.11)) The weak form (7.10) and its corresponding finite elements (7.11) are implemented using FIREDRAKE extruded mesh functionality [MBM+16]. A direct solver based on an LU preconditioner is used. In Fig. 7.4 and Tables B.6, B.7, B.8 the errors for $(e_w, \boldsymbol{e}_\theta, \boldsymbol{E}_\kappa, \boldsymbol{e}_\gamma)$ are reported. As one can notice, the conjectured error estimates (7.12) are recovered for all variables.

Results for the mixed weak symmetry formulation (AFW elements (7.14)) Formulation (7.13) and its elements (7.14) are considered here. A direct solver fails for high order cases (i.e. $k = 3$). For this reason a generalized minimal residual method GMRES [SS86] is used with restart number of iterations equal to 100. In Fig. 7.5 and Tables B.9, B.10, B.11 the errors for variables $(e_w, \boldsymbol{e}_\theta, \boldsymbol{E}_\kappa, \boldsymbol{e}_\gamma)$ are reported. The errors for $(e_w, \boldsymbol{e}_\theta, \boldsymbol{e}_\gamma)$ respect the conjectured result (7.15). Variable $\boldsymbol{E}_\kappa$ exhibits a superconvergence phenomenon for the case $k = 1$. In [AL14] no numerical study was carried out for the case $k = 1$. The BDM elements might be responsible for such superconvergence. The convergence order of $(\boldsymbol{E}_\kappa, \boldsymbol{e}_\gamma)$ deteriorates for $k = 3$ for the finest mesh. This must be linked to errors due to the underlying large saddle-point problem. Indeed in [AL14] a hybridization method is used to transform the saddle-point problem into a positive definite one. The results for the Lagrange multiplier are reported in Fig. 7.5e and Table B.12. For this variable, an order 2 of convergence is observed for all cases.

Results for dual mixed formulation (CGDG elements (7.21)) For this formulation the boundary conditions are imposed strongly on $e_w, \boldsymbol{e}_\theta$. A direct solver based on an LU preconditioner is used. In Fig. 7.6 and Tables B.13 the errors are reported. Conjecture 7 is verified for this test.

7.4.3 Numerical test for the Kirchhoff plate

The weak form (7.18) and the finite elements (7.16) are considered. The HHJ elements were included in FENICS and FIREDRAKE thanks to the contribution of Lizao Li [Li18]. Two

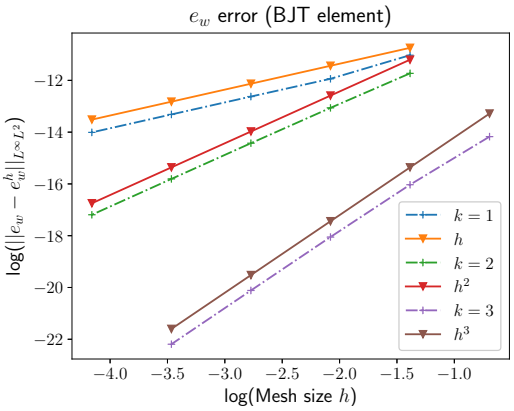

(a) $L^\infty_{\Delta t}(L^2(\Omega))$ error for e_w

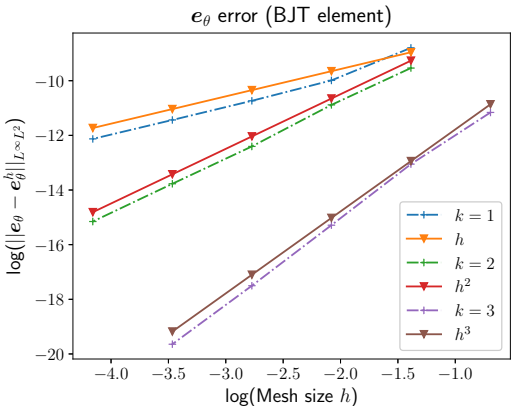

(b) $L^\infty_{\Delta t}(L^2(\Omega, \mathbb{V}))$ error for $\boldsymbol{e}_\theta$

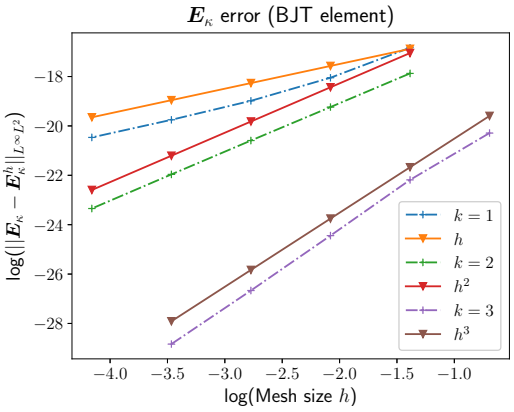

(c) $L^\infty_{\Delta t}(L^2(\Omega, \mathbb{S}))$ error for $\boldsymbol{E}_\kappa$

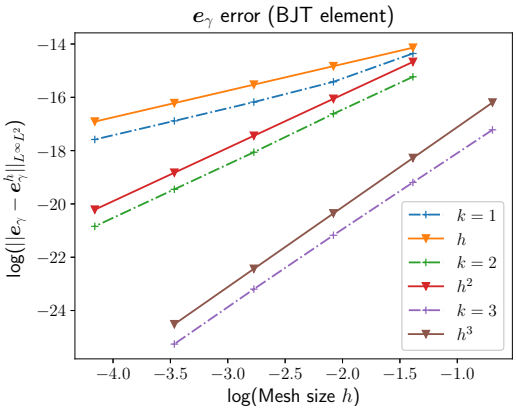

(d) $L^\infty_{\Delta t}(L^2(\Omega, \mathbb{V}))$ error for $\boldsymbol{e}_\gamma$

Figure 7.4: Error for the clamped Mindlin plate (BJT elements).

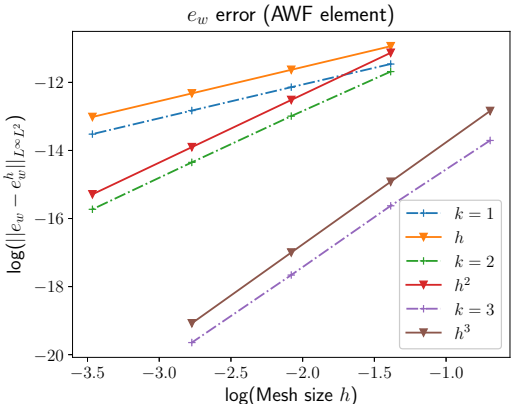

(a) $L^\infty_{\Delta t}(L^2(\Omega))$ error for e_w

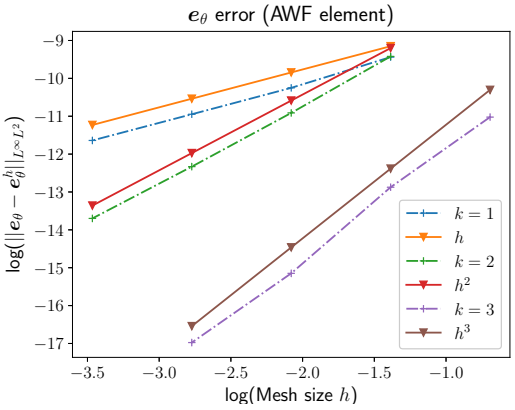

(b) $L^\infty_{\Delta t}(L^2(\Omega, \mathbb{V}))$ error for $\boldsymbol{e}_\theta$

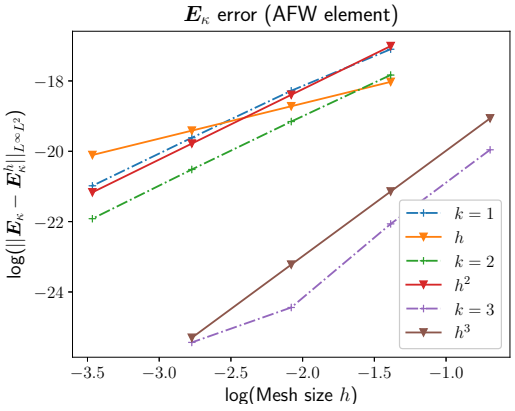

(c) $L^\infty_{\Delta t}(L^2(\Omega, \mathbb{M}))$ error for $\boldsymbol{E}_\kappa$

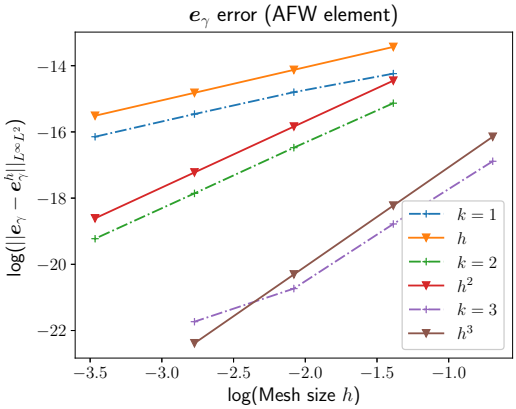

(d) $L^\infty_{\Delta t}(L^2(\Omega, \mathbb{V}))$ error for $\boldsymbol{e}_\gamma$

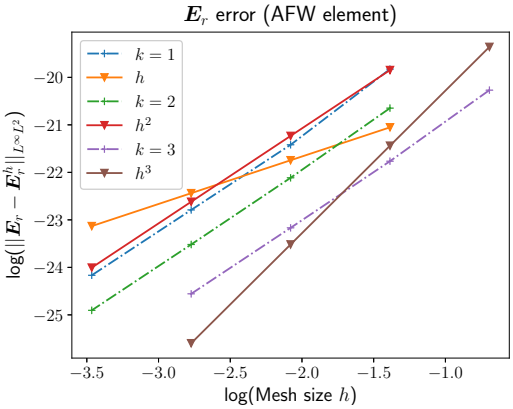

(e) $L^\infty_{\Delta t}(L^2(\Omega, \mathbb{K}))$ error for $\boldsymbol{E}_r$

Figure 7.5: Error for the clamped Mindlin plate (AFW elements).

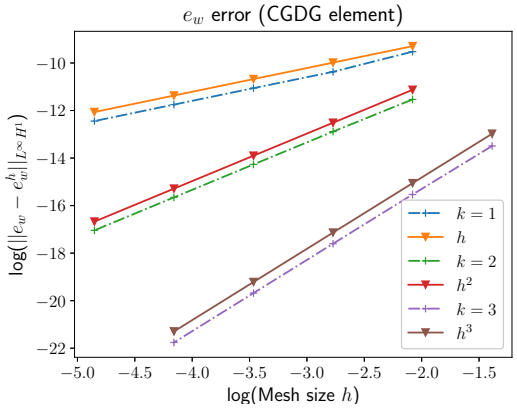

(a) $L^\infty_{\Delta t}(H^1(\Omega))$ error for e_w

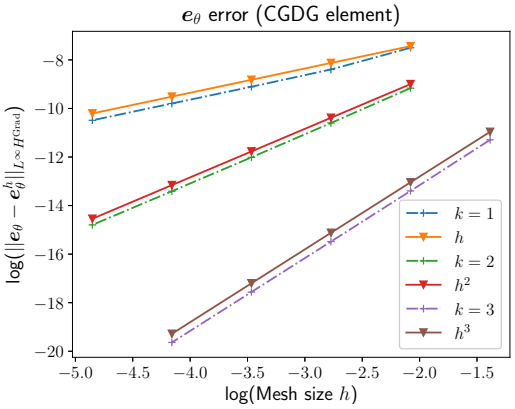

(b) $L^\infty_{\Delta t}(H^{\mathrm{Grad}}(\Omega,\mathbb{V}))$ error for $\boldsymbol{e}_\theta$

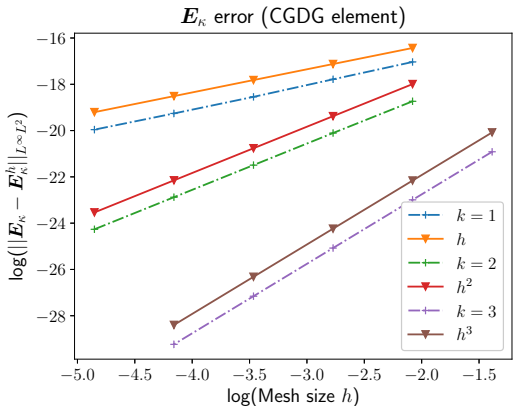

(c) $L^\infty_{\Delta t}(L^2(\Omega,\mathbb{S}))$ error for $\boldsymbol{E}_\kappa$

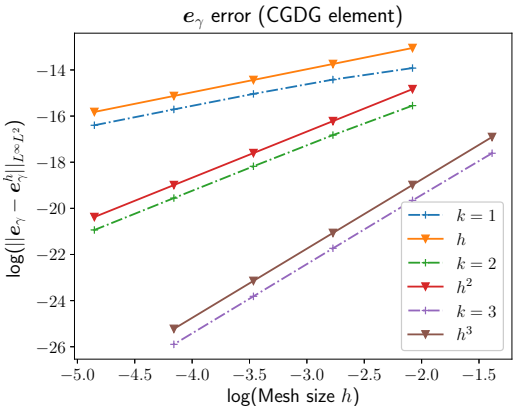

(d) $L^\infty_{\Delta t}(L^2(\Omega))$ error for $\boldsymbol{e}_\gamma$

Figure 7.6: Error for the clamped Mindlin plate (CGDG elements).

numerical tests are performed to verify these elements. Both tests are solved using a direct solver with an LU preconditioner.

7.4.3.1 Simply supported test

An analytical solution for simply supported Kirchhoff plates is readily available. Consider the following solution of problem (4.20) under simply supported conditions on a square unitary domain $\Omega = (0,1) \times (0,1)$

$$w^{\text{ex}}(x,y,t) = \sin(\pi x)\sin(\pi y)\sin(t), \quad (x,y) \in \Omega.$$

The forcing term is given by

$$f = (4D\pi^4 - \rho b)\sin(\pi x)\sin(\pi y)\sin(t), \quad D = \frac{E_Y b^3}{12(1-\nu^2)}.$$

The corresponding variables in the port-Hamiltonian framework are

$$e_w^{\text{ex}} = \partial_t w^{\text{ex}}, \quad \boldsymbol{E}_\kappa^{\text{ex}} = \mathcal{D}\nabla^2 w^{\text{ex}},$$

under simply supported boundary conditions

$$e_w|_{\partial\Omega} = 0, \qquad \boldsymbol{E}_\kappa : (\boldsymbol{n} \otimes \boldsymbol{n})|_{\partial\Omega} = 0.$$

Variables $(e_w^{\text{ex}}, \boldsymbol{E}_\kappa^{\text{ex}})$ under excitation f solve problem (4.36). The physical parameters used in simulation are reported in Table 7.3.

Plate parameters			
E	ρ	ν	b
136 [GPa]	5600 [kg/m^3]	0.3	0.001 [m]

Table 7.3: Physical parameters for the Kirchhoff plate.

Results for the HHJ elements (7.16) Results are shown in Fig. 7.7 and Tables B.16, B.17 and B.18. The conjectured error estimates are respected.

Results for the dual mixed formulation (BellDG3 elements) The results are reported in Fig. 7.8 and Tab. B.19. The error is computed in the $L^\infty(H^2(\Omega))$ norm for e_w and in the $L^\infty(L^2(\Omega,\mathbb{S}))$ norm for $\boldsymbol{E}_\kappa$. The convergence of the proposed elements is higher than linear, with a rate approaching 1.50 for the finest meshes. It is difficult to interpret this rate of convergence with respect to known convergence results. In particular the convergence rate for the Bell element (measured in the H^2-norm) for the classical biharmonic problem

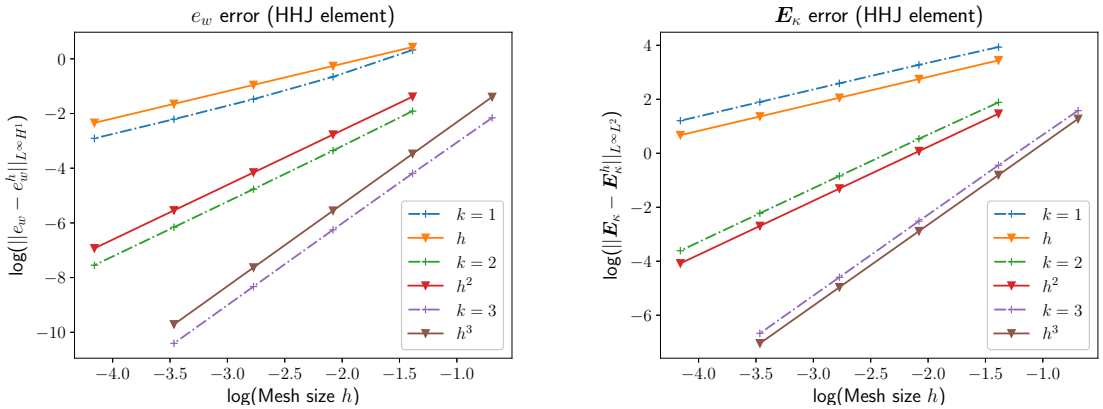

(a) $L^\infty_{\Delta t}(H^1(\Omega))$ error for e_w (b) $L^\infty_{\Delta t}(L^2(\Omega, \mathbb{S}))$ error for $\boldsymbol{E}_\kappa$

Figure 7.7: Error for the SSSS Kirchhoff plate (HHJ elements).

is 3 [Cia88]. The proposed method is not as effective as a standard discretization of the biharmonic problem.

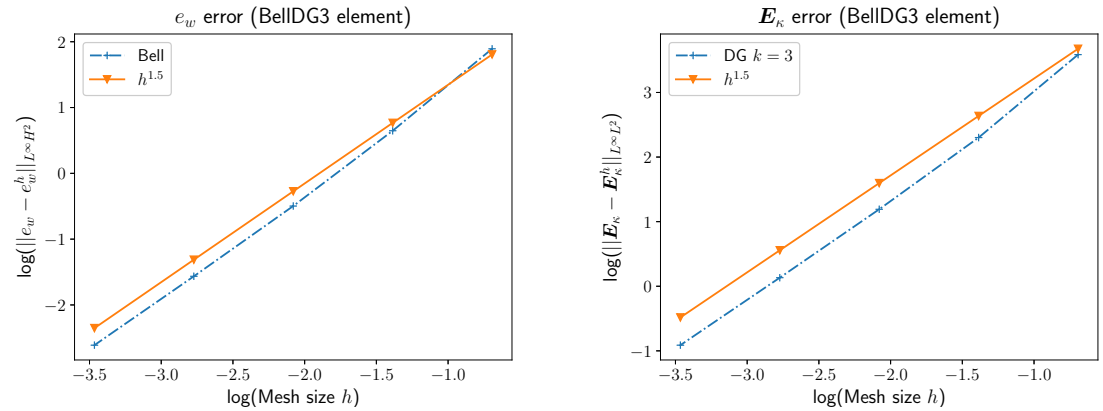

(a) $L^\infty_{\Delta t}(H^2(\Omega))$ error for e_w (b) $L^\infty_{\Delta t}(L^2(\Omega, \mathbb{S}))$ error for $\boldsymbol{E}_\kappa$

Figure 7.8: Error for the SSSS Kirchhoff plate (BellDG3 elements).

7.4.3.2 Mixed boundary conditions (CSFS)

We retrieve the manufactured solution for the static case from [RZ18]. Consider a square plate $\Omega = (-1, 1) \times (-1, 1)$ with simply supported top and bottom boundary, clamped left boundary and free right boundary. The stiffness tensor is the identity

$$\boldsymbol{\mathcal{D}}_b = \mathrm{Id}.$$

The density ρ and thickness b are the same as in 7.3. The static load is given by

$$f_s = 4\pi \sin(\pi x) \sin(\pi y).$$

The exact static solution is given by

$$w_s(x,y) = [(c_1 + c_2 x)\cosh(\pi x) + (c_3 + c_4 x)\sinh(\pi x) + \sin(\pi x)]\sin(\pi y).$$

The coefficients are then computed depending on the boundary conditions. For the considered case (CSFS) it is obtained

$$\begin{aligned}
c_1 &= -2\frac{\sinh(\pi) - 3\sinh(3\pi) + \pi[4\pi\sinh(\pi) + 7\cosh(\pi) - 3\cosh(3\pi)]}{5 + 8\pi^2 + 3\cosh(4\pi)},\\
c_2 &= -\frac{8\pi[2\pi\sinh(\pi) + \cosh(\pi)]}{5 + 8\pi^2 + 3\cosh(4\pi)},\\
c_3 &= \frac{10\cosh(\pi) + 6\cosh(\pi) + 16\pi[\sinh(\pi) + \pi\cosh(\pi)]}{5 + 8\pi^2 + 3\cosh(4\pi)},\\
c_4 &= \frac{2\pi(5\sinh(\pi) - 3\sinh(3\pi) + 4\pi\cosh(\pi))}{5 + 8\pi^2 + 3\cosh(4\pi)}
\end{aligned}$$

The dynamical solution is constructed as in §7.4.2, meaning that a the static solution is multiplied by a sinusoidal function in time

$$w_d(x,y) = w_s(x,y)\sin(t).$$

The dynamical force is then given by

$$f_d(x,y,t) = f_s(x,y)\sin(t) + \rho b \partial_{tt} w_d$$

For the port-Hamiltonian system the exact solution is thus given by

$$e_w^{\text{ex}} = w_s(x,y)\cos(t), \qquad \boldsymbol{E}_\kappa^{\text{ex}} = \boldsymbol{\mathcal{D}}_b \text{ Grad } \boldsymbol{\theta}_d. \tag{7.29}$$

The boundary conditions read

$$\begin{array}{rrrr}
C & S & F & S\\
e_w^{\text{ex}}|_{x=-1} = 0, & e_w^{\text{ex}}|_{y=-1} = 0, & \partial_x E_{\kappa,xx} + \partial_y E_{\kappa,xy}|_{x=1} = 0, & e_w^{\text{ex}}|_{y=1} = 0,\\
\partial_x e_w^{\text{ex}}|_{x=-1} = 0, & E_{\kappa,yy}^{\text{ex}}|_{y=-1} = 0, & E_{\kappa,xx}^{\text{ex}}|_{x=1} = 0. & E_{\kappa,yy}^{\text{ex}}|_{y=1} = 0.
\end{array} \tag{7.30}$$

Variables $(e_w^{\text{ex}}, \boldsymbol{E}_\kappa^{\text{ex}})$ under excitations f_d solve problem (6.77a).

Results for the HHJ elements (7.16) The results are reported in Fig. 7.9 and Tables B.20, B.21, B.22. Conjecture 6 is verified for all orders.

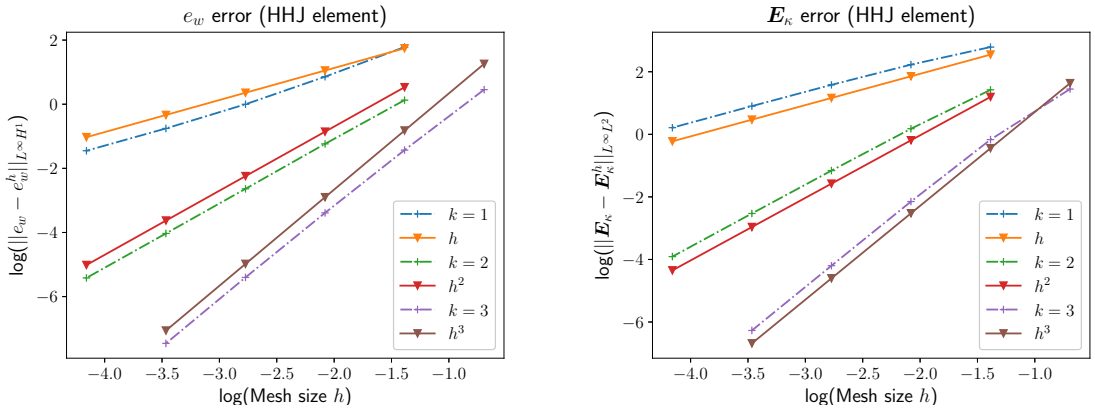

(a) $L^\infty_{\Delta t}(H^1(\Omega))$ error for e_w (b) $L^\infty_{\Delta t}(L^2(\Omega,\mathbb{S}))$ error for $\boldsymbol{E}_\kappa$

Figure 7.9: Error for the CSFS Kirchhoff plate (HHJ elements)

Results for the dual mixed formulation (BellDG3 elements) The results are reported in Fig. 7.10 and Tab. B.23. The error is computed in the $L^\infty(H^2(\Omega))$ norm for e_w and in the $L^\infty(L^2(\Omega,\mathbb{S}))$ norm for $\boldsymbol{E}_\kappa$. The convergence rate stays around 1.50 (as for the SSSS test).

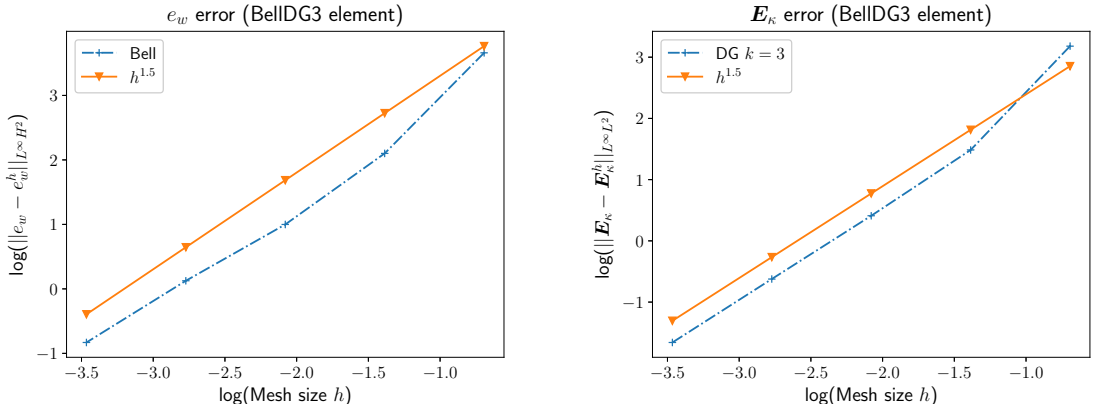

(a) $L^\infty_{\Delta t}(H^2(\Omega))$ error for e_w (b) $L^\infty_{\Delta t}(L^2(\Omega,\mathbb{S}))$ error for $\boldsymbol{E}_\kappa$

Figure 7.10: Error for the CSFS Kirchhoff plate (BellDG3 elements).

7.5 Conclusion

In this chapter, the link between mixed finite element method and pH flexible structures has been studied. It was shown that existing and non-standard elements can be used to achieve a structure-preserving discretization of the models under consideration. Apart for the dual discretization of the Kirchhoff plate, error estimates conjectures have been formulated. The numerical examples seem to confirm such conjectures. However a rigorous error analysis,

apart from the wave equation [HMS20] under uniform boundary condition, is still to be done.

Since the pH framework provides a powerful description of boundary control systems, it is important that numerical methods be capable of handling generic boundary conditions. Concerning this problem, the mixed discretization of Kirchhoff plate poses additional difficulties [BR90]. A promising methodology is detailed in [RZ18], but the dynamical case has not been considered yet.

Chapter 8

Numerical applications

> The most obvious characteristic of science is its application: the fact that, as a consequence of science, one has a power to do things. And the effect this power has had need hardly be mentioned. The whole industrial revolution would almost have been impossible without the development of science.
>
> *Richard Feynman*
> *The Meaning of It All: Thoughts of a Citizen-Scientist*

Contents

The proposed finite element discretization can be employed for different numerical applications. The chapter is organized as follows:

- a boundary stabilization problem for the Kirchhoff plate and for the irrotational shallow water equations is presented in §8.1;
- Sec. 8.2 presents a comparison between the Lagrange multiplier 6.2.1 and the virtual domain decomposition method 6.2.2 for the enforcement of mixed boundary conditions;
- a thermoelastic problem, for which an analytic solution is available, is illustrated in §8.3.

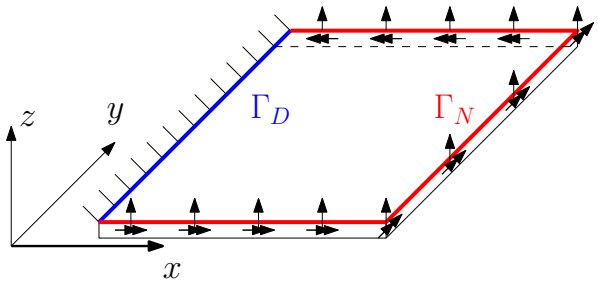

Figure 8.1: Cantilever plate subjected to a control forces on the lateral sides.

8.1 Boundary stabilization

In this section, we consider the boundary stabilization of a cantilever Kirchhoff plate and of the irrotational shallow water equations. For pHs a simple proportional gain assures asymptotic system of the system thanks to the LaSalle' invariance principle [DMSB09, Proposition 6.2]. This can be used to achieve stabilization of the undeformed configuration of the Kirchhoff plate. For the shallow water equations a reference is also added to stabilize the system around a desired fluid height.

8.1.1 Cantilever Kirchhoff plate

Consider the problem (illustrated in Fig. 8.1)

$$\begin{bmatrix} \rho h & 0 \\ \mathbf{0} & \boldsymbol{\mathcal{C}_b} \end{bmatrix} \frac{\partial}{\partial t} \begin{pmatrix} e_w \\ \boldsymbol{E}_\kappa \end{pmatrix} = \begin{bmatrix} 0 & -\operatorname{div}\operatorname{Div} \\ \operatorname{Hess} & \mathbf{0} \end{bmatrix} \begin{pmatrix} e_w \\ \boldsymbol{E}_\kappa \end{pmatrix} \qquad (x,y) \in \Omega = [0,1] \times [0,1]$$

subject to the following Dirichlet homogeneous conditions

$$\begin{aligned} \partial_t e_w|_{\Gamma_D} &= 0, \\ \partial_x e_w|_{\Gamma_D} &= 0, \end{aligned} \qquad \Gamma_D = \{x = 0\},$$

and Neumann boundary control

$$\begin{aligned} u_{\partial,q} &= \widetilde{q}_n|_{\Gamma_N} = -\boldsymbol{n} \cdot \operatorname{Div} \boldsymbol{E}_\kappa - \partial_{\boldsymbol{s}}(\boldsymbol{E}_\kappa : (\boldsymbol{n} \otimes \boldsymbol{s}))|_{\Gamma_N}, \\ u_{\partial,m} &= M_{nn}|_{\Gamma_N} = \boldsymbol{E}_\kappa : (\boldsymbol{n} \otimes \boldsymbol{n})|_{\Gamma_N}, \end{aligned} \qquad \Gamma_N = \{y = 0 \cup x = 1 \cup y = 1\}.$$

The corresponding boundary outputs read

$$\begin{aligned} y_{\partial,q} &= e_w|_{\Gamma_N}, \\ y_{\partial,m} &= \partial_{\boldsymbol{n}} e_w|_{\Gamma_N}. \end{aligned}$$

The initial conditions (compatible with the constraints) are given by

$$e_w(x,y,0) = x^2 y(y-1), \qquad \boldsymbol{E}_\kappa(x,y,0) = 0.$$

The following control law asymptotically stabilizes the system (cf. [Lag89])

$$\begin{aligned} u_{\partial,q} &= -k_q e_w|_{\Gamma_N} = -k_q y_{\partial,q}, & k_q > 0, \\ u_{\partial,m} &= -k_m \partial_{\boldsymbol{n}} e_w|_{\Gamma_N} = -k_m y_{\partial,m}, & k_m > 0. \end{aligned} \tag{8.1}$$

The discretization is performed as in (6.82). Variables e_w and $\boldsymbol{E}_\kappa$ are discretized using the Argyris element and Discontinuous Galerkin elements of order 3. A structured mesh with 6 elements per side is used. The Dirichlet conditions are imposed weakly using Lagrange multipliers (cf. (6.112) and Remark 21), that are discretized using Lagrange polynomials of order 2. The resulting system reads

$$\begin{aligned} &\begin{bmatrix} \mathbf{M}_{\rho h} & \mathbf{0} & \mathbf{0} \\ \mathbf{0} & \mathbf{M}_{\mathcal{C}_b} & \mathbf{0} \\ \mathbf{0} & \mathbf{0} & \mathbf{0} \end{bmatrix} \begin{pmatrix} \dot{\mathbf{e}}_w \\ \dot{\mathbf{e}}_\kappa \\ \dot{\boldsymbol{\lambda}}_{\Gamma_D} \end{pmatrix} = \begin{bmatrix} \mathbf{0} & -\mathbf{D}_{\text{Hess}}^\top & \mathbf{B}_{\Gamma_D} \\ \mathbf{D}_{\text{Hess}} & \mathbf{0} & \mathbf{0} \\ -\mathbf{B}_{\Gamma_D}^\top & \mathbf{0} & \mathbf{0} \end{bmatrix} \begin{pmatrix} \mathbf{e}_w \\ \mathbf{e}_\kappa \\ \boldsymbol{\lambda}_{\Gamma_D} \end{pmatrix} + \begin{bmatrix} \mathbf{B}_{w,\Gamma_N} & \mathbf{B}_{\partial_{\boldsymbol{n}} w,\Gamma_N} \\ \mathbf{0} & \mathbf{0} \\ \mathbf{0} & \mathbf{0} \end{bmatrix} \begin{bmatrix} \mathbf{u}_{\partial,q} \\ \mathbf{u}_{\partial,m} \end{bmatrix}, \\ &\begin{bmatrix} \mathbf{M}_{\Gamma_N} & \mathbf{0} \\ \mathbf{0} & \mathbf{M}_{\Gamma_N} \end{bmatrix} \begin{pmatrix} \mathbf{y}_{\partial,q} \\ \mathbf{y}_{\partial,m} \end{pmatrix} = \begin{bmatrix} \mathbf{B}_{w,\Gamma_N}^\top & \mathbf{0} & \mathbf{0} \\ \mathbf{B}_{\partial_{\boldsymbol{n}} w,\Gamma_N}^\top & \mathbf{0} & \mathbf{0} \end{bmatrix} \begin{pmatrix} \mathbf{e}_w \\ \mathbf{e}_\kappa \\ \boldsymbol{\lambda}_{\Gamma_D} \end{pmatrix}, \end{aligned} \tag{8.2}$$

where $\mathbf{B}_{\Gamma_D} = [\mathbf{B}_{w,\Gamma_D} \quad \mathbf{B}_{\partial_n w,\Gamma_D}]$. The discretization of the control law (8.1) provides

$$\begin{aligned} \mathbf{u}_{\partial,q} &= -k_q \mathbf{y}_{\partial,q} = -k_q \mathbf{M}_{\Gamma_N}^{-1} \mathbf{B}_{w,\Gamma_N}^\top \mathbf{e}_w, \\ \mathbf{u}_{\partial,m} &= -k_m \mathbf{y}_{\partial,m} = -k_m \mathbf{M}_{\Gamma_N}^{-1} \mathbf{B}_{\partial_{\boldsymbol{n}} w,\Gamma_N}^\top \mathbf{e}_w. \end{aligned} \tag{8.3}$$

System (8.2) now reads

$$\begin{bmatrix} \mathbf{M}_{\rho h} & \mathbf{0} & \mathbf{0} \\ \mathbf{0} & \mathbf{M}_{\mathcal{C}_b} & \mathbf{0} \\ \mathbf{0} & \mathbf{0} & \mathbf{0} \end{bmatrix} \begin{pmatrix} \dot{\mathbf{e}}_w \\ \dot{\mathbf{e}}_\kappa \\ \dot{\boldsymbol{\lambda}}_{\Gamma_D} \end{pmatrix} = \begin{bmatrix} -\mathbf{R}_w & -\mathbf{D}_{\text{Hess}}^\top & \mathbf{B}_{\Gamma_D} \\ \mathbf{D}_{\text{Hess}} & \mathbf{0} & \mathbf{0} \\ -\mathbf{B}_{\Gamma_D}^\top & \mathbf{0} & \mathbf{0} \end{bmatrix} \begin{pmatrix} \mathbf{e}_w \\ \mathbf{e}_\kappa \\ \boldsymbol{\lambda}_{\Gamma_D} \end{pmatrix}. \tag{8.4}$$

The matrix

$$\mathbf{R}_w = k_q \mathbf{B}_{w,\Gamma_N} \mathbf{M}_{\Gamma_N}^{-1} \mathbf{B}_{w,\Gamma_N}^\top + k_m \mathbf{B}_{\partial_{\boldsymbol{n}} w,\Gamma_N} \mathbf{M}_{\Gamma_N}^{-1} \mathbf{B}_{\partial_{\boldsymbol{n}} w,\Gamma_N}^\top \succ 0$$

is positive definitive because of the collocated input-output feature of pH systems. The energy decreases as [BMXZ18, Theorem 13]

$$\dot{H}_d = -\mathbf{e}_w^\top \, \mathbf{R}_w \, \mathbf{e}_w \leq 0.$$

Therefore, the Hamiltonian energy is a Lyapunov function and the asymptotic stability of configuration $\mathbf{e}_w = \mathbf{0}$, $\mathbf{e}_\kappa = \mathbf{0}$ is deduced using LaSalle' invariance principle.

The parameters for the numerical simulation are given in Table 8.1. The controller gains

Plate Parameters	
E	70 [GPa]
ρ	2700 [kg $\cdot$ m^3]
ν	0.35
h/L	0.05
$L_x = L_y$	1 [m]

Simulation Settings	
Integrator	Störmer-Verlet
Δt	1 [μs]
N° FE	6
FE spaces	Argyris $\times$ DG$_3$ $\times$ CG$_2$
t_{end}	5 [s]

Table 8.1: Settings and parameters for the boundary control of the Kirchhoff plate.

are set to

$$k_q = 10, \qquad k_m = 10. \tag{8.5}$$

The system is simulated using a Störmer-Verlet time integrator [HLW03] using a time step $\Delta t = 10^{-6}$ [s] for a total simulation time of $t_{\text{end}} = 5$ [s]. The Lagrange multiplier is eliminated using a projection method [BH15]. The control law is activated after 1 second. The discrete Hamiltonian goes almost to zero in 4 seconds (Fig. 8.2). Snapshots of the vertical velocity are reported in Fig. 8.3.

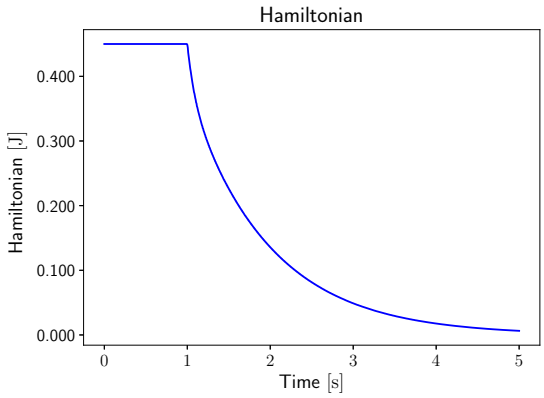

Figure 8.2: Hamiltonian trend for the cantilever Kirchhoff plate.

8.1.2 Irrotational shallow water equations

In this section we consider the boundary stabilization of a circular water tank via proportional feedback. We recall the system of equations (2.37)

$$\begin{aligned} \frac{\partial}{\partial t}\begin{pmatrix}\alpha_h \\ \boldsymbol{\alpha}_v\end{pmatrix} &= \begin{bmatrix} 0 & -\operatorname{div} \\ -\operatorname{grad} & \mathbf{0}\end{bmatrix}\begin{pmatrix} e_h \\ \boldsymbol{e}_v\end{pmatrix}, \qquad (x,y) \in \Omega = \{x^2 + y^2 \leq R\}, \\ \begin{pmatrix} e_h \\ \boldsymbol{e}_v\end{pmatrix} &= \begin{pmatrix}\delta_{\alpha_h} H \\ \delta_{\boldsymbol{\alpha}_v} H\end{pmatrix} = \begin{pmatrix}\delta_{\alpha_h} H \\ \delta_{\boldsymbol{\alpha}_v} H\end{pmatrix}, \end{aligned} \tag{8.6}$$

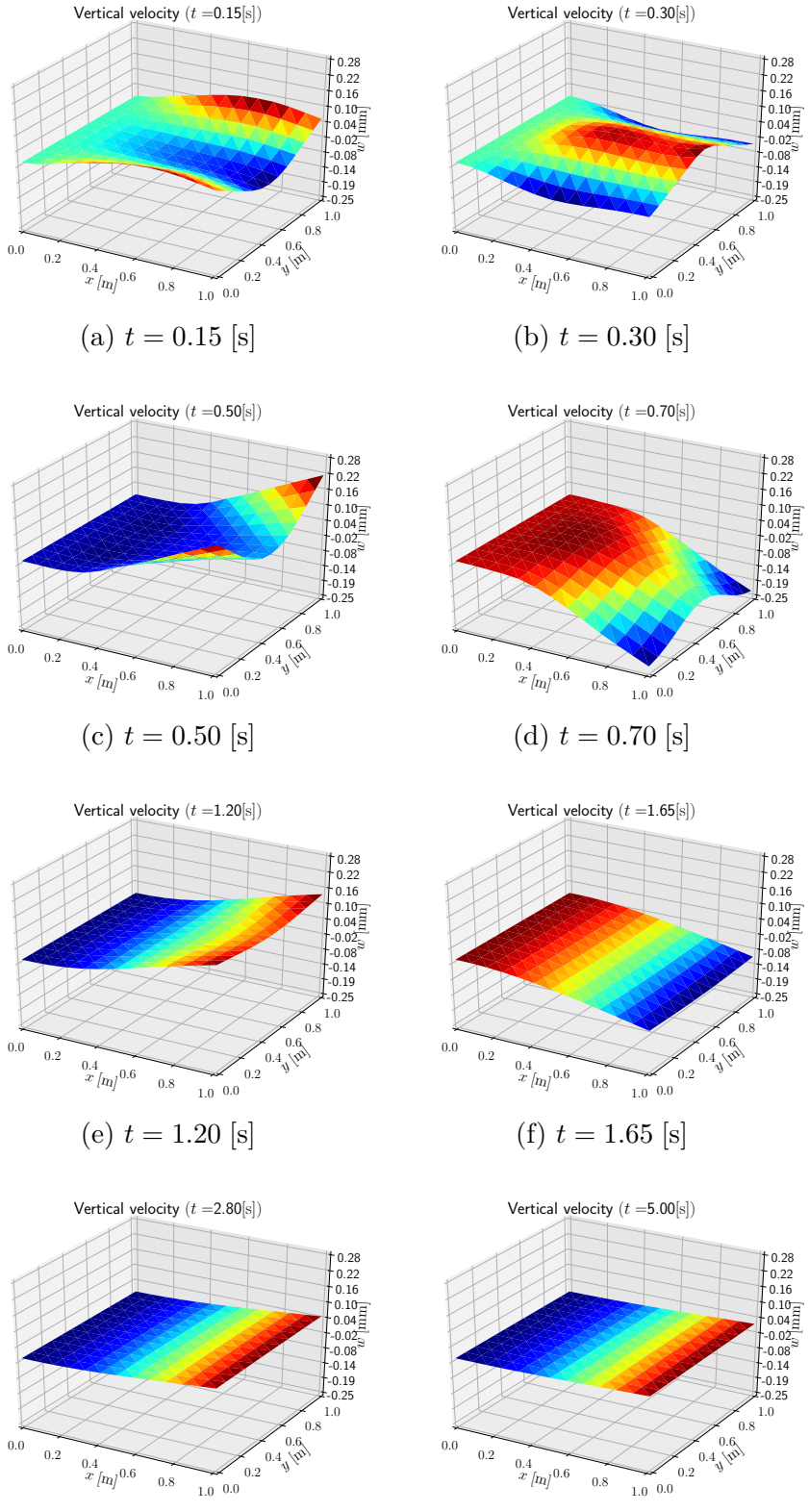

(a) $t = 0.15$ [s] (b) $t = 0.30$ [s]

(c) $t = 0.50$ [s] (d) $t = 0.70$ [s]

(e) $t = 1.20$ [s] (f) $t = 1.65$ [s]

(g) $t = 2.80$ [s] (h) $t = 5$ [s]

Figure 8.3: Snapshots at different times of the simulation of the boundary controlled cantilever Kirchhoff plate.

with

$$H(\alpha_h, \boldsymbol{\alpha}_v) = \frac{1}{2}\int_\Omega \left\{ \frac{1}{\rho}\alpha_h \left\|\boldsymbol{\alpha}_v\right\|^2 + \rho g \alpha_h^2 \right\} \, \mathrm{d}\Omega, \tag{8.7}$$

under Neumann boundary control

$$u_\partial = -\boldsymbol{e}_v \cdot \boldsymbol{n}|_{\partial\Omega} = -\frac{1}{\rho}\alpha_h \boldsymbol{\alpha}_v \cdot \boldsymbol{n}|_{\partial\Omega}. \tag{8.8}$$

The corresponding output reads

$$y_\partial = e_h|_{\partial\Omega} = (\rho g \alpha_h + \frac{1}{2\rho}\left\|\boldsymbol{\alpha}_v\right\|^2)|_{\partial\Omega}. \tag{8.9}$$

The initial conditions are

$$\begin{aligned} &\alpha_h(x,y,0) = h^{\mathrm{des}} + 10^{-1}\sin(\pi r/R)\cos(2\theta), \qquad r = \sqrt{x^2+y^2}, \qquad \theta = \arctan(y/r), \\ &\boldsymbol{\alpha}_v(x,y,0) = \mathbf{0}, \end{aligned} \tag{8.10}$$

where h^{des} is the desired fluid height. It is known that a proportional controller exponentially stabilizes the system [DSP08]. Here, we use a simple control for stabilizing the system around the desired point h^{des}

$$u_\partial = -k(y_\partial - y_\partial^{\mathrm{des}}), \qquad y_\partial^{\mathrm{des}} = \rho g h^{\mathrm{des}}, \quad k > 0. \tag{8.11}$$

This control law ensures that the Lyapunov functional

$$V = \frac{1}{2}\int_\Omega \left\{ \frac{1}{2}\rho g(\alpha_h - \alpha_h^{\mathrm{des}})^2 + \frac{1}{2\rho}\alpha_h \left\|\boldsymbol{\alpha}_v\right\|^2 \right\} d\Omega \geq 0, \tag{8.12}$$

where $\alpha_h^{\mathrm{des}} = h^{\mathrm{des}}$, has negative semi definite time derivative

$$\dot{V} = -k\int_{\partial\Omega} \left(y_\partial - y_\partial^{\mathrm{des}}\right)^2 \, \mathrm{d}\Gamma \leq 0. \tag{8.13}$$

The precompactness of the trajectories in the energy space is guaranteed since a bounded domain is considered (Rellich theorem). By the LaSalle' principle for infinite dimensional system [Hen06], the point

$$\alpha_h = h^{\mathrm{des}}, \qquad \boldsymbol{\alpha}_v = \mathbf{0}, \tag{8.14}$$

is asymptotically stable.

The discretization is performed as in (6.40). Variable α_h is discretized using Lagrange polynomials of order 1. Discontinuous Galerkin elements of order 0 defined on the domain

and on the boundary are used for $\boldsymbol{\alpha}_v, \boldsymbol{u}_\partial$.

$$\begin{aligned}\begin{pmatrix}\dot{\boldsymbol{\alpha}}_{d,h}\\ \dot{\boldsymbol{\alpha}}_{d,v}\end{pmatrix} &= \begin{bmatrix}\mathbf{0} & \mathbf{M}_h^{-1}\mathbf{D}_{\text{grad}}^\top\mathbf{M}_v^{-1}\\ -\mathbf{M}_v^{-1}\mathbf{D}_{\text{grad}}\mathbf{M}_h^{-1} & \mathbf{0}\end{bmatrix}\begin{pmatrix}\partial_{\boldsymbol{\alpha}_{d,h}}H_d(\boldsymbol{\alpha}_{d,h},\ \boldsymbol{\alpha}_{d,v})\\ \partial_{\boldsymbol{\alpha}_{d,v}}H_d(\boldsymbol{\alpha}_{d,h},\ \boldsymbol{\alpha}_{d,v})\end{pmatrix} + \begin{bmatrix}\mathbf{B}_h\\ \mathbf{0}\end{bmatrix}\mathbf{u}_\partial,\\ \mathbf{M}_\partial\mathbf{y}_\partial &= \begin{bmatrix}\mathbf{B}_h^\top & \mathbf{0}\end{bmatrix}\begin{pmatrix}\partial_{\boldsymbol{\alpha}_{d,h}}H_d(\boldsymbol{\alpha}_{d,h},\ \boldsymbol{\alpha}_{d,v})\\ \partial_{\boldsymbol{\alpha}_{d,v}}H_d(\boldsymbol{\alpha}_{d,h},\ \boldsymbol{\alpha}_{d,v})\end{pmatrix}.\end{aligned} \tag{8.15}$$

The control law (8.11), once discretized, is expressed as

$$\mathbf{u}_\partial = -k(\mathbf{y}_\partial - \mathbf{y}_\partial^{\text{des}}), \tag{8.16}$$

where $\mathbf{y}_\partial^{\text{des}} = \mathbf{M}_\partial^{-1}\int_{\partial\Omega}\rho g h^{\text{des}}\phi_\partial(s)\,\mathrm{d}\Gamma$. The closed-loop system is then

$$\begin{pmatrix}\dot{\boldsymbol{\alpha}}_{d,h}\\ \dot{\boldsymbol{\alpha}}_{d,v}\end{pmatrix} = \begin{bmatrix}-\mathbf{R}_h & \mathbf{M}_h^{-1}\mathbf{D}_{\text{grad}}^\top\mathbf{M}_v^{-1}\\ -\mathbf{M}_v^{-1}\mathbf{D}_{\text{grad}}\mathbf{M}_h^{-1} & \mathbf{0}\end{bmatrix}\begin{bmatrix}\partial_{\boldsymbol{\alpha}_{d,h}}H_d(\boldsymbol{\alpha}_{d,h},\ \boldsymbol{\alpha}_{d,v})\\ \partial_{\boldsymbol{\alpha}_{d,v}}H_d(\boldsymbol{\alpha}_{d,h},\ \boldsymbol{\alpha}_{d,v})\end{bmatrix} + \begin{bmatrix}\mathbf{B}_h\\ \mathbf{0}\end{bmatrix}k\mathbf{y}_\partial^{\text{des}}, \tag{8.17}$$

Again the matrix

$$\mathbf{R}_h = k\mathbf{B}_h\mathbf{M}_\partial^{-1}\mathbf{B}_h^\top \succ 0$$

is positive definite and the discretized Lyapunov function rate reads

$$\dot{V}_d = -\partial_{\boldsymbol{\alpha}_{d,h}}H_d(\boldsymbol{\alpha}_{d,h},\ \boldsymbol{\alpha}_{d,v})^\top\mathbf{R}_h\partial_{\boldsymbol{\alpha}_{d,h}}H_d(\boldsymbol{\alpha}_{d,h},\ \boldsymbol{\alpha}_{d,v}) \le 0.$$

Parameters	
ρ	1000 [kg · m^3]
g	10 [m/s^2]
R	1 [m]
h^{des}	1 [m]

Simulation Settings	
Integrator	Runge-Kutta 45
N° FE along R	20
FE spaces	$\text{CG}_1 \times \text{DG}_0 \times \text{DG}_0$
t_{end}	3 [s]

Table 8.2: Settings and parameters for the irrotational shallow water equations.

The parameters for the simulation are reported in Table. (8.2). The controller gain is set to $k = 10^{-3}$. The control law is activated after 0.5 seconds. The system is simulated using a Runge-Kutta method. Snapshots are collected in Fig. 8.5. The discretized Hamiltonian and Lyapunov functional trends (Fig. 8.4) clearly show that, while the Lyapunov function monotonically decreases, the Hamiltonian oscillates around the desired equilibrium.

8.2 Mixed boundary conditions enforcement

In this section the Lagrange multiplier method §6.2.1 and the virtual domain decomposition method §6.2.2 are compared for two problems:

1. a reference tracking problem for the Euler-Bernoulli beam;
2. a vibroacoustic application.

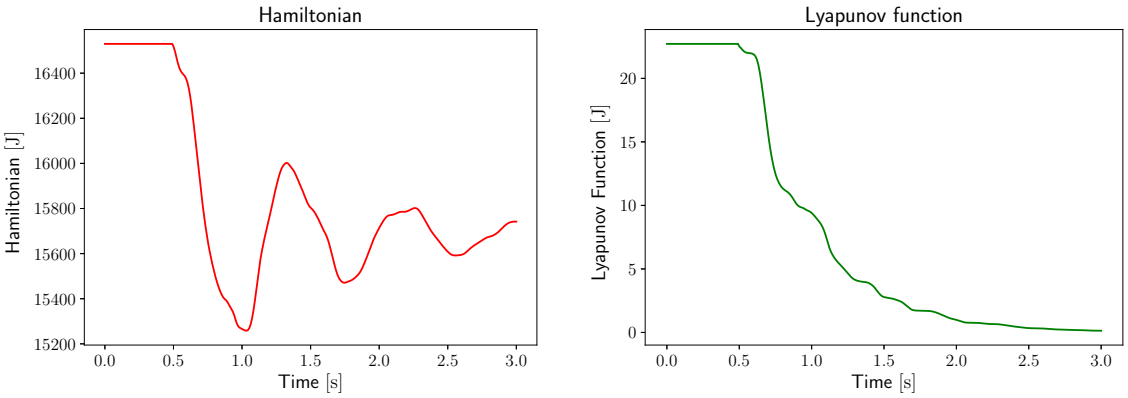

(a) Total energy (Hamiltonian) (b) Lyapunov function

Figure 8.4: Total energy and Lyapunov function for the shallow water equations.

8.2.1 Motion planning of a thin beam

Consider the motion planning problem for the Euler-Bernoulli beam [KS08, Chapter 12]

$$\partial_{tt} w + \partial_{xxxx} w = 0, \qquad x \in \Omega = \{0, 1\} \tag{8.18}$$

$$\partial_{xx} w(0,t) = 0, \qquad \partial_{xxx} w(0,t) = 0, \tag{8.19}$$

$$w^r(0,t) = \sin(\omega t), \qquad \partial_x w^r(0,t) = 0. \tag{8.20}$$

Equation (8.18) represents the Euler-Bernoulli beam (2.24) with unitary coefficients. Conditions (8.19) represent homogeneous free boundary conditions at the left side. The objective is to find controls $u_1 = w^r(1,t)$, $u_2 = \partial_x w^r(1,t)$ to match the reference outputs $y_1^r = w^r(0,t)$, $y_2^r = \partial_x w^r(0,t)$. The reference solution for this problem can be found by postulating the existence of a function of the form

$$w^r(x,t) = \sum_{k=0}^{\infty} a_k(t) \frac{x^k}{k!}.$$

Given the reference output $w^r(1,t) = \sin(\omega t)$, the reference solution assumes the form (cf. [KS08, Chapter 12] for details)

$$w^r(x,t) = \sum_{k=0}^{\infty} \omega^{2k} \frac{x^{4k}}{(4k)!} \sin(\omega t) = \frac{1}{2}[\cosh(\sqrt{\omega}x) + \cos(\sqrt{\omega}x)] \sin(\omega t). \tag{8.21}$$

The inputs that ensure the tracking of the outputs can be computed

$$\begin{aligned} w^r(1,t) &= \frac{1}{2}[\cosh(\sqrt{\omega}) + \cos(\sqrt{\omega})] \sin(\omega t), \\ \partial_x w^r(1,t) &= \frac{1}{2}[\sinh(\sqrt{\omega}) - \sin(\sqrt{\omega})] \sin(\omega t). \end{aligned} \tag{8.22}$$

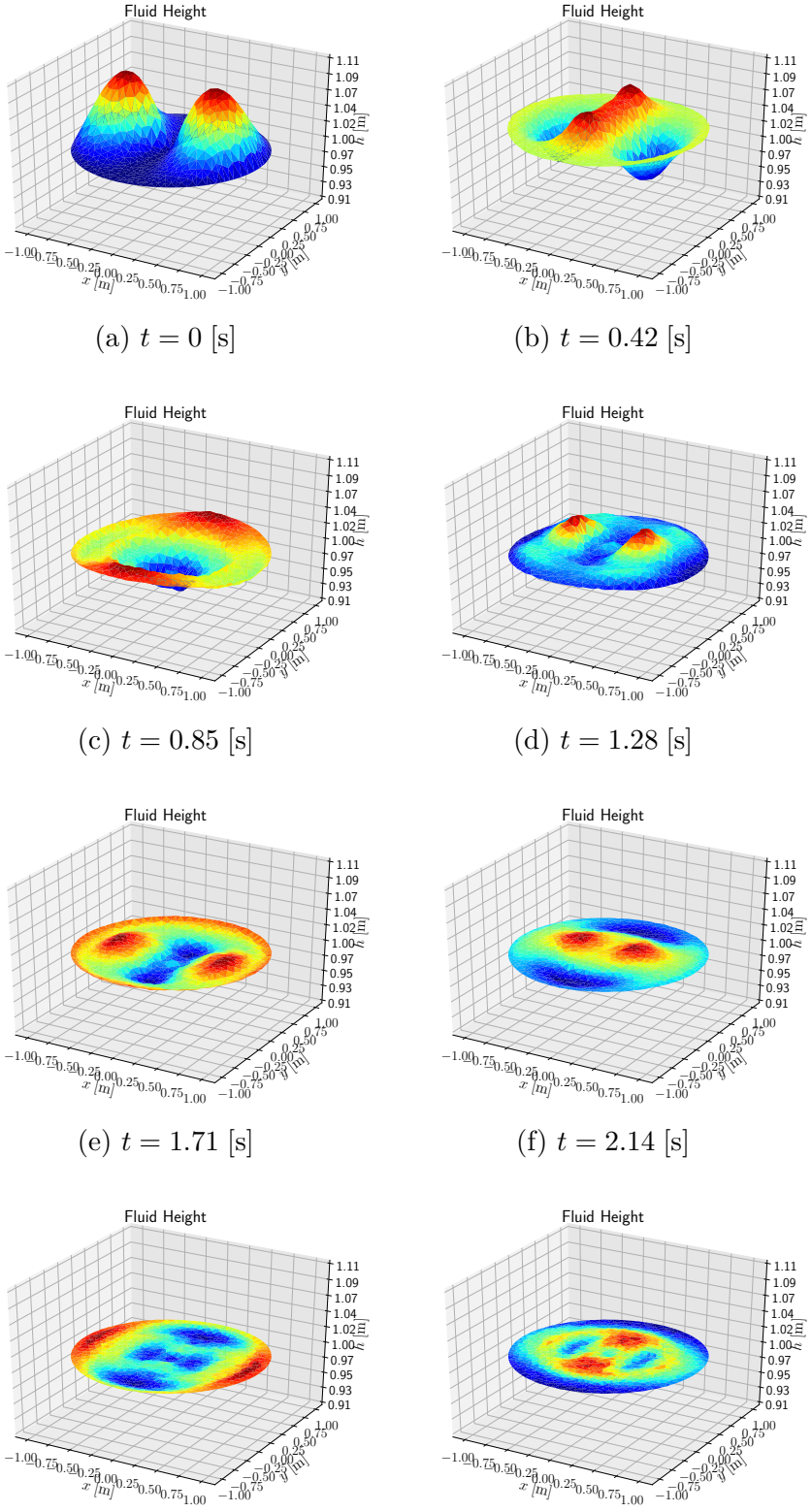

(a) $t = 0$ [s] (b) $t = 0.42$ [s]

(c) $t = 0.85$ [s] (d) $t = 1.28$ [s]

(e) $t = 1.71$ [s] (f) $t = 2.14$ [s]

(g) $t = 2.57$ [s] (h) $t = 3$ [s]

Figure 8.5: Snapshots at different times of the simulation for the boundary controlled irrotational shallow water equations.

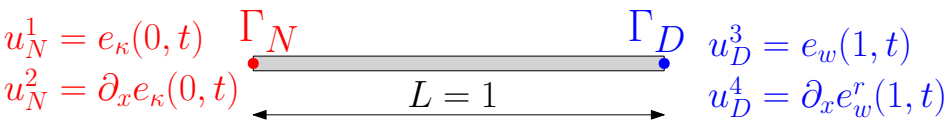

Figure 8.6: Boundary conditions for the motion planning problem.

This problem can be equivalently recast as a boundary-control pH system with mixed boundary conditions (see Fig. 8.6)

$$\frac{\partial}{\partial t}\begin{pmatrix} e_w \\ e_\kappa \end{pmatrix} = \begin{bmatrix} 0 & -\partial_{xx} \\ \partial_{xx} & 0 \end{bmatrix}\begin{pmatrix} e_w \\ e_\kappa \end{pmatrix} \tag{8.23a}$$

$$\begin{pmatrix} u_N^1 \\ u_N^2 \\ u_D^1 \\ u_D^2 \end{pmatrix} = \begin{pmatrix} e_\kappa(0,t) \\ -\partial_x e_\kappa(0,t) \\ e_w(1,t) \\ \partial_x e_w(1,t) \end{pmatrix} = \begin{pmatrix} 0 \\ 0 \\ \frac{1}{2}[\cosh(\sqrt{\omega}) + \cos(\omega)]\omega\cos(\omega t) \\ \frac{1}{2}[\sinh(\sqrt{\omega}) - \sin(\omega)]\omega\cos(\omega t) \end{pmatrix}, \tag{8.23b}$$

$$\begin{pmatrix} y_N^1 \\ y_N^2 \\ y_D^1 \\ y_D^2 \end{pmatrix} = \begin{pmatrix} -\partial_x e_w(0,t) \\ e_w(0,t) \\ \partial_x e_\kappa(1,t) \\ e_\kappa(1,t) \end{pmatrix}. \tag{8.23c}$$

The inputs assures that the outputs $y_N^1 = -\partial_x e_w(0,t)$, $y_N^2 = e_w(0,t)$ verify the desired trajectories

$$y_N^1 = -\partial_t \partial_x w^r(0,t) = 0, \qquad y_N^2 = \partial_t w^r(0,t) = \omega\cos(\omega t).$$

Next we concisely report the discretization strategy for the imposition of mixed boundary conditions.

Lagrange multipliers If Lagrange multipliers are used for the Neumann boundary condition, the following weak form is obtained

$$\begin{aligned} \langle v_w,\, \partial_t e_w\rangle_\Omega &= \langle v_w,\, -\partial_{xx} e_\kappa\rangle_\Omega\,, \\ \langle v_\kappa,\, \partial_t e_\kappa\rangle_\Omega &= \langle \partial_{xx} v_\kappa,\, e_w\rangle_\Omega + \left\langle \begin{pmatrix} \partial_{\boldsymbol{n}} v_\kappa \\ v_\kappa \end{pmatrix}, \begin{pmatrix} \lambda_N^1 \\ \lambda_N^2 \end{pmatrix} \right\rangle_{\Gamma_N} + \left\langle \begin{pmatrix} \partial_{\boldsymbol{n}} v_\kappa \\ v_\kappa \end{pmatrix}, \begin{pmatrix} u_D^1 \\ u_D^2 \end{pmatrix} \right\rangle_{\Gamma_D}. \end{aligned} \tag{8.24}$$

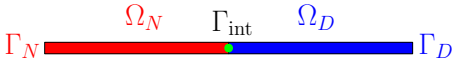

Figure 8.7: Virtual decomposition of the Euler Bernoulli beam.

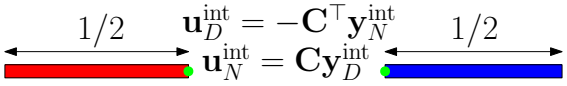

Figure 8.8: Interconnection for the Euler-Bernoulli beam.

Using a Galerkin method the following system is computed.

$$\begin{bmatrix} \mathbf{M}_w & \mathbf{0} & \mathbf{0} \\ \mathbf{0} & \mathbf{M}_\kappa & \mathbf{0} \\ \mathbf{0} & \mathbf{0} & \mathbf{0} \end{bmatrix} \begin{pmatrix} \dot{\mathbf{e}}_w \\ \dot{\mathbf{e}}_\kappa \\ \dot{\boldsymbol{\lambda}}_N \end{pmatrix} = \begin{bmatrix} \mathbf{0} & \mathbf{D}_{-\partial_{xx}}^\top & \mathbf{0} \\ -\mathbf{D}_{-\partial_{xx}} & \mathbf{0} & \mathbf{B}_{\kappa,\Gamma_N} \\ \mathbf{0} & -\mathbf{B}_{\kappa,\Gamma_N}^\top & \mathbf{0} \end{bmatrix} \begin{pmatrix} \mathbf{e}_w \\ \mathbf{e}_\kappa \\ \boldsymbol{\lambda}_N \end{pmatrix} + \begin{bmatrix} \mathbf{0} \\ \mathbf{B}_{\kappa,\Gamma_D} \\ \mathbf{0} \end{bmatrix} \mathbf{u}_D,$$
$$\mathbf{y}_D = \begin{bmatrix} \mathbf{0} & \mathbf{B}_{\kappa,\Gamma_D}^\top & \mathbf{0} \end{bmatrix} \begin{pmatrix} \mathbf{e}_p \\ \mathbf{e}_v \\ \boldsymbol{\lambda}_N \end{pmatrix}. \tag{8.25}$$

The DG1Her element (7.5) is employed for the discretization.

Virtual domain decomposition For the decomposition, the beam is split into halves (see Fig. 8.7). Applying the PFEM methodology as in 6.2.2, two finite-dimensional systems are obtained. For Ω_N the system is analogous to (6.135), while for Ω_D to (6.134).

Subdomain Ω_N

$$\begin{bmatrix} \mathbf{M}_w^{\Omega_N} & \mathbf{0} \\ \mathbf{0} & \mathbf{M}_\kappa^{\Omega_N} \end{bmatrix} \begin{pmatrix} \dot{\mathbf{e}}_{w,\Omega_N} \\ \dot{\mathbf{e}}_{\kappa,\Omega_N} \end{pmatrix} = \begin{bmatrix} \mathbf{0} & -\mathbf{D}_{\partial_{xx}}^{\Omega_N \top} \\ \mathbf{D}_{\partial_{xx}}^{\Omega_N} & \mathbf{0} \end{bmatrix} \begin{pmatrix} \mathbf{e}_{w,\Omega_N} \\ \mathbf{e}_{\kappa,\Omega_N} \end{pmatrix} + \begin{bmatrix} \mathbf{B}_{w,\Gamma_{\text{int}}}^{\Omega_N} \\ \mathbf{0} \end{bmatrix} \mathbf{u}_N^{\text{int}},$$
$$\mathbf{y}_N^{\text{int}} = \begin{bmatrix} \mathbf{B}_{w,\Gamma_{\text{int}}}^{\Omega_N \top} & \mathbf{0} \end{bmatrix} \begin{pmatrix} \mathbf{e}_{w,\Omega_N} \\ \mathbf{e}_{\kappa,\Omega_N} \end{pmatrix}. \tag{8.26}$$

Subdomain Ω_D

$$\begin{bmatrix} \mathbf{M}_w^{\Omega_D} & \mathbf{0} \\ \mathbf{0} & \mathbf{M}_\kappa^{\Omega_D} \end{bmatrix} \begin{pmatrix} \dot{\mathbf{e}}_{w,\Omega_D} \\ \dot{\mathbf{e}}_{\kappa,\Omega_D} \end{pmatrix} = \begin{bmatrix} \mathbf{0} & \mathbf{D}_{-\partial_{xx}}^{\Omega_D} \\ -\mathbf{D}_{-\partial_{xx}}^{\Omega_D \top} & \mathbf{0} \end{bmatrix} \begin{pmatrix} \mathbf{e}_{w,\Omega_D} \\ \mathbf{e}_{\kappa,\Omega_D} \end{pmatrix} + \begin{bmatrix} \mathbf{0} & \mathbf{0} \\ \mathbf{B}_{\kappa,\Gamma_D}^{\Omega_D} & \mathbf{B}_{\kappa,\Gamma_{\text{int}}}^{\Omega_D} \end{bmatrix} \begin{pmatrix} \mathbf{u}_D \\ \mathbf{u}_D^{\text{int}} \end{pmatrix},$$
$$\begin{pmatrix} \mathbf{y}_D \\ \mathbf{y}_D^{\text{int}} \end{pmatrix} = \begin{bmatrix} \mathbf{0} & \mathbf{B}_{\kappa,\Gamma_D}^{\Omega_D \top} \\ \mathbf{0} & \mathbf{B}_{\kappa,\Gamma_{\text{int}}}^{\Omega_D \top} \end{bmatrix} \begin{pmatrix} \mathbf{e}_{w,\Omega_D} \\ \mathbf{e}_{\kappa,\Omega_D} \end{pmatrix}. \tag{8.27}$$

In order to get a system with mixed causality, systems (8.26) and (8.27) have to be interconnected using a classical gyrator interconnection. Since the velocities and rotations have to be continuous at the interface and the action-reaction principle holds for the stresses,

the appropriate interconnection reads (cf. Fig. 8.8)

$$\mathbf{u}_N^{\text{int}} = \begin{pmatrix} e_\kappa(1/2,t) \\ \partial_x e_\kappa(1/2,t) \end{pmatrix} = \begin{bmatrix} 1 & 0 \\ 0 & -1 \end{bmatrix} \begin{pmatrix} e_\kappa(1/2,t) \\ -\partial_x e_\kappa(1/2,t) \end{pmatrix} = \mathbf{C}\mathbf{y}_D^{\text{int}},$$
$$\mathbf{u}_D^{\text{int}} = \begin{pmatrix} -\partial_x e_w(L/2,t) \\ e_w(L/2,t) \end{pmatrix} = \begin{bmatrix} -1 & 0 \\ 0 & 1 \end{bmatrix} \begin{pmatrix} \partial_x e_w(1/2,t) \\ e_w(1/2,t) \end{pmatrix} = -\mathbf{C}^\top \mathbf{y}_N^{\text{int}} s$$

This interconnection establishes that the power is exchanged without loss between the two systems

$$\mathbf{u}_D^{\text{int}\,\top} \mathbf{M}_{\Gamma_{\text{int}}} \mathbf{y}_D^{\text{int}} + \mathbf{u}_N^{\text{int}\,\top} \mathbf{M}_{\Gamma_{\text{int}}} \mathbf{y}_N^{\text{int}} = 0. \tag{8.28}$$

For what concerns the choice of the approximations, System (8.26) is discretized using the HerDG1 elements (7.2), while for System (8.27) the DG1Her (7.5) elements are used.

Numerical results The settings for the numerical simulation are reported in Tab. 8.3. The frequency of the reference output is set to $\omega = 4$. The analytical solutions for the reference displacement and velocity together with their numerical discretization are plotted in Figs. 8.10 and 8.11. The displacement is retrieved from the velocity using the trapezoidal rule. The numerical predictions perfectly match the analytical solution. In Fig. 8.9 the numerical solution for the vertical displacement obtained using the virtual domain decomposition is shown.

Simulation Settings	
ODE Integrator	RK 45
DAE Integrator	IDA
N° elements	6
FE spaces (DAE)	$\text{DG}_1 \times \text{Her}$
FE spaces (ODE)	Her $\times$ DG_1 on Ω_N / $\text{DG}_1 \times$ Her on Ω_D
t_{end}	1[s]

Table 8.3: Settings for the Euler-Bernoulli motion planning problem.

8.2.2 Vibroacoustics under mixed boundary conditions

Consider the model for the propagation of sound in air 2.23

$$\begin{bmatrix} \chi_s & 0 \\ \mathbf{0} & \mu_0 \end{bmatrix} \frac{\partial}{\partial t} \begin{pmatrix} e_p \\ \boldsymbol{e}_v \end{pmatrix} = - \begin{bmatrix} 0 & \text{div} \\ \text{grad} & \mathbf{0} \end{bmatrix} \begin{pmatrix} e_p \\ \boldsymbol{e}_v \end{pmatrix}, \qquad \Omega = \{x \in [0,L], r \in [0,R], \theta = [0,2\pi)\}, \tag{8.29}$$

where $e_p \in \mathbb{R}$ and $\boldsymbol{e}_v \in \mathbb{R}^3$ denote the variations of pressure and velocity from a steady state, μ_0 is the steady state mass density, and χ_s represents a constant adiabatic compressibility factor. With x, r, θ we denote the axial, radial and tangential cylindrical coordinates. The domain is a cylindrical duct of length L and radius R. The following boundary conditions

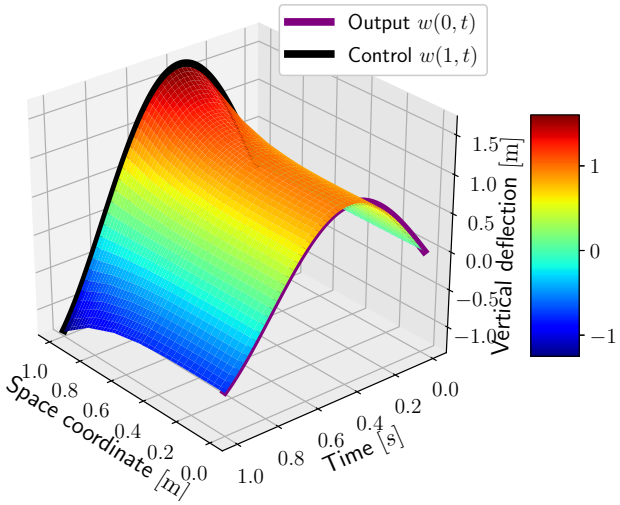

Figure 8.9: Computed vertical displacement.

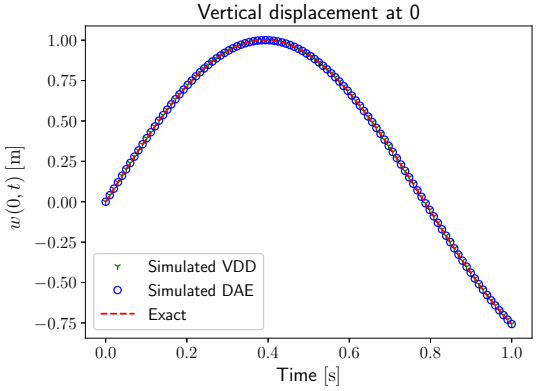

Figure 8.10: Analytical reference displacement and numerical predictions.

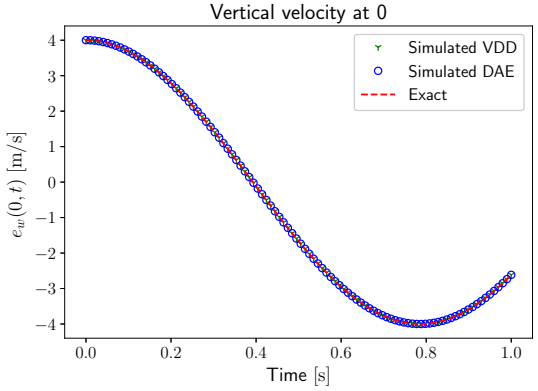

Figure 8.11: Analytical reference velocity and numerical predictions.

are imposed (see Fig. 8.12)

$$
\begin{aligned}
e_p(x,R,\theta,t) &= -\mathcal{Z}(x,t)\, e_v^r(x,R,\theta),\\
\boldsymbol{e}_v \cdot \boldsymbol{n}(0,r,\theta,t) &= -e_v^x(0,r,\theta) = -f(r),\\
\boldsymbol{e}_v \cdot \boldsymbol{n}(L,r,\theta,t) &= +e_v^x(L,r,\theta) = +f(r).
\end{aligned}
$$

For the initial boundary conditions, it is assumed

$$
\begin{aligned}
e_p^0(x,r,\theta) &= 0, \qquad & e_v^{r,0}(x,r,\theta) &= g(r),\\
e_v^{x,0}(x,r,\theta) &= f(r), \qquad & e_v^{\theta,0}(x,r,\theta) &= 0.
\end{aligned}
\tag{8.30}
$$

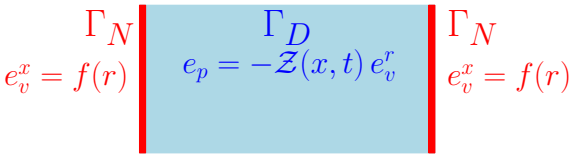

Figure 8.12: Boundary conditions for the 3D vibroacoustic problem.

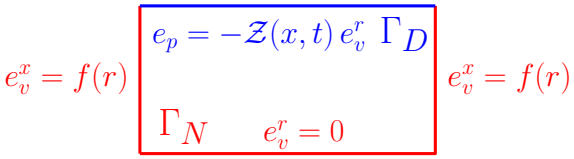

Figure 8.13: Boundary conditions for the reduced 2D vibroacoustic problem.

The impedance and the axial and radial flows expressions are the following

$$\mathcal{Z}(x,t) = \mathbb{1}\left\{\frac{1}{3}L \leq \ x \ \leq \frac{2}{3}L,\, t \geq 0.2\ t_{\text{fin}}\right\}\mu_0\, c_0,$$
$$f(r) = \left(1 - \frac{r^2}{R^2}\right) v_0,$$
$$g(r) = 16\frac{r^2}{R^4}\,(R-r)^2\, v_0.$$

The impedance operator $\mathcal{Z}$ is non invertible. If it were invertible than the impedance condition could be treated as a Robin condition. To illustrate this, consider the impedance condition

$$e_p = -\mathcal{Z}\, e_v^r.$$

Assume that $\mathcal{Z}(x,t)$ is an invertible operator. Then the impedance condition can be written as a Robin condition

$$e_v^r = -\mathcal{Z}^{-1}\, e_p,$$

that can be imposed as a Neumann condition.

This model describes the behavior of an axis-symmetrical flow subjected to an impedance condition on the lateral surface. Because of symmetry the model can be reduced to a 2D problem in polar coordinates over the domain $\Omega_{\text{r}} = \{x \in [0,L], r \in [0,R]\}$. The reduced system reads

$$\begin{bmatrix} \chi_s & 0 \\ \mathbf{0} & \mu_0 \end{bmatrix} \frac{\partial}{\partial t} \begin{pmatrix} e_p \\ \boldsymbol{e}_v \end{pmatrix} = - \begin{bmatrix} 0 & \text{div}_r \\ \text{grad}_r & \mathbf{0} \end{bmatrix} \begin{pmatrix} e_p \\ \boldsymbol{e}_v \end{pmatrix}, \qquad \text{div}_r = \begin{bmatrix} \partial_x & \partial_r + 1/r \end{bmatrix}, \quad \text{grad}_r = \begin{bmatrix} \partial_x \\ \partial_r \end{bmatrix}. \tag{8.31}$$

The boundary conditions must now account for the symmetry condition at $r = 0$, leading to the set of boundary conditions (see Fig. 8.13)

$$u_D = e_p|_{\Gamma_D} = -\mathcal{Z}(x,t)\, e_v^r(x,R), \tag{8.32}$$

$$u_N = \boldsymbol{e}_v \cdot \boldsymbol{n}|_{\Gamma_N} = \begin{cases} -f(r), & x = 0, \\ +f(r), & x = L, \\ 0, & r = 0, \end{cases} \tag{8.33}$$

where Γ_D, Γ_D denote the boundary partitions. The Hamiltonian is then computed as

$$H = \frac{1}{2}\langle e_p,\, \chi_s e_p\rangle_{\Omega_\mathrm{r}} + \frac{1}{2}\langle \boldsymbol{e}_v,\, \mu_0 \boldsymbol{e}_v\rangle_{\Omega_\mathrm{r}}$$

where $\langle\cdot,\,\cdot\rangle_{\Omega_\mathrm{r}}$ is the standard L^2-inner product in polar coordinates, defined for scalar or vector fields as

$$\langle \alpha,\, \beta\rangle_{\Omega_\mathrm{r}} = \int_{\Omega_\mathrm{r}} \alpha\cdot\beta\; r\,\mathrm{d}r\,\mathrm{d}x = \int_{\Omega_\mathrm{r}} \alpha\cdot\beta\;\; \mathrm{d}\Omega_r.$$

The power flow is obtained by application of the Stokes theorem

$$\dot{H} = \langle e_p,\, \boldsymbol{e}_v\cdot\boldsymbol{n}\rangle_{\partial\Omega_\mathrm{r}} = \int_{\partial\Omega_\mathrm{r}} e_p\;\boldsymbol{e}_v\cdot\boldsymbol{n}\;\mathrm{d}\Gamma_r = -\int_0^L \mathcal{Z}(x,t)(e_v^r)^2\; R\,\mathrm{d}x \le 0$$

where $\mathrm{d}\Gamma_r = r\,\mathrm{d}s$ is the infinitesimal surface.

In the next paragraphs we provide a concise description of the discretization procedure for the two methods.

Lagrange multipliers If a Lagrange multiplier is introduced for the Dirichlet boundary condition, the following weak form is obtained

$$\begin{aligned}
\langle v_p,\, \chi_s\partial_t e_p\rangle_{\Omega_r} &= \langle \mathrm{grad}_r v_p,\, \boldsymbol{e}_v\rangle_{\Omega_r} + \langle v_p,\, \lambda_D\rangle_{\Gamma_D} + \langle v_p,\, u_N\rangle_{\Gamma_N}\,,\\
\langle \boldsymbol{v}_v,\, \mu_0\partial_t \boldsymbol{e}_v\rangle_{\Omega_r} &= \langle \boldsymbol{v}_v,\, \mathrm{grad}_r e_p\rangle_{\Omega_r}\,,\\
0 &= -\langle v_D,\, e_p\rangle_{\Gamma_D} + \langle v_D,\, u_D\rangle_{\Gamma_D}\,,\\
\langle v_N,\, y_N\rangle_{\Gamma_N} &= \langle v_N,\, e_p\rangle_{\Gamma_N}\,,\\
\langle v_D,\, y_D\rangle_{\Gamma_D} &= \langle v_D,\, \lambda_D\rangle_{\Gamma_D}\,,
\end{aligned} \tag{8.34}$$

where v_N, v_D are the test functions associated to the output discretization and $\langle\cdot,\,\cdot\rangle_{\Gamma_*}$ is the L^2 inner product on boundary Γ_*. Introducing a Galerkin approximation for the variables, one obtains the following system

$$\begin{bmatrix}\mathbf{M}_{\chi_s} & \mathbf{0} & \mathbf{0}\\ \mathbf{0} & \mathbf{M}_{\mu_0} & \mathbf{0}\\ \mathbf{0} & \mathbf{0} & \mathbf{0}\end{bmatrix}\begin{pmatrix}\dot{\mathbf{e}}_p\\ \dot{\mathbf{e}}_v\\ \dot{\boldsymbol{\lambda}}_D\end{pmatrix} = \begin{bmatrix}\mathbf{0} & \mathbf{D}_{\mathrm{grad}}^\top & \mathbf{B}_{p,\Gamma_D}\\ -\mathbf{D}_{\mathrm{grad}} & \mathbf{0} & \mathbf{0}\\ -\mathbf{B}_{p,\Gamma_D}^\top & \mathbf{0} & \mathbf{0}\end{bmatrix}\begin{pmatrix}\mathbf{e}_p\\ \mathbf{e}_v\\ \boldsymbol{\lambda}_D\end{pmatrix} + \begin{bmatrix}\mathbf{B}_{p,\Gamma_N} & \mathbf{0}\\ \mathbf{0} & \mathbf{0}\\ \mathbf{0} & \mathbf{M}_{\Gamma_D}\end{bmatrix}\begin{pmatrix}\mathbf{u}_N\\ \mathbf{u}_D\end{pmatrix},$$
$$\begin{bmatrix}\mathbf{M}_{\Gamma_N} & \mathbf{0}\\ \mathbf{0} & \mathbf{M}_{\Gamma_D}\end{bmatrix}\begin{pmatrix}\mathbf{y}_N\\ \mathbf{y}_D\end{pmatrix} = \begin{bmatrix}\mathbf{B}_{p,\Gamma_D}^\top & \mathbf{0} & \mathbf{0}\\ \mathbf{0} & \mathbf{0} & \mathbf{M}_{\Gamma_D}\end{bmatrix}\begin{pmatrix}\mathbf{e}_p\\ \mathbf{e}_v\\ \boldsymbol{\lambda}_D\end{pmatrix}. \tag{8.35}$$

The matrices are computed as in (6.112). To impose the actual boundary conditions consider the weak form of (8.32) $u_D = -\mathcal{Z}\lambda_D = -\mathcal{Z}y_D$ [SMH19]:

$$\mathbf{M}_{\Gamma_D}\mathbf{u}_D = -\mathbf{M}_{\Gamma_D,\mathcal{Z}}\mathbf{y}_D,$$

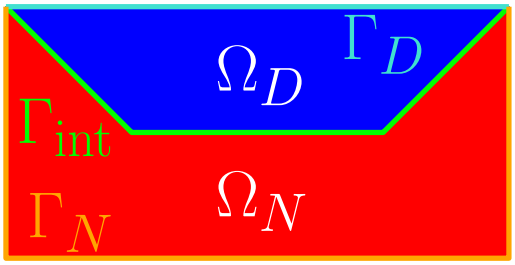

Figure 8.14: Virtual decomposition of the vibroacoustic domain.

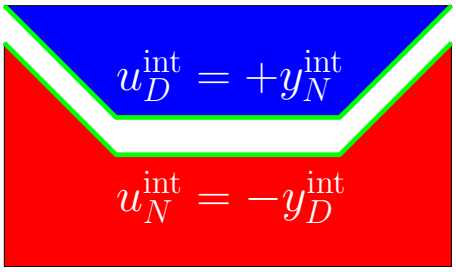

Figure 8.15: Interconnection for the vibroacoustic domain.

where $\mathbf{M}_{\Gamma_D,\mathcal{Z}}$ corresponds to the mass matrix associated to the weighted inner product $\langle v_D,\, \mathcal{Z} y_D \rangle_{\Gamma_D}$. The Neumann boundary condition is imposed by projection on the u_N space. The boundary-controlled system becomes

$$\begin{bmatrix} \mathbf{M}_{\chi_s} & \mathbf{0} & \mathbf{0} \\ \mathbf{0} & \mathbf{M}_{\mu_0} & \mathbf{0} \\ \mathbf{0} & \mathbf{0} & \mathbf{0} \end{bmatrix} \begin{pmatrix} \dot{\mathbf{e}}_p \\ \dot{\mathbf{e}}_v \\ \dot{\boldsymbol{\lambda}}_D \end{pmatrix} = \begin{bmatrix} \mathbf{0} & \mathbf{D}_{\text{grad}}^{\top} & \mathbf{B}_{p,\Gamma_D} \\ -\mathbf{D}_{\text{grad}} & \mathbf{0} & \mathbf{0} \\ -\mathbf{B}_{p,\Gamma_D}^{\top} & \mathbf{0} & -\mathbf{M}_{\Gamma_D,\mathcal{Z}} \end{bmatrix} \begin{pmatrix} \mathbf{e}_p \\ \mathbf{e}_v \\ \boldsymbol{\lambda}_D \end{pmatrix} + \begin{pmatrix} \mathbf{b}_N \\ \mathbf{0} \\ \mathbf{0} \end{pmatrix}. \tag{8.36}$$

Virtual domain decomposition In order to apply this methodology the domain has to be split into two sub-domains. The shared boundary connecting the two sub-domains can be freely chosen. For the given geometry, the separation line that provides the most regular simplicial meshes is the trapezoidal one given in Fig. 8.14.

Applying the PFEM methodology as in 6.2.2 two finite-dimensional systems are obtained. For Ω_D the system is analogous to (6.134), while for Ω_N to (6.135).

Subdomain Ω_D

$$\begin{bmatrix} \mathbf{M}_{\chi_s}^{\Omega_D} & \mathbf{0} \\ \mathbf{0} & \mathbf{M}_{\mu_0}^{\Omega_D} \end{bmatrix} \begin{pmatrix} \dot{\mathbf{e}}_{p,\Omega_D} \\ \dot{\mathbf{e}}_{v,\Omega_D} \end{pmatrix} = \begin{bmatrix} \mathbf{0} & -\mathbf{D}_{\text{div}}^{\Omega_D} \\ \mathbf{D}_{\text{div}}^{\Omega_D \top} & \mathbf{0} \end{bmatrix} \begin{pmatrix} \mathbf{e}_{p,\Omega_D} \\ \mathbf{e}_{v,\Omega_D} \end{pmatrix} + \begin{bmatrix} \mathbf{0} & \mathbf{0} \\ \mathbf{B}_{v,\Gamma_D}^{\Omega_D} & \mathbf{B}_{v,\Gamma_{\text{int}}}^{\Omega_D} \end{bmatrix} \begin{pmatrix} \mathbf{u}_D \\ \mathbf{u}_D^{\text{int}} \end{pmatrix},$$
$$\begin{bmatrix} \mathbf{M}_{\Gamma_D} & \mathbf{0} \\ \mathbf{0} & \mathbf{M}_{\Gamma_{\text{int}}} \end{bmatrix} \begin{pmatrix} \mathbf{y}_D \\ \mathbf{y}_D^{\text{int}} \end{pmatrix} = \begin{bmatrix} \mathbf{0} & \mathbf{B}_{v,\Gamma_D}^{\Omega_D \top} \\ \mathbf{0} & \mathbf{B}_{v,\Gamma_{\text{int}}}^{\Omega_D \top} \end{bmatrix} \begin{pmatrix} \mathbf{e}_{p,\Omega_D} \\ \mathbf{e}_{v,\Omega_D} \end{pmatrix}. \tag{8.37}$$

Subdomain Ω_N

$$\begin{bmatrix} \mathbf{M}_{\chi_s}^{\Omega_N} & \mathbf{0} \\ \mathbf{0} & \mathbf{M}_{\mu_0}^{\Omega_N} \end{bmatrix} \begin{pmatrix} \dot{\mathbf{e}}_{p,\Omega_N} \\ \dot{\mathbf{e}}_{v,\Omega_N} \end{pmatrix} = \begin{bmatrix} \mathbf{0} & \mathbf{D}_{\text{grad}}^{\Omega_N \top} \\ -\mathbf{D}_{\text{grad}}^{\Omega_N} & \mathbf{0} \end{bmatrix} \begin{pmatrix} \mathbf{e}_{p,\Omega_N} \\ \mathbf{e}_{v,\Omega_N} \end{pmatrix} + \begin{bmatrix} \mathbf{B}_{v,\Gamma_N}^{\Omega_N} & \mathbf{B}_{v,\Gamma_{\text{int}}}^{\Omega_N} \\ \mathbf{0} & \mathbf{0} \end{bmatrix} \begin{pmatrix} \mathbf{u}_N \\ \mathbf{u}_N^{\text{int}} \end{pmatrix},$$
$$\begin{bmatrix} \mathbf{M}_{\Gamma_N} & \mathbf{0} \\ \mathbf{0} & \mathbf{M}_{\Gamma_{\text{int}}} \end{bmatrix} \begin{pmatrix} \mathbf{y}_N \\ \mathbf{y}_N^{\text{int}} \end{pmatrix} = \begin{bmatrix} \mathbf{B}_{v,\Gamma_N}^{\Omega_N \top} & \mathbf{0} \\ \mathbf{B}_{v,\Gamma_{\text{int}}}^{\Omega_N \top} & \mathbf{0} \end{bmatrix} \begin{pmatrix} \mathbf{e}_{p,\Omega_N} \\ \mathbf{e}_{v,\Omega_N} \end{pmatrix}. \tag{8.38}$$

In order to get a system with mixed causality, systems (8.37) and (8.38) have to be interconnected using a classical gyrator interconnection. Considering that the pressure field is continuous at Γ_{int}, the outward normal verifies $\boldsymbol{n}_D|_{\Gamma_{\text{int}}} = -\boldsymbol{n}_N|_{\Gamma_{\text{int}}}$ and the corresponding degrees of freedom have to be matched, the correct interconnection reads (cf. Fig. 8.15)

$$\mathbf{u}_N^{\text{int}} = -\mathbf{y}_D^{\text{int}}, \qquad \mathbf{u}_D^{\text{int}} = \mathbf{y}_N^{\text{int}}. \tag{8.39}$$

The resulting interconnected system is written as

$$\begin{bmatrix} \mathbf{M}_{\Omega_D} & \mathbf{0} \\ \mathbf{0} & \mathbf{M}_{\Omega_N} \end{bmatrix} \begin{pmatrix} \dot{\mathbf{e}}_{\Omega_D} \\ \dot{\mathbf{e}}_{\Omega_N} \end{pmatrix} = \begin{bmatrix} \mathbf{J}_{\Omega_D} & \mathbf{C} \\ -\mathbf{C}^\top & \mathbf{J}_{\Omega_N} \end{bmatrix} \begin{pmatrix} \mathbf{e}_{\Omega_D} \\ \mathbf{e}_{\Omega_N} \end{pmatrix} + \begin{bmatrix} \mathbf{B}_{\Gamma_D}^{\Omega_D} & \mathbf{0} \\ \mathbf{0} & \mathbf{B}_{\Gamma_N}^{\Omega_N} \end{bmatrix} \begin{pmatrix} \mathbf{u}_D \\ \mathbf{u}_N \end{pmatrix},$$
$$\begin{bmatrix} \mathbf{M}_{\Gamma_D} & \mathbf{0} \\ \mathbf{0} & \mathbf{M}_{\Gamma_N} \end{bmatrix} \begin{pmatrix} \mathbf{y}_D \\ \mathbf{y}_N \end{pmatrix} = \begin{bmatrix} \mathbf{B}_{\Gamma_D}^{\Omega_N \top} & \mathbf{0} \\ \mathbf{0} & \mathbf{B}_{\Gamma_N}^{\Omega_D \top} \end{bmatrix} \begin{pmatrix} \mathbf{e}_{\Omega_1} \\ \mathbf{e}_{\Omega_2} \end{pmatrix}. \tag{8.40}$$

where $\mathbf{C} = \mathbf{B}_{\Gamma_{\text{int}}}^{\Omega_D} \mathbf{M}_{\Gamma_{\text{int}}}^{-1} \mathbf{B}_{\Gamma_{\text{int}}}^{\Omega_N \top}$. The actual boundary conditions (8.32) (8.33) can be plugged into the system leading to

$$\begin{bmatrix} \mathbf{M}_{\Omega_D} & \mathbf{0} \\ \mathbf{0} & \mathbf{M}_{\Omega_N} \end{bmatrix} \begin{pmatrix} \dot{\mathbf{e}}_{\Omega_D} \\ \dot{\mathbf{e}}_{\Omega_N} \end{pmatrix} = \begin{bmatrix} \mathbf{J}_{\Omega_D} - \mathbf{R}_{\Omega_D} & \mathbf{C} \\ -\mathbf{C}^\top & \mathbf{J}_{\Omega_N} \end{bmatrix} \begin{pmatrix} \mathbf{e}_{\Omega_D} \\ \mathbf{e}_{\Omega_N} \end{pmatrix} + \begin{pmatrix} \mathbf{0} \\ \mathbf{b}_{\Gamma_N}^{\Omega_N} \end{pmatrix}, \tag{8.41}$$

where $\mathbf{R}_{\Omega_D} = \mathbf{B}_{\Gamma_D}^{\Omega_D} \mathbf{M}_{\Gamma_D}^{-1} \mathbf{M}_{\Gamma_D,\mathcal{Z}} \mathbf{M}_{\Gamma_D}^{-1} \mathbf{B}_{\Gamma_D}^{\Omega_D \top}$ is symmetric and positive definite.

Numerical results and discussion In this section a numerical illustration of the two methodologies is presented. The Hamiltonian and the state variables trends given by the DAE (obtained from the Lagrange's multiplier method) and the ODE formulation (obtained from the virtual domain decomposition method) are compared with respect to a reference solution. The reference is set to the DAE solution on a very fine mesh. The physical parameters are provided in Tab. 8.4. The initial condition are selected according to (8.30):

$$e_p^0(x,r) = 0, \quad e_v^{x,0}(x,r) = f(r), \quad e_v^{r,0}(x,r) = g(r).$$

A radial component of the velocity allows highlighting the effect of the impedance. The velocity profile satisfies some regularity conditions so that the transition between Neumann and

Physical Parameters	
L	2 [m]
R	1 [m]
μ_0	1.225 [kg/m^3]
c_0	340 [m/s]
χ_s	7.061 [μPa]$^{-1}$
v_0	1 [m/s]

Simulation Settings	
ODE Integrator	RK 45
DAE Integrator	IDA
t_{end}	0.1[s]
FE spaces (DAE and ODE)	$\text{CG}_1 \times \text{RT}_1 \times \text{CG}_1$

Table 8.4: Settings and parameters for the vibroacoustic problem.

Dirichlet boundary conditions is smooth. In order to get a finite-dimensional discretization the fields are approximated using the following finite element families for both approaches:

- e_p is interpolated using order 1 Lagrange (Continuous Galerkin) polynomials (CG_1);
- $\boldsymbol{e}_v$ is interpolated using order 1 Raviart-Thomas polynomials (RT_1);
- Boundary variables are approximated by Lagrange polynomial of order 1 defined on the boundary Γ_D (for λ_D, u_D, y_D) or Γ_N (for u_N, y_N).

Such a choice guarantees the conformity with respect to the differential operators. The FEniCS library, that allows interpolating functions on different meshes, is used for the computations. The reference solution, obtained by using the DAE approach on a very fine mesh, is plotted in Fig. 8.16a, where the two contributions to the total energy

$$H_{p,d} \approx \frac{1}{2}\mathbf{e}_p^\top \mathbf{M}_{\chi_s}\mathbf{e}_p, \qquad H_{v,d} \approx \frac{1}{2}\mathbf{e}_v^\top \mathbf{M}_{\mu_0}\mathbf{e}_v,$$

are highlighted. The Dirichlet condition induces a continuous transfer from radial kinetic energy into pressure potential. The impedance acts by dissipating the radial component of the velocity so that only the axial flow contribution is left. The total energy at the initial time of the simulation is given only by the kinetic energy

$$H_v^0 = H_{vx}^0 + H_{vr}^0 = \frac{1}{2}\int_0^L \int_0^R \mu_0 \left\|\boldsymbol{e}_v\right\|^2 \, r \, \mathrm{d}r \, \mathrm{d}x.$$

Given the physical parameters in Tab. 8.4, the numerical values of the energy contribution are readily found

$$H_v^0 = 0.453[J], \qquad H_{vx}^0 = 0.204[J], \qquad H_{vr}^0 = 0.249[J].$$

In order to demonstrate the consistency of the two proposed approaches the following

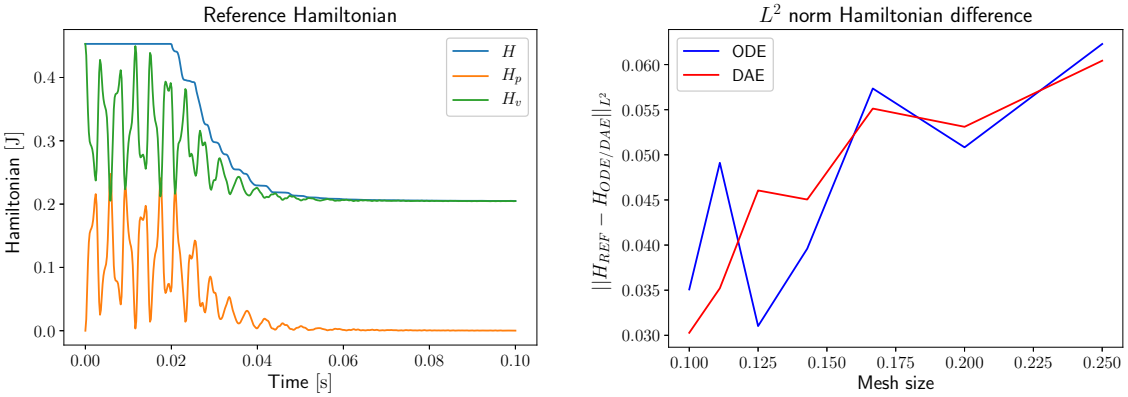

(a) Reference Hamiltonian. (b) L^2-Hamiltonian error.

Figure 8.16: Reference Hamiltonian and L^2-error.

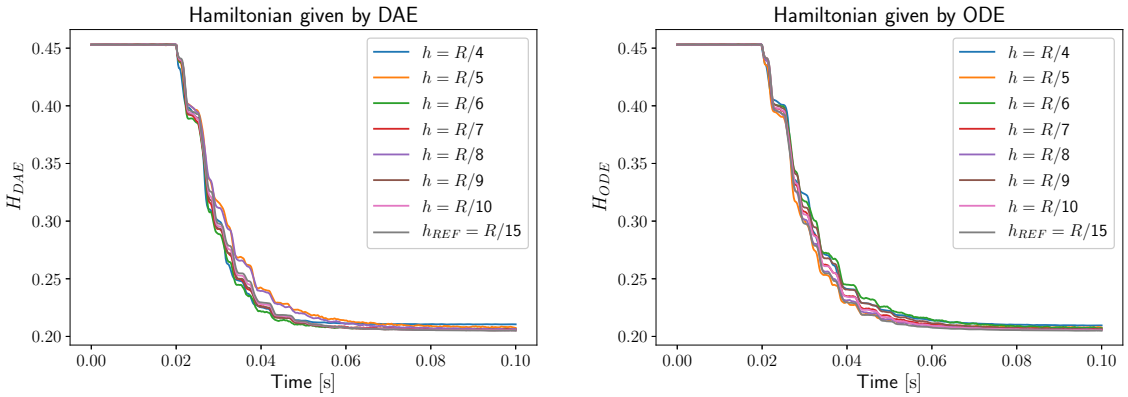

(a) DAE system (8.36). (b) ODE system (8.41).

Figure 8.17: Hamiltonian trend for different mesh size.

measures are adopted

$$\varepsilon^H_{\text{ODE/DAE}} = \frac{||H_{\text{REF}} - H_{\text{ODE/DAE}}||_{L^2}}{||H_{\text{REF}}||_{L^2}},$$
$$\varepsilon^p_{\text{ODE/DAE}} = \frac{||p_{\text{REF}} - p_{\text{ODE/DAE}}||_{L^2}}{||p_{\text{REF}}||_{L^2}},$$
$$\varepsilon^v_{\text{ODE/DAE}} = \frac{||\boldsymbol{v}_{\text{REF}} - \boldsymbol{v}_{\text{ODE/DAE}}||_{L^2}}{||\boldsymbol{v}_{\text{REF}}||_{L^2}}.$$

The total energy obtained with several meshes is shown in Figs. 8.17a, 8.17b for the DAE and ODE approaches respectively. It can be noticed that the Hamiltonian tends to the value H^0_{vx}, as expected. The overall Hamiltonian trend is well captured and even for coarse meshes the relative error does not exceed 6% (see Fig. 8.16b). The convergence of the Hamiltonian

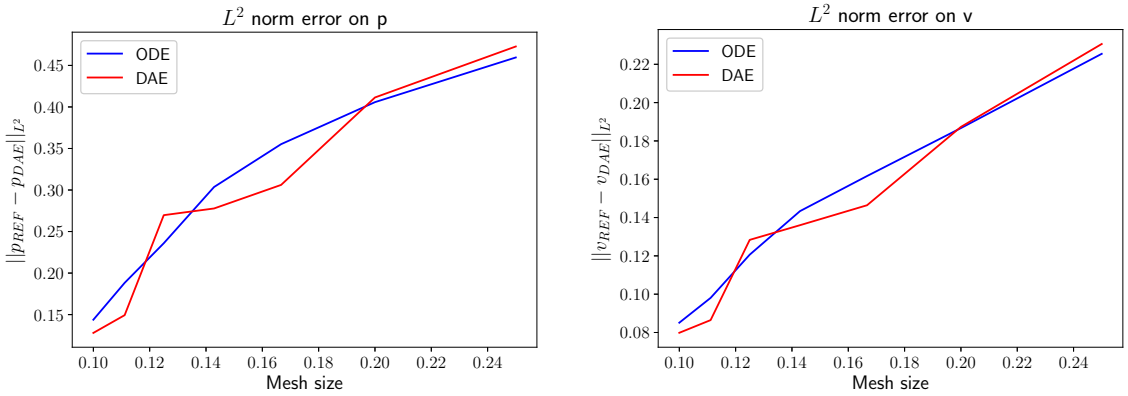

(a) L^2 pressure error.

(b) L^2 velocity error.

Figure 8.18: Error on the state variables for different mesh size.

h mesh	$\Delta t_{\text{DAE}}[s]$	$\Delta t_{\text{ODE}}[s]$
$R_{\text{ext}}/4$	98.95	124.43
$R_{\text{ext}}/5$	415.99	255.54
$R_{\text{ext}}/6$	798.24	893.63
$R_{\text{ext}}/7$	1408.76	1120.69
$R_{\text{ext}}/8$	3054.78	2271.28
$R_{\text{ext}}/9$	6929.24	5792.89
$R_{\text{ext}}/10$	12648.15	8835.09

Table 8.5: Elapsed simulation time for the vibroacoustic experiment.

is non monotonic. This is probably related to the finite elements choice. Nevertheless, both methods converge monotonically to the reference solution, as illustrated in Figs. 8.18a, 8.18b. The faster convergence of one method on the other cannot be established. For what concerns the computational cost, in Tab. 8.5 the simulation time required by each solver is shown. The ODE approach is less time consuming for sufficiently small mesh size.

8.3 Thermoelastic wave propagation

In this section the pH discretization of the Danilovskaya problem [Dan50] is performed. For this problem an analytical solution in the Laplace domain is available [Bal91]. First the classical and pH formulation are illustrated. Second the discretization strategy is discussed. Numerical results are then presented.

8.3.1 The Danilovskaya problem

The Danilovskaya problem is a one-dimensional thermoelastic model in the infinite half-space $x \geq 0$. We recall the system of equations for the thermoelastic problem in 1D:

$$\begin{aligned}
\rho\partial_{tt}u &= \partial_x(\sigma_{ET}), \qquad x \geq 0, \\
\rho c_\epsilon \partial_t T &= -\partial_x(j_Q) - C_\beta \partial_t \varepsilon, \qquad \text{where} \qquad C_\beta := T_0\beta(2\mu + 3\lambda), \\
\sigma_{ET} &= \sigma_E + \sigma_T, \\
\sigma_E &= (2\mu + \lambda)\varepsilon, \\
\sigma_T &= -C_\beta \theta, \\
\varepsilon &= \partial_x u, \\
j_Q &= -k\,\partial_x T.
\end{aligned} \tag{8.42}$$

All the variables have the same meaning as in Chapter 5. The initial conditions for this problem are all null. The system is excited by a sudden thermal heating at $x = 0$. Furthermore, the variables vanish at ∞. Consequently, the following boundary conditions apply

$$\begin{aligned}
T(0,t) &= T_1 H(t), \qquad & \sigma_{ET}(0,t) &= 0, \\
\lim_{x\to\infty} T(x,t) &= 0, \qquad & \lim_{x\to\infty} u(x,t) &= 0,
\end{aligned}$$

where $H(t)$ is the Heaviside function. Since the effect of the elastic vibration on the thermal field is weak, a dimensionless constant c_δ is usually introduced to strengthen the coupling from the mechanical to the thermal domain [RSBR16]. This dimensionless constant reads

$$c_\delta = \delta \frac{\rho c_\epsilon (2\mu + \lambda)}{\beta^2 (3\lambda + 2\mu)^2 T_0}, \tag{8.43}$$

where $\delta \in \{0, 1\}$ is a variable for switching on and off the strong coupling from the mechanical to the thermal domain. The problem can now be recast as a pH system in co-energy variables

$$\begin{bmatrix} \rho & 0 & 0 & 0 \\ 0 & (2\mu+\lambda)^{-1} & 0 & 0 \\ 0 & 0 & \rho c_\epsilon T_0 & 0 \\ 0 & 0 & 0 & 0 \end{bmatrix} \frac{\partial}{\partial t} \begin{pmatrix} e_v \\ e_\varepsilon \\ e_T \\ j_Q \end{pmatrix} = \begin{bmatrix} 0 & \partial_x & \mathcal{A}_\beta & 0 \\ \partial_x & 0 & 0 & 0 \\ -c_\delta \mathcal{A}_\beta^* & 0 & 0 & -\partial_x \\ 0 & 0 & -\partial_x & -(T_0 k)^{-1} \end{bmatrix} \begin{pmatrix} e_v \\ e_\varepsilon \\ e_T \\ \boldsymbol{j}_Q \end{pmatrix}, \tag{8.44}$$

where $\mathcal{A}_\beta(\cdot) := -\partial_x(C_\beta\,\cdot)$ (cf. Eq. (5.11)). All the variables have the same meaning as in Chapter 5. Notice that the coupling parameter c_δ breaks the Hamiltonian structure. The boundary conditions in the pH variables read

$$e_T(0,t) = \frac{T_1 - T_0}{T_0} H(t), \qquad (e_\varepsilon - C_\beta e_v)(0,t) = 0, \tag{8.45}$$

$$\lim_{x\to\infty} e_T(x,t) = 0, \qquad \lim_{x\to\infty} e_v(x,t) = 0. \tag{8.46}$$

Remark 23 (Boundary conditions for the numerical simulation)
In the numerical simulation, the vanishing conditions at ∞ (8.46) *are replaced by Neumann conditions at the extremity of the simulation domain* $\Omega = \{0, L\}$ *[RSBR16]*

$$(e_\varepsilon - C_\beta e_v)(L,t) = 0, \qquad j_Q(L,t) = 0. \tag{8.47}$$

8.3.2 Discretization of the thermoelastic system

The partitioned finite element method also applies to system (8.44). The additional difficulty resides in the discretization of the coupling operator $\mathcal{A}_\beta$. One possible strategy consists in integrating by parts the whole first line of (8.44) and the ∂_x operator in the third line. This choice leads to the following weak form for the numerical domain $\Omega = \{0, L\}$

$$\begin{aligned}
\langle v_v,\, \rho \partial_t e_v \rangle_\Omega &= -\langle \partial_x v_v,\, e_\varepsilon \rangle_\Omega + \left\langle \mathcal{A}_\beta^* v_v,\, e_T \right\rangle_\Omega + \langle \gamma_0 v_v,\, \gamma_n (e_\varepsilon - C_\beta e_T) \rangle_{\partial\Omega}\,, \\
\left\langle v_\varepsilon,\, (2\mu+\lambda)^{-1} \partial_t e_\varepsilon \right\rangle_\Omega &= +\langle v_\varepsilon,\, \partial_x e_v \rangle_\Omega\,, \\
\langle v_T,\, \rho c_\epsilon T_0 \partial_t e_T \rangle_\Omega &= -\left\langle v_T,\, \mathcal{A}_\beta^* e_v \right\rangle_\Omega + \langle \partial_x v_T,\, j_Q \rangle_\Omega - \langle \gamma_0 v_T,\, \gamma_n j_Q \rangle_{\partial\Omega}\,, \\
0 &= -\langle v_j,\, \partial_x e_T \rangle_\Omega - \left\langle v_j,\, (T_0 k)^{-1} e_j \right\rangle_\Omega\,,
\end{aligned} \tag{8.48}$$

where $v_v,\ v_\varepsilon,\ v_T,\ v_j$ are the test functions. For this discretization the boundary condition

$$e_T(0,t) = \frac{T_1 - T_0}{T_0} H(t),$$

is imposed strongly as an essential condition. The other boundary terms disappear because of (8.47). Introducing a Galerkin approximation

$$\square_v = \sum_{i=1}^{n_v} \phi_v^i \square_v^i, \qquad \square_\varepsilon = \sum_{i=1}^{n_\varepsilon} \phi_\varepsilon^i \square_\varepsilon^i, \qquad \square_T = \sum_{i=1}^{n_T} \phi_T^i \square_T^i, \qquad \square_Q = \sum_{i=1}^{n_Q} \phi_Q^i \square_Q^i, \qquad \square = \{v, e\}, \tag{8.49}$$

the following system is obtained

$$\begin{bmatrix} \mathbf{M}_\rho & \mathbf{0} & \mathbf{0} & \mathbf{0} \\ \mathbf{0} & \mathbf{M}_{(2\mu+\lambda)^{-1}} & \mathbf{0} & \mathbf{0} \\ \mathbf{0} & \mathbf{0} & \mathbf{M}_{\rho c_\epsilon T_0} & \mathbf{0} \\ \mathbf{0} & \mathbf{0} & \mathbf{0} & \mathbf{0} \end{bmatrix} \begin{pmatrix} \dot{\mathbf{e}}_v \\ \dot{\mathbf{e}}_\varepsilon \\ \dot{\mathbf{e}}_T \\ \dot{\mathbf{e}}_Q \end{pmatrix} = \begin{bmatrix} \mathbf{0} & -\mathbf{D}_{\text{grad}}^\top & \mathbf{A}_\beta & \mathbf{0} \\ \mathbf{D}_{\text{grad}} & \mathbf{0} & \mathbf{0} & \mathbf{0} \\ -c_\delta \mathbf{A}_\beta^\top & \mathbf{0} & \mathbf{0} & \mathbf{D}_{\text{grad}}^\top \\ \mathbf{0} & \mathbf{0} & -\mathbf{D}_{\text{grad}} & -\mathbf{R}_Q \end{bmatrix} \begin{pmatrix} \mathbf{e}_v \\ \mathbf{e}_\varepsilon \\ \mathbf{e}_T \\ \mathbf{e}_Q \end{pmatrix}. \tag{8.50}$$

The coupling matrix $\mathbf{A}_\beta$ arises from the discretization of the coupling operator $\mathcal{A}^*_\beta$

$$A^{mn}_\beta = \left\langle \mathcal{A}^*_\beta \phi^m_v,\, \phi^n_T \right\rangle_\Omega, \qquad m \in \{1, n_v\},\ n \in \{1, n_T\}.$$

The dissipation matrix reads

$$R^{mn}_Q = \left\langle \phi^m_Q,\, (T_0 k)^{-1} \phi^n_Q \right\rangle_\Omega, \qquad m, n \in \{1, n_j\}.$$

The other matrices are computed as in Chapter 6.

8.3.3 Numerical results

In Tab. 8.6 the parameters for the simulation are reported. The constant C_x, C_v are the characteristic length and velocity of the problem [RSBR16]. The dimensionless constant $\widehat{L}$, $\widehat{t}_{\text{end}}$ are the dimensionless length and time of the problem. For the discretization CG elements of order 1 are employed for e_v, e_T, while DG of order 0 are used for e_ε, j_Q.

Physical Parameters	
λ	$0.85\ 10^9$ [kg/(cm · s^2)]
μ	$0.56\ 10^9$ [kg/(cm · s^2)]
ρ	$7.82\ 10^{-3}$ [kg/cm^3]
c_ϵ	$4.61\ 10^6$ [cm^2/(K · s^2)]
k	$1.7\ 10^3$ [kg · cm/(K · s^3)]
β	$9.03\ 10^{-6}$ [K^{-1}]
T_0	300 [K]
L	$C_x\ \widehat{L}$
C_x	$k/(\rho c_\epsilon C_v)$
$\widehat{L}$	10

Simulation Settings	
Integrator	Crank-Nicholson
t_{end}	$C_v/C_x\ \widehat{t}_{\text{end}}$
C_v	$\sqrt{(\lambda + 2\mu)/\rho}$
$\widehat{t}_{\text{end}}$	4
Δt	$10^{-3}\ t_{\text{end}}$
FE spaces	$\text{CG}_1 \times \text{DG}_0 \times \text{CG}_1 \times \text{DG}_0$
N° FE	200

Table 8.6: Settings and parameters for the thermoelastic problem.

To assess the validity of the solution, the numerical results are compared with the analytical solution in the Laplace domain. The dimensionless displacement field $\widehat{u}$ and temperature θ are introduced

$$\widehat{u} = \frac{(\lambda + 2\mu)}{C_x C_\beta} u, \qquad \widehat{T} = \frac{T - T_0}{T_0}.$$

The solution in the Laplace domain for the dimensionless variable is given by [Bal91]

$$\begin{aligned} \widehat{T}(s) &= \frac{1}{s(C_1^2 - C_2^2)}[(C_1^2 - s^2)\exp(-C_1\widehat{x}) - (C_2^2 - s^2)\exp(-C_2\widehat{x})], \\ \widehat{u}(s) &= -\frac{1}{s(C_1^2 - C_2^2)}[C_1\exp(-C_1\widehat{x}) - C_2\exp(-C_2\widehat{x})], \end{aligned} \tag{8.51}$$

where $\widehat{x} = x/C_x$ is the dimensionless space variable and C_1, C_2 are given by

$$\begin{aligned} C_1(s) &= \left[\frac{s}{2}[(1+\delta+s) + [(1+\delta+s)^2 - 4s]^{\frac{1}{2}}]\right]^{\frac{1}{2}}, \\ C_2(s) &= \left[\frac{s}{2}[(1+\delta+s) - [(1+\delta+s)^2 - 4s]^{\frac{1}{2}}]\right]^{\frac{1}{2}}. \end{aligned} \tag{8.52}$$

In Figs. 8.19, 8.20 the analytical and numerical displacement and temperature at $\widehat{x} = 1$ are compared for weak $\delta = 0$ and strong coupling $\delta = 1$. The inverse of the Laplace transform is computed using the de Hoog method [dHKS82] (available trough the `invertlaplace` function of the `mpmath` Python library). The displacement is retrieved from the velocity field using the trapezoidal rule. The numerical solution matches the analytical one, thus assessing the validity of the model (8.44) and its discretization (8.50). In Figs. 8.21 and 8.22 the numerical solutions for the displacement and dimensionless temperature are reported for weak $\delta = 0$ and strong coupling $\delta = 1$.

8.4 Conclusion

In this chapter the Partitioned Finite Element method has been employed for a number of problems. Thanks to this method, a structured and general numerical implementation of interconnected infinite-dimensional system is available. For what concerns the mixed boundary conditions enforcement, there is a point that require further investigation: the usage of Lagrange multiplier for the weak imposition of the boundary conditions is absolutely non trivial since the subspace employed for the multiplier has to be carefully designed [Pit79, Pit80, Pit81, GH92]. As a general guideline, the Lagrange multiplier space must not impose too many boundary conditions to the discrete solution, in order to fulfill the inf-sup condition [Jol03].

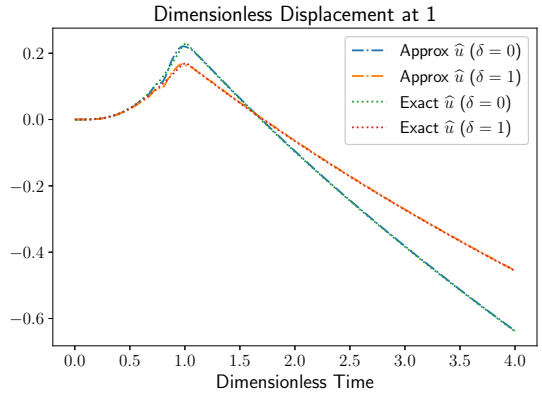

Figure 8.19: Dimensionless displacement ($\widehat{x} = 1$).

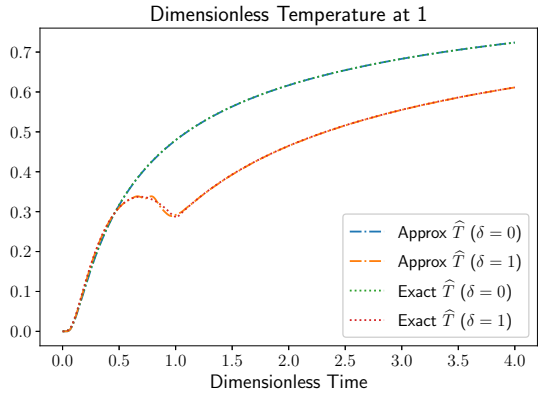

Figure 8.20: Dimensionless temperature ($\widehat{x} = 1$).

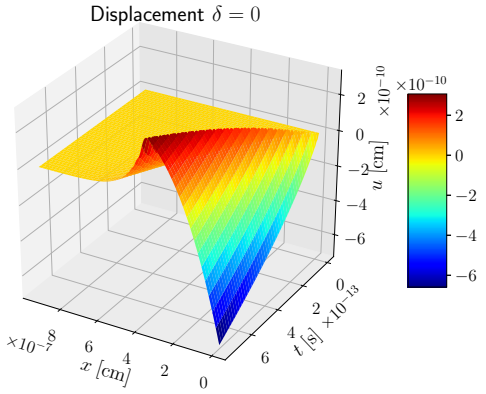

(a) $\delta = 0$

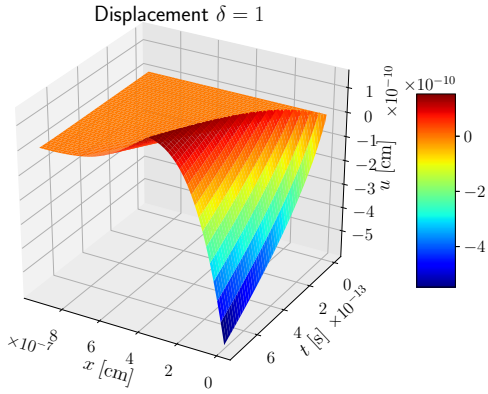

(b) $\delta = 1$

Figure 8.21: Displacement solution for the Danilovskaya problem.

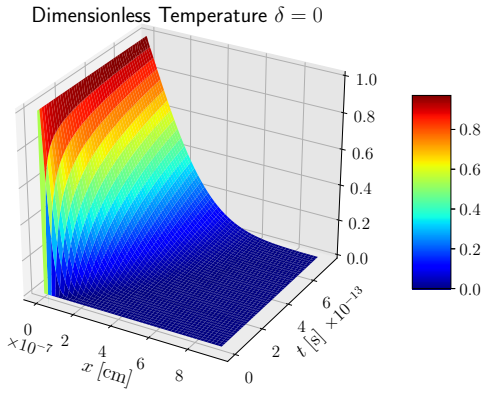

(a) $\delta = 0$

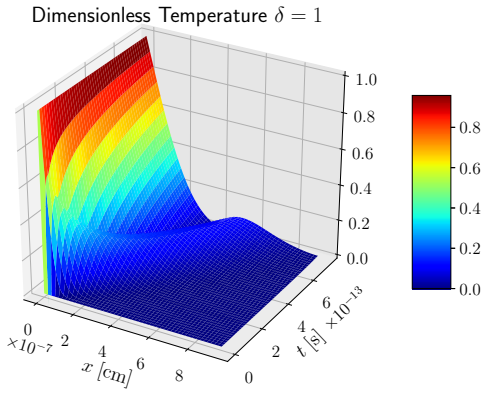

(b) $\delta = 1$

Figure 8.22: Temperature solution for the Danilovskaya problem.

Part IV

Port-Hamiltonian flexible multibody dynamics

Chapter 9

Modular multibody systems in port-Hamiltonian form

One of my earliest memories of something that caught my attention was of a steam locomotive. I guess mainly because they have so many moving parts that are out in the open. You can watch the valves moving back and forth — the driving rods.

Jim Peebles

Contents

In this chapter, the pH framework is combined with a floating frame description of the flexible dynamics under large rigid body displacements. Starting from the general equation for the rigid flexible dynamics of a floating body, an equivalent port-Hamiltonian system is found by appropriate selection of the canonical momenta. The flexible behavior is based on the linear elasticity assumption making it possible to include all kinds of linear models. The problem is then written as a coupled system of

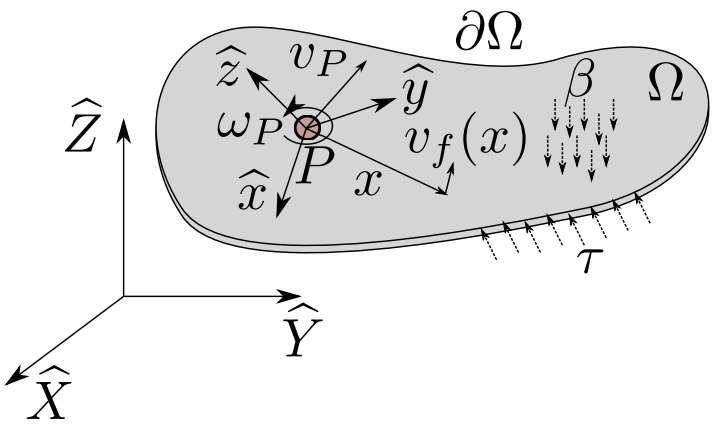

Figure 9.1: Thin floating body undergoing a surface traction $\boldsymbol{\tau}$ and body force density $\boldsymbol{\beta}$

ordinary and partial differential equations (ODEs and PDEs), extending the general definition of finite-dimensional port-Hamiltonian descriptor systems provided in [MM19]. The modularity feature of pH systems makes the proposed approach analogous to a substructuring technique: each individual component can be interconnected to the other bodies using standard interconnection of pH systems, as it is done in [MMS07]. This feature allows the use of modeling platforms like SIMULINK® or MODELICA®. The constraints are imposed on the velocities, leading to a quasi-linear index 2 differential-algebraic port-Hamiltonian system (pHDAE) [Ste06, BMXZ18]. In the linear case, the algebraic constraints can be eliminated, preserving the overall pH structure, using null space methods [LBS08]. As a floating frame formulation is used, model reduction techniques can be employed to lower the computational complexity of the model [CBG16, EKLS+18].

The chapter is organized in the following manner. In Section 9.1 the classical equations of a flexible floating body are recalled. Using the properties of the cross product, the equations are recast in a form closer to the pH structure. Section 9.2 details the pH formulation of a floating flexible body by introducing the proper canonical momenta. In Section 9.3 the PFEM is detailed for the elastodynamics problem. The procedure is easily extended to flexible floating bodies. The particular case of thin planar beams is detailed. Section 9.4 explains how to interconnect models together using classical pH interconnection.

9.1 Flexible dynamics of a floating body

The coupled ODE-PDE system representing the motion of a single flexible body is here recalled. Then, by exploiting the properties of the cross product, the system of equations is rephrased to highlight the port-Hamiltonian structure.

9.1.1 Classical model

Consider an open connected set $\Omega \subseteq \mathbb{R}^3$, representing a floating flexible body. The rigid dynamics is located at point P, that is not necessarily the center of mass. The velocity of a generic point is expressed by considering a small flexible displacement superimposed to the rigid motion

$$\boldsymbol{v} = \boldsymbol{v}_P + [\boldsymbol{\omega}_P]_\times \boldsymbol{x}_f + \boldsymbol{v}_f, \qquad \boldsymbol{x}_f := \boldsymbol{x} + \boldsymbol{u}_f,$$

where $\boldsymbol{x}$ is the position vector of the current point, $\boldsymbol{v}_P, \boldsymbol{\omega}_P$ are the linear and angular velocities of point P and $\boldsymbol{v}_f := \dot{\boldsymbol{u}}_f$ is the time derivative of the deformation displacement $\boldsymbol{u}_f$ (computed with respect to the body frame). These quantities are evaluated in the body reference frame $\widehat{\boldsymbol{x}}, \widehat{\boldsymbol{y}}, \widehat{\boldsymbol{z}}$ (see Fig. 9.1). The notation $[\boldsymbol{a}]_\times$ (cross map) denotes the skew-symmetric matrix associated to vector $\boldsymbol{a}$ (see Sec. A.4). The model for the classical equations derived using the least action principle can be found in [Sim06] and [Sim13, Chapter 4].

- Linear momentum balance:

$$\begin{aligned} &m\, {}^i\ddot{\boldsymbol{r}}_P + \boldsymbol{R}\,[\boldsymbol{s}_u]_\times^\top\, \dot{\boldsymbol{\omega}}_P + \boldsymbol{R}\int_\Omega \rho \ddot{\boldsymbol{u}}_f \,\mathrm{d}\Omega = \\ &\quad + \boldsymbol{R}\left\{ -[\boldsymbol{\omega}_P]_\times [\boldsymbol{\omega}_P]_\times \boldsymbol{s}_u - \int_\Omega 2\rho\,[\boldsymbol{\omega}_P]_\times \dot{\boldsymbol{u}}_f \,\mathrm{d}\Omega + \int_\Omega \boldsymbol{\beta}\,\mathrm{d}\Omega + \int_{\partial\Omega} \boldsymbol{\tau}\,\mathrm{d}\Gamma \right\} \end{aligned} \tag{9.1}$$

  where ρ is the mass density, $m = \int_\Omega \rho \,\mathrm{d}\Omega$ the total mass, $\boldsymbol{s}_u = \int_\Omega \rho \boldsymbol{x}_f \,\mathrm{d}\Omega$ the static moment. Vector ${}^i\boldsymbol{r}_P$ is the position of point P in the inertial frame and $\boldsymbol{R}$ is the rotation matrix that transforms vectors from the body frame to the inertial frame. Additionally, $\boldsymbol{\beta}$ is a density force and $\boldsymbol{\tau}$ is a surface traction, both expressed in the body reference frame.

- Angular momentum balance:

$$\begin{aligned} &[\boldsymbol{s}_u]_\times \boldsymbol{R}^\top\, {}^i\ddot{\boldsymbol{r}}_P + \boldsymbol{J}_u \dot{\boldsymbol{\omega}}_P + \int_\Omega \rho\,[\boldsymbol{x}_f]_\times \ddot{\boldsymbol{u}}_f \,\mathrm{d}\Omega + [\boldsymbol{\omega}_P]_\times \boldsymbol{J}_u \boldsymbol{\omega}_P = \\ &- \int_\Omega 2\rho\,[\boldsymbol{x}_f]_\times [\boldsymbol{\omega}_P]_\times \dot{\boldsymbol{u}}_f \,\mathrm{d}\Omega + \int_\Omega [\boldsymbol{x}_f]_\times \boldsymbol{\beta}\,\mathrm{d}\Omega + \int_{\partial\Omega} [\boldsymbol{x}_f]_\times \boldsymbol{\tau}\,\mathrm{d}\Gamma \end{aligned} \tag{9.2}$$

  where $\boldsymbol{J}_u := \int_\Omega \rho\,[\boldsymbol{x}_f]_\times^\top [\boldsymbol{x}_f]_\times \,\mathrm{d}\Omega = -\int_\Omega \rho\,[\boldsymbol{x}_f]_\times [\boldsymbol{x}_f]_\times \,\mathrm{d}\Omega$ is the inertia matrix.

- Flexibility PDE:

$$\rho \boldsymbol{R}^\top\, {}^i\ddot{\boldsymbol{r}}_P + \rho([\dot{\boldsymbol{\omega}}_P]_\times + [\boldsymbol{\omega}_P]_\times [\boldsymbol{\omega}_P]_\times)\boldsymbol{x}_f + \rho(2\,[\boldsymbol{\omega}_P]_\times \dot{\boldsymbol{u}}_f + \ddot{\boldsymbol{u}}_f) = \mathrm{Div}\,\boldsymbol{\Sigma} + \boldsymbol{\beta}, \tag{9.3}$$

  Variable $\boldsymbol{\Sigma}$ is the Cauchy stress tensor. From linear elasticity theory the infinitesimal strain is given by $\boldsymbol{\varepsilon} = \mathrm{Grad}(\boldsymbol{u}_f)$. The constitutive equation is expressed as $\boldsymbol{\Sigma} = \boldsymbol{\mathcal{D}}\boldsymbol{\varepsilon}$, where $\boldsymbol{\mathcal{D}}$ is the stiffness tensor (cf. Eq. (3.5)). This PDE requires the specifications of boundary conditions.

$$\begin{aligned} \boldsymbol{\Sigma}\cdot\boldsymbol{n}|_{\Gamma_N} &= \boldsymbol{\tau}|_{\Gamma_N}, \quad \boldsymbol{n} \text{ is the outward normal,} \\ \boldsymbol{u}_f|_{\Gamma_D} &= \bar{\boldsymbol{u}}_f|_{\Gamma_D}, \end{aligned} \tag{9.4}$$

The boundary $\partial\Omega = \overline{\Gamma}_D \cup \overline{\Gamma}_N$ is split into two subsets, one on which the surface traction is imposed (Γ_N Neumann condition) and the other where the flexible displacement is known (Γ_D Dirichlet condition).

9.1.2 Towards a port-Hamiltonian formulation

The gyroscopic terms in Eqs. (9.1), (9.2), (9.3) need some manipulations so that the skew-symmetric interconnection operator can be more easily highlighted. The following proposition shows that the classical equations can be rewritten in a more structured form.

Proposition 10
Denoting by $\boldsymbol{v}_f = \dot{\boldsymbol{u}}_f$ the derivative of the flexible displacement in the body frame, Equations. (9.1), (9.2), (9.3) can be equivalently reformulate as follows

- *Linear momentum balance:*

$$\begin{aligned} m\dot{\boldsymbol{v}}_P + [\boldsymbol{s}_u]_\times^\top \dot{\boldsymbol{\omega}}_P + \int_\Omega \rho\dot{\boldsymbol{v}}_f \,\mathrm{d}\Omega = \\ \left[m\boldsymbol{v}_P + [\boldsymbol{s}_u]_\times^\top \boldsymbol{\omega}_P + 2\int_\Omega \rho\boldsymbol{v}_f \,\mathrm{d}\Omega\right]_\times \boldsymbol{\omega}_P + \int_\Omega \boldsymbol{\beta}\,\mathrm{d}\Omega + \int_{\partial\Omega} \boldsymbol{\tau}\,\mathrm{d}\Gamma. \end{aligned} \tag{9.5}$$

- *Angular momentum balance:*

$$\begin{aligned} [\boldsymbol{s}_u]_\times \dot{\boldsymbol{v}}_P + \boldsymbol{J}_u\dot{\boldsymbol{\omega}}_P + \int_\Omega \rho\,[\boldsymbol{x}_f]_\times \dot{\boldsymbol{v}}_f \,\mathrm{d}\Omega = \\ \left[[\boldsymbol{s}_u]_\times^\top \boldsymbol{\omega}_P + 2\int_\Omega \rho\boldsymbol{v}_f \,\mathrm{d}\Omega\right]_\times \boldsymbol{v}_P + \left[[\boldsymbol{s}_u]_\times \boldsymbol{v}_P + \boldsymbol{J}_u\boldsymbol{\omega}_P + 2\int_\Omega \rho\,[\boldsymbol{x}_f]_\times \boldsymbol{v}_f \,\mathrm{d}\Omega\right]_\times \boldsymbol{\omega}_P + \\ 2\int_\Omega \left[\rho\boldsymbol{v}_P + \rho\,[\boldsymbol{x}_f]_\times^\top \boldsymbol{\omega}_P\right]_\times \boldsymbol{v}_f \,\mathrm{d}\Omega + \int_\Omega [\boldsymbol{x}_f]_\times \boldsymbol{\beta}\,\mathrm{d}\Omega + \int_{\partial\Omega} [\boldsymbol{x}_f]_\times \boldsymbol{\tau}\,\mathrm{d}\Gamma. \end{aligned} \tag{9.6}$$

- *Flexibility PDE:*

$$\rho\dot{\boldsymbol{v}}_P + \rho\,[\boldsymbol{x}_f]_\times^\top \dot{\boldsymbol{\omega}}_P + \rho\dot{\boldsymbol{v}}_f = \left[\rho\boldsymbol{v}_P + \rho\,[\boldsymbol{x}_f]_\times^\top \boldsymbol{\omega}_P + 2\rho\boldsymbol{v}_f\right]_\times \boldsymbol{\omega}_P + \mathrm{Div}\,\boldsymbol{\Sigma} + \boldsymbol{\beta}. \tag{9.7}$$

Proof. Equation (9.1) is written in the inertial frame and so it needs to be projected in the body frame. Considering that the position of point P, i.e. ${}^i\boldsymbol{r}_P$, is computed in the inertial frame and $\boldsymbol{v}_P$ in the body frame, it holds ${}^i\dot{\boldsymbol{r}}_P = \boldsymbol{R}\boldsymbol{v}_P$. The derivative of this expression gives

$${}^i\ddot{\boldsymbol{r}}_P = \boldsymbol{R}\left(\dot{\boldsymbol{v}}_P + [\boldsymbol{\omega}_P]_\times \boldsymbol{v}_P\right) \tag{9.8}$$

If (9.8) is put into (9.1), (9.2) and (9.3) and pre-multiplying Eq. (9.1) by $\boldsymbol{R}^\top$, it is obtained.

- Linear momentum balance:

$$\begin{aligned} m(\dot{\boldsymbol{v}}_P + [\boldsymbol{\omega}_P]_\times \boldsymbol{v}_P) + [\boldsymbol{s}_u]_\times^\top \dot{\boldsymbol{\omega}}_P + \int_\Omega \rho \dot{\boldsymbol{v}}_f \, \mathrm{d}\Omega = \\ - [\boldsymbol{\omega}_P]_\times [\boldsymbol{\omega}_P]_\times \boldsymbol{s}_u - \int_\Omega 2\rho [\boldsymbol{\omega}_P]_\times \boldsymbol{v}_f \, \mathrm{d}\Omega + \int_\Omega \boldsymbol{\beta} \, \mathrm{d}\Omega + \int_{\partial\Omega} \boldsymbol{\tau} \, \mathrm{d}\Gamma. \end{aligned} \tag{9.9}$$

- Angular momentum balance:

$$\begin{aligned} [\boldsymbol{s}_u]_\times (\dot{\boldsymbol{v}}_P + [\boldsymbol{\omega}_P]_\times \boldsymbol{v}_P) + \boldsymbol{J}_u \dot{\boldsymbol{\omega}}_P + \int_\Omega \rho [\boldsymbol{x}_f]_\times \dot{\boldsymbol{v}}_f \, \mathrm{d}\Omega + [\boldsymbol{\omega}_P]_\times \boldsymbol{J}_u \boldsymbol{\omega}_P = \\ - \int_\Omega 2\rho [\boldsymbol{x}_f]_\times [\boldsymbol{\omega}_P]_\times \boldsymbol{v}_f \, \mathrm{d}\Omega + \int_\Omega [\boldsymbol{x}_f]_\times \boldsymbol{\beta} \, \mathrm{d}\Omega + \int_{\partial\Omega} [\boldsymbol{x}_f]_\times \boldsymbol{\tau} \, \mathrm{d}\Gamma. \end{aligned} \tag{9.10}$$

- Flexibility PDE:

$$\rho(\dot{\boldsymbol{v}}_P + [\boldsymbol{\omega}_P]_\times \boldsymbol{v}_P) + \rho([\dot{\boldsymbol{\omega}}_P]_\times + [\boldsymbol{\omega}_P]_\times [\boldsymbol{\omega}_P]_\times)\boldsymbol{x}_f + \rho(2[\boldsymbol{\omega}_P]_\times \boldsymbol{v}_f + \dot{\boldsymbol{v}}_f) = \mathrm{Div}\, \boldsymbol{\Sigma} + \boldsymbol{\beta}, \tag{9.11}$$

Consider now the term $[\boldsymbol{\omega}_P]_\times [\boldsymbol{\omega}_P]_\times \boldsymbol{s}_u$, appearing in (9.9). Using the anticommutativity (A.12) and the fact that the cross map is skew-symmetric $[\boldsymbol{a}]_\times = -[\boldsymbol{a}]_\times^\top$ one finds

$$- [\boldsymbol{\omega}_P]_\times [\boldsymbol{\omega}_P]_\times \boldsymbol{s}_u = \left[[\boldsymbol{s}_u]_\times^\top \boldsymbol{\omega}_P\right]_\times \boldsymbol{\omega}_P.$$

Eq. (9.9) is then rewritten as

$$m\dot{\boldsymbol{v}}_P + [\boldsymbol{s}_u]_\times^\top \dot{\boldsymbol{\omega}}_P + \int_\Omega \rho \dot{\boldsymbol{v}}_f \, \mathrm{d}\Omega = \left[m\boldsymbol{v}_P + [\boldsymbol{s}_u]_\times^\top \boldsymbol{\omega}_P + 2\int_\Omega \rho \boldsymbol{v}_f \, \mathrm{d}\Omega\right]_\times \boldsymbol{\omega}_P + \int_\Omega \boldsymbol{\beta} \, \mathrm{d}\Omega + \int_{\partial\Omega} \boldsymbol{\tau} \, \mathrm{d}\Gamma. \tag{9.12}$$

The terms $[\boldsymbol{s}_u]_\times [\boldsymbol{\omega}_P]_\times \boldsymbol{v}_P$, $2\rho [\boldsymbol{x}_f]_\times [\boldsymbol{\omega}_P]_\times \boldsymbol{v}_f$, appearing in (9.10) can be rewritten using the Jacobi identity (A.13)

$$[\boldsymbol{s}_u]_\times [\boldsymbol{\omega}_P]_\times \boldsymbol{v}_P = - \left[[\boldsymbol{s}_u]_\times \boldsymbol{v}_P\right]_\times \boldsymbol{\omega}_P - \left[[\boldsymbol{s}_u]_\times^\top \boldsymbol{\omega}_P\right]_\times \boldsymbol{v}_P, \tag{9.13}$$

$$2\rho [\boldsymbol{x}_f]_\times [\boldsymbol{\omega}_P]_\times \boldsymbol{v}_f = -2\rho \left[[\boldsymbol{x}_f]_\times \boldsymbol{v}_f\right]_\times \boldsymbol{\omega}_P - 2\rho \left[[\boldsymbol{x}_f]_\times^\top \boldsymbol{\omega}_P\right]_\times \boldsymbol{v}_f \tag{9.14}$$

Eq. (9.10) is then rewritten as

$$\begin{aligned} [\boldsymbol{s}_u]_\times \dot{\boldsymbol{v}}_P + \boldsymbol{J}_u \dot{\boldsymbol{\omega}}_P + \int_\Omega \rho [\boldsymbol{x}_f]_\times \dot{\boldsymbol{v}}_f \, \mathrm{d}\Omega = \\ \left[[\boldsymbol{s}_u]_\times^\top \boldsymbol{\omega}_P + 2\int_\Omega \rho \boldsymbol{v}_f \, \mathrm{d}\Omega\right]_\times \boldsymbol{v}_P + \left[[\boldsymbol{s}_u]_\times \boldsymbol{v}_P + \boldsymbol{J}_u \boldsymbol{\omega}_P + 2\int_\Omega \rho [\boldsymbol{x}_f]_\times \boldsymbol{v}_f \, \mathrm{d}\Omega\right]_\times \boldsymbol{\omega}_P + \\ 2\int_\Omega \left[\rho \boldsymbol{v}_P + \rho [\boldsymbol{x}_f]_\times^\top \boldsymbol{\omega}_P\right]_\times \boldsymbol{v}_f \, \mathrm{d}\Omega + \int_\Omega [\boldsymbol{x}_f]_\times \boldsymbol{\beta} \, \mathrm{d}\Omega + \int_{\partial\Omega} [\boldsymbol{x}_f]_\times \boldsymbol{\tau} \, \mathrm{d}\Gamma. \end{aligned} \tag{9.15}$$

Notice that the term $2[\boldsymbol{v}_f]_\times \boldsymbol{v}_P + 2[\boldsymbol{v}_P]_\times \boldsymbol{v}_f = 0$ has been added to the equation. Using again the anticommutativity Eq. (9.11) is expressed as

$$\rho\dot{\boldsymbol{v}}_P + \rho [\boldsymbol{x}_f]_\times^\top \dot{\boldsymbol{\omega}}_P + \rho\dot{\boldsymbol{v}}_f = \left[\rho\boldsymbol{v}_P + \rho [\boldsymbol{x}_f]_\times^\top \boldsymbol{\omega}_P + 2\rho\boldsymbol{v}_f\right]_\times \boldsymbol{\omega}_P + \mathrm{Div}\, \boldsymbol{\Sigma} + \boldsymbol{\beta}. \tag{9.16}$$

Indeed, Eqs. (9.12), (9.15), (9.16) are exactly (9.5), (9.6), (9.7). □

By introducing the appropriate momenta, Eqs. (9.5), (9.6), (9.7) can be reformulated as a pH system as illustrated in the following section.

9.2 Elastic body under large rigid motion as a pH system

In this section the flexible dynamics of a floating body is written as a coupled system of ODEs and PDEs in pH form. The final form is a descriptor port-Hamiltonian system that fits and generalizes the framework detailed in [BMXZ18, MM19].

9.2.1 Energies and canonical momenta

Consider the total energy (Hamiltonian), given by the sum of kinetic and deformation energy:

$$H = H_{\text{kin}} + H_{\text{def}} = \frac{1}{2}\int_\Omega \left\{\rho||\boldsymbol{v}_P + [\boldsymbol{\omega}_P]_\times \boldsymbol{x}_f + \boldsymbol{v}_f||^2 + \boldsymbol{\Sigma} : \boldsymbol{\varepsilon}\right\} \,\mathrm{d}\Omega. \tag{9.17}$$

The inner product $\boldsymbol{A} : \boldsymbol{B} = \mathrm{Tr}(\boldsymbol{A}\boldsymbol{B}^T)$ is the tensor contraction. The momenta (usually called energy variables in the pH framework) are then computed by derivation of the Hamiltonian. As the variables belong to finite- and infinite-dimensional spaces the derivative is either a classical gradient or a variational derivative:

$$\begin{aligned}
\boldsymbol{p}_t &:= \frac{\partial H}{\partial \boldsymbol{v}_P} = m\boldsymbol{v}_P + [\boldsymbol{s}_u]_\times^\top \boldsymbol{\omega}_P + \int_\Omega \rho \boldsymbol{v}_f \,\mathrm{d}\Omega,\\
\boldsymbol{p}_r &:= \frac{\partial H}{\partial \boldsymbol{\omega}_P} = [\boldsymbol{s}_u]_\times \boldsymbol{v}_P + \boldsymbol{J}_u\boldsymbol{\omega}_P + \int_\Omega \rho\,[\boldsymbol{x}_f]_\times \boldsymbol{v}_f \,\mathrm{d}\Omega,\\
\boldsymbol{p}_f &:= \frac{\delta H}{\delta \boldsymbol{v}_f} = \rho\boldsymbol{v}_P + \rho\,[\boldsymbol{x}_f]_\times^\top \boldsymbol{\omega}_P + \rho\boldsymbol{v}_f,\\
\boldsymbol{\varepsilon} &:= \frac{\delta H}{\delta \boldsymbol{\Sigma}} = \boldsymbol{\mathcal{D}}^{-1}\boldsymbol{\Sigma} = \boldsymbol{\mathcal{C}}\boldsymbol{\Sigma},
\end{aligned} \tag{9.18}$$

where the last derivative is computed with respect to a tensor and $\boldsymbol{\mathcal{C}}$ is the compliance tensor (3.6). The relation between energy and co-energy variables is then given by

$$\begin{bmatrix}\boldsymbol{p}_t\\ \boldsymbol{p}_r\\ \boldsymbol{p}_f\\ \boldsymbol{\varepsilon}\end{bmatrix} = \underbrace{\begin{bmatrix} m\boldsymbol{I}_{3\times 3} & [\boldsymbol{s}_u]_\times^\top & \mathcal{I}_\rho^\Omega & 0\\ [\boldsymbol{s}_u]_\times & \boldsymbol{J}_u & \boldsymbol{\mathcal{I}}_{\rho x}^\Omega & 0\\ (\mathcal{I}_\rho^\Omega)^* & (\boldsymbol{\mathcal{I}}_{\rho x}^\Omega)^* & \rho & 0\\ 0 & 0 & 0 & \boldsymbol{\mathcal{C}}\end{bmatrix}}_{\mathcal{M}\text{: Mass operator}} \begin{bmatrix}\boldsymbol{v}_P\\ \boldsymbol{\omega}_P\\ \boldsymbol{v}_f\\ \boldsymbol{\Sigma}\end{bmatrix}, \tag{9.19}$$

where $\boldsymbol{I}_{3\times3}$ is the identity matrix in $\mathbb{R}^3$. The operators are defined as

$$\mathcal{I}_\rho^\Omega := \int_\Omega \rho(\cdot)\,\mathrm{d}\Omega, \qquad \boldsymbol{\mathcal{I}}_{\rho x}^\Omega := \int_\Omega \rho\,[\boldsymbol{x}_f]_\times\,(\cdot)\,\mathrm{d}\Omega,$$
$$(\mathcal{I}_\rho^\Omega)^* = \rho, \qquad (\boldsymbol{\mathcal{I}}_{\rho x}^\Omega)^* = \rho\,[\boldsymbol{x}_f]_\times^\top = -\rho\,[\boldsymbol{x}_f]_\times.$$

The mass operator $\mathcal{M}$ is a self-adjoint, positive operator. The kinetic and deformation energy can then be written as

$$H_{\mathrm{kin}} + H_{\mathrm{def}} = \frac{1}{2}\left\langle \boldsymbol{e}_{\mathrm{kd}},\, \mathcal{M}\boldsymbol{e}_{\mathrm{kd}}\right\rangle_{X_{\mathrm{kd}}} \tag{9.20}$$

where $\boldsymbol{e}_{\mathrm{kd}} = [\boldsymbol{v}_P;\, \boldsymbol{\omega}_P;\, \boldsymbol{v}_f; \boldsymbol{\Sigma}]$ and the inner product $\langle\cdot,\,\cdot\rangle_{X_{\mathrm{kd}}}$ is taken over the space

$$X_{\mathrm{kd}} = \mathbb{R}^3 \times \mathbb{R}^3 \times L^2(\Omega, \mathbb{R}^3) \times L^2(\Omega, \mathbb{R}^{3\times3}_{\mathrm{sym}})$$

Notice that the kinetic energy also depends on the flexible displacement

$$\frac{\delta H_{\mathrm{kin}}}{\delta \boldsymbol{u}_f} = [\boldsymbol{p}_f]_\times\,\boldsymbol{\omega}_P.$$

This term is responsible for a coupling between the kinematic coordinates and the velocities, as will be clear in the following section.

9.2.2 Port-Hamiltonian formulation

In order to get a complete formulation, generalized coordinates are required. It is natural to select the following variables:

- ${}^i\boldsymbol{r}_P$ the position of point P in the inertial frame of reference;
- $\boldsymbol{R}$ the direction cosine matrix that transforms vectors from the body frame to the inertial frame (other attitude parametrizations are possible, here the direction cosine matrix is considered for ease of presentation);
- $\boldsymbol{u}_f$ the flexible displacement;

In particular, following [FJL15], the direction cosine matrix is converted into a vector by concatenating its rows

$$\boldsymbol{R}_{\mathrm{v}} = \mathrm{vec}(\boldsymbol{R}^\top) = [\boldsymbol{R}_x\ \boldsymbol{R}_y\ \boldsymbol{R}_z]^\top,$$

where $\boldsymbol{R}_x, \boldsymbol{R}_y, \boldsymbol{R}_z$ are the first, second and third row of matrix $\boldsymbol{R}$. Furthermore the corresponding cross map will be given by

$$[\boldsymbol{R}_{\mathrm{v}}]_\times = \begin{bmatrix} [\boldsymbol{R}_x]_\times \\ [\boldsymbol{R}_y]_\times \\ [\boldsymbol{R}_z]_\times \end{bmatrix}, \qquad [\boldsymbol{R}_{\mathrm{v}}]_\times \in \mathbb{R}^{9\times3}.$$

The overall port-Hamiltonian formulation, equivalent to Eqs. (9.5), (9.5), (9.5), is then (omitting the external forces and torques)

$$\underbrace{\left[\begin{array}{c:c} \boldsymbol{I} & \boldsymbol{0} \\ \hdashline \boldsymbol{0} & \mathcal{M} \end{array}\right]}_{\mathcal{E}} \frac{\partial}{\partial t} \underbrace{\begin{pmatrix} {}^{i}\boldsymbol{r}_P \\ \boldsymbol{R}_{\mathrm{v}} \\ \boldsymbol{u}_f \\ \hdashline \boldsymbol{v}_P \\ \boldsymbol{\omega}_P \\ \boldsymbol{v}_f \\ \boldsymbol{\Sigma} \end{pmatrix}}_{e} = \underbrace{\left[\begin{array}{ccc:cccc} \boldsymbol{0} & \boldsymbol{0} & \boldsymbol{0} & \boldsymbol{R} & \boldsymbol{0} & \boldsymbol{0} & \boldsymbol{0} \\ \boldsymbol{0} & \boldsymbol{0} & \boldsymbol{0} & \boldsymbol{0} & [\boldsymbol{R}_{\mathrm{v}}]_\times & \boldsymbol{0} & \boldsymbol{0} \\ \boldsymbol{0} & \boldsymbol{0} & \boldsymbol{0} & \boldsymbol{0} & \boldsymbol{0} & \boldsymbol{I}_{3\times 3} & \boldsymbol{0} \\ \hdashline -\boldsymbol{R}^\top & \boldsymbol{0} & \boldsymbol{0} & \boldsymbol{0} & [\widehat{\boldsymbol{p}}_t]_\times & \boldsymbol{0} & \boldsymbol{0} \\ \boldsymbol{0} & -[\boldsymbol{R}_{\mathrm{v}}]_\times^\top & \boldsymbol{0} & [\widehat{\boldsymbol{p}}_t]_\times & [\widehat{\boldsymbol{p}}_r]_\times & \mathcal{I}_{p_f}^{\Omega} & \boldsymbol{0} \\ \boldsymbol{0} & \boldsymbol{0} & -\boldsymbol{I}_{3\times 3} & \boldsymbol{0} & -(\mathcal{I}_{p_f}^{\Omega})^* & \boldsymbol{0} & \mathrm{Div} \\ \boldsymbol{0} & \boldsymbol{0} & \boldsymbol{0} & \boldsymbol{0} & \boldsymbol{0} & \mathrm{Grad} & \boldsymbol{0} \end{array}\right]}_{\mathcal{J}} \underbrace{\begin{pmatrix} \partial_{\boldsymbol{r}_P} H \\ \partial_{\boldsymbol{R}_{\mathrm{v}}} H \\ \delta_{\boldsymbol{u}_f} H \\ \hdashline \boldsymbol{v}_P \\ \boldsymbol{\omega}_P \\ \boldsymbol{v}_f \\ \boldsymbol{\Sigma} \end{pmatrix}}_{z}. \tag{9.21}$$

Variables $\widehat{\boldsymbol{p}}_t, \widehat{\boldsymbol{p}}_r$ are defined as

$$\begin{aligned} \widehat{\boldsymbol{p}}_t &= \boldsymbol{p}_t + \int_\Omega \rho \boldsymbol{v}_f \, \mathrm{d}\Omega, \\ \widehat{\boldsymbol{p}}_r &= \boldsymbol{p}_r + \int_\Omega \rho \, [\boldsymbol{x}_f]_\times \, \boldsymbol{v}_f \, \mathrm{d}\Omega. \end{aligned} \tag{9.22}$$

The operator $\mathcal{I}_{p_f}^{\Omega}$ is defined as

$$\mathcal{I}_{p_f}^{\Omega} := \int_\Omega \left\{ 2\,[\boldsymbol{p}_f]_\times + \rho\,[\boldsymbol{v}_f]_\times \right\} (\cdot) \, \mathrm{d}\Omega. \tag{9.23}$$

Its adjoint is given by

$$(\mathcal{I}_{p_f}^{\Omega})^* = \left\{ 2\,[\boldsymbol{p}_f]_\times^\top + \rho\,[\boldsymbol{v}_f]_\times^\top \right\} (\cdot) = -\left\{ 2\,[\boldsymbol{p}_f]_\times + \rho\,[\boldsymbol{v}_f]_\times \right\} (\cdot).$$

The coefficient 2 is required to compensate the contribution given by $\delta_{\boldsymbol{u}_f} H$

$$-\frac{\delta H}{\delta \boldsymbol{u}_f} - (\mathcal{I}_{p_f}^{\Omega})^* \boldsymbol{\omega}_P = \left[\rho\,[\boldsymbol{v}_P]_\times + \rho \left[[\boldsymbol{x}_f]_\times^\top \boldsymbol{\omega}_P \right]_\times + 2\rho\,[\boldsymbol{v}_f]_\times \right] \boldsymbol{\omega}_P.$$

The additional terms related to $\rho \boldsymbol{v}_f$ are associated to the Coriolis accelerations that affect the deformation field. System (9.21) fits into the framework detailed in [MM19] and extends it, since a coupled system of ODEs and PDEs is considered. The operator $\boldsymbol{\mathcal{J}}$ is skew-symmetric $\boldsymbol{\mathcal{J}}^* = -\boldsymbol{\mathcal{J}}$ over the Hilbert space

$$X = \mathbb{R}^3 \times \mathbb{R}^9 \times L^2(\Omega, \mathbb{R}^3) \times \mathbb{R}^3 \times \mathbb{R}^3 \times L^2(\Omega, \mathbb{R}^3) \times L^2(\Omega, \mathbb{R}^{3\times 3}_{\mathrm{sym}}).$$

The dynamics can be rewritten compactly as follows

$$\begin{aligned}\mathcal{E}(\boldsymbol{e})\frac{\partial \boldsymbol{e}}{\partial t} &= \mathcal{J}(\boldsymbol{e})\boldsymbol{z}(\boldsymbol{e}) + \mathcal{B}_\Omega(\boldsymbol{e})\boldsymbol{u}_\Omega + \mathcal{B}_r(\boldsymbol{e})\boldsymbol{u}_\partial,\\ \boldsymbol{y}_\Omega &= \mathcal{B}_\Omega^*(\boldsymbol{e})\boldsymbol{z}(\boldsymbol{e}),\\ \boldsymbol{y}_r &= \mathcal{B}_r^*(\boldsymbol{e})\boldsymbol{z}(\boldsymbol{e}),\\ \boldsymbol{u}_\partial &= \mathcal{B}_\partial \boldsymbol{z}(\boldsymbol{e}) = \boldsymbol{\Sigma}\cdot\boldsymbol{n}|_{\partial\Omega} = \boldsymbol{\tau}|_{\partial\Omega},\\ \boldsymbol{y}_\partial &= \mathcal{C}_\partial \boldsymbol{z}(\boldsymbol{e}) = \boldsymbol{v}_f|_{\partial\Omega},\end{aligned} \tag{9.24}$$

where $\boldsymbol{u}_\Omega = \boldsymbol{\beta}$. Using definitions (9.18), it follows that the Hamiltonian satisfies

$$\partial_{\boldsymbol{e}} H = \boldsymbol{\mathcal{E}}^* \boldsymbol{z}. \tag{9.25}$$

Adopting the same nomenclature as in [MM19], $\boldsymbol{e}$ contains the state and $\boldsymbol{z}$ contains the effort functions. The operators verify $\mathcal{E} = \mathcal{E}^*$, $\mathcal{J} = -\mathcal{J}^*$. The control operators are expressed as

$$\begin{aligned}\mathcal{B}_\Omega &= \begin{bmatrix}\boldsymbol{0} & \boldsymbol{0} & \boldsymbol{0} & \mathcal{I}^\Omega & \boldsymbol{\mathcal{I}}_x^\Omega & \boldsymbol{I} & \boldsymbol{0}\end{bmatrix}^\top,\\ \mathcal{B}_r &= \begin{bmatrix}\boldsymbol{0} & \boldsymbol{0} & \boldsymbol{0} & \mathcal{I}^\Gamma & \boldsymbol{\mathcal{I}}_x^\Gamma & \boldsymbol{0} & \boldsymbol{0}\end{bmatrix}^\top,\end{aligned}$$

where

$$\begin{aligned}\mathcal{I}^\Omega &:= \int_\Omega (\cdot)\,\mathrm{d}\Omega, \qquad & \boldsymbol{\mathcal{I}}_x^\Omega &:= \int_\Omega [\boldsymbol{x}_f]_\times (\cdot)\,\mathrm{d}\Omega,\\ \mathcal{I}^\Gamma &:= \int_{\partial\Omega} (\cdot)\,\mathrm{d}\Gamma, \qquad & \boldsymbol{\mathcal{I}}_x^\Gamma &:= \int_{\partial\Omega} [\boldsymbol{x}_f]_\times (\cdot)\,\mathrm{d}\Gamma.\end{aligned}$$

The distributed control operator $\mathcal{B}_\Omega$ is compact. The boundary traction force acts on the rigid part through the compact operator $\mathcal{B}_r$. Notice that by definition of adjoint (see Appendix A), the vector $\boldsymbol{y}_r$ represents the rigid body velocity at the boundary

$$\boldsymbol{y}_r = (\boldsymbol{v}_P + [\boldsymbol{x}_f]_\times^\top \boldsymbol{\omega}_P)|_{\partial\Omega},$$

while $\boldsymbol{y}_\Omega$ represents the velocity field in the domain

$$\boldsymbol{y}_\Omega = \boldsymbol{v}_P + [\boldsymbol{x}_f]_\times^\top \boldsymbol{\omega}_P + \boldsymbol{v}_f.$$

The power balance is naturally embedded in the dynamics

$$\begin{aligned}\dot{H}(\boldsymbol{e}) &= \langle \partial_{\boldsymbol{e}} H, \partial_t \boldsymbol{e}\rangle_X = \langle \mathcal{E}^*\boldsymbol{z}, \partial_t \boldsymbol{e}\rangle_X,\\ &= \langle \boldsymbol{z}, \mathcal{E}\partial_t \boldsymbol{e}\rangle_X, \quad \text{Adjoint definition},\\ &= \langle \boldsymbol{z}, \mathcal{J}\boldsymbol{z} + \mathcal{B}_d(\boldsymbol{e})\boldsymbol{u}_d + \mathcal{B}_r(\boldsymbol{e})\boldsymbol{u}_\partial\rangle_X,\\ &= \langle \boldsymbol{y}_\partial, \boldsymbol{u}_\partial\rangle_{L^2(\partial\Omega,\mathbb{R}^3)} + \langle \mathcal{B}_d^*\boldsymbol{z}, \boldsymbol{u}_d\rangle_X + \langle \mathcal{B}_r^*\boldsymbol{z}, \boldsymbol{u}_\partial\rangle_X, \quad \text{I.B.P. on } \mathcal{J},\\ &= \langle \boldsymbol{y}_\partial + \boldsymbol{y}_r, \boldsymbol{u}_\partial\rangle_{L^2(\partial\Omega,\mathbb{R}^3)} + \langle \boldsymbol{y}_d, \boldsymbol{u}_d\rangle_{L^2(\Omega,\mathbb{R}^3)},\end{aligned} \tag{9.26}$$

where the integration by parts (Stokes theorem) has been used

$$\int_\Omega \boldsymbol{\Sigma} : \mathrm{Grad}(\boldsymbol{v}_f)\ \mathrm{d}\Omega + \int_\Omega \mathrm{Div}(\boldsymbol{\Sigma}) \cdot \boldsymbol{v}_f\ \mathrm{d}\Omega = \int_{\partial\Omega} (\boldsymbol{\Sigma} \cdot \boldsymbol{n}) \cdot \boldsymbol{v}_f\ \mathrm{d}\Gamma = \langle \boldsymbol{y}_\partial, \boldsymbol{u}_\partial \rangle_{L^2(\partial\Omega,\mathbb{R}^3)}. \quad (9.27)$$

The power balance equals the power due to body force and surface traction

$$\begin{aligned} \dot{H}(\boldsymbol{e}) &= \int_{\partial\Omega} \boldsymbol{\tau} \cdot \boldsymbol{v}\ \mathrm{d}\Gamma + \int_\Omega \boldsymbol{\beta} \cdot \boldsymbol{v}\ \mathrm{d}\Omega, \qquad \boldsymbol{v} := \boldsymbol{v}_P + [\boldsymbol{\omega}_P]_\times \boldsymbol{x}_f + \boldsymbol{v}_f, \\ &= \int_{\partial\Omega} \boldsymbol{u}_\partial \cdot \boldsymbol{v}\ \mathrm{d}\Gamma + \int_\Omega \boldsymbol{u}_\Omega \cdot \boldsymbol{v}\ \mathrm{d}\Omega. \end{aligned} \quad (9.28)$$

Remark 24
Even if three dimensional elasticity has been taken as example up to this point, other models are easily considered. Beam and plate models are described by appropriate differential operators that replace the Div, Grad *appearing in* (9.21) *(see §9.3.3). For example in the case of the Kirchhoff plate the three-dimensional divergence is replaced by a planar divergence for the membrane behavior and a double divergence for the flexural behavior.*

Remark 25
Conservative forces are easily accounted for by introducing an appropriate potential energy. For example if the gravity force is considered, the corresponding potential energy reads

$$H_{\mathrm{pot}} = \int_\Omega \rho g\, {}^i r_z\ \mathrm{d}\Omega = \int_\Omega \rho g \left[{}^i r_{P,z} + \boldsymbol{R}_z \boldsymbol{x}_f \right]\ \mathrm{d}\Omega,$$

where ${}^i r_z$ *is the vertical location of a generic point computed in the inertial frame. The associated co-energy variables are easily obtained*

$$\begin{aligned} &\partial_{\boldsymbol{r}_P} H_{\mathrm{pot}} = mg\, \widehat{\boldsymbol{Z}}, \quad \widehat{\boldsymbol{Z}} \text{ is the inertial frame vertical direction}, \\ &\partial_{\boldsymbol{R}_{\mathrm{v}}} H_{\mathrm{pot}} = [\boldsymbol{0}_{(3,1)},\ \boldsymbol{0}_{(3,1)},\ \int_\Omega \rho g \boldsymbol{x}_f^\top\ \mathrm{d}\Omega]^\top, \\ &\delta_{\boldsymbol{u}_f} H_{\mathrm{pot}} = \rho g\, \boldsymbol{R}_z^\top. \end{aligned}$$

These contributions correspond to the forcing terms due to gravity.

Remark 26
The linear elasticity hypothesis does not allow including the effect of non-linearities due to large deformations. However, geometric stiffening could be considered by adding a potential energy associated to centrifugal forces [YSGU88].

Remark 27
If case of vanishing deformations $\boldsymbol{u}_f \equiv 0$*, the Newton-Euler equations on the Euclidean group*

$SE(3)$ are retrieved [CHR18]

$$\frac{d}{dt}\begin{pmatrix} {}^i\boldsymbol{r}_P \\ \boldsymbol{R}_\mathrm{v} \\ \boldsymbol{p}_t \\ \boldsymbol{p}_r \end{pmatrix} = \begin{bmatrix} \mathbf{0} & \mathbf{0} & \boldsymbol{R} & \mathbf{0} \\ \mathbf{0} & \mathbf{0} & \mathbf{0} & [\boldsymbol{R}_\mathrm{v}]_\times \\ -\boldsymbol{R}^\top & \mathbf{0} & \mathbf{0} & [\boldsymbol{p}_t]_\times \\ \mathbf{0} & -[\boldsymbol{R}_\mathrm{v}]_\times^\top & [\boldsymbol{p}_t]_\times & [\boldsymbol{p}_r]_\times \end{bmatrix} \begin{pmatrix} \partial_{\boldsymbol{r}_P} H \\ \partial_{\boldsymbol{R}_\mathrm{v}} H \\ \boldsymbol{v}_P \\ \boldsymbol{\omega}_P \end{pmatrix},$$

where

$$\begin{pmatrix} \boldsymbol{p}_t \\ \boldsymbol{p}_r \end{pmatrix} = \begin{bmatrix} m\boldsymbol{I} & [\boldsymbol{s}]_\times^\top \\ [\boldsymbol{s}]_\times & \boldsymbol{J} \end{bmatrix} \begin{pmatrix} \boldsymbol{v}_P \\ \boldsymbol{\omega}_P \end{pmatrix}, \qquad \boldsymbol{p} = \boldsymbol{M}\boldsymbol{v}.$$

The kinetic energy is then given by $H_\mathrm{kin} = \frac{1}{2}\boldsymbol{v}^\top \boldsymbol{M}\boldsymbol{v}$. This system can be written in standard pH form as $\dot{\boldsymbol{x}} = \boldsymbol{J}(\boldsymbol{x})\partial_{\boldsymbol{x}} H$.

9.3 Discretization procedure

To discretize the equation, the dual mixed formulation 7.3 is used to highlight as boundary control the Neumann condition. This means that the forces at the boundary appear as inputs. The uncontrolled system corresponds to the free conditions, meaning that the body is floating.

9.3.1 Illustration for the Elastodynamics problem

Recall the port-Hamiltonian representation in co-energy variables of linear elasticity 3.16

$$\underbrace{\begin{bmatrix} \rho & \mathbf{0} \\ \mathbf{0} & \boldsymbol{\mathcal{C}} \end{bmatrix}}_{\mathcal{M}} \frac{\partial}{\partial t}\begin{pmatrix} \boldsymbol{e}_v \\ \boldsymbol{E}_\varepsilon \end{pmatrix} = \underbrace{\begin{bmatrix} \mathbf{0} & \mathrm{Div} \\ \mathrm{Grad} & \mathbf{0} \end{bmatrix}}_{\mathcal{J}} \begin{pmatrix} \boldsymbol{e}_v \\ \boldsymbol{E}_\varepsilon \end{pmatrix} + \underbrace{\begin{bmatrix} \boldsymbol{I} \\ \mathbf{0} \end{bmatrix}}_{\mathcal{B}_\Omega} \boldsymbol{u}_\Omega,$$

where $\boldsymbol{u}_\Omega$ corresponds to a distributed force. Assuming Neumann boundary conditions (the normal traction $\boldsymbol{\tau}$ is known at the boundary), this system can be written compactly as a boundary control system

$$\begin{aligned} \mathcal{M}\frac{\partial \boldsymbol{e}}{\partial t} &= \mathcal{J}\boldsymbol{e} + \mathcal{B}_\Omega \boldsymbol{u}_\Omega, \\ \boldsymbol{y}_\Omega &= \mathcal{B}_\Omega^* \boldsymbol{e}, \\ \boldsymbol{u}_\partial &= \boldsymbol{E}_2 \cdot \boldsymbol{n}|_{\partial\Omega}, \\ \boldsymbol{y}_\partial &= \boldsymbol{e}_1|_{\partial\Omega}. \end{aligned} \tag{9.29}$$

The system is defined over the state space

$$X = L^2(\Omega, \mathbb{R}^3) \times L^2(\Omega, \mathbb{R}^{3\times 3}_\mathrm{sym}).$$

The total energy is then computed as an inner product modulated by the mass operator $H = \frac{1}{2}\langle \boldsymbol{e},\ \boldsymbol{\mathcal{M}}\boldsymbol{e}\rangle_X$.The power balance is computed by applying the Stokes theorem (9.27)

$$\dot{H} = \langle \boldsymbol{e}, \mathcal{M}\partial_t \boldsymbol{e}\rangle_X = \langle \boldsymbol{y}_\partial, \boldsymbol{u}_\partial\rangle_{L^2(\partial\Omega,\mathbb{R}^3)} + \langle \boldsymbol{y}_\Omega, \boldsymbol{u}_\Omega\rangle_{L^2(\Omega,\mathbb{R}^3)}. \tag{9.30}$$

So the system is lossless and passive with storage function given by the total energy. Once the system is put into weak form and an integration by parts is applied on the Div operator, it is obtained

$$\begin{aligned}
\langle \boldsymbol{v}_v,\ \rho\partial_t \boldsymbol{e}_v\rangle_{L^2(\Omega,\mathbb{R}^3)} &= -\langle \mathrm{Grad}(\boldsymbol{v}_v),\ \boldsymbol{E}_\varepsilon\rangle_{L^2(\Omega,\mathbb{R}^{3\times3}_{\mathrm{sym}})} + \langle \boldsymbol{v}_v,\ \boldsymbol{u}_\Omega\rangle_{L^2(\Omega,\mathbb{R}^3)} + \langle \boldsymbol{v}_v,\ \boldsymbol{u}_\partial\rangle_{L^2(\partial\Omega,\mathbb{R}^3)}\,, \\
\langle \boldsymbol{V}_\varepsilon,\ \boldsymbol{\mathcal{C}}\partial_t \boldsymbol{E}_\varepsilon\rangle_{L^2(\Omega,\mathbb{R}^{3\times3}_{\mathrm{sym}})} &= \langle \boldsymbol{V}_\varepsilon,\ \mathrm{Grad}(\boldsymbol{e}_v)\rangle_{L^2(\Omega,\mathbb{R}^{3\times3}_{\mathrm{sym}})}\,.
\end{aligned} \tag{9.31}$$

The output equation is discretized considering test function $\boldsymbol{v}_\partial$ defined over the boundary

$$\langle \boldsymbol{v}_\partial,\ \boldsymbol{y}_\partial\rangle_{L^2(\partial\Omega,\mathbb{R}^3)} = \langle \boldsymbol{w}_\partial,\ \boldsymbol{e}_v\rangle_{L^2(\partial\Omega,\mathbb{R}^3)}\,. \tag{9.32}$$

If a Galerkin method is applied then corresponding test and trial functions are discretized using the same basis

$$\begin{aligned}
\boldsymbol{v}_v(\boldsymbol{x}) &= \sum_{i=1}^{n_v} \boldsymbol{\phi}_v^i(\boldsymbol{x}) v_v^i, & \boldsymbol{V}_\varepsilon(\boldsymbol{x}) &= \sum_{i=1}^{n_\varepsilon} \boldsymbol{\Phi}_\varepsilon^i(\boldsymbol{x}) v_\varepsilon^i, & \boldsymbol{w}_\partial(\boldsymbol{s}) &= \sum_{i=1}^{n_\partial} \boldsymbol{\phi}_\partial^i(\boldsymbol{s}) w_\partial^i, \\
\boldsymbol{e}_v(\boldsymbol{x},t) &= \sum_{i=1}^{n_v} \boldsymbol{\phi}_v^i(\boldsymbol{x}) e_v^i(t), & \boldsymbol{E}_\varepsilon(\boldsymbol{x},t) &= \sum_{i=1}^{n_\varepsilon} \boldsymbol{\Phi}_\varepsilon^i(\boldsymbol{x}) e_\varepsilon^i(t), & \boldsymbol{u}_\partial(\boldsymbol{s},t) &= \sum_{i=1}^{n_\partial} \boldsymbol{\phi}_\partial^i(\boldsymbol{s}) u_\partial^i(t),
\end{aligned}$$

where $\boldsymbol{x} \in \Omega,\ \boldsymbol{s} \in \partial\Omega$. A finite-dimensional pH system is readily obtained

$$\begin{aligned}
\underbrace{\begin{bmatrix} \mathbf{M}_\rho & \mathbf{0} \\ \mathbf{0} & \mathbf{M}_{\boldsymbol{\mathcal{C}}} \end{bmatrix}}_{\mathbf{M}} \begin{pmatrix} \dot{\mathbf{e}}_v \\ \dot{\mathbf{e}}_\varepsilon \end{pmatrix} &= \underbrace{\begin{bmatrix} \mathbf{0} & -\mathbf{D}_{\mathrm{Grad}}^\top \\ \mathbf{D}_{\mathrm{Grad}} & \mathbf{0} \end{bmatrix}}_{\mathbf{J}} \begin{pmatrix} \mathbf{e}_v \\ \mathbf{e}_\varepsilon \end{pmatrix} + \underbrace{\begin{bmatrix} \mathbf{M}_v \\ \mathbf{0} \end{bmatrix}}_{\mathbf{B}_\Omega} \mathbf{u}_\Omega + \underbrace{\begin{bmatrix} \mathbf{B}_v \\ \mathbf{0} \end{bmatrix}}_{\mathbf{B}_\partial} \mathbf{u}_\partial, \\
\mathbf{M}_v \widetilde{\mathbf{y}}_\Omega &= \begin{bmatrix} \mathbf{M}_v & \mathbf{0} \end{bmatrix} \begin{pmatrix} \mathbf{e}_v \\ \mathbf{e}_\varepsilon \end{pmatrix}, \\
\mathbf{M}_\partial \widetilde{\mathbf{y}}_\partial &= \begin{bmatrix} \mathbf{B}_v^\top & \mathbf{0} \end{bmatrix} \begin{pmatrix} \mathbf{e}_v \\ \mathbf{e}_\varepsilon \end{pmatrix}.
\end{aligned} \tag{9.33}$$

The matrices are defined as follows

$$\begin{aligned}
M_\rho^{ij} &= \left\langle \boldsymbol{\phi}_v^i,\ \rho\boldsymbol{\phi}_v^j \right\rangle_{L^2(\Omega,\mathbb{R}^3)}, & M_\partial^{lk} &= \left\langle \boldsymbol{\phi}_\partial^l,\ \boldsymbol{\phi}_\partial^k \right\rangle_{L^2(\partial\Omega,\mathbb{R}^3)}, \\
M_{\boldsymbol{\mathcal{C}}}^{mn} &= \langle \boldsymbol{\Phi}_\varepsilon^m,\ \boldsymbol{\mathcal{C}}\boldsymbol{\Phi}_\varepsilon^n\rangle_{L^2(\Omega,\mathbb{R}^{3\times3}_{\mathrm{sym}})}, & D_{\mathrm{Grad}}^{mi} &= \left\langle \boldsymbol{\Phi}_\varepsilon^m,\ \mathrm{Grad}\,\boldsymbol{\phi}_v^i \right\rangle_{L^2(\Omega,\mathbb{R}^{3\times3}_{\mathrm{sym}})}, \\
M_v^{ij} &= \left\langle \boldsymbol{\phi}_v^i,\ \boldsymbol{\phi}_v^j \right\rangle_{L^2(\Omega,\mathbb{R}^3)}, & B_v^{ik} &= \left\langle \boldsymbol{\phi}_1^i,\ \boldsymbol{\phi}_\partial^k \right\rangle_{L^2(\partial\Omega,\mathbb{R}^3)},
\end{aligned} \tag{9.34}$$

where $i,j \in \{1,n_1\}$, $m,n \in \{1,n_2\}$, $l,k \in \{1,n_\partial\}$. System (9.33) is rewritten compactly as

$$\begin{aligned} \mathbf{M}\dot{\mathbf{e}} &= \mathbf{J}\mathbf{e} + \mathbf{B}_\Omega \mathbf{u}_\Omega + \mathbf{B}_\partial \mathbf{u}_\partial, \\ \mathbf{y}_\Omega &:= \mathbf{M}_v \widetilde{\mathbf{y}}_\Omega = \mathbf{B}_\Omega^\top \mathbf{e}, \\ \mathbf{y}_\partial &:= \mathbf{M}_\partial \widetilde{\mathbf{y}}_\partial = \mathbf{B}_\partial^\top \mathbf{e}. \end{aligned} \tag{9.35}$$

Remark 28 (Connection with standard discretization)
A standard finite element discretization of linear elastodynamics provides a system of the form

$$\mathbf{M}_\rho \ddot{\mathbf{q}} + \mathbf{K}\mathbf{q} = \mathbf{M}_v \mathbf{u}_\Omega + \mathbf{B}_v \mathbf{u}_\partial, \tag{9.36}$$

where $\mathbf{M}_\rho$, $\mathbf{M}_v$, $\mathbf{B}_v$ *are defined as in* (9.34). *Since the stiffness matrix* $\mathbf{K}$ *is symmetric and positive definite, it admits the following non unique factorization [HJ12]*

$$\mathbf{K} = \mathbf{D}_{\text{Grad}}^\top \mathbf{M}_{\mathcal{C}}^{-1} \mathbf{D}_{\text{Grad}}.$$

Now consider the following new variables

$$\mathbf{e}_v := \dot{\mathbf{q}}, \qquad \mathbf{e}_\varepsilon := \mathbf{M}_{\mathcal{C}}^{-1} \mathbf{D}_{\text{Grad}} \mathbf{q}.$$

Then Sys. (9.36) *can be rewritten as*

$$\begin{bmatrix} \mathbf{M}_\rho & \mathbf{0} \\ \mathbf{0} & \mathbf{M}_{\mathcal{C}} \end{bmatrix} \begin{pmatrix} \dot{\mathbf{e}}_v \\ \dot{\mathbf{e}}_\varepsilon \end{pmatrix} = \begin{bmatrix} \mathbf{0} & -\mathbf{D}_{\text{Grad}}^\top \\ \mathbf{D}_{\text{Grad}} & \mathbf{0} \end{bmatrix} \begin{pmatrix} \mathbf{e}_v \\ \mathbf{e}_\varepsilon \end{pmatrix} + \begin{bmatrix} \mathbf{M}_v \\ \mathbf{0} \end{bmatrix} \mathbf{u}_\Omega + \begin{bmatrix} \mathbf{B}_v \\ \mathbf{0} \end{bmatrix} \mathbf{u}_\partial, \tag{9.37}$$

which is exactly (9.33). *The reader may also consult [CF05, Theorem 2] for the equivalence of standard and mixed finite elements for elastodynamics problems.*

9.3.2 Discretized rigid-flexible port-Hamiltonian dynamics

The same methodology is applied to system (9.24). If corresponding test functions w, state e and effort functions z are discretized using the same bases, then a finite-dimensional pHDAE system is obtained (after integration by parts of the Div operator)

$$\begin{aligned} \mathbf{E}(\mathbf{e})\dot{\mathbf{e}} &= \mathbf{J}(\mathbf{e})\mathbf{z}(\mathbf{e}) + \mathbf{B}_\Omega(\mathbf{e})\mathbf{u}_\Omega + \mathbf{B}_\partial(\mathbf{e})\mathbf{u}_\partial, \\ \mathbf{y}_\Omega &:= \mathbf{M}_1 \widetilde{\mathbf{y}}_\Omega = \mathbf{B}_\Omega^\top \mathbf{z}(\mathbf{e}), \\ \mathbf{y}_\partial &:= \mathbf{M}_\partial \widetilde{\mathbf{y}}_\partial = \mathbf{B}_\partial^\top \mathbf{z}(\mathbf{e}). \end{aligned} \tag{9.38}$$

The computation of vector $\mathbf{z}$ is based on the discrete Hamiltonian gradient:

$$\frac{\partial H_d}{\partial \mathbf{e}} = \mathbf{E}^\top \mathbf{z}, \qquad H_d = H_{d,\text{kin}} + H_{d,\text{def}} + H_{d,\text{pot}}.$$

This relation represents the finite-dimensional counterpart of (9.25). For the deformation and kinetic energy, it is straightforward to find the link between the state and effort functions

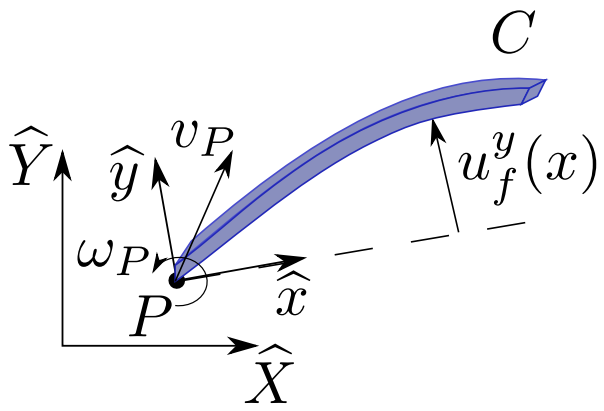

Figure 9.2: Floating beam. The rigid motion is located at point P

since those energies are quadratic in the state variable:

$$H_{d,\text{kin}} + H_{d,\text{def}} = \frac{1}{2}\mathbf{e}_{\text{kd}}^{\top}\,\mathbf{M}_{\text{kd}}\,\mathbf{e}_{\text{kd}} \longrightarrow \mathbf{z}_{\text{kd}} = \mathbf{e}_{\text{kd}}, \tag{9.39}$$

where $\mathbf{e}_{\text{kd}} = [\mathbf{v}_P; \boldsymbol{\omega}_P; \mathbf{v}_f; \boldsymbol{\Sigma}]$ and $\mathbf{M}_{\text{kd}}$ is the discretization of the mass operator $\boldsymbol{\mathcal{M}}$ given in Eq (9.19). The only term that requires additional care is the potential energy and particularly the variational derivative of the Hamiltonian with respect to the deformation displacement $\boldsymbol{z}_u = \delta_{\boldsymbol{u}_f} H$. Consider the continuous power balance associated to the flexible displacement

$$\dot{H}_u = \int_\Omega \frac{\partial \boldsymbol{u}_f}{\partial t} \cdot \boldsymbol{z}_u \,\mathrm{d}\Omega = \int_\Omega \frac{\partial \boldsymbol{u}_f}{\partial t} \cdot \frac{\delta H}{\delta \boldsymbol{u}_f} \,\mathrm{d}\Omega$$

The deformation displacement and its corresponding effort variable are discretized using the same basis, i.e. $\boldsymbol{u}_f = \boldsymbol{\phi}_u^{\top}\mathbf{u}_f$, $\boldsymbol{z}_u = \boldsymbol{\phi}_u^{\top}\mathbf{z}_u$. The discrete Hamiltonian rate assumes two equivalent expressions

$$\dot{H}_{u,d}(\mathbf{u}_f) = \begin{cases} \dot{\mathbf{u}}_f^{\top}\mathbf{M}_u\,\mathbf{z}_u, \\ \dot{\mathbf{u}}_f^{\top}\dfrac{\partial H_d}{\partial \mathbf{u}_f}, \end{cases}$$

where $\mathbf{M}_u = \int_\Omega \boldsymbol{\phi}_u\,\boldsymbol{\phi}_u^{\top}\,\mathrm{d}\Omega$. To preserve the power balance at the discrete level, $\mathbf{z}_u = \mathbf{M}_u^{-1}\frac{\partial H_d}{\partial \mathbf{u}_f}$ must hold.

Remark 29

The set Γ_D for the Dirichlet condition has to be non empty, otherwise the deformation field is allowed for rigid movement, leading to a singular mass matrix. To enforce that, test and state shape functions are chosen so as to verify an homogeneous Dirichlet condition (cf. [AS86] for a detailed discussion on this topic).

9.3.3 Application to thin planar beams

A thin planar flexible beam is considered as mechanical model. The dependence of the canonical momenta on the deformation field is neglected. This hypothesis usually applies in the floating frame formulation, since the deformations are small. P is placed at the origin of the local frame $P : \{x = 0\}$, while C is the ending point of the beam $C : \{x = L\}$ (see Fig. 9.2). The beam has length L, Young modulus E, density ρ, cross section A and second moment of area I. The model in strong form for a flexible beam is then written compactly as

$$\begin{aligned} \begin{bmatrix} \boldsymbol{I} & \boldsymbol{0} \\ \boldsymbol{0} & \mathcal{M} \end{bmatrix} \begin{pmatrix} \dot{\boldsymbol{q}} \\ \dot{\boldsymbol{p}} \end{pmatrix} &= \begin{bmatrix} \boldsymbol{0} & \mathcal{J}_{qp} \\ -\mathcal{J}_{qp}^* & \mathcal{J}_p \end{bmatrix} \begin{pmatrix} \partial_{\boldsymbol{q}} H \\ \boldsymbol{p} \end{pmatrix} + \begin{bmatrix} \boldsymbol{0} \\ \mathcal{B}_r \end{bmatrix} \boldsymbol{u}_\partial, \\ \boldsymbol{u}_\partial &= \mathcal{B}_\partial \boldsymbol{p}, \\ \boldsymbol{y}_\partial &= \mathcal{C}_\partial \boldsymbol{p}, \end{aligned} \tag{9.40}$$

The state and boundary vectors are expressed as

$$\begin{aligned} \boldsymbol{q} &= [{}^i\boldsymbol{r}_P,\ \boldsymbol{R}_{\mathrm{v}},\ \boldsymbol{u}_f]^\top \\ \boldsymbol{p} &= [v_P^x,\ v_P^y,\ \omega_P^z,\ v_f^x,\ v_f^y,\ n_x,\ m_x]^\top, \\ \boldsymbol{u}_\partial &= [F_P^x,\ F_P^y,\ T_P^z,\ F_C^x,\ F_C^y,\ T_C^z]^\top, \\ \boldsymbol{y}_\partial &= [v_P^x,\ v_P^y,\ \omega_P^z,\ v_C^x,\ v_C^y,\ \omega_C^z]^\top. \end{aligned}$$

The state contains the generalized coordinates $\boldsymbol{q}$, the linear and angular velocity $v_P^x,\ v_P^y,\ \omega_P^z$ at point P, the deformation velocity $v_f^x,\ v_f^y$ and the traction and bending stress $n_x,\ m_x$. The boundary input contains the forces and torques acting at the extremities of the beam, while the boundary output contains the corresponding conjugated variables (velocities and angular velocities). The deformation field has to be constrained, to prevent rigid movement (see Remark 29). The appropriate selection of the boundary condition for the deformation field is an unavoidable problem that depends on the particular case under consideration. Depending on the application, cantilever or simply supported boundary conditions may be considered

$$\text{Cantilever} \begin{cases} u_f^x(x=0) = 0, \\ u_f^y(x=0) = 0, \\ \partial_x u_f^y(x=0) = 0, \end{cases} \qquad \text{Simply supported} \begin{cases} u_f^x(x=0) = 0, \\ u_f^y(x=0) = 0, \\ u_f^y(x=L) = 0. \end{cases}$$

Partitioning the $\boldsymbol{p}$ vector into rigid $\boldsymbol{p}_r = [v_P^x,\ v_P^y,\ \omega_P^z]^\top$ and flexible part $\boldsymbol{p}_f = [v_f^x,\ v_f^y,\ n_x,\ m_x]^\top$, the mass operator is then structured as follows

$$\mathcal{M} = \left[\begin{array}{c|c} \mathcal{M}_{rr} & \mathcal{M}_{rf} \\ \hline \mathcal{M}_{fr} & \mathcal{M}_{ff} \end{array}\right] = \left[\begin{array}{ccc|cccc} m & 0 & 0 & \mathcal{I}_\rho^L & 0 & 0 & 0 \\ 0 & m & s^x & 0 & \mathcal{I}_\rho^L & 0 & 0 \\ 0 & s^x & J^{zz} & 0 & \mathcal{I}_{\rho x}^L & 0 & 0 \\ \hline (\mathcal{I}_\rho^L)^* & 0 & 0 & \rho A & 0 & 0 & 0 \\ 0 & (\mathcal{I}_\rho^L)^* & (\mathcal{I}_{\rho x}^L)^* & 0 & \rho A & 0 & 0 \\ 0 & 0 & 0 & 0 & 0 & (EA)^{-1} & 0 \\ 0 & 0 & 0 & 0 & 0 & 0 & (EI)^{-1} \end{array}\right], \tag{9.41}$$

where $s^x = \int_0^L \rho A x \, \mathrm{d}x$ is the static moment, $J^{zz} = \int_0^L \rho A x^2 \, \mathrm{d}x$ is the moment of inertia, $\mathcal{I}^L_\rho := \int_0^L \rho A(\cdot) \, \mathrm{d}x$, $\mathcal{I}^L_{\rho x} := \int_0^L \rho A x(\cdot) \, \mathrm{d}x$. Differently from standard Lagrangian formulations, the mass operator includes the coefficients $(EA)^{-1}$ and $(EI)^{-1}$. These coefficients represent the compliance of the beam and appear in the mass operator to include the deformation energy

$$H_{\mathrm{def}} = \frac{1}{2} \int_0^L \frac{1}{EA} n_x^2 + \frac{1}{EI} m_x^2 \, \mathrm{d}\Omega.$$

The interconnection operator is found by adapting the cross product to the planar case:

$$\mathcal{J}_p(\boldsymbol{e}) = \left[\begin{array}{c|c} \mathcal{J}_{rr} & \mathcal{J}_{rf} \\ \hline \mathcal{J}_{fr} & \mathcal{J}_{ff} \end{array}\right] = \left[\begin{array}{ccc|cccc} 0 & 0 & +\widehat{p}^y_t & 0 & 0 & 0 & 0 \\ 0 & 0 & -\widehat{p}^x_t & 0 & 0 & 0 & 0 \\ -\widehat{p}^y_t & +\widehat{p}^x_t & 0 & -\mathcal{I}^L_{p^y_f} & +\mathcal{I}^L_{p^x_f} & 0 & 0 \\ \hline 0 & 0 & +(\mathcal{I}^L_{p^y_f})^* & 0 & 0 & \partial_x & 0 \\ 0 & 0 & -(\mathcal{I}^L_{p^x_f})^* & 0 & 0 & 0 & -\partial_{xx} \\ 0 & 0 & 0 & \partial_x & 0 & 0 & 0 \\ 0 & 0 & 0 & 0 & \partial_{xx} & 0 & 0 \end{array}\right], \tag{9.42}$$

where $\widehat{p}^x_t, \widehat{p}^y_t$ are the modified canonical momenta components (see (9.22)) and

$$\mathcal{I}^L_{p^x_f} := \int_0^L \left\{2p^x_f + \rho A v^x_f\right\}(\cdot) \, \mathrm{d}x, \qquad \mathcal{I}^L_{p^y_f} := \int_0^L \left\{2p^y_f + \rho A v^y_f\right\}(\cdot) \, \mathrm{d}x.$$

The control operator reads

$$\mathcal{B}_r = \begin{bmatrix} \boldsymbol{I}_{3\times 3} & \boldsymbol{\tau}_{CP}^\top \\ \boldsymbol{0}_{4\times 3} & \boldsymbol{0}_{4\times 3} \end{bmatrix} \qquad \text{with} \quad \boldsymbol{\tau}_{CP} = \begin{bmatrix} 1 & 0 & 0 \\ 0 & 1 & L \\ 0 & 0 & 1 \end{bmatrix}. \tag{9.43}$$

The discretization procedure detailed in §9.3 is extended to this case, considering that the differential operators are

$$\mathcal{J}_{\mathrm{Div}} = \begin{bmatrix} \partial_x & 0 \\ 0 & -\partial_{xx} \end{bmatrix}, \qquad \mathcal{J}_{\mathrm{Grad}} = \begin{bmatrix} \partial_x & 0 \\ 0 & \partial_{xx} \end{bmatrix}.$$

These two operators play the same role as Div, Grad. The 2 PDEs associated to the first and second line of $\mathcal{J}_{\mathrm{Div}}$ are integrated by parts once and twice respectively, so that the boundary forces and momenta are naturally included in the discretized system as inputs. The finite-

dimensional system then reads

$$\begin{bmatrix} \mathbf{I} & \mathbf{0} & \mathbf{0} \\ \mathbf{0} & \mathbf{M}_{rr} & \mathbf{M}_{rf} \\ \mathbf{0} & \mathbf{M}_{fr} & \mathbf{M}_{ff} \end{bmatrix} \begin{pmatrix} \dot{\mathbf{q}} \\ \dot{\mathbf{p}}_r \\ \dot{\mathbf{p}}_f \end{pmatrix} = \begin{bmatrix} \mathbf{0} & \mathbf{J}_{qr}(\mathbf{q}) & \mathbf{J}_{qf} \\ \mathbf{J}_{rq}(\mathbf{q}) & \mathbf{J}_{rr}(\mathbf{p}) & \mathbf{J}_{rf}(\mathbf{p}) \\ \mathbf{J}_{fq} & \mathbf{J}_{fr}(\mathbf{p}) & \mathbf{J}_{ff} \end{bmatrix} \begin{pmatrix} \partial_{\mathbf{q}} H \\ \mathbf{p}_r \\ \mathbf{p}_f \end{pmatrix} + \begin{bmatrix} \mathbf{0} \\ \mathbf{B}_r \\ \mathbf{B}_f \end{bmatrix} \mathbf{u}_\partial,$$
$$\mathbf{y}_\partial = \begin{bmatrix} \mathbf{0} & \mathbf{B}_r^\top & \mathbf{B}_f^\top \end{bmatrix} \begin{pmatrix} \mathbf{q} \\ \mathbf{p}_r \\ \mathbf{p}_f \end{pmatrix}, \tag{9.44}$$

Matrix $\mathbf{B}_r = [\mathbf{I}_{3\times 3} \quad \boldsymbol{\tau}_{CP}^\top]$ accounts for the effect of boundary forces on the rigid part. Matrix $\mathbf{B}_f$ is the result of the integration by parts

$$\mathbf{B}_f = \begin{bmatrix} \mathbf{0}_{n_f^{vx}\times 3} & \boldsymbol{\phi}_{v_f^x}(L) & \mathbf{0}_{n_f^{vx}} & \mathbf{0}_{n_f^{vx}} \\ \mathbf{0}_{n_f^{vy}\times 3} & \mathbf{0}_{n_f^{vy}} & \boldsymbol{\phi}_{v_f^y}(L) & \partial_x \boldsymbol{\phi}_{v_f^y}(L) \\ \mathbf{0}_{n_f^{\sigma x}\times 3} & \mathbf{0}_{n_f^{\sigma x}} & \mathbf{0}_{n_f^{\sigma x}} & \mathbf{0}_{n_f^{\sigma x}} \\ \mathbf{0}_{n_f^{\sigma y}\times 3} & \mathbf{0}_{n_f^{\sigma y}} & \mathbf{0}_{n_f^{\sigma y}} & \mathbf{0}_{n_f^{\sigma y}} \end{bmatrix},$$

where $\boldsymbol{\phi}_{v_f^x}$, $\boldsymbol{\phi}_{v_f^y}$ are the shape functions for v_f^x, v_f^y and $\boldsymbol{\phi}_{v_f^x}$. Fields v_f^x, v_f^y, n_x, m_x are approximated using $n_f^{vx}, n_f^{vy}, n_f^{\sigma x}, n_f^{\sigma y}$ degrees of freedom respectively. System (9.44) can be rewritten compactly as

$$\begin{aligned} \mathbf{E}\dot{\mathbf{e}} &= \mathbf{J}(\mathbf{e})\mathbf{z}(\mathbf{e}) + \mathbf{B}_\partial \mathbf{u}_\partial, \\ \mathbf{y}_\partial &= \mathbf{B}_\partial^\top \mathbf{z}. \end{aligned} \tag{9.45}$$

This model describes the motion of a flexible floating beam that undergoes small deformations.

9.4 Multibody systems in pH form

In Sections §9.2, and §9.3, the pH formulation of a single flexible floating body in infinite- and finite-dimensional form was presented. The construction of a multibody system is accomplished by exploiting the modularity of the port-Hamiltonian framework. Each element of the system is interconnected to the others by means of classical pH interconnections.

9.4.1 Interconnections of pHDAE systems

Consider two generic pHDAE systems of the form

$$\begin{cases} \mathbf{E}_i \dot{\mathbf{e}}_i = \mathbf{J}_i \mathbf{z}_i(\mathbf{e}_i) + \mathbf{B}_i^{\text{int}} \mathbf{u}_i^{\text{int}} + \mathbf{B}_i^{\text{ext}} \mathbf{u}_i^{\text{ext}} \\ \mathbf{y}_i^{\text{int}} = \mathbf{B}_i^{\text{int}\top} \mathbf{z}_i \\ \mathbf{y}_i^{\text{ext}} = \mathbf{B}_i^{\text{ext}\top} \mathbf{z}_i \end{cases} \qquad \forall i = 1, 2. \tag{9.46}$$

where $\partial_{\mathbf{e}_i} H_i = \mathbf{E}_i^\top \mathbf{z}_i$. Systems of this kind arise from the discretization of formulation (9.24). The interconnection uses the internal control $\mathbf{u}_i^{\text{int}}$. An interconnection is said to be power preserving if and only if the following holds

$$\langle \mathbf{u}_1^{\text{int}},\ \mathbf{y}_1^{\text{int}} \rangle + \langle \mathbf{u}_2^{\text{int}},\ \mathbf{y}_2^{\text{int}} \rangle = 0, \tag{9.47}$$

which expresses that the power going out from one system flows in the other in a lossless manner. Two interconnections are of interest when coupling system: the gyrator and transformer interconnections.

Gyrator interconnection The gyrator interconnection reads

$$\mathbf{u}_1^{\text{int}} = -\mathbf{C}\mathbf{y}_2^{\text{int}}, \qquad \mathbf{u}_2^{\text{int}} = \mathbf{C}^\top \mathbf{y}_1^{\text{int}}.$$

This interconnection verifies (9.47) and provides the system

$$\begin{bmatrix} \mathbf{E}_1 & \mathbf{0} \\ \mathbf{0} & \mathbf{E}_2 \end{bmatrix} \begin{pmatrix} \dot{\mathbf{e}}_1 \\ \dot{\mathbf{e}}_2 \end{pmatrix} = \begin{bmatrix} \mathbf{J}_1 & -\mathbf{B}_1^{\text{int}} \mathbf{C} \mathbf{B}_2^{\text{int}\top} \\ \mathbf{B}_2^{\text{int}} \mathbf{C} \mathbf{B}_1^{\text{int}\top} & \mathbf{J}_2 \end{bmatrix} \begin{pmatrix} \mathbf{z}_1 \\ \mathbf{z}_2 \end{pmatrix} + \begin{bmatrix} \mathbf{B}_1^{\text{ext}} & \mathbf{0} \\ \mathbf{0} & \mathbf{B}_2^{\text{ext}} \end{bmatrix} \begin{pmatrix} \mathbf{u}_1^{\text{ext}} \\ \mathbf{u}_2^{\text{ext}} \end{pmatrix}$$
$$\begin{pmatrix} \mathbf{y}_1^{\text{ext}} \\ \mathbf{y}_2^{\text{ext}} \end{pmatrix} = \begin{bmatrix} \mathbf{B}_1^{\text{ext}\top} & \mathbf{0} \\ \mathbf{0} & \mathbf{B}_2^{\text{ext}\top} \end{bmatrix} \begin{pmatrix} \mathbf{z}_1 \\ \mathbf{z}_2 \end{pmatrix}.$$

Transformer interconnection The transformer interconnection reads

$$\mathbf{u}_1^{\text{int}} = -\mathbf{C}\mathbf{u}_2^{\text{int}}, \qquad \mathbf{y}_2^{\text{int}} = \mathbf{C}^\top \mathbf{y}_1^{\text{int}}.$$

Again, this interconnection verifies (9.47). After the interconnection the final system is differential algebraic:

$$\begin{bmatrix} \mathbf{E}_1 & \mathbf{0} & \mathbf{0} \\ \mathbf{0} & \mathbf{E}_2 & \mathbf{0} \\ \mathbf{0} & \mathbf{0} & \mathbf{0} \end{bmatrix} \begin{pmatrix} \dot{\mathbf{e}}_1 \\ \dot{\mathbf{e}}_2 \\ \dot{\boldsymbol{\lambda}} \end{pmatrix} = \begin{bmatrix} \mathbf{J}_1 & \mathbf{0} & -\mathbf{B}_1^{\text{int}} \mathbf{C} \\ \mathbf{0} & \mathbf{J}_2 & \mathbf{B}_2^{\text{int}} \\ \mathbf{C}^\top \mathbf{B}_1^{\text{int}\top} & -\mathbf{B}_2^{\text{int}\top} & \mathbf{0} \end{bmatrix} \begin{pmatrix} \mathbf{z}_1 \\ \mathbf{z}_2 \\ \boldsymbol{\lambda} \end{pmatrix} + \begin{bmatrix} \mathbf{B}_1^{\text{ext}} & \mathbf{0} \\ \mathbf{0} & \mathbf{B}_2^{\text{ext}} \\ \mathbf{0} & \mathbf{0} \end{bmatrix} \begin{pmatrix} \mathbf{u}_1^{\text{ext}} \\ \mathbf{u}_2^{\text{ext}} \end{pmatrix}$$
$$\begin{pmatrix} \mathbf{y}_1^{\text{ext}} \\ \mathbf{y}_2^{\text{ext}} \end{pmatrix} = \begin{bmatrix} \mathbf{B}_1^{\text{ext}\top} & \mathbf{0} & \mathbf{0} \\ \mathbf{0} & \mathbf{B}_2^{\text{ext}\top} & \mathbf{0} \end{bmatrix} \begin{pmatrix} \mathbf{z}_1 \\ \mathbf{z}_2 \\ \boldsymbol{\lambda} \end{pmatrix}.$$

9.4.2 Application to multibody systems of beams

Once a discretized system is obtained, lossless joints can be modeled as a transformer interconnection. A common example is a revolute joint between two beams. Considering discretization (9.45), the boundary control input $\mathbf{u}_{\partial,i}$ may be split into interconnection variables $\mathbf{u}_i^{\text{int}}$ and external variables $\mathbf{u}_i^{\text{ext}}$, i.e. $\mathbf{u}_{\partial,i} = [\mathbf{u}_i^{\text{int}};\ \mathbf{u}_i^{\text{ext}}]$. The same splitting applies to the output. In

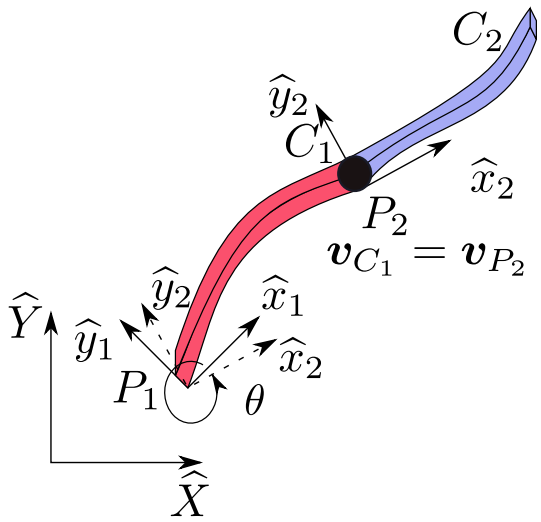

Figure 9.3: Two beams interconnected by an hinge

this case the interconnection variables are

$$\mathbf{u}_1^{\text{int}} = [F_{C_1}^x,\, F_{C_1}^y]^\top := \mathbf{F}_{C_1}, \qquad \mathbf{y}_1^{\text{int}} = [v_{C_1}^x,\, v_{C_1}^y]^\top := \mathbf{v}_{C_1},$$
$$\mathbf{u}_2^{\text{int}} = [F_{P_2}^x,\, F_{P_2}^y]^\top := \mathbf{F}_{P_2}, \qquad \mathbf{y}_2^{\text{int}} = [v_{P_2}^x,\, v_{P_2}^y]^\top := \mathbf{v}_{P_2}.$$

The interconnection matrix is the relative rotation matrix between the two local frames

$$\mathbf{R}(\theta) = \begin{bmatrix} \cos(\theta) & -\sin(\theta) \\ \sin(\theta) & \cos(\theta) \end{bmatrix}, \qquad \theta(t) = \theta(0) + \int_0^t (\omega_{P_2}^z - \omega_{P_1}^z)\, \mathrm{d}\tau. \tag{9.48}$$

The transformer interconnection

$$\mathbf{u}_1^{\text{int}} = -\mathbf{R}(\theta)\mathbf{u}_2^{\text{int}}, \qquad \mathbf{y}_2^{\text{int}} = \mathbf{R}(\theta)^\top \mathbf{y}_1^{\text{int}}, \tag{9.49}$$

imposes the constraints on the velocity level and gives rise to a quasi-linear index 2 pHDAE:

$$\begin{bmatrix} \mathbf{E}_1 & \mathbf{0} & \mathbf{0} \\ \mathbf{0} & \mathbf{E}_2 & \mathbf{0} \\ \mathbf{0} & \mathbf{0} & \mathbf{0} \end{bmatrix} \begin{pmatrix} \dot{\mathbf{e}}_1 \\ \dot{\mathbf{e}}_2 \\ \dot{\boldsymbol{\lambda}} \end{pmatrix} = \begin{bmatrix} \mathbf{J}_1(\mathbf{e}_1) & \mathbf{0} & -\mathbf{B}_1^{\text{int}}\mathbf{R} \\ \mathbf{0} & \mathbf{J}_2(\mathbf{e}_2) & \mathbf{B}_2^{\text{int}} \\ \mathbf{R}^\top \mathbf{B}_1^{\text{int}\top} & -\mathbf{B}_2^{\text{int}\top} & \mathbf{0} \end{bmatrix} \begin{pmatrix} \mathbf{z}_1 \\ \mathbf{z}_2 \\ \boldsymbol{\lambda} \end{pmatrix} + \begin{bmatrix} \mathbf{B}_{\partial 1}^{\text{ext}} & \mathbf{0} \\ \mathbf{0} & \mathbf{B}_{\partial 2}^{\text{ext}} \\ \mathbf{0} & \mathbf{0} \end{bmatrix} \begin{pmatrix} \mathbf{u}_1^{\text{ext}} \\ \mathbf{u}_2^{\text{ext}} \end{pmatrix},$$
$$\begin{pmatrix} \mathbf{y}_1^{\text{ext}} \\ \mathbf{y}_2^{\text{ext}} \end{pmatrix} = \begin{bmatrix} \mathbf{B}_{\partial 1}^{\text{ext}\top} & \mathbf{0} & \mathbf{0} \\ \mathbf{0} & \mathbf{B}_{\partial 2}^{\text{ext}\top} & \mathbf{0} \end{bmatrix} \begin{pmatrix} \mathbf{z}_1 \\ \mathbf{z}_2 \\ \boldsymbol{\lambda} \end{pmatrix}. \tag{9.50}$$

Remark 30

The constraints are imposed at a velocity level to preserve the pH structure. It is well-known that a drift appears in this case. For linear systems it is possible to use the Gear-Gupta-

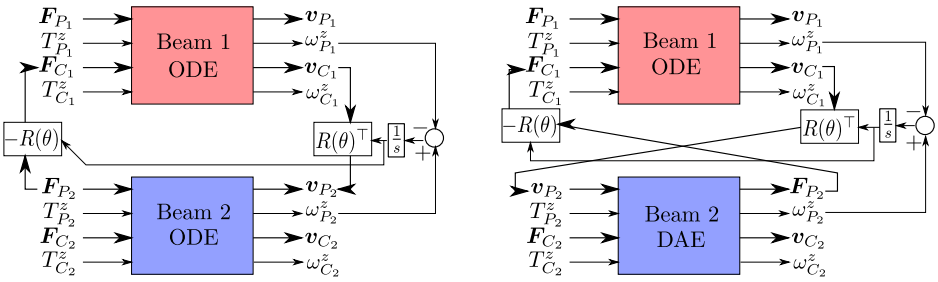

Figure 9.4: Block diagrams representing the transformer interconnection (9.49) (left) and the equivalent gyrator interconnection (9.52) (right)

Leimkuhler formulation to preserve the pH structure and enforce the constraints directly on the positions [Sch19]. In the non-linear case, stabilization technique may be introduced to avoid drifting phenomena [BL08, LB08].

The same result can be obtained by using a pHDAE system and a gyrator interconnection. To illustrate this, consider the pHDAE obtained by interchanging the role of output and input of the second system $\mathbf{u}_2^{\text{int}} \leftrightarrow \mathbf{y}_2^{\text{int}}$. The output then plays the role of a Lagrange multiplier. The input $\mathbf{u}_2^{\text{int}}$ is now considered as Lagrange multiplier $\boldsymbol{\lambda}_2$ and the output $\mathbf{y}_2^{\text{int}}$ plays the role of $\mathbf{u}_2^{\text{int}}$. The discretized system assumes the following differential-algebraic structure

$$\begin{aligned}
\begin{bmatrix} \mathbf{E}_2 & \mathbf{0} \\ \mathbf{0} & \mathbf{0} \end{bmatrix} \begin{pmatrix} \dot{\mathbf{e}}_2 \\ \dot{\boldsymbol{\lambda}}_2 \end{pmatrix} &= \begin{bmatrix} \mathbf{J}_2(\mathbf{e}_2) & \mathbf{B}_2^{\text{int}} \\ -\mathbf{B}_2^{\text{int}\top} & \mathbf{0} \end{bmatrix} \begin{pmatrix} \mathbf{z}_2 \\ \boldsymbol{\lambda}_2 \end{pmatrix} + \begin{bmatrix} \mathbf{0} \\ \mathbf{I} \end{bmatrix} \mathbf{u}_2^{\text{int}} + \begin{bmatrix} \mathbf{B}_2^{\text{ext}} \\ \mathbf{0} \end{bmatrix} \mathbf{u}_2^{\text{ext}}, \\
\mathbf{y}_2^{\text{int}} &= \begin{bmatrix} \mathbf{0} & \mathbf{I} \end{bmatrix} \begin{pmatrix} \mathbf{z}_2 \\ \boldsymbol{\lambda}_2 \end{pmatrix}, \\
\mathbf{y}_2^{\text{ext}} &= \begin{bmatrix} \mathbf{B}_2^{\text{ext}\top} & \mathbf{0} \end{bmatrix} \begin{pmatrix} \mathbf{z}_2 \\ \boldsymbol{\lambda}_2 \end{pmatrix}.
\end{aligned} \tag{9.51}$$

This system is improper, since the input appears in the algebraic part. Now, a gyrator interconnection is used to model the hinged joint

$$\mathbf{u}_1^{\text{int}} = -\mathbf{R}(\theta)\mathbf{y}_2^{\text{int}}, \qquad \mathbf{u}_2^{\text{int}} = \mathbf{R}(\theta)^\top \mathbf{y}_1^{\text{int}}. \tag{9.52}$$

The resulting differential-algebraic system is exactly (9.50), which is proper. The equivalence between the two representations is represented in Fig. 9.4. This approach allows the modular construction of systems of arbitrary complexity. Other kinds of lossless joints (prismatic, spherical) can be modeled by appropriate interconnections. The system can then be simulated by using specific DAE solvers [BCP95].

9.4.3 The linear case: substructuring and model reduction

If the angular velocities and the relative orientations are small then the system may be linearized about a particular geometrical configuration. Omitting the partition related to the

generalized coordinates $\mathbf{q}$ and partitioning the system into rigid and flexible dynamics, the resulting equations are then expressed as

$$\begin{bmatrix} \mathbf{M}_{rr} & \mathbf{M}_{rf} & \mathbf{0} \\ \mathbf{M}_{fr} & \mathbf{M}_{ff} & \mathbf{0} \\ \mathbf{0} & \mathbf{0} & \mathbf{0} \end{bmatrix} \begin{pmatrix} \dot{\mathbf{p}}_r \\ \dot{\mathbf{p}}_f \\ \dot{\boldsymbol{\lambda}} \end{pmatrix} = \begin{bmatrix} \mathbf{0} & \mathbf{0} & \mathbf{G}_r^\top \\ \mathbf{0} & \mathbf{J}_{ff} & \mathbf{G}_f^\top \\ -\mathbf{G}_r & -\mathbf{G}_f & \mathbf{0} \end{bmatrix} \begin{pmatrix} \mathbf{p}_r \\ \mathbf{p}_f \\ \boldsymbol{\lambda} \end{pmatrix} + \begin{bmatrix} \mathbf{B}_r \\ \mathbf{B}_f \\ \mathbf{0} \end{bmatrix} \mathbf{u}. \tag{9.53}$$

The Hamiltonian is now a quadratic function of the state variables $H = \frac{1}{2}\mathbf{p}^\top \mathbf{M}\mathbf{p}$ [BMXZ18]. The modular construction of complex multi-body systems is then analogous to a substructuring technique [dKRV08], where the velocities and forces are linked at the interconnection points. Such system can be reduced using Krylov subspace method directly on the DAE formulation [EKLS+18]. The basic idea relies on the construction of a subspace $\mathbf{V}_f^{\text{red}}$ for the vector $\mathbf{p}_f$ such that $\mathbf{p}_f \approx \mathbf{V}_f^{\text{red}} \mathbf{p}_f^{\text{red}}$. The reduced system then reads

$$\begin{bmatrix} \mathbf{M}_{rr} & \mathbf{M}_{rf}^{\text{red}} & \mathbf{0} \\ \mathbf{M}_{fr}^{\text{red}} & \mathbf{M}_{ff}^{\text{red}} & \mathbf{0} \\ \mathbf{0} & \mathbf{0} & \mathbf{0} \end{bmatrix} \begin{pmatrix} \dot{\mathbf{p}}_r \\ \dot{\mathbf{p}}_f^{\text{red}} \\ \dot{\boldsymbol{\lambda}} \end{pmatrix} = \begin{bmatrix} \mathbf{0} & \mathbf{0} & \mathbf{G}_r^\top \\ \mathbf{0} & \mathbf{J}_{ff}^{\text{red}} & \mathbf{G}_f^{\text{red}\top} \\ -\mathbf{G}_r & -\mathbf{G}_f^{\text{red}} & \mathbf{0} \end{bmatrix} \begin{pmatrix} \mathbf{p}_r \\ \mathbf{p}_f^{\text{red}} \\ \boldsymbol{\lambda} \end{pmatrix} + \begin{bmatrix} \mathbf{B}_r \\ \mathbf{B}_f^{\text{red}} \\ \mathbf{0} \end{bmatrix} \mathbf{u}, \tag{9.54}$$

where the second row has been pre-multiplied by $\mathbf{V}_f^{\text{red}\top}$. Alternatively, a null space matrix can employed to eliminate the Lagrange multiplier and preserve the port-Hamiltonian structure. Consider the pHDAE (9.53), where the differential and algebraic parts are explicitly separated

$$\begin{aligned} \mathbf{M}\dot{\mathbf{p}} &= \mathbf{J}\mathbf{p} + \mathbf{G}^\top \boldsymbol{\lambda} + \mathbf{B}\mathbf{u}, \\ \mathbf{0} &= \mathbf{G}\mathbf{p}, \end{aligned} \tag{9.55}$$

and consider a matrix $\mathbf{P}$ that satisfies

$$\text{range}\{\mathbf{P}\} = \text{null}\{\mathbf{G}\}.$$

Then, the range of $\mathbf{P}$ automatically satisfies the constraints. Considering the transformation $\hat{\mathbf{p}} = \mathbf{P}\mathbf{p}$ and pre-multiplying the system by $\mathbf{P}^\top$ an equivalent ODE is obtained

$$\widehat{\mathbf{M}}\, \dot{\hat{\mathbf{p}}} = \widehat{\mathbf{J}}\, \hat{\mathbf{p}} + \widehat{\mathbf{B}}\, \mathbf{u},$$

with $\widehat{\mathbf{M}} = \mathbf{P}^\top \mathbf{M}\mathbf{P}$, $\widehat{\mathbf{J}} = \mathbf{P}^\top \mathbf{J}\mathbf{P}$, $\widehat{\mathbf{B}} = \mathbf{P}^\top \mathbf{B}$. The computation of $\mathbf{P}$ can be performed by QR decomposition of matrix $\mathbf{G}$ [LBS08]. A pH system in standard form is then obtained considering the variable change $\hat{\mathbf{x}} = \widehat{\mathbf{M}}\hat{\mathbf{p}}$

$$\dot{\hat{\mathbf{x}}} = \widehat{\mathbf{J}}\widehat{\mathbf{Q}}\, \hat{\mathbf{x}} + \widehat{\mathbf{B}}\mathbf{u}, \qquad \widehat{\mathbf{Q}} := \widehat{\mathbf{M}}^{-1}.$$

Once an equivalent ODE formulation is obtained the concepts and ideas presented in [CBG16] can be used to reduce the flexible dynamics.

9.5 Conclusion

A port-Hamiltonian formulation for the flexible multibody dynamics has been discussed. The equations of motions proposed in the paper are obtained by direct manipulation of pre-existing results, unveiling the Hamiltonian structure of the floating frame of reference formulation.

The discretization procedure uses a mixed finite element method, hence, the stress distribution is available without any post-processing. This is a valuable characteristic of this framework, as the stress distribution is the most important variable for preliminary analysis of mechanical components.

This approach allows treating different models and their interconnections in a common framework. This formulation works with any kind of rigid joints and could be easily extended for any kind of flexible joints. The construction of multibody system becomes completely modular and well suited for control applications.

In the following chapter, the proposed formulation is tested for some benchmark problems.

Chapter 10

Validation

The logic of validation allows us to move between the two limits of dogmatism and skepticism.

The Model of the Text: Meaningful Action Considered as a Text
Paul Ricœur

Contents

Numerical simulations are collected in this chapter to assess the correctness of the proposed formulation for flexible multibody dynamics in pH form. Two main sections compose the chapter: the first one is dedicated to systems composed of beams, the second involves thin plates as mechanical components. The Firedrake python library [RHM+17] is employed to construct the finite-dimensional discretization.

10.1 Beam systems

The examples presented in this section make use of Euler Bernoulli beam model (9.44). To discretize the system, Lagrange polynomial of order one and Hermite polynomials of order 3 are used for v_f^x and v_f^y respectively. Discontinuous Galerkin elements of order 0 and 1 are selected for n_x and m_x respectively. This choice corresponds to the HerDG1 element (7.2) for the bending behavior and to the CGDG element (7.21) for the truss behavior.

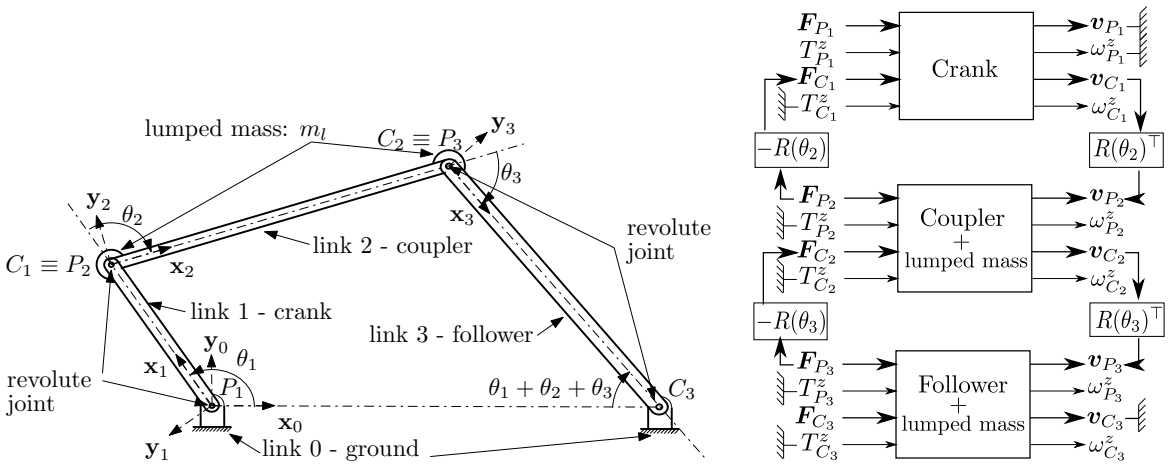

Figure 10.1: Four-bar mechanism illustration (left) and block diagram used for the eigenvalues analysis (right)

Table 10.1: Four-bar mechanism links properties: each link is a uniform beam with mass density $\rho = 2714\,[\mathrm{kg/m^3}]$ and Young modulus $E = 7.1\,10^{10}\,[\mathrm{N/m^2}]$.

i	0	1	2	3
Name	ground	crank	coupler	follower
Length L_i [m]	0.254	0.108	0.2794	0.2705
Cross section A_i [m^2]	–	$1.0774\,10^{-4}$	$4.0645\,10^{-5}$	$4.0645\,10^{-5}$
Flexural rigidity $(EI)_i$ [Nm^2]	–	11.472	0.616	0.616

The first example concerns the computation of eigenvalues of a four-bar mechanism for different geometrical configuration. The second example is a rotating crank-slider. In this case the non-linearities cannot be neglected. The third example is a hinged beam undergoing external excitations so that the out-of-plane motion becomes important. For all the examples, each beam is discretized using 2 elements.

10.1.1 Linear analysis of a four-bar mechanism

The four-bar mechanism has one degree of freedom and represents a closed chain of bodies. The data, taken from [KL90, CDPGA17], are recalled in Table 10.1. In Fig. 10.1 the mechanism and the corresponding block diagram used for constructing the final pH system with transformer interconnections between subsystems are presented. The lumped masses are directly included in the coupler and follower model considering a simple modification of the rigid mass matrix

$$\mathbf{M}_{rr}^{i+m_l}[1:2,1:2] = \mathbf{M}_{rr}^{i}[1:2,1:2] + \mathbf{I}_{2\times 2} m_l,$$

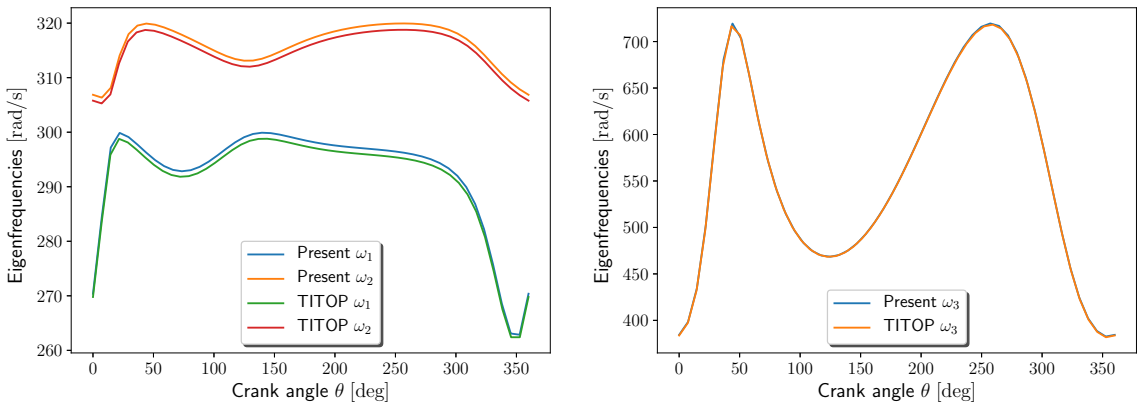

Figure 10.2: Eigenvalues $\omega_i,\ i = 1, 2, 3$ for the four-bar mechanism for varying crank angle.

where $i = 2, 3$ denotes the coupler or follower model. Given a certain crank angle θ_1 the relative angles between the different links are found by solving the two kinematic constraints

$$L_1 \cos(\theta_1) + L_2 \cos(\theta_1 + \theta_2) + L_3 \cos(\theta_1 + \theta_2 + \theta_3) = L_0,$$
$$L_1 \sin(\theta_1) + L_2 \sin(\theta_1 + \theta_2) + L_3 \sin(\theta_1 + \theta_2 + \theta_3) = 0.$$

Once the angles describing the geometrical configuration are known, the transformer interconnection (9.49) is applied to insert a revolute joint between adjacent links. For the deformation field a cantilever condition is imposed for each beam. The resulting system is then constrained to ground by imposing to following equalities

$$\mathbf{v}_{P_1} = \mathbf{0}, \quad \omega^z_{P_1} = 0, \quad \mathbf{v}_{C_3} = \mathbf{0}.$$

The resulting system is expressed in pH form as $\mathbf{E}\dot{\mathbf{e}} = \mathbf{J}\mathbf{e}$. The eigenfrequencies are then found by solving the generalized eigenvalue problem $\mathbf{E}\boldsymbol{\Phi}\boldsymbol{\Lambda} = \mathbf{J}\boldsymbol{\Phi}$. Since $\mathbf{J}$ is skew-symmetric the eigenvalues will be imaginary $\boldsymbol{\Lambda} = j\boldsymbol{\Omega}$. The first three pulsations are reported in Fig. 10.2 for different values of the crank angle θ_1. The results match those of [CDPGA17] (labeled as TITOP in the figure), assessing the validity of the linear model.

10.1.2 Rotating crank-slider

To verify the non-linear planar model a crank-slider rotating at high speed is considered. The example is retrieved from [ES18]. The crank is considered as rigid, with length $L_{\text{cr}} = 0.15$ [m] and rotates at a constant angular rate $\omega_{\text{cr}} = 150$ [rad/s]. The flexible coupler has length $L_{\text{cl}} = 0.3$ [m] and a circular cross section whose diameter is $d_{\text{cl}} = 6$ [mm]. Its Young modulus and density are given by $E_{\text{cl}} = 0.2\ 10^{12}$ [Pa], and $\rho_{\text{cl}} = 7870$ [kg/m^3]. The slider has a total mass equal to half the mass of the coupler $m_{\text{sl}} = 0.033$ [kg]. A simply supported condition is supposed for the coupler deformation field. This choice is motivated by the fact that the slider has a large inertia and does not allow elastic displacement at the tip.

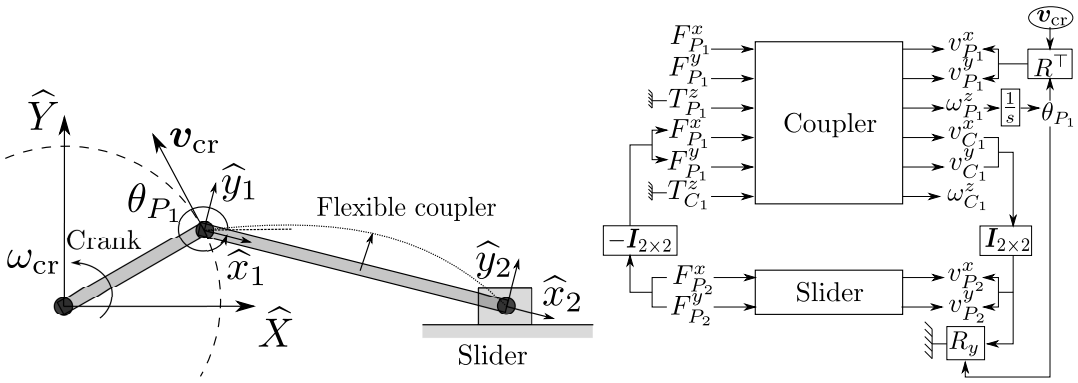

Figure 10.3: Crank slider illustration (left) and block diagram (right)

An illustration of the system and the block diagram used to construct the model are provided in Fig. 10.3. To construct the crank slider a transfomer interconnection is first used to connect the slider to the flexible coupler. The motion of the slider is then computed in the coupler reference frame. Then the sliding constraint, that requires the vertical velocity of the slider to be null in the inertial frame, is imposed as follows

$$0 = \sin(\theta_{P_1}) v^x_{P_2} + \cos(\theta_{P_1}) v^y_{P_2} = \mathbf{R}_y(\theta_{P_1}) \mathbf{v}_{P_2},$$

where $\mathbf{R}_y$ is the second line of the rotation matrix and θ_{P_1} is the angle defining the orientation of the coupler. The rigid crank velocity at the endpoint

$$\mathbf{v}_{\text{cr}}(t) = -\omega_{\text{cr}} L_{\text{cr}} \sin(\omega_{\text{cr}} t) \widehat{\mathbf{X}} + \omega_{\text{cr}} L_{\text{cr}} \cos(\omega_{\text{cr}} t) \widehat{\mathbf{Y}}$$

has to be written in the coupler reference frame to get the input

$$\mathbf{u}_{\text{cl}} = \mathbf{R}(\theta_{P_1})^\top \mathbf{v}_{\text{cr}}.$$

The resulting system is a quasi linear index-2 DAE of the form

$$\begin{bmatrix} \mathbf{M} & \mathbf{0} & \mathbf{0} \\ \mathbf{0} & \mathbf{0} & \mathbf{0} \\ \mathbf{0} & \mathbf{0} & \mathbf{0} \end{bmatrix} \begin{pmatrix} \dot{\mathbf{e}} \\ \dot{\boldsymbol{\lambda}}_0 \\ \dot{\boldsymbol{\lambda}}_u \end{pmatrix} = \begin{bmatrix} \mathbf{J}(\mathbf{e}) & \mathbf{G}_0^\top(\theta_{P_1}) & \mathbf{G}_u^\top \\ -\mathbf{G}_0(\theta_{P_1}) & \mathbf{0} & \mathbf{0} \\ -\mathbf{G}_u & \mathbf{0} & \mathbf{0} \end{bmatrix} \begin{pmatrix} \mathbf{e} \\ \boldsymbol{\lambda}_0 \\ \boldsymbol{\lambda}_u \end{pmatrix} + \begin{bmatrix} \mathbf{0} \\ \mathbf{0} \\ \mathbf{R}(\theta_{P_1})^\top \end{bmatrix} \mathbf{v}_{\text{cr}}.$$

Setting the initial conditions properly is of utmost importance for a DAE solver. For this problem the beam is supposed undeformed at the initial time. The initial conditions for the rigid movement are then found using basic kinematics considerations. The system is then solved using the IDA algorithm available in the Assimulo library [AFÅ15]. The computational performances for this test case are reported in Tab. 10.2 In Fig. 10.4 the midpoint deformation displacement $u^x_f(L_{\text{cl}/2})$, $u^y_f(L_{\text{cl}/2})$, normalized with respect to the coupler length, is reported. The resulting vertical displacement is in accordance with the results presented in [ES18]. The horizontal displacement exhibits high oscillations because of the higher eigenfrequencies of the longitudinal movement. This is due to the fact that null initial conditions are imposed

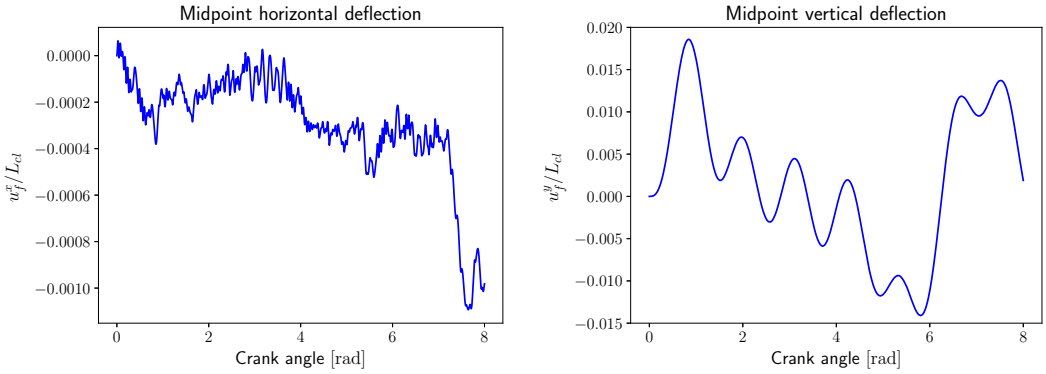

Figure 10.4: Coupler midpoint horizontal (left) and vertical (right) displacement

Table 10.2: Computational performances for the crank slider.

Solver	Elapsed simulation time	Average Δt	Final time
IDA	12.14 [s]	$4.98\,10^{-7}$ [s]	$0.053\,10^{-4}$ [s]

on the deformation [Sim06]. In order to obtain a smoother solution, the initial deformation has to be computed from the rigid initial condition.

10.1.3 Hinged spatial beam

A spatial beam rotating about a spherical joint is considered (see Fig. 10.5). This example was considered in [Car00, ES18]. The physical parameters are briefly recalled in Table 10.3. The spherical joint constraint is imposed by setting to zero the linear velocity, while a cantilever is imposed for the deformation field as the tip is free. For the first 10.2 [s] a torque $M_z = 200$ [N/mm] is applied about the vertical axis. Then, an impulsive force $F_z = 100$ [N] is applied at the tip of the beam at 15 [s], to excite the out-of-plane movement. The system is solved using an implicit Runge-Kutta method of the Radau IIA family (see Tab. 10.4 for the computational performance of this test case). The simulation results, provided in Fig. 10.6, correspond to the total energy and the angular velocity measured in the inertial vertical direction. The result matches with the provided references. Indeed the non-linearities associated to the gyroscopic terms are small as the maximum angular velocity is equal to 0.1 [rad/s] $\approx$ 5 [deg/s].

Table 10.3: Physical parameters for the hinged spatial beam.

Length	Cross section	Inertia moment	Density	Young modulus
141.45 [mm]	9.0 [mm^2]	6.75 [mm^4]	7800 [kg/mm^3]	2.1 10^6 [N/m^2]

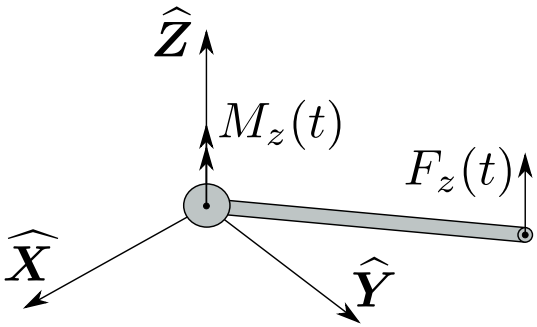

Figure 10.5: Spatial beam on a spherical joint.

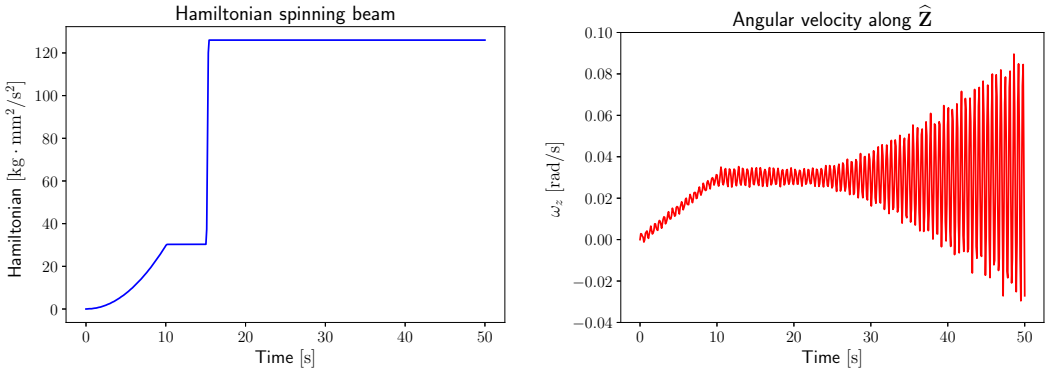

Figure 10.6: Simulation results: kinetic energy (left) and angular velocity about the vertical inertial direction (right).

10.2 Plate systems

In this section, the Kirchhoff plate model is considered in multibody applications. In the first example a cantilever plate is interconnected to a rigid rod, welded to one side of the plate. The discretization is achieved using the same finite elements as in §8.1.1. This example is not compared with previously published material, because of the lack of similar simulations in the literature. The second example concerns the computation of frequencies of a cantilever plate with in domain actuation. This mechanical system is taken from the experimental setup employed in [PSB+20]. The Hellan-Hermann-Johnson elements are used to discretize the plate.

Table 10.4: Computational performances for the hinged spatial beam.

Solver	Elapsed simulation time	Average Δt	Final time
Radau IIA	21.14 [s]	6 10^{-4} [s]	50 [s]

10.2.1 Boundary interconnection with a rigid element

In this section the interconnection of an infinite- and finite-pH system is explained in both the infinite- and finite-dimensional settings. This paradigm provides an easy way to construct an arbitrarily complex system, given its basic components. Infinite- and finite-dimensional can be coupled together, making it possible to construct models for complex applications. The interconnection of a flexible plate and a rigid rod along one side of the plate is taken as an illustrative example.

10.2.1.1 Infinite-dimensional setting

Consider an infinite-dimensional pH system (or distributed pH system, dpH) and a finite-dimensional pH system denoted by equations

$$\text{dpH} \qquad \begin{aligned} \partial_t \boldsymbol{x}_1 &= \mathcal{J}\,\delta_{\boldsymbol{x}_1} H_1, \\ \boldsymbol{u}_{\partial,1} &= \mathcal{B}_\partial\,\delta_{\boldsymbol{x}_1} H_1, \\ \boldsymbol{y}_{\partial,1} &= \mathcal{C}_\partial\,\delta_{\boldsymbol{x}_1} H_1, \end{aligned} \tag{10.1}$$

$$\text{pH} \qquad \begin{aligned} \dot{\mathbf{x}}_2 &= \mathbf{J}\nabla_{\mathbf{x}_2} H_2 + \mathbf{B}\mathbf{u}_2, \\ \mathbf{y}_2 &= \mathbf{B}^\top \nabla_{\mathbf{x}_2} H_2, \end{aligned} \tag{10.2}$$

where $\mathbf{x} \in \mathbb{R}^n, \mathbf{u}_2, \mathbf{y}_2 \in \mathbb{R}^m$ and $\boldsymbol{x}_1 \in X$, $\boldsymbol{u}_{\partial,1} \in U$, $\boldsymbol{y}_{\partial,1} \in Y = U'$ belong to some Hilbert spaces (the prime denotes the topological dual of a space) and $\mathcal{B}_\partial : X \to U$, $\mathcal{C}_\partial : X \to Y$ are boundary operators. The duality pairings for the boundary ports are denoted by

$$\langle \boldsymbol{u}_{\partial,1},\, \boldsymbol{y}_{\partial,1} \rangle_{U\times Y}\,, \qquad \langle \mathbf{u}_2,\, \mathbf{y}_2 \rangle_{\mathbb{R}^m}\,.$$

For the interconnection, consider the compact operator $\mathcal{W} : Y \to \mathbb{R}^m$ and the following power-preserving interconnection

$$\mathbf{u}_2 = -\mathcal{W}\,\boldsymbol{y}_{\partial,1}, \qquad \boldsymbol{u}_{\partial,1} = \mathcal{W}^*\,\mathbf{y}_2, \tag{10.3}$$

where $\mathcal{W}^*$ denotes the adjoint of $\mathcal{W}$ (cf. Fig. 10.7).

As an illustration, a rigid rod welded to the plate is considered (see Fig. 10.8). The rigid rod, undergoing small displacements about the z axis and small rotations about the x axis, can be written as a pH system in co-energy variables with structure

$$\begin{bmatrix} m^{\text{rod}} & 0 \\ 0 & J_G^{\text{rod}} \end{bmatrix} \frac{d}{dt} \begin{pmatrix} v_G \\ \omega_G \end{pmatrix} = \begin{pmatrix} F_z \\ T_x \end{pmatrix} = \mathbf{u}_{\text{rod}}, \qquad \mathbf{y}_{\text{rod}} = \begin{pmatrix} v_G \\ \omega_G \end{pmatrix}, \tag{10.4}$$

with v_G, ω_G, J_G^{rod} the linear velocity, angular velocity and rotary inertia about G, the center of mass, m^{rod} the total mass and F_z, T_x the force along z and the torque along x. The Hamiltonian reads $H_{\text{rod}} = \frac{1}{2}\left(M_G\, {v_G}^2 + J_G\, {\omega_G}^2\right)$. The rod is welded to a rectangular thin plate of sides L_x, L_y on side $x = L_x$. The boundary variables for the plate involved in the

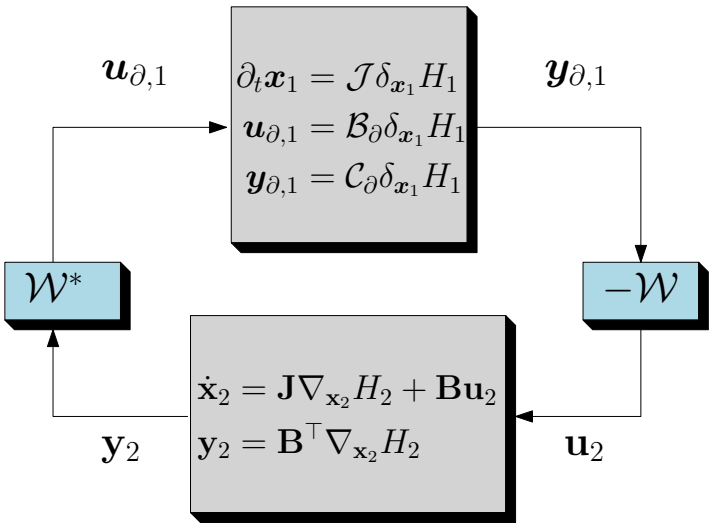

Figure 10.7: Boundary interconnection between an infinite- and a finite-dimensional pH system.

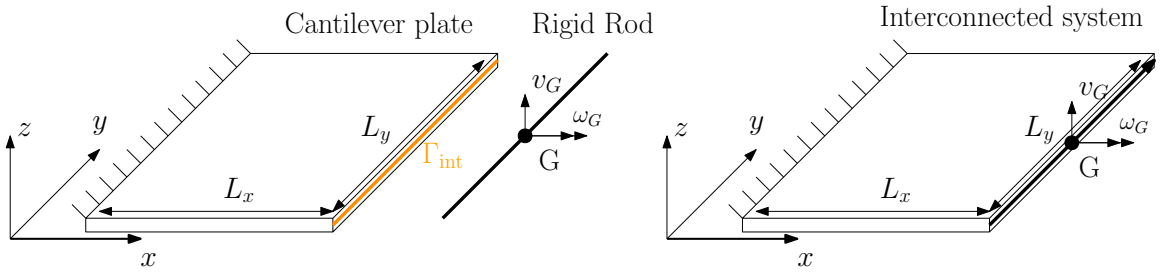

Figure 10.8: Interconnection of a Kirchhoff plate along its boundary.

interconnection are

$$u_{\partial,w_t} = \partial_t w(x = L_x, y, t), \qquad y_{\partial,w_t} = \widetilde{q}_n(x = L_x, y, t),$$

where w is the vertical displacement and $\widetilde{q}_n$ is the effective shear force (4.41a). The space Y is the space of square-integrable functions with support

$$\Gamma_{\text{int}} = \{(x, y) |\, x = L_x, 0 \leq y \leq L_y\}\,.$$

The compact interconnection operator then reads

$$\mathcal{W} y_{\partial,w_t} = \begin{pmatrix} \int_{\Gamma_{\text{int}}} y_{\partial,w_t}\, \mathrm{d}s \\ \int_{\Gamma_{\text{int}}} (y - L_y/2)\, y_{\partial,w_t}\, \mathrm{d}s \end{pmatrix}. \tag{10.5}$$

The adjoint operator is then obtained considering that $\mathbf{u}_{\text{rod}} = \mathcal{W} y_{\partial,w_t}$ and that the inner product of $\mathbb{R}^m$ is easily converted to an inner product on the space $L^2(\Gamma_{\text{int}})$ (square-integrable

functions on Γ_{int})

$$\begin{aligned}\langle \mathcal{W} y_{\partial,w_t},\ \mathbf{y}_{\text{rod}}\rangle_{\mathbb{R}^m} &= \langle \mathcal{W}^* \mathbf{y}_{\text{rod}},\ y_{\partial,w_t}\rangle_{L^2(\Gamma_{\text{int}})}\,,\\ \mathcal{W}^* \mathbf{y}_{\text{rod}} &= v_G + \omega_G\,(y - L_y/2)\,.\end{aligned}$$

The interconnection (10.3) will ensure that the two components are connected in a power-preserving manner.

10.2.1.2 Finite-dimensional setting

Consider a rectangular plate of size L_x, L_y, clamped at $\Gamma_D = \{(x,y)|\ x = 0,\ 0 \le y \le L_y\}$, and welded to a rigid rod on $\Gamma_{\text{int}} = \{(x,y)|\ x = L_x,\ 0 \le y \le L_y\}$. By imposing the boundary conditions weakly as in (8.2), a finite dimensional system is obtained

$$\begin{aligned}\text{Diag}\begin{bmatrix}\mathbf{M}_{\rho h}\\ \mathbf{M}_{\mathcal{C}_b}\\ \mathbf{0}\\ \mathbf{0}\end{bmatrix}\begin{pmatrix}\dot{\mathbf{e}}_w\\ \dot{\mathbf{e}}_\kappa\\ \dot{\boldsymbol{\lambda}}_{\Gamma_D}\\ \dot{\boldsymbol{\lambda}}_{\widetilde{q}_n,\,\Gamma_{\text{int}}}\end{pmatrix} &= \begin{bmatrix}\mathbf{0} & -\mathbf{D}_{\text{Hess}}^\top & \mathbf{B}_{\Gamma_D} & \mathbf{B}_{w,\Gamma_{\text{int}}}\\ \mathbf{D}_{\text{Hess}} & \mathbf{0} & \mathbf{0} & \mathbf{0}\\ -\mathbf{B}_{\Gamma_D}^\top & \mathbf{0} & \mathbf{0} & \mathbf{0}\\ -\mathbf{B}_{w,\Gamma_{\text{int}}}^\top & \mathbf{0} & \mathbf{0} & \mathbf{0}\end{bmatrix}\begin{pmatrix}\mathbf{e}_w\\ \mathbf{e}_\kappa\\ \boldsymbol{\lambda}_{\Gamma_D}\\ \boldsymbol{\lambda}_{\widetilde{q}_n,\,\Gamma_{\text{int}}}\end{pmatrix} + \begin{bmatrix}\mathbf{0}\\ \mathbf{0}\\ \mathbf{0}\\ \mathbf{M}_{\Gamma_{\text{int}}}\end{bmatrix}\mathbf{u}_{\partial,w_t},\\ \mathbf{M}_{\Gamma_{\text{int}}}\mathbf{y}_{\partial,w_t} &= \begin{bmatrix}\mathbf{0} & \mathbf{0} & \mathbf{0} & \mathbf{M}_{\Gamma_{\text{int}}}\end{bmatrix}\begin{pmatrix}\mathbf{e}_w\\ \mathbf{e}_\kappa\\ \boldsymbol{\lambda}_{\Gamma_D}\\ \boldsymbol{\lambda}_{\widetilde{q}_n,\,\Gamma_{\text{int}}}\end{pmatrix},\end{aligned} \tag{10.6}$$

where the Lagrange multiplier $\boldsymbol{\lambda}_{\Gamma_D}$ contains both the reaction forces and torques whereas $\boldsymbol{\lambda}_{\widetilde{q}_n,\,\Gamma_{\text{int}}}$ contains only the reaction force $\widetilde{q}_n$ along the interconnected boundary Γ_{int}. The rigid rod is written compactly as

$$\begin{aligned}\mathbf{M}_{\text{rod}}\dot{\mathbf{e}}_{\text{rod}} &= \mathbf{u}_{\text{rod}},\\ \mathbf{y}_{\text{rod}} &= \mathbf{e}_{\text{rod}},\end{aligned} \tag{10.7}$$

where $\mathbf{e}_{\text{rod}} = [v_G\ \omega_G]^\top$, $\boldsymbol{M}_{\text{rod}} = \text{Diag}(M_G,\, J_G)$. The final system is obtained considering the weak form of interconnection (10.5)

$$\mathbf{u}_{\text{rod}} = -\mathbf{W}\mathbf{y}_{\partial,w_t}, \qquad \mathbf{M}_{\Gamma_{\text{int}}}\mathbf{u}_{\partial,w_t} = \mathbf{W}^\top \mathbf{y}_{\text{rod}}. \tag{10.8}$$

The interconnection matrix $\mathbf{W}$ is obtained once the operator $\mathcal{W}^*$ is set into weak form

$$\begin{aligned}\mathbf{W}^{\top ij} &= \left\langle \boldsymbol{\phi}^i_{w_t},\ \mathcal{W}^*\boldsymbol{\phi}^j_{\mathbb{R}^2}\right\rangle_{L^2(\Gamma_{\text{int}})},\\ \mathbf{W}^{\top i} &= \int_{\Gamma_{\text{int}}} [\boldsymbol{\phi}^i_{w_t} \quad \phi^i_{w_t}(y - L_y/2)]\ \mathrm{d}s,\end{aligned}$$

where $\boldsymbol{\phi}^j_{\mathbb{R}^2}\ \forall j = \{1,2\}$ is the canonical basis of $\mathbb{R}^2$, and $\phi^i_{w_t}\ \forall i = \{1, n_\partial\}$ is the approximation basis for the boundary variable. Then the augmented system is found plugging (10.8) into

(10.6)

$$\text{Diag}\begin{bmatrix}\mathbf{M}_{\rho h}\\ \mathbf{M}_{\mathcal{C}_b}\\ \mathbf{0}\\ \mathbf{0}\\ \mathbf{M}_{\text{rod}}\end{bmatrix}\begin{pmatrix}\dot{\mathbf{e}}_w\\ \dot{\mathbf{e}}_\kappa\\ \dot{\boldsymbol{\lambda}}_{\Gamma_D}\\ \dot{\boldsymbol{\lambda}}_{\widetilde{q_n},\,\Gamma_{\text{int}}}\\ \dot{\mathbf{e}}_{\text{rod}}\end{pmatrix}=\begin{bmatrix}\mathbf{0} & -\mathbf{D}_{\text{Hess}}^\top & \mathbf{B}_{\Gamma_D} & \mathbf{B}_{w,\Gamma_{\text{int}}} & \mathbf{0}\\ \mathbf{D}_{\text{Hess}} & \mathbf{0} & \mathbf{0} & \mathbf{0} & \mathbf{0}\\ -\mathbf{B}_{\Gamma_D}^\top & \mathbf{0} & \mathbf{0} & \mathbf{0} & \mathbf{0}\\ -\mathbf{B}_{w,\Gamma_{\text{int}}}^\top & \mathbf{0} & \mathbf{0} & \mathbf{0} & \mathbf{W}^\top\\ \mathbf{0} & \mathbf{0} & \mathbf{0} & -\mathbf{W} & \mathbf{0}\end{bmatrix}\begin{pmatrix}\mathbf{e}_w\\ \mathbf{e}_\kappa\\ \boldsymbol{\lambda}_{\Gamma_D}\\ \boldsymbol{\lambda}_{\widetilde{q_n},\,\Gamma_{\text{int}}}\\ \mathbf{e}_{\text{rod}}\end{pmatrix}. \tag{10.9}$$

10.2.1.3 Numerical Simulation

To validate this approach, numerical simulations on system (10.9) are carried out. A plate clamped in $x = 0$ is considered. A final time equal to $t_{\text{end}} = 10$ [ms] is taken and a vertical distributed force, given by the formula

$$f_w = \begin{cases} 10^5\left(y + 10\,(y - L_y/2)^2\right)\ \text{[Pa]}, & \forall\, t < 0.2\,t_{\text{end}},\\ 0, & \forall\, t \geq 0.2\,t_{\text{end}},\end{cases} \tag{10.10}$$

acts on the plate. The rigid rod has mass $M = 50$ [kg] and length $L_{\text{rod}} = 1$ [m]. The plate parameters and settings for the discretization (a uniform grid is taken) are provided in Table 10.5. The finite element discretization is the same as in 8.1.1. The constraints are eliminated considering a projection method [BH15].

Plate Parameters	
E	70 [GPa]
ρ	2700 [kg/m^3]
ν	0.35
h	0.05 [m]
$L_x,\ L_y$	1 [m]

Simulation Settings	
Integrator	Runge-Kutta 45
t_{end}	10 [ms]
N° FE	6
FE space	Argyris $\times$ DG$_3$ $\times$ CG$_2$

Table 10.5: Simulation settings and parameters.

Snapshots of simulations without and with the rigid rod are reported in Figs. 10.10, 10.11. The deformations undergone by the plate are clearly affected by the presence of the rod: the maximum deformation as well as the Hamiltonian value (cf. Fig. 10.9), once the excitation is removed, are lower when the rigid rod is present. The interconnected side remains straight during the whole simulation, meaning that the constraints are respected.

10.2.2 Actuated plate

In this section, the experimental setup presented in [PSB+20] is modeled using the pH framework. The setup is composed by a cantilever plate controlled by means of two proof-mass actuators and a mirror used to reflect a laser beam for measuring the end-point deflection (see Fig. 10.12). This system can be constructed modularly considering each component separately.

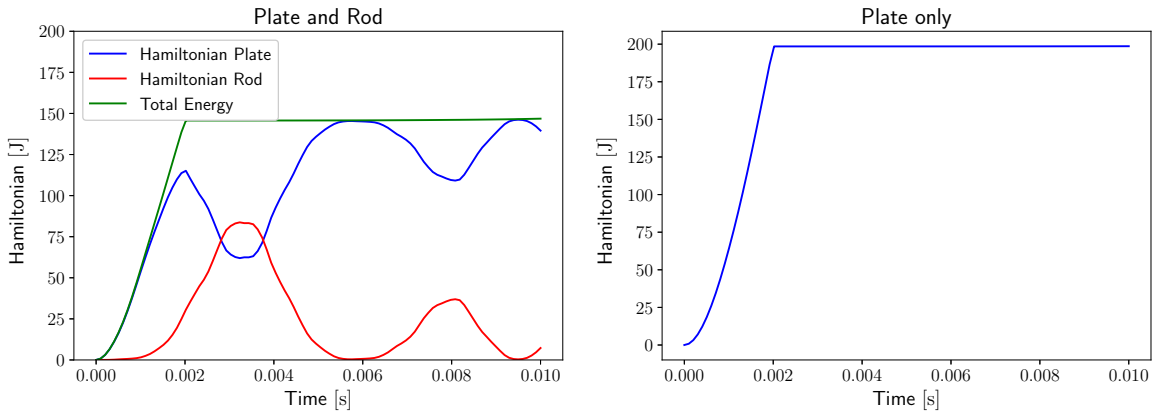

(a) Plate and rod (b) Plate only

Figure 10.9: Hamiltonian trend for the interconnection of a cantilever plate with a rigid rod (left). For comparison the same simulation is performed without including the rod (right).

10.2.2.1 Modular modelling of the system

In this section, the model for each component is detailed. The final system is obtained by imposing the appropriate transformer interconnections.

Cantilever plate The cantilever plate is modelled as in Sec. 8.1.1. The difference is that now the forces at the free boundary are null and that the other components interact with the plate system by means of reaction forces within the domain $\Omega = (0, L_x) \times (0, L_y)$. The forces exerted by the external components can be modelled by a delta distribution. Then the continuous model can be written as the following system in distributional form

$$\begin{bmatrix} \rho h & 0 \\ \mathbf{0} & \boldsymbol{\mathcal{C}_b} \end{bmatrix} \frac{\partial}{\partial t} \begin{pmatrix} e_w \\ \boldsymbol{E}_\kappa \end{pmatrix} = \begin{bmatrix} 0 & -\operatorname{div}\operatorname{Div} \\ \operatorname{Hess} & \mathbf{0} \end{bmatrix} \begin{pmatrix} e_w \\ \boldsymbol{E}_\kappa \end{pmatrix} + \sum_{i=1}^{n_{\text{comp}}} \begin{bmatrix} 1 & -\partial_y & \partial_x \\ \mathbf{0} & \mathbf{0} & \mathbf{0} \end{bmatrix} \delta(\boldsymbol{x} - \boldsymbol{x}_{P_i}) \mathbf{u}_{P_i},$$
$$\mathbf{y}_{P_i} = \delta(\boldsymbol{x} - \boldsymbol{x}_{P_i}) \begin{bmatrix} 1 & \mathbf{0} \\ \partial_y & \mathbf{0} \\ -\partial_x & \mathbf{0} \end{bmatrix} \begin{pmatrix} e_w \\ \boldsymbol{E}_\kappa \end{pmatrix}, \qquad \forall i \in \{1, n_{\text{comp}}\} \tag{10.11}$$

where n_{comp} is the number of external components, $\boldsymbol{x}_{P_i}$ is the attachment point of the i-th component, $\mathbf{u}_{P_i} = [F^z_{P_i}\ T^x_{P_i}\ T^y_{P_i}]^\top$ contains the external force along z and the external torques along x and y. The torques undergo a derivation, analogously to what happens for the effective shear force at the boundary (cf. Eq. (4.41a)). This derivation affects $\delta(\boldsymbol{x} - \boldsymbol{x}_{P_i})$, the Dirac delta placed at $\boldsymbol{x}_{P_i}$. In the adjoint of the control operator the derivation operator

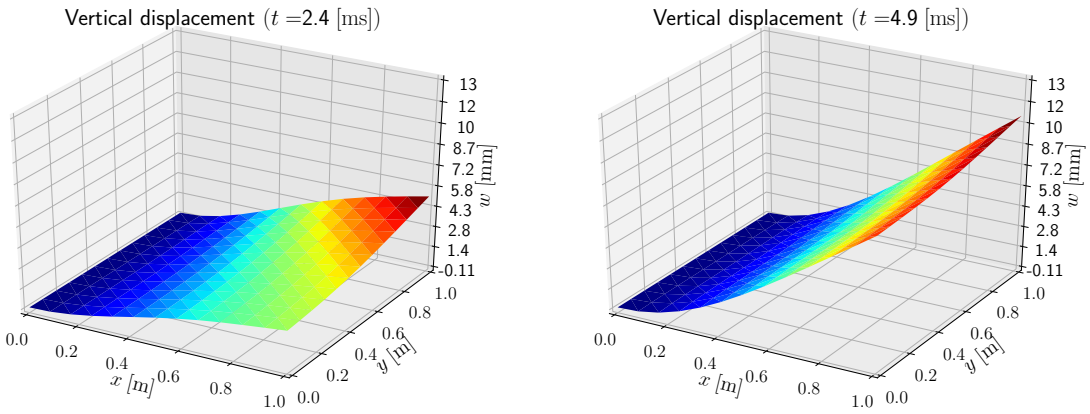

(a) $t = 0.25\ t_{\text{end}}$ (b) $t = 0.5\ t_{\text{end}}$

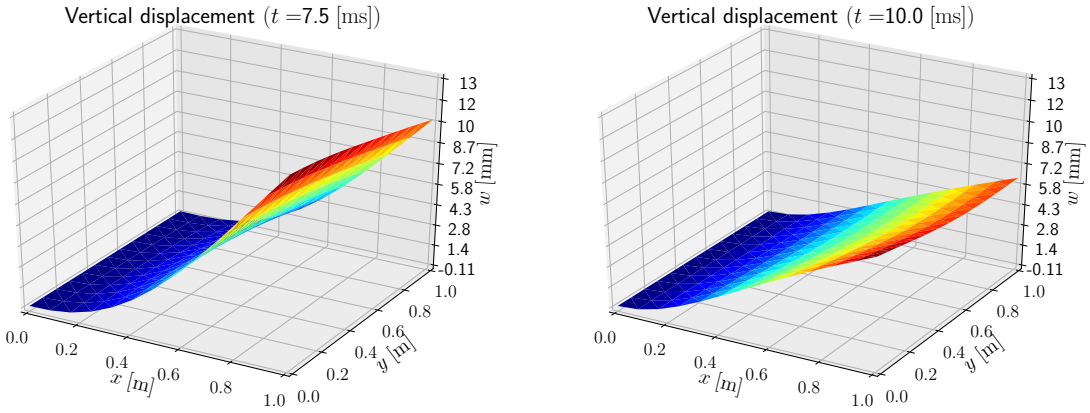

(c) $t = 0.75\ t_{\text{end}}$ (d) $t = t_{\text{end}}$

Figure 10.10: Snapshots at 4 different times of a cantilever plate undergoing solicitation (10.10).

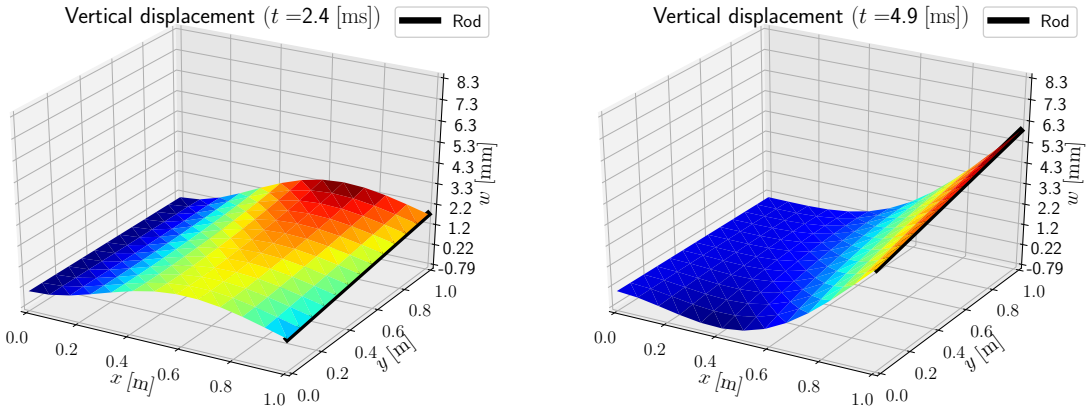

(a) $t = 0.25\ t_{\text{end}}$ (b) $t = 0.5\ t_{\text{end}}$

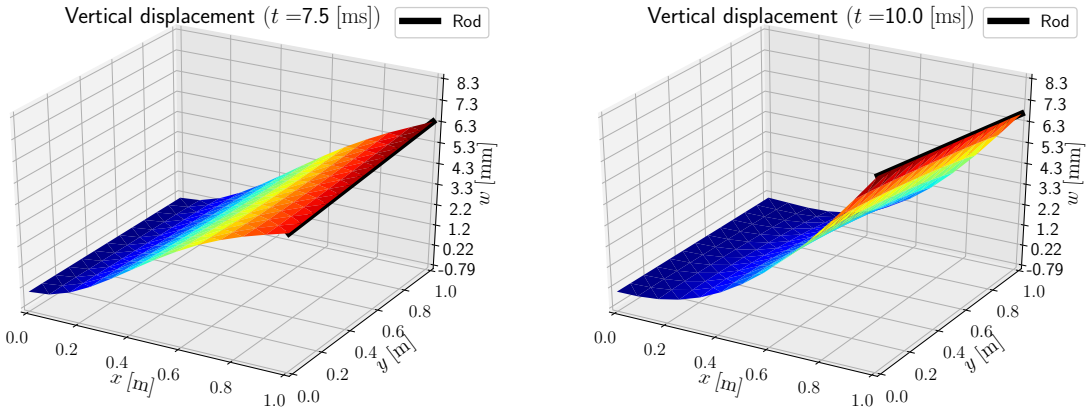

(c) $t = 0.75\ t_{\text{end}}$ (d) $t = t_{\text{end}}$

Figure 10.11: Snapshots at 4 different times of a cantilever plate and a rigid rod undergoing solicitation (10.10). Notice the different deformation amplitude with respect to Fig. 10.10.

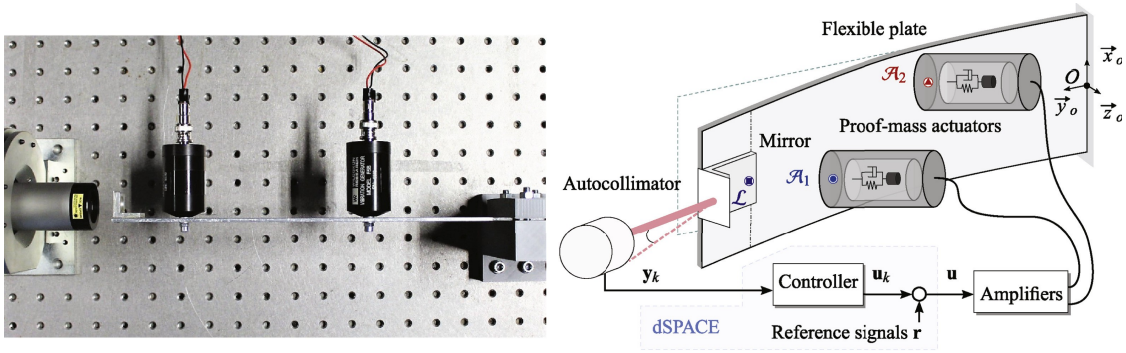

Figure 10.12: Experimental setup used in [PSB+20]. Top down photo of the system (left), schematic diagram of the setup (right).

and the Dirac distribution swap their positions

$$\mathcal{B}_{\Omega,i} = \begin{bmatrix} 1 & -\partial_y & \partial_x \end{bmatrix} \delta(\boldsymbol{x} - \boldsymbol{x}_{P_i}), \qquad \mathcal{B}^*_{\Omega,i} = \delta(\boldsymbol{x} - \boldsymbol{x}_{P_i}) \begin{bmatrix} 1 \\ \partial_y \\ -\partial_x \end{bmatrix}.$$

This is rigorously justified using the integration by parts

$$\begin{aligned} \langle e_w, \mathcal{B}_{\Omega,i}\mathbf{u}_{P_i} \rangle_{L^2(\Omega)} &= \int_\Omega e_w \begin{bmatrix} 1 & -\partial_y & \partial_x \end{bmatrix} \delta(\boldsymbol{x} - \boldsymbol{x}_{P_i}) \mathbf{u}_{P_i} \, \mathrm{d}\Omega \\ &= \int_\Omega \delta(\boldsymbol{x} - \boldsymbol{x}_{P_i}) \begin{bmatrix} 1 \\ \partial_y \\ -\partial_x \end{bmatrix} e_w \cdot \mathbf{u}_{P_i} = \left\langle \mathcal{B}^*_{\Omega,i} e_w, \, \mathbf{u}_{P_i} \right\rangle_{L^2(\Omega)} \end{aligned} \tag{10.12}$$

The model is subject to the following homogeneous boundary conditions

$$\begin{aligned} \partial_t e_w|_{\Gamma_D} = 0, \qquad & -\boldsymbol{n} \cdot \mathrm{Div}\, \boldsymbol{E}_\kappa - \partial_{\boldsymbol{s}}(\boldsymbol{E}_\kappa : (\boldsymbol{n} \otimes \boldsymbol{s}))|_{\Gamma_N} = 0, \\ \partial_x e_w|_{\Gamma_D} = 0, \qquad & \boldsymbol{E}_\kappa : (\boldsymbol{n} \otimes \boldsymbol{n})|_{\Gamma_N} = 0, \end{aligned}.$$

where $\Gamma_D = \{y = 0\}$, and $\Gamma_N = \{x = 0 \cup x = L_x \cup y = L_y\}$. The flexible plate is then discretized using the Hellan-Herrmann-Johnson elements 7.16. The Dirac distribution is approximated by the following boxcar function

$$\delta^{\mathrm{app}}(\boldsymbol{x} - \boldsymbol{x}_{P_i}) = \begin{cases} 4\, h_x h_y, & |x - x_{P_i}| \le h_x \;\text{ and }\; |y - y_{P_i}| \le h_y, \\ 0, & \text{elsewhere}, \end{cases} \tag{10.13}$$

where h_x, h_y are the mesh sizes along x and y respectively. In particular 8 elements are taken along the x direction and 60 for the y direction. The following finite-dimensional model is then obtained

$$\begin{aligned}\text{Diag}\begin{bmatrix}\mathbf{M}_{\rho h}\\ \mathbf{M}_{\mathcal{C}_b}\\ \mathbf{0}\end{bmatrix}\begin{pmatrix}\dot{\mathbf{e}}_w\\ \dot{\mathbf{e}}_\kappa\\ \dot{\boldsymbol{\lambda}}_{\Gamma_D}\end{pmatrix} &= \begin{bmatrix}\mathbf{0} & -\mathbf{D}_{\text{HHJ}}^\top & \mathbf{G}_{\Gamma_D}^\top\\ \mathbf{D}_{\text{HHJ}} & \mathbf{0} & \mathbf{0}\\ -\mathbf{G}_{\Gamma_D} & \mathbf{0} & \mathbf{0}\end{bmatrix}\begin{pmatrix}\mathbf{e}_w\\ \mathbf{e}_\kappa\\ \boldsymbol{\lambda}_{\Gamma_D}\end{pmatrix} + \sum_{i=1}^{n_{\text{comp}}}\begin{bmatrix}\mathbf{B}_{\Omega,i}\\ \mathbf{0}\\ \mathbf{0}\end{bmatrix}\mathbf{u}_{P_i},\\ \mathbf{y}_{P_i} &= \begin{bmatrix}\mathbf{B}_{\Omega,i}^\top & \mathbf{0} & \mathbf{0}\end{bmatrix}\begin{pmatrix}\mathbf{e}_w\\ \mathbf{e}_\kappa\\ \boldsymbol{\lambda}_{\Gamma_D}\end{pmatrix}, \qquad \forall i \in \{1, n_{\text{comp}}\}.\end{aligned} \tag{10.14}$$

Matrix $\mathbf{D}_{\text{HHJ}}$ represents the discretization of the bilinear form (7.17). Matrix $\mathbf{G}_{\Gamma_D}$ collects the degrees of freedom subject to the boundary condition. If the degrees of freedom are ordered so that nodes subject to boundary conditions are placed after the non constrained degrees of freedom, this matrix takes the form $\mathbf{G}_{\Gamma_D} = [\mathbf{0} \quad \mathbf{I}]$. Recalling the property of the derivative of the delta distribution

$$\delta'[\phi] = -\delta[\phi'],$$

where the apostrophe denotes a generic derivative, matrix $\mathbf{B}_{\Omega,i}$ is computed as

$$\mathbf{B}_{\Omega,i}^j = \int_\Omega \delta^{\text{app}}(\boldsymbol{x} - \boldsymbol{x}_{P_i})\begin{bmatrix}1 & \partial_y & -\partial_x\end{bmatrix}\phi_w^j \,\mathrm{d}\Omega, \qquad \forall j \in \{1, n_w\}, \tag{10.15}$$

where ϕ_w^j, $\forall j \in \{1, n_w\}$ is the test function associated to e_w.

Proof-mass actuator model A proof-mass actuator is mathematically modelled by a hollow cylinder casing of mass m_{c_i}, $i \in \{1, 2\}$ and inertia with respect to the center of mass $\mathbf{J}_{c_i} = \text{Diag}(J_{c_i}^{xx},\ J_{c_i}^{yy})$. The casing is connected to a spring-damper-mass system of stiffness k_i, damping c_i and internal mass m_i. The overall model for this system is written in co-energies pH form as

$$\begin{aligned}\begin{bmatrix}m_{c_i} & 0 & 0 & 0 & 0\\ 0 & J_{c_i}^{xx} & 0 & 0 & 0\\ 0 & 0 & J_{c_i}^{yy} & 0 & 0\\ 0 & 0 & 0 & m_i & 0\\ 0 & 0 & 0 & 0 & k_i\end{bmatrix}\begin{pmatrix}\dot{v}_{c_i}\\ \dot{\omega}_{c_i}^x\\ \dot{\omega}_{c_i}^y\\ \dot{v}_i\\ \dot{\Delta x}_i\end{pmatrix} &= \begin{bmatrix}c_i & 0 & 0 & -c_i & k_i\\ 0 & 0 & 0 & 0 & 0\\ 0 & 0 & 0 & 0 & 0\\ -c_i & 0 & 0 & c_i & -k_i\\ -k_i & 0 & 0 & k_i & 0\end{bmatrix}\begin{pmatrix}v_{c_i}\\ \omega_{c_i}^x\\ \omega_{c_i}^y\\ v_i\\ \Delta x_i\end{pmatrix} + \begin{bmatrix}1 & 0 & 0\\ 0 & 1 & 0\\ 0 & 0 & 1\\ 0 & 0 & 0\\ 0 & 0 & 0\end{bmatrix}\mathbf{u}_{A_i},\\ \mathbf{y}_{A_i} &= \begin{bmatrix}1 & 0 & 0 & 0 & 0\\ 0 & 1 & 0 & 0 & 0\\ 0 & 0 & 1 & 0 & 0\end{bmatrix}\begin{pmatrix}v_{c_i}\\ \omega_{c_i}^x\\ \omega_{c_i}^y\\ v_i\\ \Delta x_i\end{pmatrix},\end{aligned} \tag{10.16}$$

where v_{c_i} is the velocity of the casing at its center of mass, $\omega_{c_i}^x$, $\omega_{c_i}^y$ are the angular velocities of the casing, v_i is the velocity of the internal mass and Δx_i is the elongation of the spring. $\boldsymbol{u}_{A_i} = [F_{A_i}^z,\ T_{A_i}^x,\ T_{A_i}^y]^\top$ are the external forces and torques acting on the casing.

Mirror model The mirror is a simple L-shaped rigid body with mass m_m, static moment s_m^x and inertia $\mathbf{J}_m = \mathrm{Diag}(J_m^{xx}, J_m^{yy})$

$$\begin{aligned} \begin{bmatrix} m_m & s_m^x & 0 \\ s_m^x & J_m^{xx} & 0 \\ 0 & 0 & J_m^{yy} \end{bmatrix} \begin{pmatrix} \dot{v}_m \\ \dot{\omega}_m^x \\ \dot{\omega}_m^y \end{pmatrix} &= \begin{bmatrix} 1 & 0 & 0 \\ 0 & 1 & 0 \\ 0 & 0 & 1 \end{bmatrix} \mathbf{u}_M, \\ \mathbf{y}_M &= \begin{bmatrix} 1 & 0 & 0 \\ 0 & 1 & 0 \\ 0 & 0 & 1 \end{bmatrix} \begin{pmatrix} v_m \\ \omega_m^x \\ \omega_m^y \end{pmatrix}, \end{aligned} \tag{10.17}$$

where v_m is the velocity of the mirror at its center of mass and $\omega_{c_i}^x$, $\omega_{c_i}^y$ its angular velocities. $\mathbf{u}_M = [F_M^z,\ T_M^x,\ T_M^y]^\top$ are the external forces and torques acting on the mirror.

Assembly of the model The overall model is obtained interconnecting each component to the others by means of transformer interconnections

$$\begin{aligned} \mathbf{u}_{P_1} &= -\mathbf{u}_{A_1}, & \mathbf{y}_{P_1} &= \mathbf{y}_{A_1}, & &\text{First actuator,} \\ \mathbf{u}_{P_2} &= -\mathbf{u}_{A_2}, & \mathbf{y}_{P_2} &= \mathbf{y}_{A_2}, & &\text{Second actuator,} \\ \mathbf{u}_{P_3} &= -\mathbf{u}_M, & \mathbf{y}_{P_3} &= \mathbf{y}_M, & &\text{Mirror.} \end{aligned}$$

10.2.2.2 Numerical results

The objective is the computation of the natural frequencies to assess the final model in comparison with [PSB+20]. For this reason, the damping of the proof-mass actuators c_i is neglected. Once all the components have been assembled together, the overall system takes the form

$$\mathbf{E}\dot{\mathbf{x}} = \mathbf{J}\mathbf{x}.$$

where $\mathbf{E} = \mathrm{Diag}(\mathbf{M},\ \mathbf{0})$. The parameters of each subsystem, retrieved from [San19], are reported in Table 10.6. In Fig. 10.13 the eigenvectors ψ_w associated to e_w and corresponding eigenfrequencies ω_i are reported. Their values and corresponding eigenvectors match those reported in [PSB+20, San19]. The mutual interaction between the flexible plate and the actuators dynamics is particularly evident for the first three frequencies. Above the third frequency, the actuators have little importance in the overall frequency response.

10.3 Conclusion

In this chapter the proposed formulation for multibody dynamics has been tested. The employment of finite elements leads to large sparse systems to be solved. To limit the computational complexity of these models, model reduction techniques can be incorporated. While for linear pHDAE systems consolidated methodologies exist [EKLS+18], for non linear

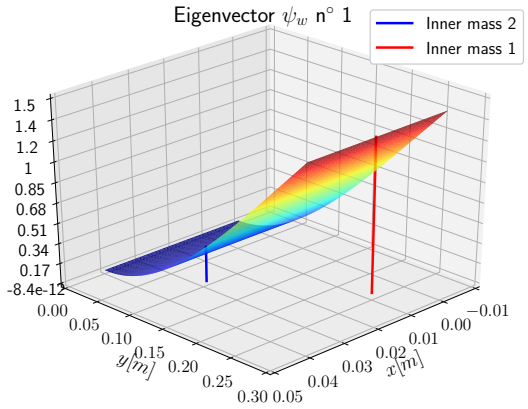

(a) 1st bending mode $\omega_1 = 10.21$ [Hz]

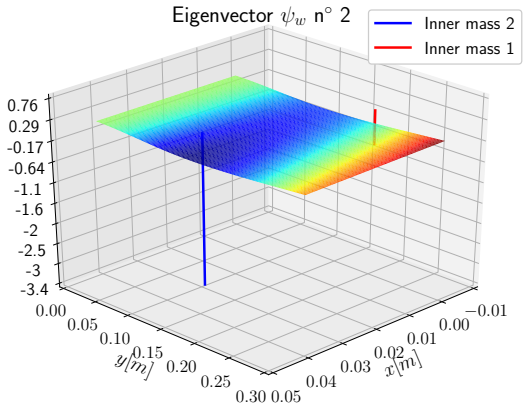

(b) 1st actuator mode $\omega_2 = 32.82$ [Hz]

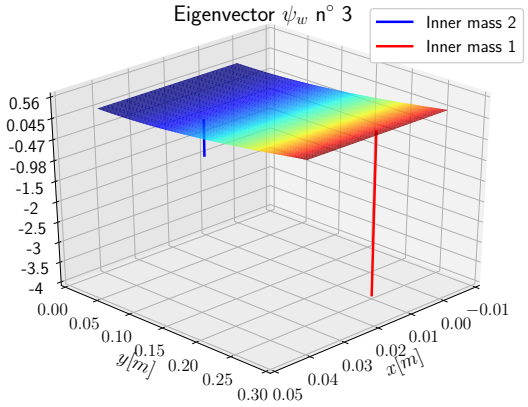

(c) 2nd actuator mode $\omega_3 = 34.89$ [Hz]

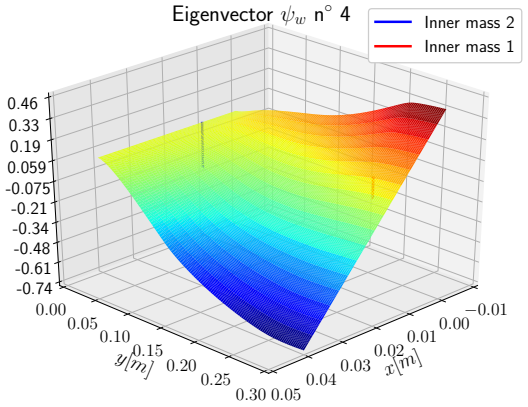

(d) 1st torsional mode $\omega_4 = 47.30$ [Hz]

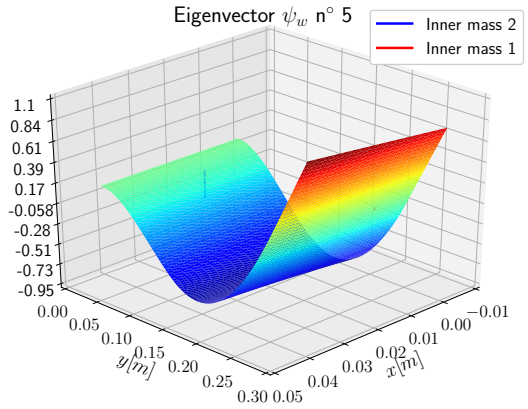

(e) 2nd bending mode $\omega_5 = 64.41$ [Hz]

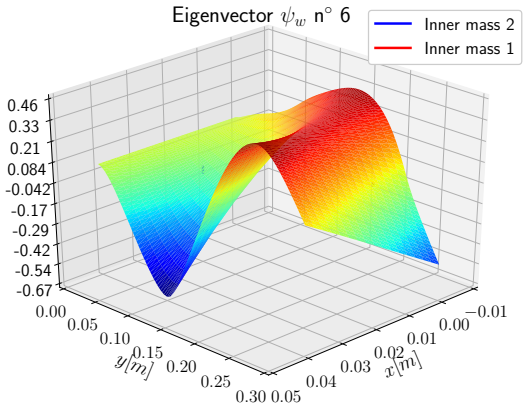

(f) 2nd torsional mode $\omega_6 = 118.09$ [Hz]

Figure 10.13: Eigenvectors for the experimental test-bench in [PSB+20]

Subsystem	Parameter	Description	Value
Flexible Plate	ρ	Density	2692 [kg/m^3]
	E	Young modulus	69 [GPa]
	ν	Poisson's ratio	0.33
	L_y	Length	28 [cm]
	L_x	Width	4 [cm]
	h	Thickness	3 [mm]
Proof-mass Actuators	m_i	Mass of the moving mass	23.6 [g]
	m_{c_i}	Casing mass	182.7 [g]
	$J_{c_i}^{xx}$	Casing inertia along x	0.3 [g $\cdot$ m^2]
	$J_{c_i}^{yy}$	Casing inertia along y	0.3 [g $\cdot$ m^2]
	k_i	Stiffness	1026 [N/m]
	$\boldsymbol{x}_{A_1} = \boldsymbol{x}_{P_1}$	Location 1st actuator	$[-1 \quad 25 \quad 0]^\top$ [cm]
	$\boldsymbol{x}_{A_2} = \boldsymbol{x}_{P_2}$	Location 2st actuator	$[1 \quad 10.5 \quad 0]^\top$ [cm]
Mirror	m_m	Mirror mass	23.4 [g]
	s_m^x	Static moment	-0.338 [g $\cdot$ m]
	J_m^{xx}	Mirror inertia along x	0.008 [g $\cdot$ m^2]
	J_m^{yy}	Mirror inertia along y	0.058 [g $\cdot$ m^2]
	$\boldsymbol{x}_M = \boldsymbol{x}_{P_3}$	Location mirror	$[0 \quad 28 \quad 0]^\top$ [cm]

Table 10.6: Parameters for each subsystem

differential-algebraic systems solutions are not yet available. To avoid the problem of dealing with large-scale systems, spectral methods can be equivalently used to achieve a structure preserving discretization made up of small and dense matrices. The time-domain simulations of the resulting systems have been accomplished using ready-to-use solvers. A rigorous numerical analysis represents an important future development. In particular, numerical methods capable of preserving important structural properties in discrete time have been studied for rigid body dynamics [CHR18] and generic ODE [KL19] and DAE [MM19] pH systems. These methods could be fruitfully employed in the proposed framework.

Conclusion

Conclusions and future directions

Je n'ai cherché de rien prouver, mais de bien peindre et d'éclairer bien ma peinture.

André Gide
Préface de L'Immoraliste

This work has investigated the benefits of the pH formalism as a physics-based modelling paradigm. Particular attention has been devoted to continuum mechanics models. These models are of hyperbolic nature and exhibit a partitioned structure when rephrased in pH form. This partitioned structure is intimately connected with an abstract integration by parts formula. These two concepts are crucial to demonstrate the well-posedness of linear pHs on multi-dimensional domains [Skr19]. Furthermore, they are at the core of the proposed finite element based discretization strategy. Because it is based on the partitioned structure of the problem, this methodology goes under the name of Partitioned Finite Element Method. As far as the system under consideration possesses this partitioned structure, the method remains applicable. Hence, it is not restricted to hyperbolic systems but can be extended to parabolic systems [SHM19b]. Non-linearities associated to the Hamiltonian are easily handled as well, since the constitutive law are discretized separately from the dynamics. The proposed discretization has been implemented using finite elements. There is a clear connection between the Partitioned Finite Element Method, mixed finite elements and standard finite elements discretization. For this reason a number of known finite elements can be used to achieve a structure-preserving discretization. Many conjectures for the error estimates are proposed and validated through numerical experiments, assessing the validity and the performance of the numerical schemes. The developed algorithms can be used to develop model-based control strategies. This is illustrated by means of the simple damping injection method. An application field that strongly benefits from the modularity of pHs is the dynamics of multibody system. It was shown that classical Lagrangian models based on the floating frame of reference paradigm can be recast as a coupled system of ODEs and PDEs in pH form. The floating frame of reference formulation is employed since it allows incorporating all linear mechanical models discussed in this thesis. The discretization used is then similar to a standard discretization with reduced integration of the stresses. It is then possible to connect together subcomponents to model mechanisms modularly.
There are many points that require further investigations. Possible future directions concern the following topics.

Modelling Only linear plate models have been formulated as pH systems. It is of interest to see how thin linear structures on manifolds, i.e. shells, can be formulated in terms of Hamiltonian systems. Boundary values problems have been formulated for the membrane problem and the Koiter shell [Cia00]. It should be possible to formulate these problems as

Hamiltonian systems by making use of differential geometry tools. To avoid the use of differential geometry, tangential differential calculus [DZ11] may also be employed. This framework has been successfully adopted to provide an intrinsic formulation of Kirchhoff [SF19a] and Mindlin [SF19b] shell problems.
For what concerns non linear models, it would be of great interest to see if the Föppl–von Kármán equations, describing the large deformations of thin plates [BTTD15], admit a pH reformulation.

Discretization Some issues deserve a deeper analysis concerning the discretization of plate models. The Kirchhoff plate discretization is achieved using a Dual-Mixed discretization and the non-conforming HHJ method. The first method is computationally expensive and for this reason has not been analyzed in the literature. For the second strategy, inhomogeneous boundary conditions in the presence of free boundary conditions are not easy to handle. To cope with the limitations of these two methodologies, the discretization proposed in [RZ18] may be used. This formulation allows using C^0-functions to approximate this problem with generic inhomogeneous boundary conditions. It would be of great interest to extend this method for the dynamic case.
For the Mindlin plate, a key point to address is the shear locking phenomenon. Mixed finite element allows constructing approximations of the static problem that are not affected by this phenomenon [BadVMR13]. For the dynamical case things get more complicated as the thickness plays a role also in the inertial terms.
A complete convergence study for the boundary-controlled wave equation is carried out in [HMS20]. Rigorous convergence studies for the models proposed in this work should be performed as well.
For the numerical implementation finite elements approximation has been used. However, spectral methods could be used as well. This would provide discretized systems of small dimension with dense matrices, drastically reducing the computational burdens. In particular modal analysis techniques may be employed to construct approximation for given frequency bandwidth.

Model reduction Model reduction strategies have not been addressed in this manuscript. Given the size of the matrices arising from the discretization, this remains a fundamental issue. Promising methodologies, relying on Proper Orthogonal Decomposition and H_2-optimal subspaces for non-linear pHODE [CBG16] and on Krylov methods for linear pHDAE [EKLS+18], are already available. In practice it is of interest to reduce the system accurately in a limited frequency bandwidth, representative of the system and instrumentation dynamics [Vui14]. Structure-preserving frequency limited model reduction techniques have been recently extended to pH systems [XJ20]. It would be of great interest to apply these techniques to the models proposed in this work.

Flexible multibody dynamics The proposed formulation gives rise to a stiff differential-algebraic system of index two. The resolution of these kind of problems is notoriously hard [BCP95]. There is a need for reliable and efficient computational tools for the time-integration. Methods preserving the passive nature of the system are of course preferable.
Another interesting topic would be the inclusion of large deformations. In principle, this should be possible using a co-rotational formulation or substructuring techniques [WH88].

Control The pH framework has proven to be rather effective for the design of control laws for non-linear systems [OGC04] and 1-dimensional boundary control PDEs [MLGR20]. A still open subject is the introduction of performance specifications in the pH formalism. Performance specifications are usually expressed in the frequency domain. For infinite-dimensional systems, recent works address the implementation of controllers based on H_∞ techniques [AN18, AN20]. These strategies are applicable to parabolic and hyperbolic PDEs. For pH systems, it would be of interest to see if robust and passivity-based control can be combined together. Furthermore it would be important to consider the case of non-collocated controls and observations [CR16]. By introducing appropriate state estimators [YY19], it should be possible to reconstruct the conjugated input to guarantee a passive output feedback.

Appendix A

Mathematical tools

A.1 Differential operators

The space of all, symmetric and skew-symmetric $d \times d$ matrices are denoted by $\mathbb{M}, \mathbb{S}, \mathbb{K}$ respectively. The space of $\mathbb{R}^d$ vectors is denoted by $\mathbb{V}$. $\Omega \subset \mathbb{R}^d$ is an open connected set. For a scalar field $u : \Omega \to \mathbb{R}$ the gradient is defined as

$$\operatorname{grad}(u) = \nabla u := \left(\partial_{x_1} u \dots \partial_{x_d} u\right)^\top.$$

For a vector field $\boldsymbol{u} : \Omega \to \mathbb{V}$, with components u_i, the gradient (Jacobian) is defined as

$$\operatorname{grad}(\boldsymbol{u})_{ij} := (\nabla \boldsymbol{u})_{ij} = \partial_{x_i} u_j.$$

The symmetric part of the gradient operator Grad (i.e. the deformation gradient in continuum mechanics) is thus given by

$$\operatorname{Grad}(\boldsymbol{u}) := \frac{1}{2}\left(\nabla \boldsymbol{u} + (\nabla \boldsymbol{u})^\top\right) \in \mathbb{S}.$$

The Hessian operator of u is then computed as follows

$$\operatorname{Hess}(u) = \nabla^2 u = \operatorname{Grad}(\operatorname{grad}(u)).$$

For a tensor field $\boldsymbol{U} : \Omega \to \mathbb{M}$, with components u_{ij}, the divergence is a vector, defined column-wise as

$$\operatorname{Div}(\boldsymbol{U}) = \nabla \cdot \boldsymbol{U} := \left(\sum_{i=1}^{d} \partial_{x_i} u_{ij}\right)_{j=1,\dots,d}.$$

The double divergence of a tensor field $\boldsymbol{U}$ is then a scalar field defined as

$$\operatorname{div}(\operatorname{Div}(\boldsymbol{U})) := \sum_{i=1}^{d}\sum_{j=1}^{d} \partial_{x_i}\partial_{x_j} u_{ij}.$$

Definition 7 (Formal adjoint, Def. 5.80 [RR04])
Consider the differential operator defined on Ω

$$\mathcal{L}(\boldsymbol{x}, \partial) = \sum_{|\alpha| \le k} a_\alpha(\boldsymbol{x}) \partial^\alpha, \tag{A.1}$$

where $\alpha := (\alpha_1, \dots, \alpha_d)$ *is a multi-index of order* $|\alpha| := \sum_{i=1}^{d} \alpha_i$, a_α *are a set of real scalars and* $\partial^\alpha := \partial_{x_1}^{\alpha_1} \dots \partial_{x_d}^{\alpha_d}$ *is a differential operator of order* $|\alpha|$ *resulting from a combination of spatial derivatives. The formal adjoint of* $\mathcal{L}$ *is the operator defined by*

$$\mathcal{L}^*(\boldsymbol{x}, \partial)u = \sum_{|\alpha| \leq k} (-1)^\alpha \partial^\alpha (a_\alpha(\boldsymbol{x}) u(\boldsymbol{x})). \tag{A.2}$$

The importance of this definition lies in the fact that

$$\langle \phi,\, \mathcal{L}(\boldsymbol{x}, \partial)\psi \rangle_\Omega = \langle \mathcal{L}^*(\boldsymbol{x}, \partial)\phi,\, \psi \rangle_\Omega \tag{A.3}$$

for every $\phi, \psi \in C_0^\infty(\Omega)$. If the assumption of compact support is removed, then (A.3) no longer holds; instead the integration by parts yields additional terms involving integrals over the boundary $\partial\Omega$. However, these boundary terms vanish if ϕ and ψ satisfy certain restrictions on the boundary.

A.2 Integration by parts

Theorem 7 (Integration by parts for tensors)
Consider a smooth tensor-valued function $\boldsymbol{A} \in \mathbb{R}^{d\times d}$ *and vector-valued function* $\boldsymbol{b} \in \mathbb{V} = \mathbb{R}^d$. *The following integration by parts formula holds*

$$\int_\Omega \{\mathrm{Div}(\boldsymbol{A}) \cdot \boldsymbol{b} + \boldsymbol{A} : \mathrm{grad}(\boldsymbol{b})\} \, \mathrm{d}\Omega = \int_\Omega \mathrm{div}(\boldsymbol{A}\boldsymbol{b}) \, \mathrm{d}\Omega = \int_{\partial\Omega} (\boldsymbol{A}^\top \boldsymbol{n}) \cdot \boldsymbol{b} \, \mathrm{d}S, \tag{A.4}$$

where $\boldsymbol{n}$ *is the outward normal at the boundary and* $\mathrm{d}S$ *the infinitesimal surface.*

Proof. Consider the components expression of Eq. (A.4)

$$\begin{aligned}
\int_\Omega \{\mathrm{Div}(\boldsymbol{A}) \cdot \boldsymbol{b} + \boldsymbol{A} : \mathrm{grad}(\boldsymbol{b})\} \, \mathrm{d}\Omega &= \int_\Omega \sum_{i=1}^{d} \sum_{j=1}^{d} \{(\partial_{x_i} A_{ij}) b_j + A_{ij} (\partial_{x_i} b_j)\} \, \mathrm{d}\Omega, \\
&= \int_\Omega \sum_{i=1}^{d} \sum_{j=1}^{d} \partial_{x_i} (A_{ij} b_j) \, \mathrm{d}\Omega = \int_\Omega \mathrm{div}(\boldsymbol{A}\boldsymbol{b}) \, \mathrm{d}\Omega, \\
&= \int_{\partial\Omega} \sum_{i=1}^{d} \sum_{j=1}^{d} (n_i A_{ij}) b_j \, \mathrm{d}S = \int_{\partial\Omega} (\boldsymbol{A}^\top \boldsymbol{n}) \cdot \boldsymbol{b} \, \mathrm{d}S.
\end{aligned} \tag{A.5}$$

□

The previous result can be specialized for symmetric tensor field [BBF+13, Chapter 1].

Theorem 8 (Integration by parts for symmetric tensors)
Consider a smooth tensor-valued function $\boldsymbol{M} \in \mathbb{S} = \mathbb{R}^{d\times d}_{sym}$ *and vector-valued function* $\boldsymbol{b} \in \mathbb{V} =$

$\mathbb{R}^d$. *Then, it holds*

$$\int_\Omega \{\mathrm{Div}(\boldsymbol{M})\cdot\boldsymbol{b}+\boldsymbol{M}:\mathrm{Grad}(\boldsymbol{b})\}\ \mathrm{d}\Omega=\int_\Omega \mathrm{div}(\boldsymbol{M}\boldsymbol{b})\ \mathrm{d}\Omega=\int_{\partial\Omega}(\boldsymbol{M}\,\boldsymbol{n})\cdot\boldsymbol{b}\ \mathrm{d}S. \tag{A.6}$$

Proof. Consider the components expression of Eq. (A.6)

$$\int_\Omega \{\mathrm{Div}(\boldsymbol{M})\cdot\boldsymbol{b}+\boldsymbol{M}:\mathrm{Grad}(\boldsymbol{b})\}\ \mathrm{d}\Omega=\int_\Omega \sum_{i=1}^{d}\sum_{j=1}^{d}\left\{(\partial_{x_i}M_{ij})b_j+M_{ij}\frac{1}{2}(\partial_{x_i}b_j+\partial_{x_j}b_i)\right\}\ \mathrm{d}\Omega, \tag{A.7}$$

The term $M_{ij}\frac{1}{2}(\partial_{x_i}b_j+\partial_{x_j}b_i)$ can be manipulated exploiting the symmetry of the tensor $\boldsymbol{M}$

$$\begin{aligned}\sum_{i=1}^{d}\sum_{j=1}^{d}\frac{1}{2}(M_{ij}\partial_{x_i}b_j+M_{ij}\partial_{x_j}b_i)&=\sum_{i=1}^{d}\sum_{j=1}^{d}\frac{1}{2}(M_{ij}\partial_{x_i}b_j+M_{ji}\partial_{x_i}b_j),\\&=\sum_{i=1}^{d}\sum_{j=1}^{d}\frac{1}{2}(M_{ij}+M_{ji})\partial_{x_i}b_j \qquad \text{Since } \boldsymbol{M} \text{ is symmetric,}\\&=\sum_{i=1}^{d}\sum_{j=1}^{d}M_{ij}\partial_{x_i}b_j=\boldsymbol{M}:\mathrm{grad}(\boldsymbol{b})\end{aligned} \tag{A.8}$$

Then it holds

$$\int_\Omega \{\mathrm{Div}(\boldsymbol{M})\cdot\boldsymbol{b}+\boldsymbol{M}:\mathrm{Grad}(\boldsymbol{b})\}\ \mathrm{d}\Omega=\int_\Omega \{\mathrm{Div}(\boldsymbol{M})\cdot\boldsymbol{b}+\boldsymbol{M}:\mathrm{grad}(\boldsymbol{b})\}\ \mathrm{d}\Omega \tag{A.9}$$

Using Eq (A.4) then

$$\begin{aligned}\int_\Omega \{\mathrm{Div}(\boldsymbol{M})\cdot\boldsymbol{b}+\boldsymbol{M}:\mathrm{Grad}(\boldsymbol{b})\}\ \mathrm{d}\Omega&=\int_\Omega \{\mathrm{Div}(\boldsymbol{M})\cdot\boldsymbol{b}+\boldsymbol{M}:\mathrm{grad}(\boldsymbol{b})\}\ \mathrm{d}\Omega,\\&=\int_{\partial\Omega}(\boldsymbol{M}^\top\boldsymbol{n})\cdot\boldsymbol{b}\ \mathrm{d}S, \qquad \text{Since } \boldsymbol{M} \text{ is symmetric,}\\&=\int_{\partial\Omega}(\boldsymbol{M}\,\boldsymbol{n})\cdot\boldsymbol{b}\ \mathrm{d}S.\end{aligned} \tag{A.10}$$

This concludes the proof. □

A.3 Bilinear forms

Definition 8 (Skew-symmetric bilinear form)
A bilinear form on the Hilbert space H

$$\begin{aligned}b: H\times H &\longrightarrow \mathbb{R},\\(\boldsymbol{v},\boldsymbol{u}) &\longrightarrow b(\boldsymbol{v},\boldsymbol{u}),\end{aligned}$$

is skew-symmetric iff

$$b(\boldsymbol{v}, \boldsymbol{u}) = -b(\boldsymbol{u}, \boldsymbol{v}).$$

A.4 Properties of the cross product

We denote by $[\boldsymbol{a}]_\times$ the skew symmetric map associated to vector $\boldsymbol{a} = [a_x, a_y, a_z]^\top$

$$[\boldsymbol{a}]_\times = \begin{bmatrix} 0 & -a_z & a_y \\ a_z & 0 & -a_x \\ -a_y & a_x & 0 \end{bmatrix} \tag{A.11}$$

This map allows rewriting the cross product as a matrix vector product $\boldsymbol{a} \wedge \boldsymbol{b} = [\boldsymbol{a}]_\times \boldsymbol{b}$. The cross product satisfies the anticommutativity property

$$[\boldsymbol{a}]_\times \boldsymbol{b} = -[\boldsymbol{b}]_\times \boldsymbol{a}, \qquad \boldsymbol{a}, \boldsymbol{b} \in \mathbb{R}^3. \tag{A.12}$$

Furthermore, it satisfies the Jacobi Identity

$$[\boldsymbol{a}]_\times ([\boldsymbol{b}]_\times \boldsymbol{c}) + [\boldsymbol{b}]_\times ([\boldsymbol{c}]_\times \boldsymbol{a}) + [\boldsymbol{c}]_\times ([\boldsymbol{a}]_\times \boldsymbol{b}) = 0, \qquad \boldsymbol{a}, \boldsymbol{b}, \boldsymbol{c} \in \mathbb{R}^3. \tag{A.13}$$

A.5 Index of a differential-algebraic system

When dealing with differential-algebraic systems an important notion is the index.

Definition 9
The index of a DAE is the minimum number of differentiation steps required to transform a DAE into an ODE.

Consider for simplicity a generic linear pH system arising from the weak imposition of the boundary conditions or from a multibody application. The equations are

$$\begin{aligned} \mathbf{M}\dot{\mathbf{e}} &= \mathbf{J}\mathbf{e} + \mathbf{G}^\top \boldsymbol{\lambda} + \mathbf{B}\mathbf{u}, \\ \mathbf{0} &= -\mathbf{G}\mathbf{e}. \end{aligned}$$

Matrix $\mathbf{M}$ is squared and invertible and matrix $\mathbf{G}$ is full row rank. If the second equation is derived twice in time, then it is obtained

$$\dot{\boldsymbol{\lambda}} = -(\mathbf{G}\mathbf{M}^{-1}\mathbf{G}^\top)^{-1}\mathbf{G}\mathbf{M}^{-1}(\mathbf{J}\dot{\mathbf{e}} + \mathbf{B}\dot{\mathbf{u}}).$$

Therefore, the system index is two.

Appendix B

Supplementary material: tabulated results of Chapter 7

$\frac{1}{h}$	$\|\|e_w - e_w^h\|\|_{L^\infty(H^2)}$ Error	Order	$\|\|e_\kappa - e_\kappa^h\|\|_{L^\infty(L^2)}$ Error	Order
4	2.03e-01	—	7.58e-02	—
8	4.39e-02	2.21	1.90e-02	1.99
16	1.02e-02	2.09	4.77e-03	1.99
32	2.52e-03	2.02	1.19e-03	1.99
64	6.27e-04	2.00	2.98e-04	1.99
128	1.56e-04	2.00	7.47e-05	1.99

Table B.1: Euler Bernoulli convergence result for the HerDG1 scheme.

$\frac{1}{h}$	$\|\|e_w - e_w^h\|\|_{L^\infty(L^2)}$ Error	Order	$\|\|e_\kappa - e_\kappa^h\|\|_{L^\infty(H^2)}$ Error	Order
4	1.61e-02	—	7.48e-01	—
8	4.05e-03	1.99	1.88e-01	1.99
16	1.01e-03	1.99	4.71e-02	1.99
32	2.53e-04	1.99	1.17e-02	1.99
64	6.34e-05	1.99	2.94e-03	1.99
128	1.58e-05	1.99	7.37e-04	1.99

Table B.2: Euler Bernoulli convergence result for the DG1Her scheme.

$\frac{1}{h}$	$\|\|e_w - e_w^h\|\|_{L^\infty(H^1)}$ Error	Order	$\|\|e_\kappa - e_\kappa^h\|\|_{L^\infty(H^1)}$ Error	Order
4	5.93e-01	—	4.16e-00	—
8	2.57e-01	1.20	2.08e-00	0.99
16	1.26e-01	1.02	1.04e-00	0.99
32	6.29e-02	1.00	5.22e-01	0.99
64	3.14e-02	1.00	2.61e-01	0.99
128	1.57e-02	1.00	1.30e-01	0.99

Table B.3: Euler Bernoulli convergence result for the CGCG scheme $k = 1$.

$\frac{1}{h}$	$\|\|e_w - e_w^h\|\|_{L^\infty(H^1)}$		$\|\|e_\kappa - e_\kappa^h\|\|_{L^\infty(H^1)}$	
	Error	Order	Error	Order
4	5.66e-02	—	4.20e-01	—
8	1.38e-02	2.03	1.05e-01	1.99
16	3.34e-03	2.05	2.65e-02	1.99
32	8.16e-04	2.03	6.62e-03	1.99
64	2.01e-04	2.01	1.65e-03	1.99
128	5.01e-05	2.00	4.14e-04	2.00

Table B.4: Euler Bernoulli convergence result for the CGCG scheme $k = 2$.

$\frac{1}{h}$	$\|\|e_w - e_w^h\|\|_{L^\infty(H^1)}$		$\|\|e_\kappa - e_\kappa^h\|\|_{L^\infty(H^1)}$	
	Error	Order	Error	Order
2	3.16e-02	—	2.19e-01	—
4	4.04e-03	2.97	2.80e-02	2.96
8	5.06e-04	2.99	3.51e-03	2.99
16	6.33e-05	3.00	4.39e-04	2.99
32	7.91e-06	3.00	5.50e-05	2.99
64	1.26e-06	2.64	6.88e-06	2.99

Table B.5: Euler Bernoulli convergence result for the CGCG scheme $k = 3$.

$\frac{1}{h}$	$\|\|e_w - e_w^h\|\|_{L^\infty(L^2)}$		$\|\|\boldsymbol{e}_\theta - \boldsymbol{e}_\theta^h\|\|_{L^\infty(L^2)}$		$\|\|\boldsymbol{E}_\kappa - \boldsymbol{E}_\kappa^h\|\|_{L^\infty(L^2)}$		$\|\|\boldsymbol{e}_\gamma - \boldsymbol{e}_\gamma^h\|\|_{L^\infty(L^2)}$	
	Error	Order	Error	Order	Error	Order	Error	Order
4	1.62e-05	—	1.51e-04	—	4.89e-08	—	5.83e-07	—
8	6.52e-06	1.31	4.59e-05	1.71	1.45e-08	1.75	2.01e-07	1.53
16	3.28e-06	0.98	2.17e-05	1.07	5.69e-09	1.34	9.41e-08	1.09
32	1.64e-06	0.99	1.07e-05	1.01	2.63e-09	1.10	4.64e-08	1.02
64	8.24e-07	0.99	5.39e-06	1.00	1.29e-09	1.02	2.31e-08	1.00

Table B.6: Mindlin plate convergence result for the BJT scheme $k = 1$.

$\frac{1}{h}$	$\|\|e_w - e_w^h\|\|_{L^\infty(L^2)}$		$\|\|\boldsymbol{e}_\theta - \boldsymbol{e}_\theta^h\|\|_{L^\infty(L^2)}$		$\|\|\boldsymbol{E}_\kappa - \boldsymbol{E}_\kappa^h\|\|_{L^\infty(L^2)}$		$\|\|\boldsymbol{e}_\gamma - \boldsymbol{e}_\gamma^h\|\|_{L^\infty(L^2)}$	
	Error	Order	Error	Order	Error	Order	Error	Order
4	8.05e-06	—	7.22e-05	—	1.72e-08	—	2.42e-07	—
8	2.12e-06	1.92	1.87e-05	1.94	4.42e-09	1.96	6.06e-08	2.00
16	5.42e-07	1.96	4.09e-06	2.19	1.14e-09	1.95	1.43e-08	2.07
32	1.36e-07	1.99	1.04e-06	1.97	2.89e-10	1.97	3.56e-09	2.00
64	3.41e-08	1.99	2.62e-07	1.99	7.26e-11	1.99	8.88e-10	2.00

Table B.7: Mindlin plate convergence result for the BJT scheme $k = 2$.

$\frac{1}{h}$	$\|\|e_w - e_w^h\|\|_{L^\infty(L^2)}$		$\|\|\boldsymbol{e}_\theta - \boldsymbol{e}_\theta^h\|\|_{L^\infty(L^2)}$		$\|\|\boldsymbol{E}_\kappa - \boldsymbol{E}_\kappa^h\|\|_{L^\infty(L^2)}$		$\|\|\boldsymbol{e}_\gamma - \boldsymbol{e}_\gamma^h\|\|_{L^\infty(L^2)}$	
	Error	Order	Error	Order	Error	Order	Error	Order
2	6.98e-07	—	1.42e-05	—	1.54e-09	—	3.31e-08	—
4	1.09e-07	2.67	2.14e-06	2.72	2.31e-10	2.73	4.61e-09	2.84
8	1.44e-08	2.91	2.29e-07	3.22	2.42e-11	3.25	6.36e-10	2.85
16	1.83e-09	2.97	2.05e-08	3.19	2.62e-12	3.20	8.44e-11	2.91
32	2.30e-10	2.99	2.94e-09	3.08	3.00e-13	3.12	1.07e-11	2.97

Table B.8: Mindlin plate convergence result for the BJT scheme $k = 3$.

$\frac{1}{h}$	$\|\|e_w - e_w^h\|\|_{L^\infty(L^2)}$		$\|\|\boldsymbol{e}_\theta - \boldsymbol{e}_\theta^h\|\|_{L^\infty(L^2)}$		$\|\|\boldsymbol{E}_\kappa - \boldsymbol{E}_\kappa^h\|\|_{L^\infty(L^2)}$		$\|\|\boldsymbol{e}_\gamma - \boldsymbol{e}_\gamma^h\|\|_{L^\infty(L^2)}$	
	Error	Order	Error	Order	Error	Order	Error	Order
4	1.05e-05	—	7.96e-05	—	3.75e-08	—	6.54e-07	—
8	5.33e-06	0.98	3.53e-05	1.17	1.15e-08	1.70	3.73e-07	0.80
16	2.68e-06	0.99	1.75e-05	1.00	3.02e-09	1.92	1.92e-07	0.95
32	1.34e-06	0.99	8.80e-06	0.99	7.71e-10	1.97	9.72e-08	0.98

Table B.9: Mindlin plate convergence result for the AFW scheme $k = 1$.

$\frac{1}{h}$	$\|\|e_w - e_w^h\|\|_{L^\infty(L^2)}$		$\|\|\boldsymbol{e}_\theta - \boldsymbol{e}_\theta^h\|\|_{L^\infty(L^2)}$		$\|\|\boldsymbol{E}_\kappa - \boldsymbol{E}_\kappa^h\|\|_{L^\infty(L^2)}$		$\|\|\boldsymbol{e}_\gamma - \boldsymbol{e}_\gamma^h\|\|_{L^\infty(L^2)}$	
	Error	Order	Error	Order	Error	Order	Error	Order
4	8.43e-06	—	8.10e-05	—	1.80e-08	—	2.68e-07	—
8	2.28e-06	1.88	1.82e-05	2.15	4.79e-09	1.90	6.99e-08	1.93
16	5.85e-07	1.96	4.41e-06	2.04	1.22e-09	1.96	1.75e-08	1.99
32	1.47e-07	1.98	1.12e-06	1.97	3.03e-10	2.01	4.47e-09	1.97

Table B.10: Mindlin plate convergence result for the AFW scheme $k = 2$.

$\frac{1}{h}$	$\|\|e_w - e_w^h\|\|_{L^\infty(L^2)}$		$\|\|\boldsymbol{e}_\theta - \boldsymbol{e}_\theta^h\|\|_{L^\infty(L^2)}$		$\|\|\boldsymbol{E}_\kappa - \boldsymbol{E}_\kappa^h\|\|_{L^\infty(L^2)}$		$\|\|\boldsymbol{e}_\gamma - \boldsymbol{e}_\gamma^h\|\|_{L^\infty(L^2)}$	
	Error	Order	Error	Order	Error	Order	Error	Order
2	1.11e-06	—	1.63e-05	—	2.14e-09	—	4.63e-08	—
4	1.63e-07	2.77	2.56e-06	2.67	2.61e-10	3.04	6.96e-09	2.73
8	2.13e-08	2.93	2.63e-07	3.28	2.42e-11	3.42	9.90e-10	2.81
16	2.93e-09	2.86	4.24e-08	2.63	8.99e-12	1.43	3.64e-10	1.44

Table B.11: Mindlin plate convergence result for the AFW scheme $k = 3$.

	$\|\|\boldsymbol{E}_r - \boldsymbol{E}_r^h\|\|_{L^\infty(L^2)}$					
	$k = 1$		$k = 2$		$k = 3$	
$\frac{1}{h}$	Error	Order	Error	Order	Error	Order
4	2.45e-09	—	1.07e-09	—	1.57e-09	—
8	4.98e-10	2.29	2.48e-10	2.11	3.52e-10	2.15
16	1.26e-10	1.97	6.11e-11	2.02	8.67e-11	2.02
32	3.19e-11	1.98	1.52e-11	1.99	2.16e-11	2.00

Table B.12: Mindlin plate convergence result for the Lagrange multiplier $\boldsymbol{E}_r$.

$\frac{1}{h}$	$\|\|e_w - e_w^h\|\|_{L^\infty(H^1)}$		$\|\|\boldsymbol{e}_\theta - \boldsymbol{e}_\theta^h\|\|_{L^\infty(H^{\mathrm{Grad}})}$		$\|\|\boldsymbol{E}_\kappa - \boldsymbol{E}_\kappa^h\|\|_{L^\infty(L^2)}$		$\|\|\boldsymbol{e}_\gamma - \boldsymbol{e}_\gamma^h\|\|_{L^\infty(L^2)}$	
	Error	Order	Error	Order	Error	Order	Error	Order
8	7.30e-05	—	5.52e-04	—	3.99e-08	—	9.02e-07	—
16	3.13e-05	1.22	2.26e-04	1.28	1.88e-08	1.08	5.47e-07	0.72
32	1.57e-05	0.99	1.11e-04	1.02	8.84e-09	1.09	2.94e-07	0.89
64	7.87e-06	0.99	5.57e-05	0.99	4.31e-09	1.03	1.50e-07	0.97
128	3.94e-06	0.99	2.78e-05	0.99	2.14e-09	1.01	7.55e-08	0.99

Table B.13: Mindlin plate convergence result for the CGDG scheme $k = 1$.

$\frac{1}{h}$	$\|\|e_w - e_w^h\|\|_{L^\infty(H^1)}$		$\|\|\boldsymbol{e}_\theta - \boldsymbol{e}_\theta^h\|\|_{L^\infty(H^{\mathrm{Grad}})}$		$\|\|\boldsymbol{E}_\kappa - \boldsymbol{E}_\kappa^h\|\|_{L^\infty(L^2)}$		$\|\|\boldsymbol{e}_\gamma - \boldsymbol{e}_\gamma^h\|\|_{L^\infty(L^2)}$	
	Error	Order	Error	Order	Error	Order	Error	Order
8	9.78e-06	—	1.04e-04	—	7.30e-09	—	1.77e-07	—
16	2.53e-06	1.95	2.49e-05	2.07	1.85e-09	1.97	4.93e-08	1.84
32	6.35e-07	1.99	6.06e-06	2.04	4.63e-10	1.99	1.27e-08	1.95
64	1.58e-07	1.99	1.50e-06	2.01	1.15e-10	2.00	3.21e-09	1.98
128	3.97e-08	2.00	3.74e-07	2.00	2.89e-11	2.00	8.06e-10	1.99

Table B.14: Mindlin plate convergence result for the CGDG scheme $k = 2$.

$\frac{1}{h}$	$\|\|e_w - e_w^h\|\|_{L^\infty(H^1)}$		$\|\|\boldsymbol{e}_\theta - \boldsymbol{e}_\theta^h\|\|_{L^\infty(H^{\mathrm{Grad}})}$		$\|\|\boldsymbol{E}_\kappa - \boldsymbol{E}_\kappa^h\|\|_{L^\infty(L^2)}$		$\|\|\boldsymbol{e}_\gamma - \boldsymbol{e}_\gamma^h\|\|_{L^\infty(L^2)}$	
	Error	Order	Error	Order	Error	Order	Error	Order
4	1.38e-06	—	1.24e-05	—	8.24e-10	—	2.24e-08	—
8	1.79e-07	2.94	1.51e-06	3.03	1.03e-10	2.99	2.90e-09	2.94
16	2.26e-08	2.98	1.88e-07	3.00	1.28e-11	3.00	3.64e-10	2.99
32	2.83e-09	2.99	2.36e-08	2.99	1.60e-12	3.00	4.54e-11	3.00
64	3.54e-10	2.99	2.95e-09	2.99	2.00e-13	3.00	5.67e-12	3.00

Table B.15: Mindlin plate convergence result for the CGDG scheme $k = 3$.

$\frac{1}{h}$	$\|\|e_w - e_w^h\|\|_{L^\infty(H^1)}$		$\|\|\boldsymbol{E}_\kappa - \boldsymbol{E}_\kappa^h\|\|_{L^\infty(L^2)}$	
	Error	Order	Error	Order
4	1.38e-00	—	5.11e+01	—
8	5.17e-01	1.41	2.64e+01	0.95
16	2.28e-01	1.18	1.33e+01	0.98
32	1.09e-01	1.05	6.68e-00	0.99
64	5.45e-02	1.01	3.34e-00	0.99

Table B.16: Kirchhoff plate convergence result for the HHJ scheme $k = 1$ (SSSS test).

$\frac{1}{h}$	$\|\|e_w - e_w^h\|\|_{L^\infty(H^1)}$		$\|\|\boldsymbol{E}_\kappa - \boldsymbol{E}_\kappa^h\|\|_{L^\infty(L^2)}$	
	Error	Order	Error	Order
4	1.47e-01	—	6.58e-00	—
8	3.48e-02	2.08	1.70e-00	1.94
16	8.51e-03	2.03	4.31e-01	1.98
32	2.11e-03	2.00	1.08e-01	1.99
64	5.28e-04	2.00	2.70e-02	1.99

Table B.17: Kirchhoff plate convergence result for the HHJ scheme $k = 2$ (SSSS test).

$\frac{1}{h}$	$\|\|e_w - e_w^h\|\|_{L^\infty(H^1)}$		$\|\|\boldsymbol{E}_\kappa - \boldsymbol{E}_\kappa^h\|\|_{L^\infty(L^2)}$	
	Error	Order	Error	Order
2	1.15e-01	—	4.85e-00	—
4	1.51e-02	2.92	6.42e-01	2.91
8	1.92e-03	2.97	8.10e-02	2.98
16	2.41e-04	2.99	1.01e-02	2.99
32	3.02e-05	2.99	1.26e-03	3.00

Table B.18: Kirchhoff plate convergence result for the HHJ scheme $k = 3$ (SSSS test).

$\frac{1}{h}$	$\|\|e_w - e_w^h\|\|_{L^\infty(H^2)}$		$\|\|\boldsymbol{E}_\kappa - \boldsymbol{E}_\kappa^h\|\|_{L^\infty(L^2)}$	
	Error	Order	Error	Order
2	6.63e-00	—	3.60e+01	—
4	1.91e-00	1.79	9.99e-00	1.85
8	6.08e-01	1.64	3.29e-00	1.60
16	2.09e-01	1.54	1.14e-00	1.52
32	7.34e-02	1.50	4.01e-01	1.50

Table B.19: Kirchhoff plate convergence result for the BellDG3 scheme (SSSS test).

$\frac{1}{h}$	$\|\|e_w - e_w^h\|\|_{L^\infty(H^1)}$		$\|\|\boldsymbol{E}_\kappa - \boldsymbol{E}_\kappa^h\|\|_{L^\infty(L^2)}$	
	Error	Order	Error	Order
4	5.94e-00	—	1.62e+01	—
8	2.35e-00	1.33	9.27e-00	0.81
16	9.98e-01	1.23	4.86e-00	0.93
32	4.69e-01	1.08	2.46e-00	0.98
64	2.34e-01	1.00	1.23e-00	0.99

Table B.20: Kirchhoff plate convergence result for the HHJ scheme $k = 1$ (CSFS test).

$\frac{1}{h}$	$\|\|e_w - e_w^h\|\|_{L^\infty(H^1)}$		$\|\|\boldsymbol{E}_\kappa - \boldsymbol{E}_\kappa^h\|\|_{L^\infty(L^2)}$	
	Error	Order	Error	Order
4	1.13e-00	—	4.14e-00	—
8	2.90e-01	1.96	1.19e-00	1.79
16	7.14e-02	2.02	3.13e-01	1.93
32	1.77e-02	2.00	7.96e-02	1.97
64	4.43e-03	2.00	2.00e-02	1.98

Table B.21: Kirchhoff plate convergence result for the HHJ scheme $k = 2$ (CSFS test).

$\frac{1}{h}$	$\|\|e_w - e_w^h\|\|_{L^\infty(H^1)}$		$\|\|\boldsymbol{E}_\kappa - \boldsymbol{E}_\kappa^h\|\|_{L^\infty(L^2)}$	
	Error	Order	Error	Order
2	1.57e-00	—	4.25e-00	—
4	2.39e-01	2.71	8.44e-01	2.33
8	3.37e-02	2.82	1.16e-01	2.85
16	4.50e-03	2.90	1.49e-02	2.95
32	5.76e-04	2.96	1.89e-03	2.98

Table B.22: Kirchoff plate convergence result for the HHJ scheme $k = 3$ (CSFS test).

$\frac{1}{h}$	$\|\|e_w - e_w^h\|\|_{L^\infty(H^2)}$		$\|\|\boldsymbol{E}_\kappa - \boldsymbol{E}_\kappa^h\|\|_{L^\infty(L^2)}$	
	Error	Order	Error	Order
2	3.88e+01	—	2.40e+01	—
4	8.17e-00	2.24	4.41e-00	2.44
8	2.71e-00	1.58	1.50e-00	1.54
16	1.13e-00	1.25	5.36e-01	1.49
32	4.35e-01	1.38	1.90e-01	1.49

Table B.23: Kirchhoff plate convergence result for the BellDG3 scheme (CSFS test).

Appendix C

Implementation using FEniCS and Firedrake

In this appendix, the main tools needed for implementing PFEM in FEniCS and Firedrake libraries are illustrated. It is assumed to a recent version of FEniCS and Firedrake is available, either through local installation (Anaconda or installation from source for FEniCS and virtual Python environment for Firedrake) or through Docker containers. Additional information concerning the installation can be found at https://fenicsproject.org/download/ for FEniCS and https://www.firedrakeproject.org/download.html for Firedrake.

This tutorial is by no means a complete introductory tutorial. It is intended to provide the general commands needed for the implementation of PFEM and to highlight similarities and differences between FEniCS and Firedrake. For readers interested in a comprehensive documentation, the FEniCS developers have written a book to explain the functioning of the library [LMW+12], whereas the Firedrake developers employ illustrative tutorials[1].

In this appendix, boxes colored in red are used for FEniCS, cyan for Firedrake, gray for identical commands in both libraries and green for implementations based on Scipy. The FEniCS or Firedrake library is assumed to be loaded through the star import:

```
from fenics import *
```

or

```
from firedrake import *
```

Furthermore, the Numpy library and some methods of the Scipy sparse library are needed[2]:

```
import numpy as np
from scipy.sparse import csr_matrix
from scipy.sparse import lil_matrix
```

[1] https://www.firedrakeproject.org/documentation.html
[2] https://www.scipy.org/

```
from scipy.sparse import vstack, hstack, block_diag
from scipy.sparse.linalg import eigs
```

As an illustration we consider the discretization of the Mindlin plate using the CGDG elements (7.21). We first illustrate how to compute the mass and interconnection matrices. Then, the construction of the boundary control matrix is explained by retrieving a SCIPY sparse matrix from the matrix computed by FENICS or FIREDRAKE.

Creation of a mixed function space

For the discretization of pHs one has to use a mixed function space, i.e. a collection of more than one function space. Consider the creation of the Mindlin plate CGDG elements (7.21) on a unit square simplicial mesh with 40 elements per side.

Mixed function space in FENICS

```
n_el  = 40
mesh  = UnitSquareMesh(n_el, n_el)
P_w   = FiniteElement('CG', triangle, 1)          # vertical velocity
P_th  = VectorElement('CG', triangle, 1)          # angular velocity
P_kap = VectorElement('DG', triangle, 0, dim=3)   # bending momenta
P_gam = VectorElement('DG', triangle, 0)          # shear stress
elem  = MixedElement([P_w, P_th, P_kap, P_gam])
V     = FunctionSpace(mesh, elem)
```

Mixed function space in FIREDRAKE

```
n_el  = 40
mesh  = UnitSquareMesh(n_el, n_el)
V_w   = FunctionSpace(mesh, "CG", 1)
V_th  = VectorFunctionSpace(mesh, "CG", 1)
V_kap = VectorFunctionSpace(mesh, "DG", 0, dim=3)
V_gam = VectorFunctionSpace(mesh, "DG", 0)
V     = MixedFunctionSpace([V_w, V_th, V_kap, V_gam])
```

The space `V_kap` has dimension 3 since it corresponds to variable $\boldsymbol{E}_\kappa \in \mathbb{R}^{2\times 2}_{\text{sym}} \cong \mathbb{R}^3$, ($\cong$ stands for isomorphic).

Definition of variational forms

The precedent commands create a mixed function space that can be used to construct variational forms trough the Unified Form Language[3] [ALO+14] (UFL). UFL is a core component

[3] https://readthedocs.org/projects/fenics-ufl/downloads/pdf/latest/

of FEniCS and has been adopted in Firedrake as well. It is an expressive domain-specific language for abstractly representing (finite element) variational formulations of differential equations. In particular, this language defines a syntax for the integration of variational forms over various domains.

Given the previously defined mixed function space, consider the definition of the mass and interconnection variational forms (the implementation is the same in both libraries since UFL is a common component).

Definition of the variational forms (FEniCS & Firedrake)

```
# Physical parameters
E   = 1e12
nu  = 0.3
rho = 2600
h   = 0.1
k   = 5/6
G   = E / 2 / (1 + nu)
F   = G * h * k

# Definition of the bending curvature operator
def bending_curv(mom):
    kappa = 12. / (E * h ** 3) * ((1+nu)*mom - nu * Identity(2) * tr(mom))
    return kappa

# Test variables
v = TestFunction(V)
v_w, v_th, v_kap, v_gam = split(v)

# Co-energy variables
e = TrialFunction(V)
e_w, e_th, e_kap, e_gam = split(e)

# Convert the R^3 vector to a symmetric tensor
v_kap = as_tensor([[v_kap[0], v_kap[1]],
                   [v_kap[1], v_kap[2]]])
e_kap = as_tensor([[e_kap[0], e_kap[1]],
                   [e_kap[1], e_kap[2]]])

# Energy variables
a_w   = rho * h * e_w
a_th  = (rho * h ** 3) / 12. * e_th
a_kap = bending_curv(e_kap)
a_gam = 1. / F * e_gam
```

```
# Mass bilinear form
m_form = v_w * a_w * dx + dot(v_th, a_th) * dx + \
         inner(v_kap, a_kap) * dx + dot(v_gam, a_gam) * dx

# Interconnection bilinear form
j_form = dot(v_gam, grad(e_w)) * dx - dot(grad(v_w), e_gam) * dx + \
         inner(v_kap, sym(grad(e_th))) * dx - \
         inner(sym(grad(v_th)), e_kap) * dx + \
         dot(v_th, e_gam) * dx - dot(v_gam, e_th) * dx
```

This sample code highlights the strength of the UFL library. The expressive implementation is really close to the abstract mathematical formulation.

Matrices assemble

Once the forms have been declared, it is possible to actually construct the associated matrices. Consider the case of a clamped (i.e. Dirichlet) boundary condition. For the CGDG elements a clamped condition corresponds to essential boundary conditions. These are defined in the same way in FEniCS and Firedrake

Dirichlet boundary conditions (FEniCS & Firedrake)

```
bcs = []
bcs.append(DirichletBC(V.sub(0), Constant(0.0), "on_boundary"))
bcs.append(DirichletBC(V.sub(1), Constant((0.0, 0.0)), "on_boundary"))
```

The subspaces `V.sub(0)`, `V.sub(1)` correspond to spaces `V_w`, `V_th` associated to the vertical velocity and the angular velocity, respectively. The boundary conditions can now be incorporated in the matrices. The final assemble of the matrices is achieved in FEniCS by the following code snippet.

Matrices assemble in FEniCS

```
J, M = PETScMatrix(), PETScMatrix()
dummy = v_w * dx
assemble_system(j_form, dummy, bcs, A_tensor=J)
assemble_system(m_form, dummy, bcs, A_tensor=M)
```

Matrices are first defined as PETSc[4] matrices and forms are assembled into it. The boundary conditions have been applied to the stiffness matrix using `assemble_system` so as to preserve symmetry (a dummy right-hand side vector has been introduced to call this function). The same matrices are constructed in Firedrake by the following code

[4] https://www.mcs.anl.gov/petsc/

Matrices assemble in FIREDRAKE

```
J_ass = assemble(j_form, bcs=bcs, mat_type='aij')
M_ass = assemble(m_form, bcs=bcs, mat_type='aij')
J = J_ass.M.handle
M = M_ass.M.handle
```

The option `mat_type` specifies the desired format for the matrix representation. To get a final PETSc matrix, the AIJ format is used. The method `M.handle` provides as outputs PETSc matrices that can be manipulated by the `pesct4py` library[5].

For what concerns the ordering of the degrees of freedom, FIREDRAKE just piles up the degrees of freedom of each subspace. The final matrices have the same structure as in (6.93). For FENICS the default option is a not-natural ordering to cluster the non-zero entries closer to the diagonal. A natural ordering can be set by changing the `reorder_dofs_serial` parameter[6].

Eigenvalues computation with SLEPc

A simple test to assess the validity of the finite element discretization consists in computing the eigenvalues of the matrices, to assess the absence of spurious modes. The SLEPc library is used to this end[7] [HRV05]. Since we are interested in the lowest eigenvalues, a shift-and-invert method is used. It is known that for this problem the first normalized eigenfrequencies

$$\widehat{\omega}_i = \omega_i \, (2(1+\nu)\rho/E)^{1/2}$$

are close to 1 [DR80]. Hence, a good choice for the spectral shift is $\sigma = (2(1+\nu)\rho/E)^{-1/2}$. The following code computes the eigenvalues.

Eigenvalues computation in FENICS

```
solver = SLEPcEigenSolver(J, M)
solver.parameters["solver"] = "krylov-schur"
# Set the problem type: the J matrix is not hermitian nor positive.
solver.parameters["problem_type"] = "pos_gen_non_hermitian"
# We look for eigenvalues on the imaginary axis.
solver.parameters["spectrum"] = "target imaginary"
solver.parameters["spectral_transform"] = "shift-and-invert"
solver.parameters["spectral_shift"] = 1/((2*(1+nu)*rho)/E)**0.5
solver.solve(40)
n_conv = solver.get_number_converged()
```

[5] https://www.mcs.anl.gov/petsc/petsc4py-current/docs/apiref/index.html
[6] https://fenicsproject.discourse.group/t/ordering-of-mixed-elements/946
[7] https://slepc.upv.es/documentation/slepc.pdf

```
omega_tilde = []
for i in range(n_conv):
    lam_r, lam_i, psi_r, psi_i = solver.get_eigenpair(i)

    # Discard the zero eigenvalues due to the bcs.
    if lam_i > 1e-5:
        omega_tilde.append(lam_i *((2 * (1 + nu) * rho) / E) ** 0.5)
```

For FIREDRAKE the equivalent code snippet is the following.

Eigenvalues computation in FIREDRAKE

```
# Check for SLEPc
from firedrake.petsc import PETSc
try:
    from slepc4py import SLEPc
except ImportError:
    import sys
    warning("Unable to import SLEPc (try firedrake-update --slepc)")
    sys.exit(0)

# Options for the solver.
opts = PETSc.Options()
opts.setValue("pos_gen_non_hermitian", None)
opts.setValue("st_pc_factor_shift_type", "NONZERO")
opts.setValue("eps_type", "krylovschur")
opts.setValue("st_type", "sinvert")
opts.setValue("st_shift", 1/(((2*(1+nu)*rho)/E)**0.5))
opts.setValue("eps_target", 1/(((2*(1+nu)*rho)/E)**0.5))

# Construction of the eigensolver.
es = SLEPc.EPS().create(comm=COMM_WORLD)
es.setDimensions(40)
es.setOperators(J, M)
es.setFromOptions()
es.solve()

n_conv = es.getConverged()
psi_r, psi_i = J.getVecs()
omega_tilde = []
for i in range(n_conv):
    lam = es.getEigenpair(i, psi_r, psi_i)
    lam_i = np.imag(lam)
```

```
    if lam_i > 1e-5:
        omega_tilde.append(lam_i*((2*(1+nu)*rho)/E)**0.5)
```

In Fig. C.1 the 6 first eigenvectors are plotted. The associated eigenvalues are consistent with the results reported in [DR80].

Conversion to Scipy for direct manipulation of the boundary matrices

If boundary control has to be taken into account, it is preferable to move to SCIPY for manipulating and constructing the final matrices. Consider now the case of a Mindlin plate with Neumann boundary control. The construction of the mass and interconnection matrices is the same, without imposing any boundary conditions. For the boundary variables we choose Lagrange polynomials of order 1.

Remark 31 (Construction of the **B** matrix)
Notice that FENICS and FIREDRAKE do not support Function spaces defined on the boundary. It is therefore necessary to construct the **B** *matrix using functions defined on the domain and then eliminate the useless columns. First, we show how to construct the* **B** *matrix containing all degrees of freedom. Later on, the extraction of the boundary degrees of freedom is illustrated using SCIPY.*

Control matrix construction in FENICS

```
P_qn  = FiniteElement('CG', triangle, 1)   # shear force
P_Mnn = FiniteElement('CG', triangle, 1)   # flexural momentum
P_Mns = FiniteElement('CG', triangle, 1)   # torsional momentum
elem  = MixedElement([P_qn, P_Mnn, P_Mns])

V_u   = FunctionSpace(mesh, elem)
q_n, M_nn, M_ns = TrialFunction(V_u)

n_ver = FacetNormal(mesh)
s_ver = as_vector([-n_ver[1], n_ver[0]])

b_form = v_w * q_n * ds + dot(v_th, n_ver) * M_nn * ds + \
         dot(v_th, s_ver) * M_ns * ds
B_petsc = PETScMatrix()
assemble(b_form, B_petsc)
B = B_petsc.mat()
```

The method `mat()` in FENICS provides a PETCs matrix manageable by `petsc4py`, similarly to the method `M.handle` in FIREDRAKE.

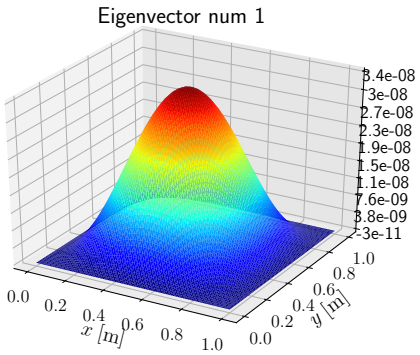

(a) $\widehat{\omega}_1 = 1.60$

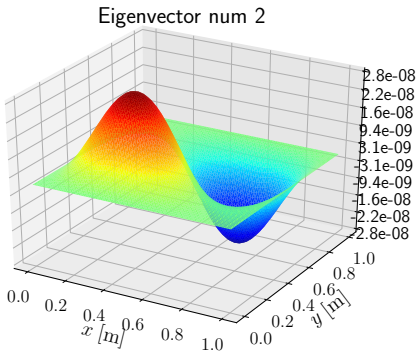

(b) $\widehat{\omega}_2 = 3.06$

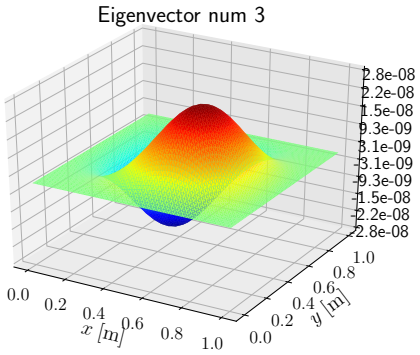

(c) $\widehat{\omega}_3 = 3.07$

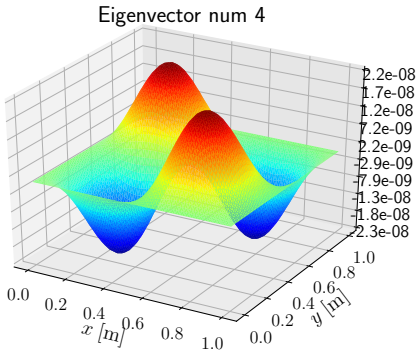

(d) $\widehat{\omega}_4 = 4.31$

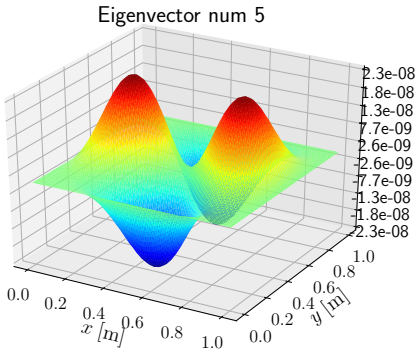

(e) $\widehat{\omega}_3 = 5.08$

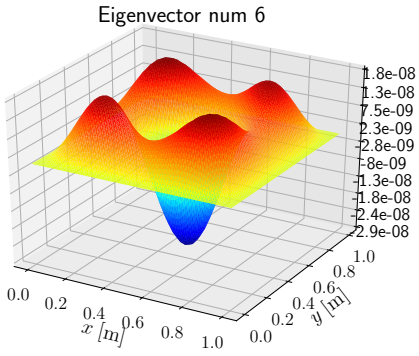

(f) $\widehat{\omega}_4 = 5.13$

Figure C.1: Eigenvectors for the clamped Mindlin plate computed with FIREDRAKE. The eigenfrequencies are normalized $\widehat{\omega} = \omega((2(1+\nu)\rho/E)^{1/2}$.

Control matrix construction in FIREDRAKE

```
V_qn  = FunctionSpace(mesh, 'CG', 1)
V_Mnn = FunctionSpace(mesh, 'CG', 1)
V_Mns = FunctionSpace(mesh, 'CG', 1)

V_u = V_qn * V_Mnn * V_Mns
q_n, M_nn, M_ns = TrialFunction(V_u)

n_ver = FacetNormal(mesh)  # outward normal to the boundary
s_ver = as_vector([-n_ver[1], n_ver[0]])  # tangent versor to the boundary

b_form = v_w * q_n * ds + dot(v_th, n_ver) * M_nn * ds + \
         dot(v_th, s_ver) * M_ns * ds
B_ass = assemble(b_form, mat_type='aij')
B = B_ass.M.handle
```

The matrix `B` computed with FENICS and FIREDRAKE has now the type `petsc4py.PETSc.Mat` and can be converted to a SCIPY sparse CSR matrix (compressed sparse row format). As anticipated in Remark 31, the zero columns associated with interior degrees of freedom have to be removed from the matrix.

Construction of the final $\mathbf{B}$ matrix (SCIPY)

```
# Conversion to CSR scipy format
B_scipy_cols = csr_matrix(B.getValuesCSR()[::-1])

# Non zero rows and columns
rows, cols = csr_matrix.nonzero(B_scipy_cols)

# Indexes of non zero columns
set_cols = np.array(list(set(cols)))

# Number of non zero columns (i.e. number of inputs)
n_u = len(set(cols))

# Initialization of the final matrix in lil folmat
# for efficient incremental construction.
B_scipy = lil_matrix((V.dim(), n_u))

for r, c in zip(rows, cols):
    # Column index in the final matrix
    ind_col = np.where(set_cols == c)[0]

    # Fill the matrix with the values
```

```
    B_scipy[r, ind_col] = B_scipy_cols[r, c]

# Convert to csr format
B_scipy.tocsr()
```

Similarly Scipy matrices in CSR format can be obtained for the mass $\mathbf{M}$ and interconnection $\mathbf{J}$ matrix, thus obtaining the final boundary controlled system

$$\mathbf{M}\dot{\mathbf{e}} = \mathbf{J}\mathbf{e} + \mathbf{B}\mathbf{u}.$$

This system can then be simulated using time integrator libraries available in Scipy[8].

Stability check of the boundary subspace

To check if the discretization of the boundary variable is appropriate, one can solve the eigenvalues problem

$$\begin{bmatrix} \mathbf{M} & \mathbf{0} \\ \mathbf{0} & \mathbf{0} \end{bmatrix} \begin{pmatrix} \boldsymbol{\psi}_e^i \\ \boldsymbol{\psi}_\lambda^i \end{pmatrix} j\omega_i = \begin{bmatrix} \mathbf{J} & \mathbf{B} \\ -\mathbf{B}^\top & \mathbf{0} \end{bmatrix} \begin{pmatrix} \boldsymbol{\psi}_e^i \\ \boldsymbol{\psi}_\lambda^i \end{pmatrix},$$

and check the consistency of the eigenvalues, i.e. no spurious modes appear.

Eigenvalues computation using Lagrange multipliers (Scipy)

```
# Conversion to scipy CSR matrices
# Important: no boundary conditions imposed
J_scipy = csr_matrix(J.getValuesCSR()[::-1])  # for fenics J.mat()
M_scipy = csr_matrix(M.getValuesCSR()[::-1])  # for fenics M.mat()

Z_mat = csr_matrix((n_u, n_u))
J_aug = vstack((hstack((J_scipy, B_scipy)), hstack((-B_scipy.T, Z_mat))))
M_aug = block_diag((M_scipy, Z_mat))

# Shift value
shift = 1/(((2*(1+nu)*rho)/E)**0.5)
# Resolution of the eigenproblem
eigenvalues, eigvectors = eigs(J_aug, k=40, M=M_aug,\
                           sigma=shift, which='LM', tol=1e-6)

omega_all = np.imag(eigenvalues)
index = omega_all >= 1e-5
omega = omega_all[index]
omega.sort()
```

[8] https://docs.scipy.org/doc/scipy/reference/integrate.html

```
omega_tilde = omega*((2*(1+nu)*rho)/E)**0.5
```

The following values are obtained

$$\widehat{\omega}_1 = 1.59, \qquad \widehat{\omega}_2 = 3.04, \qquad \widehat{\omega}_3 = 3.06,$$
$$\widehat{\omega}_4 = 4.29, \qquad \widehat{\omega}_5 = 5.05, \qquad \widehat{\omega}_6 = 5.10.$$

Since no spurious eigenvalues occur, it is legitimate to assume that the Lagrange multiplier subspace is a stable one (among others). This is just a heuristic reasoning, since the rigorous mathematical justification of the boundary subspace stability comes from the fulfillment of the *inf-sup* condition.

Concluding remarks

This appendix provides all the tools needed for constructing of the matrices and for handling uniform boundary conditions. If one has to consider mixed boundary conditions, the boundary forms and Dirichlet conditions have to be defined on a subset of the boundary (consult https://fenicsproject.org/pub/tutorial/sphinx1/._ftut1005.html for an explanation in FEniCS and https://www.firedrakeproject.org/variational-problems.html for Firedrake).

Bibliography

[AB85] D. Arnold and F. Brezzi. Mixed and nonconforming finite element methods: implementation, postprocessing and error estimates. *ESAIM: Mathematical Modelling and Numerical Analysis-Modélisation Mathématique et Analyse Numérique*, 19(1):7–32, 1985.

[Abe12] R. Abeyaratne. *Lecture Notes on the Mechanics of Elastic Solids. Volume II: Continuum Mechanics*. Cambridge, MA and Singapore, 1st edition, 2012.

[ACPC02] M. Amara, D. Capatina-Papaghiuc, and A. Chatti. Bending moment mixed method for the Kirchhoff–Love plate model. *SIAM Journal on Numerical Analysis*, 40(5):1632–1649, 2002.

[ACRMA17] S. Aoues, F.L. Cardoso-Ribeiro, D. Matignon, and D. Alazard. Modeling and control of a rotating flexible spacecraft: A port-Hamiltonian approach. *IEEE Transactions on Control Systems Technology*, 27(1):355–362, 2017.

[AFÅ15] C. Andersson, C. Führer, and J. Åkesson. Assimulo: A unified framework for ODE solvers. *Mathematics and Computers in Simulation*, 116(0):26 – 43, 2015.

[AFS68] J.H. Argyris, I. Fried, and D.W. Scharpf. The TUBA family of plate elements for the matrix displacement method. *The Aeronautical Journal (1968)*, 72(692):701–709, 1968.

[AFW07] D. Arnold, R. Falk, and R. Winther. Mixed finite element methods for linear elasticity with weakly imposed symmetry. *Mathematics of Computation*, 76(260):1699–1723, 2007.

[AL00] G. Avalos and I. Lasiecka. Boundary controllability of thermoelastic plates via the free boundary conditions. *SIAM Journal on Control and Optimization*, 38(2):337–383, 2000.

[AL14] D. Arnold and J. Lee. Mixed methods for elastodynamics with weak symmetry. *SIAM Journal on Numerical Analysis*, 52(6):2743–2769, 2014.

[ALO+14] M.S. Alnæs, A. Logg, K.B. Ølgaard, M.E. Rognes, and G.N. Wells. Unified form language: A domain-specific language for weak formulations of partial differential equations. *ACM Trans. Math. Softw.*, 40(2), March 2014.

[AN18] P. Apkarian and D. Noll. Structured H^∞-control of infinite-dimensional systems. *International Journal of Robust and Nonlinear Control*, 28(9):3212–3238, 2018.

[AN20] P. Apkarian and D. Noll. Boundary control of partial differential equations using frequency domain optimization techniques. *Systems & Control Letters*, 135:104577, 2020.

[APCL15] D. Alazard, J.A. Perez, C. Cumer, and T. Loquen. Two-input two-output port model for mechanical systems. In *AIAA Science and Technology Forum and Exposition. Kissimmee, Florida*, 2015.

[Arn90] D. Arnold. Mixed finite element methods for elliptic problems. *Computer Methods in Applied Mechanics and Engineering*, 82(1):281 – 300, 1990. Proceedings of the Workshop on Reliability in Computational Mechanics.

[AS86] O.P. Agrawal and A.A. Shabana. Application of deformable-body mean axis to flexible multibody system dynamics. *Computer Methods in Applied Mechanics and Engineering*, 56(2):217–245, 1986.

[Aug20] B. Augner. Well-posedness and stability for interconnection structures of port-Hamiltonian type. In Joachim Kerner, Hafida Laasri, and Delio Mugnolo, editors, *Control Theory of Infinite-Dimensional Systems*, pages 1–52, Cham, 2020. Springer International Publishing.

[AW02] D. Arnold and R. Winther. Mixed finite elements for elasticity. *Numerische Mathematik*, 92(3):401–419, 2002.

[AW19] D. Arnold and S. W. Walker. The Hellan-Herrmann-Johnson method with curved elements, 2019. arXiv preprint arXiv:1909.09687.

[BadVMR13] L. Beirão da Veiga, D. Mora, and R. Rodríguez. Numerical analysis of a locking-free mixed finite element method for a bending moment formulation of Reissner-Mindlin plate model. *Numerical Methods for Partial Differential Equations*, 29(1):40–63, 2013.

[Bal91] M. Balla. Analytical study of the thermal shock problem of a half-space with various thermoelastic models. *Acta Mechanica*, 89(1):73–92, Mar 1991.

[BAPBM19a] A. Brugnoli, D. Alazard, V. Pommier-Budinger, and D. Matignon. Interconnection of the Kirchhoff plate within the port-Hamiltonian framework. In *Proceedings of the 59th IEEE Conference on Decision and Control*, Dec 2019.

[BAPBM19b] A. Brugnoli, D. Alazard, V. Pommier-Budinger, and D. Matignon. Partitioned finite element method for the Mindlin plate as a port-Hamiltonian system. *IFAC-PapersOnLine*, 52(2):88 – 95, 2019. 3rd IFAC Workshop on Control of Systems Governed by Partial Differential Equations CPDE 2019.

[BAPBM19c] A. Brugnoli, D. Alazard, V. Pommier-Budinger, and D. Matignon. Port-Hamiltonian formulation and symplectic discretization of plate models. Part I: Mindlin model for thick plates. *Applied Mathematical Modelling*, 75:940 – 960, Nov 2019. https://doi.org/10.1016/j.apm.2019.04.035.

[BAPBM19d] A. Brugnoli, D. Alazard, V. Pommier-Budinger, and D. Matignon. Port-Hamiltonian formulation and symplectic discretization of plate models. Part II: Kirchhoff model for thin plates. *Applied Mathematical Modelling*, 75:961 – 981, Nov 2019. https://doi.org/10.1016/j.apm.2019.04.036.

[BAPBM20] A. Brugnoli, D. Alazard, V. Pommier-Budinger, and D. Matignon. Port-hamiltonian flexible multibody dynamics. *Multibody System Dynamics*, Oct 2020. https://doi.org/10.1007/s11044-020-09758-6.

[BAPBM21] A. Brugnoli, D. Alazard, V. Pommier-Budinger, and D. Matignon. Structure-preserving discretization of port-Hamiltonian plate models. Accepted for the 24st International Symposium on Mathematical Theory of Networks and Systems, Aug 2021.

[BBF+13] D. Boffi, F. Brezzi, M. Fortin, et al. *Mixed finite element methods and applications*, volume 44. Springer, 2013.

[BCP95] K.E. Brenan, S.L. Campbell, and L.R. Petzold. *Numerical Solution of Initial-Value Problems in Differential-Algebraic Equations*. Society for Industrial and Applied Mathematics, 1995.

[BCRHK20] A. Brugnoli, F. L. Cardoso-Ribeiro, G. Haine, and P. Kotyczka. Partitioned finite element method for power-preserving structured discretization with mixed boundary conditions. In *Proceedings of the 21st IFAC World Congress*, volume 53, pages 7647–7652, 2020.

[BDJ05] E. Bécache, G. Derveaux, and P. Joly. An efficient numerical method for the resolution of the Kirchhoff-Love dynamic plate equation. *Numerical Methods for Partial Differential Equations*, 21(2):323–348, 2005.

[BDM85] F. Brezzi, J.Jr. Douglas, and L.D. Marini. Two families of mixed finite elements for second order elliptic problems. *Numerische Mathematik*, 47:217–236, 1985.

[Bel69] K. Bell. A refined triangular plate bending finite element. *International Journal for Numerical Methods in Engineering*, 1(1):101–122, 1969.

[BGL05] M. Benzi, G. H. Golub, and J. Liesen. Numerical solution of saddle point problems. *Acta Numerica*, 14:1–137, 2005.

[BH15] P. Benner and J. Heiland. Time-dependent Dirichlet conditions in finite element discretizations. *ScienceOpen Research*, 2015.

[BHSV20] A. Brugnoli, G. Haine, A. Serhani, and X. Vasseur. Numerical approximation of port-Hamiltonian systems for hyperbolic or parabolic PDEs with boundary control. *arXiv preprint arXiv:2007.08326*, 2020. Under Review.

[Bio56] M.A. Biot. Thermoelasticity and irreversible thermodynamics. *Journal of Applied Physics*, 27(3):240–253, 1956.

[BJT00] E. Bécache, P. Joly, and C. Tsogka. An analysis of new mixed finite elements for the approximation of wave propagation problems. *SIAM Journal on Numerical Analysis*, 37(4):1053–1084, 2000.

[BJT01] E. Bécache, P. Joly, and C. Tsogka. A new family of mixed finite elements for the linear elastodynamic problem. *SIAM Journal on Numerical Analysis*, 39:2109–2132, 06 2001.

[BL08] O.A. Bauchau and A. Laulusa. Review of contemporary approaches for constraint enforcement in multibody systems. *Journal of Computational and Nonlinear Dynamics*, 3(1), 2008.

[BMXZ18] C. Beattie, V. Mehrmann, H. Xu, and H. Zwart. Linear port-Hamiltonian descriptor systems. *Mathematics of Control, Signals, and Systems*, 30(4):17, 2018.

[Bor70] J.P. Boris. Relativistic plasma simulation-optimization of a hybrid code. In *Proceedings of the Fourth Conference on Numerical Simulation of Plasmas*, pages 3–67, 1970.

[BR90] H. Blum and R. Rannacher. On mixed finite element methods in plate bending analysis. *Computational Mechanics*, 6(3):221–236, May 1990.

[Bre08] F. Brezzi. *Mixed finite elements, compatibility conditions, and applications.* Springer, 2008.

[BTTD15] S. Bilbao, O. Thomas, C. Touzé, and M. Ducceschi. Conservative numerical methods for the full von Kármán plate equations. *Numerical Methods for Partial Differential Equations*, 31(6):1948–1970, 2015.

[Car73] D. E. Carlson. Linear thermoelasticity. In C. Truesdell, editor, *Linear Theories of Elasticity and Thermoelasticity: Linear and Nonlinear Theories of Rods, Plates, and Shells*, pages 297–345. Springer, Berlin, Heidelberg, 1973.

[Car00] A. Cardona. Superelements modelling in flexible multibody dynamics. *Multibody System Dynamics*, 4(2):245–266, Aug 2000.

[CBG16] S. Chaturantabut, C. Beattie, and S. Gugercin. Structure-preserving model reduction for nonlinear port-Hamiltonian systems. *SIAM Journal on Scientific Computing*, 38(5):B837–B865, 2016.

[CDPGA17] J. Chebbi, V. Dubanchet, J.A. Perez Gonzalez, and D. Alazard. Linear dynamics of flexible multibody systems. *Multibody System Dynamics*, 41(1):75–100, Sep 2017.

[CF05] G. Cohen and S. Fauqueux. Mixed spectral finite elements for the linear elasticity system in unbounded domains. *SIAM Journal on Scientific Computing*, 26(3):864–884, 2005.

[CH58] J.W. Cahn and J.E. Hilliard. Free energy of a nonuniform system. I. Interfacial free energy. *The Journal of Chemical Physics*, 28(2):258–267, 1958.

[CH20] L. Chen and X. Huang. Finite elements for divdiv-conforming symmetric tensors. *arXiv preprint arXiv:2005.01271*, 2020.

[Cha62] P. Chadwick. On the propagation of thermoelastic disturbances in thin plates and rods. *Journal of the Mechanics and Physics of Solids*, 10(2):99–109, 1962.

[CHR18] E. Celledoni, E.H. Høiseth, and N. Ramzina. Passivity-preserving splitting methods for rigid body systems. *Multibody System Dynamics*, 44(3):251–275, 2018.

[Cia88] P.G. Ciarlet. *Mathematical Elasticity: Three-Dimensional Elasticity*. Studies in mathematics and its applications. North-Holland, 1988.

[Cia00] P.G. Ciarlet. *Mathematical elasticity: Volume III: Theory of shells*. Studies in Mathematics and Its Applications. North-Holland, May 2000.

[CMKO11] S.H. Christiansen, H.Z. Munthe-Kaas, and B. Owren. Topics in structure-preserving discretization. *Acta Numerica*, 20:1–119, 2011.

[Cou90] T.J. Courant. Dirac manifolds. *Transactions of the American Mathematical Society*, 319(2):631–661, 1990.

[CR16] F.L. Cardoso-Ribeiro. *Port-Hamiltonian modeling and control of fluid-structure system*. PhD thesis, Université de Toulouse, Dec. 2016.

[CRBML19] F.L. Cardoso-Ribeiro, A. Brugnoli, D. Matignon, and L. Lefèvre. Port-Hamiltonian modeling, discretization and feedback control of a circular water tank. In *Proceedings of the 59th IEEE Conference on Decision and Control*, Dec 2019.

[CRML18] F.L. Cardoso-Ribeiro, D. Matignon, and L. Lefèvre. A structure-preserving partitioned finite element method for the 2D wave equation. *IFAC-PapersOnLine*, 51(3):119 – 124, 2018. 6th IFAC Workshop on Lagrangian and Hamiltonian Methods for Nonlinear Control LHMNC 2018.

[CRML19] F.L. Cardoso-Ribeiro, D. Matignon, and L. Lefèvre. A partitioned finite element method for power-preserving discretization of open systems of conservation laws, 2019. arXiv preprint arXiv:1906.05965.

[CRMPB17] F.L. Cardoso-Ribeiro, D. Matignon, and V. Pommier-Budinger. A port-Hamiltonian model of liquid sloshing in moving containers and application to a fluid-structure system. *Journal of Fluids and Structures*, 69:402–427, February 2017.

[CvdSB07] J. Cervera, A.J. van der Schaft, and A. Baños. Interconnection of port-Hamiltonian systems and composition of Dirac structures. *Automatica*, 43(2):212–225, feb 2007.

[Dan50] V.I. Danilovskaya. Thermal stresses in an elastic half-space due to sudden heating of its boundary (in russian). *Prikladnaya Matematika i Mechanika*, 14:316–318, 1950.

[dHKS82] F.R. de Hoog, J.H. Knight, and A.N. Stokes. An improved method for numerical inversion of Laplace transforms. *SIAM Journal on Scientific and Statistical Computing*, 3(3):357–366, 1982.

[DHNLS99] R. Durán, L. Hervella-Nieto, E. Liberman, and J. Solomin. Approximation of the vibration modes of a plate by Reissner-Mindlin equations. *Mathematics of Computation of the American Mathematical Society*, 68(228):1447–1463, 1999.

[dKRV08] D. de Klerk, D.J. Rixen, and S.N. Voormeeren. General framework for dynamic substructuring: History, review and classification of techniques. *AIAA Journal*, 46(5):1169–1181, 2008.

[DMSB09] V. Duindam, A. Macchelli, S. Stramigioli, and H. Bruyninckx. *Modeling and Control of Complex Physical Systems*. Springer Verlag, 2009.

[DR80] D.J. Dawe and O.L. Roufaeil. Rayleigh-Ritz vibration analysis of Mindlin plates. *Journal of Sound and Vibration*, 69(3):345–359, 1980.

[DSP08] V. Dos Santos and C. Prieur. Boundary control of open channels with numerical and experimental validations. *IEEE Transactions on Control Systems Technology*, 16(6):1252–1264, 2008.

[DZ11] M.C. Delfour and J.P. Zolésio. *Shapes and geometries: metrics, analysis, differential calculus, and optimization*. Society for Industrial and Applied Mathematics, 2011.

[EK18] H. Egger and T. Kugler. Damped wave systems on networks: exponential stability and uniform approximations. *Numerische Mathematik*, 138(4):839–867, 2018.

[EKLS+18] H. Egger, T. Kugler, B. Liljegren-Sailer, N. Marheineke, and V. Mehrmann. On structure-preserving model reduction for damped wave propagation in transport networks. *SIAM Journal on Scientific Computing*, 40(1):A331–A365, 2018.

[ES18] M. Ellenbroek and J. Schilder. On the use of absolute interface coordinates in the floating frame of reference formulation for flexible multibody dynamics. *Multibody System Dynamics*, 43(3):193–208, Jul 2018.

[Fal08] R.S. Falk. Finite element methods for linear elasticity. In Daniele Boffi and Lucia Gastaldi, editors, *Mixed Finite Elements, Compatibility Conditions, and Applications*, pages 159–194. Springer Berlin Heidelberg, Berlin, Heidelberg, 2008.

[FJL15] P. Forni, D. Jeltsema, and G.A.D. Lopes. Port-Hamiltonian formulation of rigid-body attitude control. *IFAC-PapersOnLine*, 48(13):164 – 169, 2015. 5th IFAC Workshop on Lagrangian and Hamiltonian Methods for Nonlinear Control LHMNC 2015.

[Gev88] T. Geveci. On the application of mixed finite element methods to the wave equations. *ESAIM: M2AN*, 22(2):243–250, 1988.

[GH92] M.D. Gunzburger and S.L. Hou. Treating inhomogeneous essential boundary conditions in finite element methods and the calculation of boundary stresses. *SIAM Journal on Numerical Analysis*, 29(2):390–424, 1992.

[Gri11] P. Grisvard. *Elliptic Problems in Nonsmooth Domains*. Society for Industrial and Applied Mathematics, 2011.

[Gri15] M. Grinfeld. *Mathematical Tools for Physicists*. John Wiley & Sons Inc, 2nd edition, jan 2015.

[GSV18] T. Gustafsson, R. Stenberg, and J. Videman. A posteriori estimates for conforming Kirchhoff plate elements. *SIAM Journal on Scientific Computing*, 40(3):A1386–A1407, 2018.

[GTVDSM04] G. Golo, V. Talasila, A.J. Van Der Schaft, and B. Maschke. Hamiltonian discretization of boundary control systems. *Automatica*, 40(5):757–771, 2004.

[GV64] I.M. Gel'fand and N.Ya. Vilenkin. *Generalized functions: Applications of harmonic analysis*, volume 4. Academic press, 1964.

[HE09] R.B. Hetnarski and M.R. Eslami. *Thermal stresses: advanced theory and applications*, volume 158. Springer, 2009.

[Hel67] K. Hellan. Analysis of elastic plates in flexure by a simplified finite element method. *Acta Polytechnica Scandinavica*, 1967.

[Hen06] D. Henry. *Geometric theory of semilinear parabolic equations*, volume 840. Springer, 2006.

[Her67] L.R. Herrmann. Finite-element bending analysis for plates. *Journal of the Engineering Mechanics Division*, 93(5):13–26, 1967.

[HJ12] R.A. Horn and C.R. Johnson. *Matrix analysis*. Cambridge university press, 2012.

[HLW03] E. Hairer, C. Lubich, and G. Wanner. Geometric numerical integration illustrated by the Störmer–Verlet method. *Acta numerica*, 12:399–450, 2003.

[HM78] T.J.R. Hughes and J.E. Marsden. Classical elastodynamics as a linear symmetric hyperbolic system. *Journal of Elasticity*, 8(1):97–110, 1978.

[HMS20] G. Haine, D. Matignon, and A. Serhani. Numerical analysis of a structure-preserving space-discretization for an anisotropic and heterogeneous boundary controlled N-dimensional wave equation as port-Hamiltonian system. *arXiv preprint arXiv:2006.15032*, 2020.

[Hol08] D.D. Holm. *Geometric Mechanics: Part II: Rotating, Translating and Rolling*. World Scientific Publishing Company, 2008.

[HRV05] V. Hernandez, J.E. Roman, and V. Vidal. SLEPc: A scalable and flexible toolkit for the solution of eigenvalue problems. *ACM Trans. Math. Software*, 31(3):351–362, 2005.

[Hug12] T.J.R. Hughes. *The finite element method: linear static and dynamic finite element analysis*. Courier Corporation, 2012.

[Hur65] W.C. Hurty. Dynamic analysis of structural systems using component modes. *AIAA Journal*, 3(4):678–685, 1965.

[HZ97] S.W. Hansen and B.Y. Zhang. Boundary control of a linear thermoelastic beam. *Journal of Mathematical Analysis and Applications*, 210(1):182–205, 1997.

[JCLT20] G. Ju, M. Cai, J. Li, and J. Tian. Parameter-robust multiphysics algorithms for Biot model with application in brain edema simulation. *Mathematics and Computers in Simulation*, 177:385 – 403, 2020.

[Joh73] C. Johnson. On the convergence of a mixed finite-element method for plate bending problems. *Numerische Mathematik*, 21(1):43–62, 1973.

[Jol03] P. Joly. Variational methods for time-dependent wave propagation problems. In M. Ainsworth, P. Davies, D. Duncan, B. Rynne, and P. Martin, editors, *Topics in Computational Wave Propagation: Direct and Inverse Problems*, chapter 6, pages 201–264. Springer Berlin Heidelberg, Berlin, Heidelberg, 2003.

[JZ12] B. Jacob and H. Zwart. *Linear Port-Hamiltonian Systems on Infinite-dimensional Spaces*. Number 223 in Operator Theory: Advances and Applications. Springer Verlag, Germany, 2012. https://doi.org/10.1007/978-3-0348-0399-1.

[Kir18] R.C. Kirby. A general approach to transforming finite elements. *The SMAI journal of computational mathematics*, 4:197–224, 2018.

[KK15] R.C. Kirby and T. T. Kieu. Symplectic-mixed finite element approximation of linear acoustic wave equations. *Numerische Mathematik*, 130(2):257–291, Jun 2015.

[KL90] L. Kitis and R.K. Lindenberg. Natural frequencies and mode shapes of flexible mechanisms by a transfer matrix method. *Finite Elements in Analysis and Design*, 6(4):267 – 285, 1990.

[KL19] P. Kotyczka and L. Lefèvre. Discrete-time port-Hamiltonian systems: A definition based on symplectic integration. *Systems & Control Letters*, 133:104530, 2019.

[KM19] R.C. Kirby and L. Mitchell. Code generation for generally mapped finite elements. *ACM Trans. Math. Softw.*, 45(4), December 2019.

[KML18] P. Kotyczka, B. Maschke, and L. Lefèvre. Weak form of Stokes-Dirac structures and geometric discretization of port-Hamiltonian systems. *Journal of Computational Physics*, 361:442 – 476, 2018.

[Kot19] P. Kotyczka. *Numerical Methods for Distributed Parameter Port-Hamiltonian Systems*. TUM University Press, 2019.

[KS08] M. Krstic and A. Smyshlyaev. *Boundary control of PDEs: A course on backstepping designs*, volume 16. Society for Industrial and Applied Mathematics, 2008.

[KZ15] M. Kurula and H. Zwart. Linear wave systems on n-d spatial domains. *International Journal of Control*, 88(5):1063–1077, 2015. https://www.tandfonline.com/doi/abs/10.1080/00207179.2014.993337.

[KZvdSB10] M. Kurula, H. Zwart, A.J. van der Schaft, and J. Behrndt. Dirac structures and their composition on Hilbert spaces. *Journal of mathematical analysis and applications*, 372(2):402–422, 2010. https://doi.org/10.1016/j.jmaa.2010.07.004.

[Lag89] J.E. Lagnese. *Boundary Stabilization of Thin Plates*. Society for Industrial and Applied Mathematics, 1989.

[LB08] A. Laulusa and O.A. Bauchau. Review of classical approaches for constraint enforcement in multibody systems. *Journal of computational and nonlinear dynamics*, 3(1), 2008.

[LBS08] S. Leyendecker, P. Betsch, and P. Steinmann. The discrete null space method for the energy-consistent integration of constrained mechanical systems. Part III: Flexible multibody dynamics. *Multibody System Dynamics*, 19(1):45–72, Feb 2008.

[Lee12] J. Lee. *Mixed methods with weak symmetry for time dependent problems of elasticity and viscoelasticity.* PhD thesis, University of Minnesota, 2012.

[LGZM05] Y. Le Gorrec, H. Zwart, and B. Maschke. Dirac structures and boundary control systems associated with skew-symmetric differential operators. *SIAM Journal on Control and Optimization*, 44(5):1864–1892, 2005.

[Li18] L. Li. *Regge finite elements with applications in solid mechanics and relativity.* PhD thesis, University of Minnesota, 2018.

[LMW+12] A. Logg, K.A. Mardal, G.N. Wells, et al. *Automated Solution of Differential Equations by the Finite Element Method*. Springer, 2012.

[LPKL12] L.D. Landau, L.P. Pitaevskii, A.M. Kosevich, and E.M. Lifshitz. *Theory of Elasticity*. Butterworth Heinemann, third edition, Dec 2012.

[LR00] R. Lifshitz and M. L. Roukes. Thermoelastic damping in micro-and nanomechanical systems. *Physical review B*, 61(8):5600, 2000.

[Mar81] J.E. Marsden. *Lectures on geometric methods in mathematical physics*. CBMS-NSF Regional Conference Series in Applied Mathematics. SIAM, 1981.

[MBM+16] A.T.T. McRae, G.T. Bercea, L. Mitchell, D.A. Ham, and C.J. Cotter. Automated generation and symbolic manipulation of tensor product finite elements. *SIAM Journal on Scientific Computing*, 38(5):S25–S47, 2016.

[Min51] R.D. Mindlin. Influence of rotatory inertia and shear on flexural motions of isotropic elastic Plates. *Journal of Applied Mechanics*, 18:31–38, March 1951.

[MLGR20] A. Macchelli, Y. Le Gorrec, and H. Ramirez. Exponential stabilisation of port-Hamiltonian boundary control systems via energy-shaping. *IEEE Transactions on Automatic Control*, pages 1–1, 2020.

[MLGRZ16] A. Macchelli, Y. Le Gorrec, H. Ramírez, and H. Zwart. On the synthesis of boundary control laws for distributed port-Hamiltonian systems. *IEEE Transactions on Automatic Control*, 62(4):1700–1713, 2016.

[MLM12] R. Moulla, L. Lefevre, and B. Maschke. Pseudo-spectral methods for the spatial symplectic reduction of open systems of conservation laws. *Journal of computational Physics*, 231(4):1272–1292, 2012.

[MM04] A. Macchelli and C. Melchiorri. Modeling and control of the Timoshenko beam. The distributed port Hamiltonian approach. *SIAM Journal on Control and Optimization*, 43(2):743–767, 2004.

[MM19] V. Mehrmann and R. Morandin. Structure-preserving discretization for port-Hamiltonian descriptor systems. In *2019 IEEE 58th Conference on Decision and Control (CDC)*, pages 6863–6868, 2019.

[MMB05] A. Macchelli, C. Melchiorri, and L. Bassi. Port-based modelling and control of the Mindlin plate. In *Proceedings of the 44th IEEE Conference on Decision and Control*, pages 5989–5994, Dec. 2005.

[MMS07] A. Macchelli, C. Melchiorri, and S. Stramigioli. Port-based modeling of a flexible link. *IEEE Transactions on Robotics*, 23:650 – 660, Sep 2007.

[MMS09] A. Macchelli, C. Melchiorri, and S. Stramigioli. Port-based modeling and simulation of mechanical systems with rigid and flexible links. *IEEE Transactions on Robotics*, 25(5):1016–1029, Oct 2009.

[Nät19] J Nättilä. Runko: Modern multi-physics toolbox for simulating plasma. *arXiv preprint arXiv:1906.06306*, 2019.

[NFFE12] C. Nowakowski, J. Fehr, M. Fischer, and P. Eberhard. Model order reduction in elastic multibody systems using the floating frame of reference formulation. *IFAC Proceedings Volumes*, 45(2):40 – 48, 2012. 7th Vienna International Conference on Mathematical Modelling.

[Nor06] A.N. Norris. Dynamics of thermoelastic thin plates: A comparison of four theories. *Journal of Thermal Stresses*, 29(2):169–195, 2006.

[NY04] G. Nishida and M. Yamakita. A higher order Stokes-Dirac structure for distributed-parameter port-Hamiltonian systems. In *Proceedings of the 2004 American Control Conference*, volume 6, pages 5004–5009 vol.6, 2004.

[OGC04] R. Ortega and E. García-Canseco. Interconnection and damping assignment passivity-based control: a survey. *European Journal of Control*, 10(5):432 – 450, 2004.

[Olv93] P. J. Olver. *Applications of Lie groups to differential equations*, volume 107 of *Graduate texts in mathematics*. Springer-Verlag New York, 2nd edition, 1993.

[PAL+16] J.A. Perez, D. Alazard, T. Loquen, C. Pittet, and C. Cumer. Flexible multibody system linear modeling for control using component modes synthesis and double-port approach. *Journal of Dynamic Systems, Measurement, and Control*, 138(12), 08 2016. 121004.

[Pas06] R. Pasumarthy. *On Analysis and Control of Interconnected Finite- and Infinite-dimensional Physical Systems*. PhD thesis, University of Twente, September 2006.

[Pir89] O.A. Pironneau. *Finite element methods for fluids*. John Wiley and Sons, 1989.

[Pit79] J. Pitkäranta. Boundary subspaces for the finite element method with Lagrange multipliers. *Numerische Mathematik*, 33(3):273–289, 1979.

[Pit80] J. Pitkäranta. Local stability conditions for the Babuška method of Lagrange multipliers. *Mathematics of Computation*, 35(152):1113–1129, 1980.

[Pit81] J. Pitkäranta. The finite element method with Lagrange multipliers for domains with corners. *Mathematics of Computation*, 37(155):13–30, 1981.

[PSB+20] V. Preda, F. Sanfedino, S. Bennani, F. Boquet, and D. Alazard. Robust and adaptable dynamic response reshaping of flexible structures. *Journal of Sound and Vibration*, 468:115086, 2020.

[PZ18] D. Pauly and W. Zulehner. The divdiv-complex and applications to biharmonic equations. *Applicable Analysis*, pages 1–52, 2018.

[PZ20] D. Pauly and W. Zulehner. The elasticity complex, 2020. arXiv preprint arXiv:2001.11007.

[Red03] J.N. Reddy. *Mechanics of laminated composite plates and shells: theory and analysis*. CRC press, 2003.

[Red06] J.N. Reddy. *Theory and analysis of elastic plates and shells*. CRC press, 2006.

[Rei47] E. Reissner. On bending of elastic plates. *Quarterly of Applied Mathematics*, 5(1):55–68, 1947.

[RHM+17] F. Rathgeber, D.A. Ham, L. Mitchell, M. Lange, F. Luporini, A.T.T. McRae, G.T. Bercea, G.R. Markall, and P.H.J. Kelly. Firedrake: automating the finite element method by composing abstractions. *ACM Transactions on Mathematical Software (TOMS)*, 43(3):24, 2017.

[RMS13] H. Ramirez, B. Maschke, and D. Sbarbaro. Irreversible port-Hamiltonian systems: A general formulation of irreversible processes with application to the CSTR. *Chemical Engineering Science*, 89:223–234, 2013.

[RR04] M. Renardy and R.C. Rogers. *An Introduction to Partial Differential Equations*. Number 13 in Texts in Applied Mathematics. Springer-Verlag New York, 2nd edition, 2004.

[RRR19] M. Ramaswamy, J.-P. Raymond, and A. Roy. Boundary feedback stabilization of the Boussinesq system with mixed boundary conditions. *Journal of Differential Equations*, 266(7):4268 – 4304, 2019.

[RRTW19] B. Rong, X. Rui, L. Tao, and G. Wang. Theoretical modeling and numerical solution methods for flexible multibody system dynamics. *Nonlinear Dynamics*, 98(2):1519–1553, Oct 2019.

[RRWY10] B. Rong, X. Rui, G. Wang, and F. Yang. Discrete time transfer matrix method for dynamics of multibody system with real-time control. *Journal of Sound and Vibration*, 329(6):627 – 643, 2010.

[RSBR16] E. Rabizadeh, A. Saboor Bagherzadeh, and T. Rabczuk. Goal-oriented error estimation and adaptive mesh refinement in dynamic coupled thermoelasticity. *Computers & Structures*, 173:187 – 211, 2016.

[RT77] P.A. Raviart and J.M. Thomas. A mixed finite element method for 2-nd order elliptic problems. In Ilio Galligani and Enrico Magenes, editors, *Mathematical Aspects of Finite Element Methods*, pages 292–315, Berlin, Heidelberg, 1977. Springer Berlin Heidelberg.

[RZ18] K. Rafetseder and W. Zulehner. A decomposition result for Kirchhoff plate bending problems and a new discretization approach. *SIAM Journal on Numerical Analysis*, 56(3):1961–1986, 2018.

[San19] F. Sanfedino. *Experimental validation of a high accuracy pointing system*. PhD thesis, Université de Toulouse, April 2019.

[SAPB+18] F. Sanfedino, D. Alazard, V. Pommier-Budinger, A. Falcoz, and F. Boquet. Finite element based N-port model for preliminary design of multibody systems. *Journal of Sound and Vibration*, 415:128 – 146, 2018.

[Sch19] L. Scholz. Condensed forms for linear port-Hamiltonian descriptor systems. *Electronic Journal of Linear Algebra*, 35:65–89, 03 2019.

[SF19a] D. Schöllhammer and T.P. Fries. Kirchhoff-Love shell theory based on tangential differential calculus. *Computational mechanics*, 64(1):113–131, 2019.

[SF19b] D. Schöllhammer and T.P. Fries. Reissner-Mindlin shell theory based on tangential differential calculus. *Computer Methods in Applied Mechanics and Engineering*, 352:172–188, 2019.

[SHM19a] A. Serhani, G. Haine, and D. Matignon. Anisotropic heterogeneous n-D heat equation with boundary control and observation: I. Modeling as port-Hamiltonian system. *IFAC-PapersOnLine*, 52(7):51 – 56, 2019. 3rd IFAC Workshop on Thermodynamic Foundations for a Mathematical Systems Theory TFMST 2019.

[SHM19b] A. Serhani, G. Haine, and D. Matignon. Anisotropic heterogeneous n-D heat equation with boundary control and observation: II. Structure-preserving discretization. *IFAC-PapersOnLine*, 52(7):57 – 62, 2019. 3rd IFAC Workshop on Thermodynamic Foundations for a Mathematical Systems Theory TFMST 2019.

[Sim99] J.G. Simmonds. Major simplifications in a current linear model for the motion of a thermoelastic plate. *Quarterly of Applied Mathematics*, 57(4):673–679, 1999.

[Sim06] B. Simeon. On Lagrange multipliers in flexible multibody dynamics. *Computer Methods in Applied Mechanics and Engineering*, 195(50–51):6993 – 7005, 2006.

[Sim13] B. Simeon. *Computational flexible multibody dynamics*. Springer, 2013.

[Skr19] N. Skrepek. Well-posedness of linear first order port-Hamiltonian systems on multidimensional spatial domains, 2019. arXiv preprint arXiv:1910.09847.

[SMH19] A. Serhani, D. Matignon, and G. Haine. Partitioned finite element method for port-Hamiltonian systems with boundary damping: Anisotropic heterogeneous 2D wave equations. *IFAC-PapersOnLine*, 52(2):96 – 101, 2019. 3rd IFAC Workshop on Control of Systems Governed by Partial Differential Equations CPDE 2019.

[SS86] Y. Saad and M.H. Schultz. Gmres: A generalized minimal residual algorithm for solving nonsymmetric linear systems. *SIAM Journal on Scientific and Statistical Computing*, 7(3):856–869, 1986.

[SS17] M. Schöberl and K. Schlacher. Variational Principles for Different Representations of Lagrangian and Hamiltonian Systems. In Hans Irschik, Alexander Belyaev, and Michael Krommer, editors, *Dynamics and Control of Advanced Structures and Machines*, pages 65–73. Springer International Publishing, 2017.

[Ste95] R. Stenberg. On some techniques for approximating boundary conditions in the finite element method. *Journal of Computational and Applied Mathematics*, 63(1-3):139–148, 1995.

[Ste06] A. Steinbrecher. *Numerical Solution of Quasi-Linear Differential-Algebraic Equations and Industrial Simulation of Multibody Systems.* PhD thesis, TU Berlin, 01 2006.

[SvdSS12] M. Seslija, A.J. van der Schaft, and J.M.A. Scherpen. Discrete exterior geometry approach to structure-preserving discretization of distributed-parameter port-Hamiltonian systems. *Journal of Geometry and Physics*, 62(6):1509–1531, 2012.

[TRLGK18] V. Trenchant, H. Ramírez, Y. Le Gorrec, and P. Kotyczka. Finite differences on staggered grids preserving the port-Hamiltonian structure with application to an acoustic duct. *Journal of Computational Physics*, 373, 06 2018.

[TW09] M. Tucsnak and G. Weiss. *Observation and control for operator semigroups.* Birkhäuser Advanced Texts: Basler Lehrbücher. Birkhäuser Verlag, Basel, 2009.

[TWK59] S. Timoshenko and S. Woinowsky-Krieger. *Theory of plates and shells.* Engineering societies monographs. McGraw-Hill, 1959.

[TWRLG20] J. Toledo, Y. Wu, H. Ramírez, and Y. Le Gorrec. Observer-based boundary control of distributed port-Hamiltonian systems. *Automatica*, 120, 2020.

[TYBK90] T.M. Tan, A. Yousuff, L.Y. Bahar, and M. Konstantinidis. A modified finite element-transfer matrix for control design of space structures. *Computers & Structures*, 36(1):47 – 55, 1990.

[vdS06] A.J. van der Schaft. Port-Hamiltonian systems: an introductory survey. *Proceedings oh the International Congress of Mathematicians, Vol. 3, 2006-01-01, ISBN 978-3-03719-022-7, pags. 1339-1366*, Jan 2006.

[vdSM02] A.J. van der Schaft and B. Maschke. Hamiltonian formulation of distributed-parameter systems with boundary energy flow. *Journal of Geometry and Physics*, 42(1):166 – 194, 2002.

[Vil07] J.A. Villegas. *A Port-Hamiltonian Approach to Distributed Parameter Systems.* PhD thesis, University of Twente, May 2007.

[VNLF16] N.M.T. Vu, R. Nouailletas, F. Lefèvre, and F. Felici. Plasma q-profile control in tokamaks using a damping assignment passivity-based approach. *Control Engineering Practice*, 54:34 – 45, 2016.

[Vui14] P. Vuillemin. *Frequency-limited model approximation of large-scale dynamical models*. PhD thesis, Université de Toulouse, 2014.

[VZLGM09] J.A. Villegas, H. Zwart, Y. Le Gorrec, and B. Maschke. Exponential stability of a class of boundary control systems. *IEEE Transactions on Automatic Control*, 54(1):142–147, 2009.

[WH88] S.C. Wu and E.J. Haug. Geometric non-linear substructuring for dynamics of flexible mechanical systems. *International Journal for Numerical Methods in Engineering*, 26(10):2211–2226, 1988.

[WN03] T.M. Wasfy and A.K. Noor. Computational strategies for flexible multibody systems. *Applied Mechanics Reviews*, 56(6):553–613, 11 2003.

[Wri09] P. Wriggers. Mixed finite element methods - theory and discretization. In Carsten Carstensen and Peter Wriggers, editors, *Mixed Finite Element Technologies*, pages 131–177. Springer Vienna, Vienna, 2009.

[XJ20] K. Xu and Y. Jiang. Structure-preserving interval-limited balanced truncation reduced models for port-Hamiltonian systems. *IET Control Theory Applications*, 14(3):405–414, 2020.

[Yee66] K. Yee. Numerical solution of initial boundary value problems involving Maxwell's equations in isotropic media. *IEEE Transactions on Antennas and Propagation*, 14(3):302–307, 1966.

[You90] K.D. Young. Distributed finite-element modeling and control approach for large flexible structures. *Journal of Guidance, Control, and Dynamics*, 13(4):703–713, 1990.

[YSGU88] A. Yigit, R.A. Scott, and A. Galip Ulsoy. Flexural motion of a radially rotating beam attached to a rigid body. *Journal of Sound and Vibration*, 121(2):201 – 210, 1988.

[YY19] A. Yaghmaei and M.J. Yazdanpanah. Structure preserving observer design for port-Hamiltonian systems. *IEEE Transactions on Automatic Control*, 64(3):1214–1220, 2019.

Résumé — Malgré l'abondante littérature sur le formalisme port-Hamiltonienne (pH), les problèmes d'élasticité en deux ou trois dimensions géométriques n'ont presque jamais été considérés. Cette thèse vise à étendre l'approche port-Hamiltonienne (pH) à la mécanique des milieux continus. L'originalité apportée réside dans trois contributions majeures. Tout d'abord, la nouvelle formulation pH des modèles de plaques et des phénomènes thermoélastiques couplés est présentée. L'utilisation du calcul tensoriel est obligatoire pour modéliser les milieux continus et l'introduction de variables tensorielles est nécessaire pour obtenir une description pH équivalente qui soit intrinsèque, c'est-à-dire indépendante des coordonnées choisies. Deuxièmement, une technique de discrétisation basée sur les éléments finis et capable de préserver la structure du problème de la dimension infinie au niveau discret est développée et validée. La discrétisation des problèmes d'élasticité nécessite l'utilisation d'éléments finis non standard. Néanmoins, l'implémentation numérique est réalisée grâce à des bibliothèques open source bien établies, fournissant aux utilisateurs externes un outil facile à utiliser pour simuler des systèmes flexibles sous forme pH. Troisièmement, une nouvelle formulation pH de la dynamique multicorps flexible est dérivée. Cette reformulation, valable sous de petites hypothèses de déformations, inclut toutes sortes de modèles élastiques linéaires et exploite la modularité intrinsèque des systèmes pH.

Mots clés : Systèmes port-Hamiltonien, méchanique des solides, discretisation symplectique, méthode des éléments finis, dynamique multicorps

---

Abstract — Despite the large literature on port-Hamiltonian (pH) formalism, elasticity problems in higher geometrical dimensions have almost never been considered. This work establishes the connection between port-Hamiltonian distributed systems and elasticity problems. The originality resides in three major contributions. First, the novel pH formulation of plate models and coupled thermoelastic phenomena is presented. The use of tensor calculus is mandatory for continuum mechanical models and the inclusion of tensor variables is necessary to obtain an equivalent and intrinsic, i.e. coordinate free, pH description. Second, a finite element based discretization technique, capable of preserving the structure of the infinite-dimensional problem at a discrete level, is developed and validated. The discretization of elasticity problems requires the use of non-standard finite elements. Nevertheless, the numerical implementation is performed thanks to well-established open-source libraries, providing external users with an easy to use tool for simulating flexible systems in pH form. Third, flexible multibody systems are recast in pH form by making use of a floating frame description valid under small deformations assumptions. This reformulation include all kinds of linear elastic models and exploits the intrinsic modularity of pH systems.

Keywords: Port-Hamiltonian systems, continuum mechanics, structure preserving discretization, finite element method, multibody dynamics.
